Zbigniew Zembaty
Mario De Stefano   *Editors*

Seismic Behaviour and Design of Irregular and Complex Civil Structures II

Springer

Geotechnical, Geological and Earthquake Engineering

Volume 40

More information about this series at

Zbigniew Zembaty • Mario De Stefano
Editors

Seismic Behaviour and Design of Irregular and Complex Civil Structures II

Springer

Editors
Zbigniew Zembaty
Faculty of Civil Engineering
Opole University of Technology
Opole, Poland

Mario De Stefano
Department of Architecture (DiDA)
University of Florence
Florence, Italy

Preface

Structural regularity was a logical preference for traditional civil engineering design when the hand, static calculations motivated early researchers to simplify structural models. What is more, application of the simplified separate, planar models of the actual three-dimensional structures in most cases resulted in a conservative design. However, when it comes to modern structural dynamics and earthquake engineering, the results of similar simplifications are quite the opposite. The actual three-dimensional seismic response of irregular structures generates substantial additional design burdens compared to the results of direct applications of simple planar, code formulas. The same is true when it comes to complications in the seismic load models resulting from the wave propagation effects, i.e. spatial, non-uniform excitations or rotational ground motion. To address such formulated research aims, contributions coming from modern seismology are also required. In most cases, accounting for these effects will increase the seismic design load. Nonlinear effects during strong motion excitations, as well as modern passive and active control of irregular structures, require yet more advanced research methodology. Furthermore, major seismic codes are still in the need of improvement regarding both regularity criteria and analysis methods. That is why these effects are being intensively studied.

This book presents a second collection of the state-of-the-art papers devoted to these subjects and published within the framework of the Springer *Geotechnical, Geological and Earthquake Engineering* series. The first book[1] appeared in 2013 and had a positive response, particularly from the earthquake engineering community. The second volume contains 30 reviewed and edited contributions presented during the 7th *European Workshop on the Seismic Behaviour of Irregular and Complex Structures*, which took place in Opole, Poland, on October 17–18, 2014.

---

[1] Lavan O., De Stefano M. (editors), Seismic Behaviour and Design of Irregular and Complex Structures, Springer, Geotechnical, Geological and Earthquake Engineering, Dordrecht, 2013 (http://www.springer.com/gp/book/9789400753761).

Forty participants from 15 countries took part in this successful event organized as in the earlier workshops, by Working Group (WG) 8 of the European Association for Earthquake Engineering: *Seismic Behaviour of Irregular and Complex Structures*, as well as by the Polish Group for Seismic and Paraseismic Engineering affiliated to the Polish Academy of Sciences and by the Faculty of Civil Engineering, Opole University of Technology. Previous conferences which took place in Capri, Italy (1996); Istanbul, Turkey (1999); Florence, Italy (2002); Thessaloniki, Greece (2005); Catania, Italy (2008); and Haifa, Israel (2011) also resulted in published proceedings. This conference cycle has already established itself as a valuable venue for exchanging of ideas in the area of irregularity issues in earthquake engineering.

The book consists of 30 chapters and is divided into 3 parts:

- The first part, devoted to the complexity issues of ground motion modelled as wave propagation effect, consists of seven papers referring to seismic engineering and modern seismology issues.
- The second part, consisting of 20 chapters, covers the key area of structural irregularity effects on seismic response, both the horizontal ones, leading to structural torsion and vertical setbacks often leading to the amplification of the overall seismic response.
- The third part consists of three papers devoted to active and passive control of the irregular structures.

Opole, Poland   Zbigniew Zembaty
Florence, Italy   Mario De Stefano

Contents

Part III   Seismic Control and Monitoring of Irregular Structures

Contributors

Asimina M. Athanatopoulou Department of Civil Engineering, Aristotle University, Thessaloniki, Macedonia, Greece

Francesca Barbagallo Department of Civil Engineering and Architecture, University of Catania, Catania, Italy

André Belejo Oregon State University, Corvallis, OR, USA

Jan Benčat University Research Centre, University of Žilina, Žilina, Slovakia

Rita Bento ICIST, Instituto Superior Técnico, Universidade de Lisboa, Lisbon, Portugal

Piotr Bobra Faculty of Civil Engineering, Opole University of Technology, Opole, Poland

Melina Bosco Department of Civil Engineering and Architecture, University of Catania, Catania, Italy

Yael Daniel AJS Consulting Engineers, Haifa, Israel

Mario De Stefano Department of Architecture (DiDA), University of Florence, Florence, Italy

Peter Fajfar Faculty of Civil and Geodetic Engineering, University of Ljubljana, Ljubljana, Slovenia

Tomasz Falborski Faculty of Civil and Environmental Engineering, Gdańsk University of Technology, Gdańsk, Poland

Giovanna A.F. Ferrara Department of Civil Engineering and Architecture, University of Catania, Catania, Italy

Kenji Fujii Department of Architecture and Civil Engineering, Chiba Institute of Technology, Narashino, Chiba, Japan

Giada Gasparini Department DICAM, University of Bologna, Bologna, Italy

George K. Georgoussis Department of Civil Engineering Educators, School of Pedagogical and Technological Education (ASPETE), Attica, Greece

M.R. Ghayamghamian International Institute of Earthquake Engineering and Seismology, Tehran, Iran

Aurelio Ghersi Department of Civil Engineering and Architecture, University of Catania, Catania, Italy

M. Hashemifard International Institute of Earthquake Engineering and Seismology, Tehran, Iran

Robert Jankowski Faculty of Civil and Environmental Engineering, Gdańsk University of Technology, Gdańsk, Poland

Leszek R. Jaroszewicz Institute of Applied Physics, Military University of Technology, Warsaw, Poland

Erol Kalkan Earthquake Science Center, United States Geological Survey, Menlo Park, CA, USA

Suraj N. Khante Applied Mechanics Department, Government College of Engineering, Amravati, Maharashtra, India

Dietlinde Köber Reinforced Concrete Department, Technical University of Bucharest, Bucharest, Romania

Seweryn Kokot Faculty of Civil Engineering, Opole University of Technology, Opole, Poland

Aleksandra Korzec Institute of Hydro-Engineering Polish Academy of Sciences, Gdańsk-Oliwa, Poland

Jerzy K. Kowalski m-Soft Ltd., Warsaw, Poland

Zbigniew Krajewski Institute of Applied Physics, Military University of Technology, Warsaw, Poland

Anna Kurzych Institute of Applied Physics, Military University of Technology, Warsaw, Poland

Alessandra La Brusco Department of Architecture (DiDA), University of Florence, Florence, Italy

Oren Lavan Faculty of Civil and Environmental Engineering, Technion – Israel Institute of Technology, Haifa, Israel

Grigorios E. Manoukas Department of Civil Engineering, Aristotle University, Thessaloniki, Macedonia, Greece

Valentine Mariani Department of Architecture (DiDA), University of Florence, Florence, Italy

Edoardo M. Marino Department of Civil Engineering and Architecture, University of Catania, Catania, Italy

Rutuja S. Meshram Applied Mechanics Department, Government College of Engineering, Amravati, Maharashtra, India

G.R. Nouri Department of Civil Engineering, Faculty of Engineering, Kharazmi University, Tehran, Iran

Filip Pachla Institute of Structural Mechanics, Cracow University of Technology, Cracow, Poland

Michele Palermo Department DICAM, University of Bologna, Bologna, Italy

Zdzisław Pawlak Institute of Structural Engineering, Poznań University of Technology, Poznań, Poland

Iztok Peruš Faculty of Civil and Geodetic Engineering, University of Ljubljana, Ljubljana, Slovenia

Juan C. Reyes Department of Civil and Environmental Engineering, Universidad de los Andes, Bogota, Colombia

Andrea C. Riaño Department of Civil and Environmental Engineering, Universidad de los Andes, Bogota, Colombia

Andrea Rossi Rose School, EUCENTRE, Pavia, Italy

Pier Paolo Rossi Department of Civil Engineering and Architecture, University of Catania, Catania, Italy

Stefano Silvestri Department DICAM, University of Bologna, Bologna, Italy

Klemen Sinkovič Faculty of Civil and Geodetic Engineering, University of Ljubljana, Ljubljana, Slovenia

Barbara Sołtysik Faculty of Civil and Environmental Engineering, Gdańsk University of Technology, Gdańsk, Poland

Andrea Spagnoli Department of Civil, Environmental, Land Management, Engineering and Architecture, Parma University, Parma, Italy

Paola R. Stramondo Department of Civil Engineering and Architecture, University of Catania, Catania, Italy

Waldemar Świdziński Institute of Hydro-Engineering Polish Academy of Sciences, Gdańsk-Oliwa, Poland

Marco Tanganelli Department of Architecture (DiDA), University of Florence, Florence, Italy

Tadeusz Tatara Institute of Structural Mechanics, Cracow University of Technology, Cracow, Poland

Krzysztof P. Teisseyre Institute of Geophysics, Polish Academy of Sciences, Warsaw, Poland

Roman Teisseyre Institute of Geophysics, Polish Academy of Sciences, Warsaw, Poland

Amfilohios Throumoulopoulos Department of Civil Engineering, Aristotle University, Thessaloniki, Macedonia, Greece

Tomaso Trombetti Department DICAM, University of Bologna, Bologna, Italy

Stefania Viti Department of Architecture (DiDA), University of Florence, Florence, Italy

Elżbieta Wdowicka Polytechnic Faculty, Higher Vocational State School (PWSZ), Kalisz, Poland

Jacek Wdowicki Polytechnic Faculty, Higher Vocational State School (PWSZ), Kalisz, Poland

Kinga Woźniczko DHV HYDROPROJEKT Sp. z o.o., Warszawa, Poland

Dan Zamfirescu Reinforced Concrete Department, Technical University of Bucharest, Bucharest, Romania

Zbigniew Zembaty Faculty of Civil Engineering, Opole University of Technology, Opole, Poland

Part I
Ground Motion, Rotations and Wave Propagation Effects

Chapter 1
A General Procedure for Selecting and Scaling Ground Motion Records for Nonlinear Analysis of Asymmetric-Plan Buildings

Juan C. Reyes, Erol Kalkan, and Andrea C. Riaño

Abstract In performance assessment and design verification of complex structural systems including base-isolated buildings, high-rise structures and structures utilizing advanced lateral force resisting components (e.g., viscous dampers), nonlinear response history analysis (RHA) is now a common engineering tool to estimate seismic demands. Today, majority of ground motion selection and scaling methods are suitable for symmetric plan buildings with first-mode dominant response. There is, therefore, a need for a robust method to select and scale records for nonlinear RHAs of asymmetric-plan buildings with significant torsional response. Presented here is a generalized ground motion selection and scaling procedure called modal pushover-based (MPS) procedure. The proposed procedure explicitly considers structural strength, determined from pushover curves, and determines a scaling factor for each record to match a target value of roof displacement. The accuracy and efficiency of the procedure is evaluated by using computer models of symmetric- and asymmetric-plan buildings subjected to one or two horizontal components of ground motions. Analyses for one component of ground motions were conducted for five existing symmetric-plan buildings of 4, 6, 13, 19 and 52 stories; for two components of ground motion, 48 single-story systems and 10 multi-story buildings were analysed. Also examined here is the ASCE/SEI 7 scaling procedure for comparison purposes. This study clearly shows that the MPS procedure provides much superior results in terms of accuracy [true estimates

J.C. Reyes (✉) • A.C. Riaño
Department of Civil and Environmental Engineering, Universidad de los Andes, Carrera 1 Este No. 19A-40, Bogota, Colombia
e-mail: jureyes@uniandes.edu.co

E. Kalkan
Earthquake Science Center, United States Geological Survey, Menlo Park, CA, USA
e-mail: ekalkan@usgs.gov

of expected median engineering demand parameters (EDPs)] and efficiency (reduced record-to-record variability of EDPs) than the ASCE/SEI 7 scaling procedure.

Keywords Scaling seismic records • Modal pushover based scaling • Nonlinear analysis • Asymmetric-plan buildings • Selecting seismic records

1.1 Introduction

Performance-based procedures for evaluating existing buildings and proposed designs of new buildings in the U.S. require response history analyses (RHAs) for an ensemble of earthquake records to determine EDPs for validation of a targeted performance criterion. Earthquake records selected for RHAs often need to be scaled to a seismic hazard level considered.

Kalkan and Chopra (2009) developed the modal pushover-based scaling (MPS) procedure for selecting and scaling earthquake ground motion records in a form convenient for evaluating existing structures and proposed designs of new structures. This procedure explicitly considers structural strength, obtained from the first-"mode" pushover curve, and determines a scaling factor for each record to match a target value of the deformation of the first-"mode" inelastic SDF system. The MPS procedure has been proven to be accurate and efficient for low-, medium- and high-rise buildings with symmetric plan (Kalkan and Chopra 2010, 2011, 2012) subjected to one component of ground motion. Recently, Reyes and Chopra (2011a, b, 2012) extended the MPS procedure for one component (mentioned above) to two horizontal components of ground motion.

Reyes and Quintero (2014) proposed a new version of the MPS procedure for single-story asymmetric-plan buildings. Reyes et al. (2014) extended this procedure to multi-story asymmetric-plan buildings. In this investigation, the developed procedure is compared against the ASCE/SEI 7-10 (ASCE7 henceforth) ground motion scaling procedure for 3D analysis. Based on results from nine multi-story asymmetric-plan buildings with various plan shapes, it is shown that the MPS procedure provides much superior results in terms of accuracy and efficiency than the ASCE/SEI 7-10 ground motion scaling procedure.

1.2 Modal Pushover-Based Scaling (MPS) Procedure

The MPS procedure is implemented here in three phases: (1) computation of target roof displacement and pushover analyses, (2) scaling phase, and (3) selection phase. The step-by-step procedure is presented here in a general form (Reyes et al. 2014).

1.2.1 Target Roof Displacement and Pushover Analyses

1. For a given site, define the target spectra $\hat{A}_x$ and $\hat{A}_y$, in this study taken as the median of the 5-percent damped pseudo-acceleration response spectra of two components of the ground motions.
2. Compute the natural frequencies ω_n (periods T_n) and modes ϕ_n of the first few modes of linear-elastic vibration of the building. For each ground motion component direction (x or y), identify the first, second and third modes as the three modes with the largest effective modal mass.
3. Develop the base shear-roof displacement, $V_{bn} - u_{rn}$, relationship or pushover curve by nonlinear static analysis of the building subjected to the nth-"mode" invariant force distribution:

$$s_n^* = \left[\begin{array}{c} \mathbf{m}\phi_{xn} \\ \mathbf{m}\phi_{yn} \\ \mathbf{I}_o\phi_{\theta n} \end{array} \right]$$

where $\mathbf{m}$ is a diagonal matrix of order N with $m_{jj} = m_j$, the mass lumped at the jth floor level; $\mathbf{I}_o$ is a diagonal matrix of order N with $I_{ojj} = I_{oj}$, the moment of inertia of the jth floor diaphragm about a vertical axis through the center of mass (C.M.); and subvectors ϕ_{xn}, ϕ_{yn}, and $\phi_{\theta n}$ of the nth mode ϕ_n represent x, y and θ components of ground motion, respectively. This step should be implemented only for the first three "modes" in the direction under consideration; this step could be omitted for the higher-"modes" if they are treated as linear-elastic (Chopra 2007).
4. Idealize the $V_{bn} - u_{rn}$ pushover curve as a bilinear or trilinear curve, as appropriate, and convert it into the force-deformation, $(F_{sn}/L_n) - D_n$, relationship for the nth-"mode" inelastic SDF system using well-known formulations [10]:

$$\frac{F_{sn}}{L_n} = \frac{V_{bn}}{M_n^*} \quad D_n = \frac{u_{rn}}{\Gamma_n\phi_{rn}}$$

where F_{sn} is a nonlinear hysteretic function of the nth modal coordinate and M_n^* is the effective modal mass for the nth-"mode" (Chopra 2007).

$$\Gamma_n = \frac{L_n}{M_n} = \frac{\phi_n^T\mathbf{M}\mathbf{\iota}}{\phi_n^T\mathbf{M}\phi_n} \quad \mathbf{M} = \left[\begin{array}{ccc} \mathbf{m} & 0 & 0 \\ 0 & \mathbf{m} & 0 \\ 0 & 0 & \mathbf{I}_o \end{array} \right] \quad \mathbf{\iota}_x = \left[\begin{array}{c} \mathbf{1} \\ \mathbf{0} \\ \mathbf{0} \end{array} \right] \quad \mathbf{\iota}_y = \left[\begin{array}{c} \mathbf{0} \\ \mathbf{1} \\ \mathbf{0} \end{array} \right]$$

$\mathbf{1}$ and $\mathbf{0}$ are vectors of dimension N with all elements equal to one and zero, respectively; and ϕ_{rn} is the value of ϕ_n at the roof.
5. Establish the target roof displacement $\hat{u}_r$. For a system with known T_n, damping ratio ξ_n, and force-deformation curve (Step 3), determine the peak deformation

D_n for the nth-"mode" inelastic SDF system due to each of the unscaled ground motions $\ddot{u}_g(t)$ by solving:

$$\ddot{D}_n(t) + 2\xi_n\omega_n\dot{D}_n(t) + \frac{F_{sn}}{L_n} = -\ddot{u}_g(t) \rightarrow D_n$$

Determine $\hat{D}_n$ as the median of the D_n values. Calculate roof displacement in the direction under consideration of the nth-"mode" as $\hat{u}_{rn} = \Gamma_n\phi_{rn}\hat{D}_n$, and compute the roof displacement in the direction under consideration $\hat{u}_r$ from values of $\hat{u}_{rn}$ using a suitable modal combination method (e.g., complete quadratic combination). In practical applications, target deformation $\hat{D}_n$ can be computed as $\hat{D}_n = C_{Rn}\hat{D}_{no}$, where C_{Rn} is the inelastic deformation ratio, estimated from empirical equations (Chopra and Chintanapakdee 2004), $\hat{D}_{no} = (T_n/2\pi)^2\hat{A}_n$ and $\hat{A}_n$ is the target pseudo-spectral acceleration at period T_n.

1.2.2   Scaling Phase

6. Compute the scale factor SF for each record in the direction under consideration by solving the following nonlinear equation: $u_r - \hat{u}_r = 0$, where u_r is the peak roof displacement in the direction under consideration from the scaled records. Because this equation is nonlinear, SF cannot be determined a priori, but requires an iterative procedure as shown below:

   (a) Select an initial value of the scale factor SF, and compute deformation $D_n(t)$ for the nth-"mode" inelastic SDF due to the scaled record by solving: $\ddot{D}_n(t) + 2\xi_n\omega_n\dot{D}_n(t) + F_{sn}/L_n = -SF \times \ddot{u}_g(t) \rightarrow D_n(t)$

   (b) Compute roof displacement of the nth-"mode" in the direction under consideration: $u_{rn}(t) = \Gamma_n\phi_{rn}D_n(t)$

   (c) Compute roof displacement in the direction under consideration:

   $$u_r = max\left(\left|\sum_n u_{rn}(t)\right|\right)$$

   (d) Estimate error: $\varepsilon = u_r - \hat{u}_r$

   (e) Adjust the value of the scale factor SF, and repeat steps "a" to "d" until ε is less than a tolerance value.

In this study, step 6 was implemented by a numerical algorithm. By developing steps "a" to "e", separately for the x and y components of the record, scale factors SF_x and SF_y are determined. Note that pushover curves (step 4), and target roof displacement (step 5) will be different for the two horizontal components of the ground motion.

1.2.3 Selection Phase

7. Select the first k records with the lower values of:

$$Error = \sum_{i=4}^{6} \left(\left| SF_x A_x(T_i) - \hat{A}_x(T_i) \right| + \left| SF_y A_y(T_i) - \hat{A}_y(T_i) \right| \right)$$

where $\hat{A}_x$ and $\hat{A}_y$ are vectors of spectral values $\hat{A}_i$ at different periods T_i ($T_i = T_4$, T_5, T_6); A_x and A_y are vectors of spectral values for the unscaled records over the same periods.

1.3 Point of Comparison (Benchmark)

The benchmark or comparison point of an EDP is defined in this study as the median value of EDPs obtained from nonlinear RHAs of the structure subjected to a large set of unscaled records. The accuracy and efficiency of the MPS and ASCE7 procedures are examined by comparing their median EDP estimates from subset of records against the benchmark values, and by comparing record-to-record variability of the EDPs.

1.4 Study Cases for One Component RHAs

For a single horizontal component of ground motion, the MPS procedure scales each record by a factor such that the deformation of the first-"mode" inelastic SDF system matches a target value of the inelastic deformation. When steps 1 thru 6 of the procedure shown in Sect. 1.2 are implemented for one-component of ground motion, the following simplifications may be made: (1) Only the fundamental mode in the direction of analysis is used in steps 3 thru 6; (2) Target deformation $\hat{D}_1$ may be used instead of a target roof displacement $\hat{u}_r$; (3) In order to compute the scale factor SF in step 6, the nonlinear equation may be written as $D_1 - \hat{D}_1 = 0$; (4) The selection phase (step 7) may consider only the unscaled spectral values at the second mode in the direction of analysis instead of the spectral values at T_4, T_5 and T_6. These simplifications may reduce significantly the computational time.

A large group of representative buildings in California were selected to study the one-component MPS and the ASCE7 procedure. This group consists of three existing low- and mid-rise steel special moment resisting frame (SRMF) buildings with 4, 6 and 13 stories, and two existing tall steel SRMF buildings having 19 and 52 stories. A description of these structures and complete details of their analytical models are reported in Kalkan and Chopra (2011, 2012). For these studies a total of 21 near-fault
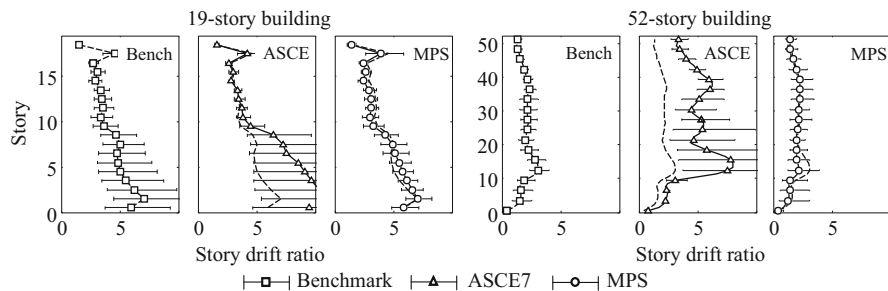
Fig. 1.1 Inter-story drift ratios in percentage for the 19- and 52-story buildings. In each case the marker and the horizontal line represent the median value of the EDP $\pm$ σ, assuming a log-normal distribution

strong ground motions were selected. These motions were recorded during seismic events with moment magnitude $M_W \geq 6.5$ at fault distances $R_{RUP} \leq 12$ km. Selected records are listed in Table 1 of Kalkan and Chopra (2011, 2012)

For those five buildings, the median values of EDPs attributable to sets of seven ground motions scaled by the two methods—MPS and ASCE7—were computed by nonlinear RHAs of the buildings and compared against the benchmark EDP values. Representative results for two tall buildings are shown in Fig. 1.1. For the 19-story building, the first three panels of this figure show the benchmark (abbreviated as Bench) EDPs, and EDPs for the ASCE7 and MPS procedures, respectively. The next three panels display similar results for the 52-story building. The markers and horizontal lines represent the median EDP value $\pm$ one standard deviation σ assuming a lognormal distribution. For comparison purposes, the median benchmark values are kept in all sub-plots as a dashed line. The ASCE7 scaling method grossly overestimates the inter-story drift ratios (IDRs) at almost all floors; for example, IDRs are overestimated by as much as 80 % for the 19-story building, and almost 170 % for the 52-story building. In contrast, IDRs obtained from MPS differ from the benchmark results by less than 10 % in most cases. Furthermore, the dispersion in EDPs as a result of the seismic records scaled according to the ASCE7 procedure is much larger than those from the MPS procedure.

Similar results were observed for the other three buildings analysed (low- and mid-rise buildings); these results are not shown due to space limitations. Additional findings can be found in Kalkan and Chopra (2011, 2012).

1.5 Study Cases for Two Components RHAs

The accuracy and efficiency of the MPS procedure for multi-story symmetric-plan buildings subjected to two components of ground motions was examined using a computer model of an existing 9-story steel moment frame building (Reyes and Chopra 2011b). For asymmetric-plan buildings, two categories of hypothetical

$\bigcirc$ corner c1 $\diamondsuit$ x-girder $\triangle$ y-girder $\bullet$ center of mass $+$ center of stiffness
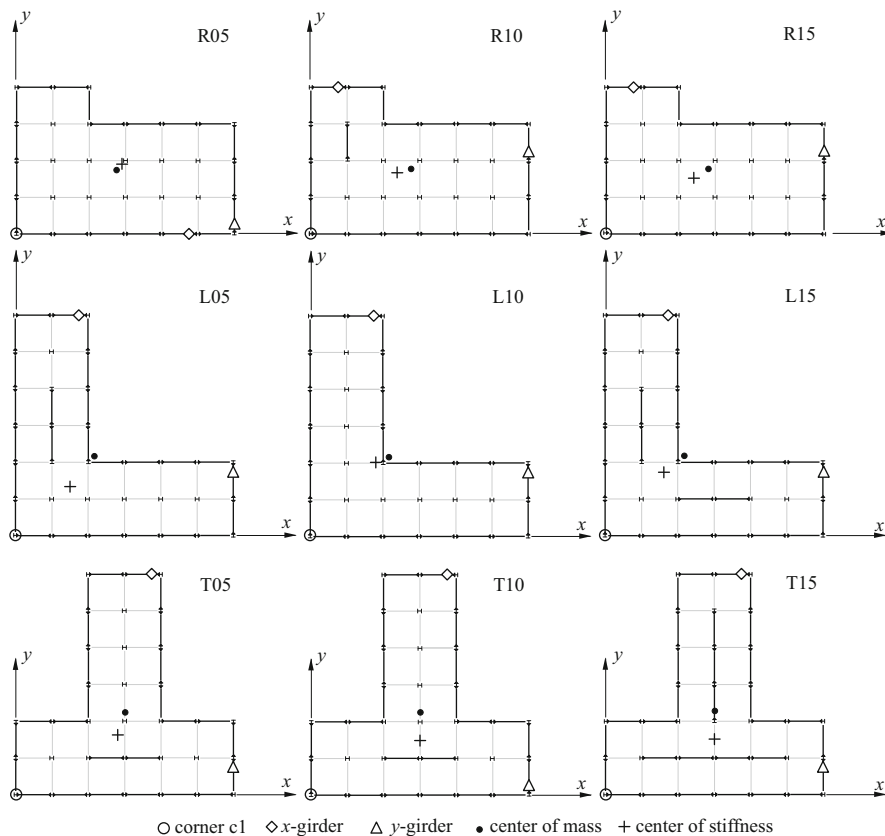
Fig. 1.2 Plan views of the nine multi-story asymmetric-plan buildings

buildings were considered: single-story and multi-story buildings. The single-story buildings modelled are 48 structures with fundamental vibration periods T_n equal to 0.2, 0.5, 1 and 2 s, and with yield strength reduction factors R equal to 2, 3, 5, and a value that leads to linear elastic design. Their lateral resisting system consists of buckling restrained braced frames with non-moment-resisting beam–column connections. The structures considered in the multi-story buildings category are nine steel SMRF buildings with 5, 10 and 15 stories. Their plan shapes are shown in Fig. 1.2, where the moment resisting frames are highlighted. The buildings are identified by the letters R, L and T followed by the number of stories: plan R is approximately rectangular, plan T is symmetric about the x axis, and plan L is un-symmetric about both x and y axis. Further details of their structural systems including the fundamental periods, mode shapes, torsional irregularity factors etc. can be found in Reyes and Quintero (2014) and Reyes et al. (2015).

For the single-story buildings, the 30 near-fault records selected were recorded from nine shallow crustal earthquakes with moment magnitude $M_W = 6.7 \pm 0.2$
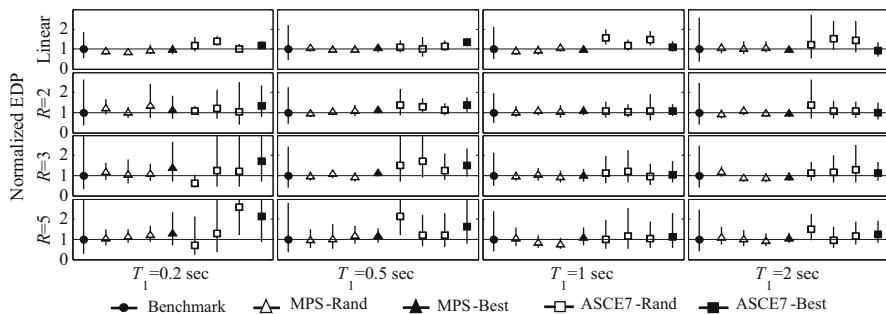
Fig. 1.3 Normalized roof displacement (EDP) at point c2 along x-direction of the L-shaped plan single-story buildings (see Fig. 1.2). For each set the marker and the *vertical line* represent the median value of the EDP ± one standard deviation, assuming a log-normal distribution
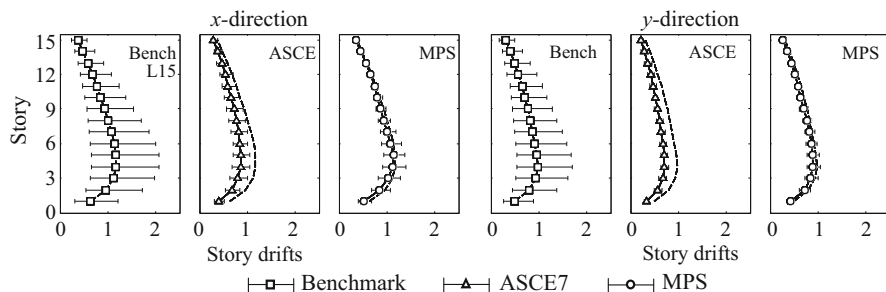
Fig. 1.4 Inter-story drift ratios in percentage along x- and y-direction at corner c1 of the L-shaped plan 15-story building (see Fig. 1.2). In each case the marker and the horizontal line represent the median value of the EDP ± σ, assuming a log-normal distribution

recorded at distances (R_{RUP}) ranging from 0.1 to 15 km. The seismic scenario for multi-story buildings consists of 30 far-field ground motion records populated from seven shallow crustal earthquakes with moment magnitude $M_W = 6.7 \pm 0.2$ at distances ranging from 20 to 30 km. The selected seismic records are listed in Table 1 in Reyes and Quintero (2014) and Reyes et al. (2015).

The procedure developed in Sect. 1.2 is compared against the ASCE7 scaling procedure. Representative results from single-story buildings and 15-story building are shown in Figs. 1.3 and 1.4, respectively. These structures have L-shaped plan with significant plan irregularity. Figure 1.3 includes three sets of seven records randomly selected (called "MPS-Rand" and "ASCE7-Rand") and one set of seven records selected by implementing an improved selection procedure (called "MPS-Best" and "ASCE7-Best"). Roof displacements (normalized by the corresponding benchmark results) obtained from sets "MPS-Rand" (Fig. 1.3) are accurate, and show a low "record-to-record" and "set-to-set" variability. Only displacements are unsuccessfully estimated for short-period structures designed for high values of yield strength reduction factors. A considerable improvement in accuracy and

"record-to-record" variability is obtained when sets "MPS-Best" (Fig. 1.3) are used for estimating the roof displacements; in this case, the errors are not greater than 20 %. Roof displacements obtained from sets "ASCE7-Rand" (Fig. 1.3) are in general less accurate and show a large "record-to-record" and "set-to-set" variability; overestimation of roof displacements is as high as 40 %.

Figure 1.4 shows story drifts at a selected corner of the building (c1 in Fig. 1.2) from records scaled and selected according to MPS and ASCE7 procedures together with benchmark values. This figure confirms that for the multi-story case (L15 building), the records scaled according to the MPS procedure lead to more accurate estimates of median values of EDPs than ASCE7 scaling procedure. The maximum discrepancies encountered by scaling records according to the ASCE7 procedure are reduced when these records are scaled by the MPS procedure; for example, the error in story drifts decreases from 28 % to 8 %. Due to limited space, we only show here a representative set of results; additional findings can be found in Reyes and Quintero (2014) and Reyes et al. (2015).

1.6   Conclusions

This paper presents summary of a general procedure for selecting and scaling ground motion records for nonlinear response history analyses of asymmetric-plan buildings with significant plan irregularity. Based on results from multiple study cases, it is clearly shown that the modal-pushover-based (MPS) procedure provides much superior computation of EDPs in terms of accuracy and efficiency as compared to the ASCE7 scaling method. This superiority is evident in two respects. First, the ground motions scaled according to the extended MPS procedure provide median values of EDPs that are much closer to the benchmark values than is achieved by the ASCE7. Second, the dispersion (or record to-record variability) in the EDPs due to seven scaled records around the median is much smaller when records are scaled by the MPS procedure compared to the ASCE7 procedure.

References

Chopra AK (2007) Dynamics of structures: theory and applications to earthquake engineering, 4th edn. Prentice-Hall, Englewood Cliffs, pp 403–445

Chopra AK, Chintanapakdee C (2004) Inelastic deformation ratios for design and evaluation of structures: single-degree-of-freedom bilinear systems. ASCE J Struct Eng 130(9):1309–1319

Kalkan E, Chopra AK (2009) Modal pushover-based ground motion scaling procedure for nonlinear response history analysis of structures. In: Proceedings of the Structural Engineers Association of California Convention, San Diego, CA, 2009

Kalkan E, Chopra AK (2010) Practical guidelines to select and scale earthquake records for nonlinear response history analysis of structures, U.S. Geological Survey Open-File Report 2010-1068. Available at http://pubs.usgs.gov/of/2010/1068/. Accessed 22 Jan 2015

Kalkan E, Chopra AK (2011) Modal-pushover-based ground-motion scaling procedure. J Struct Eng 137(3):298–310

Kalkan E, Chopra AK (2012) Evaluation of modal pushover-based scaling of one component of ground motion: tall buildings. Earthq Spectra 28(4):1469–1493

Reyes JC, Chopra AK (2011a) Three-dimensional modal pushover analysis of buildings subjected to two components of ground motion, including its evaluation for tall buildings. Earthq Eng Struct Dyn 40:789–806

Reyes JC, Chopra AK (2011b) Evaluation of three-dimensional modal pushover analysis for asymmetric-plan buildings subjected to two components of ground motion. Earthq Eng Struct Dyn 40:1475–1494

Reyes JC, Chopra AK (2012) Modal pushover-based scaling of two components of ground motion records for nonlinear RHA of buildings. Earthq Spectra 28(3):1243–1267

Reyes JC, Quintero O (2014) Modal pushover-based scaling of earthquake records for nonlinear analysis of single-story asymmetric-plan buildings. Earthq Eng Struct Dyn 43:1005–1021

Reyes JC, Riaño AC, Kalkan E, Arango CM (2015) Extending modal pushover-based scaling (MPS) procedure for nonlinear response history analysis of multi-story unsymmetric-plan buildings. Eng Struct 88:125–137

Chapter 2
Prediction of the "Average" Peak Nonlinear Seismic Response of Asymmetric Buildings Under Bi-directional Ground Motion Acting at an Arbitrary Angle of Incidence

Kenji Fujii

Abstract In this study the "reduced response spectrum" is introduced for the prediction of the "average" response of all possible angle of incidence, and the "average" peak seismic response of an asymmetric building under horizontal bi-directional ground motion, acting at an arbitrary angle of incidence, is predicted based on the procedure proposed in Fujii (Bull Earthq Eng 12:909–938, 2014). In this study, the following two definitions of the "reduced response spectrum" are examined; (A) the geometric mean spectrum of the horizontal major and minor components, and (B) the square root of the average of squares spectrum from all possible angle of incidence. In the numerical example, nonlinear time-history analyses of a four-storey torsionally stiff asymmetric building are carried out considering the various directions of seismic inputs, and these results are compared with the predicted results. The results show that the predicted "average" peak response displacement for the flexible-side frame satisfactorily agrees with the average of the time-history analyses results, either definition of the "reduced response spectrum".

Keywords Asymmetric building • Bi-directional ground motion • Geometric mean spectrum • Pushover analysis • Equivalent SDOF model

2.1 Introduction

In designing new buildings for earthquake resistance or when conducting seismic evaluation of existing buildings, a horizontal ground motion is applied to each of the main orthogonal axes of the buildings. However, for the seismic assessment of

K. Fujii (✉)
Department of Architecture and Civil Engineering, Chiba Institute of Technology,
2-17-1 Tsudanuma, Narashino, Chiba 275-0016, Japan
e-mail: kenji.fujii@it-chiba.ac.jp

asymmetric buildings this procedure may be inadequate because the most critical direction of incidence of the seismic input, which would produce the largest response, may be different from the direction of the building's main orthogonal axes, and the major component of ground motion may act in any direction.

For this purpose the author has proposed a simplified procedure to predict the largest peak seismic response of an asymmetric building subjected to horizontal bi-directional ground motion acting at an arbitrary angle of incidence (Fujii 2014). In this procedure, the response spectra of the two horizontal ground motion components are assumed to be identical. The response spectrum of the horizontal minor component is assumed to be the same as that of the major component. These assumptions may be valid for a conservative prediction of the "largest" peak responses. Even though this idealization is simple, it may be too conservative for use in the seismic assessment of structures. Besides, as Beyer and Boomer has noted in their study (Beyer and Boomer 2007), that the "average", or the median, structural response of all possible angle of incidence should be considered from the aspect of the probabilistic seismic hazard assessment (PSHA) lather than the "largest", or the maximum, structural response.

One of the very simple approaches to predict the "average" peak response is using the response spectrum, which is somehow reduced considering the variation of response spectrum of all orientation, and apply the procedure proposed in previous study (Fujii 2014). However how to define the "reduced response spectrum" for the better prediction of the "average" responses remains problem. One of the candidate of the reduced response spectrum is the geometric mean spectrum of orthogonal components (Beyer and Boomer 2006, 2007), because it is commonly used as horizontal component definition in a ground motion prediction equation. The another candidate of the reduced response spectrum is, from the aspect of structural response, the square root of the average of squares spectrum from all possible angle of incidence, because the sum of squares of velocity spectrum of two orthogonal components is strongly related to the seismic input energy of structure.

In this study the "reduced response spectrum" is introduced for the prediction of the "average" response of all possible angle of incidence, and then the "average" peak seismic response of an asymmetric building under horizontal bi-directional ground motion, acting at an arbitrary angle of incidence, is predicted based on the procedure proposed in Fujii (2014). In this study, two definitions of the "reduced response spectrum" are examined.

In the numerical example, nonlinear time-history analyses of a four-storey torsionally stiff (TS) asymmetric building are carried out considering various directions of seismic inputs, and these results are compared with the predicted results.

2.2 Description of the Procedure

2.2.1 Definition of the "Reduced Response Spectrum"

In this study, the "reduced response spectrum" is introduced for the prediction of the "average" peak response. The definition of the "reduced response spectrum" is illustrated in Fig. 2.1.

A set of orthogonal axes U-V in the X-Y plane is considered, with the U-axis being the principal axis of the first modal response (Fujii 2010, 2011). The asymmetric buildings are N-storey buildings, with $3N$ degrees of freedom ($3N$-DOFs) oriented for the multi-storey model presented here. Another set of orthogonal axes ξ-ζ in the X-Y plane is considered, with the ξ and ζ axes being the axes of the horizontal major and minor components of the seismic input, respectively.

It is assumed that the pseudo acceleration spectra of the ξ and ζ components, $_pS_{A\xi}(T)$ and $_pS_{A\zeta}(T)$, respectively, are similar (Fig. 2.1b).

The ratio of $_pS_{A\zeta}(T)$ to $_pS_{A\xi}(T)$, γ, is constant, as shown in Eq. 2.1.

$$\gamma = {_pS_{A\zeta}}(T) / {_pS_{A\xi}}(T) = \text{const.} \tag{2.1}$$

The thick dotted circles in Fig. 2.1a show the simplified seismic inputs of each direction for the prediction of the "average" peak response, while the thin dotted circle in this figure shows the simplified seismic input for the prediction of the "largest" peak response. Note that in the previous study (Fujii 2014), the spectrum of the major component $_pS_{A\xi}(T)$ is used to predict the "largest" peak response. In this study, $_pS_{A\xi}(T)$ is replaced by the reduced response spectrum $_p\overline{S}_{AU}(T)$ as shown in Fig. 2.1b.

In this study, the following two definitions of the "reduced response spectrum" are examined; (A) the geometric mean spectrum of the horizontal major and minor components, and (B) the square root of the average of squares spectrum from all possible angle of incidence.
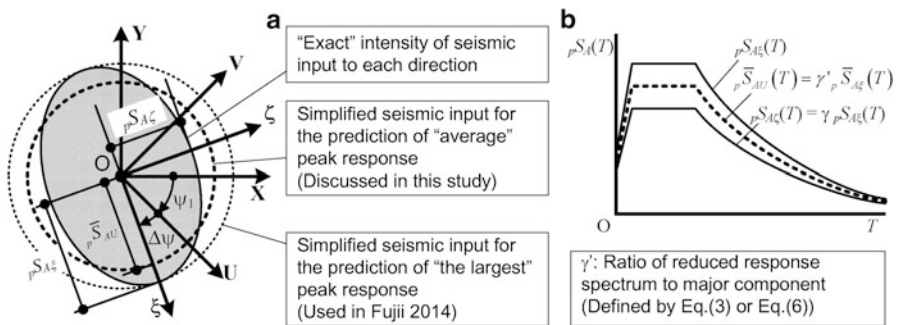
Fig. 2.1 Definition of the "reduced response spectrum" for the prediction of the "average" peak response. (**a**) Intensity of seismic input to each direction. (**b**) Reduced response spectrum

If the reduced response spectrum $_p\overline{S}_{AU}(T)$ is defined as the geometric mean spectrum of the horizontal major and minor components, $_p\overline{S}_{AU}(T)$ is calculated from Eq. 2.2.

$$_p\overline{S}_{AU}(T) = \sqrt{_pS_{A\xi}(T)\,_pS_{A\zeta}(T)}. \tag{2.2}$$

Substituting Eq. 2.1 into Eq. 2.2, the ratio of reduced response spectrum to major component, γ', is obtained as in Eq. 2.3.

$$\gamma' = {}_p\overline{S}_{AU}(T)/_pS_{A\xi}(T) = \sqrt{\gamma}. \tag{2.3}$$

Note that in general, the geometric mean spectrum of orthogonal components depends on the angle of incidence considered, as discussed in Boore et al. (2006) and Beyer and Boomer (2007). However in this study, the geometric mean spectrum of the horizontal major and minor components, defined as Eq. 2.2, is used as the one definition of the reduced response spectrum for the simplicity.

Another definition of the reduced response spectrum considered in this paper is expressed as Eq. 2.4.

$$_p\overline{S}_{AU}(T) = \sqrt{\frac{1}{\pi}\int_0^\pi \left\{_pS_{AU}(T, \Delta\psi)\right\}^2 d\Delta\psi}. \tag{2.4}$$

$$\begin{aligned}\left\{_pS_{AU}(T, \Delta\psi)\right\}^2 &= \left\{_pS_{A\xi}(T)\right\}^2 \cos^2(\Delta\psi) + \left\{_pS_{A\zeta}(T)\right\}^2 \sin^2(\Delta\psi) \\ &= \left\{\cos^2(\Delta\psi) + \gamma^2 \sin^2(\Delta\psi)\right\}^2 \left\{_pS_{A\xi}(T)\right\}^2.\end{aligned} \tag{2.5}$$

In Eq. 2.4, $_pS_{AU}(T, \Delta\psi)$ is the pseudo acceleration spectrum of the U-component, and $\Delta\psi$ is the angle between the U and ξ axes as shown in Fig. 2.1.

Substituting Eq. 2.5 into Eq. 2.4, the ratio γ' is obtained as in Eq. 2.6.

$$\gamma' = \sqrt{(1 + \gamma^2)/2}. \tag{2.6}$$

Note that from the comparisons of Eqs. 2.3 and 2.6, the reduced spectrum defined as (B) the square root of the average of squares spectrum from all possible angle of incidence (Eq. 2.6) is larger than that defined as (A) the geometric mean spectrum of the horizontal major and minor components (Eq. 2.3). Therefore, the prediction of the "average" response by using Eq. 2.6 will result more conservative than that by using Eq. 2.3.

2.2.2 Outline of Simplified Procedure

An outline of the proposed procedure to predict the "average" peak response is summarized in Fig. 2.2. The fundamental assumptions of the proposed procedure are as follows:

1. The spectra of the two horizontal ground motion components are assumed to be identical to the reduced response spectrum $_p\overline{S}_{AU}(T)$;
2. The building oscillates predominantly in a single mode in each set of orthogonal directions;
3. The principal directions of the first and second modal responses are almost orthogonal.

Note that these assumptions are the same as the procedure proposed previously in Fujii (2014) except for the use of the reduced response spectrum. Therefore, the details of the procedure are the same as shown in previous study (Fujii 2014), except for the seismic input.

2.3 Numerical Examples

2.3.1 Building Model

The building investigated in this study was a four-storey asymmetric building model as shown in Fig. 2.3. This building model, with bi-directional eccentricity, is the Model-B1 in previous study (Fujii 2014). Each frame structure was designed according to the weak-beam strong-column concept. The longitudinal reinforcements of the concrete sections were determined so that the potential hinges were located at all the beam-ends and bottoms of the columns, and the structural wall in the first storey. Sufficient shear reinforcement was assumed to be provided to prevent premature shear failure. The base shear coefficients obtained from the planar pushover analysis in both the X and Y-directions, which were the values when the roof displacement reached 1 % of the total height H_N, were 0.522 and 0.455, respectively. Further details of this model can be found in previous study (Fujii 2014).

Figure 2.4 shows the natural modes of the building model in the elastic range. Here, T_{ke} is the kth natural period in the elastic range, ψ_{ke} is the angle of incidence of the principal direction of the kth modal response in the elastic range with its tangent given by Eq. 2.7, and $R_{\rho ke}$ is the torsional index of the kth mode (Fujii 2014) in the elastic range, as defined by Eq. 2.8.

STEP 1: Pushover Analysis (1st Mode)

MDOF Model

Displacement-Based Mode-Adaptive Pushover Analysis

1st Mode Vector $\Gamma_{1U}\varphi_1$:Variable

Mass matrix: **M**, Displacement: **d**
Restoring force: $\mathbf{f_R}$

Note: Principal direction of the first modal response (U-Dir.) is determined based on the first mode vector at each nonlinear stage.

Reduction

Equivalent SDOF Model (1st Mode)

D_{1U}^* A_{1U}^*

U

Excitation

D_{1U}^*

$D_{1U}^* = \Gamma_{1U}\varphi_1{}^{\mathbf{T}}\mathbf{Md}/M_{1U}^*, A_{1U}^* = \Gamma_{1U}\varphi_1{}^{\mathbf{T}}\mathbf{f_R}/M_{1U}^*$
$M_{1U}^* = \Gamma_{1U}{}^2\varphi_1{}^{\mathbf{T}}\mathbf{M}\varphi_1$

STEP 2: Prediction of Peak Response (1st Mode)

Capacity curve:
A_{1U}^*-D_{1U}^* relationship (Results of STEP 1)

Demand curve:
Reduced response spectrum

$A_{1U}^*, {}_pS_A$ Demand

Capacity

Predicted peak ($D_{1U}^*{}_{max}, A_{1U}^*{}_{max}$)

D_{1U}^*, S_D

STEP 3: Pushover Analysis (2nd Mode)

MDOF Model

2nd Mode Vector $\Gamma_{2V}\varphi_2$:Determined in terms of $\Gamma_{1U}\varphi_1$ at $D_{1U}^*{}_{max}$

Pushover Analysis
:Invariant force distribution $\mathbf{P_2} = \mathbf{M}(\Gamma_{2V}\varphi_2)$

Reduction

Equivalent SDOF Model (2nd Mode)

D_{2V}^* V A_{2V}^*

Excitation

D_{2V}^*

$D_{2V}^* = \Gamma_{2V}\varphi_2{}^{\mathbf{T}}\mathbf{Md}/M_{2V}^*, A_{2V}^* = \Gamma_{2V}\varphi_2{}^{\mathbf{T}}\mathbf{f_R}/M_{2V}^*$
$M_{2V}^* = \Gamma_{2V}{}^2\varphi_2{}^{\mathbf{T}}\mathbf{M}\varphi_2$

STEP 4: Prediction of Peak Response (2nd Mode)

Capacity curve:
A_{2V}^*-D_{2V}^* relationship (Results of STEP 3)

Demand curve:
Reduced response spectrum (same as STEP 2)

$A_{2V}^*, {}_pS_A$ Demand

Capacity

D_{2V}^*, S_D

Predicted peak ($D_{2V}^*{}_{max}, A_{2V}^*{}_{max}$)

STEP 5: Prediction of the "average" peak response at each frame

Force Distribution:

$$\begin{cases} \mathbf{P_U^{\pm}} = \mathbf{M}\left(\Gamma_{1U}\varphi_1 A_{1U}^*{}_{max} \pm 0.5\Gamma_{2V}\varphi_2 A_{2V}^*{}_{max}\right) \\ \mathbf{P_V^{\pm}} = \mathbf{M}\left(\pm 0.5\Gamma_{1U}\varphi_1 A_{1U}^*{}_{max} + \Gamma_{2V}\varphi_2 A_{2V}^*{}_{max}\right) \end{cases}$$

Predicted "average" peak responses: Envelope of four pushover analyses results

Fig. 2.2 Outline of the proposed procedure for the prediction of the "average" peak response
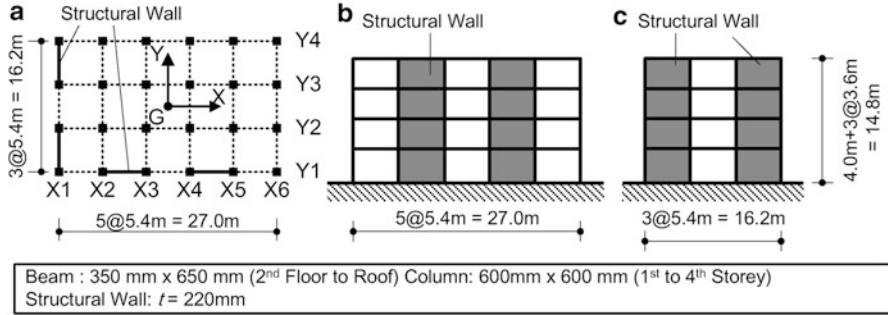
Fig. 2.3 Four-storey building model considered for the numerical examples. (**a**) Plan. (**b**) Elevation (frame Y1). (**c**) Elevation (frame X1)
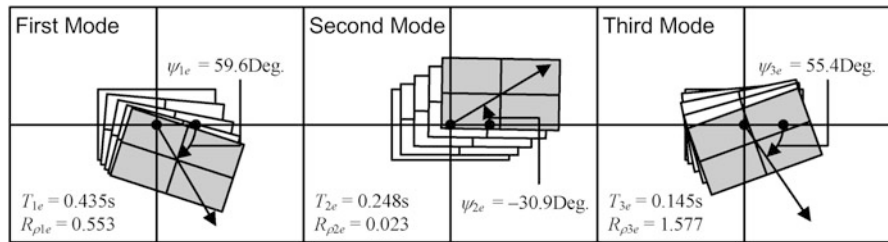
Fig. 2.4 Shape of the first three natural modes of the building model in the elastic range

$$\tan \psi_{ke} = -\sum_j m_j \phi_{Yjke} \Big/ \sum_j m_j \phi_{Xjke}, \qquad (2.7)$$

$$R_{\rho ke} = \sqrt{\sum_j I_j \phi_{\Theta jke}{}^2 \Big/ \sum_j m_j \left(\phi_{Xjke}{}^2 + \phi_{Yjke}{}^2\right)}, \qquad (2.8)$$

$$\boldsymbol{\varphi}_{\mathbf{ke}} = \{ \phi_{X1ke} \quad \cdots \quad \phi_{XNke} \quad \phi_{Y1ke} \quad \cdots \quad \phi_{YNke} \quad \phi_{\Theta 1ke} \quad \cdots \quad \phi_{\Theta Nke} \}^{\mathbf{T}}. \qquad (2.9)$$

In Eqs. 2.7, and 2.8, m_j and I_j are the mass and mass moment of inertia of the jth floor, respectively. As shown in this figure, the principal directions of the first and second modal responses of the building model are almost orthogonal; the angle between the principal directions of the first two modes is 90.6°. This figure also shows that the first mode is predominantly translational ($R_{\rho 1e} < 1$) and the second mode is almost purely translational ($R_{\rho 2e} \ll 1$), while the third mode is predominantly torsional ($R_{\rho 3e} > 1$). Because the first and second modes are predominantly translational ($R_{\rho 1e}, R_{\rho 2e} < 1$) in the building models, this is classified as a torsionally stiff (TS) system in this study, as is discussed in previous study (Fujii 2014).
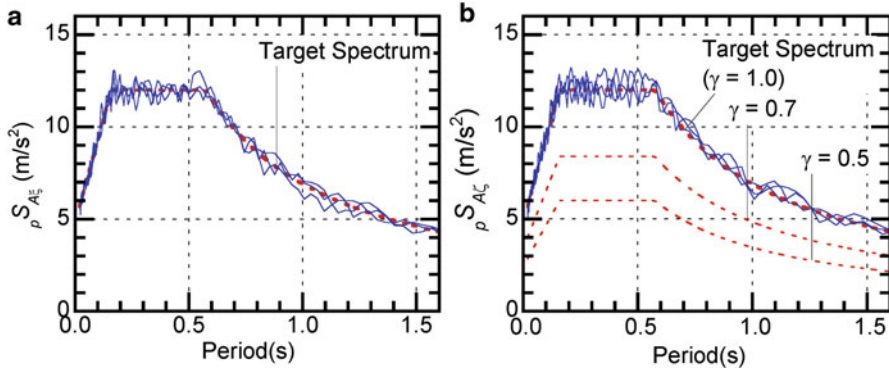
Fig. 2.5 Elastic acceleration response spectra for simulated ground motion. (**a**) "Major" component. (**b**) "Minor" component

2.3.2 Ground Motion

In this study, the seismic excitation was considered to be bi-directional in the X–Y plane, and three sets of artificial ground motions were generated. Note that these three sets of artificial ground motions were the same as those used in the previous study (Fujii 2014).

The elastic response spectra of the artificial ground motions with 5 % critical damping are shown in Fig. 2.5. In this study, the "minor" component was scaled by the multiplying parameter $\gamma = 0.0$ (unidirectional excitation), 0.5, 0.7 and 1.0, to investigate the influence of the ratio of the spectra for the horizontal minor to major components. According to López et al. (2006), this ratio varies between 0.63 and 0.81, and the average of this ratio is 0.70. Therefore, the case $\gamma = 0.7$ may be considered as the most realistic case in real ground motion.

In this study, nonlinear time-history analyses were carried out for various values of the parameter γ and various directions of incidence of the seismic input. ψ, the angle of incidence of the "major" component with respect to the X-axis, varied at 15° intervals from $(\psi_1 - 90)°$ to $(\psi_1 + 90)°$, where $\psi_1 (=59.7°)$ was the angle of incidence of the U-axis corresponding to the predicted "largest" peak equivalent displacement of the first modal response $D_{1U}{}^*{}_{max}$ shown in the previous study (Fujii 2014).

2.3.3 Comparisons of the Predicted and Time History Analyses Results

Figure 2.6 compares the predicted "average" peak roof displacement with the results of time-history analyses, and Fig. 2.7 also compares the predicted "average" peak storey drift of the flexible-edge frames (frames Y4 and X6) with the time

Fig. 2.6 Comparisons of the peak roof displacement at each frame. (**a**) γ = 0.0 (unidirectional excitation). (**b**) γ = 0.5, (**c**) γ = 0.7, (**d**) γ = 1.0
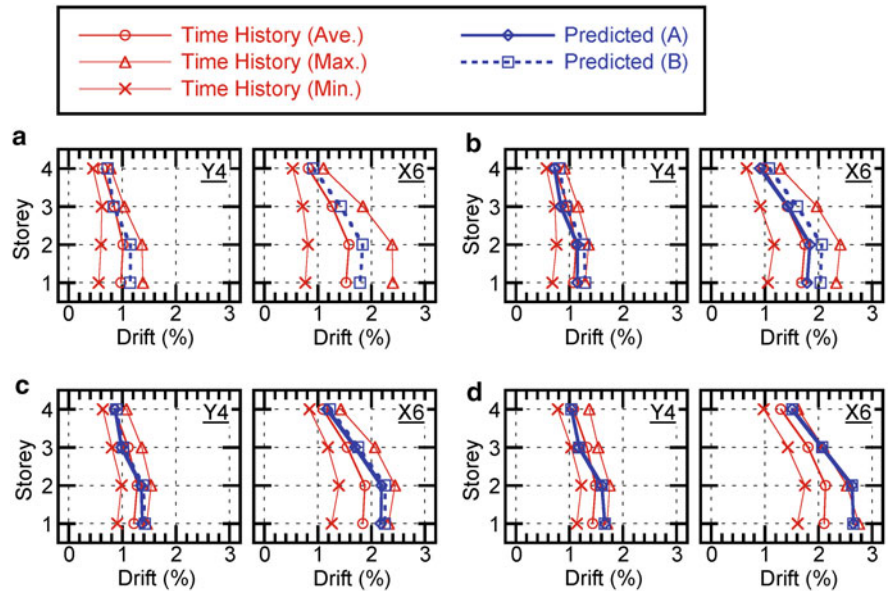
Fig. 2.7 Comparisons of the peak drift at the flexible-edge frame. (**a**) γ = 0.0. (**b**) γ = 0.5, (**c**) γ = 0.7, (**d**) γ = 1.0

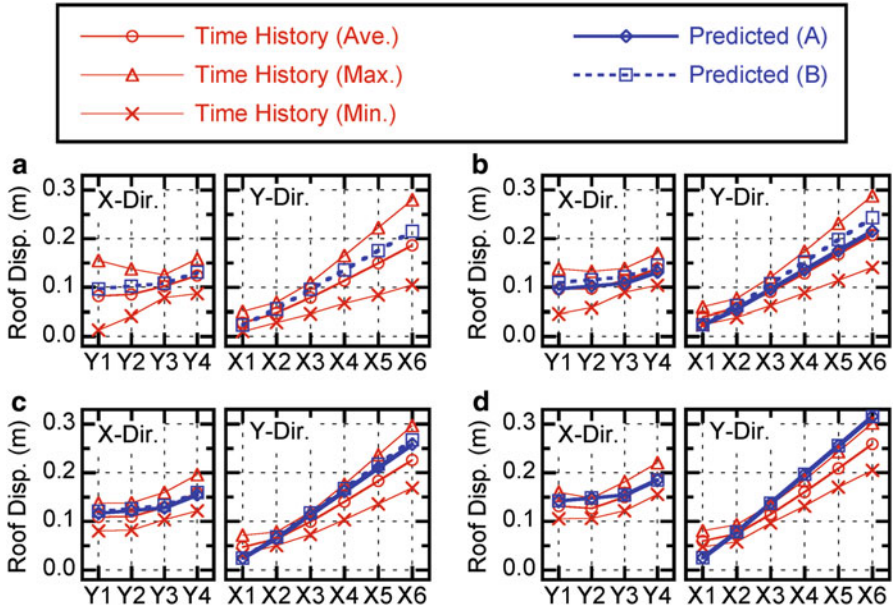history analyses results. The predicted results by using the geometric mean spectrum (predicted (A)), and the square root of the average of squares spectrum (predicted (B)) are also shown. Note that in case of $\gamma = 0.0$ (unidirectional excitation), the predicted results from the geometric mean spectrum (predicted (A)) are not shown in these figures, because the predicted results show zero responses.

As shown in these figures, the predicted peak responses by using both spectra (predicted (A) and (B)) agree well with the average of time history analyses results for $\gamma = 0.5$, 0.7 and 1.0; the differences of predicted responses between (A) and (B) are negligibly small when $\gamma = 0.7$, and in case of $\gamma = 0.5$, the plots of "predict (B)" results show approximately 10 % larger (more conservative) responses than "predict (A)" results. While in case of $\gamma = 0.0$ (unidirectional excitation), the plots of "predict (B)" results are close to the average of time history analyses results. Therefore, in case of the spectral ratio γ is larger than 0.5, either the geometric mean spectrum or the square root of the average of squares spectrum may be used as the "reduced response spectrum", for the prediction of the "average" peak response of all possible angle of incidence.

2.4 Conclusions

In this study the reduced response spectrum is introduced for the prediction of the "average" response of all possible angle of incidence, and then the "average" peak seismic response of an asymmetric building under horizontal bi-directional ground motion, acting at an arbitrary angle of incidence, is predicted based on the procedure proposed in Fujii (2014). In this study, two definitions of the "reduced response spectrum" are examined; one is the geometric mean spectrum of the horizontal major and minor components, and the other is the square root of the average of squares spectrum from all possible angle of incidence.

In the numerical example, nonlinear time-history analyses of a four-storey TS asymmetric building were carried out considering various directions for the seismic inputs. The results showed that the predicted "average" peak response displacement for the flexible-side frame satisfactorily agreed with the average of the time-history analyses results, either definition of the "reduced response spectrum", when the spectral ratio of the minor to the major components is larger than 0.5.

For the prediction of the "average" peak response under "real" horizontal bi-directional ground motion whose spectral shape of both components are different, the author think GMRot50, the median of geometric mean spectrum of all possible angle of incidence, proposed by Boore et al. (2006), may be used as the "reduced spectrum". Further investigation is needed for the applicability of this procedure under "real" horizontal bi-directional ground motion.

Erratum to "Prediction of the largest peak nonlinear seismic response of asymmetric buildings under bi-directional excitation using pushover analyses"

Unfortunately, there were some errors in the previous study (Fujii 2014), which is the key paper for this article. The correct versions of Eqs. 17 and 19 are shown below.

$$_nD_{2V}{}^* = \frac{\Gamma_{2Vie}\boldsymbol{\varphi_{2ie}}^{\mathbf{T}}\mathbf{M}_n\mathbf{d}}{M_{2Vie}{}^*}, \,_nA_{2V}{}^* = \frac{\Gamma_{2Vie}\boldsymbol{\varphi_{2ie}}^{\mathbf{T}}{}_n\mathbf{f_R}}{M_{2Vie}{}^*}, \tag{17}$$

$$\begin{cases} \mathbf{P_U}^{\pm} = \mathbf{M}\left(\Gamma_{1Uie}\boldsymbol{\varphi_{1ie}}A_{1U}{}^*{}_{max} \pm 0.5\Gamma_{2Vie}\boldsymbol{\varphi_{2ie}}A_{2V}{}^*{}_{max}\right) \\ \mathbf{P_V}^{\pm} = \mathbf{M}\left(\pm 0.5\Gamma_{1Uie}\boldsymbol{\varphi_{1ie}}A_{1U}{}^*{}_{max} + \Gamma_{2Vie}\boldsymbol{\varphi_{2ie}}A_{2V}{}^*{}_{max}\right) \end{cases}. \tag{19}$$

References

Beyer K, Boomer JJ (2006) Relationships between median values and between aleatory variabilities for different definitions of the horizontal component of motion. Bull Seismol Soc Am 96(4A):1512–1522

Beyer K, Boomer JJ (2007) Selection and scaling of real accelerograms for bi-directional loading: a review of current practice and code provisions. J Earthq Eng 11:13–45

Boore DM, Watson-Lamprey J, Abrahamson NA (2006) Orientation-independent measures of ground motion. Bull Seismol Soc Am 96(4A):1502–1511

Fujii K. (2010) Seismic assessment of asymmetric buildings considering the critical direction of seismic input. Paper presented at the 14th European conference on earthquake engineering, paper no. 0623, Ohrid, Macedonia, 30 Aug–3 Sep 2010

Fujii K (2011) Nonlinear static procedure for multi-story asymmetric frame buildings considering bidirectional excitation. J Earthq Eng 15:245–273

Fujii K (2014) Prediction of the largest peak nonlinear seismic response of asymmetric buildings under bi-directional excitation using pushover analyses. Bull Earthq Eng 12:909–938

López A, Hernández JJ, Bonilla R, Fernández A (2006) Response spectra for multicomponent structural analysis. Earthq Spectra 22:85–113

Chapter 3
Evaluation of Torsional Component of Ground Motion by Different Methods Using Dense Array Data

G.R. Nouri, M.R. Ghayamghamian, and M. Hashemifard

Abstract In addition to the structural torsional effects coming from the horizontal asymmetry of the building structure one can also meet with the direct torsional ground excitations of the building. The dynamic analyses of structures have been carried out by neglecting the excitation by the rotational ground motions in engineering practice largely caused by the lack of recorded torsional ground motions. Using dense array data is one of the approaches has been developed to produce torsional component of ground motion. In this paper, by using the data of Chiba dense array and applying three methods of Time Derivation, Finite Difference and Geodetic, torsional motion are estimated and compared. In this array, accelerometers are placed densely with separation distances between 5 and 300 m. The results showed that the peak torsional ground motion which was computed by Time Derivation method is larger than which was computed by Geodetic method.

Peak torsional ground motion values that are estimated by Finite Difference method show smaller values than those computed by Time Derivation for long separation distances (>20 m). However, the values estimated from the Finite Difference and Time Derivation methods are relatively close for short separation distances. Also, the effects of peak ground acceleration and magnitude of events on the torsional motions have been investigated and the relationship between PGA and the maximum torsional motion for different methods has been proposed.

Keywords Torsional motion • Seismic dense array • Geodetic method • Time derivation method • Finite difference method

G.R. Nouri (✉)
Department of Civil Engineering, Faculty of Engineering, Kharazmi University, Tehran, Iran
e-mail: r.nouri@khu.ac.ir

M.R. Ghayamghamian • M. Hashemifard
International Institute of Earthquake Engineering and Seismology, Tehran, Iran
e-mail: mrgh@iiees.ac.ir; majid_hashemifard@yahoo.com

3.1 Introduction

Strong ground motion consists of three components of translation along x, y and z axes and three components of rotation about these axes and also six components of strain. In general, three main approaches have been developed to extract rotational motions: one is a numerical simulation of the field of radiation from the source mechanism (Aki 1986; Haskell 1969). The second approach is measuring rotational components indirectly by translational components. In preliminary studies, researchers tried to propose a relation between translational and rotational components using one seismic station (Newmark 1969; Ghafory-Ashtiany and Singh 1986). Also, indirect measurements of rotational motions using a seismo-meter array have been studied by several investigators (Niazi 1986; Oliveira and Bolt 1989; Spudich et al. 1995; Bodin et al. 1997; Li et al. 2004; Huang 2003; Ghayamghamian and Nouri 2007).

The third approach is measuring rotational components directly by rotational sensors. Ring laser gyroscopes have become one of the most important instruments for measuring rotation (Nigbor 1994; Takeo 1998). Suryanto et al. (2006) present for the first time a comparison of array-derived rotations with direct measurements of rotations. Their research showed that the overall fit between direct and array-derived measurements is surprisingly good.

Ghayamghamian and Nouri (2007) studied the rotational ground motions and their dependence on seismic parameters, using Chiba dense array data, and a possibility of estimating torsional ground motion from translational records was investigated. They computed torsional motion from the difference of two translational records on the ground. Also, the effect of torsional ground motion on structural response was studied by Ghayamghamian et al. (2009). The torsional motion was estimated by a geodetic method using data of Chiba dense array. The results showed that the increase in the displacements of symmetric or asymmetric buildings due to torsional excitation of the ground is largest for structures with very short translational periods (less than about 0.3 s) and small frequency ratios ($\Omega < 1$). For such structures, the accidental eccentricities e_a resulting from torsional ground motions were found to be larger than those proposed by the design codes.

In this paper, data are collected from the Chiba dense array to estimate the torsional ground motion. Due to closely spaced instruments in Chiba array and regular arrangement of instruments at two inner rings, the better estimation of torsional motion can be achieved using multiple stations up to high frequencies.

To compute torsional motion, three methods, namely, Time Derivation, Finite Difference and Geodetic are deployed and the results compared to each other. Also, variations of the maximum torsional motion with peak ground acceleration and magnitude of earthquake are investigated in these three methods.

3.2   Chiba Dense Array

A 3-D array system has been installed at Chiba, an experimental station of the Institute of Industrial Science, University of Tokyo, in 1982 (Fig. 3.1). The topographical conditions of the site are generally simple, with the ground surface being almost flat. In this array, seismometers and accelerometers are placed, with a minimum separation distance of 5 m, both on the ground surface and in boreholes. The array system is composed of 15 boreholes with 44 three-component accelerometers, 9 are densely arranged. Stations C1–C4 and P1–P4 are respectively placed on circles with radii of 5 and 15 m with respect to station C0, which is placed at the center of these two rings (Katayama et al. 1990). Nine events recorded with high signal-to-noise ratios (SNR), and wide ranges of magnitudes and PGAs were selected (Ghayamghamian and Nouri 2007). Specifications of these events, are given in Table 3.1.

3.3   Estimation of Torsional Motion

In this paper, three methods have been applied to estimate the torsional motion using translational components which include Time Derivation, Finite Difference and Geodetic methods.
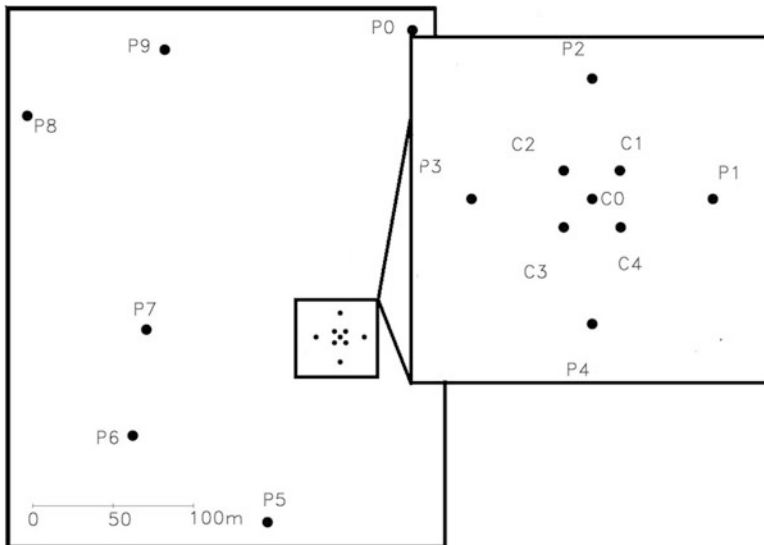
Fig. 3.1 Chiba array configuration and reference system

Table 3.1 Specification of selected events

Event no.	Focal depth (km)	Distance (km)	PGA		M_{JMA}	SNR at C0 (%)
			NS	EW		
33	73.3	104.5	52	60	6.5	98.6
37	57.9	44.7	400	293	6.7	99.8
42	47.6	37.9	117	79	5.2	98.7
46	55.3	47.7	57	71	5.6	98.5
47	55.7	55.2	32	34	6.0	98.1
81	96.0	42.2	71	86	6.0	98.7
82	69.0	62.4	38	51	5.3	97.2
84	50.0	40.2	91	121	5.4	98.8
87	92.0	52.4	91	94	5.9	99.0

3.3.1 Time Derivation Method

Ghafory-Ashtiany and Singh (1986) obtained following expression for computation of ground rotational acceleration by using the Eq. 3.1.

$$\psi_k(t) = -\frac{1}{c_j}\frac{d}{dt}\big[\ddot{X}_j(t) - \ddot{X}_i(t)\big] \tag{3.1}$$

Where, $\psi_k(t)$ is the rotation about the k-axis, X_i and X_j are displacements along the x and y axes and x_i ‹x_j and x_k are principle axes. Also c_j is shear wave velocity in direction x_j.

3.3.2 Finite Difference Method

The average torsional motions can be approximated from the difference of two translational records in an array of stations.

$$\psi_z = \frac{1}{2}\left(\frac{\ddot{u}_2(t) - \ddot{u}_1(t)}{\Delta y} - \frac{\ddot{v}_2(t) - \ddot{v}_1(t)}{\Delta x}\right) \tag{3.2}$$

where, $\psi_z(t)$ is torsional acceleration, $\ddot{u}_j(t)$ and $\ddot{v}_j(t)$ are translational accelerations along the x and y axes respectively related to a station pair (j = 1,2).

This method has been used for computing torsional motion in various researches (Huang 2003; Ghayamghamian and Nouri 2007; Hao 1996; Ghayamghamian and Motosaka 2003). This estimation of torsional motion is the first order accuracy and can be done especially when the stations are distributed regularly in the ideal cross shaped array.

3.3.3 Geodetic Method

Spudich et al. (1995) introduced a geodetic method that can estimate torsional motion using multiple stations with higher precision. In the framework of classical elasticity, and further assuming infinitesimal deformations, displacement of a point r is related to that of a neighboring point $r+\delta r$:

$$u(r + \delta r) = u(r) + G\delta r = u(r) + \varepsilon \delta r + \omega \times \delta r \qquad (3.3)$$

where G, ε, ω are the displacement-gradient matrix, strain and rotation respectively. Using the displacement-gradient matrix G, one can compute strains and rotations. The G matrix is given by

$$G = \begin{pmatrix} \partial_x u_x & \partial_y u_x & \partial_z u_x \\ \partial_x u_y & \partial_y u_y & \partial_z u_y \\ \partial_x u_z & \partial_y u_z & \partial_z u_z \end{pmatrix} \qquad (3.4)$$

The relation between rotational and translational motions is obtained through the application of the curl operator ($\nabla \times$) to the displacement by:

$$\begin{pmatrix} \omega_x \\ \omega_y \\ \omega_z \end{pmatrix} = \frac{1}{2}\nabla \times u(r) = \frac{1}{2}\begin{pmatrix} \partial_x u_z - \partial_z u_y \\ \partial_z u_x - \partial_x u_z \\ \partial_x u_y - \partial_y u_x \end{pmatrix} \qquad (3.5)$$

where ω_x, ω_y, ω_z are rotations about x, y and z axes. At least three stations must be used to determine the horizontal-displacement gradient using this method. This method was applied to studying the dynamic deformations induced by the Landers earthquake (M = 7.4, 1992) and recorded by the Parkfield seismic array (UPSAR) in California. In addition, Suryanto et al. (2006) used the same method to compare array-derived torsional ground motion with direct-ring laser measurements and found the two to be in good agreement.

3.4 Comparison Between Results of the Methods

By using the three above mentioned methods, the torsional ground acceleration was calculated and compared with each other. For this purpose, maximum torsional motion and standard deviation values have been used. Torsional motion for one station, pairs of stations with different separation distances and two rings of accelerometers (C0, C1–C4) and (C0, P1–P4) are calculated by Time Derivation, Finite Difference and Geodetic methods respectively. Figure 3.2 shows comparison of standard derivation and the maximum values of torsional motion obtained from that three methods for selected events. Comparison between the results of various
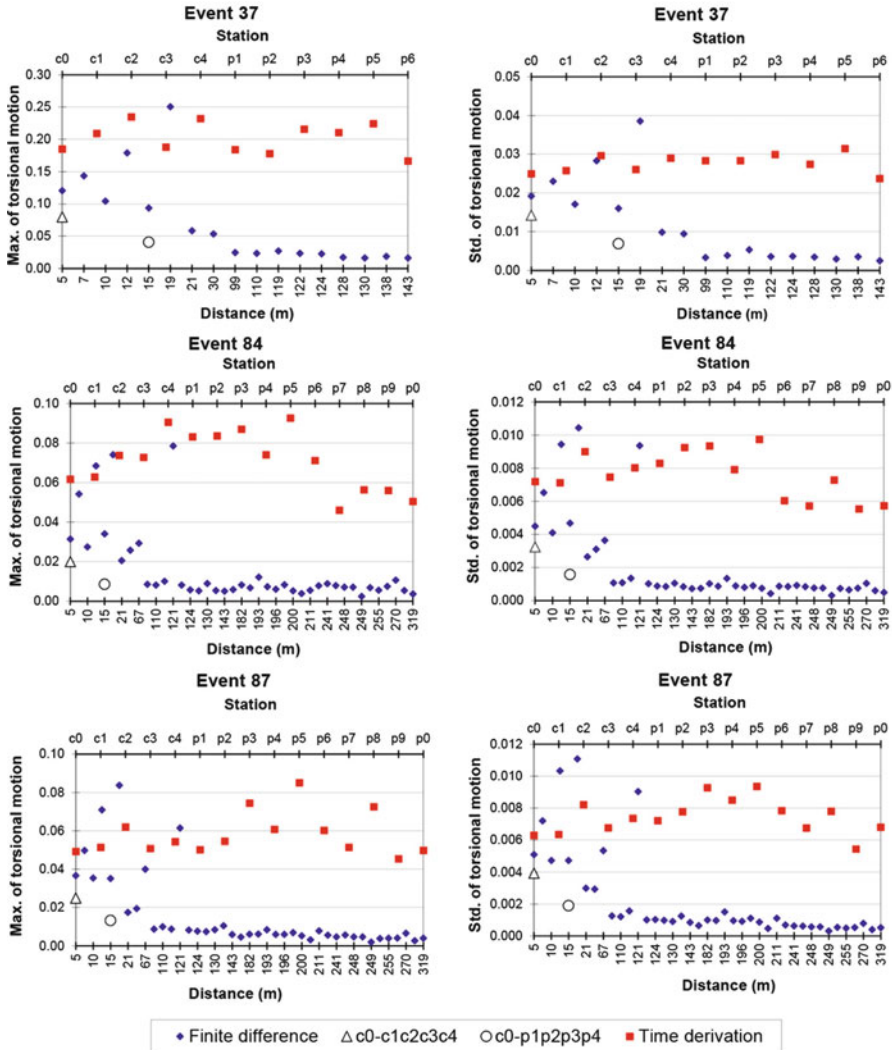
Fig. 3.2 Comparison of maximum torsional motion and standard deviation in the different methods for selected events

events demonstrate that torsional component values strongly depend on the earthquake characteristics.

Maximum torsional component and standard derivation values belong to the event 37 that possesses the maximum value of peak ground acceleration (PGA = 400 gal) and magnitude of earthquake ($M_{JMA} = 6.5$). As illustrated in Fig. 3.2, standard derivation and maximum torsional motion values are extremely sensitive to the separation distance of stations and decrease as the distance increases in the Finite Difference method. This procedure is independent of the peak ground acceleration and magnitude of earthquake.

Values obtained from the Time Derivation method are larger than the ones from Finite Difference method with separation distance larger than 20 m as shown in Fig. 3.2. The ratio of values computed by these two methods are 6–8 at far separation distances. However, for short separation distances they demonstrate close values.

It is clear that the maximum values of torsional motion as estimated by the Time Derivation method are larger than those computed by the Geodetic method. Also, larger values of torsional motion for the Geodetic method can be observed compared with those for Finite Difference method that the separation distances are far.

Array-derived torsional motions are subjected to an important limitation. The instruments should be as close as possible for the calculated linear approximations to be as close as possible to the true gradients. Bodin et al. (1997) showed that to obtain array-gradient estimates accurate to within ~90 % of true gradients, the array dimensions must be less than one quarter-wavelength of the dominant energy in the wave train. Later, Langston (2007a, b) indicated that the accuracy order of finite difference approximation depends also on the geometry of the array. He found that the station spacing must be ~10 % of a horizontal wavelength to obtain 90 % accuracy, and these finite difference estimates are in first- and second-order of accuracy for irregular and regular arrays, respectively. Regarding estimated large-wave velocity (Yamazaki and Turker 1992) and the very closely spaced instruments in the Chiba array, the torsional motions can be accurately evaluated for the two closely spaced rings (C0, C1–C4) and (C0, P1–P4) up to the high-frequency range (<11 Hz).

3.5   Effects of Peak Ground Acceleration and Magnitude of Earthquake

It has been tried to establish a relationship between the translational and torsional components due to existing problems in recording torsional motion. In this section variations of the maximum torsional motion with peak ground acceleration are investigated in the three methods. The mean estimated values of both inner and outer rings in the Geodetic method are used. As shown in Fig. 3.3, with increasing peak ground acceleration, maximum of torsional motion also increases. However, these changes are small in events with low peak ground acceleration and maximum torsional motion will increase significantly with increasing translational acceleration. It is seen that, there is a linear correlation between maximum values of the two components with an acceptable accuracy by examining the relationship between the maximum translational and torsional components.

Magnitude of earthquake is also one of its characteristics. Chiba dense array data covers a wide range of magnitudes and changes of the maximum torsional motion with events magnitude in the three methods are shown in Fig. 3.3. The results demonstrate that maximum torsional motion values changes partially until magnitude 6.5, however, after this value we can see a sudden increase. As illustrated,
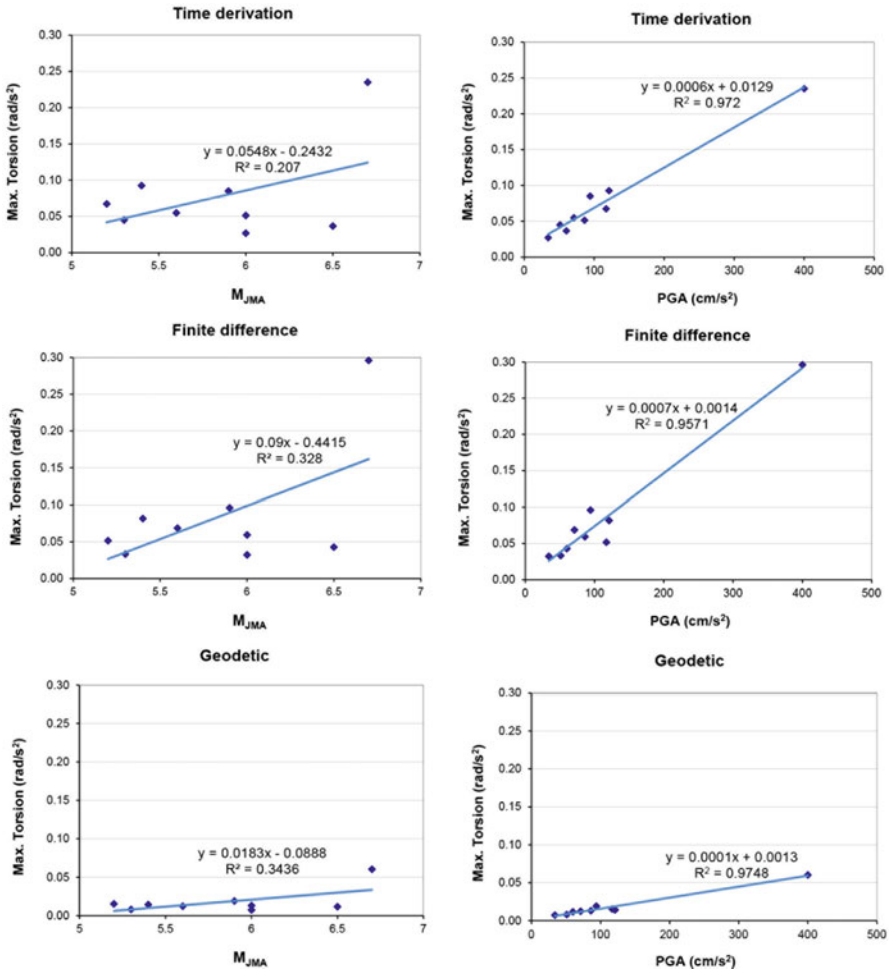
Fig. 3.3 Variations of the maximum torsional motion with peak ground acceleration and magnitude of earthquakes

there is no determined relationship between magnitude of earthquake and maximum torsional motion.

3.6 Conclusions

Translational motions of seismic arrays were applied for estimating torsional motion. In this study, torsional ground accelerations were estimated by three methods, namely, Time Derivation, Finite Difference and Geodetic method using

data of Chiba dense array. Then, the maximum torsional motion and standard deviation values of the three methods were compared. The results showed that the peak torsional ground motion which was computed by Time Derivation method is larger than those was computed by Geodetic method. Peak torsional ground motion values that were estimated by Finite difference method show smaller values than which were computed by Time derivation for long separation distances (>20 m). However, the values estimated from the Finite Difference and Time derivation methods are close to each other for short separation distances. The results revealed that, there is a linear correlation between maximum values of translational and torsional components for all three methods.

References

Aki K (1986) Seismic displacement near a fault. Geophys Res 73:5359–5376

Bodin P, Gomberg J, Sing SK, Santoyo M (1997) Dynamic deformations of shallow sediments in the valley of Mexico, part I: three-dimensional strains and rotations recorded on a seismic array. Bull Seismol Soc Am 87:528–539

Ghafory-Ashtiany M, Singh MP (1986) Structural response for six correlated earthquake components. Earthq Eng Struct Dyn 14:103–119

Ghayamghamian MR, Motosaka M (2003) The effects of torsion and motion cou-pling in site response estimation. J Earthq Eng Struct Dyn 32(5):691–709

Ghayamghamian MR, Nouri GR (2007) On the characteristics of ground motion rotational components using Chiba dense array data. Earthq Eng Struct Dyn 36:1407–1427

Ghayamghamian M, Nouri G, Igel H, Tobita T (2009) The effect of torsional ground motion on structural response: code recommendation for accidental eccentricity. Bull Seismol Soc Am 99:1261–1270

Hao H (1996) Characteristics of torsional ground motion. Earthq Eng Struct Dyn 25:599–610

Haskell NA (1969) Elastic displacements in the near-field of a propagating fault. Bull Seismol Soc Am 59:865–908

Huang BS (2003) Ground rotational motions of the 1999 Chi-Chi, Taiwan earthquake as inferred from dense array observations. Geophys Res Lett 30:1307–1310

Katayama T, Yamazaki F, Nagata S (1990) Development of strong motion database for the Chiba seismometer array, s.l.: University of Tokyo.

Langston A (2007a) Spatial gradient analysis of linear seismic array. Bull Seismol Soc Am 97:268–280

Langston A (2007b) Wave gradiometry in two dimensions. Bull Seismol Soc Am 97:401–416

Li H, Sun L, Wang S (2004) Improved approach for obtaining rotational components of seismic motion. Nucl Eng Des 232:131–137

Newmark NM (1969) Torsion in symmetrical buildings. In: Proceedings of the 4th World Conference on Earthquake Engineering, Santiago, Chile

Niazi M (1986) Inferred displacements, velocities and rotations of a long rigid foundation located at el centro differential array site during the 1979 imperial valley, California, earthquake. Earthq Eng Struct Dyn 14:531–542

Nigbor RL (1994) Six-degree-of-freedom ground-motion measurement. Bull Seismol Soc Am 84:1665–1669

Oliveira CS, Bolt BA (1989) Rotational components of surface strong ground motion. Earthq Eng Struct Dyn 18:517–528

Spudich P et al (1995) Transient stresses at Parkfield, California, produced by the M7.4 Landers earthquake of June 28, 1992: observations from the UPSAR dense seismograph array. J Geophys Res 100:675–690

Suryanto W et al (2006) First comparison of array-derived rotational ground motions with direct ring laser measurements. Bull Seismol Soc Am 96:2059–2071

Takeo M (1998) Ground rotational motions recorded in near-source region of earth-quakes. Geophys Res Lett 25:789–792

Yamazaki F, Turker T (1992) Spatial variation study on earthquake ground motion observed by the Chiba array. In: Madrid, Proceeding of the Tenth World Conference on Earthquake Engineering

Chapter 4
Estimation of Rotational Ground Motion Effects on the Bell Tower of Parma Cathedral

Zbigniew Zembaty, Andrea Rossi, and Andrea Spagnoli

Abstract The purpose of this paper is to present results of calculations of seismic response of the old Parma Bell Tower with and without the rotational, rocking seismic effects as modeled in the European seismic code: Eurocode 8 (part 6: Towers, Masts and Chimneys). A detailed, finite element model of the tower was prepared, which led to the solution of its eigen problem and to conventional dynamic, response modal analysis. Next a simplified rod model, equivalent to the detailed finite element model was prepared, taking into account soil compliance as well as the rocking excitation effects. The results of computations show rather substantial, 30–40 % contribution of the rocking excitations in the overall seismic response.

Keywords Response spectra • Rotational ground motion • Seismic rocking excitations • Eurocode 8 • Tower shaped structures

4.1 Introduction

Formally one can define three rotational components of the surface, seismic ground motion. These are two rotations ψ, θ about the two horizontal axes x, y and rotation φ about vertical axis z (see Fig. 4.1).

Among them, particularly important can be rotation θ about the horizontal axis y, perpendicular to the epicentral direction. For this direction there are numerous

Z. Zembaty (✉)
Faculty of Civil Engineering, Opole University of Technology, ul. Proszkowska 76, 45-061 Opole, Poland
e-mail: z.zembaty@po.opole.pl

A. Rossi
Rose School, EUCENTRE, via Ferrata 1, 27100 Pavia, Italy
e-mail: andre.red@hotmail.it

A. Spagnoli
Department of Civil, Environmental, Land Management, Engineering and Architecture, Parma University, via Università, 12, 43121 Parma, Italy
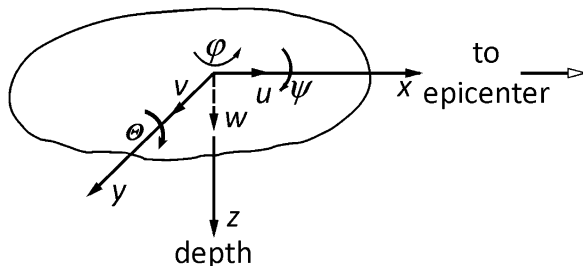e-mail: spagnoli@unipr.it

Fig. 4.1 Coordinate system at the ground surface and the rotational components of seismic ground motion

models suggesting the seismic rocking excitations from the body and surface waves propagation, general spatial seismic effects and including (or excluding) the local soil conditions (see e.g. Falamarz-Sheikhabadi and Ghafory-Ashtiany 2012; Kalkan and Grazer 2007; Trifunac 1982; Castellani and Zembaty 1996).

The first attempt of modeling the rotational effects in form of typical response spectrum format can be found in Eurocode 8, part 6 devoted to chimneys, masts and towers, 2005 (see also: Zembaty 2009). In this code the rotational response spectra about Cartesian axes $x, y, \& z$ on the ground surface are modeled as functions of shear wave velocity at the ground surface and the traditional Eurocode 8, translational design response spectra (2004). The response spectrum of the rocking component θ about the horizontal axis y (Fig. 4.1) is given by formula A.1 of Eurocode 8 part 6 (2005):

$$R_y^\theta(T) = \frac{1.7\pi S_e(T)}{\nu_S T} \tag{4.1}$$

where T is the natural period, v_S equals average shear wave velocity in the top 30 m of the local soil, while $S_e(T)$ stands for the elastic translational response spectrum. In Eurocode 8 (2004), $S_e(T)$ it is given by formula 3.2.2.2:

$$S_e(T) = a_g \cdot \begin{cases} S \cdot \left[1 + \dfrac{T}{T_B} \cdot (2,5\eta - 1)\right] & \text{if } 0 \le T \le T_B \\[2mm] S \cdot 2,5 \cdot \eta & \text{if } T_B \le T \le T_C \\[2mm] S \cdot 2,5 \cdot \eta \cdot \left(\dfrac{T_C}{T}\right) & \text{if } T_C \le T \le T_D \\[2mm] S \cdot 2,5 \cdot \eta \cdot \left(\dfrac{T_C \cdot T_D}{T^2}\right) & \text{if } T > T_D \end{cases} \tag{4.2}$$

in which T_B, T_C, T_D and S represent local site conditions as well as two types of ground motions (far and near field) while a_g is the horizontal design acceleration.

In Fig. 4.2 the plots of response spectra type 1 and type 2 are shown as functions of natural period T. The type 1 response spectrum is similar to the response spectrum of the actual Italian seismic code NTC (2008). The type 2 response spectrum was included in present analysis for comparison.
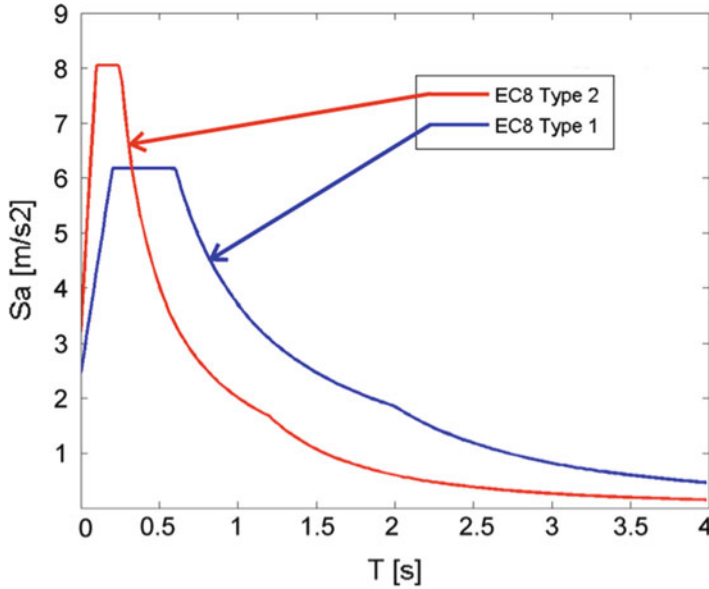
Fig. 4.2 Plots of response spectra type 1 and 2 for 5 % damping ratio

Practical applications of formula 1 with Eq. 4.2 require first to solve the eigen problem of the structure and next the application of the mode superposition technique in respective implementation of the response spectrum methodology. Usually first two to three modes are enough to reach satisfactory accuracy for symmetric slender towers (e.g. circular chimneys) under horizontal seismic excitations. The inclusion of up to four to five modes makes it possible to ensure that the required convergence of the mode superposition method was achieved. This calculation procedure can be carried out using one of many programs implementing Finite Element Method in structural dynamics. So far however **none of the commercial FEM programs allows to include rotational**, **excitation seismic effects**, **in particular in format of an acceleration response spectrum**. For this reason, in this paper, slender tower is first modelled using SAP 2000 program to solve its eigen problem and compute its response to horizontal seismic excitations using translational response spectrum. Next an equivalent, simplified model of the tower is formulated as a Timoshenko beam and calculated for the combined rotational and horizontal excitations. The Timoshenko beam model allows to include appropriate combination of shear and bending characteristic for the old masonry towers which is the case of seismic vibrations of the Parma Cathedral Bell Tower.

4.2   Formulation of the Problem

Consider matrix equation of motion of a structure modeled as a plane, discrete system under horizontal excitations u(t).

$$M\ddot{q} + C\dot{q} + Kq = -M\ddot{u}(t) \tag{4.3}$$

where matrix $\mathbf{M}$ is diagonal and contains discrete masses m_j of the modelled structure, $\mathbf{K}$ is the stiffness matrix, $\mathbf{C}$ is the damping matrix. Its solution can be obtained using mode superposition method and Duhamel integral as follows:

$$q_j = \sum_{i=1}^{n} w_{ji}\eta_i \int_0^t \ddot{u}(\tau)h_i(t-\tau)d\tau \tag{4.4}$$

where h_i stands for modal impulse response function

$$h_i(t) = \frac{1}{\omega_{id}}e^{-\omega_i t}\sin(\omega_{id}t) \tag{4.5}$$

$\omega_i = 2\pi/T_i$ is the angular natural frequency of mode i-th, T_i natural period, w_{ji} j-th element of the i-th eigen vector, ω_{id} damped natural frequency $\omega_{id} = \omega_i\sqrt{\left(1-\xi_j^2\right)}$ and η_i modal participation factor:

$$\eta_i = \frac{w_i^{Tr}M\mathbf{1}}{w_i^{Tr}Mw_i} \tag{4.6}$$

in which $\mathbf{w}_i$ is modal vector i, bold symbol $\mathbf{1}$ denotes vector containing values of 1 and Tr stands for vector transposition.

Adding rotational excitations $\theta(t)$ about horizontal axis y (rocking) leads to following form of Eq. 4.3 (see e.g. [5]):

$$M\ddot{q} + C\dot{q} + Kq = -\left[M\ddot{u}(t) + \{m_jH_j\}\ddot{\Theta}(t)\right] \tag{4.7}$$

in which symbol $\{m_jH_j\}$ represents a vector containing values of the multiplications of discrete masses m_j by their respective heights H_j above the ground surface.

It should be noted that the structure rests on a compliant soil described by rotational stiffness k_Θ (Fig. 4.2).

Applying the response spectrum method one can assess the displacements q_j at the height H_j for a given mode i, separately for horizontal excitations:

$$max \, q_{ji}^{hor} \cong \left| w_{ji}\eta_i^{hor}\frac{1}{\omega_i^2}S_a(\omega_i, \xi_i) \right| \tag{4.8}$$

and for the rotational excitations

$$max \, q_{ji}^{rot} \cong \left| w_{ji}\eta_i^{rot}\frac{1}{\omega_i^2}S_a^{\ddot{\theta}}(\omega_i, \xi_i) \right| \tag{4.9}$$

in which S_a and $S_a^{\ddot{\theta}}$ denote horizontal and rotational, acceleration response spectra respectively, while

Fig. 4.3 A simplified model of a slender tower under horizontal-rotational excitations
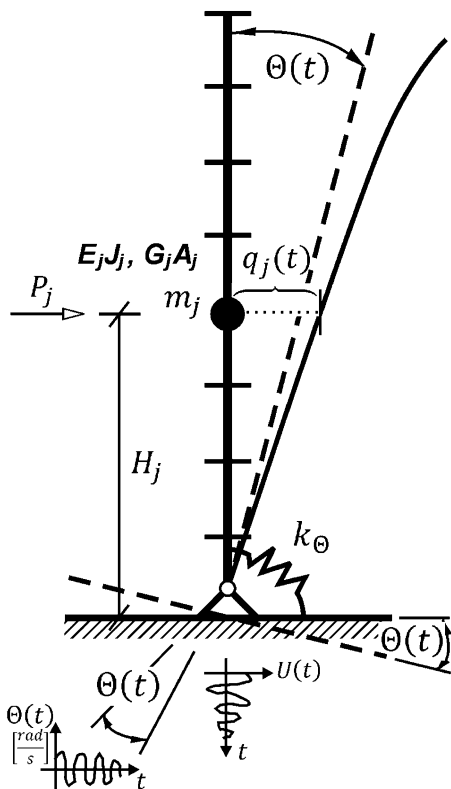
$$\eta_i^{hor} = \frac{w_i^{Tr} M \mathbf{1}}{w_i^{Tr} M w_i} \tag{4.10a}$$

$$\eta_i^{rot} = \frac{w_i^{Tr} M H}{w_i^{Tr} M w_i} \tag{4.10b}$$

represent modal participation factors calculated differently for the horizontal and the rotational excitations and $\mathbf{H}$ is a vector containing the heights H_j of the discrete masses m_j above the ground (Fig. 4.3).

Applying, for the slender tower, with well separated natural frequencies, the familiar SRSS rule to combine the responses in the succeeding modes, and assuming hypothetically that the same rule also holds when combining the responses from horizontal and rotational excitations, one can asses max response at H_j height

$$max\, \boldsymbol{q}_j \cong \sqrt{\sum\nolimits_{i=1}^{n} \left(max\, \boldsymbol{q}_{ji}^{hor} \right)^2 + \sum\nolimits_{i=1}^{n} \left(max\, \boldsymbol{q}_{ji}^{rot} \right)^2} \tag{4.11}$$

The rocking effects on slender towers will be best observed in the base shear and overturning moment. They can be calculated from the equivalent pseudo-static, horizontal forces associated with each discrete mass m_j:

$$P_{ji} = m_j w_{ji} \eta_i S_a(\omega_i, \xi_i) \tag{4.12}$$

These pseudo-static forces are calculated in a different way for the horizontal and rotational excitations. Thus symbol η_i in Eq. 4.12 is given either by Eq. 4.10a or 4.10b, while symbol S_a stands either for horizontal acceleration response spectrum or for the rotational one $S_a^{\ddot\Theta}$.

Summing down all the pseudo-static forces gives the base shear force associated with the natural mode i. Using basic formulas of the mode superposition method, after some algebra, respective base shear calculated for mode i equals:

$$F_{base[i]} = \frac{\left(\sum_k m_k w_{ki}\right)^2}{\sum_k m_k w_{ki}^2} S_a(\omega_i, \xi_i) \tag{4.13}$$

Summing down moments of the pseudo-static forces with respect to the ground surface, gives the overturning moment of the mode i:

$$M_{base[i]} = \sum_j H_j P_{ji} \tag{4.14}$$

The total base shear and total overturning moments due to horizontal and rotational effects are calculated using the SRSS rule the same way as in Eq. 4.11.

4.3 Response of Parma Bell Tower to Horizontal-Rocking Excitations

4.3.1 Description of Parma Bell Tower and Its Dynamic Properties

The bell tower of Parma cathedral (Fig. 4.4) was built in the twelfth century.

It is 64.25 m high and has hollow square cross-section of 7.72 m side. The thickness of the masonry wall decreases along the height, from 1.40 to 1.05 m (Fig. 4.5). There are two series of openings: one small at mid-height and one large at the top. The structure is composed of an outer and inner masonry wall of clay bricks infilled with a sort of conglomerate made of brick and stone rubble. The foundation is a masonry block about 6.00 m deep and 11.70 m wide. The soil underneath the tower consists of alluvial deposits with prevailing slimy clays, clayey sandy slimes and slimy sands. The respective site type has been determined as C according to Eurocode 8, part 1, (2005), classification.

Fig. 4.4 Parma cathedral and its bell tower. The photograph on the *left* (Courtesy of photo Vaghi/ CSAC, Università di Parma/Photography Section)

4.3.2 Dynamic Properties of the Parma Bell Tower

First a 3D, finite element model of the Parma Tower was prepared using SAP 2000. The masonry walls were modeled using the so called "shell thick element" type to represent both shear and bending, prevailing in the seismic response of these types of structures. The foundation block was modeled using the "solid" elements type. The number of finite elements equalled 488 of the shell type, and 243 of the solid type. Then the eigen problem was calculated and the fundamental natural period T_1 was calculated equal to 1.366 s. This natural period does not differ much from the experimental results of Roberto Cerioni et al. (1996), using a 3D FEM model, that is: $T_1 = 1.374$ s.
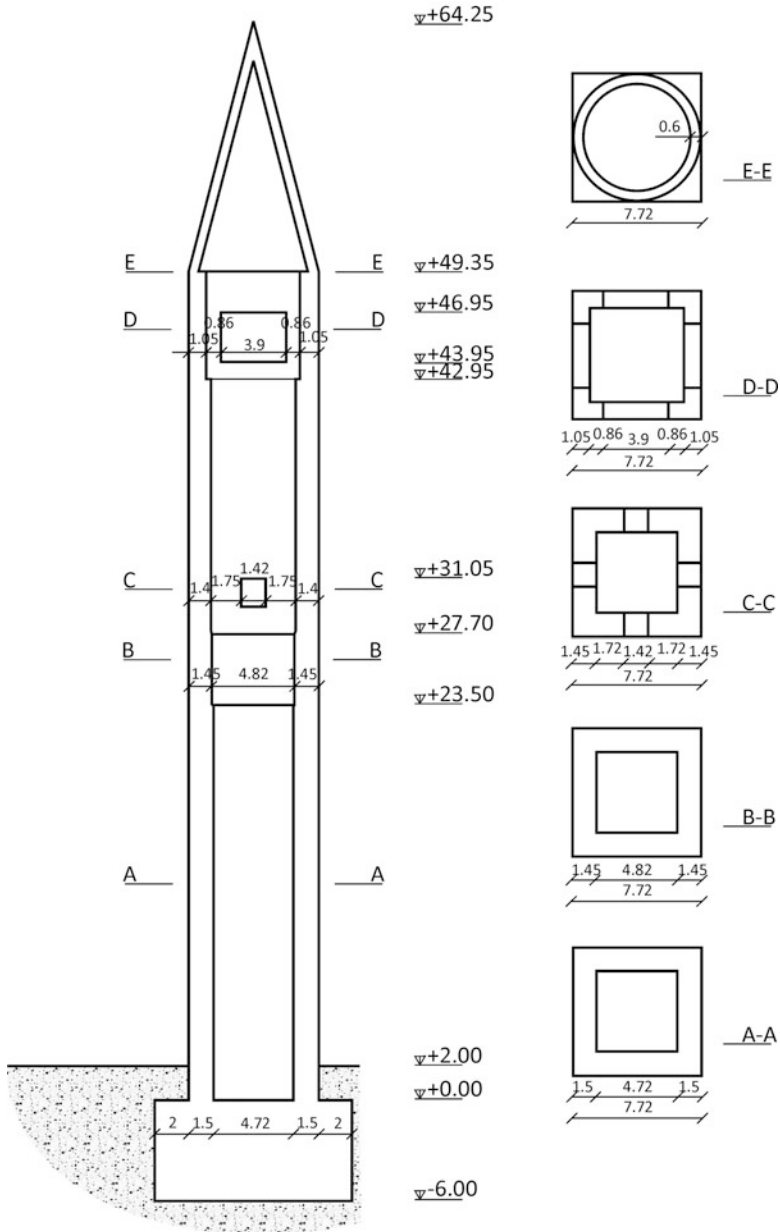
Fig. 4.5 Detailed cross-sections of the Parma Cathedral Bell Tower

4.3.3 Results of the Analysis of the Response

Since so far, the rotational excitations are not included in any of the commercial seismic engineering FEM software, respective simplified model of the tower structure should be build "manually". To model slender towers one can use a beam or frame element. Taking into account a combined shear and bending, constituting seismic response of typical masonry towers it was decided to use a plane Timoshenko beam model of the tower.

In order to calibrate the beam model of the tower a criterion of equal displacements under horizontal seismic excitations was chosen. The tip displacements of the tower were calculated using the 3D FEM model and using the Timoshenko beam and respective tip displacements were compared. After multiple trials and errors appropriate values of EJ and GA constant along the beam height were chosen, so that the differences in the tip displacements of the 3D FEM model and the simplified beam model is minimized. As a result the, values of $E=3 \cdot 10^9$ Pa and $G= 1.36 \cdot 10^9$ Pa were obtained. The Poisson ratio ν was assumed as equal to 0.1.

The foundation at the base of the structure was built in form of a simple cuboid. It was introduced to the vibrating system as an additional moment of inertia I^θ, equal to: 34,782,246 kg m^2 and rotational soil compliance which was calculated taking into account the foundation area and sub-soil properties. Applying classic formulas for the elastic half space respective rotational stiffness k_θ equals $1.94 \cdot 10^{12}$ N·m/rad (Fig. 4.3).

As a result of tuning of the simplified beam model, as described above, the first natural period was obtained as equal to $T_1 = 1.366$ s – the same as the one from 3D FEM model of SAP 2000.

To model the horizontal excitations the response spectrum of Eq. 4.2 was used for type 1 and 2 of the response spectra (Fig. 4.2), while respective rocking excitations were modeled using Eq. 4.1. Peak ground acceleration $a_g = 2.146$ m/s^2 and the site category C were assumed with following parameters of the response spectra: $T_B = 0.2$ s, $T_C = 0.6$ s, $T_D = 2$ s, $S = 1.15$ for type 1 spectrum and $T_B = 0.1$ s, $T_C = 0.25$ s, $T_D = 1.2$ s, $S = 1.5$ for type 2 spectrum. Respective damping correction factor was assumed as equal to 1 ($\xi = 5$ %).

The numerical analyses were carried out in Matlab for the respective Timoshenko beam model. Two specific cases were compared. First, when only horizontal excitations are assumed, and second, when the seismic excitations are assumed as simultaneously acting horizontal and rocking effects. The base shear and overturning moments are compared in Table 4.1. It can be seen from Table 4.1 that the effect of rocking excitations on the overall seismic response is substantial in case of the rather flexible soil representing the Parma tower site. As a result of including the rocking effects the tip displacements increased of about 24 %, while the base shear and overturning moments of 30–40 % and about 25 % respectively.

In Figs. 4.6 and 4.7 detailed plots of the shear forces and bending moments along the height of the tower are shown for type 1 and 2 response spectra.

Table 4.1 Seismic horizontal 'h' and rocking 'r' excitation effects on tip displacements, base shear and overturning moments for the Parma Cathedral Bell Tower under type 1 and 2 EC-8 response spectra

Type of response	Type of excitations	Value of the response		Increase	
		Type 1	Type 2	Type 1	Type 2
Tip displacements	'h'	0.2711 m	0.132412 m	23.72 %	24.53 %
	'h' + 'r'	0.3354 m	0.164893 m		
Base shear	'h'	6,674,260 N	5,773,605 N	31.31 %	40.16 %
	'h' + 'r'	8,763,971 N	8,092,285 N		
Overturning moments	'h'	1.95E+08 N	1.04E+08 Nm	24.37 %	27.84 %
	'h' + 'r'	2.45E+08 N	1.33E+08 Nm		
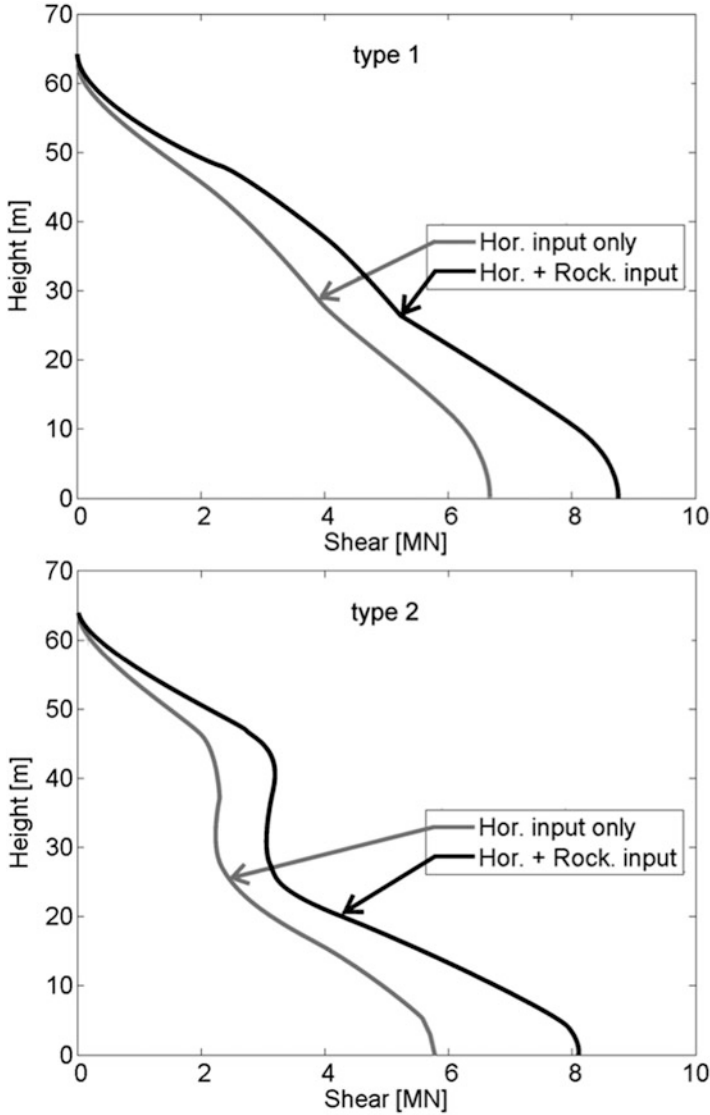
Fig. 4.6 Plot of the shear forces along the height of the tower

It is interesting to note from Figs. 4.6 and 4.7 that the shear and bending moment responses for type 1 and type 2 response spectra are substantially different. The main reason is the different contribution of the higher than the first mode for both spectra. This can clearly be seen in Tables 4.2 and 4.3 showing contributions of the first five modes in the "total" response at selected heights of the tower. The "total" response was computed in this case by including in the computations 20 modes. The higher modes (particularly second and the third) generate greater pseudo-static
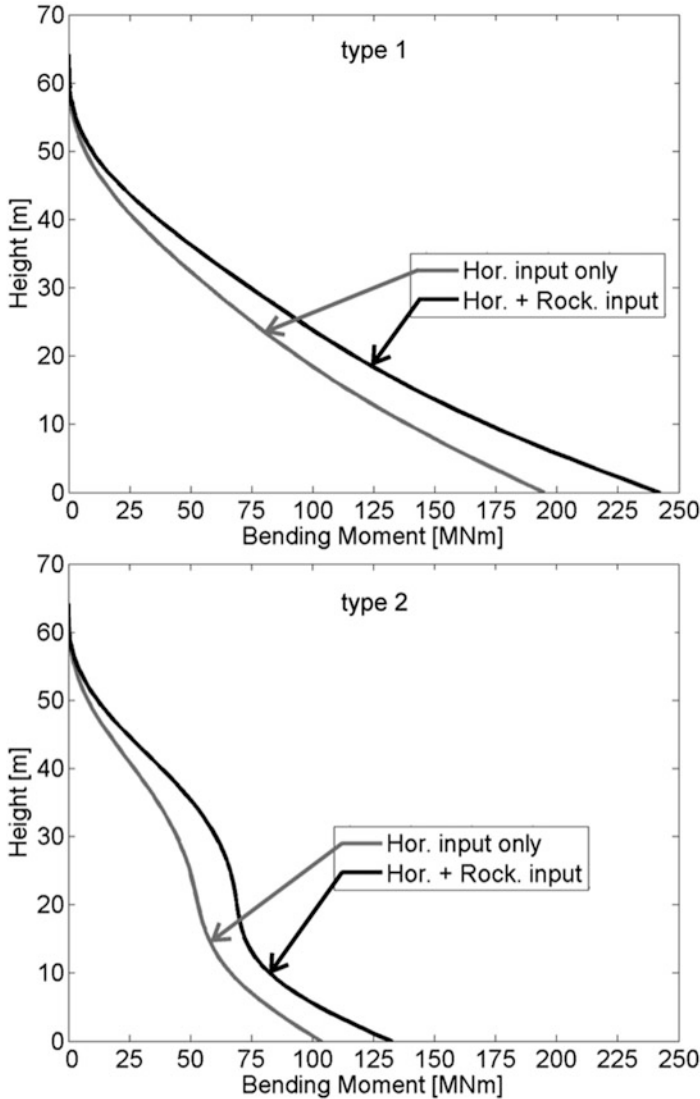
Fig. 4.7 Plot of the bending moments along the height of the tower

forces in the upper part of the tower. This difference can be seen in the shapes of the plots of shear and moments from Figs. 4.6 and 4.7 for type 1 and type 2 spectra.

When slender towers are under a combined horizontal and rocking excitations, including also the rotational soil compliance, one can argue that the heavy weights of the tower finite elements, acting on the eccentricities caused by the horizontal displacements of the tower, may substantially increase respective bending moments. For this reason this well known second order effect (P-Δ) has been included here by adding an additional overturning moment at the base of the

Table 4.2 Contribution of the first five modes in the total response of the tower at selected heights, for type 1 response spectrum (z = height, S = shear force, M = bending moment)

z [m]	F	Mode '1' only % of total	Modes '1'+'2' % of total	Modes up to three % of total	Modes up to four % of total	Modes up to five % of total
39.93	S	77.12	99.09	99.09	99.09	99.82
	M	58.59	96.54	96.54	99.91	99.93
30.17	S	96.18	97.00	97.00	99.75	99.78
	M	79.05	99.79	99.79	99.91	99.99
25.56	S	96.40	97.63	97.63	99.72	99.88
	M	87.21	99.93	99.93	99.95	99.99
0	S	72.26	97.45	97.45	99.42	99.82
	M	96.97	99.90	99.90	99.99	100.00

Table 4.3 Contribution of the first five modes in the total response of the tower at selected heights, for type 2 response spectrum (z = height, S = shear force, M = bending moment)

z [m]	F	Mode '1' only % of total	Modes '1'+'2' % of total	Modes up to three % of total	Modes up to four % of total	Modes up to five % of total
39.93	S	43.21	96.06	96.06	96.06	99.35
	M	26.90	90.77	90.77	99.75	99.83
30.17	S	72.75	76.40	76.40	98.20	98.40
	M	46.22	99.05	99.05	99.58	99.97
25.56	S	74.99	80.63	80.63	97.78	99.17
	M	58.54	99.59	99.59	99.68	99.95
0	S	37.37	91.19	91.19	97.92	99.41
	M	84.58	99.03	99.03	99.89	99.98

structure equal to the sum of the product of the nodal horizontal displacements and respective weights of the lumped masses. The result was checked for the excitations of up to the peak ground accelerations $a_g = 2.146$ m/s$^2 = 0.22$ g, which approximately corresponds to the design for MM intensity of about VIII. It was found that in the case of the Parma Cathedral Bell Tower the P-Δ effects did not exceed 1.2 % (Rossi 2012).

4.4 Conclusion

This paper presents results of a numerical analysis of combined horizontal-rocking seismic effects on an old masonry Parma Bell Tower. Since standard Finite Element programs are not capable to include rotational excitations, a simplified, Timoshenko beam model of the tower was formulated. A numerical analysis in Matlab was carried out using the Eurocode 8 part 6, (2005), model of the rotational seismic

effects. It was found that for the Parma Bell Tower situated on soil C and at the design intensity level defined by accelerations a_g=2.146 m/s^2 the rocking effects are substantial, increasing the base shear for 33 % and the overturning moments for about 25 %. It was also checked that for this level of excitations the second order effects coming from the P-Δ effects are not substantial (about 1.2 %).

The rotational seismic effects are under early stage investigations (see e.g. Lee et al. 2009; Igel et al. 2012) so the formulas of EC-8 part 6 should still be calibrated by more experimental data. Until the rotational data coming from strong intensive records are gathered using special modern rotational devices (Lee et al. 2009; Igel et al. 2012), the approximate formulas of EC-8 part 6, (2005), need to be applied in the engineering practice.

References

Castellani A, Zembaty Z (1996) Comparison between earthquake rotation spectra obtained by different experimental sources. Eng Struct 18(4):597–603

CEN, Comité Européen de Normalisation (2004) Eurocode 8: design of structures for earthquake resistance. Part 1: general rules, seismic actions and rules for buildings. CEN (Comite Europeen de Normalisation), EN 1998-1. Brussels, Belgium

CEN, Comité Européen de Normalisation (2005) Eurocode 8: design of structures for earthquake resistance. Part 6: towers, masts and chimneys. CEN (Comite Europeen de Normalisation), EN 1998-6. Brussels, Belgium

Cerioni R, Brighenti R, Donida G (1996) Seismic analysis of masonry towers: the bell-tower of the Parma Cathedral, Studi e Ricerche – Vol. 17, Scuola di Specializzazione in Costruzioni in C. A., Fratelli Pesenti, Politecnico di Milano, Italia

Falamarz-Sheikhabadi G-A (2012) Approximate formulas for rotational effects in earthquake engineering. J Seismol 16:815–827

Igel H, Brokesova J, Evans J, Zembaty Z (2012) Preface to special issue on "Advances in rotational seismology: instrumentation, theory, observations and engineering". J Seismol 16:571–572

Kalkan E, Grazer V (2007) Coupled tilt and translational ground motion response spectra. J Struct Eng ASCE 133(5):609–619

Lee WHK, Celebi M, Todorovska M, Igel H (2009) Introduction to the special issue on rotational seismology and engineering applications. Bull Seismol Soc Am 99(2B):945–957

NTC (2008) New Italian design code for constructions, "Nuove Norme Tecniche per le Costruzioni" of 14 January 2008

Rossi A (2012) Rotational seismic effects on slender towers with the application of Eurocode 8 Part 6 MsC thesis, Parma University. pp. 1–279.

Trifunac M (1982) A note on rotational components of earthquake motions for incident body waves. Soil Dyn Earthq Eng 1:11–19

Zembaty Z (2009) Rotational seismic load defintion in eurocode 8, part 6, for slender tower-shaped structures. Bull Seismol Soc Am 99(2B):1483–1485

Chapter 5
FOSREM: Fibre-Optic System for Rotational Events and Phenomena Monitoring: Construction, Investigation and Area of Application

Leszek R. Jaroszewicz, Anna Kurzych, Zbigniew Krajewski, Jerzy K. Kowalski, and Krzysztof P. Teisseyre

Abstract This paper reviews our expertise with construction, investigation and simulation of the fibre optic interferometric device named FOSREM (Fibre-Optic System for Rotational Events and Phenomena Monitoring). The presented device was designed for a direct monitoring of rotational components emitted during seismic events as well as existing in irregular and complex structures. The construction of the FOSREM utilizes the Sagnac fibre interferometer in a minimum optical gyro configuration. This approach causes that FOSREM is complete insensitivity to linear motions, and it enables to measure directly the rotational components. In order to make FOSREM mobile and autonomous device we were focused on decreasing size to the $36 \times 36 \times 16$ cm dimension and implementing special FORS – Telemetric Server which enables to control FOSREM remotely via Internet. The laboratory investigation of our system indicated that it keeps the theoretical sensitivity equal to $2 \cdot 10^{-8}$ rad/s/Hz$^{1/2}$ and accuracy no less than $6 \cdot 10^{-9}$–$5 \cdot 10^{-5}$ rad/s in a frequency band from 0 Hz to the upper frequency between 2.56 and 328.12 Hz, respectively. FOSREM protects linear changes of sensitivity in the above detection frequency bandpass and has the maximum values of rotation rate possible to record without "overshoot" equal to 10 rad/s due to an innovative electronic system.

L.R. Jaroszewicz (✉) • A. Kurzych • Z. Krajewski
Institute of Applied Physics, Military University of Technology, 2 Gen. Sylwestra Kaliskiego St., 00-908 Warsaw, Poland
e-mail: jarosz@wat.edu.pl

J.K. Kowalski
m-Soft Ltd., 9-4 Sotta "Sokoła" St., 02-790 Warsaw, Poland

K.P. Teisseyre
Institute of Geophysics, Polish Academy of Sciences, 64 Księcia Janusza St., 01-452 Warsaw, Poland

5.1   Introduction

Investigation of seismic rotational phenomena has been started theoretically for over 30 years (Lee et al. 2009). The atypical observations which appeared after earthquakes like strange, rotational deformations of movements or tombs gave reasons to research the mechanism of their formation (Kozak 2009). They were interpreted as an interaction of seismic waves with components of media which they pass through. Further considerations have been focused on the existence of seismic rotational phenomena in grained rocks in a form of rotational events, as well as seismic rotational waves (Droste and Teisseyre 1997). These deliberations have been developed in the case of rocks with microstructure, defects (Eringen 1999; Teisseyre and Boratynski 2002) or without any internal structure (Teisseyre 2005; Teisseyre et al. 2005; Teisseyre and Górski 2009).

Whereas one of the most important problem of the seismic behaviour of irregular constructions in-plane is the existence of difficulties with controlling horizontal rotation of these structures. The existence of such rotations has a direct influence on torsional effects in structures as well as inter-story drift. Nowadays there are a lot of advanced materials which enable constructing complicated, innovative and very high structures. These constructions require unique and precise devices for continuously monitoring structural responses (Cowsik et al. 2009).

The two above paragraphs indicated that new innovative instruments to measure the rotational components of earthquakes as well as to monitor real rotation effects in engineering constructions are necessary. Measurements of rotational motions obtained by a special array or set of conventional seismometers are sensitive to linear motions (Teisseyre and Nagahama 1999; Jaroszewicz et al. 2003). In our opinion, the sensors based on the Sagnac effect (Sagnac 1913) seem to be the most proper in the pointed out application fields. The main advantage of such approach is possibility to measure rotational motions in a direct way (Jaroszewicz et al. 2014; Kurzych et al. 2014). Moreover it does not require an external reference frame for its measurements. The first review about application of the commercial available fibre optic gyroscope (FOG) for the measurement of rotations in structural engineering can be found in (Schreiber et al. 2009) as well as in (Zembaty et al. 2013) for stiffness reconstruction.

However, the direct FOG application for such investigation is connected with data processing problems because FOG output gives angles instead of angular velocity which parameter is optimized according to minimize the drift phenomenon. For above reasons we constructed two devices: the Autonomous Fibre-Optic Rotational Seismograph (AFORS) and Fibre-Optic System for Rotational Events and Phenomena Monitoring (FOSREM). The first one was used for direct recording the rotational components of seismic events (Jaroszewicz et al. 2011, 2014; Kurzych et al. 2014) and initially for continuous monitoring of the 'horizontal

building's rotation (Jaroszewicz et al. 2013a) while the second will be applied in area of strong-motion seismology and to monitor engineering construction.

This paper describes and summarizes our broad experience in construction and application of above mentioned systems.

5.2 Construction of the Rotational Fibre Optic Interferometric Devices

The constructed rotational fibre optic interferometric devices (AFORS and FOSREM) contain generally two parts: Optical Head and electronic system. The Optical Head contains fibre optic interferometer where the Sagnac effect generates a phase shift. The Sagnac effect is a result of difference between two equal beams propagating around closed optical path, in an opposite direction. After recombination of these two beams the Sagnac phase shift induced by a rotational rate Ω perpendicular to a plane of sensor is equal to (Post 1967):

$$\Delta\varphi = \frac{4\pi RL}{\lambda c}\Omega = \frac{1}{S_o}\Omega \tag{5.1}$$

where: L – length of the fibre in the sensor loop, R – sensor loop diameter, λ – wavelength of the source, c – velocity of the light in the vacuum, S_o – optical constant of the interferometer.

The above dependence allows to measure rotations in a direct way and without any external reference frame because the Sagnac phase shift does not depend on a centre rotation location as well as a sensor plane shape (Post 1967). For above reasons sensors based on the Sagnac effect seem to be appropriate to measure rotational effects, perturbations and inter-story drifts in buildings.

We designed AFORS's/FOSREM's Optical Head according to the FOG minimal configuration, as is shown in Fig. 5.1. It consists of the: superluminescent diode (SLED) (*Exalos*, Schlieren, Switzerland; with $\Delta B = 31.2$ nm, $\lambda_0 = 1305.7$ nm and P $= 9.43$ mW), two X-type couplers (*Phoenix Photonics*, Birchington, UK; with $\alpha = 0.20$ dB), depolarizer (AFORS: *Phoenix Photonics;* with DOP <5 % and $\alpha = 0.20$ dB), isolator (*FCA*, Niepołomice, Poland; with $\alpha = 0.34$ dB and 39 dB isolation), detector (*Optoway Technology*, Taiwan; with S $= 0.9$ A/W), two fibre-optic polarizers mounted in-line (*Phoenix Photonics;* with $\varepsilon = 43$ dB and $\alpha = 0.45$ dB each) and phase modulator. (*Piezomechanik*, Germany). The wideband, low coherence SLED protects the proper method for eliminating the polarization influence on the sensor work and emits the high optical power, which it affects the system sensitivity. The second coupler has been added after the polarizer to ensure that both counter-propagating beams pass through the same path in the sensor loop (Udd and Spillman 2011). The polarizers assure that the two light waves return to the first coupler in the same polarization. This configuration
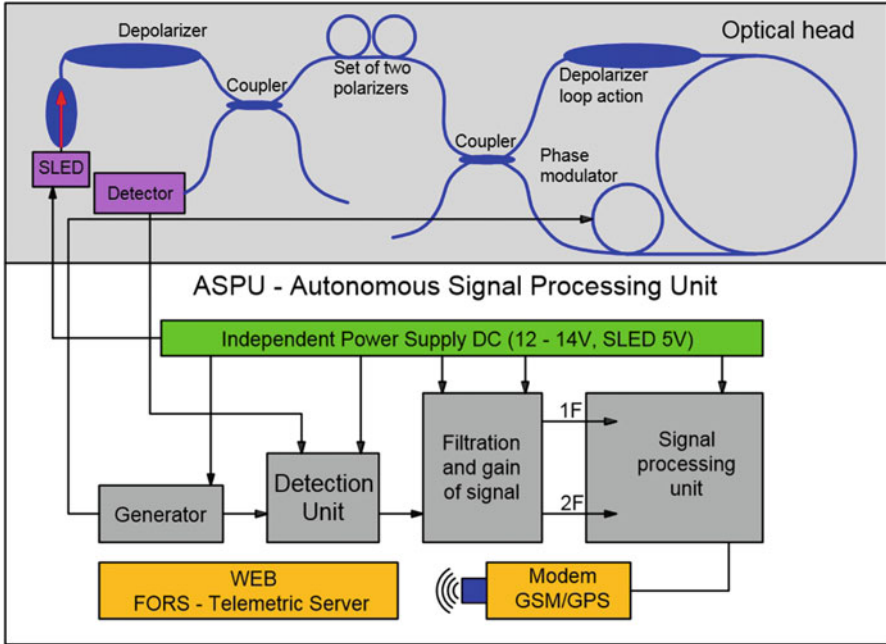
Fig. 5.1 The block diagram of the AFORS/FOSREM construction (*upper* part presents the optical head and the *lower* presents electronic system)

guarantees that the only nonreciprocal effect in the system is the Sagnac effect. In the next part of this paper we presented all reasonable causes of the selection exactly above parameters of the optical elements.

The electronic system, presented in lower part of Fig. 5.1, is named Autonomous Signal Processing Unit – ASPU (*m-Soft Ltd.*, Warsaw, Poland). It allows to calculate and record information about rotation motions which is obtained directly from the measured Sagnac phase shift. Generally, the ASPU protects selection of the first ($A_{1\omega}$) and the second ($A_{2\omega}$) amplitude of the harmonic output signal [u(t)], which enables to assign rotation rate according to the relation of (Jaroszewicz et al. 2011):

$$\Omega = S_o \cdot \arctan[S_e \cdot u(t)] = S_o \cdot \arctan\left[S_e \cdot \frac{A_{1\omega}}{A_{2\omega}}\right] \qquad (5.2)$$

where S_e – the electrical constant related to parameters of the applied components and obtained during the sensor calibration together with determining the optical constant S_o. The calibration process is wide described in (Krajewski 2005; Jaroszewicz et al. 2011). The electronic part uses quartz oscillator which determines the basic detection time equals 4.7104 ms for AFORS. The multiplication of this time gives opportunity to choose the frequency from 0 Hz to the upper chosen value between 0.84 and 106.15 Hz, and above band range is named "detection

frequency bandpass" in the next part of this paper. It should be underlined that this feature of AFORS/FOSREM allows to detect rotational movements in extremely low frequencies, even equal to 0 Hz, it is significant advantage of optical devices in comparison to the mechanical devices, which have limited so-called bandwidth, connected with their mechanical nonlinear frequency characteristic. According to *A Glossary for Rotational Seismology* (Lee 2009), the bandwith is a range between high-pass and low-pass cut-off frequencies and often meant as the portion of frequency-response amplitude spectrum that is approximately flat.

It should be underlined that it is completely another approach in comparison to the method used in the FOG where measurement of the angular changes is obtained by applying the time integration of the angular rates. Moreover, the ASPU sends records to a GSM/GSP modem connected with WEB special FORS – Telemetric Server. This server enables to make AFORS and FOSREM remotely control via internet including needful system corrections, software upgrade, data storage as well as changes of the working parameters.

The sensitivity of the designed sensors is the most significant parameter due to apply them to measure rotational effects. Theoretical considerations (Ostrzyżek 1989) reach to conclusion that the optimization of the Optical Head elements, which a main goal is maximization of the sensor sensitivity, requires selection of such parameters as: radius of the sensor loop, optical power and wavelength of the light source, length of the fibre and total losses of the optical path. These parameters have the most meaningful effect on the system sensitivity.

In our first devices, named AFORS-1,-2,-3, the optical fibre of 15 km – SMF-28e$^+$ was wound on the 0.63 m diameter sensor loop which has been made of a special composite material with permalloy particles for shielding the sensor from external magnetic field. Based on all above described configuration and consideration finally we obtained the accuracy for AFORSs as is shown in Fig. 5.2. As one can see AFORS-1 and AFORS-2 have similar accuracy, only about half of the order worse than theoretically calculated their sensitivity for given detection frequency bandpass. Unfortunately, for AFORS-3 accuracy is more than three times worse and this system may be used in limited application. Such deterioration is connected with problems of applied electronic part in AFORS-3. Because all AFORSs use "open configuration" for rotation rate calculation according to the formula (5.2), the parameters of the sensor loop determine directly the maximum values of rotation rate possible to record without "overshoot" which is equal to 0.02 rad/s.

The AFORS-1 (Fig. 5.3) has been installed in the Książ seismological observatory in Poland since July 2010 with its continuous monitoring via Internet basing on the application FORS – Telemetric Server.

In Fig. 5.4 we presented example of the rotational event recorded after the Honshu earthquake M = 9.0 which took place on March 11th 2011, at 5 h 46 min 23 s.

The system of next two devices AFORS-2 and AFORS-3 have been initially used to measure rotation response of engineering constructions. We used two seismographs in order to have one as the reference system. The summarized results of this investigation are presented in Fig. 5.5 as amplitude of building rotation measured at different building floors caused by ground moves after tramp pass through street in distance about 50 m from and parallel to long building wall.
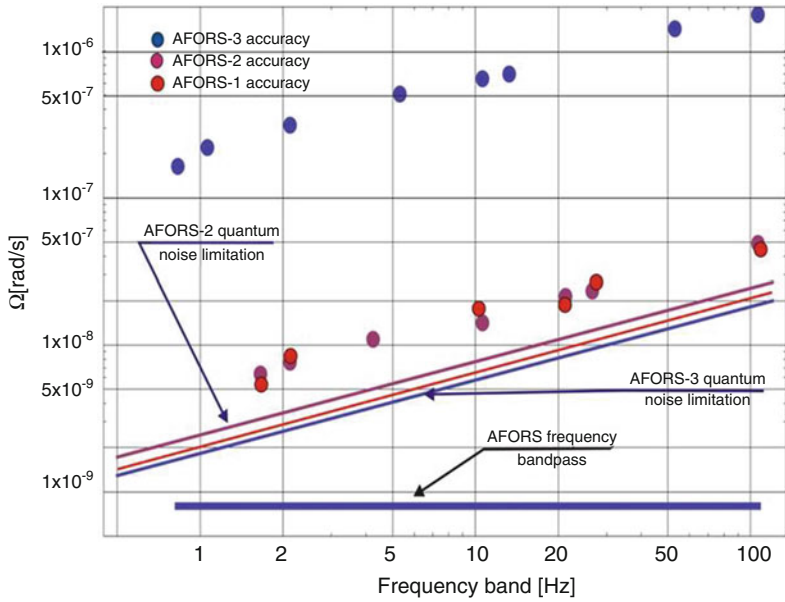
Fig. 5.2 The accuracy measured in Warsaw, Poland for the chosen detection frequency bandpass (0.84–106.15 Hz) for AFORSs
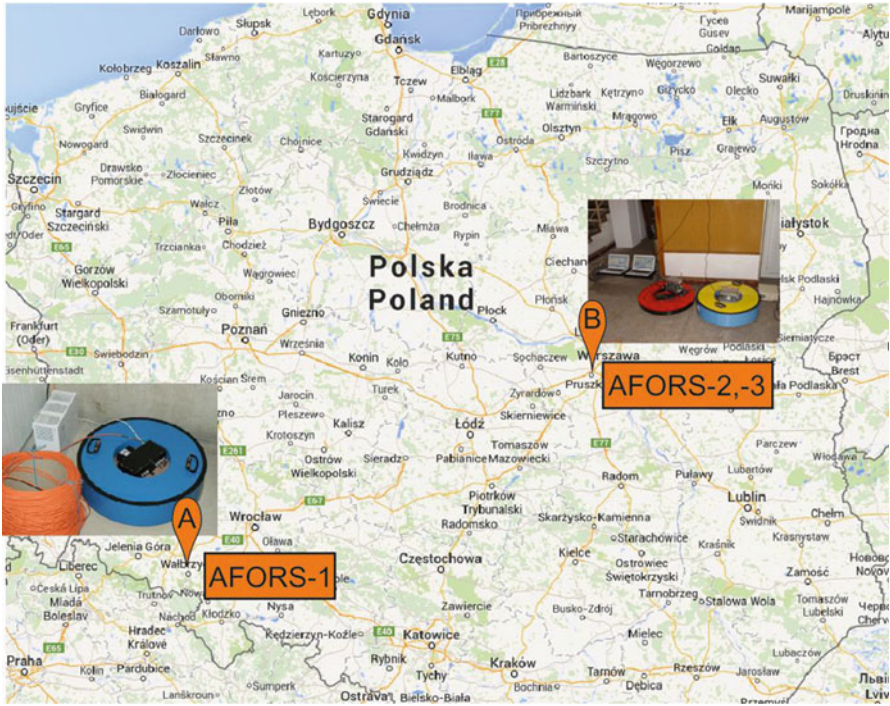
Fig. 5.3 GOOGLE map with current devices localization
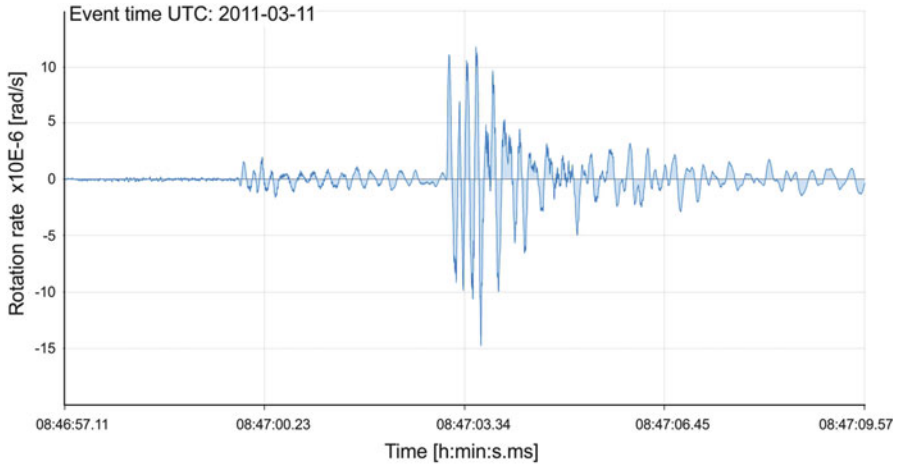
Fig. 5.4 The plot of the seismic event recorded in Książ, Poland on March 11th 2011, starting from 8 h 46 min, after the Honshu earthquake M = 9.0, times UTC (Jaroszewicz et al. 2013a)
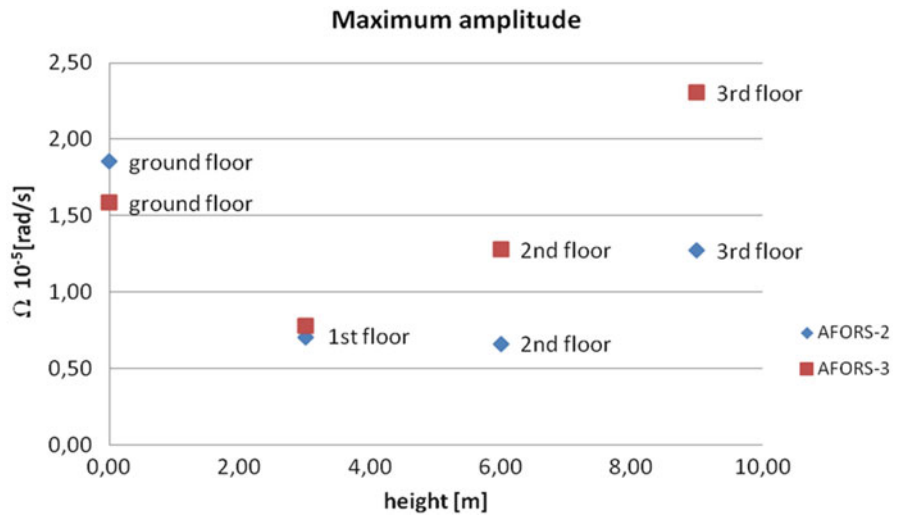
Fig. 5.5 The data recorded on different floors as the response for ground moves (Jaroszewicz et al. 2013b)

Nevertheless, our investigations which were carried out by AFORS's pointed out that we have to construct a new mobile system. The main reasons for such assumption were the noticeable disadvantages of AFORS's application in structural engineering which are: extremely high cost (uses only for limited applications), problem with verification of their proper operations, single axis rotation measurements and errors under high temperatures (above 60 °C) as well as transport complications due to large dimensions of the devices.

For above-mentioned reasons a new Fibre-Optic System for Rotational Events and Phenomena Monitoring (FOSREM) has been performed which should give more practical device. It should be emphasised that FOSREM gives possibilities to measure rotational effects in a wide range of frequencies and rotational rates. Moreover, we focused on decreasing size of the sensor to $36 \times 36 \times 16$ cm dimension. Thus we decided to record data about rotation motions during the earthquakes in seismological observatory by AFORS systems due to high accuracy and sufficient detection frequency bandpass for seismic application while our new system FOSREM will be applied to investigate engineering construction rotation response as well as to operate during strong-motions earthquakes.

5.3 Simulated and Experimental Results of FOSREM

The sensitivity of the designed sensors described the lowest value of the measured angular velocity in a set detection frequency bandpass. It means the velocity in which the quotient of the output power to the noises is equal to one. To precisely estimate the main parameters of sensors we have made simulations which enabled to design FOSREM. A few of our previous investigations (Jaroszewicz et al. 2013b) carried out by AFORSs were disturbed by high temperature. Thus, in this paper we included discussion about the influence of the temperature on the system operating as well.

The dependence between sensitivity and optical power of the light source shows that sensitivity increases with increasing the source optical power. The relation presented in Fig. 5.6a shows that the most advantageous value of optical power is near 10 mW which corresponds to apply in FOSREM SLED diode with a optical power P = 9.43 mW.

To enlarge the sensitivity one can apply the shorter wavelength of light source (see Fig. 5.6b). Although higher attenuation is related with shorter wavelength. Therefore operating in the second telecommunication window seems to be the optimal solution.

In the FOSREM construction we were also focused on decreasing size of the sensors. Dimensions of the first two FOSREM devices are equal to the $47 \times 23 \times 36$ cm (similar to the size of a flight hand luggage – Fig. 5.7a), however next devices will have size equals $36 \times 36 \times 16$ cm which considerably enlarges their mobility (Fig. 5.7b). It enables to carry out the planned measurements simply and without transport complications. Additionally, we designed a mechanical protection of the Optical Head, as is shown in Fig. 5.7b, printed on 3D Printer (MakerBot Replicator 2X).

Such approach requires, at first, analysis of the fibre length and the sensor loop radius selection. To define the optimal fibre length we performed simulation which is shown in Fig. 5.8. The simulation was prepared for 1305.7 nm wavelength of the light source and 16.3 dB system losses as well as the sensitivity of the photodiode equals 0.9 A/W. The simulation shows that the selection fibre length of 5 km is the
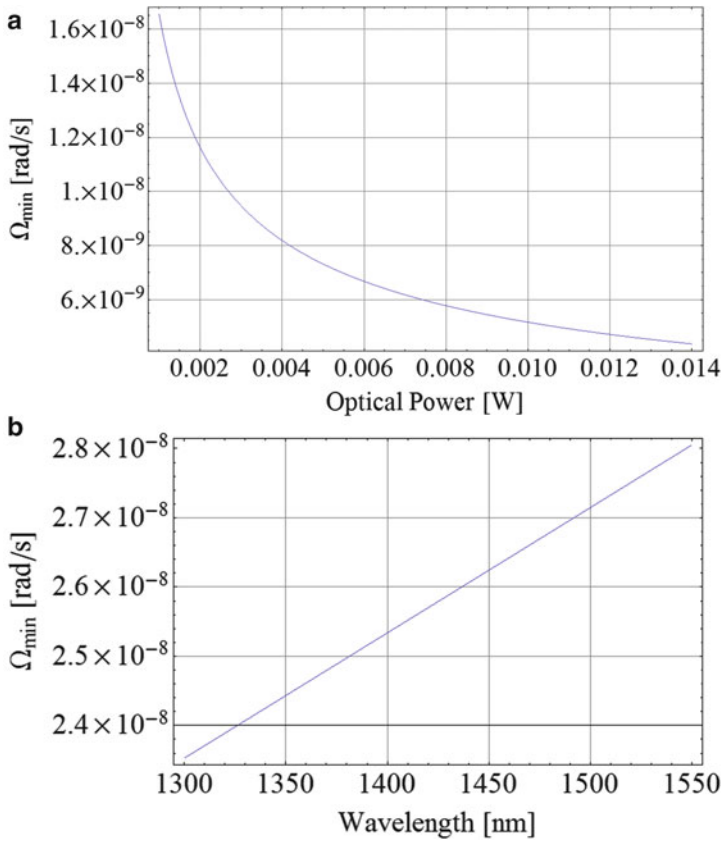
Fig. 5.6 Influence of the light source parameters on sensor sensitivity: (**a**) The sensor sensitivity vs. optical power of the source; (**b**) The sensor sensitivity vs. wavelength of the source
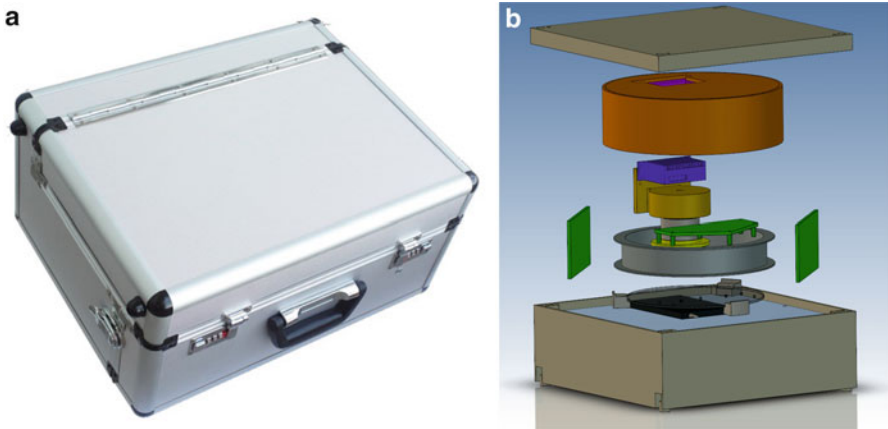
Fig. 5.7 Package of the designed sensor: (**a**) total size of the first two sensors; (**b**) 3D visualization of the new sensor with all components, colour: *beige* – package, *dark* – depolarizer, *grey* – sensor loop, *green* – electronic parts, *yellow* – modulator, *blue* – SLED diode, *orange* – sensor's mechanical protection and acoustic isolation

a

b
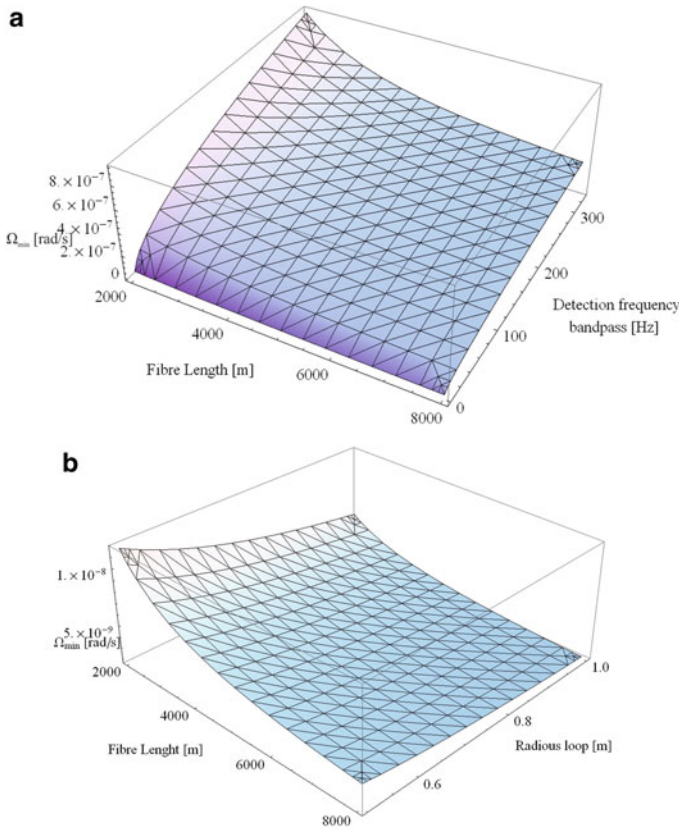
Fig. 5.8 Influence of fibre length and radius loop on the sensor sensitivity: (**a**) correlation between fibre length, detection frequency bandpass and sensor sensitivity; (**b**) correlation between fibre length, radius loop and sensor sensitivity

most optimal length for obtaining minimal rate of rotation rates in entire detection frequency bandpass. The Sagnac effect increases with the length of the optical fibre. Although the optical fibre introduces an attenuation which decreases the level of signal. The sensitivity is at the same level in the entire detection frequency bandpass for fibre length of 5 km. The fibre length of 5 km and 0.12 m radius of sensor loop enable to achieve sensitivity about $2 \cdot 10^{-8}$ rad/s/Hz$^{1/2}$. FOSREM uses quartz oscillator, which determines the basic detection time equals 1.5234 ms, thus above sensitivity should protect the accuracy no less than $6 \cdot 10^{-9}$–$5 \cdot 10^{-5}$ rad/s in a frequency band from 0 Hz to the upper frequency between 2.56 and 328.12 Hz, respectively. To perform the sensor loop in FOSREM we wound optical fibre to an aluminum reel (the grey one in Fig. 5.7b) in a double-quadrupole mode (Dai et al. 2002) for the thermal stabilization of the sensor's work. One should noticed that this method of winding can cause growth of the attenuation. For the reasons above we decided that 5 km is the most optimal length.

The total losses of the optical path (α) have the main influence on system sensitivity (see simulation in Fig. 5.9). Due to the above we made assumption that total losses of the Optical Head should be below value of 17 dB (where 9 dB is theoretical minimum losses) because it protects the system sensitivity at expected level. The value of the system losses higher than 17 dB causes rapid increase of the minimum measured rotation. In first two FOSREM constructions we obtained losses equals about 16 dB which contain: losses on all fibre splices (about 2 dB), attenuation in the sensor loop about 1.65 dB, losses on the couplers 9 dB resulting from the minimum configuration, losses on the other optical elements such as the polarizer and the depolarizer about 3.65 dB. Moreover, it should be underlined that the selected radius of the sensor loop does not introduce additional macrobending losses.

Figure 5.10 shows correlation between temperature, detection frequency band and the minimal measured rotation rate. As one can see Ω is stable in temperature range between 260 and 333 K. Such results are contradicting our previous
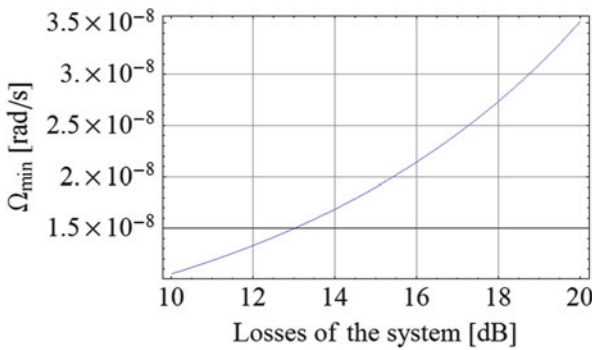

Fig. 5.9 The sensor sensitivity vs. optical system losses
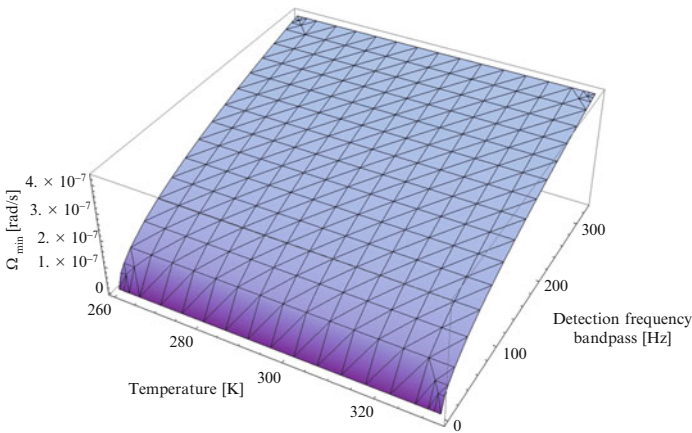

Fig. 5.10 Correlation between temperature, detection frequency bandpass and sensor sensitivity

measurements where recorded data was disturbed by the high temperature (Jaroszewicz et al. 2013b). However in the AFORS we used optical fibre of 15 km which could introduce higher temperature fluctuation in the system and polarization instability caused by the temperature perturbations while the presented simulation in Fig. 5.10 was performed for sensor with optical fibre of 5 km.

The presented simulations indicate that FOSREM sensitivity depends on the various parameters. Our considerations allow to design very promising device which will be applied to the investigation of rotation motions, displacements and inter-story drifts of civil engineering structures.

Finally, in order to carry out some experimental measurements we have placed the first constructed prototype of FOSREM on a rotational table (Fig. 5.11). The presented results in Fig. 5.12 show measurement of Earth rotation component in Warsaw (equal to $4.45 \cdot 10^{-5}$ rad/s) for different value of detection frequencies bandpass for tentatively calibrated our device. We carried out measurements using four selected upper frequencies: 0.01 Hz, 10.25 Hz, 109.38 and maximal – 328.12 Hz, respectively.

Because engineering applications need system which is able to detect rotation rate as high as 10 rad/s, the reconstruction of ASPU according to special electronic procedure (prepared as an patent application) gives for FOSREM the expected maximum value of rotation rate possible to record without "overshoot" up to above mentioned value, also.

The main purpose of presenting these results was to demonstrate a wide usefulness of our instruments. We are convinced that AFORS and FOSREM parameters give opportunity to record highly interesting rotational events or phenomena.
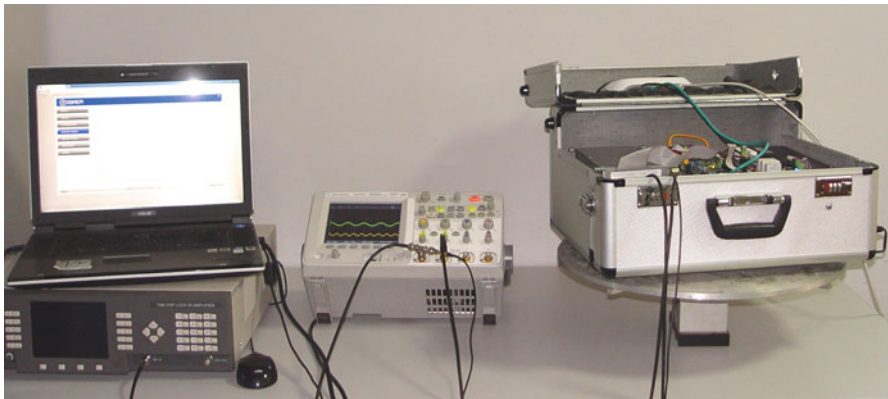

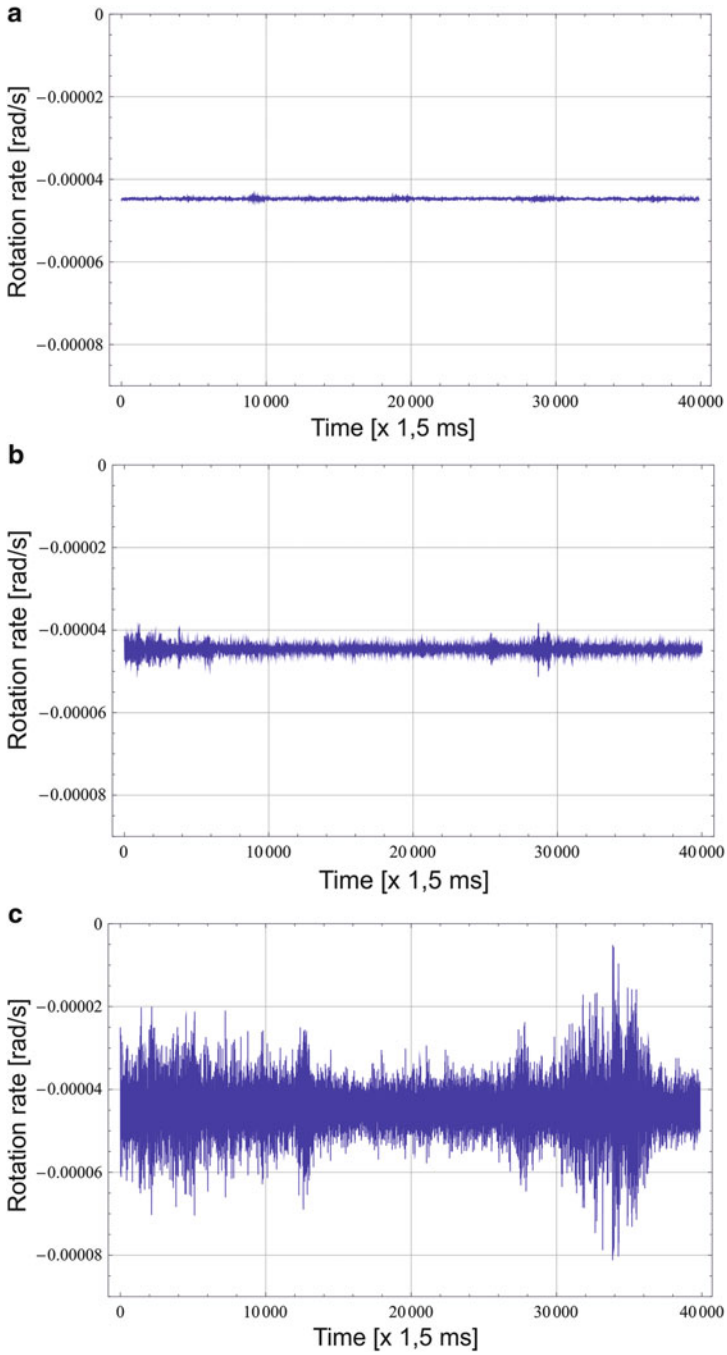**Fig. 5.11** The laboratory set to measure rotational motions by FOSREM

Fig. 5.12 Example of measured Earth rotation rate component in Warsaw at various detection frequency bandpass: (**a**) 0.01 Hz; (**b**) 10.25 Hz; (**c**) 109.38 Hz; (**d**) 328.12 Hz
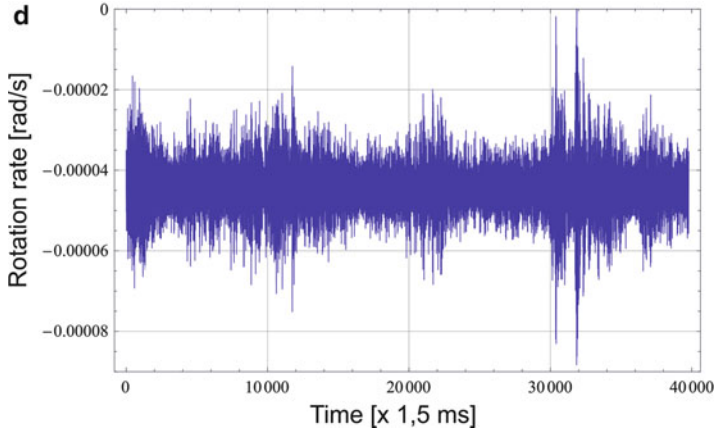
Fig. 5.12 (continued)

5.4   Conclusions

In this paper we presented the most promising interferometric sensor construction to monitor continuously the rotational effects of complicated engineering constructions as well as to measure effects in engineering strong-motion seismology area – FOSREM. It is unique and innovative device which utilizes the Sagnac effect. This technique allows to measure the rotational effects directly and without any reference frame. It is very important during the earthquakes when nothing is stable.

The included simulations have enabled to design the FOSREM and have shown that selected parameters of the optical elements are appropriate to obtain enough accuracy (no less than $6 \cdot 10^{-9}$–$5 \cdot 10^{-5}$ rad/s) for the seismic application. Moreover, the FOSREM operates in the wide range of the detection frequency bandpass from 0 Hz to the chosen upper frequency range from 2.56 to 328.12 Hz with maximum value of detected rotation rate of the order of 10 rad/s. The designed FOSREM construction is mobile and the electric part makes it totally remotely controlled via Internet and it allows to obtain immediate information about recorded events. All FOSREM advantages indicate that it is proper device to apply it in the investigation of rotational effects in engineering structures.

Moreover, presented data shows the proper work of AFROSs as a system for rotational motion detection and they are very promising for the future investigation of rotational events in Książ seismological observatory. We are collecting continuously records about seismic evens and they are under scientific processing and will be published in papers linked with seismological science.

We believe that our devices can significantly influence seismological science.

References

Cowsik R, Madziwa-Nussinov T, Wagoner K, Wiens D, Wysossion M (2009) Performance characteristics of a rotational seismometer for near-field and engineering applications. Bull Seismol Soc Am 99(2B):1181–1189

Dai X, Zhao X, Cai B, Yang G, Zhou K, Liu C (2002) Quantitative analysis of the Shupe reduction in a fiberoptic Sagnac interferometer. Opt Eng 41:1155–1156

Droste Z, Teisseyre R (1997) Rotational and displacemental components of ground motion as deduced from data of the azimuth system of seismographs. Publ Inst Geophys Pol Acad Sci M-1(97):157–167

Eringen AC (1999) Microcontinuum field theories, vol 1, Foundations and Solids. Springer, New York

Jaroszewicz LR, Krajewski Z, Solarz L, Marć P, Kostrzyński T (2003) A new area of the fiber-optic sagnac interferometer application. In: Proceedings of International Microwave and Optoelectronics Conference IMOC-2003, Iguazu Falls, Brazil, 20–23 Sep 2003

Jaroszewicz LR, Krajewski Z, Kowalski H, Mazur G, Zinówko P, Kowalski JK (2011) AFORS autonomous fibre-optic rotational seismograph: design and application. Acta Geophys 59:578–596

Jaroszewicz LR, Krajewski Z, Teisseyre KP (2013a) The possibility of a continuous monitoring of the horizontal buildings' rotation by the fiber-optic rotational seismograph AFORS type. In: Lavan O, De Stefano M (eds) Seismic behaviour and design of irregular and complex civil structures. Springer, Heidelberg, pp 339–351

Jaroszewicz LR, Krajewski Z, Matysik M, Kowalski KJ (2013b) Investigation of building rotation motion using autonomous fibre rotational seismographs. Paper presented at the 3rd International Workshop on Rotational Seismology – 3IWoRS, Christchurch, 22–25 Sep 2013

Jaroszewicz LR, Krajewski Z, Kowalski KJ, Kurzych A, Raszewski R (2014) AFORS – autonomous fiber optic rotational seismograph as a system for continuous monitoring the rotational seismic events. Adv Mater Res 909:444–449

Kozak JT (2009) Tutorial on earthquake rotational effects: historical examples. Bull Seismol Soc Am 99:998–1010

Krajewski Z (2005) Fiber optic Sagnac interferometer as device for rotational effect investigation connected with seismic events. Dissertation, Military University of Technology

Kurzych A, Jaroszewicz LR, Krajewski Z, Teisseyre KP, Kowalski JK (2014) Fibre optic system for monitoring rotational seismic phenomena. Sensors 14:5459–5469

Lee WHK, Celebi M, Todorovska MI, Igel H (2009) Introduction to the special issue on rotational seismology and engineering applications. Bull Seismol Soc Am 99:945–957

Leee WHK (2009) A glossary for rotational seismology. Bull Seismol Soc Am 99:1082–1090

Ostrzyżek A (1989) Accuracy analyze of the angle speed measurement in the fibre optic gyroscope. Dissertation, Military University of Technology

Post EJ (1967) Sagnac effect. Rev Mod Phys 39:475–493

Sagnac G (1913) The light ether demonstrated by the effect of the relative wind in ether into a uniform rotation interferometer. Acad Sci 95:708–710

Schreiber KU, Velikoseltsev A, Carr AJ, Franco-Anaya R (2009) The application fibre optic gyroscope for the measurement of rotations in structural engineering. Bull Seismol Soc Am 99(2B):1207–1214

Teisseyre R (2005) Asymmetric continuum mechanics: deviations from elasticity and symmetry. Acta Geophys 53(2):115–126

Teisseyre R, Boratynski W (2002) Continuum with self-rotation nuclei: evolution of defect fields and equations of motion. Acta Geophys 50(2):223–229

Teisseyre R, Górski M (2009) Transport in fracture processes: fragmentation and slip. Acta Geophys 57(3):583–599

Teisseyre R, Nagahama H (1999) Micro-inertia continuum: rotations and semi-waves. Acta Geophys Pol 47:259–272

Teisseyre R, Białecki M, Górski M (2005) Degenerated mechanics in a homogeneous continuum: potentials for spin and twist. Acta Geophys 53(3):219–230

Udd E, Spillman BW (2011) Fiber optic sensors. Wiley, Hoboken

Zembaty Z, Kokot S, Bobra P (2013) Application of rotation rate sensors in an experiment of stiffness 'reconstruction'. Smart Mater Struct 22: doi: 10.1088/0964-1726/22/7/077001

Chapter 6
Application of Rotation Rate Sensors in Measuring Beam Flexure and Structural Health Monitoring

Zbigniew Zembaty, Seweryn Kokot, and Piotr Bobra

Abstract This paper presents a new approach to measure and monitor structural vibrations in civil and seismic engineering which uses new rotational sensors which can measure flexural vibrations of a beam axis. First a rotation rate sensor (measuring rotational velocity) is tested with respect to its ability to follow changes of strains in a beam during its vibrations. Next a system of rotation rate sensors is applied to effectively reconstruct stiffness variations of a simple, cantilever beam. It is demonstrated that the rotation rate sensors can be used to effectively reconstruct three unknown stiffness drops of a cantilever beam under harmonic vibrations. Both experiments are carried out using small plexi beams in laboratory scale. At this moment the rotational sensors are still rather expensive and with limited range and accuracy. However with the time passing by, their quality will improve and prices decrease making them very effective instruments in seismic engineering and health monitoring of structural systems.

6.1 Introduction

Structural Health Monitoring (*SHM*) is a rapidly developing, new branch of civil engineering, which originated in the second half of twentieth century in other fields of engineering, particularly in the machine and aero industry, due to a particular need of constant monitoring of important machines and structural systems. One of the key problems of *SHM* in civil engineering is to conclude about the state of structures based on monitoring their dynamic response to various types of excitations (harmonic, wind, seismic, ambient etc.). Using respective response

Z. Zembaty (✉) • S. Kokot • P. Bobra
Faculty of Civil Engineering, Opole University of Technology,
ul. Proszkowska 76, 45-758 Opole, Poland
e-mail: z.zembaty@po.opole.pl; s.kokot@po.opole.pl; p.bobra@po.opole.pl

measurements one can retrieve natural frequencies and modes of the structure and use them in modal analyses leading to damage assessment and localizations. However when one is trying to locate damages in structures by observing changes in the natural modes it appears that the observed stiffness losses are much better reflected in the variations of spatial derivatives of the modes than in the modes themselves. On the other hand, numerical differentiation of the measured natural modes introduces such substantial noise, that in spite of using special smoothing techniques, effective damage localization is still very difficult (see e.g. papers by Maek and DeRoeck 1999; Ndambi et al. 2002). For some time however, new techniques of directly measuring angle variations appeared (see e.g. Meydan 1997) and nowadays matured to achieve angle resolution of $10^{-3\circ}$. Thus, in addition to transversal accelerations, now it is possible to measure angle variations along the bar axis during vibrations of the structures. This way, the changes in curvature of the axes of the bars of the structures can be obtained almost directly. Numerical simulations aiming at investigations of potential advantages of these new angular measurements have already appeared in the literature, and the effectiveness of including the rotations in conventional modal analysis was confirmed (Abdo and Hori 2002; Kokot and Zembaty 2009b). The measurements of beam axis rotations make it also possible to retrieve respective strains for the same beam in bending.

This paper investigates the advantages of using the rotation rate sensors in monitoring beam vibrations in bending. First, selected results of an experiment in which strains of a beam in harmonic flexural, vibrations are assessed based on the measurements of rotational velocity of the beam axis are presented. Next, results of another experiment are presented, in which rotation rate sensors are used to reconstruct stiffness changes of a beam under harmonic flexural vibrations.

6.2 Beam Under Flexural Vibrations

Consider equation of motion of a uniform cantilever beam $(EJ(x) = EJ = const, m(x) = m = const)$ under kinematic excitations (Fig. 6.1):

$$EJ\left[\frac{\partial^4 w}{\partial x^4} + \kappa \frac{\partial^4 w}{\partial x^4} \dot{w}\right] + \mu m \dot{w} + \mu m \ddot{w} = -m\ddot{u}(t) \qquad (6.1)$$

where 'dot' stands for differentiation with respect to time, $\ddot{u}(t)$ is the acceleration of the kinematic motion of the beam, κ, μ are constants reflecting the participation of the damping proportional to stiffness and mass respectively.

Applying mode superposition method (e.g. Chopra 2011) leads to following solution
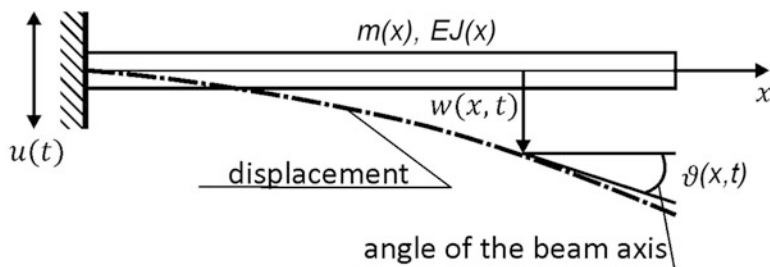
Fig. 6.1 Cantilever beam under vertical, kinematic excitations

$$w(x,t) = -\sum_{j=1}^{\infty} \wp_j \psi_j(x) \int_{-\infty}^{\infty} h_j(\tau)\ddot{u}(t-\tau)d\tau \qquad (6.2)$$

in which

$$\wp_j = \frac{\int_0^L \psi_j(x)dx}{\int_0^L \psi_j^2(x)dx} \qquad (6.3)$$

is the modal participation factor, $\psi_j(x)$ stands for the "j-th" mode shape, while $h_j(t)$ is the impulse response function of the "j-th" natural mode of vibration:

$$h_j(t) = \frac{1}{\omega_{jd}}\exp\left[-\xi_j\omega_j t\right]\sin\left(\omega_{jd}t\right) \qquad (6.4)$$

where $\omega_{jd} = \sqrt{(1-\xi_j^2)}$ is the damped natural frequency and $\xi_j = \mu/(2\omega_j) + \kappa\omega_j/2$ is the modal damping ratio. Equation 6.2 can be used to obtain its spatial derivative i.e. the angle of the axis rotation:

$$\vartheta(x,t) = \frac{\partial w(x,t)}{\partial x} = -\sum_{j=1}^{\infty} \wp_j \psi_j'(x) \int_{-\infty}^{\infty} h_j(\tau)\ddot{u}(t-\tau)d\tau \qquad (6.5)$$

and second derivative, which is proportional to bending moment

$$\vartheta'(x,t) = \frac{\partial^2 w(x,t)}{\partial x^2} = \frac{M}{EJ} = \frac{1}{\rho} = -\sum_{j=1}^{\infty} \wp_j \psi_j''(x) \int_{-\infty}^{\infty} h_j(\tau)\ddot{u}(t-\tau)d\tau \qquad (6.6)$$

Using the Fourier transform one may re-write Eq. 6.2 in frequency domain as follows

$$W(x, \omega) = -\sum_{j=1}^{\infty} \wp_j \psi_j H_j(\omega) U_{accel}(\omega) \tag{6.7}$$

where $H_j(\omega)$ stands for frequency response function of the "j-th" mode of vibration

$$H_j(\omega) = \int_{-\infty}^{\infty} \ddot{u}(\tau) e^{-i\omega\tau} d\tau = \frac{1}{\omega_j^2 - \omega^2 + 2i\xi_j\omega_j\omega} \tag{6.8}$$

in which $i = \sqrt{(-1)}$ and $U_{accel}(\omega)$ denotes Fourier transform of the excitation accelerations $\ddot{u}(t)$

$$U_{accel}(\omega) = \int_{-\infty}^{\infty} \ddot{u}(\tau) e^{-i\omega\tau} d\tau \tag{6.9}$$

In case of steady-state vibrations the minus signs in formulas (6.1, 6.5, and 6.7) can be dropped. Applying the rules of time and spatial differentiation of formula (6.2) into its frequency domain form (6.7), one can obtain velocity of the angle of the beam axis $\dot{\vartheta}$ denoted in frequency domain as θ_{vel}:

$$\theta_{vel}(x, \omega) = \sum_{j=1}^{\infty} \wp_j \psi'_j(x) i\omega H_j(\omega) U_{accel}(\omega) \tag{6.10}$$

Assume now that the beam has a rectangular $b \times h$ cross-section. For such the Euler-Bernoulli beam the maximum strain (on the beam surface) equals

$$\varepsilon = \pm \frac{h}{2} \frac{\partial^2 w}{\partial x^2} \tag{6.11}$$

Thus applying Eq. 6.5 the maximum strain can be obtained in frequency domain as follows

$$\varepsilon(x, \omega) = \pm \frac{h}{2} \sum_{j=1}^{\infty} \wp_j \psi''_j(x) H_j(\omega) U_{accel}(\omega) \tag{6.12}$$

Comparing Eq. 6.12 with 6.10 gives formula for the beam surface strain in terms of rotational velocity written in frequency domain

$$\varepsilon(x, \omega) = \theta_{vel}(x, \omega) \frac{h}{2i\omega} \frac{\sum_{j=1}^{\infty} \wp_j \psi''_j(x) H_j(\omega)}{\sum_{j=1}^{\infty} \wp_j \psi'_j(x) H_j(\omega)} \tag{6.13}$$

For harmonic vibrations one may substitute amplitude of rotation rate am (θ_{vel}) obtaining phase shifted maximum strain. Thus the final formula to be used in the

comparisons of the amplitude of rotation rate and the amplitude of maximum strain takes form

$$am(\varepsilon) = |\varepsilon(x,\omega)| = am(\theta_{vel})\frac{h}{2}\left|\frac{1}{i\omega}\frac{\sum_{j=1}^{\infty}\wp_j\psi_j''(x)H_j(\omega)}{\sum_{j=1}^{\infty}\wp_j\psi_j'(x)H_j(\omega)}\right| \qquad (6.14)$$

6.3 Experiment 1: Obtaining Strain from Rotational Velocity of the Beam Axis

The small scale, laboratory models to study structural rotations should be chosen in such a way, that the resulting rotations are large enough to represent typical rotations of structures in full scale. After an analysis what was available, it was decided to perform experiments on small span, cantilever beams made of plexiglass excited by kinematic harmonic excitations (Fig. 6.2).

It should be noted that such small beams are much easier to excite in laboratory conditions by using kinematic excitation, than exerting the actuator motion on them. For this reason a heavy, long span, simply supported steel beam was prepared to act as a support for the analysed plexiglass beam. The steel beam was excited in vertical direction by the actuator controlled by HBM Instron system, while the
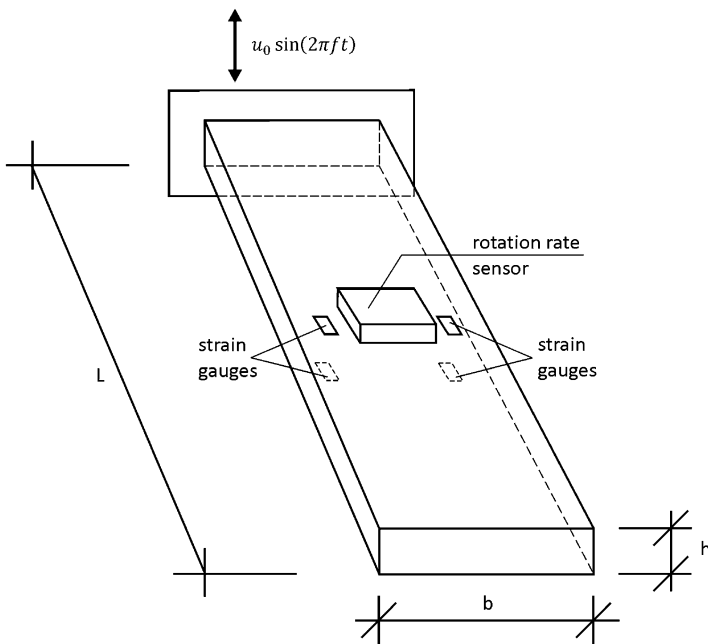
Fig. 6.2 Schematic view of the plexi beam under vertical, harmonic, kinematic excitations with four gauges and rotational sensor mounted in its mid span
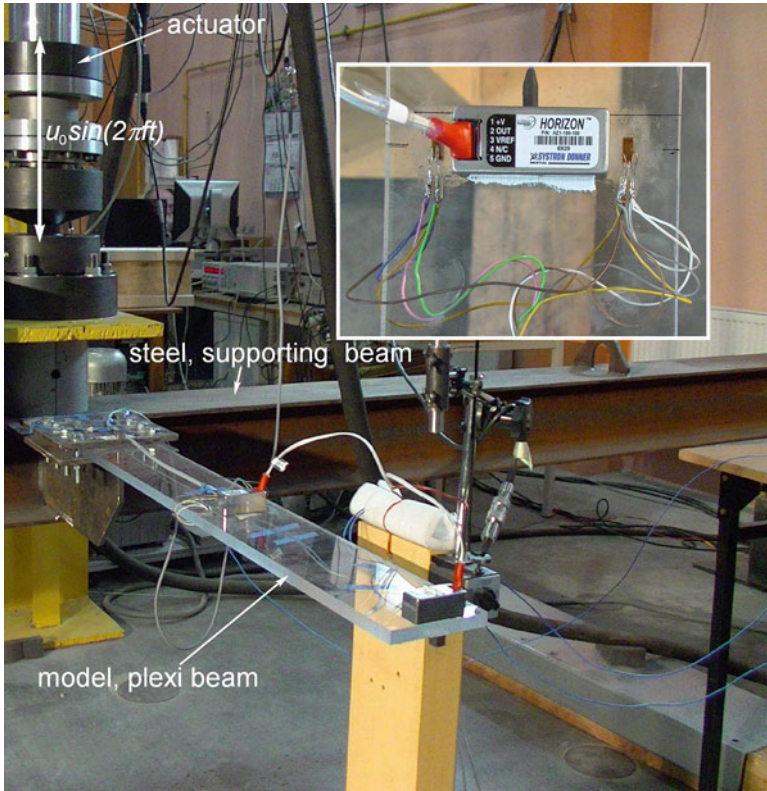
Fig. 6.3 Illustration of the experimental set-up to measure rotations and strains

Table 6.1 Comparison of measured and calculated amplitudes of rotation rates and strains

			Amplitude of strains		
Frequency	Amplitude of excitation accelerations	Amplitude of rotation rate	Measured	Calculated (Eq. 6.14 and column 3 as input)	Calculated using FEM
[Hz]	[m/s^2]	[deg/s]			
1	2	3	4	5	6
4.50	0.5454	2.70	1.45E-05	1.37E-05	1.36E-05
5.25	0.7727	6.88	3.14E-05	3.07E-05	3.05E-05
5.70	0.9655	12.85	5.91E-05	5.36E-05	5.58E-05

analysed, plexiglass beam was clamped at the mid-span of the steel beam (Fig. 6.3). This solution made it possible to excite kinematic vibrations of the plexiglass beam. To measure rotations the Systron Donner sensor HZ-100-100 ($\pm$100 °/s range) was applied. The harmonic motion of the actuator was controlled by Instron system, while data acquisition was done by multi-channel system "MCG Plus" of Hottinger.

The material data of plexiglass are as follows: density $\rho = 1{,}318.7\ \text{kg/m}^3$ and Young modulus $E = 4.51$ GPa. In Table 6.1 selected results of this experiment are shown.

The differences among the strains obtained from rotation rate and directly measured reached about 5–9 % which can be explained by the differences between simplified, continuous dynamic model of the cantilever beam and its actual experimental realization as well as various forms of noises present in this experiment.

6.4   Reconstruction of Flexural Stiffness of a Beam Under Harmonic Vibrations from the Rotations of Its Axis

Consider familiar equation of motion of a discrete dynamic system under harmonic excitations with frequency p [rad/s] and vector of excitation amplitudes $\mathbf{P}_0$:

$$\mathbf{M}\ddot{\mathbf{q}} + \mathbf{K}^d\mathbf{q} = \mathbf{P}_0 e^{ipt} \tag{6.15}$$

where superscript 'd' indicates that the structure vibrates in a 'damaged' state with its original, stiffness matrix $\mathbf{K}$ reduced to $\mathbf{K}^d$ due to the accumulated damages, while the matrix of inertia $\mathbf{M}$ stays unchanged. It is also assumed that structural response is small and out of the resonance frequencies zones, so that damping effects may be neglected. Such situation occurs for example for the cracked reinforced concrete structures (e.g. Zembaty et al. 2006). In Fig. 6.4, a fragment of a beam structure under harmonic excitations is presented. The structure is divided into finite elements *k-1*, *k*, *k+1* etc. The generalized coordinates q_i, q_{i+1}, q_{i+2}, are assumed along the measurement directions and include also rotational degrees of freedom.

Fig. 6.4 Fragment of a beam structure under harmonic excitations with translational and rotational degrees of freedom
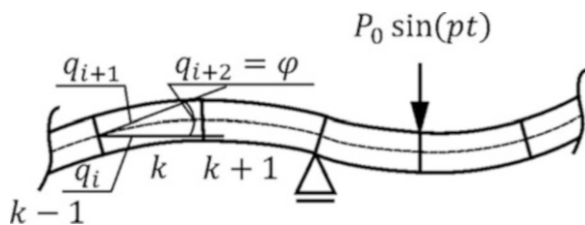
Equation 6.15 can be solved using familiar algebraic matrix equation with respect to the unknown response amplitude vector u:

$$\left(\mathbf{K}^d - p^2\mathbf{M}\right)\mathbf{u} = \mathbf{P}_0 \tag{6.16}$$

The global stiffness matrix can calculated using the Finite Element Method (FEM) with contributions from all respective finite elements:

$$\mathbf{K}^d = \sum_{i=1}^{n} \mathbf{K}_i^{de} = \sum_{i=1}^{n} \alpha_i \mathbf{K}_i^{ue} \tag{6.17}$$

where n is the number of all discretized elements. At this stage one can introduce the key parameters of this analysis which are non-dimensional stiffness reduction factors α_i which describe relative stiffness loss due to accumulated damages ($0 \le \alpha_i \le 1$). Substituting Eq. 6.17 into Eq. 6.16 one obtains:

$$\left(\sum_{i}^{n} \alpha_i \mathbf{K}_i^{ue} - p^2 \mathbf{M} \right) \mathbf{u} = \mathbf{P}_0 \tag{6.18}$$

Equation 6.18 can be applied to find the vector of the amplitudes of displacements $\mathbf{u}$ in terms of the vector of driving force amplitudes $\mathbf{P}_0$, when the FEM model of the structure is prepared.

Consider now the norm J measuring difference between vectors of the amplitudes $\mathbf{u}^c$ calculated using Finite Element Method and the vector of amplitudes $\mathbf{u}^m$ measured in the actual structure:

$$J(\boldsymbol{\alpha}) = \sum_{j=1}^{n_d} \left(\frac{u_j^c(\boldsymbol{\alpha}) - u_j^m}{u_j^m} \right)^2 \tag{6.19a}$$

where n_d is the number of measured displacement amplitudes. Finding minimum of Eq. 6.19a the vector of stiffness reduction factors $\boldsymbol{\alpha}$ describing the actual state of damage can be obtained. This reconstruction procedure requires the structure to be excited and to acquire all the amplitudes along dynamic degrees of freedom of the structure. Classic FEM analysis of beams and frames defines structural response usually only in terms of translational coordinates, while the rotational degrees of freedom are removed from the global stiffness matrix by static condensation. Thus one can easily include rotational coordinates in the analyses by keeping selected, required rotational degrees of freedom (not condensing them out). In this case instead of Eq. 6.19a we will have

$$J_{dr}(\boldsymbol{\alpha}) = \sum_{j=1}^{n_{dr}} \left(\frac{u_j^c(\boldsymbol{\alpha}) - u_j^m}{u_j^m} \right)^2 \tag{6.19b}$$

where n_{dr} denotes the number of translational and additional, rotational degrees of freedom. A comparison of the effectiveness of minimization of functionals given by Eq. 6.19a or 6.19b using Genetic Algorithms and Levenberg-Margquardt local search (GA L-M) was subject of a detailed numerical analysis in the paper by Kokot and Zembaty (2009b). When analyzing reconstructions of multiple stiffness two measures of its effectiveness can be defined:

- Weighted Average Error (WAE):

$$\text{WAE} = \sqrt{\sum_{i=1}^{n_e} \left(\frac{\alpha_i^a - \alpha_i^d}{\alpha_i^d} \right)^2} \tag{6.20}$$

measuring averaged difference between computed and assumed vectors of stiffness reduction factors (the averaging summation takes place over all the discretized elements n_e).

- Maximum Error (ME) between actual and measured stiffness distribution:

$$\text{ME} = \max_i \left| \alpha_i^a - \alpha_i^d \right| \tag{6.21}$$

The above symbols α_i with superscripts a and d denote respectively the 'assumed' and 'detected' stiffness losses.

6.5 Experiment 2: Reconstruction of Stiffness Variations of a Cantilever Beam

The tests were carried out using the same experimental set up as previously, but with two types of plexiglass beams: the 'intact' beam and a beam with three drops of stiffness (Fig. 6.5).

To measure translational vibrations three miniature accelerometers PCB 333B52 were installed underneath the beam. The angular motions were measured using three rotation rate sensors HZ 100-100 installed on top of the beam. All sensors were glued at points corresponding to the nodes of the finite element. The mass losses from the reductions of the beam cross-sections were compensated by gluing nuts to the beam (see Fig. 6.6).
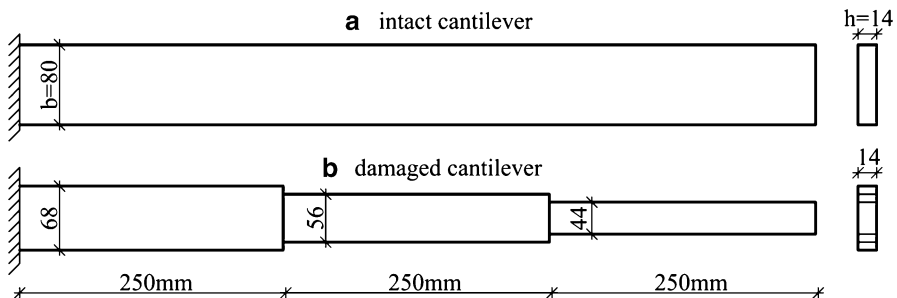

Fig. 6.5 The geometry of the beam investigated in experiment '2' – in intact and the in the 'damaged' state defined by three stiffness reductions
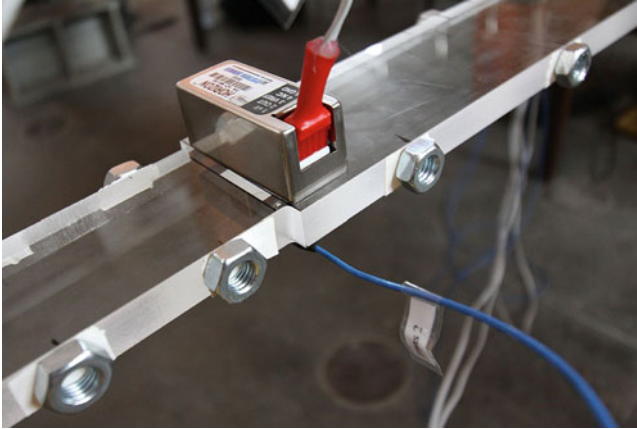
Fig. 6.6 Detail of the beam with angular sensor HZ 100-100 installed at the beam stiffness drop and the additional, compensating masses (nuts)
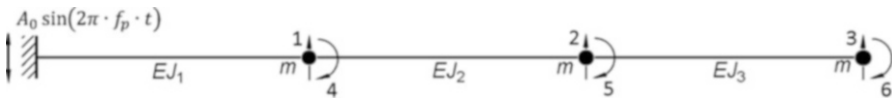
Fig. 6.7 Dynamic model of the cantilever beam vibrating under vertical, kinematic, harmonic excitations

The detailed scheme of the vibrating beam together with all the translational and rotational degrees of freedom is shown in Fig. 6.7. Two models of the 750 mm long plexiglass beam were measured and analysed: the first "intact" one, with constant cross section b = 80 mm and h = 14 mm (see upper part of Fig. 6.5) and the second, "damaged" one, with decreased cross sections (see lower part of Fig. 6.5), leading to 15 % drops of stiffness.

The fundamental, natural frequency of the tested cantilever beam (with all the sensors attached) equalled 6.90 Hz while for the "damaged" one 6.23 Hz. This was important to know before the experiment started, as the "reconstruction" method described in Chap. 2, by definition avoids vibrations close to resonances (Kokot and Zembaty 2009a, b).

The tests were carried out by measuring harmonic vibrations of the plexiglass beams for various excitation frequencies (from 3.5 to 7.5 Hz), outside the resonance zones, at low excitation level (amplitude of displacements at the fixed end was equal to 0.5 mm). The minimization in the stiffness reconstruction process was carried out using the hybrid optimization procedure described in detail in the paper by Kokot and Zembaty (2009a). First a specific number of 6,000 generations in the genetic algorithm allowed to reach the vicinity of the global minimum. Next the Levenberg-Marquardt local search method was involved to fine-tune the solution.

Table 6.2 Stiffness reduction factors for a beam with three stiffness reductions under harmonic kinematic excitations at frequency 4.5 Hz

	α_1	α_2	α_3
Actual stiffness reduction	0.85	0.70	0.55
Detected stiffness reduction	0.86	0.67	0.54

Two solutions were studied in detail: with three measured translation accelerations only and with three rotation rates only. Results for excitation frequency $p_f = 4.5$ Hz and amplitude of the beam tip response equal to about 0.5 mm, are shown in Table 6.2. The errors of reconstruction equalled: WAE $= 2.48$ % and ME $= 3.87$ %.

6.6 Conclusions

This paper reports the results of early stage, laboratory experiments of the application of modern rotation rate sensors to measure and monitor of structural vibrations in civil and seismic engineering. Following positive recommendations from numerical simulations (Abdo and Hori 2002; Kokot and Zembaty 2009b), both experiments demonstrated the ability of modern rotation rate sensors to be effectively applied in measuring structural vibrations and in difficult, stiffness "reconstructions" of practical structural health monitoring.

This is a good prognostic for future application of rotation rate sensors not only to directly measure rotations of key structural elements, but also to follow strains and monitor distributed damages of some civil engineering structures. More details about the reported experiments can be found in the recent paper by Zembaty et al. (2013).

References

Abdo MA-B, Hori M (2002) A numerical study of structural damage detection using changes in the rotation of mode shapes. J Sound Vib 251:227–239
Chopra AK (2011) Dynamics of structures, theory and application to earthquake engineering. Prentice Hall, Englewood Cliffs
Kokot S, Zembaty Z (2009a) Damage reconstruction of 3d frames using genetic algorithms with Levenberg-Marquardt local search. Soil Dyn Earthq Eng 29:311–323

Kokot S, Zembaty Z (2009b) Vibration based stiffness reconstruction of beams and frames by observing their rotations under harmonic excitations – a numerical analysis. Eng Struct 31:1581–1588

Maeck J, De Roeck G (1999) Dynamic bending and torsional stiffness derivation from modal curvatures and torsion rates. J Sound Vib 225:153–170

Meydan T (1997) Recent trends in linear and angular accelerometers. Sensors Actuators A Phys 59:43–50

Ndambi J-M, Vantomme J, Harri K (2002) Damage assessment in reinforced concrete beams using eigen frequencies and mode shape derivatives. Eng Struct 24:501–515

Zembaty Z, Kowalski M, Pospisil S (2006) Dynamic identification of a reinforced concrete frame in progressive states of damage. Eng Struct 28:668–681

Zembaty Z, Kokot S, Bobra P (2013) Application of rotation rate sensors in an experiment of stiffness 'reconstruction'. Smart Mater Struct. doi:10.1088/0964-1726/22/7/077001

Chapter 7
Asymmetric Continuum with Shear and Rotation Strains Including Quantum Synchronous Processes

Roman Teisseyre

Abstract We shortly explain why the rotations strains should be included together with the shear strains in the theory of solid continuum; the related arguments are based both on the experimental and theoretical levels. In the presented Asymmetric Continuum Theory the wave propagation mechanism appears in a logical way with the respective shear and rotation strains. In this logical approach we include, beside the shear strains, also the rotation strains and their related wave propagation with shear and rotation strain interactions.

Further, we try to explain how to describe a fracture process with a help of the quantum theory and with some synchronous motions. The synchronous quantum processes permit to explain the fracture mechanism and also may include a problem of the lightning and aurora events.

This attempt might join the quantum processes with a fracture event appearing inside the elastic continuum with shear and rotation strains and with the synchronous quantum mechanism; this is a new approach joining the improved classic theory with the quantum events, which lead together to the synchronous processes.

Keywords Quantum process • Shear and rotation strains • Theoretical investigation • Asymmetric continuum theory • Seismology

7.1 Continuum with Shear and Rotation Strains

In Continuum Asymmetric Theory we may prove only the existence of displacement derivatives. The true displacements would always lead to a slip motions along some fault, thus, we should underline that the recorded displacements belong only

R. Teisseyre (✉)

Institute of Geophysics, Polish Academy of Sciences, Warsaw, Poland
e-mail: rt@igf.edu.pl

to the displacement derivatives (Fig. 7.1). Further on, we present equations for deviatoric shear and rotation strains.

For measurements:

$$u_k \approx \frac{\partial u_k}{\partial x_i} \Delta x_i, \mathrm{i} = k \pm 1 \tag{7.1}$$

where Δx_i is the length of a seismograph rigid platform and displacement, $\vec{u}_k$, is an apparent displacement.

The rotation and shear strains – included in our theory, should be measured with a special recording system.

In order to explain the wave propagation mechanism we can present the time period sequence of shear and rotation strain maxima; here, we present this sequence for a radial propagation (Fig. 7.1).
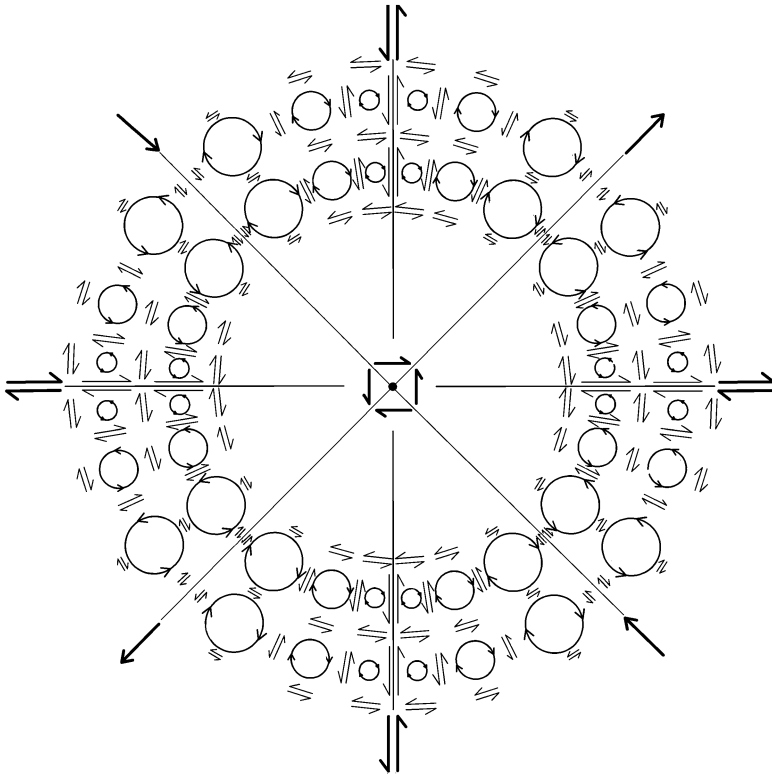

Fig. 7.1 Propagation pattern of the shear and rotation strains; the maxima of the shear and rotation strains along the sequence of five respective time intervals

In the classic definition for the elastic regime we have for strain components: E_{ik}-total, $\hat{E}_{(ik)}$- shear, and, $\breve{E}_{[ik]}$- rotation strains:

$$E_{ik} = \hat{E}_{(ik)} + \breve{E}_{[ik]} = \frac{\partial u_k}{\partial x_i} \tag{7.2a}$$

At constant pressure and without external forces we have the relations:

$$\mu \frac{\partial^2 \hat{E}_{(ni)}}{\partial x_s \partial x_s} - \rho \frac{\partial^2 \hat{E}_{(ni)}}{\partial t^2} = 0 \;, \quad \mu \frac{\partial^2 \breve{E}_{[ni]}}{\partial x_s \partial x_s} - \rho \frac{\partial^2 \breve{E}_{[ni]}}{\partial t^2} = 0 \tag{7.2b}$$

where we remind the summation convention at the repeated indexes:

We may remark that, in general, the rotation strain amplitudes might be quite low, however, the derivatives of the shear and rotation strains should fulfill the Maxwell-like relations (Teisseyre 2009, 2011, 2013; Teisseyre and Teisseyre-Jeleńska 2014).

For the energy, related to the shear and rotation strains, we may write at a constant pressure:

$$\begin{aligned} \mathrm{E} &= \sum S_{ik} E_{ik} = 2\mu \left(\sum_{i,k} E_{(ik)} E_{(ik)} + \sum_{i,k} E_{[ik]} E_{[ik]} \right) \\ &\approx 2\mu \sum_{i,k} E_{(ik)} E_{(ik)} \;, \quad i \neq k \end{aligned} \tag{7.3}$$

as the energy related to rotation strains could be neglected here.

The vector form of the rotation strains, $E_{[ik]}$, could be defined as:

$$E_{[i]} = \left\{ E_{[23]}, \; E_{[31]}, \; E_{[12]} \right\} \tag{7.4a}$$

While the deviatoric shear strains, $\hat{E}_{(ik)} = E_{(ik)} - \frac{1}{3}\delta_{ik}E_{(ss)}$, could be also presented in a vector form in this specific coordinate system:

$$\hat{E}_{(i)} = \left\{ \hat{E}_{(23)}, \hat{E}_{(31)}, \hat{E}_{(12)} \right\} \;, \quad \text{for} \quad \hat{E}_{(ik)} = E_{(ik)} - \frac{1}{3}\delta_{ik}E_{(ss)} \tag{7.4b}$$

However, in the system $\{x, ict\}$ we may present this relation using the basic 4D invariant Dirac tensors:

$$\boldsymbol{\gamma}^1 = \begin{bmatrix} 0 & 0 & 0 & -1 \\ 0 & 0 & 1 & 0 \\ 0 & 1 & 0 & 0 \\ -1 & 0 & 0 & 0 \end{bmatrix}, \quad \boldsymbol{\gamma}^2 = \begin{bmatrix} 0 & 0 & -1 & 0 \\ 0 & 0 & 0 & -1 \\ -1 & 0 & 0 & 0 \\ 0 & -1 & 0 & 0 \end{bmatrix},$$

$$\boldsymbol{\gamma}^3 = \mathrm{i} \begin{bmatrix} 0 & 0 & 0 & 1 \\ 0 & 0 & 1 & 0 \\ 0 & -1 & 0 & 0 \\ -1 & 0 & 0 & 0 \end{bmatrix}, \quad \boldsymbol{\gamma}^4 = \mathrm{i} \begin{bmatrix} 1 & 0 & 0 & 0 \\ 0 & 1 & 0 & 0 \\ 0 & 0 & -1 & 0 \\ 0 & 0 & 0 & -1 \end{bmatrix} \tag{7.5a}$$

$$\gamma^4\gamma^2\gamma^3 = \begin{bmatrix} 0 & -1 & 0 & 0 \\ -1 & 0 & 0 & 0 \\ 0 & 0 & 0 & -1 \\ 0 & 0 & -1 & 0 \end{bmatrix} \tag{7.5b}$$

Thus, these complex deviatoric shear strains with a help of these Dirac tensors (7.5a, 7.5b) can be presented as follows::

$$E_{(\lambda\kappa)} = E_{(1)}\gamma^1 + E_{(2)}\gamma^2 + E_{(3)}\gamma^4\gamma^2\gamma^3 \tag{7.6a}$$

where for the 4D strain tensor, $E_{(\lambda\kappa)}$, we shall write:

$$E_{(\lambda\kappa)} = \begin{bmatrix} 0 & -E_{(3)} & -E_{(2)} & -E_{(1)} \\ -E_{(3)} & 0 & E_{(1)} & -E_{(2)} \\ -E_{(2)} & E_{(1)} & 0 & -E_{(3)} \\ -E_{(1)} & -E_{(2)} & -E_{(3)} & 0 \end{bmatrix} \tag{7.6b}$$

The related wave equations for these strains, $E_{\lambda\kappa} = E_{(\lambda\kappa)} + iE_{[\lambda\kappa]}$, with the velocity, $\frac{c}{\kappa} \equiv V \equiv \sqrt{\mu/\rho}$, can be presented as follows:

$$\frac{\partial^2 E_{\lambda\mu}}{\partial x_n \partial x_n} - \frac{\kappa^2 \partial^2 E_{\lambda\mu}}{c^2 \partial t^2} = Y_{\lambda\mu} \quad \leftrightarrow \quad WE_{\lambda\mu} = Y_{\lambda\mu} \tag{7.7a}$$

Of course, we may return to the equations in a vector form with $E_i = \hat{E}_{(i)} + i\breve{E}_{[i]}$ (with the similarly defined external vector, Ys):

$$\frac{\partial^2}{\partial x_n \partial x_n} E_s - \frac{\kappa^2 \partial^2}{c^2 \partial t^2} E_s = Y_s \; , \quad \text{or} \quad WE_s = Y_s \tag{7.7b}$$

This relation for the complex vectors, can lead us to the Maxwell-like equations for $V = \frac{c}{\kappa}$, and current $J_S = 0$:

$$\varepsilon_{spq}\frac{\partial \breve{E}_{[q]}}{\partial x_p} - \frac{1}{V}\frac{\partial \hat{E}_{(s)}}{\partial t} = 0, \quad \varepsilon_{spq}\frac{\partial \hat{E}_{(q)}}{\partial x_p} + \frac{1}{V}\frac{\partial \breve{E}_{[s]}}{\partial t} = 0 \quad , \quad \text{or :}$$
$$\text{rot } \breve{E} - \frac{\chi}{c}\frac{\partial \hat{E}}{\partial t} = 0 \; , \quad \text{rot } \hat{E} + \frac{\chi}{c}\frac{\partial \breve{E}}{\partial t} = 0 \; ; \quad \frac{c}{\chi} = V = \sqrt{\frac{\mu}{\rho}} \tag{7.8}$$

These relations are quite similar to those for the electro-magnetic fields; the difference relates only to propagation velocity, which for the electro-magnetic fields relates to the light velocity.

The presented expression (7.8) leads directly to the Eqns. 7.7a, b.

7.2 Synchronous Quantum Processes

The basic element of quantum theory, at the thermodynamic equilibrium, is the black body radiation described by the Planck relation:

$$e(\lambda) = \frac{8\pi\nu h}{\lambda^4} \left(\exp\left(\frac{\nu h}{KT}\right) - 1 \right)^{-1} \quad \text{or} \quad e(\nu) = \frac{8\pi\nu^5 h}{c^4} \left(\exp\left(\frac{\nu h}{KT}\right) - 1 \right)^{-1} \quad (7.9)$$

where, e, is the energy radiated per unit wave length, λ; ν means frequency, $\nu = c/\lambda$, and h is the Planck constant; K – the Boltzmann constant and T – temperature, c – light velocity.

This energy can be related to the resonance frequency; the classical question of the black body radiation, that is, the radiation in thermodynamic equilibrium-fundaments of quantum mechanics.

Of course the synchronous quantum related processes appear in all radiation processes; the most basic phenomena in our world. However, here we will consider only these synchronous quantum processes which appear due to the deformation fields, that is related to the shear and rotation strains, and which lead to the Planck black body radiation. The resonance frequency means here the minima of fracture resistances at thermodynamic equilibrium, Fig. 7.2. At this conditions the basic unit energy, $h\nu$, and related black body radiation (7.9) may approach us to some synchronous processes. First we may imagine that, a distribution of the high shear strains forming the local micro-fractures, could be approximated by the parallel and local micro-displacements; thus, searching their continuum description, we might present these micro-displacements as situated along a group of the parallel lines. Thus, in this way, we may equivalently describe the micro-displacements, formed due to the shear strains, as a dense group of a continual distribution of the parallel lines.
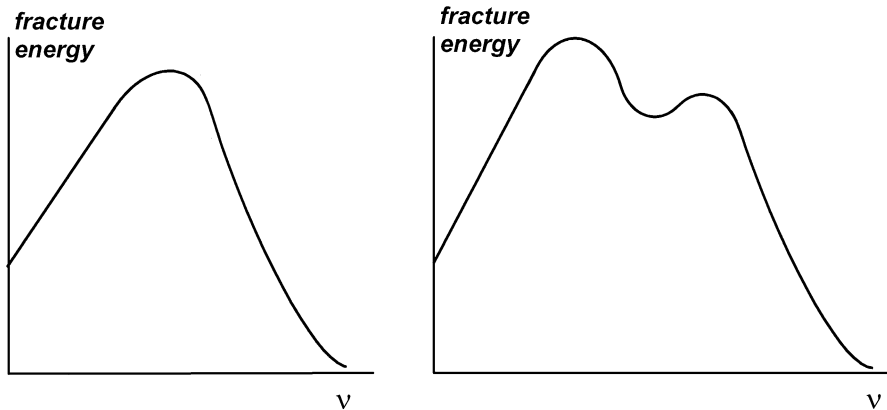

Fig. 7.2 Resonance frequency, or frequencies, at thermodynamic equilibrium: these maxima mean the minima of fracture resistances

The presented way leads us from the parallel micro-displacements up to their line continuum distributions forming the dense group; further in this way, we may achieve a continuum description of these parallel micro-events.

Thus, we may assume that before any fracture we might have a distribution of some molecular-displacements along the parallel lines processes, in such way we may approach to a fracture line and then to a fracture plane. Here, we should remind that the strain energy (Eq. 7.3) at a constant pressure is related to the sum of the strain squares, but may be limited only to the shear strains (7.3).

We may present the energy point concentrations along the distributed points at the almost parallel lines being formed before a fracture. Such energies concentrated along these lines appear due to the precursory processes and are related mainly to the shear strains:

$$\hat{E}_{(sk)} \rightarrow \sum_S \hat{E}_{(Sk)} \quad - \quad \text{a sum related to parallel lines} \quad (7.10)$$

which means a concentrations of strains along the almost parallel lines, S, forming a group leading to a plane, a sum $\sum_S$ or the parallel lines forming a big group around the central fracture pass plane.

The expression for such energy concentration may be presented as concentration of the shear strains:

$$E = \sum S_{ik}E_{ik} = 2\mu \left(\sum_{i,k} \hat{E}_{(ik)}\hat{E}_{(ik)} + \sum_{i,k} \breve{E}_{[ik]}\breve{E}_{[ik]} \right)$$
$$\approx 2\mu \sum_{i,k} \hat{E}_{(ik)}\hat{E}_{(ik)} \quad (7.11)$$

and from the another side, this basic energies along the mentioned above synchronous lines concentrated along an expected fracture plane can be presented as follows:

$$E = \left[\sum_{S,k} G_{Sk} \int_{-x_s^0}^{x_s^0} \exp\{-g_s[|x_s - x_s^0|]\}dx_s^0 \right]^2 [\exp\{-g(t-t_0)\}]^2 \frac{8\pi\nu h}{\lambda^4} \left(\exp\left(\frac{\nu h}{KT}\right) - 1 \right)^{-1}$$
$$(7.12a)$$

where, in order to form the energy concentration lines and further the fracture along some central plane element, we have introduced the summations along both these lines, S, and also along the perpendicular direction, k; a possible number of concentrated lines relate to a space element, that is both to the S and k directions; thus, the expected fracture plane may be related to the S_0 and k directions.

Such approach is introduced to better understand formation of the fracture plane element, however, a change of the related coefficients, G_{Sk}, g_S and g, up to the limit, G_S^0, g_S^0, g^0 (fracture level), should be observed by the changes of some other related fields, e.g., electric or magnetic ones.

Thus, when the coefficients increase to a fracture limit, $G_s \to G_s^0$ and $g_s \to g_s^0$, $g \to g^0$, we arrive to a fracture event, with the concentrated energies decreasing rapidly, when we drive apart from the fracture domain, $(X_s^0, -X_s^0; t^0)$:

$$
E^0 = \left[\sum_{S,k} G_{Sk}^0 \int_{-X_s^0}^{X_s^0} \exp\{-g_s^0 [|x_s - x_s^0|]\} dx_s^0 \right]^2 [\exp\{-g^0(t - t_0)\}]^2 \frac{8\pi\nu h}{\lambda^4} \left(\exp\left(\frac{\nu h}{KT}\right) - 1 \right)^{-1}
$$

$$(7.12b)$$

In this way, we describe an increase of the fracture energy in the time and space up to the final values related to these fracture coefficients; the resonance frequency, at thermodynamic equilibrium, presents the minimum of fracture resistance.

We assume that these considered phenomena, related to the electron motions, could remain synchronous in the adequate time and space domains. Moreover, a total fracture processes might be formed with the time/space synchronous series one after other.

The introduced synchronization means the synchronous fracture formation; a real fracture motion starts, when a density of quantum synchronous motions reach the critical level.

We should remember that the Planck quantum theory introduces the resonance wave frequency related to the black body radiation effect; basing on this approach we might try to consider a material strength minimum, as related to such resonance frequency, under the static vibration parts of load. We may illustrate the possible resonance frequencies, at thermodynamic equilibrium in Fig. 7.2; in the presented figures we present the reverse values needed for fracture, that is the reverse values of the fracture energies, at the synchronous fracture phenomena. Thus, the vertical axis relates the decrease of the fracture resistance.

Thus, we present a minimum of energy required for the fracture at a thermodynamic equilibrium. An individual fracture process at the quantum level may lead to the synchronous and collective fracture events at the critical fracture level: G_s^0, g_S^0, g^0.

Of course, the released energy leads also to the changes of the strains. We should remind the strain equations (Eq. 7.3), shear and rotational, $\hat{E}_{(ni)}$, $\check{E}_{[ni]}$, and related energies.

7.3 Precursory Processes

We assume, that at the fracture processes, we should have for their synchronous motions at the different positions in space and time, thus, there should appear a similarity of these motions. Therefore, we may deal there with some similarities related to the central line, along which we expect a fracture process.

Of course, these processes should be governed by the Shrödinger equation in its more adequate forms, which mean here the motions related to a center of synchronous field density; this process may lead to the probable fracture. Thus, especially important for prediction methods, could be the mentioned processes appearing in time and space domain.

For fracture, before and after the given event, we may have an appearance of chain of some fields governed by the Shrödinger like equations; specially important might be, here, the electric and magnetic signals.

As mentioned above, a real fracture starts when the quantum synchronous density reaches the critical level. However, already before some fracture event, there can appear also the collective electron motions under even not great synchronous concentration. In this way there can appear some electric and magnetic precursors, governed by these quantum processes and joined to the Maxwell relations.

We can believe that some electric or magnetic signals may appear due to these energy releases appearing at the beginning of these synchronous processes, thus, even beneath the critical concentration.

We assume that the considered phenomena related to the electron motions could remain synchronous in the adequate time and space domains. Of course, a total fracture process may be formed with the time/space synchronous series appearing one after other with much smaller velocities.

In this way we may obtain also the space/time fracture center at $t = t_0$, $x_s = x_s^0$ (which even may move), and where this synchronization means a synchronous fracture formation; a real fracture motion starts when a density of quantum synchronous motions reach the critical density: G_s^C.

We may remark that, in general, the rotation strains might be quite low, however, the derivatives of the shear and rotation strains should fulfill the Maxwell-like relations (Teisseyre 2013; Teisseyre and Teisseyre-Jeleńska 2014).

In the classic definition for the elastic regime we should remained the strain energy concentration and the line synchronous energy concentration (7.12a, 7.12b)

For a search related to the energy concentrations we should pay an attention to the electric and magnetic fields; the related joined expressions may be write as follows (Teisseyre and Teisseyre-Jeleńska 2014):

$$S_{(kl)} = \lambda \delta_{kl} E_{ss} + 2\mu E_{(kl)} + \vartheta \delta_{kl} G + \vartheta G_{(kl)} + \delta_{kl} G^E \sqrt{\sum_k E_k^2}$$

$$S_{[kl]} = 2\mu E_{[kl]} + \vartheta \varepsilon_{kls} G_s + \vartheta G_{[kl]} \quad , \quad \vartheta = (1, \pm \, \mathrm{i})$$

$$(7.13)$$

where for the dielectric materials, we should consider the **electrostriction**, G^E, related to the random electrical domains; $\vartheta = (1, \pm \, \mathrm{i})$

The most possible relations between these fields could be combined together in the following way:

$$\alpha\big(S_{(kl)} - \lambda\delta_{kl}E_{ss} - 2\mu E_{(kl)}\big) = \chi^s_{(kl)}E_s + f^s_{(kl)}\Pi_s + d^{ij}_{(kl)}\Pi_{ij} + g\delta_{kl}G^E\sqrt{\sum_k E^2_k}$$

$$\eta\big(S_{[kl]} - 2\mu E_{[kl]}\big) = \chi^s_{[kl]}M_s + f^s_{[kl]}\Pi_s + d^{ij}_{[kl]}\Pi_{ij}$$

(7.14)

where we have introduced the unknown parameters:

$$\alpha, \ \chi^s_{(kl)}, \ f^s_{(kl)}, \ d^{ij}_{(kl)}, \ g \quad \text{and} \quad \eta, \ \xi^s_{[kl]}, \ f^s_{[kl]}, \ d^{ij}_{[kl]}$$

However again, this expression could be written in the more general forms with a number of independent equations, with $\alpha \rightarrow \quad \alpha = \alpha_1 + \alpha_2 + \alpha_3 + \alpha_4$ (see Eq. 7.14), and $\eta \rightarrow \eta_1 + \eta_2 + \eta_3$ (see Eq. 7.14), as follows:

$$\alpha_1\big(S_{(kl)} - \lambda\delta_{kl}E_{ss} - 2\mu E_{(kl)}\big) = \chi^s_{(kl)}E_s, \quad \eta_1\big(S_{[kl]} - 2\mu E_{[kl]}\big) = \chi^s_{[kl]}M_s$$

$$\alpha_2\big(S_{(kl)} - \lambda\delta_{kl}E_{ss} - 2\mu E_{(kl)}\big) = f^s_{(kl)}\Pi_s, \quad \eta_2\big(S_{[kl]} - 2\mu E_{[kl]}\big) = f^s_{[kl]}\Pi_s$$

$$\alpha_3\big(S_{(kl)} - \lambda\delta_{kl}E_{ss} - 2\mu E_{(kl)}\big) = d^{ij}_{(kl)}\Pi_{ij}, \quad \eta_3\big(S_{[kl]} - 2\mu E_{[kl]}\big) = d^{ij}_{[kl]}\Pi_{ij}$$

(7.15)

$$\alpha_4\big(S_{(kl)} - \lambda\delta_{kl}E_{ss} - 2\mu E_{(kl)}\big) = g\delta_{kl}G^E\sqrt{\sum_k d\,E^2_k}$$

where we remind the summation convention at the repeated indexes.

These relations may present the origin of the different waves, which propagate according to the Maxwell–like equations, but with the different velocities: ones related to the strain fields and others to the electro/magnetic fields. These separate waves might inform us on their common source processes, but such task can be quite difficult. Here, some help may be related to the fact that the related signals, shifted in time due to the differences between these wave velocities, should present some similarities and should have similar frequencies. Thus, such task might inform us on the source processes; nevertheless, we remark that in the most cases it could be very difficult to achieve the positive results. Here, first of all, we should mentions the papers and achievements of the prof. Varotsos group (see some related references, Varotsos et al. 1986, 2006, 2011).

References

Teisseyre R (2009) Tutorial on new development in physics of rotation motions. Bull Seismol Soc Am 99(2B):1132–1136

Teisseyre R (2011) Why rotation seismology: confrontation between classic and asymmetric theories. Bull Seismol Soc Am 101(4):1683–1691

Teisseyre R (2013) Molecular Transport in in Fracture Processes. Acta Geophys 61(1):18e–25

Teisseyre R, Teisseyre-Jeleńska M (2014) Asymmetric continuum: extreme processes in solids and fluids. Springer, Berlin/Heidelberg, p 180

Varotsos PA, Alexopoulos KD (1986) Thermodynamics of point defects and their relation with bulk properties. North-Holland, Amsterdam, p 474

Varotsos PA, Sarlis NV, Skordas ES, Tanaka HK, Lazaridou MS (2006) Entropy of seismic electric signals: analysis in natural time under time reversal. Phys Rev E 73:031114

Varotsos PA, Sarlis NV, Skordas ES (2011) Natural time analysis: the new view of time. In: Precursory seismic electric signals, earthquakes and other complex time-series. Springer, Berlin/Heidelberg, p 205

Part II
Seismic Analysis and Design of Irregular Structures

Chapter 8
Seismic Assessment of RC Frame Buildings

Klemen Sinkovič, Iztok Peruš, and Peter Fajfar

Abstract In the chapter, the N2 method and the non-linear dynamic analysis (NDA) are applied for the assessment of seismic performance of two variants of a 4-storey reinforced concrete (RC) frame building. The first variant is represented by the bare frames, whereas in the second variant infill panels are included in the upper three storeys, thus creating a soft first storey structure. In one direction, the results clearly show the detrimental effect of infills which generate a storey mechanism instead of a global mechanism which occurs in the case of the bare frame structure. In the other direction, a story mechanism occurs also in the case of the bare frame structure. The infills shift the mechanism from the third to the first storey. There is good agreement of the results obtained by the N2 method and NDA. The results indicate that both variants of the building are able to survive the design ground motion.

Keywords Seismic performance assessment • Nonlinear analysis • Seismic demand • Structural capacity • Reinforced concrete frame buildings

8.1 Introduction

For the assessment of seismic performance of buildings subjected to strong earthquakes, nonlinear analysis is needed. The most complex analysis method is the non-linear dynamic analysis (NDA), which is used mainly in research and for analysis of some important structures. It requires several analyses with different accelerograms and additional data on the mathematical model (hysteretic and damping models). For practical application, pushover-based methods, e.g. the N2 method (Fajfar 2000), implemented in Eurocode 8 – Part 1 (EC8-1, CEN 2004a), are better suited. In this chapter both the NDA and the N2 method are used for the seismic performance assessment of a four-storey reinforced concrete (RC) frame

---

K. Sinkovič (✉) • I. Peruš • P. Fajfar

Faculty of Civil and Geodetic Engineering, University of Ljubljana, Jamova cesta 2, 1000 Ljubljana, Slovenia

e-mail: Klemen.Sinkovic@ikpir.fgg.uni-lj.si; Iztok.Perus@ikpir.fgg.uni-lj.si; Peter.Fajfar@ikpir.fgg.uni-lj.si

structure, representing an existing building built before modern seismic codes have been adopted. In the first variant, the bare frame structure is analysed, whereas in the second variant infill panels are included in the upper three storeys, thus creating a soft first storey structure. In the chapter the main results are presented and discussed.

8.2   Methodology

The expected seismic performance of a building is estimated by comparing the demand and the capacity of the structure.

In the case of the N2 method, the determination of demand has been well established. If the influence of higher modes in elevation and in plan (torsion) is not important, the basic version of the method, implemented in EC8-1, can be used. By performing the pushover analysis up to the target displacement, determined according to a well-known procedure, seismic demand for any relevant quantity can be determined.

On the other hand, for the time being, a widely accepted approach for the assessment of the capacity at the level of the whole structure does not exist. Existing standards and codes do not provide a clear definition of the seismic capacity of the structure. Usually, it is conservatively assumed that the structure fails when the near collapse (NC) limit state is attained. This limit state does not represent a physical collapse of the building (which is extremely difficult to predict) but a complete economic failure. An option for the definition of the NC limit state at the level of the structure is a similar definition as in the case of individual elements, i.e. at a 20 % drop of the lateral resistance of the structure. However, this definition, which seems to be the most appropriate, cannot be applied in nonlinear dynamic analysis and also not in a pushover analysis with simplified models, e.g. in the case of models without strength-degradation. A more practical definition is based on the assumption that the NC limit state of the structure is reached when the first important vertical element reaches the NC limit state. This definition of capacity was used in our study. The capacity of the structure in terms of roof displacement and storey drift was determined based on the ultimate rotation capacity (i.e. the NC limit state) of the most critical column. The relation between different quantities corresponds to the results of the pushover analysis at the moment when the ultimate rotation of the most critical column is attained.

For the ultimate rotation the empirical expressions provided in the current version of Eurocode 8 – Part 3 (EC8-3, CEN 2005) for the ultimate chord rotation θ_{um} were used. Originally, the formulas were proposed by Panagiotakos and Fardis (2001).

$$\theta_{um} = 0.016 \cdot (0.3^{\nu})$$

$$\cdot \left[\frac{\max(0.01; \omega')}{\max(0.01; \omega)} f_c\right]^{0.225} \left(\min\left(9; \frac{L_v}{h}\right)\right)^{0.35} 25^{\left(\alpha \rho_{sx} \frac{f_{yw}}{f_c}\right)} \left(1.25^{100\rho_d}\right) \quad (8.1)$$

For the meaning of symbols and for different reductions of capacity for elements designed according to out-of-dated codes please consult EC8-3. Since best estimates are used, no safety factor γ_{el} is included in Eq. 8.1. According to the current version of EC8-3, for the RC members without detailing for earthquake resistance, the value in Eq. 8.1 is divided by a factor of 1.2. In members with smooth (plain) longitudinal bars without lapping in the vicinity of the end region where yielding is expected, the ultimate chord rotation θ_{um} is further multiplied by a factor of 0.8. For columns, the resulting values of θ_{um} are between about 3 % and 4 %.

In the case of the NDA, a set of 30 accelerograms was selected with the mean elastic acceleration spectrum similar to the EC8-1 spectrum, used in the N2 analysis (Vukobratović and Fajfar 2015, Fig. 8.2). Seismic assessment is based on the same quantities as in the case of the N2 analysis. Seismic demand is represented by median values determined by NDA. For the determination of seismic capacities based on NDA an incremental dynamic analysis (IDA) is needed. Since this is an extremely time consuming procedure, in our study the same capacities as in the case of N2 were used also in the case of NDA.

8.3 Assessment of Seismic Performance of 4-storey RC Building

8.3.1 Description of the Example Building and Mathematical Modelling

The example structure is a 4-storey RC building that was designed on the basis of the design practice and codes which were used in Italy between the 1950s and the 1970s (Celarec et al. 2012). The structure is double-symmetric with storey height 3.0 m. In Fig. 8.1 the global geometry and the cross-sections of the building are presented. Note that the cross-sections of the columns are decreasing along the height of the building. The masses amount to 182.3 t in the first three storeys, and 193.3 t in the top storey. The total weight of the building is $W = 7261$ kN. The variants of the building without infills and with them (in the upper three storeys) were analysed.

The mean value of concrete compressive strength amounted to $f_{cm} = 33$ MPa and the yield strength of the steel reinforcement amounted to $f_{ym} = 370$ MPa (smooth reinforcement). In RC columns shear reinforcement $A_{sw}/s = \Phi6/30$ cm was used, which was at the time of building construction a usual requirement for shear
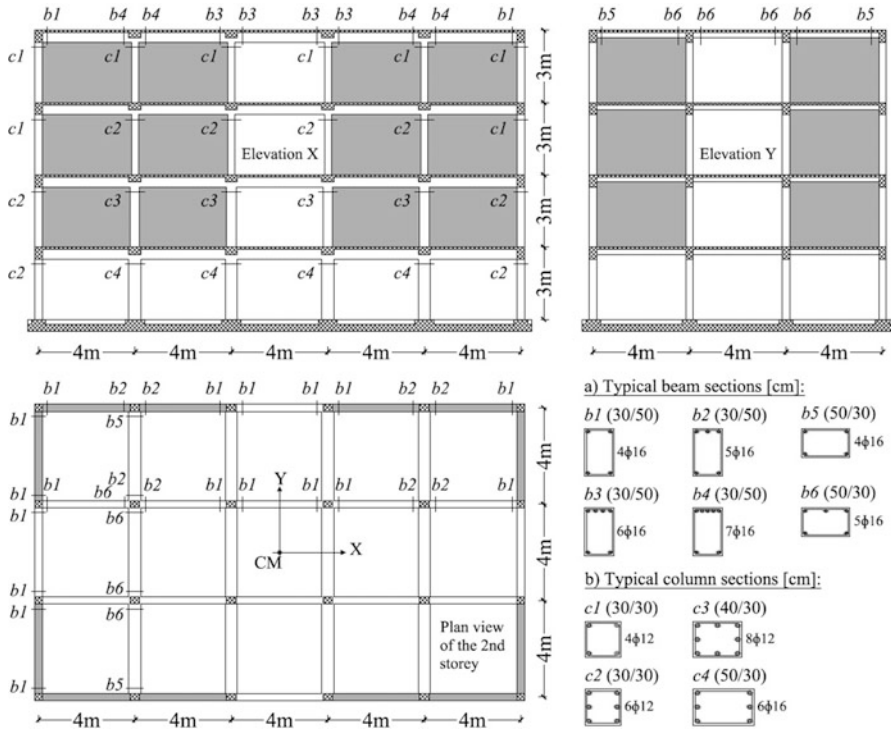
Fig. 8.1 The elevation views, the plan view of the second storey and typical reinforcement of beams and columns of the example building

reinforcement. The amount of longitudinal reinforcement in the individual columns and beams is shown in Fig. 8.1.

All the analysis were performed with OpenSees (2013), using the PBEE-toolbox (2010), which is a simple yet effective tool for the seismic analysis of RC frames by using simplified non-linear models. A simplified non-linear 3D model of RC frame structure was made. The effective width of the beams was considered according to Eurocode 2 (EC2, CEN 2004b). Fixed supports of columns at the bottom level were assumed. The RC slabs were assumed to be rigid in their planes and completely flexible out of plane. Masses were concentrated in the centre of mass at each storey. Accidental eccentricity was not taken into account. Second order ($P - \Delta$) effect was considered.

The inelastic flexural behaviour of beams and columns was modelled by one-component lumped plasticity elements. Plastic hinges were defined by moment-rotation relationship schematically shown in Fig. 8.4b). For beams, the plastic hinge was used for major axis bending only. For columns, two independent plastic hinges for bending about the two principal axes were used. The interaction between axial force and bending moment was not considered. Yield moment M_y was determined for each element by analysing the cross-section of the element.

Fig. 8.2 The elastic acceleration spectrum for $a_g = 0.29\ g$ and soil type B, spectra for individual accelerograms and mean spectrum
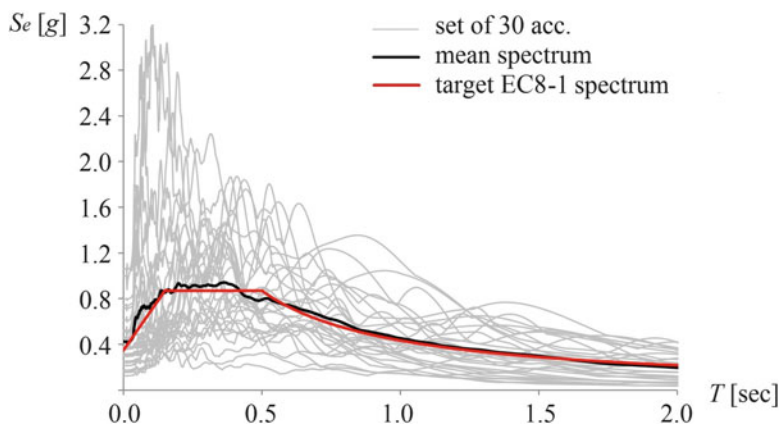
Cracked sections were modelled according to EC8-1 by using the elastic flexural properties of elements equal to one-half of the corresponding stiffness of the un-cracked elements. The ultimate rotation θ_{um} was determined according to Eq. 8.1.

The infills were modelled by means of diagonal struts. The details of the modelling do not influence the results.

For NDA, all analyses were performed on the same MDOF structural model as the N2 analysis. Stiffness degrading hysteretic behaviour was used (material »Hysteretic« in OpenSees). The parameter β, which controls the unloading stiffness, was equal to 0.5. Rayleigh damping ($\xi = 5\ \%$), proportional to mass and instantaneous stiffness was applied (considering the first two vibration periods).

In the mathematical model used in this study, it was assumed that the elements do not fail in shear. In order to confirm this assumption, the results should be checked in order to identify possible shear failures of elements, especially columns. The discussion on shear capacity is out of the scope of this chapter. However, it should be mentioned that, in the case of the investigated building, all elements passed the check.

Seismic demand is defined by EC8-1 for the design ground acceleration $a_g = 0.29\ g$, for soil type B (resulting in peak ground acceleration PGA $= 0.35\ g$) and for 5 % damping (Fig. 8.2).

8.3.2 Seismic Performance Assessment

The analyses were performed for two variants of the building, each for two directions of ground motion. The N2 analysis for the Y direction of the bare
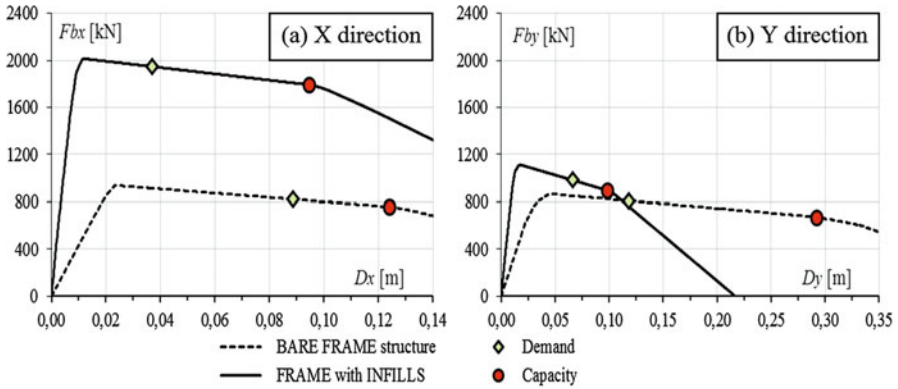
**Fig. 8.3** The pushover curves with indicated demand and capacity

frame structure is shown more in details, whereas for the other analyses only the results are shown in Figs. 8.3 and 8.5.

In the N2 method, the lateral loads for the pushover analysis were determined based on the first mode shape. The pushover curve for the bare frame building in the Y direction is shown in Fig. 8.3b), where the NC limit state of the building, defined as the state when the first column attains its NC limit state, is marked. The results of the pushover analysis indicate that the interior column C4 in the first storey is the first column that fails in flexure ($\theta_{um} = 0.031$) at the roof displacement $D_{NC} = 29.2$ cm. The corresponding storey drift ratio of the first storey is equal to $\delta_{NC.1} = 9.5$ cm/300 cm $= 0.032$. The spectral acceleration corresponding to the capacity amounts to $S_{a.NC} = 1.25$ g, and PGA $= 0.86\,g$ (see Fig. 8.4a). Several columns in the first three storeys fail soon after the failure of the first column, so the detailed results are sensitive to the details of the modelling.

Demand is based on the EC8-1 elastic spectrum presented in Fig. 8.2. The fundamental effective period amounts to $T_{eff} = 0.86$ s, resulting in the elastic spectral acceleration $S_e = 0.50\,g$. The target displacement of the SDOF system $D_{t.SDOF} = 9.3$ cm is defined by the intersection point of the line representing the period and the elastic demand spectrum (see Fig. 8.4a). The corresponding target roof displacement of the MDOF structure is equal to $D_{t.MDOF} = D_{t.SDOF} \times \Gamma = 9.3\,\text{cm} \times 1.26 = 11.8\,\text{cm}\,(\Gamma = 1.26)$, whereas the storey drift ratio of the first storey is equal to $\delta_{t.1} = 3.5\,\text{cm}/300\,\text{cm} = 0.012$. The distribution of storey drifts over the height of the structure is shown in Fig. 8.5. A global plastic mechanism over the first three stories is formed. A comparison of capacity and demand in terms of PGA, roof displacement and storey drift ratio suggest that the building is able to survive the design earthquake (Table 8.1). The storey drift ratio is shown for the first storey, where the critical column is located. Very similar values apply for the second and the third storey.

a) The N2 method:
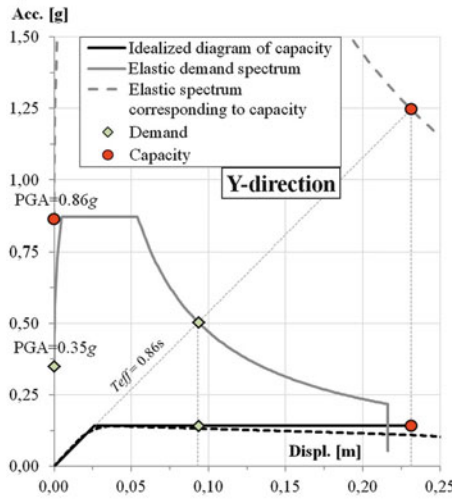
b) The damage of the building:
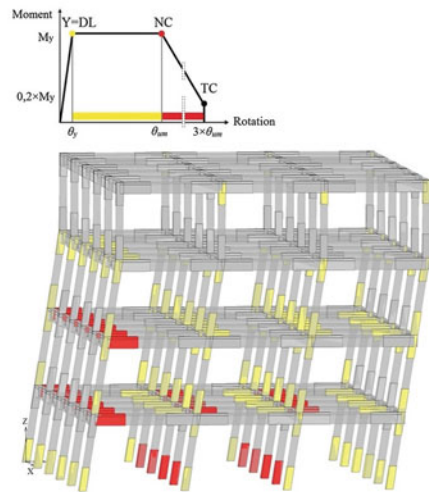
Fig. 8.4 (**a**) Comparison of capacity and demand for the equivalent SDOF system in AD format and (**b**) the damage in plastic hinges at the NC limit state for bare frame building in Y direction
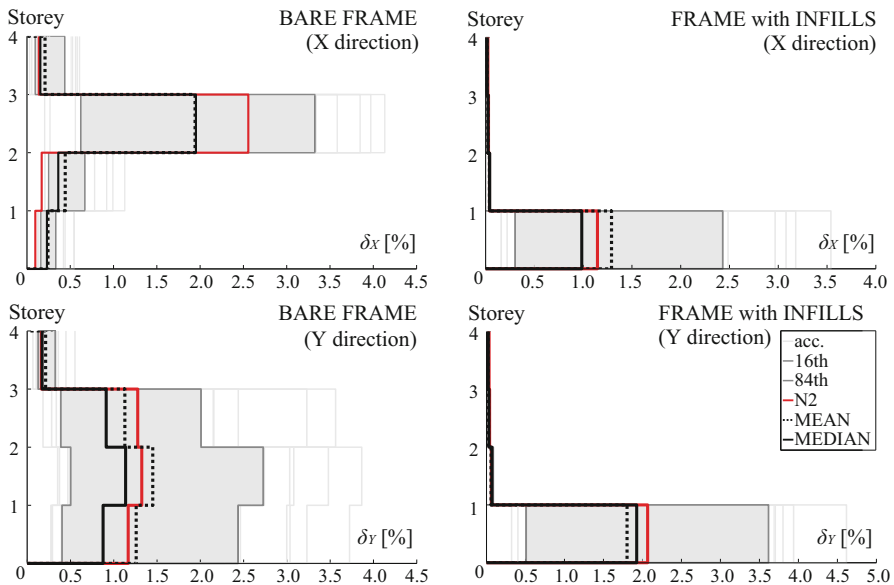
Fig. 8.5 Seismic demand in terms of storey drift ratios

The results for other three analyses, presented in Figs. 8.3 and 8.5, demonstrate that in all three cases storey mechanisms are formed. In the case of the bare frame structure in X-direction, the critical storey is the third storey (due to the change in the stiffness of columns). In the case of the infilled frames with the open first storey the mechanism forms in the first storey, as expected.

Table 8.1 Comparison between capacity (*C*) and demand (*D*) in terms of roof displacements and storey drift ratios (for third storey in the case of bare frame in X direction and for the first storey in other cases)

		Bare frame			Frame with infills		
		C	D	C/D	C	D	C/D
Analysis		X direction					
N2	PGA [g]	0.49	0.35	1.40	0.83	0.35	2.39
	Roof disp. [cm]	12.4	8.9	1.40	9.5	3.7	2.55
	St. drift ratio [%]	3.8	2.6	1.47	3.1	1.1	2.68
NDA	Roof disp. [cm]	12.4	7.9	1.56	9.5	3.2	2.96
	St. drift ratio [%]	3.8	1.9	1.91	3.1	1.0	3.10
Analysis		Y direction					
N2	PGA [g]	0.86	0.35	2.48	0.52	0.35	1.48
	Roof disp. [cm]	29.2	11.8	2.48	9.8	6.6	1.48
	St. drift ratio [%]	3.2	1.2	2.73	3.1	2.1	1.51
NDA	Roof disp. [cm]	29.2	11.0	2.64	9.8	6.2	1.57
	St. drift ratio [%]	3.2	0.9	3.61	3.1	1.9	1.62

Mean and median values of displacements and storey drift ratios were determined by NDA. For the demand in terms of storey drift ratios, the results of individual analyses, the mean and the median values, and the values of 16th and 84th percentiles are shown in Fig. 8.5.

The comparisons between capacity and demand are presented in Table 8.1. In the case of NDA, the same values for capacity were considered as in the case of the N2 method. Median values were used for demand.

8.4 Discussion and Conclusions

In the Y direction, the results indicate a detrimental effect of infills, which generate a storey mechanism instead of a global mechanism which occurs in the case of the bare frame structure. In the X direction, a story mechanism occurs in both variants of the structure. The third storey is critical for the bare frame (due to a change of stiffness and strength), whereas in the case of the partially infilled structure the mechanism occurs in the first storey. In the X direction, the influence of infills is beneficial. In all cases the capacity is larger than the demand corresponding to the design ground motion. However, it should be noted that average values for all quantities were used in analyses. If uncertainties were taken into account (by safety factors), the bare frame structure in X-direction and the partially infilled structure in Y direction would not pass the check.

There is a good agreement of the results obtained by the N2 method and NDA. Both methods are able to demonstrate the potential weaknesses of the structure.

References

Celarec D, Ricci P, Dolšek M (2012) The sensitivity of seismic response parameters to the uncertain modelling variables of masonry-infilled reinforced concrete frames. Eng Struct 35:165–177

CEN (2004a) EN 1998-1:2004 Eurocode 8: design of structures for earthquake resistance – part 1: general rules, seismic actions and rules for buildings. European Committee for Standardisation, Brussels, Belgium

CEN (2004b) EN 1992-1-1:2004 Eurocode 2: design of concrete structures – part 1-1: general rules and rules for buildings. European Committee for Standardisation, Brussels, Belgium

CEN (2005) EN 1998-3:2005/AC:2010 Eurocode 8: design of structures for earthquake resistance – part 3: assessment and retrofitting of buildings. European Committee for Standardisation, Brussels, Belgium

Dolšek M (2010) PBEE toolbox user's manual. The Institute of Structural Engineering, Earthquake Engineering and Construction IT (IKPIR). Available via: http://ice4risk.slo2projekt.info/publications.html

Fajfar P (2000) A nonlinear analysis method for performance-based seismic design. Earthq Spectra 16(3):573–592

OpenSees (2013) Open system for earthquake engineering simulation. Pacific Earthquake Engineering Research Center (PEER). Available via: http://opensees.berkley.edu/

Panagiotakos TB, Fardis MN (2001) Deformations of reinforced concrete members at yielding and ultimate. ACI Struct J 98(2):135–148

Vukobratović V, Fajfar P (2015) A method for the direct determination of approximate floor response spectra for SDOF inelastic structures. Bull Earthq Eng 13(5):1405–1424

Chapter 9
Torsional Index of an Asymmetric Building Based on Mode Shape

Kenji Fujii

Abstract It is essential to carry out three-dimensional analyses considering all possible directions of seismic input, when conducting seismic assessment of an asymmetric building. For this purpose, the author has proposed a simplified procedure to predict the largest peak seismic response of an asymmetric building subjected to horizontal bi-directional ground motion acting at an arbitrary angle of incidence. In the proposed simplified procedure, the largest peak response is predicted from the response of two independent equivalent single-degree-of-freedom models representing the first and second modes and combination of pushover analyses. However, it is unclear which conditions an asymmetric building should satisfy for the applicability of the proposed procedure. In this study, a torsional index is defined based on each mode shape, and the applicability of the proposed procedure is discussed based on the torsional index. The advantages of the proposed torsional index are as follows: (a) it is related to the effective (equivalent) modal mass ratio which represents the contribution of each modal response to the whole response, and (b) it is easily extended for an multi-storey asymmetric building, and (c) there is the clear relationship between torsional indices of two different modes and the angle between the principal directions of two modes. The numerical results show that the proposed simplified procedure is at least applicable to torsionally stiff systems for both orthogonal directions, while it is questionable for torsionally flexible systems.

Keywords Asymmetric building • Torsional index • Eigenvalue analysis • Effective modal mass ratio • Principal direction of modal response

K. Fujii (✉)
Department of Architecture and Civil Engineering, Chiba Institute of Technology,
2-17-1 Tsudanuma, Narashino, Chiba 275-0016, Japan
e-mail: kenji.fujii@it-chiba.ac.jp

9.1 Introduction

In designing of new building for earthquake resistance or when conducting seismic assessment of an asymmetric building, horizontal ground motion is applied to each of the main orthogonal axes of building. However, this procedure may be inadequate because the most critical direction of incidence of the seismic input, which would produce the largest response, may be different from the direction of the building's main orthogonal axis and the major component of the ground motion may act in any direction. Therefore it is essential to carry out three-dimensional analyses considering all the possible directions of seismic input. For this purpose, the author has proposed a simplified procedure to predict the largest peak seismic response of an asymmetric building subjected to horizontal bi-directional ground motion acting at an arbitrary angle of incidence (Fujii 2014). In this proposed procedure, the largest peak response of an asymmetric building is predicted based on (a) peak responses of two independent equivalent single-degree-of-freedom (SDOF) models representing the first and second modal response and (b) combination of pushover analyses considering the bi-directional excitations.

There are two critical assumptions in the procedure (Fujii 2014). The first is that the building oscillates predominantly in a single mode in each set of orthogonal directions, and the second is that the principal directions of the first and second modal responses are almost orthogonal. However, it is unclear which conditions an asymmetric building should satisfy for the applicability of the procedure.

In this study, a torsional index is defined based on each mode shape, and the relationship of the parameters of the asymmetric building model (eccentricity ratio, radius ratios of gyration torsional stiffness) to the proposed torsional index is investigated. The applicability of the procedure (Fujii 2014) is discussed based on the torsional index.

9.2 Definition of the Torsional Index Based on Mode Shape

9.2.1 Natural Modes of a Single-Storey Asymmetric Building Model

The building model investigated in this study is a simple, single-storey asymmetric building model, shown in Fig. 9.1. The equation of motions for undamped free vibration of this model is shown as Eq. 9.1, and rotational displacement z ($= r\theta$) is used instead of rotational angle θ.
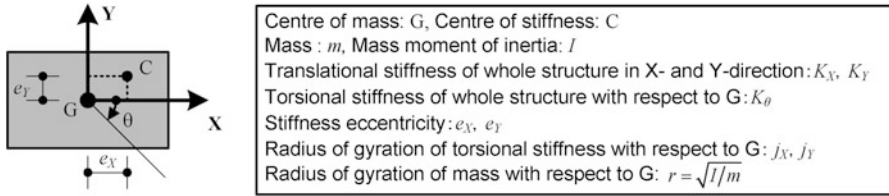
Centre of mass: G, Centre of stiffness: C
Mass : m, Mass moment of inertia: I
Translational stiffness of whole structure in X- and Y-direction: K_X, K_Y
Torsional stiffness of whole structure with respect to G: K_θ
Stiffness eccentricity: e_X, e_Y
Radius of gyration of torsional stiffness with respect to G: j_X, j_Y
Radius of gyration of mass with respect to G: $r = \sqrt{I/m}$
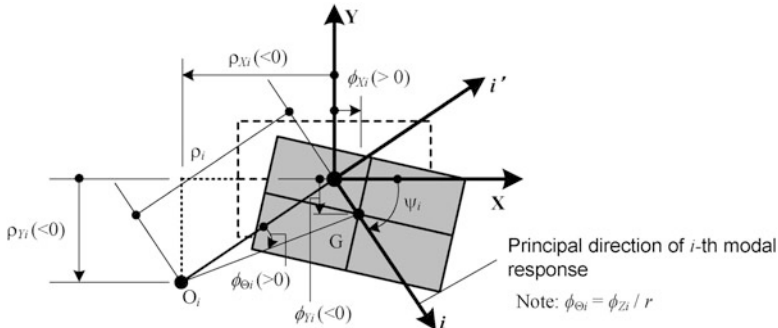
Fig. 9.1 Single-storey asymmetric building model

Fig. 9.2 Natural mode of a single-storey asymmetric building model

$$\left\{ \begin{array}{c} \ddot{x} \\ \ddot{y} \\ \ddot{z} \end{array} \right\} + \left[\begin{array}{ccc} \omega_{0X}{}^2 & 0 & \omega_{0X}{}^2 E_Y \\ 0 & \omega_{0Y}{}^2 & -\omega_{0Y}{}^2 E_X \\ \omega_{0X}{}^2 E_Y & -\omega_{0Y}{}^2 E_X & \omega_{0\theta}{}^2 \end{array} \right] \left\{ \begin{array}{c} x \\ y \\ z \end{array} \right\} = \left\{ \begin{array}{c} 0 \\ 0 \\ 0 \end{array} \right\}, \qquad (9.1)$$

$$\omega_{0X}{}^2 = K_X/m, \omega_{0Y}{}^2 = K_Y/m, \omega_{0\theta}{}^2 = K_\theta/I, E_X = e_X/r, E_Y = e_Y/r, \qquad (9.2)$$

where ω_{0X}, ω_{0Y} are the uncoupled natural circular frequencies of translational oscillation in the X and Y directions, respectively, $\omega_{0\theta}$ is the uncoupled natural circular frequency of rotational oscillation with respect to the centre of mass G (*not* to the centre of stiffness C), and E_X, E_Y are the eccentricity ratio, respectively. The natural mode of a single-storey asymmetric building model $\boldsymbol{\varphi_i}$, obtained from eigenvalue analysis, is shown in Fig. 9.2.

$$\boldsymbol{\varphi_i} = \{ \phi_X \quad \phi_Y \quad \phi_Z \}^{\mathbf{T}}. \qquad (9.3)$$

In Fig. 9.2, O_i (ρ_{Xi}, ρ_{Yi}) is the centre of rotation of the ith mode determined from Eq. 9.4, and therefore the distance from O_i to G is expressed by Eq. 9.5.

$$\rho_{Xi} = r(\phi_{Yi}/\phi_{Zi}), \rho_{Yi} = -r(\phi_{Xi}/\phi_{Zi}), \qquad (9.4)$$

$$\rho_i = \sqrt{\rho_{Xi}{}^2 + \rho_{Yi}{}^2} = r\sqrt{\phi_{Xi}{}^2 + \phi_{Yi}{}^2}/|\phi_{Zi}|. \qquad (9.5)$$

Considering a set of orthogonal i-i' axes in the X-Y plane, where the i-axis is the principal axis of the ith modal response, the tangent of ψ_i, the angle of incidence of the i-axis with respect to the X-axis, is determined from Eq. 9.6.

$$\tan \psi_i = -\phi_{Yi}/\phi_{Xi}. \qquad (9.6)$$

The effective (equivalent) modal mass ratio of ith mode in the X- and Y-directions, $m_{iX}{}^*$ and $m_{iY}{}^*$, respectively, is determined from Eq. 9.7.

$$m_{iX}{}^* = \frac{\phi_{Xi}{}^2}{\phi_{Xi}{}^2 + \phi_{Yi}{}^2 + \phi_{Zi}{}^2}, m_{iY}{}^* = \frac{\phi_{Yi}{}^2}{\phi_{Xi}{}^2 + \phi_{Yi}{}^2 + \phi_{Zi}{}^2}. \qquad (9.7)$$

9.2.2 Torsional Index of Each Mode

Based on the equations developed above, the torsional index based on the mode shape is formulated. The effective modal mass ratio ith mode in its principal direction, $m_i{}^*$, is determined from Eq. 9.8.

$$m_i{}^* = m_{iX}{}^* + m_{iY}{}^* = \frac{\phi_{Xi}{}^2 + \phi_{Yi}{}^2}{\phi_{Xi}{}^2 + \phi_{Yi}{}^2 + \phi_{Zi}{}^2}. \qquad (9.8)$$

Equation 9.8 can be rewritten in form of Eq. 9.9, considering Eq. 9.5.

$$m_i{}^* = \frac{1}{1 + \phi_{Zi}{}^2/\left(\phi_{Xi}{}^2 + \phi_{Yi}{}^2\right)} = \frac{1}{1 + (r/\rho_i)^2}. \qquad (9.9)$$

It is very important to note that $m_i{}^*$ only depends on the ratio (r/ρ_i). Thus, the torsional index of the ith mode, $R_{\rho i}$, is defined by Eq. 9.10.

$$R_{\rho i} = \frac{r}{\rho_i} = \frac{|\phi_{Zi}|}{\sqrt{\phi_{Xi}{}^2 + \phi_{Yi}{}^2}}. \qquad (9.10)$$

It can be seen that $m_i{}^*$ is unity when $R_{\rho i}$ is zero (purely translational), while $m_i{}^*$ is close to zero when $R_{\rho i}$ is significantly large. Therefore, the terms "predominantly translational" and "predominantly torsional" can be defined using $R_{\rho i}$; the "predominantly translational" mode is the mode when $R_{\rho i} < 1$, while the "predominantly torsional" mode is the mode when $R_{\rho i} > 1$.

Note that this torsional index $R_{\rho i}$ is easily extended for a multi-storey building, as discussed in previous study (Fujii 2014). The definition of $R_{\rho i}$ for a multi-storey building is shown in Appendix.

9.3 Characteristics of the Torsional Index for Each Mode

9.3.1 Relationship of the Torsional Indices for the Three Modes

The sum of the effective modal mass ratio in each X- and Y-direction for all three modes is obtained as in Eq. 9.11.

$$\sum_{i=1}^{3} m_{iX}{}^* = 1, \ \sum_{i=1}^{3} m_{iY}{}^* = 1. \tag{9.11}$$

Therefore, the sum of $m_i{}^*$ of all three modes is obtained from Eq. 9.12 as:

$$\sum_{i=1}^{3} m_i{}^* = \sum_{i=1}^{3} \frac{1}{1 + R_{\rho i}{}^2} = 2 \tag{9.12}$$

Assuming the third mode is predominantly the torsional mode ($R_{\rho 3} < 1$), $m_3{}^*$ must be smaller than 1/2. In which case, the sum $\left(m_1{}^* + m_2{}^*\right)$ must be larger than 3/2, while $m_1{}^*, m_2{}^*$ must have a value from 0 to 1. Therefore, the relationship shown in Eq. 9.13 is obtained.

$$\text{If } R_{\rho 3} > 1, \ \frac{1}{2} \leq \frac{1}{1 + R_{\rho 1}{}^2} \leq 1, \ \text{ and } \ \frac{1}{2} \leq \frac{1}{1 + R_{\rho 2}{}^2} \leq 1. \tag{9.13}$$

As a result, we have the interesting findings shown in Eq. 9.14.

$$\text{If } R_{\rho 3} > 1, \ 0 \leq R_{\rho 1} \leq 1, \ \text{ and } \ 0 \leq R_{\rho 2} \leq 1. \tag{9.14}$$

Equation 9.14 implies that, in the case of the single-storey asymmetric building model, only one mode can be the predominantly torsional mode; if the third mode is the predominantly torsional mode, the other two modes must be predominantly translational modes.

9.3.2 Relationship Between the Torsional Indices of the First and Second Modes and the Angles Between the Principal Directions of the Two Different Modes

One of the critical assumptions of the procedure, presented in previous study (Fujii 2014), is that the principal directions of the first two modes are almost orthogonal. In this section, the relationship between $R_{\rho i}, R_{\rho j}$ ($i \neq 1$) and the angles between the

principal directions of the two different modes, is investigated. A unit vector $\boldsymbol{\alpha_i}$ parallel to the principal direction of ith modal response is defined by Eq. 9.15.

$$\boldsymbol{\alpha_i} = \{ \cos\psi_i \quad -\sin\psi_i \quad 0 \}^{\mathbf{T}} = \left\{ \frac{\phi_{Xi}}{\sqrt{\phi_{Xi}^2 + \phi_{Yi}^2}} \quad -\frac{\phi_{Yi}}{\sqrt{\phi_{Xi}^2 + \phi_{Yi}^2}} \quad 0 \right\}^{\mathbf{T}}. \quad (9.15)$$

Therefore, the cosine of $\Delta\psi_{ij}$, the angle between the principal direction of the first and second modes, can be determined from Eq. 9.16.

$$\cos\Delta\psi_{ij} = \frac{\boldsymbol{\alpha_i} \cdot \boldsymbol{\alpha_j}}{|\boldsymbol{\alpha_i}||\boldsymbol{\alpha_j}|} = \frac{\phi_{Xi}\phi_{Xj} + \phi_{Yi}\phi_{Yj}}{\sqrt{\phi_{Xi}^2 + \phi_{Yi}^2}\sqrt{\phi_{Xj}^2 + \phi_{Yj}^2}}. \quad (9.16)$$

The orthogonal conditions of $\boldsymbol{\varphi_i}$ and $\boldsymbol{\varphi_j}$ can be written in the form of Eq. 9.17.

$$\phi_{Xi}\phi_{Xj} + \phi_{Yi}\phi_{Yj} + \phi_{Zi}\phi_{Zj} = 0. \quad (9.17)$$

From Eqs. 9.16 and 9.17, an interesting relationship between $R_{\rho i}$, $R_{\rho j}$ and $\Delta\psi_{ij}$ is obtained as shown in Eq. 9.18.

$$\left| \cos\Delta\psi_{ij} \right| = \left| \frac{\phi_{Zi}}{\sqrt{\phi_{Xi}^2 + \phi_{Yi}^2}} \frac{\phi_{Zj}}{\sqrt{\phi_{Xj}^2 + \phi_{Yj}^2}} \right| = R_{\rho i}R_{\rho j}. \quad (9.18)$$

It is clear from this equation that if the product of the torsional indices in the ith and jth modes, $R_{\rho i}$, $R_{\rho j}$, is close to zero $\left(R_{\rho i}R_{\rho j} \ll 1 \right)$, the principal directions of the two modes are almost orthogonal.

9.3.3 Effective Modal Mass Ratios of the First and Second Modes

Another critical assumption of the presented procedure (Fujii 2014) is that the building oscillates predominantly in a single mode in each set of orthogonal directions. In this section, the validity of this assumption is discussed based on the torsional index. Considering another set of orthogonal U-V axes in the X-Y plane, where the U-axis is the principal axis of the first modal response, the effective modal mass ratio of the first mode with respect to the U-axis, m_{1U}^{*}, and the second modal response with respect to the V-axis, m_{2V}^{*}, can be expressed as follows:

$$m_{1U}{}^* = m_1{}^* = \frac{1}{1 + R_{\rho 1}{}^2}, \tag{9.19}$$

$$m_{2V}{}^* = \frac{(\phi_{X2} \sin \psi_1 + \phi_{Y2} \cos \psi_1)^2}{\phi_{X2}{}^2 + \phi_{Y2}{}^2 + \phi_{Z2}{}^2} = \frac{1}{1 + R_{\rho 2}{}^2} \sin^2 \Delta \psi_{12}. \tag{9.20}$$

From Eq. 9.19, it is evident that if the first mode is predominantly the translational mode ($R_{\rho 1} < 1$), the equivalent first modal mass ratio in the U-direction $m_{1U}{}^*$ is the largest of all three modes in that direction; in such a case, the building oscillates predominantly in the first mode when the unidirectional excitation acts in the U-direction. For the second modal response, Eq. 9.20 can be rewritten as Eq. 9.21 taking into consideration Eq. 9.18.

$$m_{2V}{}^* = \frac{1}{1 + R_{\rho 2}{}^2}\left(1 - \cos^2 \Delta \psi_{12}\right) = \frac{1}{1 + R_{\rho 2}{}^2}\left\{1 - \left(R_{\rho 1} R_{\rho 2}\right)^2\right\}. \tag{9.21}$$

This equation implies that if the first and second modes are predominantly translational modes ($R_{\rho 1} < 1$ and $R_{\rho 2} < 1$), the building oscillates principally in the second mode when the unidirectional excitation acts in the V-direction.

9.4   Numerical Investigations

9.4.1   Model Parameters

In the numerical investigation, a parametric study is carried out by considering the various parameters of the asymmetric building model. The radius ratio of gyration for the torsional stiffness with respect to the X- and Y-axes, J_X and J_Y, respectively, is defined by Eq. 9.22.

$$J_X = \frac{j_X}{r} = \sqrt{\frac{K_\theta / K_X}{I/m}} = \frac{\omega_{0\theta}}{\omega_{0X}}, J_Y = \frac{j_Y}{r} = \sqrt{\frac{K_\theta / K_Y}{I/m}} = \frac{\omega_{0\theta}}{\omega_{0Y}}. \tag{9.22}$$

In this parametric study, E_X, E_Y varied from 0.05 to 0.95 at intervals of 0.05, while J_X, J_Y varied from 0.10 to 1.95 at intervals of 0.05 (with the condition $J_Y \geq J_X$). Note that the cases that do not satisfy the conditions shown as Eq. 9.23 are eliminated because in such cases the torsional stiffness with respect to the centre of stiffness, K'_θ shown in Eq. 9.24, will be a negative value.

$$(E_Y / J_X)^2 + (E_X / J_Y)^2 \leq 1. \tag{9.23}$$

$$K'_\theta = K_\theta - K_X e_Y{}^2 - K_Y e_X{}^2. \qquad (9.24)$$

In this parametric study, all analytical models are categorized into three cases; Case 1 ($J_Y \geq J_X \geq 1$), Case 2 ($J_Y \geq 1 \geq J_X$) and Case 3 ($1 \geq J_Y \geq J_X$).

9.4.2 Results and Discussions

Figures 9.3, 9.4, and 9.5 show the plot of torsional indices of the three modes for each case. As shown in Fig. 9.3, for all the models categorized in Case 1 the first and second modes are predominantly translational modes ($R_{\rho 1} < 1$ and $R_{\rho 2} < 1$) and the third mode is predominantly a torsional mode ($R_{\rho 3} < 1$). It should be pointed out that all the plots in Fig. 9.3a satisfy the following condition.
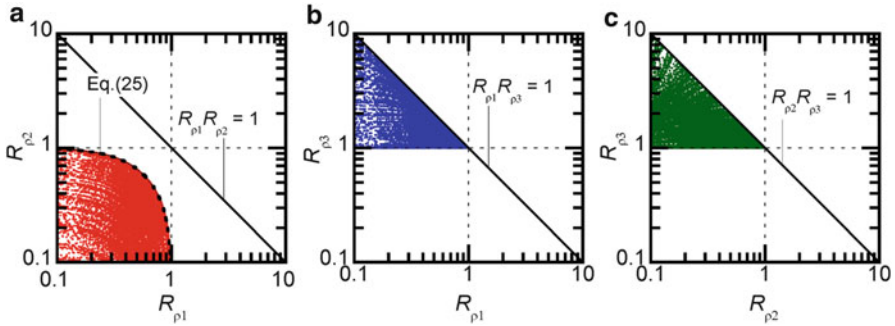

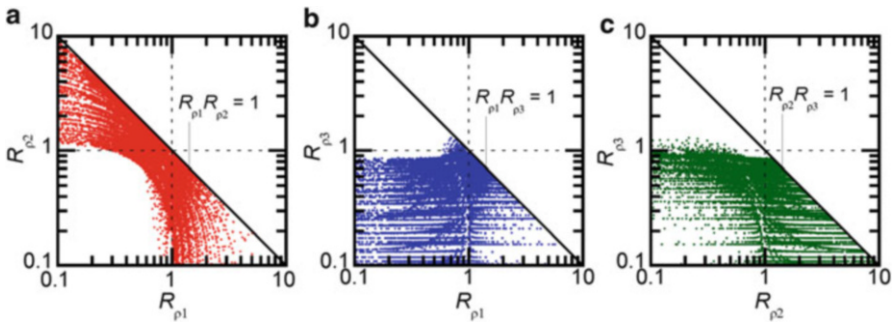**Fig. 9.3** Plots of the torsional indices for all modes in Case 1

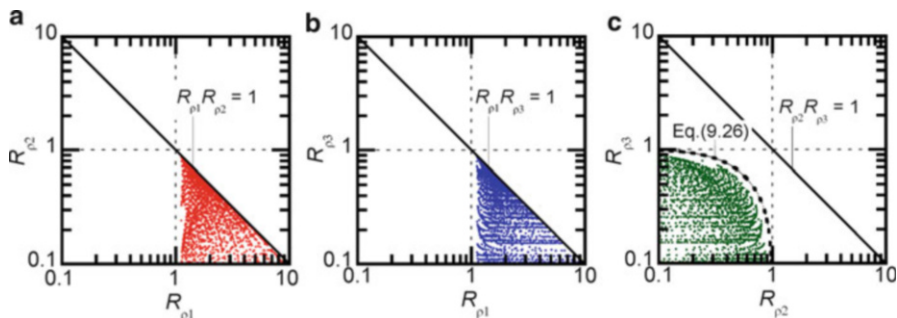**Fig. 9.4** Plots of the torsional indices for all modes in Case 2

Fig. 9.5 Plots of the torsional indices for all modes in Case 3

$$\frac{1}{1 + R_{\rho 1}{}^2} + \frac{1}{1 + R_{\rho 2}{}^2} \geq \frac{3}{2}. \tag{9.25}$$

However, in Cases 2 (shown in Fig. 9.4) and 3 (shown in Fig. 9.5), the first mode is predominantly a torsional mode; in Case 2, either the first or second mode is predominantly a torsional mode ($R_{\rho 1}$ or $R_{\rho 2}$ may larger than 1), while in Case 3, $R_{\rho 1}$ is always larger than 1, and $R_{\rho 2}$ and $R_{\rho 3}$ are smaller than 1. It should be pointed out again that all the plots in Fig. 9.5c satisfy the following condition (Eq. 9.26), which is similar to that shown in Fig. 9.3a.

$$\frac{1}{1 + R_{\rho 2}{}^2} + \frac{1}{1 + R_{\rho 3}{}^2} \geq \frac{3}{2}. \tag{9.26}$$

Figure 9.6 shows the relationship between $m_{1U}{}^*$ and $m_{2V}{}^*$ for all three cases. As expected from the results shown in Figs. 9.3, 9.4, and 9.5 and Eqs. 9.19 and 9.20, $m_{1U}{}^*$ and $m_{2V}{}^*$ are larger than 0.5 for all models categorized in Case 1 ($J_Y \geq J_X \geq 1$); as shown in Fig. 9.6a, the sum of $m_{1U}{}^*$ and $m_{2V}{}^*$ is larger than 3/2 for most models of Case 1. In contrast, $m_{1U}{}^*$ and $m_{2V}{}^*$ may be smaller than 1/2 in the other cases, especially in Case 3, where $m_{1U}{}^*$ is smaller than 1/2 for all models and $m_{2V}{}^*$ may be between 0 and 1. This implies that most models in Cases 2 and 3 may not oscillate predominantly in the first mode when the unidirectional excitation acts in the U-direction.

From these results it may be concluded that the two critical assumptions of the simplified procedure (Fujii 2014) are valid only in Case 1 ($J_Y \geq J_X \geq 1$).

Note that the classification of systems as either TS or TF systems is based on the ratio of the uncoupled torsional mode to the lateral frequencies $\Omega_{\theta X}$, $\Omega_{\theta Y}$ of the corresponding torsionally balanced system, defined by Eq. 9.27 (Hejal and Chopra 1987).
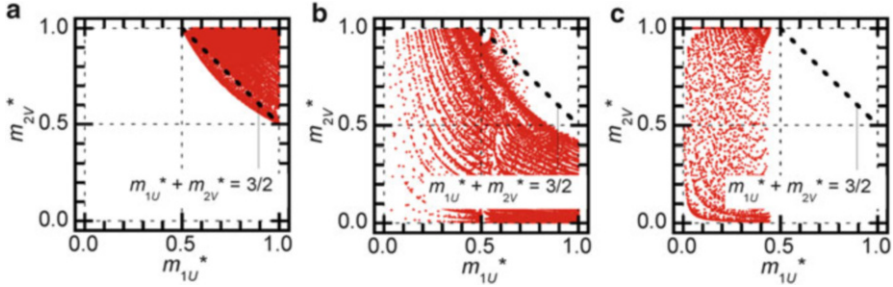
Fig. 9.6 Plots of $m_{1U}{}^*$ and $m_{2V}{}^*$ in the three cases. (**a**) Case 1. (**b**) Case 2. (**c**) Case 3

$$\Omega_{\theta X} = \omega_{0\theta}{}'/\omega_{0X}, \Omega_{\theta Y} = \omega_{0\theta}{}'/\omega_{0Y}. \tag{9.27}$$

In Eq. 9.27, $\omega_{0\theta}{}'$ is the uncoupled natural circular frequency of rotational oscillation with respect to the centre of stiffness. According to Hejal and Chopra (1987), the system $\Omega_{\theta X}$, $\Omega_{\theta Y} > 1$ is classified as a TS system in both the X- and Y-directions.

Because the torsional stiffness with respect to the centre of stiffness K_{θ}', defined by Eq. 9.24, is smaller than K_{θ}, $\Omega_{\theta X}$ is smaller than J_X (and also $\Omega_{\theta Y}$ is smaller than J_Y). If $\Omega_{\theta X}$ is larger than unity, J_X is then larger than unity (and if $\Omega_{\theta Y}$ is larger than unity, J_Y is then larger than unity). This implies that all the systems classified as TS systems for both the X- and Y-directions are included in Case 1 in this parametric study.

Therefore, the simplified procedure (Fujii 2014) may be applicable at least for TS systems for both orthogonal directions. However the applicability of the procedure is questionable for TF systems, because the two critical assumptions in the procedure are invalid for most of them.

9.5 Conclusions

In this study, a torsional index is defined based on each mode shape, and the relationship of the parameters for an asymmetric building model and the proposed torsional index is investigated. Then the applicability of the simplified procedure (Fujii 2014) is then discussed based on the torsional index. The numerical results show that the simplified procedure (Fujii 2014) may be applicable at least for TS systems for both orthogonal directions, while the applicability of the procedure is questionable for TF systems.

The advantages of the proposed torsional index are as follows: (a) it is related to the effective modal mass ratio which represents the contribution of each modal response to the whole response, and (b) it is easily extended for an multi-storey asymmetric building, and (c) there is the clear relationship between torsional indices of two different modes and the angle between the principal directions of

two modes. Therefore, the index proposed herein is suitable to discuss the applicability of the simplified procedure (Fujii 2014).

Appendix: Definition of Torsional Index for a Multi-storey Building

Consider a N-storey asymmetric building, the torsional index of the ith mode, $R_{\rho i}$, can be defined by Eq. 9.28.

$$R_{\rho i} = \sqrt{\left(\sum_{j=1}^{N} I_j \phi_{\Theta ji}{}^2 \right) \Big/ \left(\sum_{j=1}^{N} m_j \phi_{Xji}{}^2 + \sum_{j=1}^{N} m_j \phi_{Yji}{}^2 \right)}, \qquad (9.28)$$

$$\boldsymbol{\varphi_i} = \{ \begin{array}{ccccccccc} \phi_{X1i} & \cdots & \phi_{XNi} & \phi_{Y1i} & \cdots & \phi_{YNi} & \phi_{\Theta 1i} & \cdots & \phi_{\Theta Ni} \end{array} \}^{\mathbf{T}}. \qquad (9.29)$$

In Eq. 9.28, m_j and I_j are mass and mass moment of inertia of the jth floor, respectively, and $\phi_{Xji}, \phi_{Yji}, \phi_{\Theta ji}$ are the X, Y and rotational component of jth floor of ith mode vector $\boldsymbol{\varphi_i}$. Note that Eq. 9.10 is equivalent to Eq. 9.28: Eq. 9.10 is easily obtained from Eq. 9.28 by considering the case $N = 1$.

References

Fujii K (2014) Prediction of the largest peak nonlinear seismic response of asymmetric buildings under bi-directional excitation using pushover analyses. Bull Earthq Eng 12:909–938

Hejal R, Chopra AK (1987) Earthquake response of torsionally-coupled buildings. Earthquake Engineering Research Center, report no. UCB/EERC-87/20, College of Engineering, University of California at Berkeley

Chapter 10
An Approximate Method for Assessing the Seismic Response of Irregular in Elevation Asymmetric Buildings

George K. Georgoussis

Abstract An approximate procedure is presented for assessing the seismic response of irregular in elevation asymmetric buildings. The procedure is based on the concept of the equivalent single story system, which has been introduced by the author in earlier papers for assessing the response of uniform in height buildings, and retains the simplicity of the corresponding methodology. Frequencies and peak values of base resultant forces of multi story buildings with large setbacks, classified by Eurocode 8 as irregular structures, may be predicted by the proposed approximate method when the excitation is characterized by response spectra. The center of stiffness of the equivalent single story system defines the modal center of rigidity, and its coincidence with the mass axis of the real building specifies a structure which sustains an almost translational response into the elastic phase. Besides, such a structural configuration retains this response into the inelastic phase when the strength assignment of all lateral load resisting bents is stiffness proportional. The accuracy of the proposed procedure is first illustrated in mixed-bent-type eight-story elastic structures, which are characterized by EC8-2004 as irregular in elevation structures, and comparisons are made with the accurate results obtained by response spectrum analyses using the SAP2000 computer program. The inelastic response of these structures, when the strength of various bents is determined by a planar static analysis under a code lateral loading, is investigated under the Loma Prieta (1989) and Imperial Valley (1940) ground motions.

Keywords Irregular buildings • Inelastic response • Modal centre of rigidity

G.K. Georgoussis (✉)
Department of Civil Engineering Educators, School of Pedagogical and Technological Education (ASPETE), N. Heraklion, 14121 Attica, Greece
e-mail: ggeorgo@tee.gr

10.1 Introduction

It has been shown in author's earlier papers (Georgoussis 2009, 2010, 2012) that basic dynamic data (frequencies, resultant base shears and torques) of uniform multi-story mixed-bent-type eccentric structures may be found by analyzing equivalent single story modal systems. This type of analysis represents an extension of a similar procedure presented in past for the analysis of proportionate multi-story buildings (Kan and Chopra 1977; Hejal and Chopra 1989; Athanatopoulou et al. 2006). The stiffness of the elements of the equivalent single story modal system is based on the element frequencies of the bent-subsystems that provide the lateral resistance of a given structure. These frequencies are determined from the corresponding individual bents when they are assumed to carry, as planar frames, the mass of the complete structure. In the case of uniform structures composed by very dissimilar bents, a higher accuracy of the aforementioned analysis can be attained with the use of the effective element frequencies, which are based on the element frequencies, but, also, take into account the ratio of the effective modal mass of the individual bent to the corresponding mass of the uncoupled multistory system (Georgoussis et al. 2013a; Georgoussis 2014). The efficiency of the aforementioned effective frequencies is now examined in eccentric buildings with large setbacks.

The main property of the centre of the element stiffnesses of the equivalent single story modal system, which defines the modal center of rigidity (m-CR), is that when it lies on the mass axis, the response of elastic uniform building structures, asymmetric in plan, is basically translational. Besides, this response is preserved into the post-elastic phase, where the structure is stressed beyond the elastic limits, provided that the strength assignment of its resisting bents is stiffness proportional. In other words, this response is obtained when the building is detailed as a planar structure under a code load (Georgoussis 2014; Georgoussis et al. 2013b). This is attributed to the almost concurrent yielding of all resisting elements, which preserves the translational response, attained at the end of the elastic phase, to the post elastic one. This response is evident in eccentric single story systems. Reviewing the literature, it can be seen that systems, with coincident the centres of mass and rigidity and elasto-plastic elements having a strength distribution proportional to the stiffness distribution (usually called torsionally balanced (TB) models) present a purely translational inelastic response under strong ground excitations. For this reason they are used as 'reference' models in relevant studies (Correnza et al. 1994; Chandler et al. 1996; Wong and Tso 1994). This behaviour is attained because yielding is initiated at the same instant for all elements and the element force balance about CM is preserved into the inelastic phase, leading to a translational response throughout the ground shaking (De Stefano and Pintucchi 2008; Anagnostopoulos et al. 2013).

The first objective of this study is to demonstrate that the same type of analysis can be accurately applied for the assessment of frequencies and base shears of asymmetric multistory buildings with abrupt mass discontinuities, which are classified by EC8-2004 as irregular structures. As shown in the following sections, the

prediction of base torques is not as accurate as in the case of uniform buildings, but, the predicted optimum location of m-CR is quite reasonable. Note here, that EC8-2004 and other modern country codes specify a full three-dimensional dynamic analysis for irregular in elevation structures. There are no recommendations of how the practicing engineer can assess the fundamental frequency by a simple formula or methodology and there are not provisions which allow the structural detailing by a pseudo-static structural design against an equivalent lateral load. Only in the case of buildings with a fairly even distribution of mass (regular buildings) the codes provide simple expressions for calculating the fundamental frequency and allow for a pseudo-static structural design.

The second objective is to demonstrate that when (i) the mass axis of setback buildings passes through (or in a close distance from) m-CR, and (ii) the strength assignment of the various bents is stiffness proportional (that is, it is based on a planar static analysis under a set of lateral forces simulating an equivalent 'seismic loading'), the response of the mentioned structures into the inelastic phase is basically translational. Such a response has already been shown in uniform structures (Georgoussis 2014; Georgoussis et al. 2013b), but at present it is demonstrated in structures with a mass irregularity. Common 8-story setback buildings are examined under two characteristic ground motions (Loma Prieta (1989) and Imperial Valley (1940)), selected from the strong ground motion database of the Pacific Earthquake Engineering Research (PEER) Center (http://peer.berkely.edu) and scaled to a PGA=0.5 g.

10.2   Asymmetric Setback Buildings and Modelling

A typical mono-symmetric multistory building with a setback is shown in Fig. 10.1. The building is uniform over the height H_b, which defines the base structure and has a uniformly distributed mass, equal to m_b per floor, and a radius of gyration equal to r_b. Above this level, it has a setback forming a uniform tower structure of a reduced floor plan with a height equal to H_t, a mass per floor equal to m_t and a radius of gyration equal to r_t. Each floor consists of a rigid slab (deck) and at present the centers of mass (CM) at each floor are assumed to lie on the same vertical line (mass axis) which is passing through the centroids of all decks. All bents (rigid frames, shear walls, coupled wall systems, etc.) extend up to the top of the building.

The methodology to analyze elastic setback buildings, like that of Fig. 10.1, is outlined in an author's earlier paper (Georgoussis 2011). The backbone of this method is similar to that applied to uniform over the height systems (Georgoussis 2009, 2010, 2012). In brief, in mono-symmetric systems, the peak elastic response of medium height buildings can be derived by analyzing two equivalent single-story modal systems, each of which has a mass equal to the k-mode effective mass, $M_k^*(k = 1, 2)$, of the uncoupled multi-story structure, and it is supported by elements with a stiffness equal to the product of M_k^* with the first mode (when $k = 1$) or
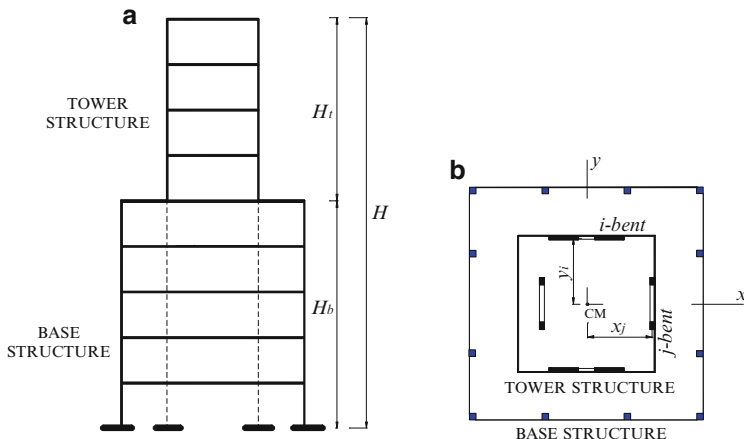
Fig. 10.1 (**a**) Multistory setback building with (**b**) an asymmetric structural configuration

second mode (when $k = 2$) squared element frequencies of the corresponding real bents of the assumed multi-story structure. For an excitation along the y-direction, the effective mass M_k^* can be simply taken equal to that corresponding to the same direction $\left(M_{yk}^*\right)$. At present this procedure is also applied and in a slightly modified version, by using the effective element frequencies (instead of the element frequencies), as they are defined in earlier papers (Georgoussis et al. 2013a; Georgoussis 2014). Under these assumptions, the undamped equation of motion of the k-mode equivalent single story system, in a coordinate system with the origin at the center of mass (Fig. 10.1b), is as follows:

$$\mathbf{M}_k^* \ddot{\mathbf{U}}_k + \mathbf{K}_k^* \mathbf{U}_k = -\mathbf{M}_k^* \mathbf{\iota} \ddot{u}_g \tag{10.1}$$

where

$\mathbf{M}_k^* = M_{yk}^* \begin{bmatrix} 1 & 0 \\ 0 & r_{ek}^2 \end{bmatrix}$ is the effective k-mode mass matrix,

$\mathbf{U}_k = \left\langle u_k \quad \theta_k \right\rangle^{\mathrm{T}}$ is the corresponding modal displacement vector at CM

$\mathbf{K}_k^* = \begin{bmatrix} k_y^* & k_{yw}^* \\ k_{wy}^* & k_w^* \end{bmatrix}_k$ is the effective k-mode stiffness matrix

$\mathbf{\iota}^{\mathrm{T}} = \left\langle 1 \quad 0 \right\rangle^{\mathrm{T}}$ is the influence vector, and

$$\begin{aligned}
k_{yk}^* &= \Sigma k_{jk}^* = M_{yk}^* \Sigma \omega_{jk}^2 \\
k_{wk}^* &= \Sigma x_j^2 k_{jk}^* + \Sigma y_i^2 k_{ik}^* = M_{yk}^* \Sigma \left(x_j^2 \omega_{jk}^2 + y_i^2 \omega_{ik}^2\right) \\
k_{ywk}^* &= k_{wyk}^* = \Sigma x_j k_{jk}^* = M_{yk}^* \Sigma x_j \omega_{jk}^2
\end{aligned} \tag{10.2}$$

The quantities ω_{jk} and ω_{ik} are the element frequencies of the j and i-bents, aligned along the y- and x-directions at distances x_j and y_i respectively. The

accuracy of this procedure is also investigated by using the effective element frequencies $\overline{\omega}_{jk}$ and $\overline{\omega}_{ik}$ (instead of ω_{jk} and ω_{ik}), which are defined as follows:

$$\overline{\omega}_{jk}^2 = \omega_{jk}^2\left(M_{jk}^*/M_{yk}^*\right), \overline{\omega}_{ik}^2 = \omega_{ik}^2\left(M_{ik}^*/M_{xk}^*\right) \tag{10.3}$$

It is evident that when the lateral stiffness of a given building is composed by the same type of bents (e.g. flexural shear walls), the aforementioned effective element frequencies are respectively equal to the element frequencies ω_{jk} and ω_{ik}. The radius of gyration of the equivalent single story system r_{ek} is taken equal to $\overline{r}_{ek}r_b$, where $\overline{r}_{ek}$ represents a Rayleigh's quotient, given as (Georgoussis 2011):

$$\overline{r}_{ek} = \left(\omega_{yk}/\omega_{ryk}\right)\left(\text{or } \overline{r}_{ek} = \left(\omega_{xk}/\omega_{rxk}\right)\right) \tag{10.4}$$

where ω_{yk} (or ω_{xk}) is the k-mode frequency of the uncoupled multistory structure in the y-direction (or x-direction) and ω_{ryk} (or ω_{rxk}) the corresponding frequency of the same structure when the mass in the floors of the tower section is reduced to $m_{rt} = (r_t/r_b)^2 m_t$. It has been shown (Georgoussis 2011) that in common setback buildings, the ratio $\overline{r}_{ek}$ is very little dependent on the type of the lateral load resisting system (frame, wall, dual system). Therefore, any of the expressions of Eq. 10.4 may be used for practical applications, but it is advisable to use the mean value of these expressions, since this averaging procedure utilizes the response of the structure in both directions.

Note here that the coupled Eq. 10.1, for the first mode $(k = 1)$ single-story system, provides the response quantities of the first two modes of vibration. Therefore, when the plan configuration produces an uncoupled stiffness matrix in Eq. 10.1, the first two modes of vibration (translational and rotational) are decoupled and the response for a low height building will be practically translational. In fact, this condition specifies that the first mode center of rigidity (m-CR) of the corresponding single-story system coincides with CM. As, in general, the x-coordinate of m-CR can be determined from the condition: $k_{ywk}^*\left(= k_{wyk}^*\right) = 0$, i.e.:

$$x_{m-CR} = \Sigma\left(x_j\omega_{j1}^2\right)/\Sigma\left(\omega_{j1}^2\right) \tag{10.5}$$

minimum seismic torsion is expected in low or medium height structures (where the first two modes of vibration virtually determine their response) when the location of m-CR coincides with CM. Such structural configurations may be seen as torsionally balanced systems. The second objective of the paper is to demonstrate that such setback buildings retain this translational response into the post elastic phase when they are detailed as planar structures under a code horizontal load.
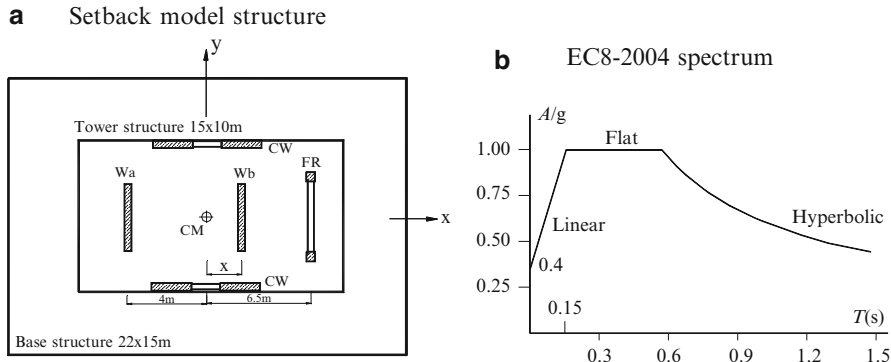
a   Setback model structure

b   EC8-2004 spectrum

Fig. 10.2 (**a**) Example setback building, (**b**) EC8-2004 design spectrum

10.3   Buildings Studied

To illustrate the application and accuracy of the proposed method, the example setback building shown in Fig. 10.2a was analyzed. This is an 8-story mono-symmetric building, which is divided in two substructures: the base structure represents a uniform building system composed by floors of 22×15 m, while the tower substructure is composed by floors of reduced dimensions 15×10 m. The lateral load resisting system, extending up to the top of the building, is composed by dissimilar bents: two structural walls (Wa and Wb) and a moment resisting frame (FR) are aligned along the y-direction and a pair of coupled-wall bents (CW) is oriented along the x-axis of symmetry. The structural walls Wa and Wb are of cross sections 30x500cm, the moment resisting frame FR consists of two 75×75 cm columns, 5 m apart, connected by beams of a cross section 40×70 cm, while the CW bents are composed two 30×300 cm walls, 5 m apart, connected by lintel beams of a cross section 25×90 cm at the floor levels. The latter bents are located symmetrically to CM at the edges of the floors of the tower structure, that is at distances equal to ± 5 m. The mass of the base floors is $m_b = 264 \mathrm{kNs}^2/\mathrm{m}$, the radius of gyration about CM is $r_b = 7.687$ m and the corresponding quantities of the tower structure are equal to $m_t = 120$ $\mathrm{kNs}^2/\mathrm{m}$ and $r_t = 5.204$ m respectively. The story height is 3.5 m and the modulus of elasticity (E) is assumed equal to 20×10^6 kN/m^2, typical for concrete structures. The centers of mass of the floor slabs lie on a same vertical line, which passes through the centroids of all the orthogonal floor plans of the example structure.

Three models of the aforementioned example building are examined. In the first model (T2–B6) the tower structures consists of two floors, in the second model (T4–B4) of four floors and, finally, in the third model (T6–B2) the tower structure consists of six floors. For each model different structural configurations are examined as follows: wall Wa and frame FR are assumed to be located at fixed positions, the first on the left of CM in a distance equal to 4 m and the second on the right of CM at a distance of 6.5 m, while the second wall Wb is taking all the possible locations along the x-axis within the limits of the tower section.

At first the periods/frequencies of the assumed models, for all possible locations of Wb, are examined. The accuracy of the proposed approximate procedure to predict periods of vibrations is investigated by comparison with the results derived from the computer program SAP2000-V11. In the computer analyses, the out of plane stiffness of the bents was neglected and in the wide column analogy used to simulate the CW bents the clear span of the coupling beams was increased by the depth of the beams (Coull and Puri 1968). To apply the proposed method, the first pair of element frequencies of the various bent-subsystems is required, and also the effective modal masses of the uncoupled system. For example, denoting with M the total mass of the second model structure ($M = 4m_b + 4m_t = 1536$ kNs^2/m for T4–B4), these quantities for the bents of this model were found by means of the SAP2000 program as follows:

Walls Wa, Wb: $\omega_{w1} = 5.092$/s, $\omega_{w2} = 23.994$/s, frame FR: $\omega_{f1} = 3.033$/s, $\omega_{f2} = 8.483$/s, coupled walls CW: $\omega_{cw1} = 5.372$/s, $\omega_{cw2} = 19.592$/s, and the first two effective modal masses of the uncoupled system are: $\overline{M}_{y1}^* = M_{y1}^*/M = 0.588$ and $\overline{M}_{y2}^* = 0.265$. The radius of gyration r_{ek} ($k = 1,2$), computed as described in the previous section, was found equal to $r_{e1} = 0.742*r_b = 5.704$ m and $r_{e2} = 0.871*r_b = 6.695$ m for the first and second mode equivalent single story systems respectively.

When the proposed method is based on the effective element frequencies, these quantities are found: $\overline{\omega}_{w1} = 5.044/s$, $\overline{\omega}_{w2} = 24.442/s$ for walls Wa, Wb and: $\overline{\omega}_{f1} = 3.412/s$, $\overline{\omega}_{f2} = 6.122/s$ for frame FR (for the coupled walls CW the effective frequencies are equal to the element frequencies as above).

The inelastic response of the assumed model structures was also investigated under two characteristic ground motions (Loma Prieta (1989) and Imperial Valley (1940)), selected from the strong ground motion database of the Pacific Earthquake Engineering Research (PEER) Center (http://peer.berkely.edu) and scaled to a PGA = 0.5 g (unidirectional excitations along the y-axis). For all the possible locations of Wb, inelastic analyses, by means of the computer program SAP2000-V11, were performed to evaluate top rotations and base shears and torques. The strength assignment of all bents of the assumed models is based on a planar static analysis, along the x and y directions, under an external lateral loading with the floor forces determined from Eq. 4.11 of EC8-2004 and summing to a base (design) shear equal to 20 % of the total weight of the structure.

10.4   Model Frequencies and Observed Nonlinear Seismic Response

The first four periods of vibration of the model setback structures, computed by the proposed method on the grounds of the element frequencies (red lines) and, also, on the grounds of the effective element frequencies (green lines) for different locations of the Wb (indicated by the normalized coordinate $\overline{x} = x/r_b$), are shown in

Fig. 10.3, together with the accurate SAP2000 computer values (black lines). It is evident that the first pair of frequencies is closer to the accurate computer results when the proposed method is based on the effective element frequencies (the green lines are closer to the black ones for the first and second periods of vibration), while the predicted second pair of frequencies is more accurate when the proposed method is based on the element frequencies (the red lines are closer to black ones for the second pair -third and fourth- periods of vibration).

Interpreting these observations, it seems that best data are provided by the proposed method when the first mode equivalent single-story system is formulated on the basis of the effective element frequencies, while best results are obtained from the second mode system when it is based on element frequencies. The results of this analysis (base shears and torques), in relation to the EC-8 acceleration spectrum (Fig. 10.2b), are shown in Fig. 10.4 by green lines, together with the results obtained by analyzing the 3D structures with the SAP2000 software (black lines). For comparison reasons the data obtained from the proposed method on the basis of only the element frequencies (for both equivalent single story modal systems) are also shown in Fig. 10.4 with red lines.

The response of the inelastic setback structures under the Loma Prieta (component Corralitos 000, 1989) and Imperial Valley (component ElC180, 1940) excitations, are shown in Fig. 10.5. Note here that the strength of all models is determined by a planar static analysis under a set of floor forces determined from Eq. 4.11 of EC8-2004. In order to compare elastic and inelastic behaviors, the elastic responses of the assumed models under the same excitations are also presented in this figure.

Three response parameters, obtained by time history analyses assuming a 5 % damping ratio, are shown: top rotations, normalized base shears and normalized base torques. The red lines represent the peak elastic response (top rotations: θ_e, are shown by dashed lines, normalized base shears: $\overline{V}_e = V_e/V_d$ (V_d: the design base shear equal to 20 % of the total weight) by solid lines and normalized base torques: $\overline{T}_e = T_e/r_b V_d$ by dotted lines). The corresponding black lines represent the peak inelastic behavior $\left(\theta_{in}, \overline{V}_{in} = V_{in}/V_d, \overline{T}_{in} = T_{in}/r_b V_d\right)$. Envisaging Fig. 10.5 it can be seen that minimum values of base torques and top rotations are observed when the location of wall Wb receives values close to those predicted from Eq. 10.5, by equating x_{m-CR} to zero. For the assumed models T2-B6, T4-B4 and T6-B2, the predicted optimum locations of FR are found equal to $\overline{x} = 0.133$, 0.168 and 0.12 respectively.

10.5   Conclusions

In this work, the torsional seismic behaviour of mass irregular asymmetric buildings was assessed using an approximate simplified procedure which has been used in the past for the analysis of uniform multi-story building. Frequencies of mono-symmetric, medium height setback buildings, composed by dissimilar bents, can be
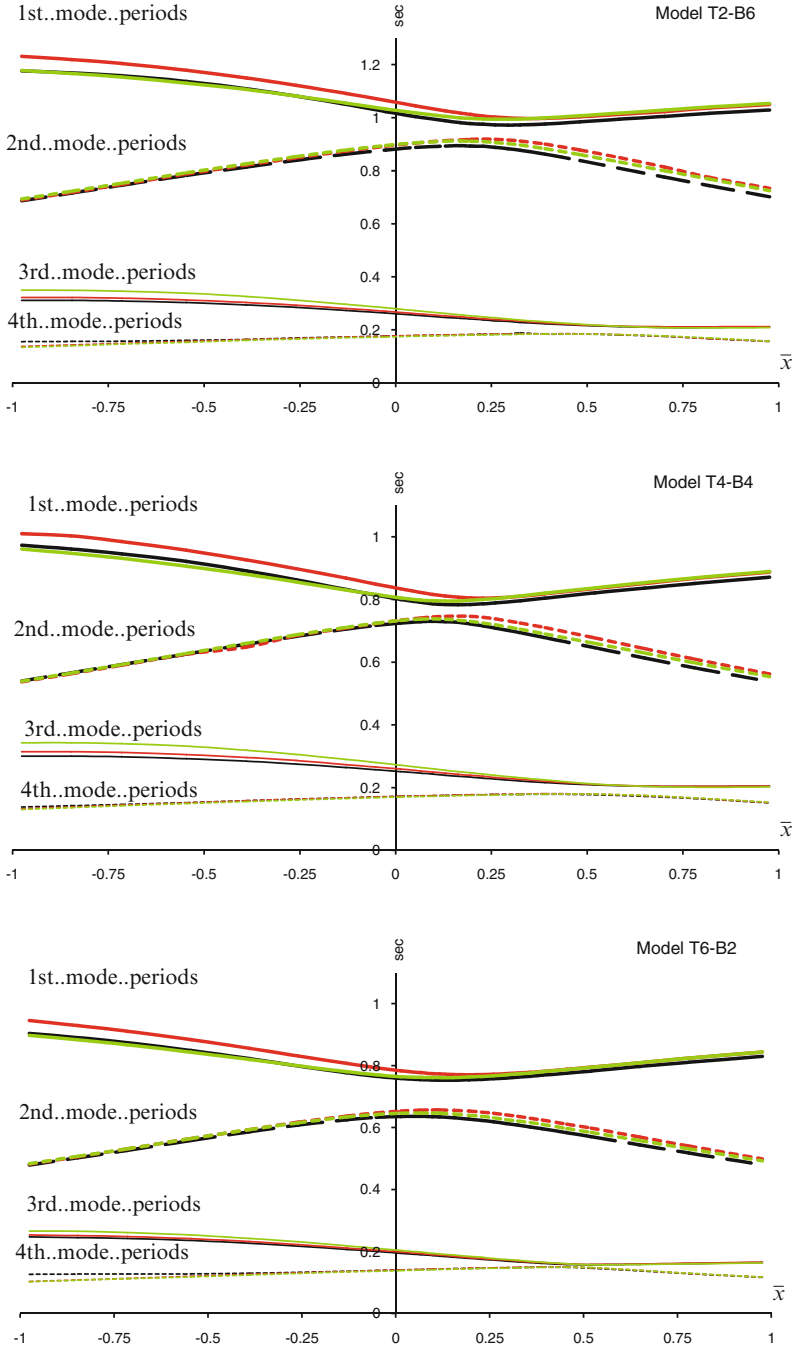
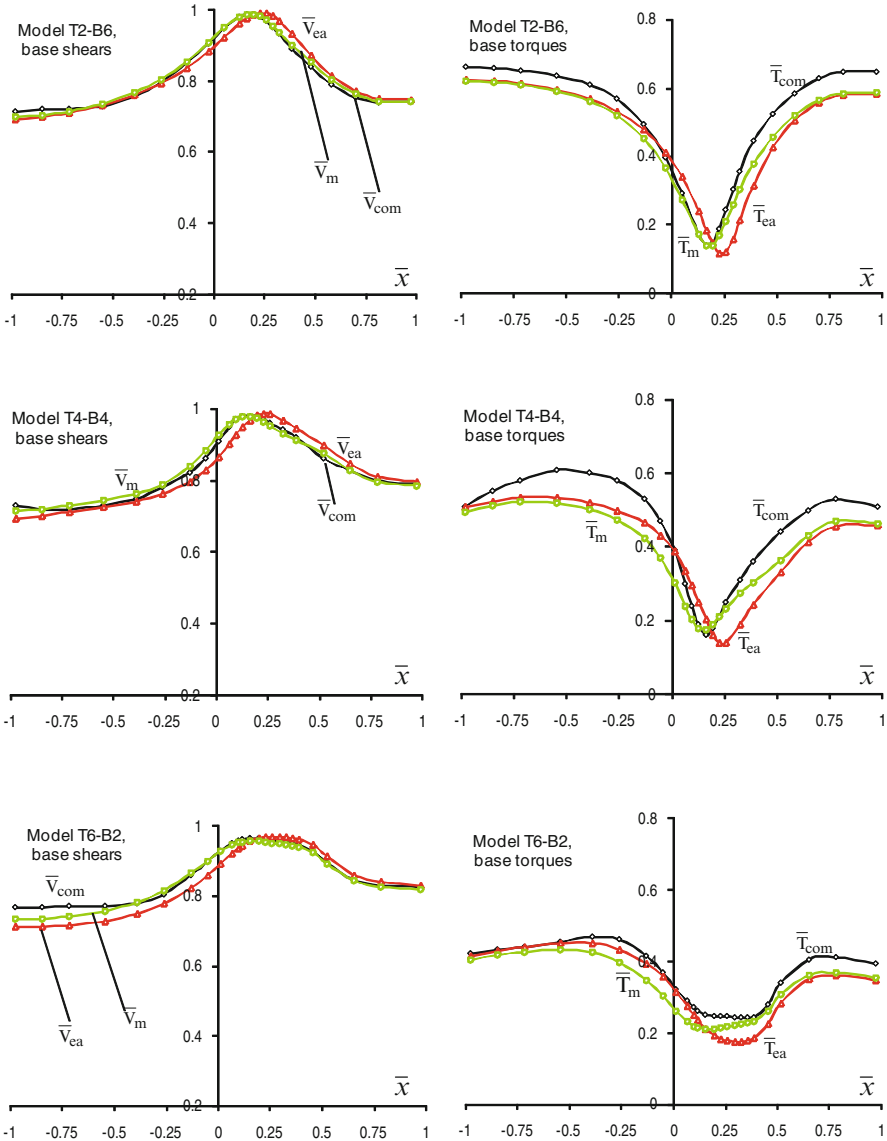**Fig. 10.3** Periods of vibration of setback models

Fig. 10.4 Peak base shears and torques of setback models

estimated with reasonable accuracy from the analysis of two equivalent, single-story modal systems, the masses of which are determined from the first two vibration modes of the uncoupled multi-story structure and the stiffnesses of the resisting elements are determined from the corresponding individual bents when they are assumed to carry, as planar frames, the mass of the complete structure. This
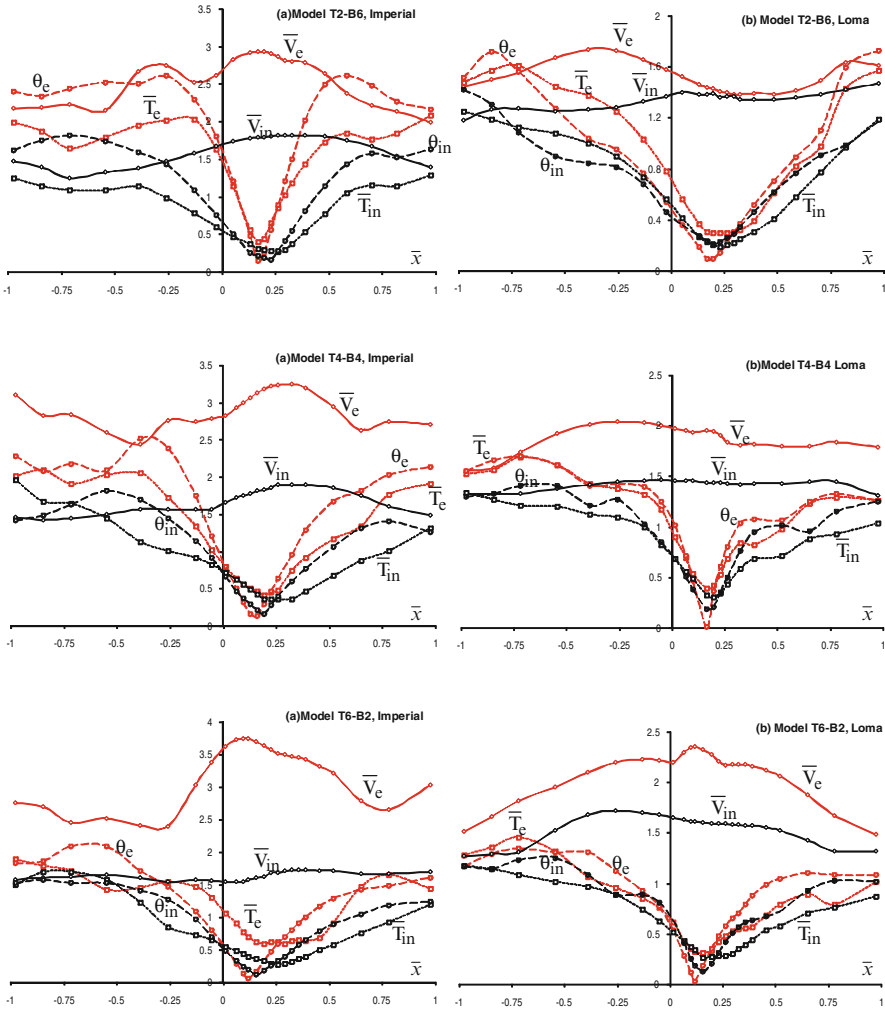
Fig. 10.5 Top rotations ($*10^{-2}$, rads), base shears and torques of setback models

simple analysis provides also quite reasonable estimates of the resultant base shears of the setback buildings and, to some extent, of the base torques. Quite reasonable is also the prediction of the location of the first mode center of rigidity. The main property of this point is that when it is within a close distance from the mass axis, the response of elastic buildings is virtually translational. This behavior is preserved in the inelastic phase, when the strength assignment of the lateral load resisting bents is derived from a planar static analysis, as a consequence of the almost concurrent yielding of these bents. This is demonstrated in common 8-story setback buildings under two characteristic ground motions.

References

Anagnostopoulos SA, Kyrkos MT, Stathopoulos KG (2013) Earthquake induced torsion in buildings: critical review and state of the art. The 2013 World Congress on Advances in Structural Engineering and Mechanics (ASEM13), Jeju, Sept 8–12

Athanatopoulou AM, Makarios T, Anastassiadis K (2006) Earthquake analysis of isotropic asymmetric multistory buildings. Struct Des Tall Spec Build 15:417–443

Chandler AM, Duan XN, Rutenberg A (1996) Seismic torsional response: assumptions, controversies and research progress. Eur Earthq Eng 1:37–51

Correnza JC, Hutchinnson GL, Chandler AM (1994) Effect of transverse load-resisting elements on inelastic earthquake response of eccentric-plan buildings. Earthq Eng Struct Dyn 23:75–89

Coull A, Puri RD (1968) Analysis of pierced shear walls. J Struct Eng ASCE 94(1):71–82

De Stefano M, Pintucchi B (2008) A review of research on seismic behaviour of irregular building structures since 2002. Bull Earthq Eng 6:285–308

Georgoussis GK (2009) An alternative approach for assessing eccentricities in asymmetric multistory structures 1: elastic systems. Struct Des Tall Spec Build 18(2):181–202

Georgoussis GK (2010) Modal rigidity center: its use for assessing elastic torsion in asymmetric buildings. Earthq Struct Int J 1(2):163–175

Georgoussis GK (2011) Simplified dynamic analysis of eccentric buildings with a setback. 1: the effect of mass irregularity. Struct Des Tall Spec Build 20:911–927

Georgoussis G (2012) Seismic analysis of non-proportionate eccentric buildings. Adv Mater Res 450–451:1482–1488

Georgoussis G (2014) Modified seismic analysis of multistory asymmetric elastic buildings and suggestions for minimizing the rotational response. Earthq Struct Int J 7(1):039–052

Georgoussis G, Tsompanos A, Makarios T, Papalou A (2013a) Optimum structural configuration of irregular buildings. 1: elastic systems. The 2013 World Congress on Advances in Structural Engineering and Mechanics (ASEM13), Jeju, Sept 8–12

Georgoussis G, Tsompanos A, Makarios T, Papalou A (2013b) Optimum structural configuration of irregular buildings. 2: inelastic systems. The 2013 World Congress on Advances in Structural Engineering and Mechanics (ASEM13), Jeju, Sept 8–12

Hejal R, Chopra AK (1989) Earthquake analysis of a class of torsionally-coupled buildings. Earthq Eng Struct Dyn 18:305–323

Kan CL, Chopra AK (1977) Elastic earthquake analysis of torsionally coupled multistorey buildings. J Struct Div ASCE 103(4):821–838

Wong CM, Tso WK (1994) Inelastic seismic response of torsionally unbalanced systems designed using elastic dynamic analysis. Earthq Eng Struct Dyn 23:777–798

Chapter 11
Application of Nonlinear Static Procedures for the Seismic Assessment of a 9-Storey Asymmetric Plan Building

André Belejo and Rita Bento

Abstract The Seismic Assessment of a 9-storey asymmetric plan building is performed through recent Nonlinear Static Procedures (NSPs). Among these methods two multimode methods are included: the Modal Pushover Analysis (MPA) and the Improved Modal Pushover Analysis (IMPA). The IMPA is a multimode procedure that has the advantage of redefining the lateral load applied, when comparing with multimode current methods; hence, instead of consider the elastic deformed shape when applying the pushover load pattern, it is possible to consider the deformed shape of the structure when behaving inelastically. The IMPA was proposed in the past and was successfully applied in the seismic assessment of bridges. Thus, the main objective of this work is to test IMPA in buildings. For this purpose the seismic demands of an asymmetric plan building, considering both components of ground motion acting simultaneously, are herein estimated by means of IMPA and compared with Nonlinear Dynamic Analyses (NDA), MPA and two other NSPs that are proposed in American and European seismic codes (ASCE/SEI 41-06 NSP and N2 method respectively). The results are obtained in terms of lateral displacements profiles, interstorey drifts, normalized top displacements and shear forces.

Keywords Improved modal pushover analysis • Torsion • Asymmetric-plan building • Nonlinear static procedures • Nonlinear dynamic analysis

A. Belejo (✉)
Oregon State University, Corvallis, OR, USA
e-mail: belejoa@onid.oregonstate.edu

R. Bento
ICIST, Instituto Superior Técnico, Universidade de Lisboa, Av. Rovisco Pais,
1049-001 Lisbon, Portugal
e-mail: rita.bento@tecnico.ulisboa.pt

11.1   Introduction

The IMPA, introduced by Paraskeva and Kappos (2010) for bridges, is an improved version of the MPA procedure, which has, as main characteristic, the ability to overcome the invariability of the lateral force distribution.

The IMPA is based on the MPA proposed by Chopra and Goel (2002), known as a complete version of a multi-mode pushover analysis. The MPA is a multi-run method, wherein several pushover curves are obtained from different load patterns proportional to each mode of vibration (as many as modes considered) and the final response is obtained combining the results that correspond to each pushover curve using an appropriate combination rule. This method has continuously been improved and updated: MPA was first extended to asymmetric buildings again by Chopra and Goel (2004), and recently adapted to consider both components of ground motion acting simultaneously in buildings by Reyes and Chopra (2011).

The IMPA is herein applied to assess the seismic behavior of an asymmetric plan building, along with three more NSPs: the MPA, the NSP proposed in ASCE/SEI 41-06 (ASCE 2007) and the most recent extension of N2 method developed by Kreslin and Fajfar (2012).

These procedures are applied within different seismic intensities, considering both components of ground motion acting simultaneously.

The objectives of this paper are: (i) to evaluate the accuracy of IMPA on the prediction of seismic demands of an asymmetric plan building, especially when the structure exhibits inelastic behavior; (ii) to evaluate the number of modes required by the multimode procedures in order to obtain reliable results; (iii) to compare the two multimode methods, IMPA and MPA and; (iv) to comparatively assess the accuracy of all methods herein applied: IMPA, MPA, the NSP proposed in ASCE/ SEI 41-06 and the extended N2 method, which is evaluated by comparison with nonlinear dynamic analyses (NDAs).

11.2   Nonlinear Static Procedures (NSPs)

The MPA considers a non adaptive force based pushover analysis based on modal proportional load patterns. The method takes into account the higher mode effects since in each run a different load pattern proportional to each mode of vibration of the structure is applied, and the results computed from each pushover curve are combined to obtain the final results. The complete methodology as a whole is described step by step in Reyes and Chopra (2011).

The key idea of the IMPA procedure is to use the deformed shape of the structure responding inelastically to the considered earthquake level in lieu of the elastic mode shape. So the IMPA, following the guidelines of the work performed for bridges by Paraskeva and Kappos (2010), is divided in two phases: (i) in the first phase, the seismic response is computed for each mode, as MPA does; (ii) in the

second phase, the procedure is restarted using a lateral load pattern proportional to the displacement shape vector correspondent to the peak deformation obtained in the first phase, and the process is repeated. In Belejo and Bento (2015), the method is described step by step.

The most recent version of N2 method corresponds to an extended version of the original N2 method proposed by Fajfar and Fichinger (1988) which is also described in Eurocode 8 (CEN 2004) that takes into account both the torsional and the higher modes effects, by adjusting the pushover results, computed with the original N2 method, by means of correction factors based on linear dynamic response spectrum analysis.

The ASCE/SEI 41-06 NSP is based on the Displacement Coefficient method (FEMA 1997) and provides a direct numerical process for calculating the displacement demand. The method has been updated over time in American codes like FEMA 356 (ASCE 2000) and FEMA440 (ATC 2005) ending up with its final version in ASCE/SEI 41-06.

11.3 Case Study: 9-Storey Building

The building selected for this work is an asymmetric plan 9-storey frame steel building that represents the older buildings designed according to the 1985 Uniform Building Code (UBC85) and was defined and studied by Reyes (2009).

The building structure is characterized by moment resisting frames, detached in Fig. 11.1 by the identified columns, gathered with the beams that connect them; gravity frames whose function is to support the gravity loads and braced frames in the alignments C1-C8, C3-C9, C9-C12 and C14-C17 that provide a "panel effect" in those localizations. More information about the building is provided in Reyes (2009) and Belejo and Bento (2015).

11.4 Modelling Issues

The analysis software adopted in this work was SeismoStruct v6.0 (Seismosoft 2006), a downloadable fibre element based finite element software.

The 3D model representing the building under analysis was built using space frames assuming the centerline dimensions. The nonlinear behavior of the members was modeled through the use of fibre element models with each fibre characterized by the respective material relationship.

In terms od damping, the hysteretic damping was already implicitly included in the nonlinear fibre model formulation of the inelastic frame elements. On the hand, the viscous damping was modeled on the Rayleigh type with its two constants selected to give 2 % damping ratio at the fundamental period of vibration T_1 and a
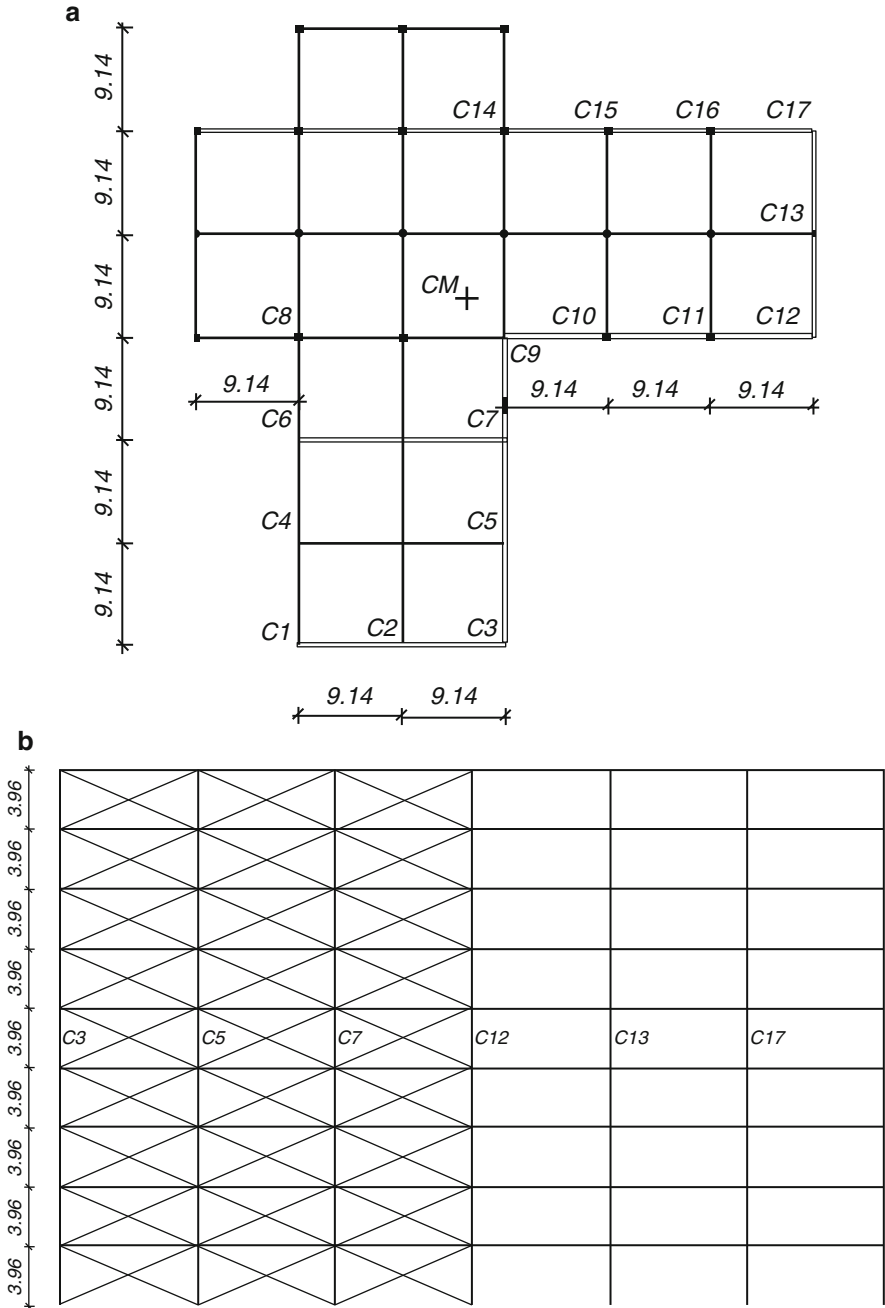
Fig. 11.1 9-storey building configuration: (**a**) in plan; (**b**) in elevation

period of $0.2T_1$, following the work performed by Reyes (2009) on a similar building.

A rigid diaphragm effect was modeled with nodal constraints under a penalty functions option. The penalty function exponent used was 10^7.

The weight of each floor was assigned as lumped mass in the nodes, corresponding to the respective tributary area.

11.5 Seismic Features

Fourteen bi-directional ground motion records were selected in order to perform NDA. Their selection was performed among the set of records used by Reyes (2009). The earthquake motion selection of these 14 records was performed by first plotting the original, non-scaled response spectrum for each earthquake motion, and comparing the spectral accelerations to the design spectral accelerations. Each earthquake motion was then scaled linearly by a scaling factor (SF), within the range of $0.2 < SF < 5.0$, in a range of spectral periods, $0.2–1.5T_1$, with the objective of obtaining a match between the scaled response spectrum and the design spectrum in a Period range of interest. The 14 motions with the smallest root-mean-square-error ($RMSE$) values, considering the geometric mean of both orthogonal directions, and their corresponding scale factor SF were recorded. The RMSE, proposed by Kottke and Rathje (2008) measures the goodness-of-fit for each response spectrum to the "target" spectrum. In this work all the records (geometric mean) were matched to the seismic hazard spectrum with the corresponding site located in Los Angeles, and considering 2 % probability of occurrence in 50 years ($P_{50} = 2$ %). The 14 matched spectra are plotted in Fig. 11.2, and Table 11.1 identifies the Earthquakes and the station where recorded.

Due to the uncertainty of knowing the position of the building relatively to the components of the records, all ground motions were assigned to the building in two

Fig. 11.2 Seismic hazard spectrum and the median response spectrum of 14 scaled ground motions
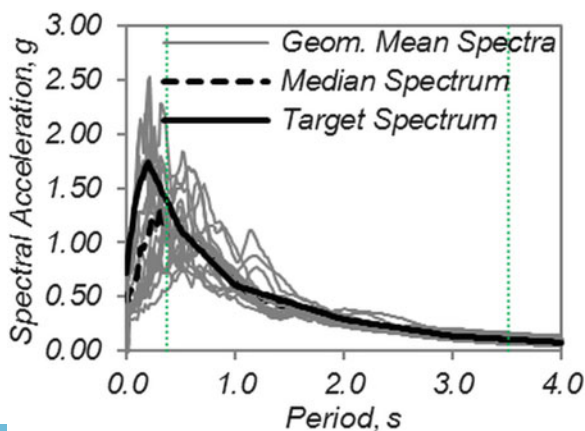
Table 11.1 Ground motion records considered

Earthquake	Station
Northridge 1994	Canyon Country
Northridge 1994	Santa Monica
Northridge 1994	Beverly Hills
Duzce 1999	Bolu
Hector Mine Oct 1999	Hec
Imperial Valley 1979	Calexico Fire Station
Kobe 1995	Shin-Osaka
Kocaeli 1999	Duzce
Landers 1992	Joshua Tree
Loma Prieta 1989	Gilroy Array #3
Loma Prieta 1989	Oakland
Loma Prieta 1989	Hollister City Hall
Loma Prieta 1989	Hollister Diff Array
Chi-Chi 1999	Chy006

Table 11.2 Periods (in seconds) and effective modal mass percentages of both buildings studied

1st set of modes				2nd set of modes			
Mode	Period (sec)	[Ux] (%)	[Uy] (%)	Mode	Period (sec)	[Ux] (%)	[Uy] (%)
1	1.87	8.2	26.4	4	0.69	1.4	2.6
2	1.69	59.3	21.1	5	0.60	6.7	4.0
3	1.57	13.1	32.8	6	0.55	2.3	4.4

different ways: "fault parallel" component of the record according to the X component of the building and "fault normal" component of the record assigned to the Y component of the building; and the opposite. Therefore the final seismic response is determined by the median of the 28 results obtained.

The median response spectrum obtained when both components of ground motion are considered is also shown in Fig. 11.2.

11.6 Numerical Results and Discussion

In this section, seismic responses obtained through the procedures abovementioned, are presented in terms of pushover curves, lateral displacement profiles, interstorey drifts, normalized top displacements and shear forces for different levels of seismic intensities, and considering both components of ground motion acting simultaneously.

The modal properties of the studied building are presented in Table 11.2, which shows the periods and the effective modal mass percentages in both X and Y directions, for the first and second set (three modes) of modes.

The results obtained attest to the torsion-dominated characteristics of the structure. The first mode is a torsional mode, the second mode shows translation along

both axes, but predominantly in the X direction, and the third mode shows translational behavior in Y direction coupled with torsion; which means that the building is torsional flexible in both directions. The second set of modes follows the modal behavior of the first set of modes.

11.6.1 Capacity Curves

In Fig. 11.3 the pushover curves obtained for the MPA (consequent first phase of IMPA for the first set of modes) are displayed for each mode considered together with the peak displacements obtained. The building is tested considering 10 % and 2 % probability of occurrence in 50 years ($P_{50} = 10$ % and $P_{50} = 2$ % respectively).
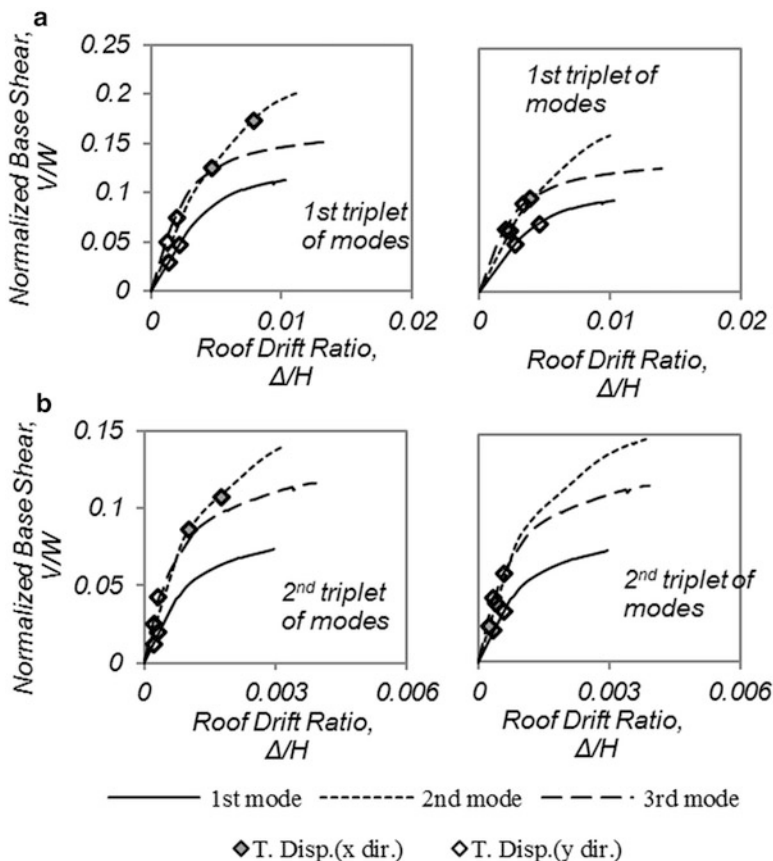
Fig. 11.3 Pushover curves used in MPA procedure: (a_1) 1st triplet of nodes in X direction; (a_2) 1st triplet of nodes in Y direction; (b_1) 2nd triplet of nodes in X direction; (b_2) 2nd triplet of nodes in Y direction
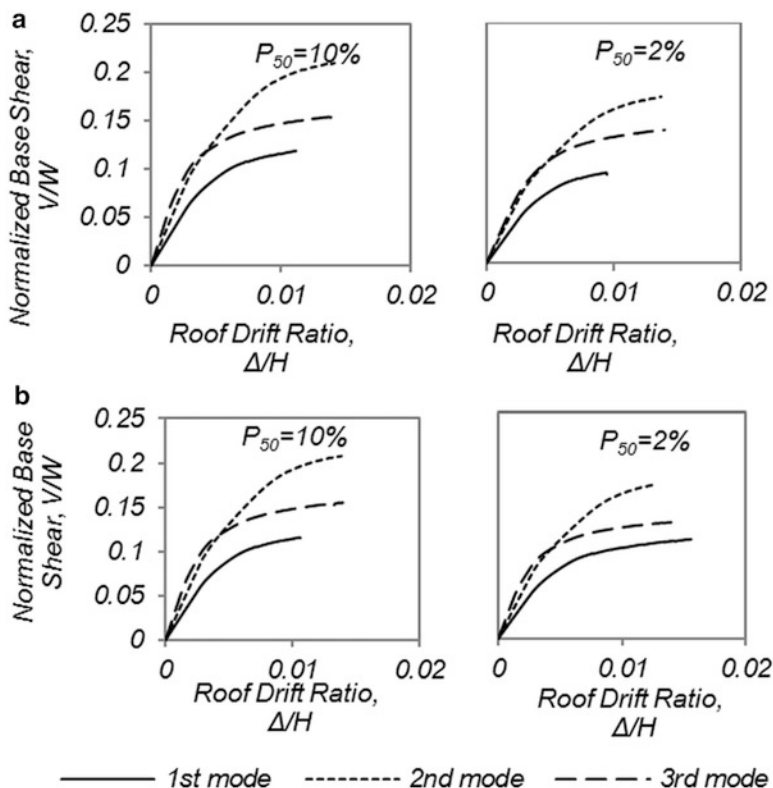
Fig. 11.4 Pushover curves of the second phase of IMPA: (**a**) X direction (**b**) Y direction

In IMPA procedure, due to the fact of being a double-run method, a second pushover curve, corresponding to each intensity and direction of ground motion, is obtained and shown in Fig. 11.4. This procedure is not performed for the second set of modes (modes 4–6) for the reason that the higher mode equivalent Single-degree-of-freedom (SDOF) systems do not have any contribution to the inelastic response when reaching the peak deformation in the first phase.

11.6.2 Number of Modes Required for MPA and IMPA

The number of modes selected has an important role in the accuracy of these methods. For that reason, MPA and IMPA were applied changing the number of modes considered: (i) only one set of modes was considered (Table 11.2) and; (ii) two sets of modes were adopted. Figure 11.5 shows how the accuracy of MPA results, in terms of displacements and internal forces, can be influenced by the number of modes considered.
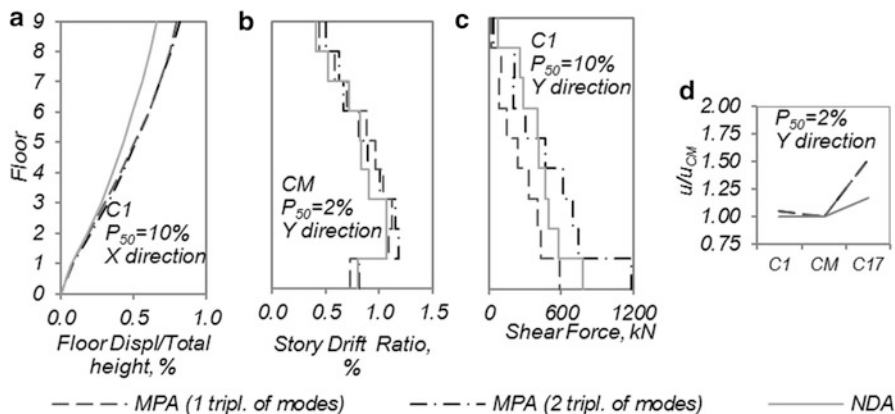
Fig. 11.5 (**a**) Lateral displacement profiles; (**b**) Interstorey drifts; (**c**) Shear forces; (**d**) Normalized top displacements

According to the results showed in Fig. 11.5, one can observe that, when considering only one set of modes, the interstorey drifts and mainly shear forces are underestimated. On the other hand, considering two sets of modes, MPA leads to conservative results.

11.6.3 Comparison Between NSPs and NDA

In this section, the seismic demands obtained through all NSPs applied are herein presented, wherein two sets of modes were considered for the multimode methods.

To study the behavior along the height of the building in both directions, lateral displacement profiles and interstorey drifts were obtained. Such results are respectively displayed in Figs. 11.6 and 11.7.

In Fig. 11.7 can be observed that all methods lead to adequate results in terms of lateral displacement profiles, being all of them slightly conservative. The accuracy shown in the results, regarding the multimode methods, is explained due to the fact that the higher modes were considered. Moreover, it is worth to mention that previous results obtained when adopting only the first set of modes for the MPA and IMPA led to less accurate results.

Extended N2 and ASCE/SEI 41-06 NSPs are generally the most conservative methods in terms of interstorey drifts.

The torsional behavior of the building was addressed through the analysis of a trend of normalized top displacements which are displayed in Fig. 11.8, and from its observation, can be stated that IMPA and MPA generally show accurate torsional behavior when compared with NDA.

With respect to Shear Forces, an extension of MPA, proposed by Reyes and Chopra (2011), based on imposing a set of displacements that are compatible with
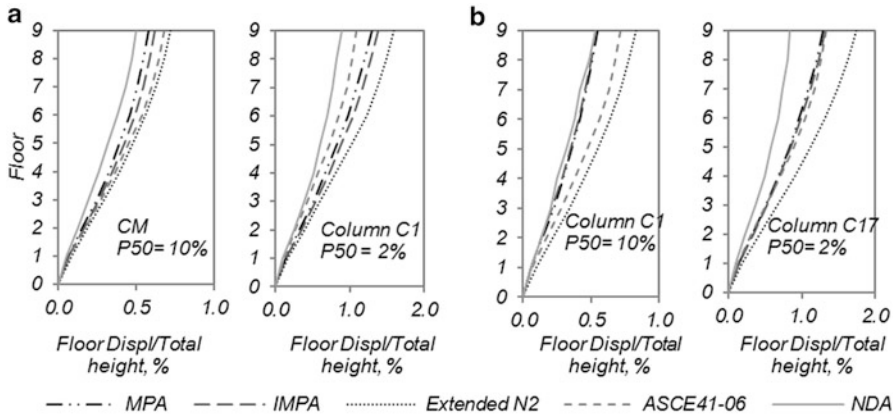
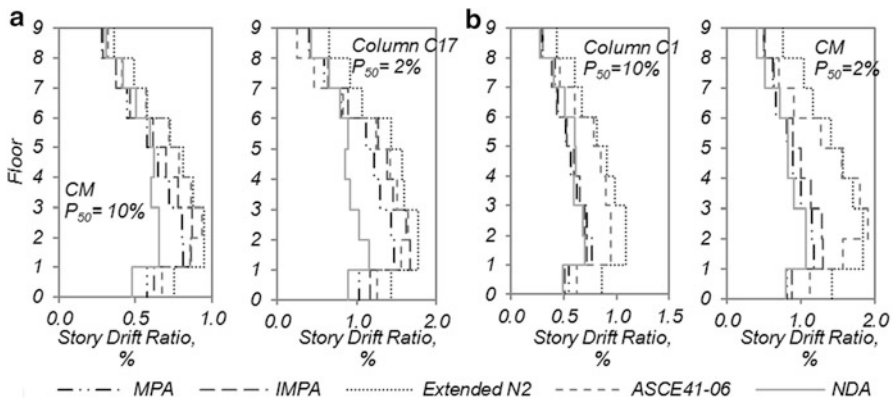**Fig. 11.6** Lateral displacement profiles: (**a**) X direction; (**b**) Y direction
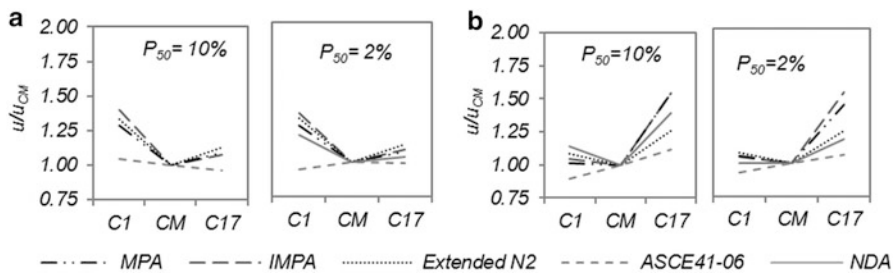

Fig. 11.7 Inter-storey drifts: (**a**) X direction; (**b**) Y direction

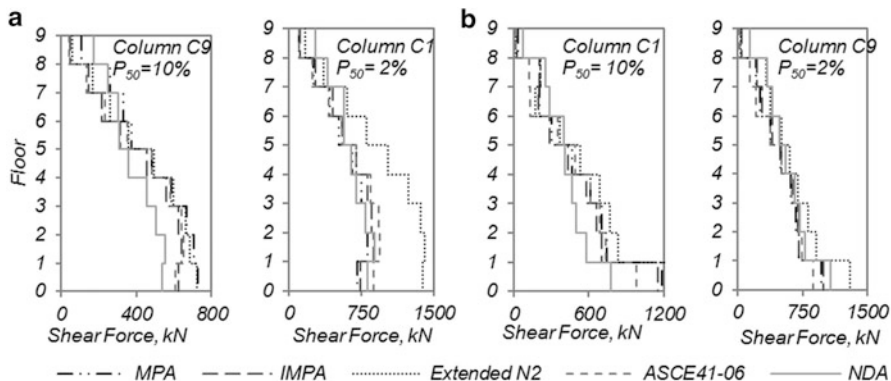**Fig. 11.8** Normalized *top* displacements: (**a**) X direction; (**b**) Y direction

Fig. 11.9 Shear forces: (**a**) X direction; (**b**) Y direction

the estimate of story drifts obtained, is applied in both multimode methods. In Fig. 11.9 the shear forces are displayed and a good match between all NSPs applied and NDA is observed.

11.7 Conclusions

In this paper, the seismic performance of an asymmetric plan building with nine stories is accessed by applying IMPA, which results obtained were evaluated and compared with the one evaluated by means of NDA. Comparisons with other current and well known NSPs as MPA, extended N2 and ASCE/SEI 41-06 NSP, were also performed. The individual performance of each one was additionally evaluated.

When compared with NDA while observing both methods, in a general view, one can conclude that there is a slight improvement with IMPA in relation to MPA when capturing torsional response of the building.

This set of results show a good match with NDA for all procedures.

Regarding to the multimode procedures, the fact of considering a greater number of modes, improved the results obtained with only one set. And it is notable that the higher modes consideration in the multi-mode procedures has an important role capturing the response of the 9-Storey building, mainly in terms of shear forces.

Regarding to the methods proposed (or extensions) in the Seismic Codes: the extended N2 captures with accuracy the torsional amplification in the buildings, contrasting with ASCE/SEI 41-06 NSP which does not capture the torsional amplification in the buildings, since it estimates linearly the response from one side of the building to the other.

Further investigation about the effectiveness of IMPA should be performed by applying the method to more buildings where the deformed shape changes substantially during pushover analysis.

References

ASCE (2000) American Society of Civil Engineers. Prestandard and commentary for the seismic rehabilitation of buildings, FEMA-356. Washington, DC

ASCE (2007) Seismic rehabilitation of existing buildings. ASCE/SEI 41-06, Reston

ATC (2005) Applied Technology Council. Improvement of nonlinear static seismic analysis procedures, FEMA440 report. Redwood City

Belejo A, Bento R (2015) Improvements in modal pushover analysis for the seismic assessment of asymmetric plan buildings. Version submitted to Soil Dynamics and Earthquake Engineering

CEN (2004) Comité Européen de Normalisation. Eurocode 8: design of structures for earthquake resistance. Part 1: general rules, seismic actions and rules for buildings. EN 1998-1:2004. Brussels

Chopra A, Goel R (2002) A modal pushover analysis procedure for estimating seismic demands for buildings. Earthq Eng Struct 31:561–582

Chopra A, Goel R (2004) A modal pushover analysis procedure to estimate seismic demands for asymmetric-plan buildings. Earthq Eng Struct Dyn 33:903–927

Fajfar P, Fischinger M (1988) N2—a method for non-linear seismic analysis of regular buildings. In: Proceedings of the 9th World conference in earthquake engineering Tokyo-Kyoto Japan 5: 111–116

FEMA (1997) Federal Emergency Management Agency. NEHRP guidelines for the seismic rehabilitation of buildings (FEMA 273). Washington, DC

Kottke A, Rathje E (2008) A semi-automated procedure for selecting and scaling recorded earthquake motions for dynamic analysis. Earthq Spectra 24(4):911–932

Kreslin M, Fajfar P (2012) The extended N2 method considering higher mode effects in both plan and elevation. Bull Earthq Eng 10:695–715

Paraskeva T, Kappos A (2010) Further development of a multimodal pushover analysis procedure for seismic assessment of bridges. Earthq Eng Struct Dyn 39(11):211–222

Reyes J (2009) Estimating seismic demands for performance-based engineering buildings. PhD dissertation, University of California, Berkeley

Reyes J, Chopra A (2011) Three-dimensional modal pushover analysis of buildings subjected to two components of ground motion, including its evaluation for tall buildings. Earthq Eng Struct Dyn 40:789–806

SeismoSoft (2006) SeismoStruct—a computer program for static and dynamic nonlinear analysis of framed structures. SeismoSoft Ltd, Pavia

Chapter 12
Seismic Assessment of an Existing Irregular RC Building According to Eurocode 8 Methods

Alessandra La Brusco, Valentine Mariani, Marco Tanganelli, Stefania Viti, and Mario De Stefano

Abstract The seismic assessment of existing buildings is an essential issue of seismic engineering. This work is focused on the evaluation of the seismic performance of existing RC buildings according to the current European Technical Codes. Alternative types of analyses, all consistent to the Code provisions, have been performed with reference to a case-study, that is a real, RC hospital building. An accurate knowledge of the building has been achieved, as a result of a collaboration between the University of Florence and the Regional Government. Both elastic and inelastic modeling, as well as static and dynamic one, have been adopted in the analysis. The global response – with special attention to torsional effects – and the seismic performance of each single member have been found with all the performed analyses. The comparison among the analyses has been performed in terms of both global and local response parameters, and the reliability of each analysis has been pointed out.

Keywords Seismic performance of existing buildings • Seismic analyses • Seismic assessment of RC structures

12.1 Introduction

The evaluation of the seismic performance of existing buildings is a crucial issue of seismic engineering. Due to its intrinsic complexity, the evaluation of seismic performance is affected by many uncertain factors even more in case of irregular buildings. Among these factors, special attention has to be paid to the intrinsic variability of the mechanical properties of materials, which can also become source of irregularity (De Stefano et al. 2013a, b, 2014a), and to the analytical procedure adopted in analysis

---

A. La Brusco (✉) • V. Mariani • M. Tanganelli • S. Viti • M. De Stefano
Department of Architecture (DiDA), University of Florence, Piazza Brunelleschi, 6, 50121 Florence, Italy
e-mail: alessandra.labrusco@unifi.it; valentina.mariani@unifi.it; marco.tanganelli@unifi.it; viti@unifi.it; mario.destefano@unifi.it

(De Luca et al. 2011; De Luca and Verderame 2011). The current European Technical Code, Eurocode 8 (EC8-3 2005), in fact, allows the designer to choose the type of analysis, according to some guidelines. It is well known that the choice about material behavior (linear or nonlinear) and type of performed analysis (static or dynamic) strongly affects the analytical reproduction of the seismic behavior of structures and, consequently, their performance prediction. In this framework, this work deals with the effects of the type of performed analysis on the seismic performance evaluation of existing buildings. The research is carried out with reference to a case-study, i.e. a real RC building, lightly irregular in plan, currently used as a hospital. The evaluation of its seismic performance is based on a wide knowledge process, that is the result of a joint agreement with the Regional Government of Tuscany.

In the first part of the paper the response of the case-study under a seismic excitation defined according to EC8 provisions has been found. Special attention has been paid to its torsional response. For slightly irregular structures, indeed, seismic codes allow to neglect torsional effects in the analysis, despite they can possibly induce not negligible amplifications in the seismic response.

In the second part of the paper the seismic performance has been evaluated according to EC8 provisions. Two different limit states, i.e. a serviceability (Damage Limitation, DL) and a ultimate one (Life Safety, LS), have been considered in the analysis. The results obtained for the seismic assessment of the case-study by performing three different types of analytical procedure are shown and compared.

12.2   Case Study

The building, having a RC skeleton, has been designed in 1976, i.e. just after the introduction of the first seismic Italian Technical Code. Therefore, the building presents some efficient design criterions, like column section reduction from foundation level to the top storey, or solid connection of the beam-column joints, although it is far away from complying the current seismic design criteria. The 3-storey building, shown in Fig. 12.1, has a regular (rectangular) plan, with one symmetric axis only.
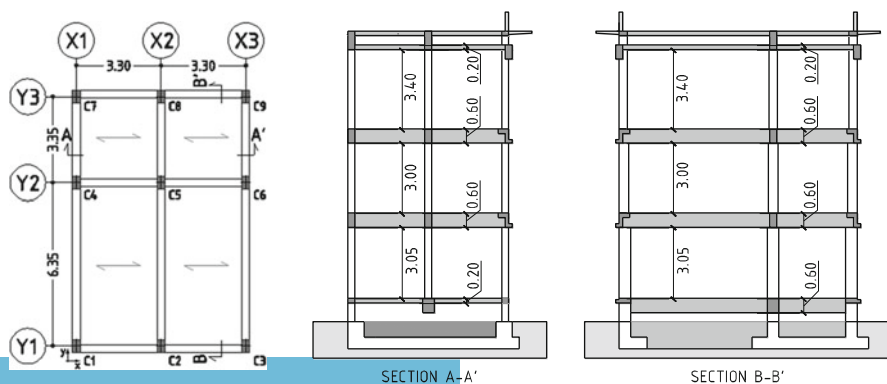

Fig. 12.1 Plan and sections (measures in meters)

Table 12.1 Cross section dimensions (in cm) of columns and beams

Columns				Beams				
Name	$b \times h$			Name	$b \times h$			
	1 st.	2 st.	3 st.		1 st.	2 st.	3 st, a	3 st, b
c_1–c_9	30×50	30×40	30×30	$x_{1,2}$ $x_{2,3}$ $x_{7,8}$ $x_{8,9}$ $y_{3,6}$ $y_{6,9}$	Z-shape		30×60	30×20
				$x_{4,5}$ $x_{5,6}$	30×60		30×80	30×20
				$y_{1,4}$, $y_{2,5}$, $y_{4,7}$; $y_{5,8}$	30×60		30×80	–

In Table 12.1 cross section dimensions of columns and beams are reported, while the area of the reinforcements is around 1 % of the cross section area. Details about number and type of rebars have been illustrated in De Stefano et al. (2014b). Some beams, having a Z-shape, have been modeled by means of a rectangular section with equivalent inertia. It should be noted that the third floor of the building consists of two different structural layers, partially coinciding. In fact two different floors, 40 cm far away each other, constitute the last storey of the building. In some alignments (X3, Y1 and Y3) two layers of beams separately support the two different floors, whilst in the other alignments (X1, X2 and Y2) a single beam supports both floors. Therefore the third floor and the related beams will be in the following distinguished with a subscript *a* or *b*, depending on weather they refer to the lower or upper layer respectively.

Mechanical properties of structural materials, i.e. concrete and steel, have been determined through destructive and not-destructive tests, according to the Italian Seismic Code provisions (NTC 2008). Three destructive tests on concrete have been performed on the columns, which have been integrated by other SonReb (sclerometric + ultrasonic methods) tests, extended even to the beams. The final compressive strength has been found by combining both destructive and SonReb results, by adopting an ad hoc *expression* (Cristofaro 2009; Cristofaro et al. 2012), which has provided a final cylindrical strength, $f_{c,mean}$ equal to 10.2 MPa. The global knowledge level achieved for the concrete structural elements has been conservatively evaluated as Knowledge Level 2 (*KL2*, $CF = 1.20$), according to EC8, associated to a Confidence Factor (*CF*) equal to 1.20, leading to a design (reduced) value of strength, f_{cd}, equal to 8.5 MPa.

Two different types of rebars, respectively ribbed and not, have been adopted for reinforcement. The reinforcement steel has been classified as FeB32K class, with a yield stress over 320 MPa and a ultimate stress over 500 MPa. Three destructive tests, one for each storey, have been done on rebars samples, according to the standard procedure (UNI EN ISO 6892 2009), returning a *mean* value, $f_{s,mean}$, equal to 385.7 MPa. Since a Knowledge Level *KL1* (*CF* equal to 1.35) has been assumed for steel, a design strength, f_{sd}, equal to 285.7 MPa has been used for analysis.

Ground mechanical properties have been determined through a geophysical site investigation, consisting in seismic refraction and down hole techniques. The results, processed using both Generalized Reciprocal Method and tomographic one, have an average shear wave velocity $V_{s,30}$ (Sirles and Viksne 1990) equal to 390 m/s. Therefore the soil has been assumed as B-type, according to NTC (2008).

12.3 Seismic Analysis

All analyses have been performed by using the computer code SAP2000 (2009). The two floors of the third level have been modeled according to the real geometry as regards the stiffness and strength distribution, while the mass (both translational and rotational) of the storey has been considered applied at the center of the storey package. The effect of the joint stiffness has been considered by introducing a rigid offset at each element end. A 50 % reduced value of the Young modulus ($E_{c,\ red} = 11{,}072$ MPa) of the concrete has been assumed, as suggested by NTC (2008). The floor stiffness has been introduced by assigning the diaphragm constraint to all nodes belonging to the same floor. Each member is modeled by an elastic finite element with terminal plastic hinges, whose properties have been defined by assigning a bi-linear moment-rotation relationship, defined by the yield and the ultimate points. Limit values of bending moment and rotation have been made according to EC8 prescriptions.

The expected maximum seismic intensity of the area, measured in terms of Peak Ground Acceleration (PGA), is provided by NTC, as well as the shape of the elastic spectrum of the case-study. To perform the dynamic analysis, two different sets of ground motions have been considered, whose average spectra closely approach the NTC (2008) one for the two considered limit states. They have been provided by Working Group Itaca (Itaca 2008), on the basis of a PGA equal to 0.25 g, a nominal life of the structure of 50 years and a magnitude between 5.5 and 6.5.

The ultimate capacity associated to LS limit state of each member is evaluated in terms of chord rotation or bending moment, depending on the type of performed analysis, for ductile mechanisms, and in terms of ultimate shear for brittle ones. Regarding the serviceability (DL) limit state, instead, a limit storey drift equal to 5‰ has been assumed.

The structural response of the case-study has been found by performing three different analyses, i.e. the linear pseudo-dynamic, the nonlinear static and the nonlinear dynamic ones. As regards the nonlinear static analysis, in recent years different improvements have been introduced (Fajfar et al. 2005; D'Ambrisi et al. 2009; Bhatt and Bento 2014) to account for structural irregularities. In the current work, anyway, the standard N2 method, as provided by EC8, has been applied.

The seismic behavior of the case-study has been described by checking both global and local response parameters. The considered global parameters are the Top Displacement (*TD*) and the torsional effects, measured as Normalized Top

Displacement (*NTD*), i.e. the top displacement at each column-line normalized to the one at the Mass Center (*MC*). The local response parameters are the ones provided by EC8 to define the seismic performance, depending on the performed analysis.

In the pseudo-dynamic linear analysis the seismic response of the case-study has been evaluated by considering the values of the spectral acceleration for the first five periods, found through a preliminary modal analysis, and then combining the consequent effects according to their participation factors. Twelve different analyses have been run for each direction, since the lateral force must be applied at MC with no eccentricity (e = 0) and with an eccentricity equal to ±5 %. In all cases the response must be combined to a quote, equal to 30 %, of the response in the orthogonal direction. The nonlinear static (pushover) analysis has been performed by considering two alternative heightwise horizontal patterns, respectively proportional to masses and to the first vibrational mode. For each pattern the two ways and a ±5 % eccentricity must be considered, with a total number of analyses equal to 12 for each direction. The nonlinear dynamic procedure consists of seven different analyses, one for each ground motion, for each direction. According to EC8 the seismic response to be considered is the maximum one for pseudo-dynamic and pushover analyses, and the *mean* one for the nonlinear dynamic analysis.

12.4   Seismic Response of the Case-Study

In order to quantify the in-plan irregularity, the eccentricity along the two main directions has been found in terms of mass, stiffness and strength. At each storey, the *MC* has been found by considering the mass of the floors and of the infill panels; the strength center has been found as a function of the concrete strength in the columns, while the center of stiffness has been determined by applying the simplified relationship proposed by Anagnastopoulos (Anagnastopoulos et al. 2013) and applied in De Stefano et al. (2015). In Table 12.2 the eccentricities between MC and the strength (e_{str}) and stiffness (e_{stiff}) centers are listed for each storey. It can be noted that, despite the building is structurally symmetric about the *Y*-direction, it has an irregular infill panels distribution, and therefore it presents an eccentricity in both directions.

Figure 12.2 shows the structural response obtained by performing the three types of analysis in terms of Top Displacement and total Base Shear. The capacity curves

Table 12.2 Strength and stiffness eccentricity at each storey

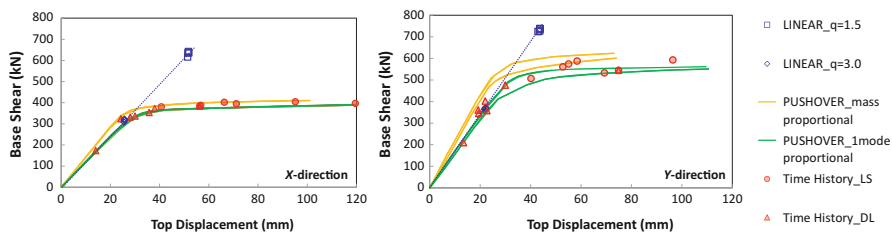| Level	X-direction		Y-direction	
	e_{str} (%)	e_{stiff} (%)	e_{str} (%)	e_{stiff} (%)
1st storey	9.00	10.71	3.33	2.23
2nd storey	7.48	9.41	5.61	5.00
3rd storey	6.08	7.95	0.76	3.17

Fig. 12.2 Seismic response of the case-study

found by performing the nonlinear static (pushover) analysis have been compared to the response found by performing the nonlinear dynamic analysis. For each ground motion, the maximum Base Shear and Top Displacement values have been extracted and reported as a point in Fig. 12.2. The nonlinear static and dynamic analyses gave consistent results, since the points fit very closely the capacity curves. The response found by performing the linear analyses refers to two different *q*-values, respectively assumed equal to 3.0 (ductile mechanisms) and equal to 1.5 (brittle mechanisms). The two families of points lye on the same line (the blue dashed line in Fig. 12.2), so evidencing the linearity of the response.

The elastic stiffness related to the elastic analysis coincides to the pushover one (first mode proportional). The families of capacity curves found by assuming the two different heighwise patterns slightly differ each other for elastic stiffness, shear and displacement capacity.

The torsional effects due to the in-plan irregularity has been checked by plotting the maximum Top Displacement at the *MC* and at each side of the case-study. Figure 12.3 shows the *NTD* at each side of the building for each considered limit state. As it was expectable, the torsional effects are larger in the serviceability limit state than in the ultimate one. The comparison of the torsional effects found by the three analysis types shows that the elastic analysis provides the larger effects in all cases. The two inelastic analyses provide similar results along the *X*-direction (larger eccentricity), while in the *Y*-direction the pushover analysis provides values of *NTD* much larger than the ones obtained by the dynamic analysis.

12.5   Seismic Performance of the Case-Study

In this section the seismic performance of the case-study has been checked according to EC8 prescriptions. The *DL* limit state has been checked in terms of maximum drift, by comparing the drift distribution provided by each analysis to the 5‰ limit imposed by EC8. Since the larger drifts occur at the flexible edge of the structure (De Stefano et al. 2014b, c), for sake of brevity in Fig. 12.4 only the drift values found at the flexible side have been shown. The dashed lines represent the maximum drift obtained by each analysis. The results provided by the linear analysis refer to a behavior factor equal to 3.0, since the maximum drift has to be
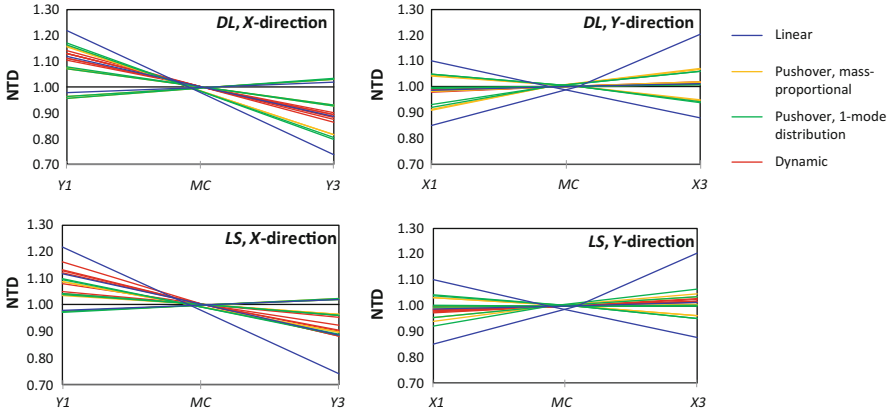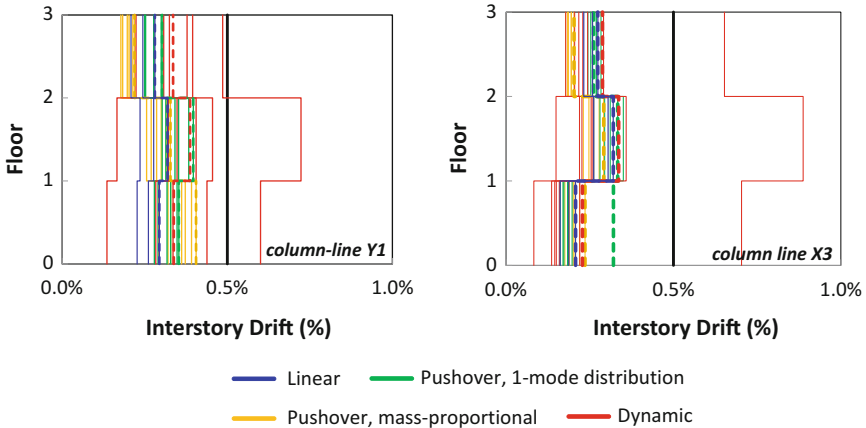
Fig. 12.3 Normalized top displacement

Fig. 12.4 Maximum drift at the flexible side of the structure at the *DL* limit state according to the three performed analyses

related to the flexural (ductile) behavior of the case-study. Concerning the nonlinear dynamic analysis, the maximum response is the *mean* value of the seven ground motions, according to EC8 prescriptions. It should be noted that the drift values provided by the dynamic analysis are very scattered, much more than the ones provided by the alternative methods.

The 5‰ limit provided by EC8 for the *DL* limit state is respected in all cases. The *LS* limit state has been studied by checking the ratio between the capacity (*C*) of each member (beams and columns) and the corresponding demand (*D*). The results found by performing each analysis are shown for the first storey only, where the maximum response has been found. In Figs. 12.5, 12.6, and 12.7 the C/D values exceeding the value of 5 have been shown with an arrow at the border of the figure.
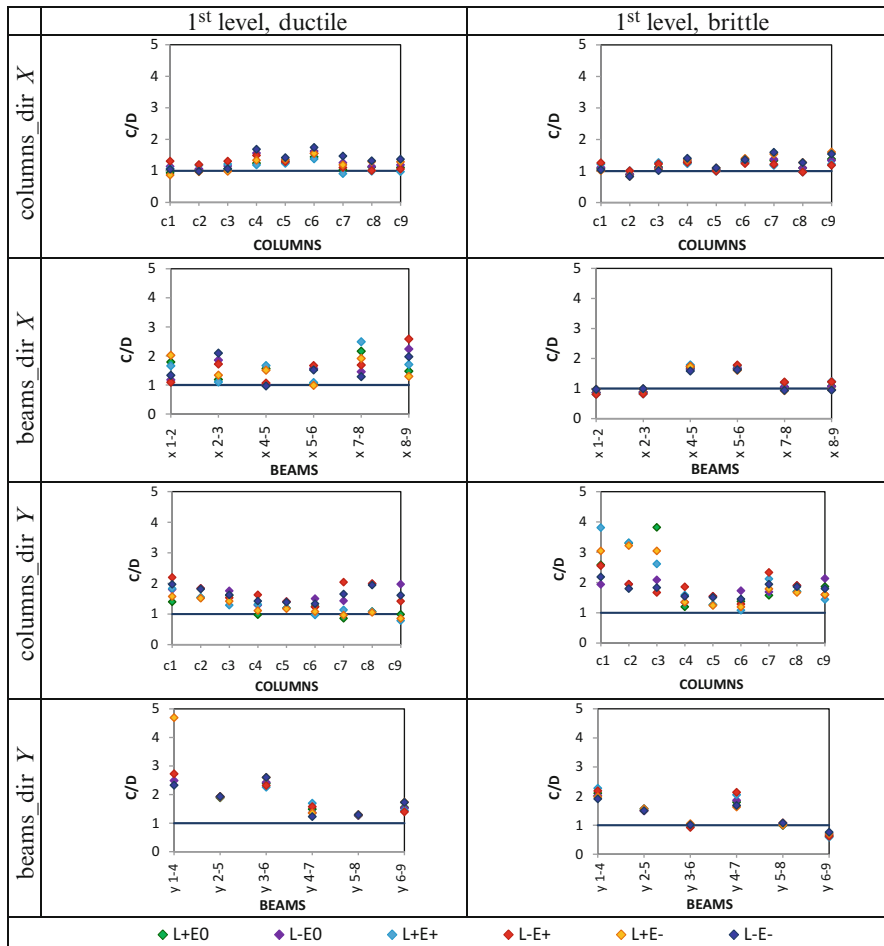
Fig. 12.5 Seismic performance of the first storey of the structure along the X and Y directions obtained by pseudo-dynamic linear analysis

Figure 12.5 shows the C/D values obtained by performing the pseudo-dynamic linear analysis for ductile and brittle mechanisms at the first storey beams and columns. It can be observed that some structural members exhibit C/D values lower than 1 both in the analyses along X and Y directions, not in compliance with the EC8 limit conditions; in particular the columns are more vulnerable to ductile failure, while beams to the brittle one.

Figure 12.6 shows the results obtained by non linear static analysis in terms of C/D values for each structural member. Once again it can be noted that the columns result more sensitive to flexural failure, whilst beams suffer more for shear failure, even if, in this case, only few beams (in the Y-direction) present C/D values lower than one.
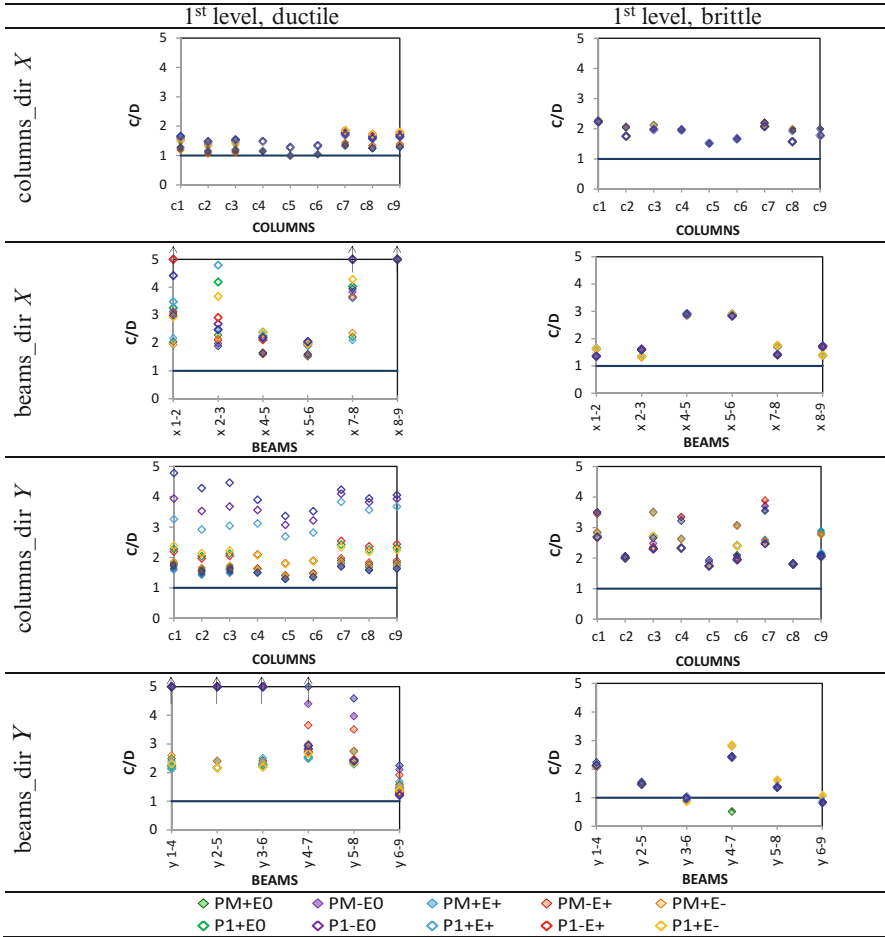
Fig. 12.6 Seismic performance of the first storey of the case study along the *X* and *Y*-directions obtained by nonlinear static analysis

Figure 12.7 shows the C/D values obtained by non linear dynamics analysis. In this case the results are very scattered, as a consequence of the influence of the seismic input on the response. Finally, Fig. 12.8 shows a comparison among the minimum values of seismic performance (ratio C/D) found by the performed analyses for columns (c) and beams (b) for brittle (brit) and ductile (duc) mechanisms respectively.

The linear analysis proves to be the most conservative, providing C/D values below the unity in many cases. The nonlinear analyses provide very similar results in some cases, as the brittle mechanism in columns, while they differ each other in the performance evaluation of beams. As it can be noted by diagrams in Fig. 12.8, the seismic performance found by performing the dynamic analysis satisfies the
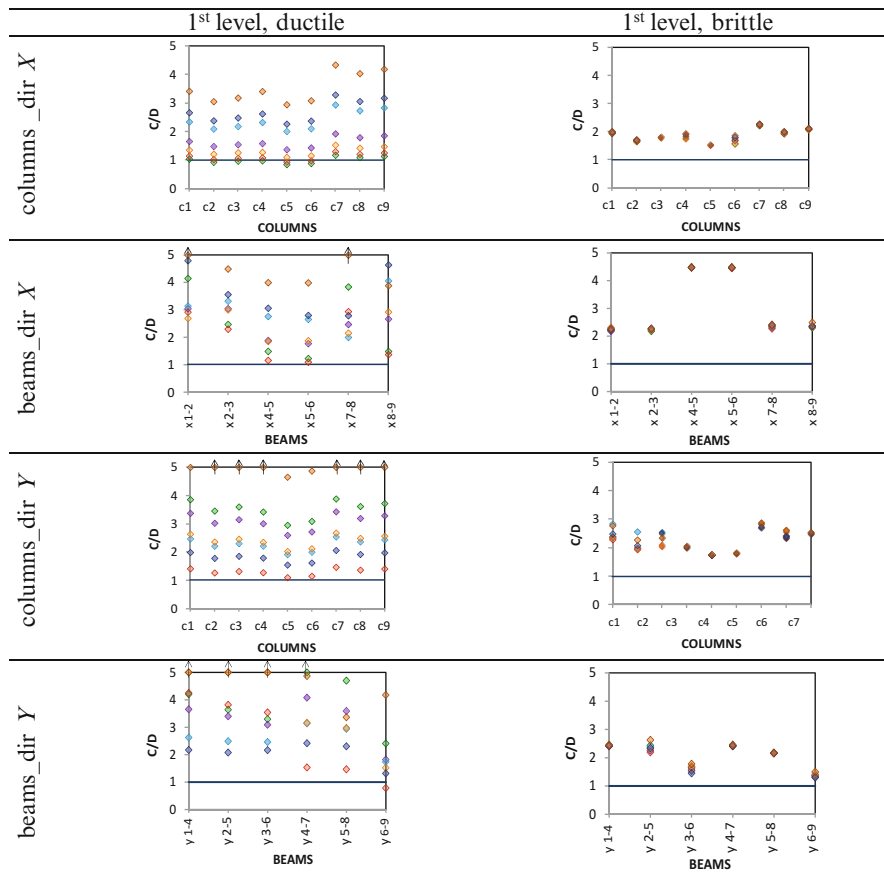
Fig. 12.7 Seismic performance of the first storey of the case study along the *X* and *Y*-directions obtained by nonlinear dynamic analysis
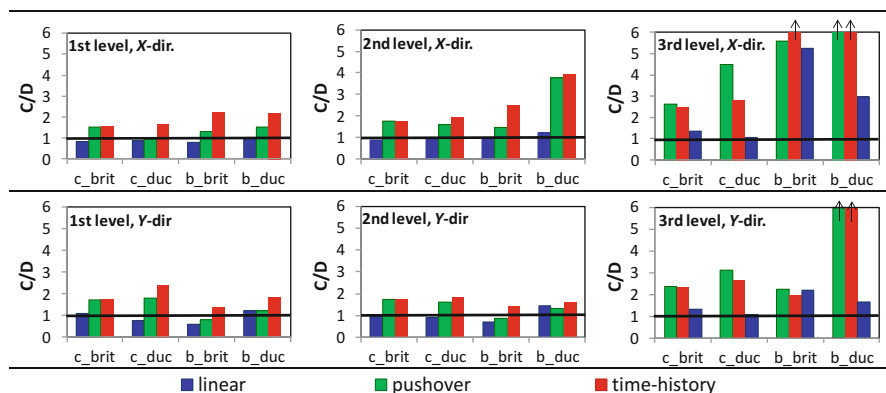

Fig. 12.8 Comparison among the performance level found by the performed analyses

EC8 requirements in all cases. When the nonlinear static analysis is performed, the brittle mechanism in the beams does not satisfy the EC8 limit conditions, while all the other requirements are respected.

12.6   Conclusive Remarks

In this work the seismic assessment of a real RC existing building has been carried out, by performing three different types of analysis, according to the current European Technical Code (EC8): the pseudo-dynamic elastic, the non-linear static and the nonlinear dynamic ones. The seismic response of the case-study has been investigated by checking both global and local response parameters. Concerning the global response of the building, *TD* and *NTD* have been checked. The nonlinear analyses provided similar results in terms of *TD*-Base Shear trends. Even the elastic analysis has approached very well the elastic results found by the nonlinear analysis, providing seismic responses (i.e. Base Shear and *TD*) which very much differ each other as a function of the assumed behavior factor, respectively equal to 1.5 (brittle mechanisms) and 3.0 (ductile mechanisms); all results, anyway, lie on the ideal axis representing the elastic response of the structure, coincident to the elastic branch of the pushover curves for horizontal forces proportional to the first mode of vibration.

The torsional response proved to be more sensitive to the type of performed analysis. As it was expectable, the torsional effects resulted larger in the serviceability limit state than in the ultimate one; the linear analysis provided larger top storey rotation than the other two analyses, in all cases. Along the *X*-direction, the one with a larger eccentricity, the two nonlinear analyses have exhibited similar results, while in the *Y*-direction the pushover analysis is more conservative than the dynamic one, since the 5 % eccentricity provided by EC8 largely covers the effective eccentricity. Concerning the serviceability limit state, the three analyses lead to similar results, providing a satisfactory response of the case-study. The seismic performance referred to the ultimate limit state, instead, has turned out to be more sensitive to the type of adopted analysis. The linear analysis resulted more conservative than the other ones, providing C/D values below the unity in many cases.

The two nonlinear analyses (pushover and dynamic) have provided very similar results in some cases, e.g. for the brittle mechanism in columns, while they differ each other in the performance evaluation of beams. Results obtained by the dynamic analysis satisfy all the EC8 requirements. When the nonlinear static analysis is adopted, instead, the brittle mechanism in the beams does not satisfy the EC8 limit values, while all the other requirements are fulfilled.

As a conclusion, the three analyses have evidenced important differences both in terms of global representation of the seismic response, including torsional effects, and in terms of local seismic performance according to the EC8 procedure. Despite

each analysis can be assumed to evaluate the seismic assessment of existing buildings, the choice of the analysis type can largely affect the final evaluation of the safety level of the building.

References

Anagnastopoulos SA, Kyrkos MT, Stathopoulos KG (2013) Earthquake induced torsion in buildings: critical review and state of art. Proc. ASEM13, Jeju Korea. Thecno-Press Journals

Bhatt C, Bento R (2014) The extended adaptive capacity spectrum method for the seismic assessment of plan asymmetric buildings. Earthq Spectra (in-press)

Cristofaro MT (2009) Metodi di valutazione della resistenza a compressione del calcestruzzo di strutture in c.a. esistenti, tesi di dottorato, Università degli Studi di Firenze (in Italian)

Cristofaro MT, D'Ambrisi A, De Stefano M, Pucinotti R, Tanganelli M (2012) Studio sulla dispersione dei valori di resistenza a compressione di edifici esistenti. Giornale Prove Non Distruttive Monitoraggio Diagnostica 2/2012:32–39, ISSN: 1721-7075 (in Italian)

D'Ambrisi A, De Stefano M, Tanganelli M (2009) Use of pushover analysis for predicting seismic response of irregular buildings: a case study. J Earthq Eng 13:1089–1100, Taylor & Francis

De Luca F, Verderame GM (2011) A practice-oriented approach for the assessment of brittle failures in existing reinforced concrete elements. Eng Struct 48:373–388

De Luca F, Verderame GM, Manfredi G (2011) La verifica di edifici esistenti in cemento armato: criticità dell'attuale approccio normativo italiano. 26° convegno nazionale AICAP, Padova 19–21 May 2011 (in Italian)

De Stefano M, Tanganelli M, Viti S (2013a) On the variability of concrete strength as a source of irregularity in elevation for existing RC buildings: a case study. Bull Earthq Eng 11(5): 1711–1726. doi:10.1007/s10518-013-9463-2, ISSN: 1573-1456

De Stefano M, Tanganelli M, Viti S (2013b) Effect of the variability in plan of concrete mechanical properties on the seismic response of existing RC framed structures. Bull Earthq Eng 11(4):1049–1060. doi:10.1007/s10518-012-9412-5, ISSN: 1573-1456

De Stefano M, Tanganelli M, Viti S (2014a) Variability in concrete mechanical properties as a source of in-plan irregularity for existing RC framed structures. Eng Struct Vol 59:161–172

De Stefano M, La Brusco A, Mariani V, Tanganelli M, Viti S (2014b) The role of structural modeling on the seismic assessment of existing RC buildings according to Eurocode 8. In: 2nd European conference on earthquake engineering and seismology. Istanbul, 25–29 Aug

De Stefano M, Tanganelli M, Viti S (2015) Torsional effects related to concrete strength variability in existing buildings: a numerical analysis. Earthq Struct 8(2):379–399

EC 8-3 (2005) Design of structures for earthquake resistance, part 3: strengthening and repair of buildings, European standard EN 1998-3. European Committee for Standardization (CEN), Brussels

Fajfar P, Marusic D, Perus I (2005) Torsional effects in the pushover-based seismic analysis of buildings. J Earthq Eng 9(6):831–854

Itaca (2008) Database of the Italian strong motions data. http://itaca.mi.ingv.it

NTC (2008) Norme tecniche per le costruzioni. D.M. Ministero Infrastrutture e Trasporti 14 gennaio 2008, G.U.R.I. 4 Febbraio 2008, Roma (in Italian)

SAP2000 Advanced 14.0.0, Structural analysis program (2009) Analysis reference manual. Computer and Structures, Berkley

Sirles C, Viksne A (1990) Site-specific shear wave velocity determinations for geotechnical engineering applications. In: Geotechnical and enviromental geophysics, vol. 3, Soc. Expl. Geophys. (Tulsa, Oklahoma), pp. 121-131

UNI EN ISO 6892-1 (2009) Materiali metallici – Prova di trazione – Parte 1: Metodo di prova a temperatura ambiente, International Organization for Standardization, Geneva

Chapter 13
The Concrete Strength Variability as Source of Irregularity for RC Existing Buildings

Stefania Viti, Marco Tanganelli, and Marco De Stefano

Abstract Existing buildings can easily present material mechanical properties which can largely vary even within a single structure. As a consequence of the high strength variability, at the occurrence of seismic events the structure may evidence unexpected phenomena, like torsional effects, with larger experienced deformations and, in turn, with reduced seismic performance. This work is focused on the reduction in seismic performance due to the concrete strength variability. The analysis has been performed on a case-study, i.e. a 3D RC framed 4 storey building. A normal distribution, compatible to a large database, has been taken to represent the concrete strength domain. Due to the introduced strength variability, a stiffness and strength eccentricity arises at the first storey of the structure, with a consequent increase in its seismic response. The capacity (C) of each column of the case study, found according to EC8 prescriptions, has been compared to the demand (D), for three different limit states. The seismic performance found by accounting for the strength variability has been compared to the one provided by the EC8 standard procedure, which has resulted to be conservative in the seismic response estimation and in the evaluation of the torsional effects, while it is not conservative in quantifying the seismic performance of the case-study.

Keywords Existing RC buildings • Concrete strength variability • Concrete mechanical properties • Seismic response of irregular structures • Torsional effects

13.1 Introduction

One of the most crucial technical issues of seismic engineering is the evaluation of the seismic safety of existing buildings, which involves a suitable characterization of actual material properties. Especially in RC buildings, the homogeneity of the material within each structure cannot be assumed, since the strength variability inside single buildings can result in *CoV* values over 30 % (Cristofaro 2009).

S. Viti (✉) • M. Tanganelli • M. De Stefano
Department of Architecture (DiDA), University of Florence, Piazza Brunelleschi, 6, 50121 Florence, Italy
e-mail: viti@unifi.it; marco.tanganelli@unifi.it; mario.destefano@unifi.it

Furthermore, an exhaustive characterization of the concrete mechanical properties is hard to achieve, since it would require a large number of destructive and not-destructive tests (Cristofaro et al. 2012).

International technical legislation provides different criteria to identify the required mechanical properties of concrete. The European technical Code, Eurocode 8 (EC8-3 2005) indicates the *mean* value of the strength domain for analysis, while it prescribes a reduced strength value (Franchin et al. 2007; Rajeev et al. 2010; Jalayer et al. 2008; Monti et al. 2007) for verification. The reduction is made by introducing a Confidence Factor (*CF*), ranging between 1.00 and 1.35 (Italian Annex) depending on the knowledge level of the structure. The safest approach provided by EC8, therefore, consists of evaluating the structural response by using the *mean* concrete strength, and to compare member forces and deformations to their limit values found by assuming a $CF = 1.35$. The amount of strength variability, as represented by *CoV*, does not affect anyway the analysis.

In this paper the concrete strength variability has been investigated on a case-study, i.e. a 4-storey RC building, as possible source of in-plan irregularity, and the torsional effects related to such irregularity have been evaluated. The concrete strength has been characterized on the base of a large database provided by the Regional Government of Tuscany (Cristofaro 2009). The strength variability has been introduced at the columns belonging to first storey only, while the other columns, as well as all the beams, are characterized by the *mean* value of the strength domain. This investigation follows some previous works made by the authors (De Stefano et al. 2013a, b, 2014) on a similar case-study, which have proved the strength variability to largely affect both the seismic demand and performance of existing buildings. In De Stefano et al. (2014) only two "extreme", very skewed, in-plan strength distributions have been considered. Therefore, only the largest possible effects related to the assumed strength variability have been found, while no information was found on the probability of occurrence of such effects. In this work, instead, a significant number (180) of different in-plan distributions have been considered, qualitatively representing all the possible combinations among the values of the strength domain. Depending on the considered in-plan strength distributions, different amounts of strength and stiffness eccentricity (Bosco et al. 2012, 2013) have been found. The maximum seismic demand erasing by the introduced eccentricity has been compared to the demand provided by EC8, assuming an accidental eccentricity of 5 %.

The capacity of each column, expressed in terms of chord rotation and shear force, has be determined with reference to three different limit states, both according to EC8 and as a function of the strength variability.

Finally, the performance of the case-study has been investigated by comparing capacity and demand in terms of chord rotation and shear force. While the chord rotation is the reference quantity for all limit states, the shear force has been considered only for the *Near Collapse* limit state. The comparison evidenced that EC8 approach for seismic performance evaluation, including the 5 % accidental eccentricity, does not cover the effects due to the considered strength variability.

13.2   The Analysis

The sample structure is a 4 story 3D reinforced concrete frame with two 4.5 m long bays in the *y*-direction and five bays 3.5 m long in the *x*-direction, as shown in Fig. 13.1. The building, designed for vertical loads only, is symmetric along both *x* and *y* directions. All the columns have a cross dimension of 30×30 cm while longitudinal beams have a dimension of 30×50 cm in both directions. Details of joints and reinforcements can be found in De Stefano et al. (2015a). A mean concrete strength (f_c), equal to 19.36 MPa, has been assumed, while the reinforcement is assumed to have the same mechanical properties as the Italian FeB38k steel (yield stress over 375 MPa, ultimate stress over 430 MPa). The strength variability has been introduced in the columns of the first storey only, by assuming a Normal distribution and three different levels of Coefficient of Variation (*CoV*), equal to 15 %, 30 % and 45 % respectively. Each strength domain is made by seven values, corresponding to different percentiles (5 %, 10 %, 20 %, 50 %, 80 %, 90 % and 95), which have been given to the 18 columns of the first storey in order to obtain the expected distribution; in each model the strength values are assorted according to the specifications listed in Fig. 13.1.

The first vibrational period of the case-study (see Table 13.1), corresponding to a translational vibration along the *y*-direction, is equal to 0.777 s. The analysis has been performed by considering one direction only for the seismic excitation, i.e. the *y*-direction. Therefore, the variability has been given along the *x*-direction.

Six groups of 30 schemes each have been considered, having the weakest position in each of the column lines of frame 2 (see Fig. 13.1). For each position of the weakest column, all the most significant strength combinations have been considered. In the assumption of the 180 layouts special attention has been paid to the "extreme" considered strength values, i.e. the values corresponding to the percentiles k05, k10, k90 and k95, that have been exhaustively combined. A more complete description of the models can be found in De Stefano et al. (2015a).

The analysis has been performed by using the computer code Seismostruct (Seismosoft 2006) and describing the cross sections through a fiber model, which has allowed to adopt different models for the concrete of the confined core (Mander et al.), the unconfined concrete of the cover (three-linear) and the reinforcement (bilinear). Contribution of floor slabs has been considered by introducing a rigid diaphragm.

The inelastic response of the case-study has been found by applying the standard N2 method, as provided by EC8. Three different limit states, i.e. Damage Limitation (*DL*), Severe Damage (*SD*) and Near Collapse (*NC*) have been considered. Each limit state has been associated to a single seismic intensity, with PGAs equal to 0.15 g, 0.20 g and 0.25 respectively. Such values of PGA been assumed on the basis of the highest seismicity occurring in Tuscany, i.e. the region where the investigation on the concrete strength (Cristofaro 2009) has been made.

The seismic input has been assumed to be represented by the elastic spectrum provided by EC8 for a soil-type *B*. Since in De Stefano et al. (2013a) has been found
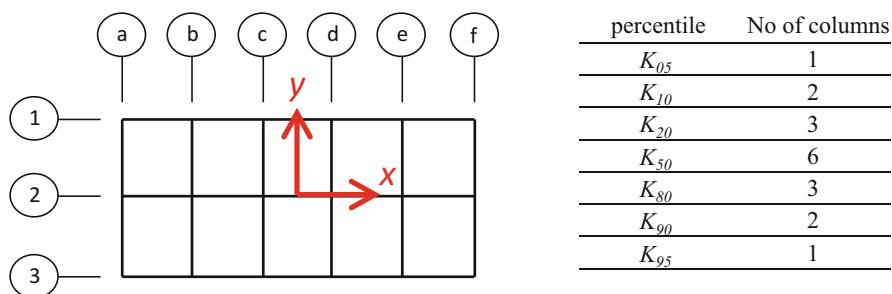
percentile	No of columns
K_{05}	1
K_{10}	2
K_{20}	3
K_{50}	6
K_{80}	3
K_{90}	2
K_{95}	1

Fig. 13.1 Case-study: plan configuration and f_c assumption at the first storey columns

Table 13.1 Periods and participating masses of the structure

	Period	Mode	Participating mass
1st period	0.777 s	Translational, y	87.42 %
2nd period	0.735 s	Translational, x	88.14 %
3rd period	0.694 s	Torsional, z	87.87 %

that the assumed horizontal pattern distribution does not significantly affect the results, in this work only one force pattern, proportional to the first vibration mode, has been considered.

## 13.3 The Introduced Eccentricity

Due to the introduced strength variability, each considered plan layout presents both a strength and a stiffness irregularity, since the Young modulus E_c is defined as a function of f_c (EC2 2002). Both strength and stiffness eccentricities have been found; the strength eccentricity, e_V, has been expressed in terms of the ultimate shear of the columns while the stiffness eccentricity, e_K, has been expressed through a simplified stiffness (K) expression (Anagnastopoulos et al. 2009), i.e. $K = (M_y H)/(6\theta_y)$. In Table 13.2 the ranges obtained for the two eccentricities are listed as a function of the assumed CoV.

Another quantity adopted to characterize the strength plan layout is the radius of gyration (Anagnastopoulos et al. 2013), which gives a measure of the strength centrifugation. Two radii of gyration have been found, i.e. based on the ultimate shear (ρ_V), and the simplified shear type behavior (ρ_K). Figure 13.2 reports their values, nondimensionalized with respect to the mass radius. Values of nondimensionalized radii of gyration, being larger than the unity, show that the building models can be classified as moderately torsionally stiff and strong.

Table 13.2 Ranges of eccentricities (e_K, e_V) due to the introduced strength variability

	$CoV = 15\ \%$		$CoV = 30\ \%$		$CoV = 45\ \%$	
	Min	Max	Min	Max	Min	Max
e_K	−1.7 %	1.7 %	−3.6 %	3.6 %	−6.1 %	+6.1 %
e_V	−0.6	+0.6 %	−1.4 %	+1.4 %	−2.8 %	+2.8 %

Fig. 13.2 Radius of gyration for the considered *CoV* strength
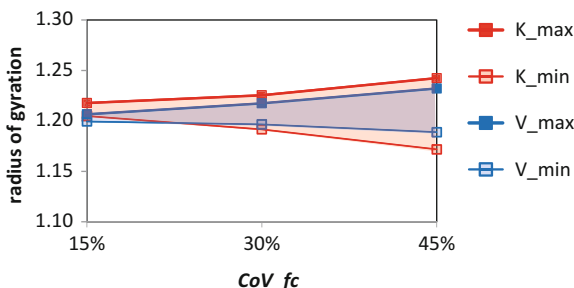
13.4   Results

The seismic response at the first storey of the case study has been studied in terms of maximum drift and shear force at each column. In Fig. 13.3 the results obtained from analysis and from EC8 standard approach, including the 5 % eccentricity, are shown for three different PGAs. Since the columns belonging to the frame 2 evidence an higher seismic response, only the results referred to such columns have been shown in this paper. A more exhaustive description of the results can be found in De Stefano et al. (2015b).

The variability in the drift response increases both with the seismic intensity and the strength variability as represented by *CoV*. Moreover, at the PGA increasing, the torsional effects arising from the introduced eccentricity increase as well, achieving their maximum amount at the side columns (column lines *a* and *f*). The structural demand provided by EC8, when the 5 % eccentricity is introduced, covers the increase in the side drift due to torsional effects. It should be reminded, anyway, that the 5 % eccentricity provided by EC8 is aimed to cover all the accidental irregularities and not the one related to the strength variability only. The shear response is not affected by torsional effects, despite it presents a large scatter due to the introduced strength variability.

Figures 13.4 and 13.5 show, in terms of chord rotation and shear force respectively, the capacity of the columns for the considered limit states. The limit values have been found by considering, for the concrete strength, both the assumed samples and the EC8 instructions. According to EC8, only one ultimate limit state, namely the *NC* one, has been considered for shear verification. The seismic performance is measured as the ratio between demand (D) and capacity (C). The seismic intensity to assume for each limit state has been selected according to the seismicity of Tuscany, since the concrete strength characterization refers to
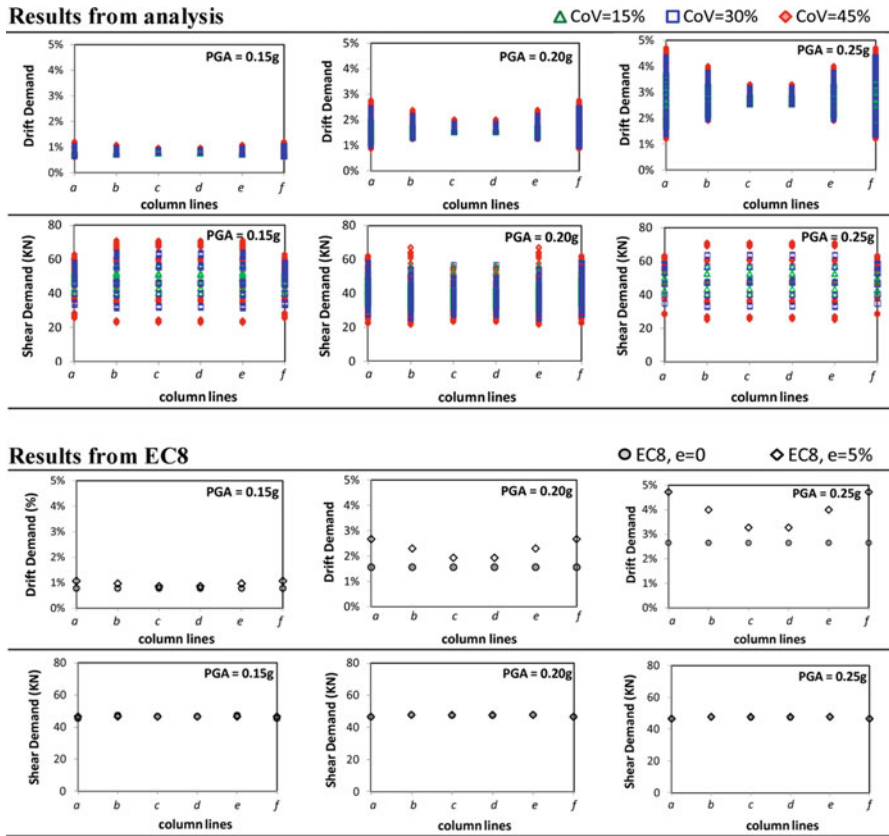
Fig. 13.3 Seismic demand (first storey, frame 2)

buildings of such area. When the ratio D/C is lower than unity the structure respects the limit provisions, while for values over unity the structure results to be not compatible with the safety requirements.

In Fig. 13.6 the obtained values of D/C are shown for the considered limit states. Both the D/C values obtained by considering the strength variability and the EC8 procedure, by accounting for the 5 % eccentricity and not, are shown for each column. It can be noted that the D/C ratio is sensitive both to PGA and *CoV*.

As regards the *DL* limit state, the seismic performance of the case-study has been evaluated for a PGA equal to 0.15 g. The ratio D/C found by considering the strength variability is below the unity only for *CoV* = 15 %. For higher *CoVs* the limit value is exceeded, approaching the value of 2 for *CoV* = 45 %. It should be noted that the EC8 approach provides D/C always below the unity if the 5 % eccentricity is not considered, while it achieves 1.25 when the eccentricity is taken into account.

The *SD* limit state has been associated to a PGA equal to 0.20 g. The performance limits are exceeded both when the EC8 approach is applied and when the
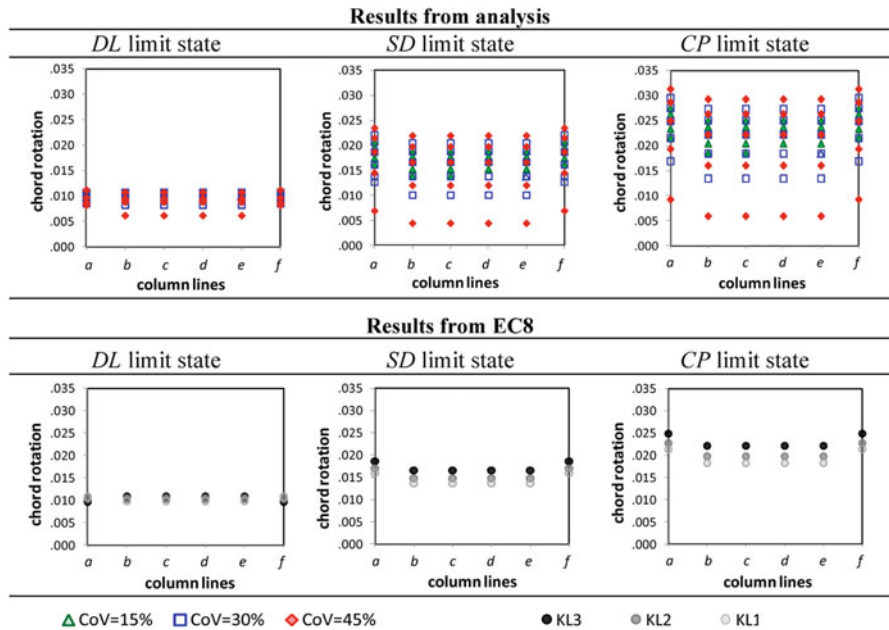
Fig. 13.4   Limit chord rotations (frame 2, first storey columns)
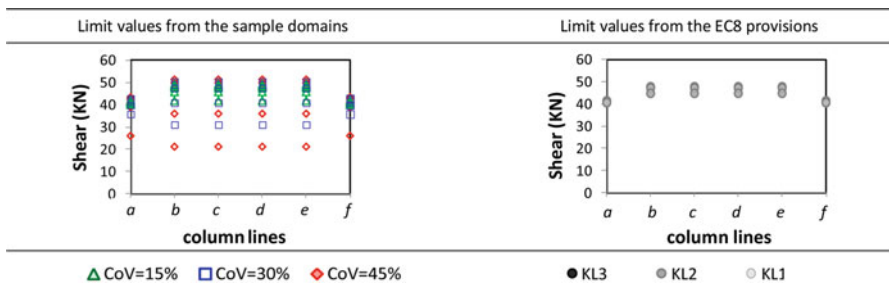

Fig. 13.5   Limit shear force (frame 2, first storey columns)

strength variability is introduced. It should be noted, anyway, that the maximum D/C value coming from the higher strength variability is 3.5 times higher than the corresponding value provided by EC8, even when the 5 % eccentricity is considered. Similar observations can be done for the *NC* limit state, associated to a PGA equal to 0.25 g.

The shear force, checked with reference to the *NC* limit state, is less sensitive to the strength variability than the chord rotation. At the increasing of the strength variability the obtained D/C ranges increase, but the final assessment of the building safety found from the analysis is similar to one provided by the EC8 approach. In all the considered limit states, the most conservative results provided by EC8,
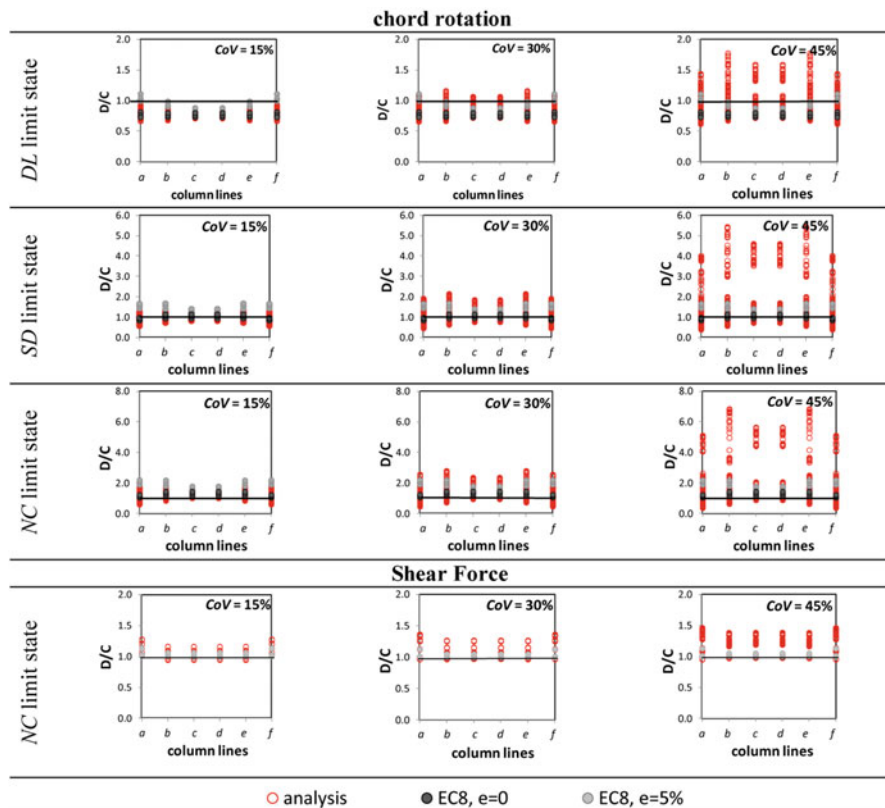
Fig. 13.6 Seismic performance of the first storey columns

i.e. obtained by assuming $KL = 3$ ($CF = 1.35$) and the 5 % eccentricity, are conservative, compared to the ones found by analysis, only for CoV below 30 %.

13.5   Conclusions

This work deals with the effects of the concrete strength variability on the seismic response of existing RC buildings. The concrete strength has been described through a 7-sample domain, having three different amounts of variability ($CoV = 15$ %, 30 %, 45 %), consistent with the experimental results found for existing building in Tuscan (Italy). 180 in-plan layouts, comprehending all the most significant strength combinations, have been considered to represent the strength distribution at the columns of the first storey. The effects of such variability have been evaluated in terms of induced eccentricity, seismic response and capacity and, therefore, in terms of seismic performance.

Due to the introduced strength variability, in fact, the building experiences both strength and stiffness eccentricity, and, consequently, a torsional response, with an increase in the demand. The increase in chord rotation is maximum at the building flexible side, with an increase of 50 % when a high PGA (PGA = 0.25 g) and CoV ($CoV = 45$ %), are considered. The shear force, instead, lightly increases at the stiffer side of the structure; such increase is scarcely sensitive to the considered PGA, while it is largely affected by the amount of the considered CoV; in fact, for $CoV = 45$ %, it achieves a maximum of 40 % for all considered PGAs.

The seismic demand found by considering the strength variability has been compared to the one provided by the standard EC8 approach, which has resulted to be conservative as regards the chord rotation, while it does not cover the increase in shear force. The seismic capacity of the first storey columns has been found, both considering the assumed strength variability and the conventional EC8 approach, for three considered limit states in terms of chord rotation and for the only CP limit state in terms of shear force. Finally, the ratio between demand (D) and capacity (C) of the case-study has been investigated. As regards the chord rotation performance, the comparison to the EC8 previsions shows different results depending on the considered limit states. For the serviceability limit state (DL), in fact, the EC8 evaluation provides similar results to those from the analysis. For a strength variability below 30 %, the maximum D/C values are close with the two approaches; when the highest value of CoV ($CoV = 45$ %) is considered, the analysis provides D/C values higher than the EC8 approach, but the final evaluation about the building safety does not change. When the ultimate limit states (SD, NC) are considered, instead, the analysis provides D/C values even three times larger than the EC8 previsions, with a consequent different evaluation of the performance. As regards EC8 previsions, the 5 % role introduced by EC8 to take into account of accidental eccentricity proved to be essential for response and performance evaluation, while the adoption of different CF values does not significantly affect the response and the performance of the case-study. When the seismic performance is evaluated in terms of shear force, the strength variability reduces the seismic performance of the structure, even if it does not affect the final evaluation of the performance acceptance of the case-study.

As a conclusion, the performed analysis proved the strength variability to be a significant source of in-plan irregularity for the case-study, affecting its seismic performance, and leading to an evaluation of its seismic assessment different from the one provided by the standard EC8 approach, even when all the most conservative assumptions have been considered (i.e. 5 % eccentricity and CF equal to 1.35).

References

Anagnastopoulos SA, Alexopoulou C, Kyrkos MT (2009) An answer to an important controversy and the need for caution when using simple models to predict inelastic earthquake response of buildings with torsion. Earthq Eng Struct Dyn 39:521–540

Anagnastopoulos SA, Kyrkos MT, Stathopoulos KG (2013) Earthquake induced torsion in buildings: critical review and state of art. Proc. ASEM13, Jeju

Bosco M, Ghersi A, Marino EM (2012) Corrective eccentricities for assessment by the nonlinear static method of 3D structures subjected to bidirectional ground motions. Earthq Eng Struct Dyn 41:1751–1773

Bosco M, Marino EM, Rossi PP (2013) An analytical method for the evaluation of the in-plan irregularity of non-regularly asymmetric buildings. Bull Earthq Eng 11:1423–1445

Cristofaro MT (2009) Metodi di valutazione della resistenza a compressione del calcestruzzo di strutture in c.a. esistenti. PhD Dissertation, Università di Firenze

Cristofaro MT, D'Ambrisi A, De Stefano M, Pucinotti R, Tanganelli M (2012) Studio sulla dispersione dei valori di resistenza a compressione del calcestruzzo di edifici esistenti. Il giornale delle prove non distruttive, monitoraggio, diagnostica., vol. 2/2012, pp. 32–39, ISSN: 1721-7075

De Stefano M, Tanganelli M, Viti S (2013a) Effect of the variability in plan of concrete mechanical properties on the seismic response of existing RC framed structures. Bull Earthq Eng. doi:10.1007/s10518-012-9412-5

De Stefano M, Tanganelli M, Viti S (2013b) On the variability of concrete strength as a source of irregularity in elevation for existing RC buildings: a case study. Bull Earthq Eng. doi:10.1007/s10518-013-9463-2

De Stefano M, Tanganelli M, Viti S (2014) Variability in concrete mechanical properties as a source of in-plan irregularity for existing RC framed structures. Eng Struct. doi:10.1016/j.engstruct.2013.10.027

De Stefano M, Tanganelli M, Viti S (2015a) Torsional effects due to concrete strength variability in existing buildings. Earthq Struct 8(2):379–399

De Stefano M, Tanganelli M, Viti S (2015b) Seismic performance sensitivity to concrete strength variability: a case-study. Earthq Struct 9(2):321–337

EC 2 (2002) Eurocode 2: design of concrete structures. European Committee for Standardization (CEN), Brussels

EC 8–3 (2005) Design of structures for earthquake resistance, part 3: strengthening and repair of buildings, European standard EN 1998-3. European Committee for Standardization (CEN), Brussels

Franchin P, Pinto PE, Rajeev P (2007) Confidence factor? J Earthq Eng 14(7):989–1007

Jalayer F, Iervolino I, Manfredi G (2008) Structural modeling: uncertainties and their influence on seismic assessment of existing RC structures. Struct Saf 32:220–228

Monti G, Alessandri S, Goretti A (2007) Livelli di conoscenza e fattori di confidenza. XII Convegno ANIDIS, L'ingegneria sismica in Italia. Pisa 10–14 Giugno 2007

Rajeev P, Franchin P, Pinto PE (2010) Review of confidence factor in EC8-Part 3: a European Code for Seismic Assessment of Existing Buildings, International Conference on Sustainable Built Environment ICSBE 2010, Kandy

Seismosoft (2006) Seismostruct version 5.2.2 – a computer program for static and dynamic nonlinear analysis of framed structures. Available online from URL: www.seismosoft.com

Chapter 14
The Influence of Axial Load Variation on the Seismic Performance of RC Buildings

Valentine Mariani, Marco Tanganelli, Stefania Viti, and Mario De Stefano

Abstract It is well known that the axial load can largely vary during a seismic event, playing an important role in the seismic performance of RC columns. In existing buildings this problem can be even more significant than in new ones, since the material can easily present poor mechanical properties. The paper is aimed at investigating the role of the axial load variation on the seismic capacity of RC columns, evaluated in terms of limit chord rotation and shear force, according to Eurocode 8. The research is performed with reference to a case-study, which is a doubly symmetric 4-storey RC framed building. The axial load variation affects both the seismic response and the capacity of the columns of the case-study, and, therefore, their seismic performance. Special attention has been paid to the role of the effective concrete strength of columns on the sensitivity of the seismic performance to the axial load variation.

Keywords Axial load variability • RC framed structures • Seismic assessment • Concrete mechanical properties • Seismic performance of existing RC buildings

14.1 Introduction

It's common knowledge that the axial load, N, plays an important role in the evaluation of the structural performance of RC columns (Abbasnia et al. 2011; Saadeghvaziri 1997). The axial load, indeed, largely affects both the seismic demand and capacity of RC buildings. Concerning the seismic demand, when the structure is subjected to a horizontal loading, e.g. a seismic action, it necessary experiences an axial load variation in its vertical elements. At the occurring of severe ground motion, in particular, some columns can be subjected to significant axial load reduction, experiencing in extreme cases traction, or conversely, they can experience a large increase in compression. Even the capacity is affected by the

V. Mariani (✉) • M. Tanganelli • S. Viti • M. De Stefano
Department of Architecture (DiDA), University of Florence, Piazza Brunelleschi, 6, 50121 Florence, Italy
e-mail: valentina.mariani@unifi.it; marco.tanganelli@unifi.it; viti@unifi.it; mario.destefano@unifi.it

axial load. For axial load higher than the "balanced" value, in fact, the ultimate bending moment progressively decreases. If the section is subjected to traction, its flexural and shear capacity is largely reduced, as well as when the section is subjected to high levels of compression. The seismic performance, being the ratio between demand (D) and capacity (C), should therefore be carefully checked taking into account the axial load variation, while the current European Technical Code (Eurocode 8, EC8), prescribes to define the capacity of the structural sections referring to the static axial load only. Furthermore, in existing buildings the sensitivity of the seismic performance to axial load variation can be even more significant than in new ones, since the material can easily present poor and uncertain mechanical properties (Cristofaro 2009; Cristofaro et al. 2012). This paper is aimed at investigating the role of the axial load variation on the seismic performance of an RC case-study building. Two different limit states, respectively a serviceability (Damage Limitation, LD) one and an ultimate (Severe Damage, SD) one, have been considered, and the chord rotation has been assumed, in both cases, as control parameter. The case-study is a doubly symmetric 4-storey RC building, designed to vertical load only, representing a typical example of pre-seismic code structure. The role of the axial load variation has been investigated in terms of seismic performance with special attention to the role of the effective strength of the columns concrete.

14.2   The Case-Study

The sample structure (De Stefano et al. 2015) is a 4-storey 3D reinforced concrete frame, symmetric along both x and y directions, with two 4.5 m long bays in the y-direction and 5 bays 3.5 m long in the x-direction, as shown in Fig. 14.1. All the columns have cross section dimensions of 30×30 cm, with 8 $\phi14$ rebars as longitudinal reinforcement and $\phi6$ stirrups with a spacing of 20 cm. Longitudinal beams have constant cross section dimensions of 30×50 cm in both directions.

The concrete has been assumed to have a *mean* strength equal to 19.36 MPa, while for the reinforcement the Italian FeB38k steel (yield stress over 375 MPa,
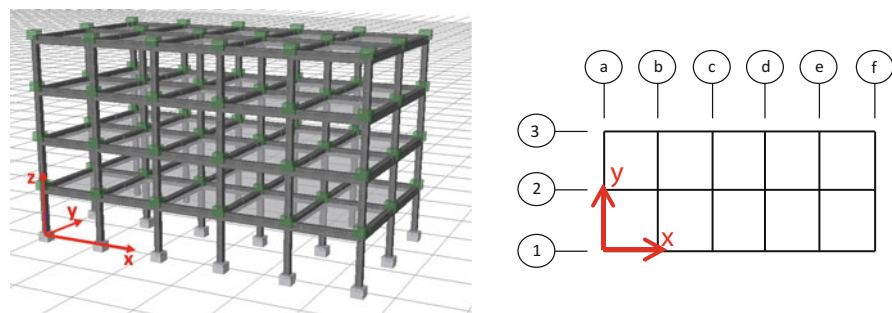

Fig. 14.1 Case-study: 3D view and plan configuration

ultimate stress over 430 MPa) has been assumed. The building is designed for vertical loads only (dead load equal to 5.9 KN/m^2, live load equal to 2.0 KN/m^2), ignoring seismic loads.

14.3 The Analysis

A nonlinear dynamic (time-history) analysis has been performed by using the computer code Seismostruct (Seismosoft 2006). A two-dimensional fiber model has been adopted for the cross sections. Each member (both columns and beams) has been described through an inelastic frame element, and a displacement-based approach has been selected for the analytical solution. In order to overcome the nonlinearity related to high amount of deformation, each member has been subdivided into four segments. The Mander et al. model (Mander et al. 1988) has been assumed for the core concrete, a three-linear model has been assumed for the unconfined concrete, and a bilinear model has been assumed for the reinforcement steel. The stiffness of floor slabs has been considered by introducing a rigid diaphragm.

The seismic input has been defined by assuming a set of seven ground motions whose mean spectrum closely fits the elastic one provided by EC8 for a soil-type B. The records were provided by Working Group Itaca (Itaca 2008), on the basis of a PGA equal to 0.25 g, a nominal life of the structure of 50 years and a magnitude between 5.5 and 6.5. Two different limit states have been considered: the *Damage Limitation* (*DL*) and the *Severe Damage* (*SD*) limit states. According to EC8 provision, a limit value equal to the yield chord rotation has been assumed for the *DL* limit state, while a limit value based on the ultimate rotation has been considered for the *LS* limit state. Both (*DL* and *SD*) limit values depend on the amount of axial load in the member. The concrete characterization, exhaustively explained in De Stefano et al. (2013a, b, 2014a) and applied in De Stefano et al. (2014b, 2015) on the same case-study, is based on a large database of experimental values of compressive strength (Cristofaro 2009); a single *mean* strength, equal to 19.36 MPa, and three different *CoV*, respectively equal to 15 %, 30 % and 45 % have been considered in the analysis. For each *CoV*, the concrete distribution has been represented by a sample of seven concrete strength values, corresponding to the percentiles of 5 %, 10 %, 20 %, 50 %, 80 %, 90 % and 95 % respectively.

14.4 Results

14.4.1 Response Sensitivity to the Axial Load Variation

The maximum and minimum axial load experienced by the case-study after the assumed set of ground motions have been checked for each frame and column line. Figure 14.2 shows the axial load variation, normalized to the value of the
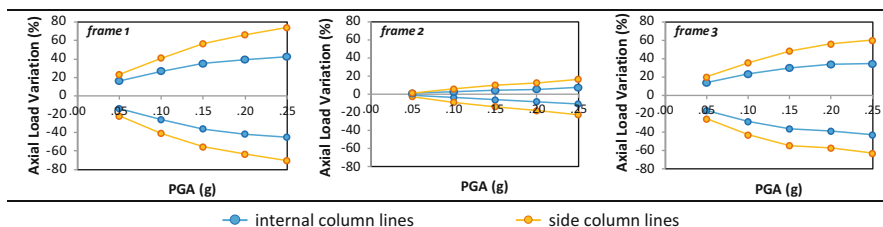
Fig. 14.2 Axial load variation in each frame of the case-study

corresponding static axial load, experienced by each column for the different considered PGAs. Since in each frame, the internal columns (column lines *b*, *c*, *d* and *e*) and the side ones (column lines *a* and *f*) experience almost the same axial load variation (De Stefano et al. 2014b), in Fig. 14.2 only two different trends have been shown, referred to the side and internal columns. The axial load variation affects more the side frames (frame 1 and 3) than the central one, since the frame 2 supports a larger amount of gravity loads. It should be noted that, despite the building is symmetric along both main axes, the axial load variation is not the same in the two side frames (frames 1 and 3); besides, in each frame, the increase and the reduction in axial load are not exactly the same.

14.4.2 Capacity Sensitivity to the Axial Load Variation

The structural capacity of existing structure in terms of ductile mechanisms is measured with reference to chord rotation. Figure 14.3 shows the capacity, in terms of chord rotation, for *DL* and *SD* limit states as a function of *N*. The limit chord rotations been found according to EC8, assuming the yield chord rotation for the *DL* limit state an ¾ of the ultimate chord rotation for the *SD* limit state. In each graph, the gray area represents the range of capacities provided by EC8, which defines the design compressive strength as the mean one reduced by the Confidence Factor CF (equal to 1.00, 1.20 and 1.35 with relation to the acheived knowledge level). As can be noted, the range of capacities provided by EC8 is smaller than the one obtained when the strength variability is considered, even for the lowest assumed *CoV* (*CoV* = 15 %). For higher values of *CoV*, more likely to be found in existing buildings (De Stefano et al. 2013a,b, 2014a), the difference between the two ranges is even larger.

14.4.3 Seismic Performance Sensitivity to the Axial Load Variation

Figures 14.4 and 14.5 show, for all the considered PGAs, the ratio between demand (D) and capacity (C), defined by considering the different strength values provided
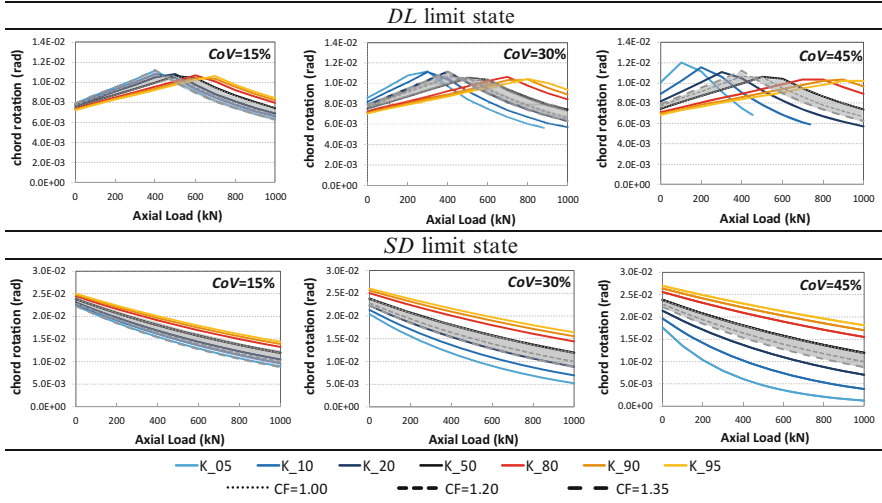
Fig. 14.3 Chord rotation for the *DL* and *SD* limit states on varying of axial load

by the domains of Fig. 14.3. For sake of brevity, results are shown for a side column and a internal one, for each frame. İn the performance evaluation the capacity has been found with reference to both the limit values of axial load (i.e. minimum and maximum) experienced by each column due to the seismic excitation; therefore, for each PGA value, the range in D/C is shown as a function of the axial load. İn Figs. 14.4 and 14.5 the results obtained for the 50 % percentile can be assumed as representative of the EC8 approach for the Knowledge Level 3 (CF = 1.00).

As can be noted, the seismic performance of the structure is very much affected by the assumed strength values, with a large increase in D/C when low percentiles (K_{05}, K_{10}) have been considered together with high *CoV*s. As regards the *DL* limit state, the case-study complies the EC8 requirements in most of the cases, for PGAs below 0.15 g, i.e. for all the seismic intensities consistent to the limit state. As regards the *SD* limit state, the assumed performance index shows to be very sensitive to the concrete strength characterization. When a low strength variability is considered (*CoV* = 15 %), in fact, the scatter in D/C is almost the same with the seven considered percentiles. On the contrary, for higher values of *CoV*, reliable with concrete strength distribution typical of real existing buildings, the scatter in D/C due to the axial load variation is very large, suggesting a significant correlation between the sensitivity to axial load and the effective strength of the column.

Figures 14.6 and 14.7 show, for the DL and SD limit states, the normalized variation ranges found by comparing each range of seismic performance to the one found by assuming the corresponding static axial load. The trend of the curves families confirms the observation made for the previous figures, i.e. the effects of the axial load variation on the seismic performance are very sensitive to the
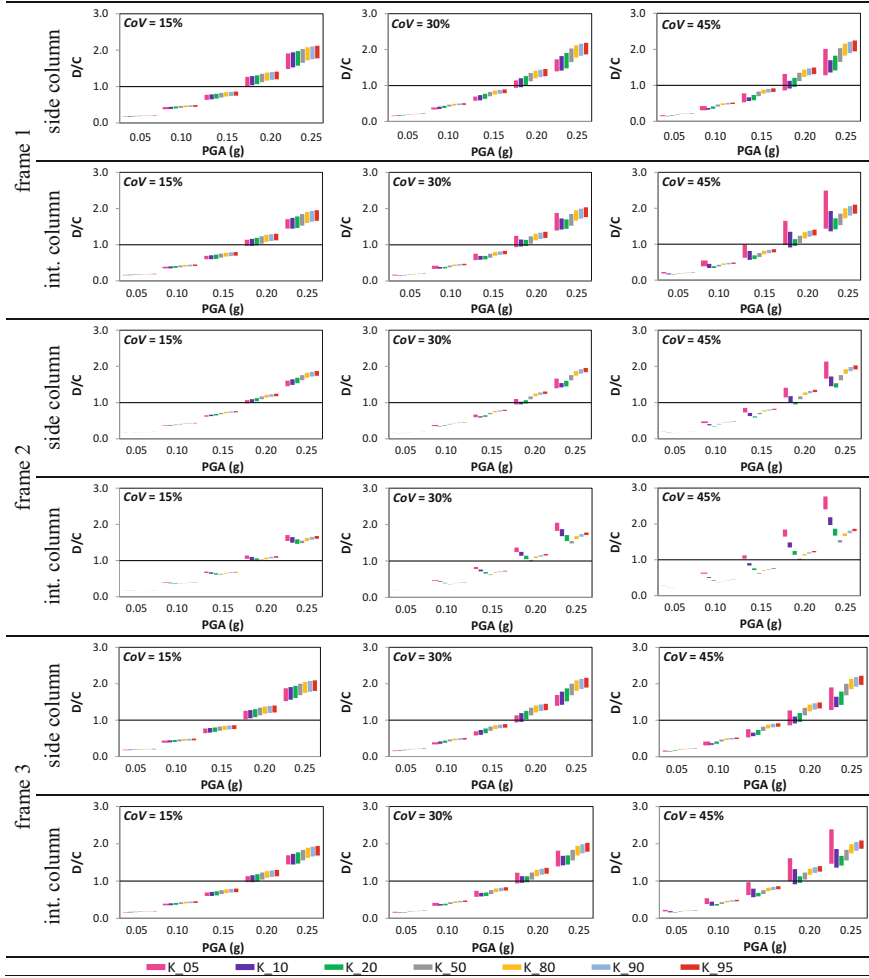
Fig. 14.4 Seismic performance: *DL* limit state

assumed concrete strength, especially for strong ground motions (high values of PGA).

14.5   Conclusions

In this paper the effects of the axial load variation on the seismic performance of RC structures have been investigated with reference to a case-study, i.e. a 4-storey RC framed building.
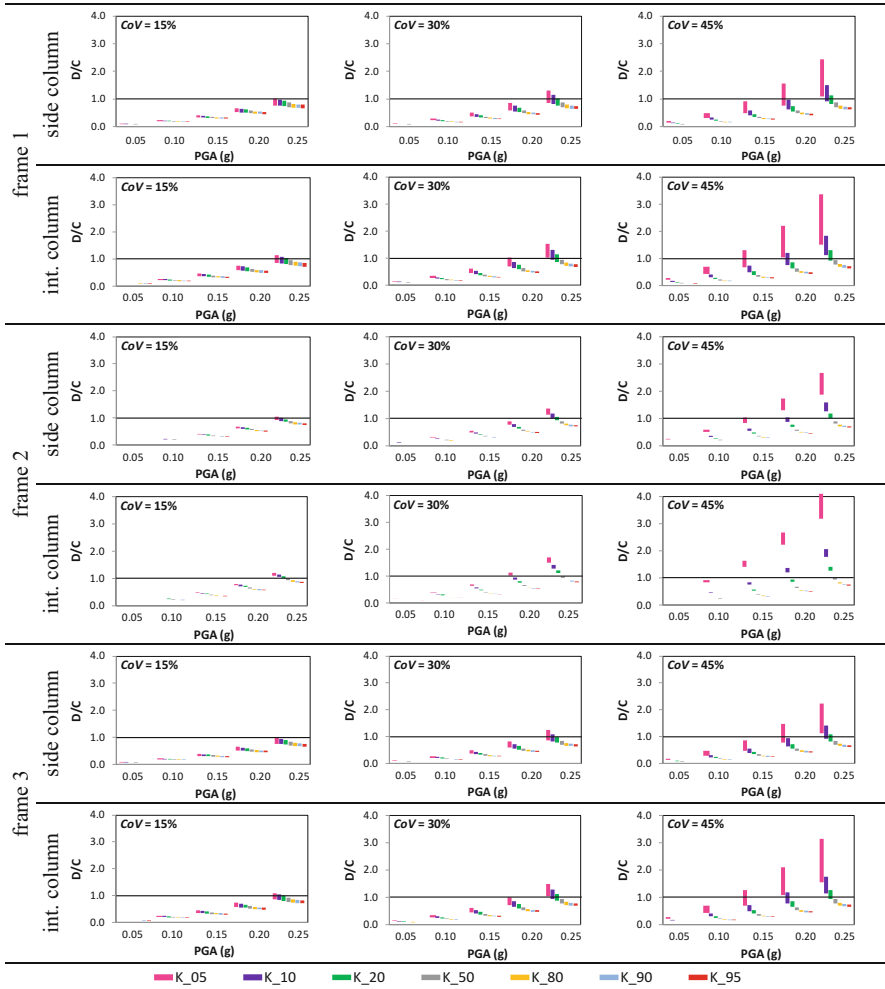
Fig. 14.5 Seismic performance: *SD* limit state (chord rotation)

The seismic performance, i.e. the ratio between demand (D) and capacity (C), has been evaluated for the columns of the first storey by considering (i) the current axial load in the columns which varies during the analysis and (ii) the static value associated to the vertical loads, according to the current practice and to the technical codes. Special attention has been paid to the role of the effective concrete strength of columns, which has been described through a Gaussian distribution, with a *mean* equal to 19.36 MPa and three different values of *Coefficient of Variation*. Each strength domain has been represented by seven values, corresponding to the percentiles of 5, 10, 20, 50, 80, 90 and 95 %. The assumed strength domains have
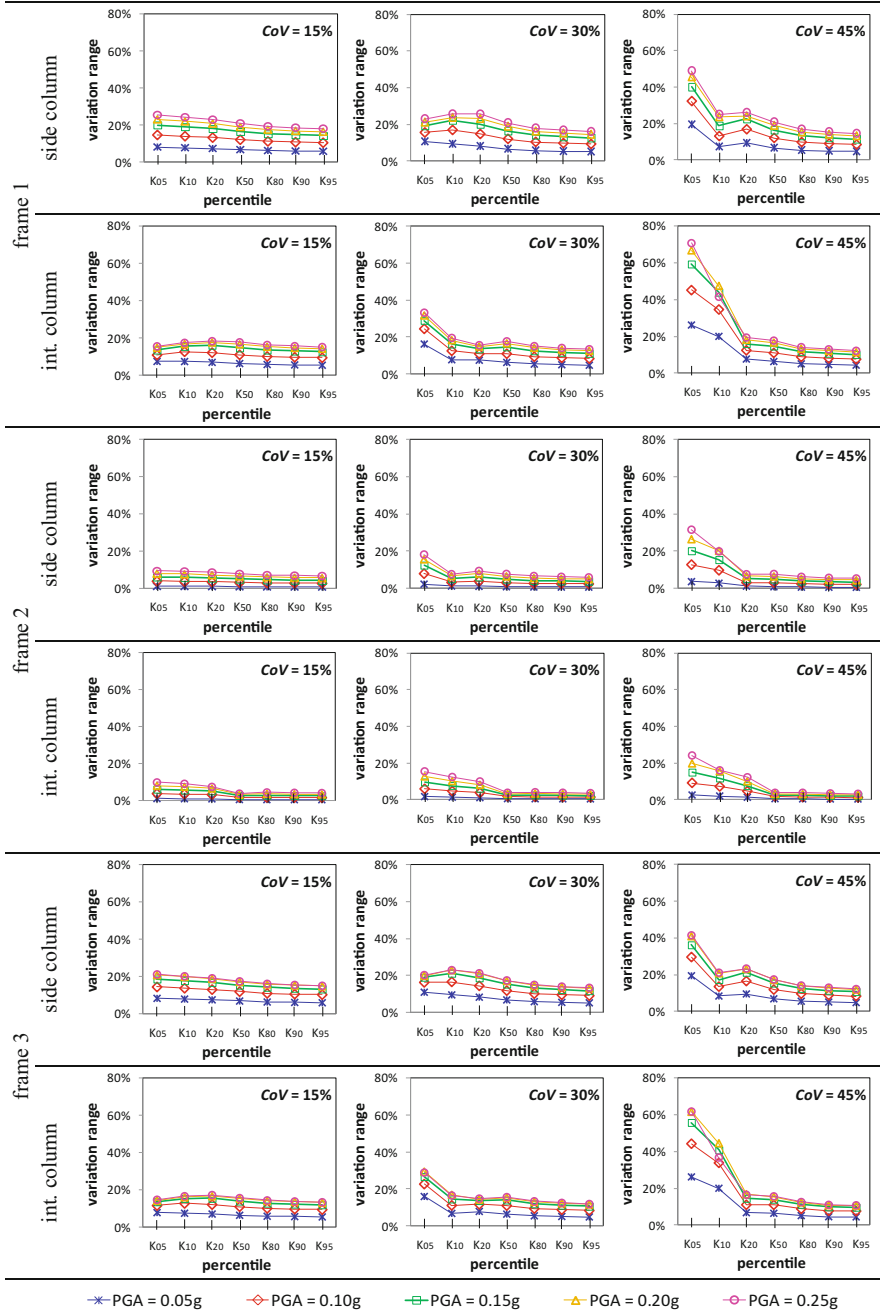
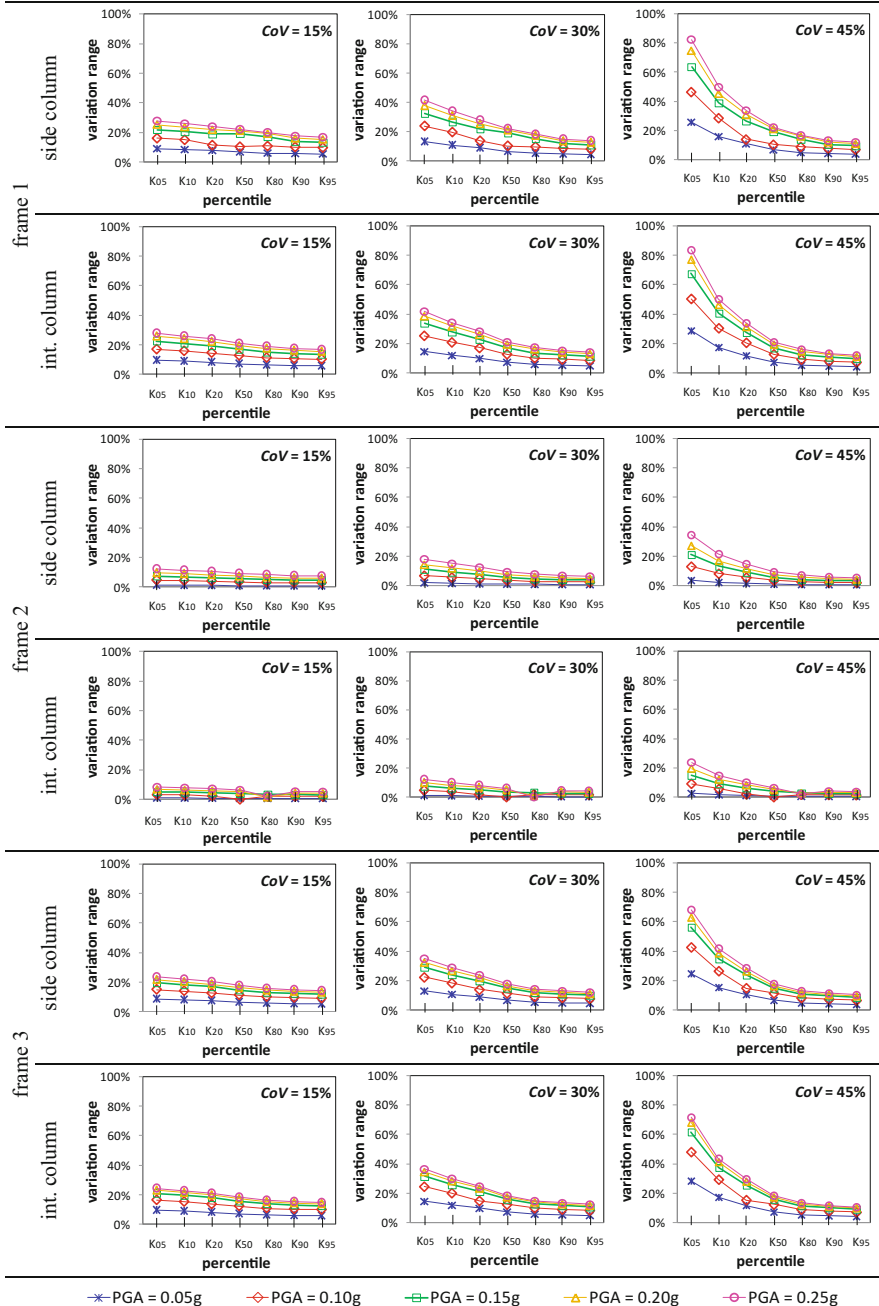**Fig. 14.6** Normalized variation ranges: *DL* limit state

Fig. 14.7 Normalized variation ranges: *SD* limit state

been compared to the conventional (reduced) values provided by EC8 as a function of the achieved Knowledge Level.

The capacity of each column for different amounts of axial load has been found in terms of chord rotation with reference to two different limit states, i.e. Damage Limitation (*DL*) and Life Safety (*SD*). Each strength value, i.e. the three values consistent to EC8 (CF = 1.00, 1.20 and 1.35 respectively) and the seven values of the assumed distribution have been considered and the scatter due to the axial load variation has been assessed in all cases.

The comparison has shown that the EC8 evaluation of the capacity of columns is not conservative when compared to the one found by assuming a concrete strength variability with a *CoV* over 15 %.

The effects of axial load variation have been finally studied in terms of seismic performance, i.e. the D/C ratio. The *SD* limit state resulted more sensitive to axial load variation, since the D/C ranges found for each strength value are larger than the ones found in the *DL* limit state. The strength variability largely affects the obtained D/C ratios in both cases.

In the *DL* limit state the effects of strength variability depend on the associated axial load. In fact, for low amount of axial load, like in the side frames, an increase in the D/C ratio can be observed at the increasing of the concrete strength. For higher level of axial load (internal frame), instead, the relationship between concrete strength and performance is difficult to predict, since the chord rotation domains have not a monotonic trend, and both the reduction in stiffness and in strength play an important role in the seismic response.

In the *SD* limit state, instead, low values of strength always induce a performance reduction. When the lowest percentiles (5 %, 10 %) are considered, together to the highest *CoV* (*CoV* = 45 %), the D/C values associated to the axial load variation largely overcome the unity. In some cases, the D/C values coming from the lowest strength percentile is four times the one found adopting the *mean* strength value, i.e. by assuming EC8 procedure.

The obtained results confirmed the importance of axial load variation in the evaluation of the seismic performance, and underlined the relationship between the effects of axial load variation and real inhomogeneous in-plan distributions of concrete strength. Both factors, i.e. the effective amount of axial load during the seismic response of the structure, and a realistic description of the concrete strength should be carefully evaluated in order to assess the seismic performance of existing buildings.

References

Abbasnia R, Mirzadeh N, Kildashti K (2011) Assessment of axial force effect on improved damage index of confined RC beam-column members. Int J Civ Eng 9(3):237–246

Cristofaro MT (2009) Metodi di valutazione della resistenza a compressione del calcestruzzo di strutture in c.a. esistenti. PhD dissertation, Università di Firenze

Cristofaro MT, D'Ambrisi A, De Stefano M, Pucinotti R, Tanganelli M (2012) Studio sulla dispersione dei valori di resistenza a compressione del calcestruzzo di edifici esistenti. Il giornale delle prove non distruttive, monitoraggio, diagnostica., vol. 2/2012, p 32–39, ISSN: 1721–7075

De Stefano M, Tanganelli M, Viti S (2013a) Effect of the variability in plan of concrete mechanical properties on the seismic response of existing RC framed structures. Bull Earthq Eng 11:1049–1060. doi:10.1007/s10518-012-9412-5

De Stefano M, Tanganelli M, Viti S (2013b) On the variability of concrete strength as a source of irregularity in elevation for existing RC buildings: a case study. Bull Earth Eng. doi:10.1007/s10518-013-9463-2

De Stefano M, Tanganelli M, Viti S (2014a) Variability in concrete mechanical properties as a source of in-plan irregularity for existing RC framed structures. Eng Struct. doi:10.1016/j.engstruct.2013.10.027

De Stefano M, Mariani V, Tanganelli M, Viti S (2014b) The influence of the axial load variation on the seismic capacity of existing RC buildings. In: Proc. 2 European Conference on Earthquake Engineering, Istanbul 2014

De Stefano M, Tanganelli M, Viti S (2015) Torsional effects due to concrete strength variability in existing buildings. Earthquake and Structures, 8(2):379–399

Itaca (2008) Database of the Italian strong motions data. http://itaca.mi.ingv.it

Mander JB, Priestley MJN, Park R (1988) Theoretical stress-strain model for confined concrete. J Struct Div ASCE 114:1804–1826

Saadeghvaziri MA (1997) Nonlinear response and modeling of RC columns subjected to varying axial load. Eng Struct 19(6):417–424

Seismosoft (2006) Seismostruct version 5.2.2 – a computer program for static and dynamic nonlinear analysis of framed structures. Available online from URL: www.seismosoft.com

Chapter 15
Parametric Study of Inelastic Seismic Response of Reinforced Concrete Frame Buildings

Asimina M. Athanatopoulou, Grigorios E. Manoukas, and Amfilohios Throumoulopoulos

Abstract The objective of this paper is to investigate the influence of strength and stiffness distribution in-plan to the nonlinear seismic behaviour of reinforced concrete frame buildings. For this purpose, two 2-storey buildings, a two-way symmetric and a one-way symmetric with eccentricity relative to the y axis, are designed applying the Modal Response Spectrum Method of analysis according to Eurocode 8. Then, the calculated reinforcement of selected elements of the two structures is modified properly in order to generate seven building models with different strength distributions. Each model is subjected to seven strong ground motions acting in two orthogonal directions. The inelastic dynamic analysis is performed for three levels of seismic intensity corresponding to minor damages, moderate damages and severe damages. The structural response is evaluated by means of local Damage Indices for each element as well as of an Overall Structural Damage Index for the whole building. Useful conclusions concerning the nonlinear response are derived.

Keywords Nonlinear Dynamic Analysis • Inelastic seismic response of R/C buildings • Center of resistance • Eccentricity • Damage index

15.1 Introduction

It is well-known that the seismic response of buildings for a given excitation depends on various factors such as the modal characteristics, the damping ratio, the eccentricity between the centers of stiffness (CS) and mass (CM), etc. Concerning the linear systems, the influence of the aforementioned factors is clearly identified and quantified. On the contrary, concerning the nonlinear range of behaviour, despite the extensive investigations conducted by several researchers

---
A.M. Athanatopoulou (✉) • G.E. Manoukas • A. Throumoulopoulos
Department of Civil Engineering, Aristotle University, University Campus,
54124 Thessaloniki, Macedonia, Greece
e-mail: minak@civil.auth.gr; grman7@otenet.gr; athroum@civil.auth.gr

worldwide, no concrete conclusions are derived so far (Paulay 1996, 1997; Myslimaj and Tso 2002; Stathopoulos and Anagnostopoulos 2005; Peruš and Fajfar 2005; De Stefano et al. 2006a, b; Anagnostopoulos et al. 2010). The inelastic deformations of the structural elements during earthquakes cause continuous modifications of the properties of the structures and as a consequence, parameters such as the structural eccentricity are no more representative of the seismic response. Thus, many researchers tried to identify additional factors that could influence the inelastic behaviour. Paulay (1996, 1997) introduced the concept of the center of resistance (CR), i.e. the point from which passes the resultant of the strengths of all vertical structural elements and examined the role of strength eccentricity (distance between CR and CM). Similar investigations were conducted by other researchers (Myslimaj and Tso 2002; Anagnostopoulos et al. 2010) too. However, no secure generalized conclusions were obtained. Furthermore, the results of some of the studies presented were contradictory.

The objective of this paper is to investigate the influence of strength and stiffness distribution in-plan to the nonlinear seismic behaviour of reinforced concrete frame buildings. For this purpose, two 2-storey buildings, a two-way symmetric and a one-way symmetric with eccentricity relative to the y axis, are designed applying the Modal Response Spectrum Method of analysis according to Eurocode 8 (CEN 2004). Then, the calculated reinforcement of selected elements of the two structures is modified properly in order to generate seven building models with different strength distributions. Each model is subjected to seven strong ground motions acting in two orthogonal directions. The inelastic dynamic analysis is performed for three levels of seismic intensity corresponding to minor damages, moderate damages and severe damages. The structural response is evaluated by means of local Damage Indices for each element as well as of an Overall Structural Damage Index for the whole building.

15.2 Elastic Analysis and Design

In the framework of the present study, two 2-storey prototype reinforced concrete buildings are designed according to Eurocodes. In particular, a two-way symmetric (SB) and a one-way symmetric building with structural eccentricity $e_s = 2.40$ m relative to the y axis (AsBCS-CR) are examined. Both buildings are frame systems according to the Eurocode 8 classification (CEN 2004, Section 5.2.2.1). Their floor plans are shown in Figs. 15.1 and 15.2, along with the cross sections dimensions. The buildings are regular in plan and in elevation, while all storey heights are 3 m. The concrete is of class C20/25 ($f_{ck} = 20$ MPa) and the reinforcement steel bars B500C ($f_{yk} = 500$ MPa) according to the Greek standards.

In addition to the self weight, distributed dead and live slab loads equal to 1.0 and 2.0 kN/m^2 respectively are considered. Besides, distributed dead load equal 1.0 kN/m^2 is applied to the slabs of the ground floor, in order to take into account the weight of masonry infill.
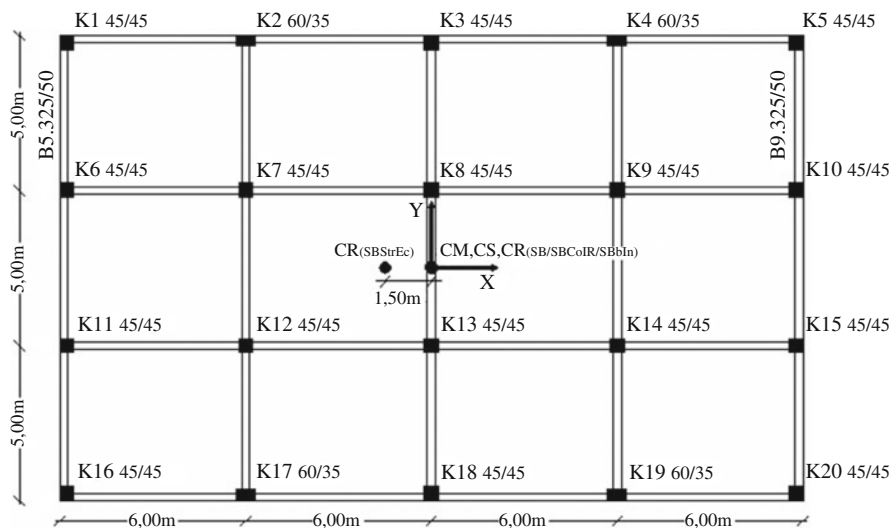
Fig. 15.1 Floor plan of the two-way symmetric building
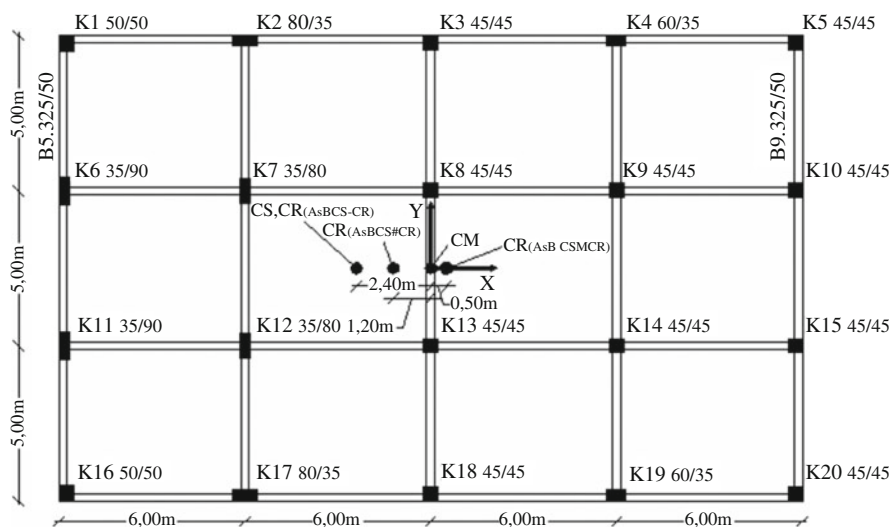

Fig. 15.2 Floor plan of the one-way symmetric building

The structural analysis and the detailing of the cross sections are conducted with the aid of appropriate software widely used by engineering practitioners in Greece. The buildings are analyzed applying the Modal Response Spectrum Analysis method (CEN 2004, Section 4.3.3.3). The behaviour factor q is taken equal to 3. Despite this low value of q, the buildings are designed to meet the Ductility Class High requirements and the capacity design provisions. The seismic hazard level

Table 15.1 Modal periods of the analyzed buildings

Mode number	Modal periods (s)	
	Two-way symmetric building	One-way symmetric building
1	0.352	0.324
2	0.335	0.323
3	0.276	0.227
4	0.118	0.104
5	0.108	0.102
6	0.090	0.065

adopted corresponds to seismic hazard level zone II of Greek territory possessing Peak Ground Acceleration equal to 0.24 g with a probability of exceedance 10 % in 50 years. The ground type is of class B (CEN 2004, Section 3.1.1). Modal analysis is also conducted using the structural analysis program SAP 2000 v.11.0.4. In Table 15.1 the modal periods of the analyzed buildings are tabulated.

15.3   Inelastic Analysis

Seven structural models – four variants of the two-way symmetric and three variants of the one-way symmetric building – are generated. In particular, the analyzed models are as follows (Figs. 15.1 and 15.2):

1. SB: the two-way symmetric prototype building as designed, without any modifications. The centers of mass (CM), stiffness (CS) and resistance (CR) coincide.
2. SBColR: the two-way symmetric prototype building with a 35 % reduction of the reinforcement of columns K7, K8, K9, K12, K13 and K14. CM, CS and CR coincide.
3. SBbmIn: the two-way symmetric prototype building with a 75 % increase of the reinforcement of all beams. CM, CS and CR coincide.
4. SBStrEc: the two-way symmetric prototype building with a 20 % reduction of the reinforcement of columns K5, K9, K10, K14, K15 and K20, as well as a 40 % increase of the reinforcement of K1, K6, K7, K11, K12 and K16. CM and CS coincide. An eccentricity $e_r = 1.50$ m between CM and CR results.
5. AsBCS-CR: the one-way symmetric prototype building as designed, without any modifications. CS and CR coincide. The eccentricity between CM and CR is equal to the structural eccentricity, i.e. $e_r = e_s = 2.40$ m.
6. AsBCS#CR: the one-way symmetric prototype building with a 25 % reduction of the reinforcement of columns K1, K2, K6, K7, K11, K12, K16 and K17. The eccentricity between CM and CR is $e_r = 1.20$ m, while e_s remains constant, i.e. $e_s = 2.40$ m.
7. AsBCSMCR: the one-way symmetric prototype building with a 35 % reduction of the reinforcement of columns K1, K2, K6, K7, K11, K12, K16 and K17, as

Table 15.2 List of seismic excitations

No	Earthquake name	Date	Station name	Magnitude (Ms)	Peak ground acceleration (g)
1	Imperial Valley, USA	15/10/1979	Calexico Fire	6.53	0.25
2	Imperial Valley, USA	15/10/1979	El Centro	6.53	0.12
3	Friuli, Italy	15/09/1976	Buia	5.91	0.12
4	Kocaeli, Turkey	17/08/1999	Arcelik	7.51	0.21
5	Loma Prieta, USA	18/10/1989	Bran	6.93	0.65
6	Kobe, Japan	16/01/1995	Takatori	6.90	0.69
7	Lefkada, Greece	14/08/2003	LEF1 (ITSAK)	6.20	0.48

well as a 50 % increase of the reinforcement of K4, K5, K9, K10, K14, K15, K19 and K20. e_r is equal to -0.50 m, while e_s remains constant, i.e. $e_s = 2.40$ m.

The whole investigation comprises a suite of seven pairs of horizontal ground motion records obtained from the PEER and the European strong motion databases (Table 15.2). The ground motions are recorded on Soil Type B according to Eurocode 8 (CEN 2004) and their magnitudes (Ms) range between 5.91 and 7.51.

The accelerograms are scaled in order to achieve three predefined levels of structural damage, as expressed through the Overall Structural Damage Index (OSDI). In particular, three different scaling factors for each ground motion are determined after successive tests, in order to achieve OSDI values equal to 0.3, 0.6 and 0.9 for the two-way symmetric prototype building (SB). It is considered that these values correspond to minor, moderate and severe damages of the structural elements respectively. The applied scaling factors, which are the same for both components of each ground motion, are tabulated in Table 15.3.

The seven generated building models are analyzed for the three intensity levels of the selected ground motions by means of Nonlinear Dynamic Analysis (NDA). All analyses are performed using the program Ruaumoko (Carr 2005).

For each seismic excitation a representative Damage Index for each critical section is calculated. In particular, the widely used Park and Ang damage index (Park and Ang 1985) modified by Kunnath et al. (1992) is used. At a given cross section the local Damage Index (DI) is given by the following equation:

$$\text{DI} = \frac{\phi_m - \phi_y}{\phi_u - \phi_y} + \frac{\beta}{M_y \cdot \phi_u} E_T \tag{15.1}$$

where φ_m is the maximum curvature observed during the load history, φ_u is the ultimate curvature capacity, φ_y is the yield curvature, E_T is the dissipated hysteretic

Table 15.3 Scaling factors applied to the accelerograms

No	Earthquake name	OSDI value for model 1		
		0.3	0.6	0.9
1	Imperial Valley, USA	1.35	2.30	3.35
2	Imperial Valley, USA	2.90	5.25	7.50
3	Friuli, Italy	3.50	5.50	7.10
4	Kocaeli, Turkey	2.80	4.60	7.15
5	Loma Prieta, USA	0.53	0.88	1.18
6	Kobe, Japan	0.53	0.90	1.03
7	Lefkada, Greece	0.70	1.05	1.69

energy, M_y is the yield moment of the cross section and β is a dimensionless constant determining the contribution of cyclic loading to damage, which is taken equal to 0.05 for the analyses conducted in the present study.

Moreover, the Overall Structural Damage Index (OSDI) of the building is computed as a weighted average of the local Damage Indices at the ends of each element. The dissipated energy is used as a weight factor:

$$\text{OSDI} = \sum_{i=1}^{n} \text{DI}_i \cdot \left(\frac{E_{Ti}}{\sum_{i=1}^{n} E_{Ti}} \right) \tag{15.2}$$

where DI_i is the local Damage Index at cross section i determined by Eq. 15.1, E_{Ti} is the energy dissipated at cross section i and n is the number of cross sections.

In Fig. 15.3 the local Damage Indices (DI) of representative structural elements of the analyzed models are shown. In particular, the mean values for the seven ground motions of DIs of four columns (K1, K5, K7, K9) and two beams (B5.3, B9.3) of the ground floor are presented. The DIs are calculated for both ends of each structural element: bottom (bot) – top (top) for columns and left (l) – right (r) for beams. From Fig. 15.3 the following observations can be made:

1. SB: DI values, which translate to ductility demands, are quite uniformly distributed along the plan. This becomes clear comparing DI values for structural elements lying at symmetrical positions (K1-K5, K7-K9, B5.3-B9.3). DI values of beams are significantly higher than those of columns, especially those of the top. Obviously, this is due to the application of the capacity design provisions. In general, the seismic response of the structure meets the codes objectives.
2. SBColR: in comparison with SB, a significant increase of the DIs of columns K7 and K9 due to the reduction of their reinforcement is observed. This is reflected to the OSDI too (see also Fig. 15.4). The uniformity of ductility demands distribution along the plan remains.
3. SBbmIn: in comparison with SB, a significant reduction of the DIs of beams due to the increase of their reinforcement is observed. This is reflected to the OSDI
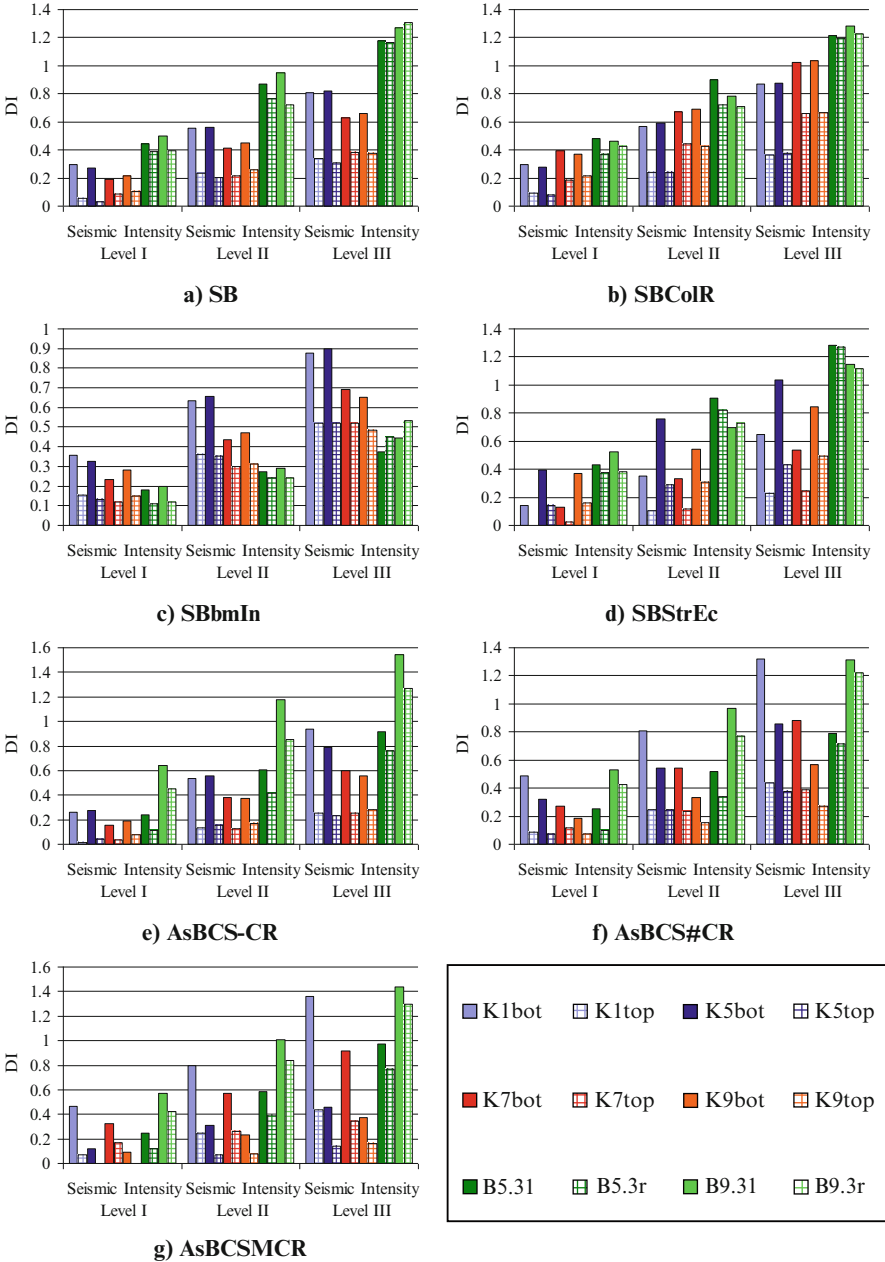
a) SB

b) SBColR

c) SBbmIn

d) SBStrEc

e) AsBCS-CR

f) AsBCS#CR

g) AsBCSMCR

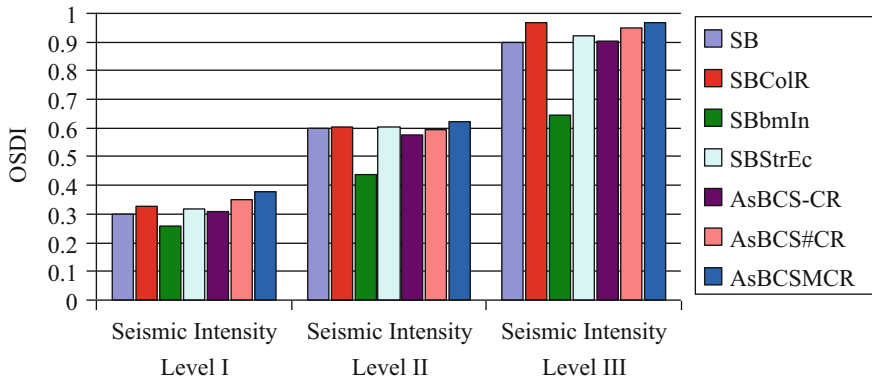**Fig. 15.3** Damage indices of structural elements

Fig. 15.4 Overall structural damage indices

too (see also Fig. 15.4). On the contrary, the DIs of columns are considerably increased, especially at the upper ends.

4. SBStrEc: in comparison with SB, a significant increase of the DIs of the weakened columns (K5, K9) and an analogous reduction of the DIs of the strengthened columns (K1, K7) occurred. With increasing intensity of earthquake excitation, the damages of the columns at the strong side increase in a larger extent with regard to those lying at the opposite side. Concerning the beams, the ductility demands of those lying at the strong side (B5.3) are increased, while of those lying at the weak side (B9.3) are reduced, especially for higher seismic intensity level.

5. AsBCS-CR: due to the capacity design, DI values of beams are significantly higher than those of columns, especially those of the top. For low seismic intensity, DI values of columns of the flexible-weak side are higher than those of the stiff-strong one. However, with increasing intensity an inversion of this trend is observed. This finding is consistent to previous studies which demonstrated that in structures experiencing extensive inelastic deformations the ductility demands are higher at the columns of the stiff side. Concerning the beams, regardless the seismic intensity, the ductility demands are higher at the flexible-weak side.

6. AsBCS#CR: in comparison with AsBCS-CR, a significant increase of the DIs of the weakened columns (K1, K7) due to the reduction of their reinforcement is observed. The transposition of the center of resistance (CR) towards the flexible-weak side implies an increase of the ductility demands of columns lying at this side too. Just like AsBCS-CR, the ductility demands of beams are significantly higher at the flexible-weak side. However, a uniform reduction of DI values is observed.

7. AsBCSMCR: in comparison with AsBCS-CR, a significant increase of the DIs of the weakened columns (K1, K7) and an analogous reduction of the DIs of the strengthened columns (K5, K9) occurred. With increasing intensity of earthquake excitation, the damages of the columns at the stiff (but no more strong)

side increase in a larger extent with regard to those lying at the opposite side. Concerning the beams, just like AsBCS-CR and AsBCS#CR, the ductility demands are significantly higher at the flexible side.

In Fig. 15.4 the mean OSDIs for the seven ground motions are shown. Concerning the models based on the two-way symmetric prototype building (SB, SBColR, SBbmIn, SBStrEc), it is apparent that the increase of the beams reinforcement (SBbmIn) leads to considerable modification of the seismic behaviour, although CR remains constant. On the contrary, the transposition of CR towards the stiff side (SBStrEc) does not affect significantly the overall structural response. This means that CR, as determined in relevant studies, i.e. without taking into account the strength of beams, is not representative of the inelastic seismic behaviour. Concerning the models AsBCS-CR, AsBCS#CR and AsBCSMCR, the transposition of CR towards the flexible side leads to an increase of the overall damage index. This finding is not consistent to previous studies (Myslimaj and Tso 2002).

15.4   Conclusions

The main conclusions derived from this study are as follows:

1. Concerning the two-way symmetric building, the ductility demands are – as expected – quite uniformly distributed in plan.
2. Concerning the one-way symmetric building for high level of seismic intensity the ductility demands are higher at the columns of the stiff side, in relevance with those lying at the flexible side. Concerning the beams, regardless the seismic intensity the ductility demands are higher at the flexible side.
3. The strength of the beams can affect significantly the inelastic seismic response of buildings. As a consequence, CR as determined in relevant studies, i.e. without taking into account the strength of the beams, is not representative of the inelastic seismic behaviour of structures.
4. In general, the ductility demands of the columns lying at the stiff side are higher than of those lying at the flexible side regardless the position of CR. When CM and CS coincide, the higher demands occur at the weak side.
5. When CR lies at the stiff side, with reducing eccentricity between CR and CM, the ductility demands of beams are uniformly reduced. When CR is transposed at the flexible side, an increase of ductility demands is observed. Anyway, the ductility demands of beams are higher at the flexible side.

References

Anagnostopoulos SA, Alexopoulou C, Stathopoulos KG (2010) An answer to an important controversy and the need for caution when using simple models to predict inelastic earthquake response of buildings with torsion. Earthq Eng Struct Dyn 39(5):521–540

Carr AJ (2005) Theory and user guide to associated programs. Ruaumoko manual, vol 1, 3. University of Canterbury, Canterbury

CEN, Comité Européen de Normalisation (2004) Eurocode 8: design of structures for earthquake resistance. Part 1: general rules, seismic actions and rules for buildings. EN 1998-1:2004. Brussels

De Stefano M, Faella G, Ramasco R (2006a) Inelastic seismic response of one-way plan-asymmetric systems under bi-directional ground motions. Earthq Eng Struct Dyn 27(4):363–376

De Stefano M, Marino EM, Rossi PP (2006b) Effect of overstrength on the seismic behaviour of multi-storey regularly asymmetric buildings. B Earthq Eng 4(1):23–42

Kunnath SK, Reinhorn AM, Lobo RF (1992) DARC version 3.0: a program for inelastic damage analysis of reinforced concrete structures. Technical Representative NCEER-92-0022. State University of New York at Buffalo, New York

Myslimaj B, Tso WK (2002) A strength distribution criterion for minimizing torsional response of asymmetric wall-type systems. Earthq Eng Struct Dyn 31(1):99–120

Park YJ, Ang AH-S (1985) Mechanistic seismic damage model for reinforced concrete. J Struct Eng 111(4):722–739

Paulay T (1996) Seismic design for torsional response of ductile buildings. B N Z Natl Soc Earthq Eng 29(3):178–198

Paulay T (1997) Seismic torsional effects on ductile structural wall systems. J Earthq Eng 1(4):721–745

Peruš I, Fajfar P (2005) On the inelastic torsional response of single-storey structures under bi-axial excitation. Earthq Eng Struct Dyn 34(8):931–941

Stathopoulos KG, Anagnostopoulos SA (2005) Inelastic torsion of multistorey buildings under earthquake excitations. Earthq Eng Struct Dyn 34(12):1449–1465

Chapter 16
Seismic Upgrading of Vertically Irregular Existing r.c. Frames by BRBs

Francesca Barbagallo, Melina Bosco, Edoardo M. Marino, Pier Paolo Rossi, and Paola R. Stramondo

Abstract In several earthquake-prone countries a large part of existing r.c. buildings had been designed before seismic codes entered into force and, therefore, considering gravity loads only. The lateral strength and stiffness of these structures are inadequate to sustain seismic action and their seismic response is aggravated by deficiencies due to vertical irregularity. In particular, the ratio of the demanded storey shear force to the lateral strength presents an irregular distribution along the height of the building. This promotes the development of a storey collapse mechanism. In this chapter, the insertion of Buckling Restrained Braces (BRBs) is proposed both for the seismic upgrading of r.c. frames designed for gravity loads and for the reduction of their vertical irregularity. The effectiveness of a design method previously proposed by the authors is investigated. The method is ruled by two parameters: the behaviour factor and the design storey drift. The design method is applied for the seismic retrofitting of a 6-storey r.c. frame considering the values of the ruling parameters in several combinations. Then, nonlinear dynamic analyses are performed to assess their influence on the seismic response of the upgraded frames.

Keywords Seismic upgrading • Design method • Buckling restrained braces • Vertical irregularity • r.c structures

16.1 Introduction

The existing r.c. buildings designed to sustain gravity loads usually have main structural elements disposed along a single direction and this makes them very flexible and weak in the orthogonal direction. Furthermore, the heightwise distributions of the lateral stiffness and shear strength of these frames are not suitable to

F. Barbagallo • M. Bosco • E.M. Marino (✉) • P.P. Rossi • P.R. Stramondo
Department of Civil Engineering and Architecture, University of Catania, V.le A. Doria, 6, 95125 Catania, Italy
e-mail: fbarbaga@dica.unict.it; mbosco@dica.unict.it; emarino@dica.unict.it; prossi@dica.unict.it; pstramon@dica.unict.it

make the drift demand widespread along the height and consistent with the capacity of the frame. In this chapter, the introduction of Buckling Restrained Braces (BRBs) is proposed for the seismic rehabilitation of these framed structures in order to increase to proper values both the lateral stiffness and the shear strength. BRBs typically consist of a ductile steel core confined by a steel tube (Uang and Nakashima 2004; Xie 2005). The brace is joined to the frame by means of the connection segments, while the yielding core and the connection segments are linked by the transition segments. The transition and connection segments have to remain elastic during cyclic loading. This is obtained by adopting for these segments cross-sectional areas larger than that of the yielding core. Therefore, the stiffness and the strength of BRBs can be varied almost independently, by choosing appropriate cross-sectional areas and lengths of the segments of the BRB, and yield stress of the steel.

BRBs, as well as other types of dampers (Daniel et al. 2013), are very promising devices for seismic protection of buildings. Indeed, BRBs can modify the distribution of the shear strength along the height so as to promote a widespread yielding of the structure and, therefore, a more favourable collapse mechanism during strong ground motions. Moreover, they can modify the distribution of the lateral stiffness along the height so that the displacements demanded by the ground motion can better fit the displacement capacity of the structure. This research develops and validates a design method for BRBs, which is applied for the seismic upgrading of an existing r.c. frame. The proposed design method aims at obtaining a more regular structural behaviour along the height and avoiding the soft storey mechanism. Afterwards the seismic response of the upgraded frames is determined by nonlinear dynamic analysis, to evaluate the increase of vertical regularity of the structure.

16.2   Proposed Design Method

The method is ruled by two parameters. The first one is the *behaviour factor q*, which determines the lateral strength to be provided by BRBs. The second parameter is the *design storey drift* $\Delta_{d,i}$, which is given as a fraction of the nominal storey drift capacity $\Delta_{l,i}$. This assumption is to take into account that, in a few storeys, drifts may be larger than those obtained by the design elastic analysis, due to some damage concentrations. The method deals with two requirements. The first one is a strength requirement aiming at providing the r.c. frame upgraded by BRBs with sufficient lateral strength, which is distributed along the height of the frame proportionally to the required storey shear. The second one is a displacement requirement aiming at reducing the displacement demand below the design value. A flowchart of the design procedure is shown in Fig. 16.1.
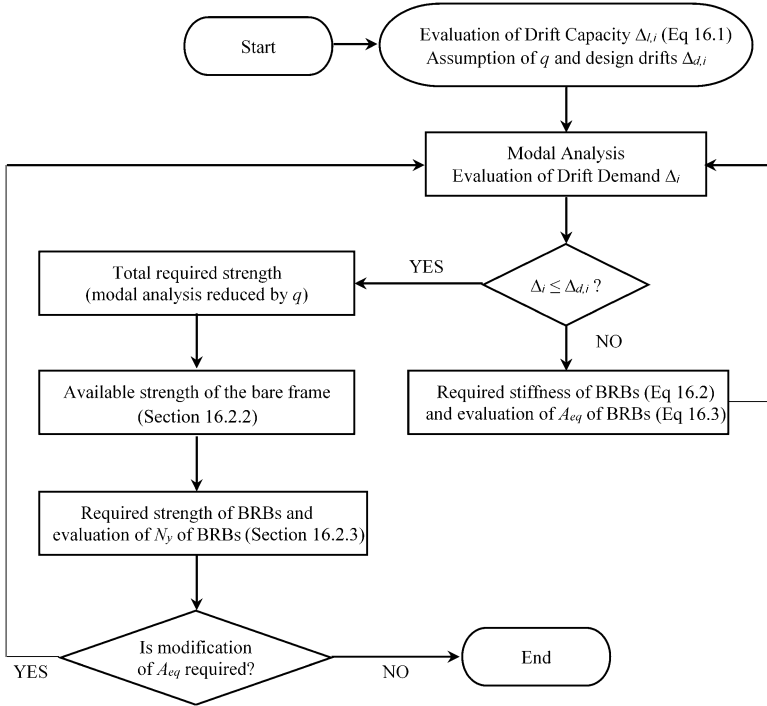
Fig. 16.1 Flowchart of the design procedure

16.2.1 Determination of the Displacement and Strength Demands

Because of the insertion of BRBs, which promotes the simultaneous yielding of all the storeys and a widespread demand along the height, the demanded drifts Δ_i can be determined for the i-th storey by the elastic analysis of the structure. This analysis is based on the elastic (unreduced) spectrum of the reference ground motion, here assumed as that having a 10 % probability of exceedance in 50 years. Afterwards, Δ_i is modified according to European seismic code EC8 (CEN 2004), to take into account that the equal displacement rule does not apply for structures whose fundamental period T_1 is smaller than T_C. After BRBs are inserted, and their stiffness is determined in compliance with the displacement requirement, the required lateral strength of the frame $V_{Ed,i}$ is calculated at each storey through the elastic analysis of the structure based on the elastic spectrum reduced by the behaviour factor q.

16.2.2 Determination of the Displacement and Strength Capacity

In this chapter, the displacement capacity is defined in terms of storey drifts corresponding to the achievement of the Significant Damage limit state in columns. The provisions of EC8 quantify the seismic performance in terms of chord rotation. EC8 defines the chord rotation capacity corresponding to Near Collapse limit state θ_{um} as the chord rotation at yielding plus plastic rotation at column failure θ_{um}^{pl}. In this chapter θ_{um} and θ_{um}^{pl} are evaluated according to EC8-Part 3 (CEN 2010), while the chord rotation at yielding is obtained as the difference between these two terms. Moreover, EC8 stipulates that the Significant Damage limit state is achieved when, somewhere in the structure, the plastic part of the chord rotation is equal to 75 % of the θ_{um}^{pl}. Thus, the displacement capacity Δ_l corresponding to the Significant Damage limit state is evaluated as:

$$\Delta_l = \left[0.75 \cdot \theta_{um}^{pl}, + \left(\theta_{um} - \theta_{um}^{pl}\right)\right] \cdot H \qquad (16.1)$$

where H is the length of the column equal to the inter-storey height of the frame. The drift Δ_l is evaluated for the ends of all the columns of the storey and the minimum value obtained is assumed as displacement capacity of the storey $\Delta_{l,i}$.

The available strength $V_{Rd,i}$ at each storey of the frame upgraded by BRBs is evaluated as the summation of two contributions. The first one is the storey shear strength provided by BRBs $V_{Rd,b,i}$, calculated as the sum of the two horizontal components of the axial forces of the braces inserted in the frame at the considered storey. The second one is the shear strength of the bare r.c. frame $V_{Rd,f,i}$ given by the sum of the shear forces transmitted by the columns of that storey when they are yielded in flexure at the two end cross-sections.

16.2.3 Design of BRBs

BRBs are designed firstly to fulfil the displacement requirement. To this end, the drift demand and the drift capacity are compared each other at every storey. Where the demand exceeds the capacity, the introduction of BRBs provides the structure with the lacking stiffness.

With regards to the total stiffness of the structure K_{req}, it is given by the summation of the stiffness of the bare r.c. frame model $K_{FR,b}$ and the stiffness of the truss model K_{Truss}. The stiffness K_{req} is evaluated as the ratio of the total shear force to the design storey drift Δ_d, while $K_{FR,b}$ is calculated as the ratio of the sum of the shear forces carried by the columns to the storey drift. Both the storey shear force and drift are determined by the elastic analysis. Given the values of these terms the stiffness of the truss model K_{Truss} can be determined as the difference between K_{req} and $K_{FR,b}$.
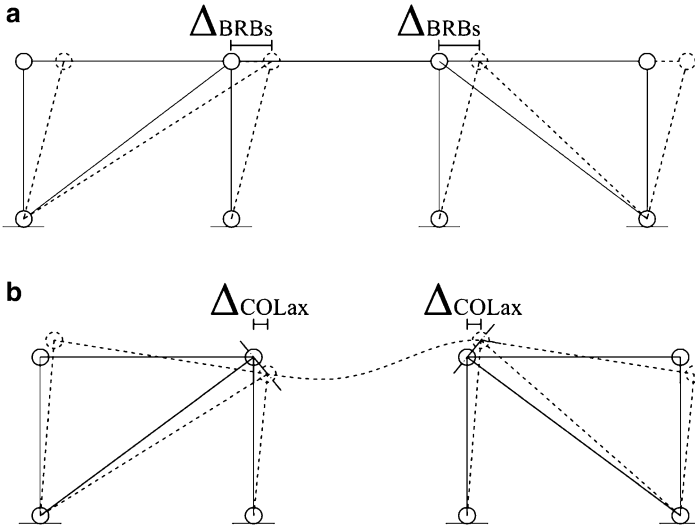
Fig. 16.2 Drifts of the truss model caused by (**a**) BRB axial deformation and (**b**) column axial deformation

Furthermore, it is considered that the total storey drift of the truss model Δ is equal to the sum of the drift caused by the axial deformations of BRBs Δ_{BRBs} (Fig. 16.2a) and that caused by the axial deformation of columns Δ_{COLax} (Fig. 16.2b). The total storey drift of the truss model Δ is calculated as the ratio between the shear force sustained by BRBs V_{BRBs}, determined by the elastic analysis, and the stiffness K_{Truss}. Focusing on the drift caused by the axial deformation of columns (Fig. 16.2b), it is evident that shortening/elongation of columns would cause also a variation in length of BRBs. But, to avoid this, columns rotate rigidly and provide the drift Δ_{COLax} that is determined by simple geometrical considerations. Finally, the drift Δ_{BRBs} is calculated as Δ minus Δ_{COLax} and the additional stiffness to be provided by BRBs to fulfil the displacement requirement is determined as:

$$K_{BRBs} = \frac{V_{BRBs}}{\Delta_{BRBs}} \tag{16.2}$$

Given the value of K_{BRBs}, the procedure determines the value of the *equivalent cross-section area* of BRBs A_{eq} by the following relation:

$$A_{eq} = \frac{1}{2} \frac{K_{BRBs} L_{BRBs}}{E \cos^2 \alpha} \tag{16.3}$$

where L_{BRBs} is the length of BRBs, E is Young's modulus of steel and α is the angle of inclination of the BRBs with respect to the beam longitudinal axis.

The design procedure has to be ran iteratively until convergence, because the insertion of the BRBs increases the frame stiffness and modifies the vibration periods and the seismic response of the frame.

After the stiffness of BRBs is calculated, their yield strength N_y is determined to fulfil the strength requirement. To this end, the required strength of the BRBs at the i-th storey, $V_{reqBRBs,i}$, is obtained as the difference between the total required strength $V_{Ed,i}$ (obtained by the elastic analysis of the frame with the spectrum reduced by q) and the shear strength of the bare r.c. frame $V_{Rd,f,i}$. The yield strength of the BRBs is calculated by the following relation:

$$N_{y,i} = \frac{V_{req,BRBs,i}}{2\cos\alpha} \tag{16.4}$$

For each BRB configuration satisfying the displacement requirement, the yield strength N_y can be obtained adopting a proper yield stress f_y, which can be obtained as the ratio between N_y and the cross-sectional area A_c of the yielding core of the BRB. However, f_y is not lower than a minimum value that is determined at each storey in order to have the BRB ductility demand not larger than 19 for the design seismic action (Merritt et al. 2003; Bosco and Marino 2013).

16.3   Case Study Structure

The described design method has been applied for the seismic upgrading of a r.c. frame extracted from a six-storey building designed to resist gravity loads only and described in Barbagallo et al. (2014). The frame has three spans 4.0 m long and the interstory height is equal to 3.2 m. The floor mass is equal to 102.37 t and the gravity loads are considered in the seismic design situation. Table 16.1 shows the dimensions of cross-sections of beams and columns. Diagonal BRBs are inserted in the lateral spans.

Beams and columns are simulated by De Saint Venant members and BRBs are modelled as trusses. All the nodes belonging to the same floor are constrained to have the same horizontal displacement. For modal response spectrum analysis, the seismic input is given by the elastic spectrum proposed by EC8 for soil type C, characterised by a peak ground acceleration a_g equal to $0.35\,g$. The confidence factor FC is assumed equal to one for both concrete and steel. The yield stress of BRBs f_y is determined by the proposed design procedure within a range of values deemed acceptable. Mechanical parameters describing the materials are summarised in Table 16.2. The design of the analysed frames is carried out considering three values of $\Delta_{d,i}$, equal to $0.6\,\Delta_{l,i}$, $0.7\,\Delta_{l,i}$, $0.8\,\Delta_{l,i}$, and three values of q, equal to 5, 6 and 7.

Table 16.1 Cross-sections dimensions ($b \times h$) of the r.c. frame members

Storey	1st	2nd	3rd	4th	5th	6th
Beams	30×60	30×60	30×60	30×60	30×60	30×60
Perimetral columns	50×30	40×30	35×30	30×30	30×30	30×30
Central columns	30×60	30×50	30×40	30×30	30×30	30×30

Table 16.2 Mechanical parameters adopted for the design of the analysed frame

	Concrete	Reinforcing steel bars	BRBs
Compressive strength	29 MPa		
Yielding strength		400 MPa	100–275 MPa
Young's modulus	30,280 MPa	210,000 MPa	210,000 MPa
Poisson's ratio	0.5	0.3	0.3

16.4   Numerical Analyses

16.4.1   Numerical Model

Nonlinear dynamic analysis of the bare and the upgraded r.c. frames have been carried out by means of the OpenSees program (Mazzoni et al. 2003), in order to evaluate the influence of the parameters q and Δ_d on the seismic performance of the frames, with particular regard to their vertical regularity.

A 2-D frame model with masses concentrated at the floor levels is set, with rigid diaphragms at each level. Because the strength contribution given by the deck to beams cannot be exactly quantified, an Elastic Beam model (EB model) and a Plastic Beam model (PB model) have been used to define a bounded behaviour. In PB model beams and columns are modelled as members constituted by elastic elements with plastic hinges at their ends. A fibre cross-section, with both concrete and steel components, is assigned to each plastic hinge whose length is equal to the depth of the cross-section. The Mander constitutive law is assigned to the concrete fibres, while an elasto-plastic with strain kinematic hardening constitutive law is assigned to the steel fibres. The parameters used for materials are summarised in Table 16.3. Instead, in EB model beams are modelled as infinitely resistant.

BRBs are modelled as truss elements with the cross-sectional area equal to the equivalent area A_{eq} obtained in design. The material model proposed by Zona and Dall'Asta (2012), which takes into account both kinematic and isotropic hardening (Rossi 2014), is used to simulate the cyclic behaviour of BRBs. Further details about the model are available in Barbagallo et al. (2014). In compliance with EC8, the nominal dead loads plus quasi-permanent live loads are assigned as initial gravity loads in the analysis. A Rayleigh viscous damping is used and set at 5 % for the first and the third mode of vibration. The P-Δ effect is considered in the analysis.

For nonlinear time-history analysis, a set of ten artificial accelerograms compatible with the EC8 elastic spectrum for soil type C and characterised by 5 %

Table 16.3 Mechanical parameters adopted for the dynamic analysis of the frames

Concrete		Reinforcing steel bars	
Compressive strength	29 MPa	Yielding strength	400 MPa
Young's modulus	30,280 MPa	Young's modulus	210,000 MPa
Strain at maximum strength	2×10^{-3}	Strain-hardening ratio	0.0066
Tensile strength	$f_{tm} = 2.28$ MPa		
Ultimate strain in tension	7.5×10^{-5}		

damping ratio and peak ground acceleration a_g equal to 0.35 g is defined. Details about the set of accelerograms may be found in Amara et al. (2014).

16.4.2 Seismic Response of the Designed Frames

The seismic performance of the analysed frames is evaluated in terms of maximum drift demand Δ_i and ratio of storey drift demand Δ_i to capacity $\Delta_{l,i}$. The values of Δ_i and $\Delta_i/\Delta_{l,i}$ are determined for each of the N storeys of the frame and for each accelerogram. Their median values over the ten accelerograms are determined for each storey and their heightwise distributions are shown in Figs. 16.3 and 16.4, respectively. The results are presented for the design storey drifts $\Delta_{d,i}$ equal to 0.6 $\Delta_{l,i}$ and 0.8 $\Delta_{l,i}$ considering both the Plastic Beam model (PB model) and the Elastic Beam model (EB model). The four curves refer to the performance of the bare frame and to that of the upgraded frames designed by q equal to 5, 6 and 7.

Figure 16.3 shows that the insertion of BRBs leads to a reduction of the maximum drift demand and, therefore, to the improvement of the seismic performance. If $\Delta_{d,i} = 0.6$ $\Delta_{l,i}$, the design of BRBs is basically ruled by the stiffness requirement. Therefore, the three considered values of q lead to similar BRBs and the upgraded frames exhibit similar seismic performances. Instead, if $\Delta_{d,i} = 0.8$ $\Delta_{l,i}$, the strength requirement controls the design of BRBs and the reduction of the storey drifts is higher for lower values of q. Furthermore, if the PB model is adopted, regardless of the adopted $\Delta_{d,i}$, some damage concentration is obtained at the lowest storeys. Instead, the EB model leads to a more regular distribution of storey drifts.

Figure 16.4 allows the determination of the values of the behaviour factor q that can be used to avoid the exceedance of the Significant Damage limit state. These values are those corresponding to maximum demand to capacity ratios $\Delta_i/\Delta_{l,i}$ not larger than 1. When $\Delta_{d,i} = 0.6$ $\Delta_{l,i}$, both for PB and for EB model, all the considered values of q lead to an acceptable seismic response. Instead, if $\Delta_{d,i} = 0.8$ $\Delta_{l,i}$, the maximum acceptable value of q is 6 for the EB model and 7 for the PB model. The most restrictive of the two values ($q = 6$) is suggested for the design of BRBs when $\Delta_{d,i} = 0.8$ $\Delta_{l,i}$ is adopted, because it is assumed that the results obtained by the PB model and EB model bound the real behaviour of the frame.

For each value of q and $\Delta_{d,i}$, the response parameters Δ_i and $\Delta_i/\Delta_{l,i}$ are normalised with respect to their maximum value along the height and then the

| ◆ Bare r.c. frame | Upgraded frames: | ○ $q = 5$ | △ $q = 6$ | ◍ $q = 7$ |

Plastic Beam Model   **Elastic Beam Model**

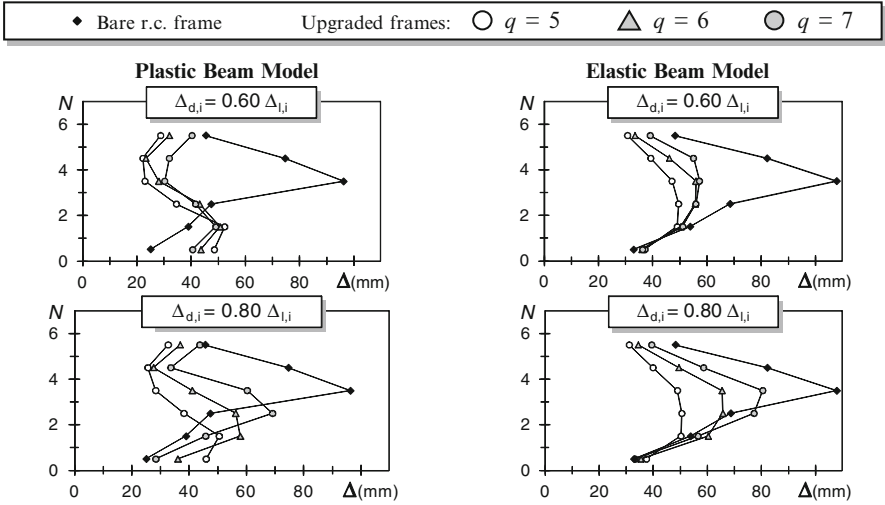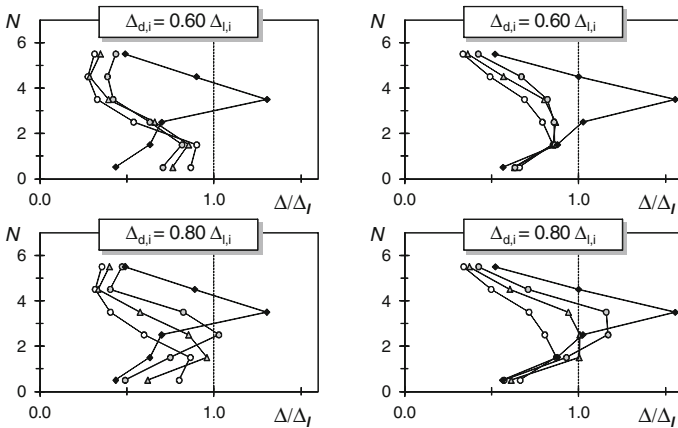**Fig. 16.3** Maximum storey drift demand

Fig. 16.4 Maximum storey drift demand to capacity ratio

means of the normalised values over the storeys Δ_m and $(\Delta/\Delta_l)_m$ are determined. If the considered Δ_i is the same at each storey, the response in terms of storey drift is perfectly regular in elevation and the mean value Δ_m of the normalised Δ_i is equal to 1. Instead, values of Δ_m smaller than 1 denote a lower level of vertical regularity of the seismic response. The same considerations apply to $(\Delta/\Delta_l)_m$ and to regularity in elevation of the response in terms of storey drift demand to capacity ratio. Figures 16.5 and 16.6 show the obtained values of Δ_m and $(\Delta/\Delta_l)_m$, which quantify the regularity of the seismic performance along the height, limited to the values of q leading to an acceptable seismic response. Each curve refers to frames designed with a fixed value of $\Delta_{d,i}$. The comparison between each curve and the value
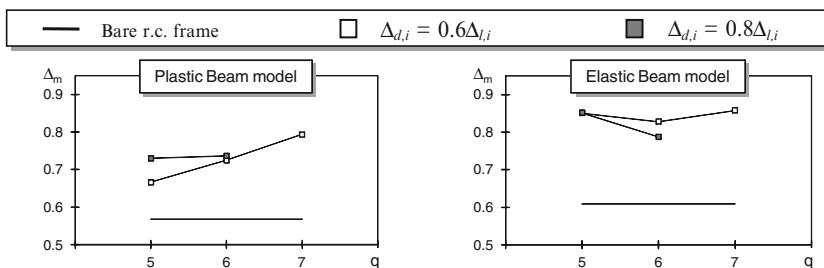
Fig. 16.5 Mean value of maximum storey drift demand
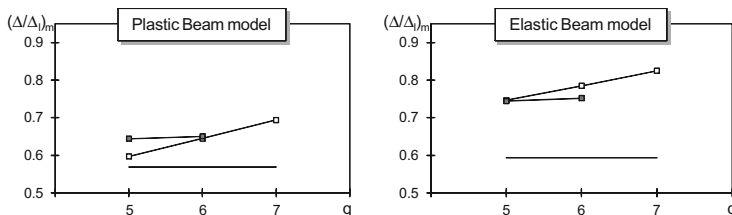
Fig. 16.6 Mean value of maximum storey drift demand to capacity ratio

obtained for the bare r.c. frame allows the evaluation of the increase of vertical regularity obtained by the upgrading by BRBs.

In all the considered cases, the values of Δ_m and $(\Delta/\Delta_l)_m$ obtained for the upgraded frames are higher than those of the bare frame. If $\Delta_{d,i} = 0.6\ \Delta_{l,i}$, the higher values of Δ_m and $(\Delta/\Delta_l)_m$ are obtained for $q = 7$. If $\Delta_{d,i} = 0.8\ \Delta_{l,i}$, with the exception of the EB model, which leads to slightly different values of Δ_m (Fig. 16.5), the obtained values of Δ_m and $(\Delta/\Delta_l)_m$ are the same for the two considered values of q. In conclusion, the proposed design procedure for the seismic upgrading of r.c. frames always increases the vertical regularity of the frames. The improvement of regularity due to the insertion of BRBs is higher when the seismic response is expressed in terms of storey drifts. Among the considered pairs of $\Delta_{d,i}$ and q, which avoid exceeding the Significant Damage limit state, the pairs $\Delta_{d,i} = 0.6\ \Delta_{l,i}$, $q = 7$ and $\Delta_{d,i} = 0.8\ \Delta_{l,i}$, $q = 5$ are those corresponding to the most regular behaviour in elevation.

16.5   Conclusions

This chapter investigates the effectiveness of a design method for seismic upgrading of existing r.c. frames by means of BRBs. The proposed design method controls the shear strength and lateral stiffness to be provided by BRBs by means of the behaviour factor q and the design storey drift Δ_d. Furthermore, it determines the

heightwise distributions of the additional strength and stiffness aiming at promoting (1) a widespread yielding of the frame and (2) a uniform exploitation of the displacement capacity. In particular, at each storey, the additional shear strength to be provided by BRBs is determined so that the ratio of the shear force demand to the total shear strength is constant along the height of the frame. Furthermore, the additional lateral stiffness is determined in such a way that the drift demand to capacity ratio is the same at all the storeys.

The effectiveness of the proposed design method is assessed on a r.c. frame originally designed for gravity loads only. Nine retrofit solutions with BRBs designed by the proposed method are analysed. In particular, Δ_d is assumed equal to 0.6, 0.7 and 0.8 times of the storey drift Δ_l corresponding to the Significant Damage limit state (drift capacity). Instead, q is assumed equal to 5, 6 and 7. The results of the nonlinear dynamic analysis demonstrate that the seismic response of the bare r.c. frame is irregular in elevation because of a significant concentration of the drift demand at the 4th storey. As a consequence, the drift demand to capacity ratio is larger than one at this storey. The insertion of the BRBs within the r.c. frame makes its seismic response more regular in elevation, mitigates the concentration of the storey drift and improves the seismic performance in terms of drift demand to capacity ratio. The obtained benefits depend on the values assumed for Δ_d and q. In particular, if Δ_d is assumed equal to 0.6 Δ_l, the storey drift demand never exceeds the capacity independently of the value of q. Instead, when Δ_d is equal to 0.8 Δ_l, a behaviour factor q not larger than 6 has to be adopted to avoid the exceedance of the Significant Damage limit state.

References

Amara F, Bosco M, Marino EM, Rossi PP (2014) An accurate strength amplification factor for the design of SDOF systems with P-Δ effects. Earthq Eng Struct Dyn 43(4):589–611

Barbagallo F, Bosco M, Ghersi A, Marino EM, Rossi PP, Stramondo PR (2014) Calibration of a design method for seismic upgrading of existing r.c. frames by BRBs. In: Proceedings of the 2nd European conference on earthquake engineering and seismology. Istanbul. 25–29 August 2014

Bosco M, Marino EM (2013) Design method and behavior factor for steel frames with buckling restrained braces. Earthq Eng Struct Dyn 42(8):1243–1263

CEN (2004) EN 1998-1, EuroCode 8: design of structures for earthquake resistance – Part 1: General rules, seismic actions and rules for buildings. European Committee for Standardization, Bruxelles

CEN (2010) EN 1998-1, EuroCode 8: design of structures for earthquake resistance – Part 3: Assessment and retrofitting of buildings. European Committee for Standardization, Bruxelles

Daniel Y, Lavan O, Levy R (2013) A simple methodology for the seismic passive control of irregular 3D frames using friction dampers. In: Lavan O, De Stefano M (eds) Seismic behaviour and design of irregular and complex civil structures, vol 24. Springer, Dordrecht, Netherlands: 285–295

Mazzoni S, McKenna F, Scott MH, Fenves GL, Jeremic B (2003) OpenSEES manual. Pacific Earthquake Engineering Research Center, University of California, Berkeley

Merritt S, Uang CM, Benzoni G (2003) Subassemblage testing of CoreBrace buckling restrained braces. Structural Systems Research Project, Report no. TR-2003/01. University of California, San Diego

Rossi PP (2014) Importance of isotropic hardening in the modeling of buckling restrained braces. J Struct Eng-ASCE 141(4), doi:10.1061/(ASCE)ST.1943-541X.0001031

Uang CM, Nakashima M (2004) Steel buckling-restrained braced frames. In: Bozorgnia Y, Bertero VV (eds) Earthquake engineering from engineering seismology to performance based engineering. CRC Press LLC, Boca Raton, Florida, USA

Xie Q (2005) State of the art of buckling restrained braces in Asia. J Constr Steel Res 61(6):727–748

Zona A, Dall'Asta A (2012) Elastoplastic model for steel buckling restrained braces. J Constr Steel Res 68(1):118–125

Chapter 17
Application of Nonlinear Static Method with Corrective Eccentricities to Steel Multi-storey Braced Buildings

Melina Bosco, Giovanna A.F. Ferrara, Aurelio Ghersi, Edoardo M. Marino, and Pier Paolo Rossi

Abstract Nonlinear static methods may be not very effective in the assessment of 3D building structures because sometimes they do not provide an accurate estimate of the deck rotations. In order to overcome this shortcoming, the authors of this chapter proposed a nonlinear static approach for asymmetric structures that is performed applying the lateral force with two different eccentricities (named corrective eccentricities) with respect to the centre of mass of the deck. In this chapter the effectiveness of the corrective eccentricity method is verified with reference to four five-storey mass eccentric steel buildings in which the seismic force is sustained by frames equipped with buckling restrained braces.

Keywords Asymmetric buildings • Multi-storey systems • Steel structures • Seismic assessment • Corrective eccentricity method

17.1 Introduction

The nonlinear static method of analysis has gained considerable popularity in recent years because it is a fair compromise between the simplicity of the linear method of analysis and the effectiveness of the nonlinear time-history analysis.

The nonlinear static method suggested in EuroCode 8 (CEN 2004; Fajfar 1999) generally provides reasonable results for planar frames (Bosco et al. 2009; Giorgi and Scotta 2013) while, in the case of in-plan irregular structures, it is effective only for torsionally-rigid systems (Bento et al. 2010; De Stefano et al. 2013, 2014; Fajfar et al. 2005; Fujii 2014; Kreslin and Fajfar 2012). Based on this consideration, methods specifically improved for 3D structures have been proposed. For instance,

M. Bosco • G.A.F. Ferrara • A. Ghersi • E.M. Marino • P.P. Rossi (✉)

Department of Civil Engineering and Architecture, University of Catania, Viale A. Doria 6, 95125 Catania, Italy

e-mail: mbosco@dica.unict.it; gferrara@dica.unict.it; aghersi@dica.unict.it; emarino@dica.unict.it; prossi@dica.unict.it

Kreslin and Fajfar (2012) developed an improved version of the N2 method called extended N2 method. The authors of this chapter have recently proposed a new approach based on a double application of the nonlinear static analysis (Bosco et al. 2012). In particular, for each considered direction of the seismic action, the nonlinear static analysis is applied with reference to two different points of the deck. The points of application of the force have been properly defined in Bosco et al. (2012) through mathematical relations based on the investigation of the seismic response of a large set of asymmetric single-storey structural systems. The resisting elements of these systems were endowed with lateral stiffness and strength in their plane only and subjected to bidirectional ground motions. The distances e_1 and e_2 between the points of application of the forces and the centre of mass C_M are named *corrective eccentricities* and the proposed nonlinear static method is called *corrective eccentricity method*. The corrective eccentricities e_1 and e_2 are calculated by simple relations as a function of the parameters that mostly influence the lateral-torsional coupling of the seismic response of asymmetric buildings. These parameters are: the rigidity eccentricity e_r (distance between the centre of rigidity C_R and C_M), the strength eccentricity e_s (distance between the centre of strength C_S and C_M), the ratio Ω_θ of the torsional to lateral frequencies of the corresponding torsionally balanced system (obtained by shifting C_M into C_R) and the ratio R_μ of the elastic shear force to the actual strength of the *corresponding planar system*. This latter system is obtained from the asymmetric system by restraining the deck rotation.

The effectiveness of the corrective eccentricity method in the prediction of the peak response of in-plan irregular buildings has been mainly tested with reference to single-storey systems (Bosco et al. 2013a). In this chapter, its effectiveness is investigated by multi-storey steel buildings. The seismic response in terms of floor displacements and storey drifts of each building is evaluated by nonlinear dynamic analysis, by the corrective eccentricity method and by the standard nonlinear static method (i.e. without corrective eccentricity). The errors committed by the two considered nonlinear static methods in the prediction of the maximum dynamic response are determined and compared.

17.2 Case Studies

The considered five storey buildings have rectangular decks with maximum dimension L and minimum dimension B equal to 30.0 and 18.0 m, respectively (Fig. 17.1). The interstorey height is equal to 3.30 m. The seismic force is sustained by frames with buckling restrained braces (BRBs) arranged in the chevron configuration. The location of the bays with buckling restrained braces is highlighted in Fig. 17.1 by double line. In order to analyse both torsionally-flexible (TF) and torsionally-rigid (TR) systems, two different plan layouts of the resisting elements are considered. In the first layout (Fig. 17.1a), all the frames with BRBs arranged along the y-axis are close to the centre of rigidity (frames Y3, Y4, Y5 and Y6). Instead, in the second
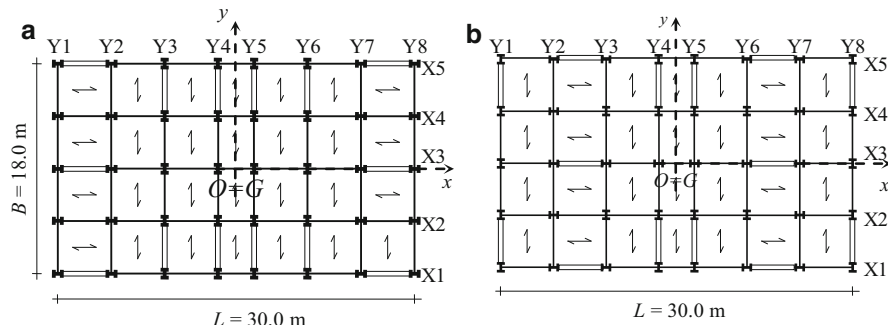
Fig. 17.1 Plan layout of the buildings (**a**) torsionally-flexible and (**b**) torsionally-rigid structures

layout (Fig. 17.1b), two of the frames with BRBs are located on the two sides of the building (frames Y1 and Y8). For all the considered systems, the braced frames are symmetrically arranged. Consequently, the centres of rigidity and those of strength are always coincident with the geometrical centre of the deck.

The storey mass is calculated according to EC8 by taking into account the dead and live loads present in the building in the seismic design situation (5.0 kN/m^2). The mass radius of gyration is equal to 10.1 m (0.337L). Masses are lumped at deck level and have the same distribution within every deck. The centres of mass of the storeys are lined up on a vertical axis and belong to the x-axis because masses are assumed symmetric with respect to this axis. Structural systems with different values of the rigidity eccentricity e_r are obtained considering different positions of C_M. Two values of the rigidity eccentricity are considered. These values are equal to $0.05L$ and $0.15L$ and are later named low (-L) and high (-H) rigidity eccentricities. Centres of mass are assumed to be on the right of the origin O. Therefore, the left side of the deck is the stiff side while the right one is the flexible side. The strength eccentricity e_s is always equal to the rigidity eccentricity.

The frames with BRBs are designed applying the seismic force to two separate planar models along the x- and y-directions. The design method adopted is that proposed in Bosco and Marino (2013). Steel grade S235 with characteristic value of the yield stress $f_y = 235$ MPa is used for all the members. The design seismic force is evaluated by the elastic spectrum proposed in EC8 for soil type C, characterised by a peak ground acceleration a_g equal to 0.35 g, and reduced by the behaviour factor q equal to 4. Beam and column cross-sections are selected among the European wide flange shapes (HEA for beams and HEB for columns). More details about the design method adopted for the frames with BRBs may be found in Bosco and Marino (2013). The design axial force of the gravity columns is evaluated according to the tributary area concept considering the load per square meter for non-seismic design situation equal to 9.2 kN/m^2.

The periods of vibration of the corresponding torsionally-balanced systems (uncoupled periods) are grouped in triplets. Each triplet contains the periods of the modes of vibration (translational and rotational) characterized by the same

Table 17.1 Uncoupled and coupled periods of the systems

Building	Uncoupled periods [s]				Coupled periods [s]			
	T_{y1}	$T_{\theta 1}$	T_{y2}	$T_{\theta 2}$	$T_{y\theta 1}$	$T_{\theta y1}$	$T_{y\theta 2}$	$T_{\theta y2}$
TF – L	0.73	0.88	0.25	0.30	0.71	0.92	0.25	0.32
TF – H	0.73	0.88	0.25	0.30	0.62	1.06	0.22	0.37
TR – L	0.73	0.58	0.25	0.20	0.74	0.57	0.26	0.20
TR – H	0.73	0.58	0.25	0.20	0.81	0.52	0.28	0.18

number of changes in the sign of the modal components. The uncoupled periods of the translational mode of vibration in the y-direction and that of the rotational mode are reported in Table 17.1 along with the (coupled) periods of vibration of the asymmetric buildings.

17.3 Modelling of the Structures

The numerical analyses are carried out by means of the OpenSees program (Mazzoni et al. 2003). The buildings are represented by means of a 3D centreline model with rigid diaphragms. Beams of the braced frames and columns are modelled by means of elements (*Beam With Hinges Elements*) which are elastic in the middle and inelastic at the ends within parts of finite length. All beam-to-column connections are pinned. BRBs are modelled by means of a single truss element. To take into account the variability of the cross-section of the BRB along the longitudinal axis, these latter members are characterised by an equivalent cross-section area A_{eq} equal to

$$A_{eq} = \frac{A_c}{\frac{L_j A_c}{L_w A_j} + \frac{L_t A_c}{L_w A_t} + \frac{L_c}{L_w}} \tag{17.1}$$

where L_w is the length of the brace, $L_c = 0.5\, L_w$ is the length of the yielding core of BRB, $L_j/2 = 0.65$ m is the length of each part of the connection segment, L_t is the length of the transition segment and $A_c/A_t = 0.5$ and $A_c/A_j = 0.3$ are the ratios of the cross-sectional area of the yielding core to the cross-sectional areas of the transition and connection segments, respectively.

The Giuffré-Menegotto-Pinto uniaxial material is assigned to the truss element. The plastic resistance of the BRBs is equal to the axial force corresponding to the yielding of the core. Therefore, the yielding stress is equal to $f_{y,eq}$.

$$f_{y,eq} = f_{ym}\frac{A_c}{A_{eq}} \tag{17.2}$$

f_{ym} being the mean value of the yield stress of the BRB (235 MPa). The post-yield stiffness ratio k_h is fixed equal to 0.053.

17.4 Seismic Analyses

The seismic analyses are performed in order to predict the seismic response of the buildings in terms of the floor displacements and storey drifts along the y-direction, which is the one affected by lateral-torsional coupling. Both nonlinear dynamic analysis (NDA) and nonlinear static (NS) analysis are performed. The seismic response obtained by the nonlinear dynamic analysis is assumed as benchmark to be predicted by the nonlinear static method of analysis. This analysis is also used to determine the seismic response of the *corresponding planar systems*. All the seismic analyses are carried out starting from a structural configuration in which the structural members have already been subjected to the gravity loads of the seismic design situation. P-Δ effects are not considered in the analysis because the interstorey drift sensitivity coefficient is lower than 0.1 for all the considered buildings (CEN 2004).

17.4.1 Dynamic Analysis

Seven ground motions are considered for the nonlinear dynamic analyses. The single ground motion consists of two accelerometric components acting along the x- and y-directions. The components of each ground motion are different from each other and compatible with the elastic response spectrum proposed in EC8 for soft soil (type C) and equivalent viscous damping ratio equal to 0.03. The accelerograms have been generated by means of the SIMQKE program (1976). The total length of the accelerogram is equal to 20 s while that of the strong motion phase is equal to 7 s, i.e. slightly lower than the minimum value suggested in EC8. Details about the choice of these accelerograms are described in Amara et al. (2014). Three levels of seismic excitation are considered. Specifically, the peak ground acceleration is set equal to 0.25 g, 0.35 g or 0.43 g.

The Rayleigh formulation is used to introduce damping. Mass and stiffness coefficients are defined so that two modes of vibration of the structures are characterised by an equivalent viscous damping ratio equal to 0.03. For planar systems, the considered modes of vibration are the first and second modes of vibration in the y-direction (i.e. T_{y1} and T_{y2} in Table 17.1). For the asymmetric systems, the first mode of vibration is that with the maximum period between $T_{y\theta1}$

and $T_{\theta y1}$ and the second mode is that with the maximum period between $T_{y\theta2}$ and $T_{\theta y2}$.

17.4.2 Pushover Analysis

For each building, the pushover analysis is performed by a set of horizontal forces applied in the y-direction and distributed along the height according to an inverted triangular load pattern. For each considered seismic excitation level, the pushover analysis is stopped when the displacement of the centre of mass of the top floor of the asymmetric system is equal to the average of the seven maximum top dynamic displacements of the corresponding planar system (*target displacement*). The present research study is intended to investigate solely the improvement caused by the corrective eccentricities to the prediction of the torsional response. Owing to this, the errors committed by the pushover analysis and regarding the translational response of the structures have been eliminated (Bosco et al. 2009). In particular, when predicting the floor displacements, the displacements provided by the push-over analysis at each storey of the building are scaled so that the displacement at the centre of mass equals the average of the maximum dynamic displacements of the corresponding planar system. When predicting the storey drifts, a similar scaling procedure is applied to the storey drifts.

17.5 Evaluation of the Corrective Eccentricities

The calculation of the corrective eccentricities e_1 and e_2 requires that the parameters e_r, e_s, Ω_θ and R_μ be determined. The rigidity eccentricity and the strength eccentricity are equal to -4.5 m (i.e. $-0.15\,L$) for systems TF-H and TR-H, while they are equal to -1.5 m (i.e. $-0.05\,L$) for systems TF-L and TR-L.

Among the methods available in literature (Bosco et al. 2013b; Calderoni et al. 2002; Doudomis and Athanatopoulou 2008; Makarios and Anastassiadis 1998a, b; Makarios 2008; Georgoussis 2009), the one proposed by Makarios and Anastassiadis (1998a, b) is used for the determination of the uncoupled torsional to lateral frequency ratios. According to this method, the uncoupled ratio $\Omega_{\theta y}$ is calculated as the ratios of the rigidity radius of gyration r_{kx} to the mass radius of gyration. This ratio is equal to 0.822 and 1.258 for the torsionally-flexible and the torsionally-rigid structures, respectively.

The parameter R_μ is determined as the ratio of the required elastic base shear $V_{b,el}$ to the actual lateral strength $V_{by,u}$ of the corresponding planar system. The elastic base shear is obtained by modal response spectrum analysis. The elastic response spectrum is that given in EC8 for soil C with peak ground acceleration a_g depending on the considered seismic excitation level (0.25 g, 0.35 g or 0.43 g). The actual lateral strength is calculated by pushover analysis, as the base shear corresponding

to the target displacement of the top floor required by the assigned seismic level. For all the considered structures, the ratios R_μ corresponding to the three considered values of a_g are equal to 2.69, 3.44 or 4.01.

The corrective eccentricities calculated on the basis of the relations proposed in Bosco et al. (2012) are reported in Table 17.2.

17.6 Results of the Numerical Analysis

In this section, a comparison is carried out between the seismic response obtained by means of the considered nonlinear static methods, i.e. the corrective eccentricity method and the standard nonlinear static method, and that obtained by nonlinear dynamic analysis. Note that the nonlinear static method without corrective eccentricity will be named as "EC8 method" for brevity even if it does not exactly coincide with the method reported in the code. Indeed, as remarked in Sect. 17.4.2, the results presented in this section correspond to the average top displacement obtained by means of the nonlinear dynamic analyses.

The in-plan distributions of the roof displacements obtained by the considered methods are compared in Fig. 17.2 with reference to systems with high eccentricity and peak ground acceleration equal to 0.35 g.

To provide a measure of the capability of the nonlinear static methods to predict the results of nonlinear dynamic analysis, the percentage error committed in the estimate of the dynamic displacement is calculated as

$$Err_i(\%) = \frac{u_i^{st} - u_i^{dyn}}{u_i^{dyn}}, i = 1 \, or \, 2 \tag{17.3}$$

where, u_i^{dyn} is the mean value of the maximum displacements obtained by nonlinear dynamic analysis, u_i^{st} is the displacement obtained by means of the nonlinear static method of analysis, and the subscript i equal to 1 or 2 denotes the stiff or the flexible side of the building. The equation above is also used to evaluate the percentage errors committed in the prediction of the storey drifts of the stiff and flexible sides. Positive values of the error indicate overestimates of the dynamic response (conservative errors), while negative values indicate underestimates of the dynamic response (unconservative errors). The variability of the errors committed at each storey is finally represented in Fig. 17.3. In particular, for each building, a bar limited by the minimum and the maximum errors is reported. Black and gray bars represent errors committed by the standard nonlinear static method or by the method of the corrective eccentricity, respectively.

Figures 17.2 and 17.3 show that when the nonlinear static method is applied according to the EC8 provisions (i.e. without corrective eccentricities), the displacements and drifts of the flexible side are well predicted for all the considered

Table 17.2 Corrective eccentricities

a_g/g	TF – L			TF – H			TR – L			TR – H		
	0.25	0.35	0.43	0.25	0.35	0.43	0.25	0.35	0.43	0.25	0.35	0.43
e_1 (m)	-1.97	-1.87	-1.79	-5.91	-5.63	-5.38	-0.86	-0.77	-0.65	-2.59	-2.30	-1.93
e_2 (m)	-1.10	-0.98	-0.86	-3.30	-2.93	-2.57	-0.22	0.120	0.53	-0.65	0.36	1.60
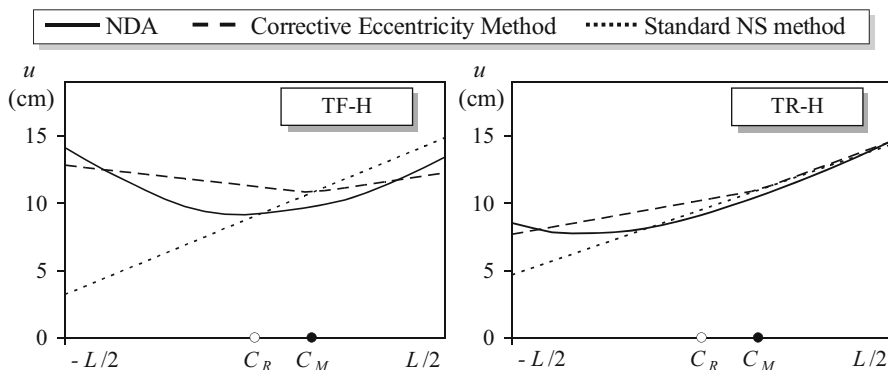
Fig. 17.2 Comparison of the top displacements obtained by the considered methods

buildings. Instead, the displacements and drifts of the stiff side are well predicted only for the structure TR-L.

The application of the corrective eccentricity method maintains the effectiveness of the EC8 method in the prediction of the displacement of the flexible side and provides a better estimate on the stiff side. In fact, in the worst case the maximum unconservative errors committed by the EC8 and corrective eccentricity methods are about 90 and 12 % in terms of floor displacements (Fig. 17.3a), and about 100 and 35 % in terms of storey drifts (Fig. 17.3b). Even if it is not shown in the figure, when the corrective eccentricity method is applied, the above mentioned maximum unconservative error in the estimate of storey drifts is committed at a single storey while the errors at the other storeys are significantly lower.

17.7   Conclusions

The chapter presents the validation of the corrective eccentricity method on a set of four multi-storey braced structures. The set of buildings includes torsionally-flexible and torsionally-rigid structures characterised by low or high rigidity and strength eccentricities. Further, three different seismic excitation levels are considered to analyse the effectiveness of the corrective eccentricity method in case of structures with moderate or high inelastic response. The effectiveness of the corrective eccentricity method is demonstrated by comparing its accuracy in predicting the nonlinear dynamic response of the analysed asymmetric buildings to that obtained by the standard application of the nonlinear static method, i.e. without corrective eccentricities. This comparison shows that the standard nonlinear static method provides a suitable prediction of the floor displacement and storey drifts only of the flexible side of the building. The corrective eccentricity method significantly enhances the prediction of floor displacement and storey drift on the stiff side of the building and the error committed in the prediction is always reasonable.
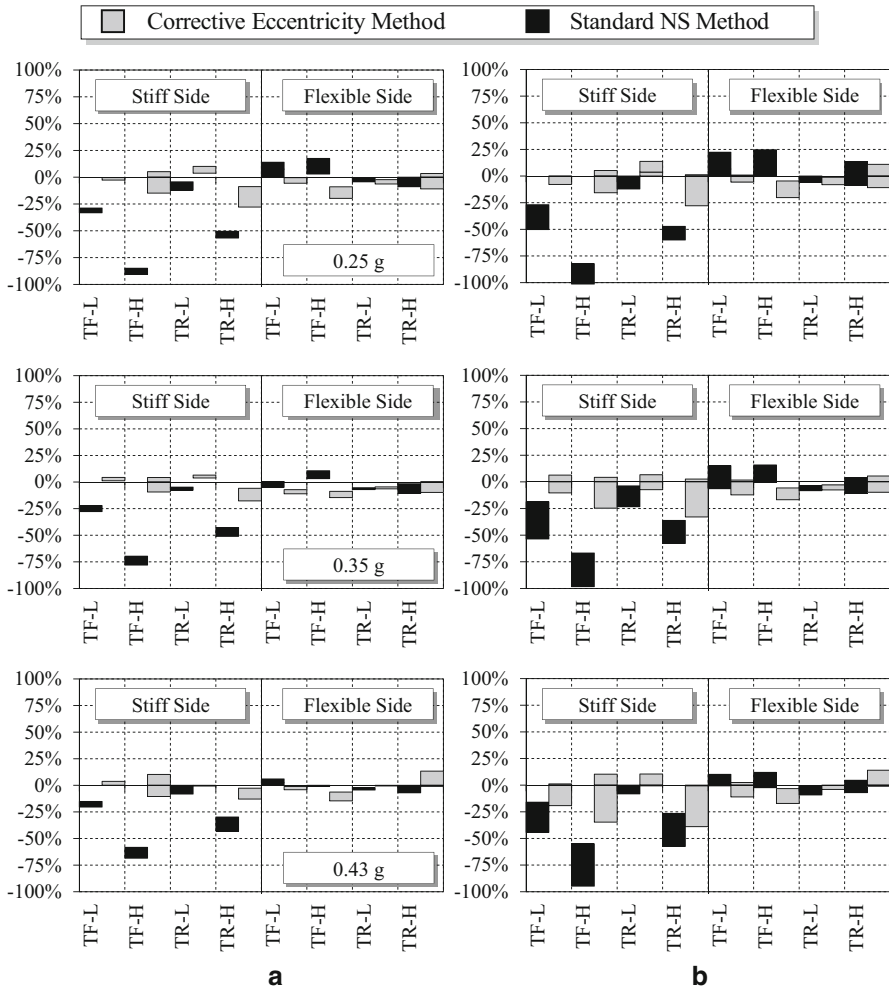
Fig. 17.3 Percentage errors in the evaluation of (**a**) floor displacements and (**b**) storey drifts

References

Amara F, Bosco M, Marino EM, Rossi PP (2014) An accurate strength amplification factor for the
    design of SDOF systems with P-Δ effects. Earthq Eng Struct Dyn 43(4):589–611
Bento R, Bhatt C, Pinho R (2010) Verification of nonlinear static procedures for a 3D irregular
    SPEAR building. Earthq Struct 1(2):177–195
Bosco M, Marino EM (2013) Design method and behavior factor for steel frames with buckling
    restrained braces. Earthq Eng Struct Dyn 42(8):1243–1263
Bosco M, Ghersi A, Marino EM (2009) On the evaluation of seismic response of structures by
    nonlinear static methods. Earthq Eng Struct Dyn 38(13):1465–1482

Bosco M, Ghersi A, Marino EM (2012) Corrective eccentricities for assessment by the nonlinear static method of 3D structures subjected to bidirectional ground motions. Earthq Eng Struct Dyn 41(13):1751–1773

Bosco M, Ghersi A, Marino EM, Rossi PP (2013a) Comparison of nonlinear static methods for the assessment of asymmetric buildings. Bull Earthq Eng 11(6):2287–2308

Bosco M, Marino EM, Rossi PP (2013b) An analytical method for the evaluation of the in-plan irregularity of non-regularly asymmetric buildings. Bull Earthq Eng 11(5):1423–1445

Calderoni B, D'Aveni A, Ghersi A, Rinaldi Z (2002) Static vs. modal analysis of asymmetric buildings: effectiveness of dynamic eccentricity formulations. Earthq Spectra 18(2):219–231

CEN, European Committee for Standardization (2004) Eurocode 8: design of structures for earthquake resistance. Part 1: general rules, seismic actions and rules for buildings. EN 1998-1:2004. Brussels, Belgium

De Stefano M, Tanganelli M, Viti S (2013) On the variability of concrete strength as a source of irregularity in elevation for existing RC buildings: a case study. Bull Earthq Eng 11(5): 1711–1726

De Stefano M, Tanganelli M, Viti S (2014) Variability in concrete mechanical properties as a source of in-plan irregularity for existing RC framed structures. Eng Struct 59(2):161–171

Doudomis IN, Athanatopoulou AM (2008) Invariant torsion properties of multistorey asymmetric buildings. Struct Des Tall Spec Build 17(1):79–97

Fajfar P (1999) Capacity spectrum method based on inelastic demand spectra. Earthq Eng Struct Dyn 28(9):979–993

Fajfar P, Marusic D, Peruš I (2005) Torsional effects in the pushover-based seismic analysis of buildings. J Earthq Eng 9:831–854

Fujii K (2014) Prediction of the largest peak nonlinear seismic response of asymmetric buildings under bi-directional excitation using pushover analyses. Bull Earthq Eng 12(2):909–938

Giorgi P, Scotta R (2013) Validation and improvement of N1 method for pushover analysis. Soil Dyn Earthq Eng 55:140–147

Kreslin M, Fajfar P (2012) The extended N2 method considering higher mode effects in both plan and elevation. Bull Earthq Eng 10:695–715

Makarios T (2008) Practical calculation of the torsional stiffness radius of multi-storey tall buildings. Struct Des Tall Spec Build 17(1):39–65

Makarios T, Anastassiadis A (1998a) Real and fictitious elastic axes of multi-storey buildings: theory. Struct Des Tall Spec Build 7(1):33–55

Makarios T, Anastassiadis A (1998b) Real and fictitious elastic axes of multi-storey buildings: applications. Struct Des Tall Spec Build 7(1):57–71

Mazzoni S, McKenna F, Scott MH, Fenves GL, Jeremic B (2003) OpenSEES command language manual. Pacific Earthquake Engineering Research Center, University of California, Berkeley

SIMQKE User Manual (1976) NISEE software library. University of California, Berkeley

Georgoussis GK (2009) An alternative approach for assessing eccentricities in asymmetric multistory buildings: 1. Elastic Systems. Struct Des Tall Spec Build 18(2):181–202

Chapter 18
Influence of the Interaction Yield Domain on Lateral-Torsional Coupling of Asymmetric Single-Storey Systems

Melina Bosco, Aurelio Ghersi, Edoardo M. Marino, and Pier Paolo Rossi

Abstract Single-storey models are widely adopted because they are able to describe the main aspects of the torsional coupling of asymmetric buildings and, at the same time, they are simple enough to enable extensive parametric analysis. Generally, single-story systems are constituted by a rigid deck, where the mass is lumped, supported by vertical resisting elements with lateral stiffness and strength in their plane only (uni-axial resisting elements). Thus, these models neglect the interaction phenomena that can be observed in actual framed structures, where the vertical resisting elements provide lateral stiffness and strength in all the horizontal directions. In this chapter, the influence of the interaction phenomena on the torsional coupling of the seismic response of asymmetric buildings predicted by nonlinear methods of analysis is investigated. Single storey systems with bi- and uni-axial resisting elements are used to simulate structures whose seismic response is affected or not by interaction phenomena. Finally, both nonlinear dynamic and nonlinear static methods of analysis are investigated.

Keywords Asymmetric buildings • Single-storey systems • Seismic assessment • Extended N2 method • Corrective eccentricity method

18.1 Introduction

The seismic response of asymmetric buildings depends on many parameters. In order to evaluate the influence of each parameter, the studies on this topic are often carried out by means of extensive parametrical analyses. An extensive parametrical study requires the adoption of simple mathematical models. For this reason, single-storey models are widely adopted to investigate the torsional behaviour of buildings

M. Bosco (✉) • A. Ghersi • E.M. Marino • P.P. Rossi
Department of Civil Engineering and Architecture, University of Catania, Viale A. Doria 6, 95125 Catania, Italy
e-mail: mbosco@dica.unict.it; aghersi@dica.unict.it; emarino@dica.unict.it; prossi@dica.unict.it

(Bosco et al. 2012). In fact, single-storey systems represent the extreme schematization of a real building and, although they do not cover some peculiarities related to the heightwise distribution of structural properties (Anagnostopoulos et al. 2010; De Stefano et al. 2013, 2014; Ghersi et al. 2007), they are able to describe the main aspects of the torsional seismic behaviour of actual asymmetric buildings which are regular in elevation (Bosco et al. 2013; De Stefano and Pintucchi 2010; Goel and Chopra 1990; Hejal and Chopra 1987; Palermo et al. 2013; Peruš and Fajfar 2005).

Generally, single-storey systems are constituted by a rigid deck, where the mass is lumped, supported by vertical resisting elements with lateral stiffness and strength in their plane only (*uni-axial resisting elements*). Based on the response of these models, four structural parameters seem to influence mostly the seismic response of asymmetric systems (Goel and Chopra 1990; Hejal and Chopra 1987; Palermo et al. 2013). These parameters are the rigidity eccentricity e_r (distance between the centre of rigidity C_R and the centre of mass C_M), the ratio Ω_θ of the torsional to lateral frequencies of the corresponding torsionally balanced system (obtained by shifting C_M into C_R), the strength eccentricity e_s (distance between the centre of strength C_S and C_M) and the ratio R_μ of the elastic strength demand to the actual strength of the system.

The single storey models with uni-axial resisting elements may be considered representative of multi-storey buildings in which the seismic forces are sustained by braced frames or shear walls. Instead, these models are less effective in simulating the response of r.c. and steel framed structures (Bosco et al. 2015). The vertical resisting elements of these structures, i.e. the columns, provide lateral stiffness and strength in all the horizontal directions and are characterised by a bi-axial yield domain such that the presence of bi-axial bending reduces their strength capacity (interaction phenomena). These aspects are neglected by uni-axial resisting elements.

In this chapter, the influence of interaction phenomena on torsional coupling of the seismic response of asymmetric buildings is investigated. Specifically, two different sets of single-storey models are considered. In the first set, the resisting elements provide lateral stiffness and strength along only one horizontal direction (either *x*- or *y*-direction of an orthogonal coordinate reference system). In the second set, the resisting elements provide lateral stiffness and strength in all the horizontal directions and possess a bi-axial yield domain (*bi-axial resisting elements*) to take into account the interaction phenomena. The seismic response of the considered models is expressed in terms of in plan distribution of displacements and is evaluated by both nonlinear dynamic and nonlinear static analyses.

18.2 The Single-Storey Models

All the analysed systems have a deck that is rectangular in plan and has dimensions, denoted as B and L, equal to 12.5 m and 29.5 m, respectively. The mass m of the deck is equal to 1416 t, while the mass radius of gyration r_m about the centre of

mass C_M is equal to $0.312\,L$. The resisting elements are located symmetrically with respect to the geometrical centre of the deck G.

The considered systems have values of Ω_θ which range from 0.6 to 1.4 with step 0.05 so as to analyse both torsionally flexible ($\Omega_\theta < 1$) and torsionally stiff systems ($\Omega_\theta > 1$). For each value of Ω_θ, several values of e_r from $-0.1\,L$ to 0 with step $0.025\,L$ are considered to include both systems with small and large rigidity eccentricity. The total lateral strength S of the systems is determined assuming values of R_μ from 1.0 to 6.0 with step 1.0. As a consequence, the considered systems may experience either moderate or large plastic deformations during the earthquake. Finally, for each value of R_μ, the total lateral strength is distributed among the resisting elements considering values of e_s from $-0.1\,L$ to $0.1\,L$ with step $0.025\,L$.

The influence of interaction phenomena is evaluated by comparing the seismic response of systems characterised by the same values of e_r, e_s, Ω_θ and R_μ and belonging to the sets of systems described in the two following Sections.

18.2.1   Systems with Uni-axial Resisting Elements

The resisting elements of the first set of systems (Fig. 18.1a) are arranged along the axes of the assumed reference system (4 along the x-axis and 8 along the y-axis). Each vertical resisting element has lateral stiffness and strength in its plane only (Fig. 18.1b) and is characterised by a bi-linear force-displacement relationship. The contribution γ_x of the resisting elements arranged along the x-axis to the total torsional stiffness of the system about the centre of rigidity C_R is equal to 20 %. This value is proper for buildings with a rectangular plan.

Structural systems with prefixed values of e_r are generated by modifying the position of C_M. The lateral stiffness $k_{xi}^{(1)}$ of the i-th resisting element along the x-direction and that $k_{yj}^{(1)}$ of the j-th element along the y-direction are modified
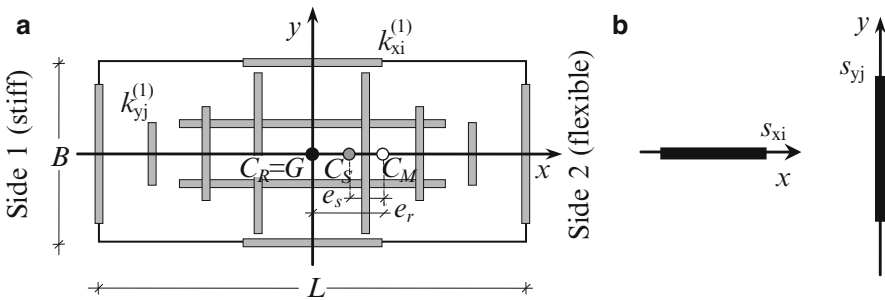
Fig. 18.1 (**a**) Plan layout of the systems of the first set; (**b**) uni-axial resistance of the resisting elements
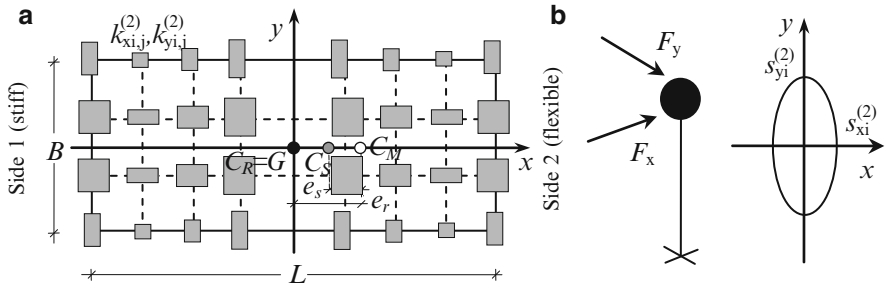
Fig. 18.2 (**a**) Plan layout of the systems of the second set; (**b**) bi-axial yield domain of the resisting elements

according to the procedure described in Ghersi and Rossi (2000) to obtain prefixed values of Ω_θ. Symmetry is maintained with respect to the x-axis.

The global lateral strength $S_x = S_y$ of the systems is assigned so as to have prefixed values of the ratio R_μ of the elastic strength demand to the actual strength of the corresponding planar system (i.e. of the system obtained by restraining the deck rotation of the basic scheme).

Then, in order to have assigned values of the strength eccentricity e_s, the lateral strength is distributed among the resisting elements according to the procedure described in Bosco et al. (2012). Furthermore, in order to consider the influence of the strength distribution on the inelastic seismic response of the systems, ten random distributions of strength s_{xi}, s_{yi} are generated for each value of e_s.

18.2.2 Systems with Bi-axial Resisting Elements

The resisting elements of the systems of the second set (Fig. 18.2a) provide lateral stiffness and strength in all the horizontal directions. The resisting elements are located at the points of the deck, which are the intersection of the axes of the resisting elements of the first set of systems.

In order to have systems which are characterised by the same values of the global parameters (e_r, e_s, Ω_θ and R_μ) of the corresponding systems of the first set, the components along the x- and y-direction of the lateral stiffness ($k_{xi,j}^{(2)}$, $k_{yi,j}^{(2)}$) and strength ($s_{xi,j}^{(2)}$, $s_{yi,j}^{(2)}$) of the resisting element which is located at the intersection of the i-th and j-th element are obtained by the relations:

$$k_{xi,\,j}^{(2)} = \frac{k_{xi}^{(1)}}{n_y^{(1)}} \qquad k_{yi,\,j}^{(2)} = \frac{k_{yj}^{(1)}}{n_x^{(1)}} \tag{18.1}$$

$$s_{xi,\,j}^{(2)} = \frac{s_{xi,\,j}^{(1)}}{n_y^{(1)}} \qquad s_{yi,\,j}^{(2)} = \frac{s_{yj}^{(1)}}{n_x^{(1)}} \tag{18.2}$$

where $n_y^{(1)} = 8$ and $n_x^{(1)} = 4$ are the number of resisting elements arranged along the y- or x-direction in the systems of the first set.

An elastic-perfectly plastic constitutive relation following the normality rule is adopted, and interaction phenomena arising in the nonlinear range of behaviour are accounted for by means of an ellipse yield domain (Fig. 18.2b).

18.3   Numerical Analyses

In order to investigate the influence of interaction phenomena on torsional coupling of the seismic response of asymmetric buildings, both pushover and nonlinear dynamic analyses are carried out.

A Rayleigh viscous damping is used for nonlinear dynamic analysis and set at 5 % for the first and the third modes of vibration. The Newmark method with parameters α and δ set at 0.25 and 0.5, respectively, is used to evaluate the dynamic response by step-by-step integration of the equations of motion. Bi-directional ground motions are used for nonlinear dynamic analysis. The accelerograms, generated by the SIMQKE computer program, are compatible with the elastic spectrum reported in Eurocode 8 for soil type C, 5 % damping ratio and peak ground acceleration a_g equal to 0.35 g. Each accelerogram is modeled by a trapezoidal envelope function with initial, central (stationary part) and final parts of 3, 22.5 and 5 s, respectively. The mean of the zero period spectral response acceleration values of the generated accelerograms is not lower than the value stipulated in Eurocode 8 and no value of the mean response spectrum is lower than 90 % of the corresponding value proposed in Eurocode 8.

The pushover analysis is carried out by applying a force along the direction of the displacements to be estimated, e.g. the y-direction. The force is applied at the centre of mass of the deck. The pushover analysis is stopped when the displacement of the centre of mass of the asymmetric system is equal to the average of the 10 maximum displacements of the corresponding planar system evaluated by nonlinear dynamic analysis.

18.4   Comparison of the Seismic Response of the Systems

Figure 18.3a shows the distribution of the maximum dynamic displacements ($u_{dyn,y}$) normalised to the maximum displacements of the corresponding planar system ($u_{pl,y}$). The results refer to a system characterised by $e_r = e_s = -0.10\,L$,
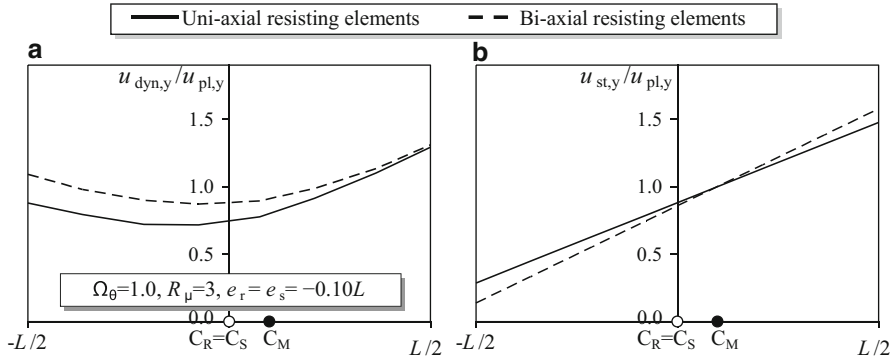
Fig. 18.3 Comparison between systems with uni- or bi-axial resisting elements (**a**) dynamic displacements; (**b**) static displacements

$R_\mu = 3$, and $\Omega_\theta = 1.0$. The solid line represents the displacements of the system with uni-axial resisting elements while the dashed line represents those of the corresponding system with bi-axial resisting elements. The figure shows that the increase in the dynamic displacements due to torsional effects on the flexible side is equal for the two systems. Instead, at the stiff side, the torsional effects cause an increase in the displacements obtained for systems with bi-axial resisting elements ($u_{\text{dyn,y}}/u_{\text{pl,y}} = 1.09$) and a reduction in the displacements for the system with uni-axial resisting elements ($u_{\text{dyn,y}}/u_{\text{pl,y}} = 0.88$).

A similar comparison is reported in Fig. 18.3b in terms of displacements obtained by the pushover analysis ($u_{\text{st,y}}$). Once again, the displacements are normalised to the maximum displacements of the corresponding planar system. The figure shows that, for the considered system, the torsional effects are more significant in the systems with bi-axial resisting elements. In fact, at the stiff side the ratio $u_{\text{st,y}}/u_{\text{pl,y}}$ is equal to 0.29 for the system with uni-axial resisting element and equal to 0.14 for the system with bi-axial resisting elements. Similarly, the ratio above is equal to either 1.48 or 1.58 at the flexible side.

Note that the results referring to $\Omega_\theta = 1.0$ have been plotted because this value of Ω_θ is proper of buildings with a framed structure, i.e. of buildings for which the bi-axial interaction phenomena may be significant.

To summarise the results obtained for the large number of structures analysed, the ratios $u_{\text{dyn,y}}/u_{\text{pl,y}}$ and $u_{\text{st,y}}/u_{\text{pl,y}}$ are first calculated at the stiff ($u_{\text{dyn1}}/u_{\text{pl}}$, $u_{\text{st1}}/u_{\text{pl}}$) and flexible ($u_{\text{dyn2}}/u_{\text{pl}}$, $u_{\text{st2}}/u_{\text{pl}}$) side for an assigned system (identified by fixed values of Ω_θ, R_μ e_s, e_r and by an assigned distribution of strength among the resisting elements). As the values of these ratios corresponding to the 10 strength distributions are always very close to one another, the average of the 10 values is considered as representative of the results corresponding to the different strength distributions.

Then, the ratios $u_{\text{dyn}}/u_{\text{pl}}$ and $u_{\text{st}}/u_{\text{pl}}$ are plotted in Figs. 18.4 and 18.5 as a function of e_r and e_s for assigned values of Ω_θ and R_μ. The grey surface refers to the ratios obtained for systems with uni-axial resisting elements; the white surface refers to
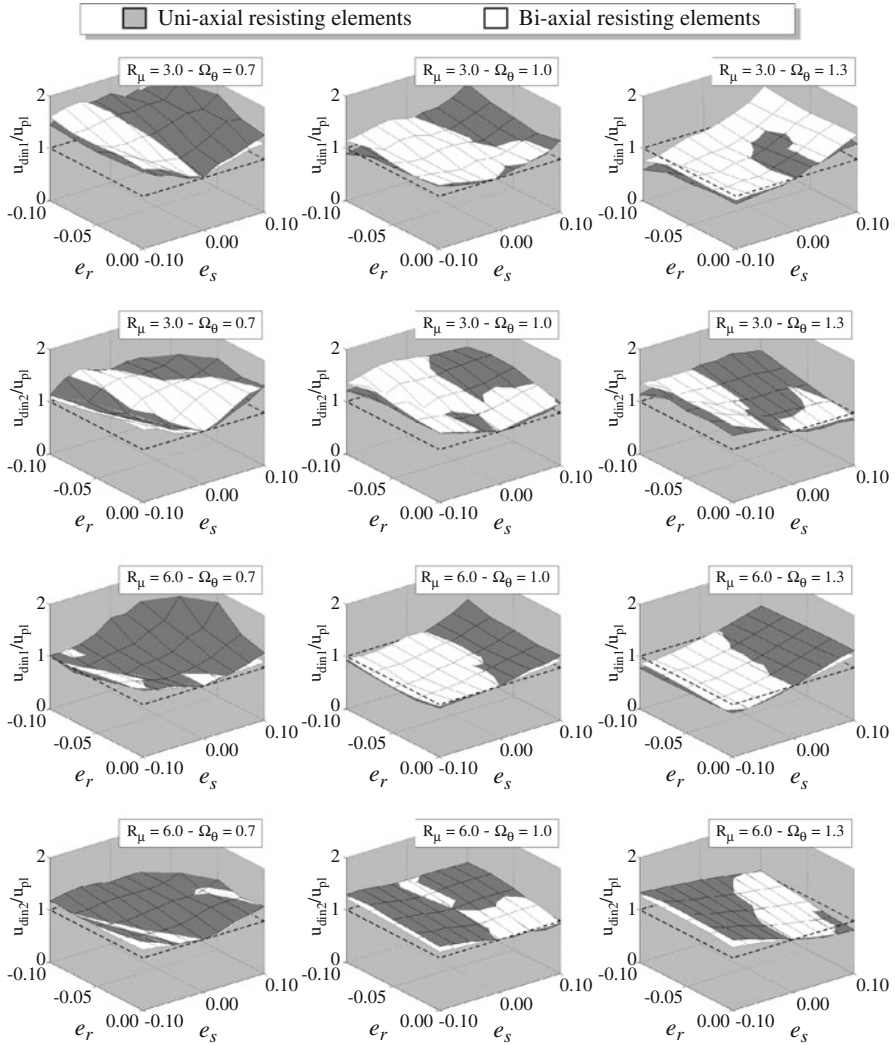
Fig. 18.4 Effects of the torsional coupling on the dynamic displacements at the stiff or flexible side of the systems

systems with bi-axial resisting element. Figure 18.4 shows that, if nonlinear dynamic analyses are carried out, the variations in the torsional response between systems belonging to the two considered sets are moderate, independently of the considered values of Ω_θ and R_μ. Instead, the interaction phenomena affect the prediction of the torsional response obtained by nonlinear static analysis significantly (Fig. 18.5). Further, the differences between the surfaces representing the two considered sets of systems increase as the ratio R_μ increases.
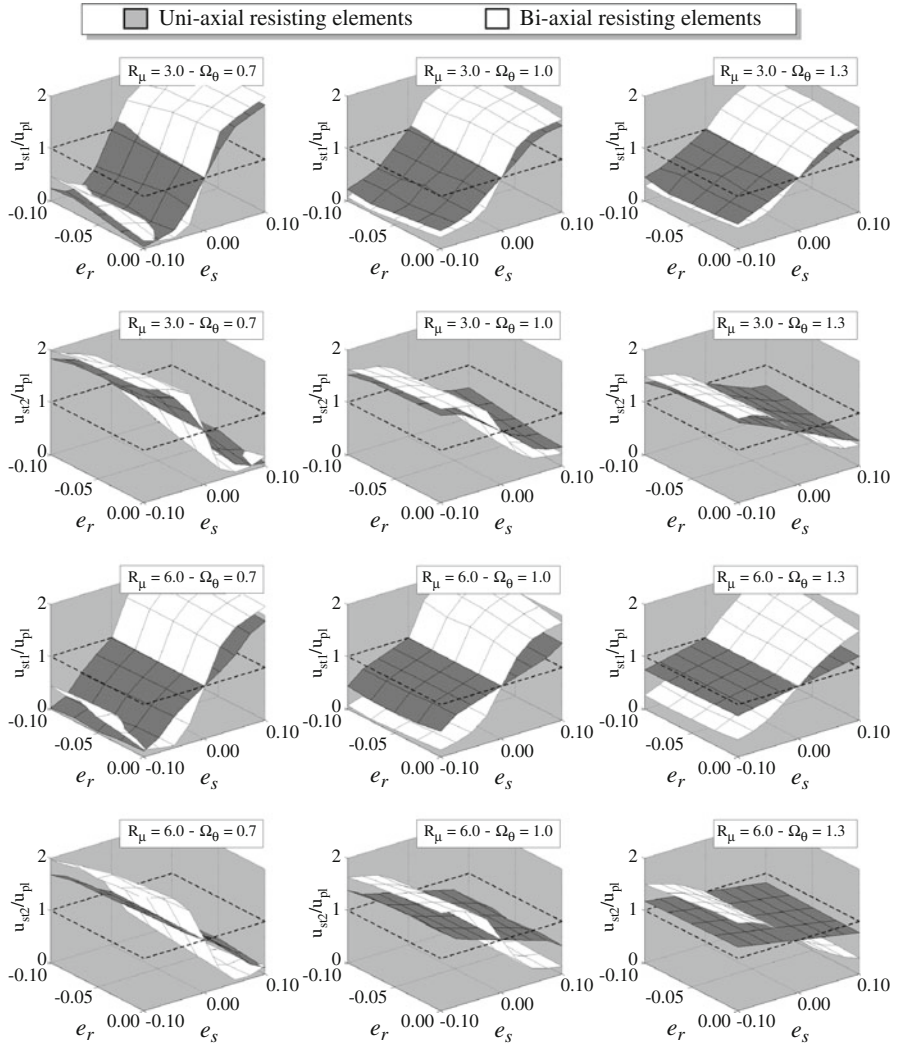
Fig. 18.5 Effects of the torsional coupling on the static displacements at the stiff or flexible side of the systems

18.5 Conclusions

The chapter analyses the influence of the interaction phenomena on torsional coupling of the seismic response of single-storey asymmetric systems. Specifically, the seismic response is determined by nonlinear dynamic and nonlinear static analysis for two sets of systems: systems with uni-axial resisting elements and bi-axial resisting elements, which neglect and take into

account the interaction phenomena, respectively. Then, the displacements of the two sides of the deck of the asymmetric systems normalised to the maximum displacement of the corresponding planar system, which are used to quantify the importance of the torsional coupling of the seismic response, are evaluated for the two sets of systems and compared.

The investigation shows that the influence of the interaction phenomena on torsional coupling effect is different depending on the method of analysis used for the prediction of seismic response. The predictions of the seismic response obtained by nonlinear dynamic analysis for systems with uni- and bi-axial resisting elements are always similar. Instead, the torsional responses predicted by nonlinear static analysis are similar only in case of systems with moderate inelastic response, while they are significantly different in case of systems that sustain a large inelastic displacement demand (large value of R_μ). Based on this consideration, nonlinear static methods for seismic response prediction calibrated by means of systems with uni-axial resisting elements should be used with caution on structures that are affected by strong interaction phenomena (for instance r.c. framed structures) and experience large inelastic deformation.

References

Anagnostopoulos SA, Alexopoulou C, Stathopoulos KG (2010) An answer to an important controversy and the need for caution when using simple models to predict inelastic earthquake response of buildings with torsion. Earthq Eng Struct Dyn 39(5):521–540

Bosco M, Ghersi A, Marino EM (2012) Corrective eccentricities for assessment by the nonlinear static method of 3D structures subjected to bidirectional ground motions. Earthq Eng Struct Dyn 41(13):1751–1773

Bosco M, Ghersi A, Marino EM, Rossi PP (2013) Comparison of nonlinear static methods for the assessment of asymmetric buildings. Bull Earthq Eng 11(6):2287–2308

Bosco M, Ferrara GAF, Ghersi A, Marino EM, Rossi PP (2015) Seismic assessment of existing r.c. framed structures with in-plan irregularity by nonlinear static methods. Earthq Struct 8(2):401–422

De Stefano M, Pintucchi B (2010) Predicting torsion-induced lateral displacements for pushover analysis: influence of torsional system characteristics. Earthq Eng Struct Dyn 39(12):1369–1394

De Stefano M, Tanganelli M, Viti S (2013) On the variability of concrete strength as a source of irregularity in elevation for existing RC buildings: a case study. Bull Earthq Eng 11(5):1711–1726

De Stefano M, Tanganelli M, Viti S (2014) Variability in concrete mechanical properties as a source of in-plan irregularity for existing RC framed structures. Eng Struct 59(2):161–171

Ghersi A, Rossi PP (2000) Formulation of design eccentricity to reduce ductility demand in asymmetric buildings. Eng Struct 22(7):857–871

Ghersi A, Marino EM, Rossi PP (2007) Static versus modal analysis: influence on inelastic response of multi-storey asymmetric buildings. Bull Earthq Eng 5(4):511–532

Goel RK, Chopra AK (1990) Inelastic seismic response of one-story asymmetric-plan systems, Report No. UCB/EERC-90/14. Earthquake Engineering Research Center, Berkeley

Hejal H, Chopra AK (1987) Earthquake response of torsionally-coupled buildings, Report No. UBC/EERC-87/20. Earthquake Engineering Research Center, Berkeley

Palermo M, Silvestri S, Gasparini G, Trombetti T (2013) Physically-based prediction of the maximum corner displacement magnification of one-storey eccentric systems. Bull Earthq Eng 11(5):1467–1491

Peruš I, Fajfar P (2005) On the inelastic torsional response of single-storey structures under bi-axial excitation. Earthq Eng Struct Dyn 34(8):931–941

Chapter 19
Improved Nonlinear Static Methods for Prediction of the Seismic Response of Asymmetric Single-Storey Systems

Melina Bosco, Aurelio Ghersi, Edoardo M. Marino, and Pier Paolo Rossi

Abstract Traditional nonlinear static methods, e.g. the original version of the N2 method implemented in Eurocode 8, are not always effective in the assessment of asymmetric structures. To overcome this shortcoming, two methods have been recently suggested by Kreslin and Fajfar and by Bosco et al. In this chapter, the two improved nonlinear static methods and the original N2 method are applied to predict the maximum seismic response of three groups of single-storey systems. Further, the systems of each group are schematised by means of two different single-storey models. In the first model, a rigid deck is sustained by resisting elements, which provide lateral stiffness and strength along only one horizontal direction. In the second model, the resisting elements provide lateral stiffness and strength in all the horizontal directions and possess a bi-axial yield domain.

Keywords Nonlinear dynamic response • Nonlinear static response • Asymmetric buildings • Single-storey systems • Modeling of resisting elements

19.1 Introduction

A proper seismic assessment of existing structures requires the comparison between the displacement capacity, i.e. the displacement corresponding to the achievement of a given limit state, and the displacement demand of the structure, i.e. the displacement caused by the ground motion. To this end, nonlinear static methods represent a powerful tool because they explicitly evaluate the inelastic response of structures and do not require the computational effort of nonlinear time-history analyses.

M. Bosco • A. Ghersi (✉) • E.M. Marino • P.P. Rossi
Department of Civil Engineering and Architecture, University of Catania, Viale A. Doria 6, 95125 Catania, Italy
e-mail: mbosco@dica.unict.it; aghersi@dica.unict.it; emarino@dica.unict.it; prossi@dica.unict.it

The nonlinear static method included in Eurocode 8, i.e. the N2 method proposed by Fajfar and his research team (Fajfar and Gašperšič 1996; Fajfar 1999), considers that the structure vibrates predominantly in a single mode. For this reason, it is suitable for predicting the response of regular planar frames, particularly if these structures are low-rise. The response of asymmetric structures, instead, always sees important contributions from more than one mode of vibration and is characterised by the simultaneous translation and rotation of the decks.

To make the nonlinear static methods reliable for the estimation of the displacement demand of plan-asymmetric structures, several researchers have proposed improvements to the standard procedure (Bento et al. 2010; Bosco et al. 2012; Chopra and Goel 2004; Fujii 2014; Kreslin and Fajfar 2012; Peruš and Fajfar 2005). These new procedures are called *improved nonlinear static methods* hereinafter.

In this chapter, the effectiveness of two improved nonlinear static methods and that of the original N2 method is investigated. The first improved method is the "*extended N2 method*" (Kreslin and Fajfar 2012). This method is based on the assumption that the results of the elastic analysis of an asymmetric structure, properly normalised, represent the upper bound of the torsional amplification of the inelastic response. The second improved method is the "*corrective eccentricity method*" (Bosco et al. 2012). According to this method, two nonlinear static analyses have to be performed for each direction of the seismic action. The lateral forces are applied to two points of the deck that are different from the centre of mass (C_M). The distances between the points where the lateral force is applied and C_M are named corrective eccentricities.

The two improved nonlinear static methods and the original N2 method are applied here to predict the maximum dynamic response of three groups of single-storey systems. Further, the systems of each group are schematised by means of two different single-storey models. In the first model, a rigid deck is sustained by resisting elements, which provide lateral stiffness and strength along only one horizontal direction (either x- or y-direction of an orthogonal coordinate reference system). In the second model, the resisting elements provide lateral stiffness and strength in all the horizontal directions. In particular, an elastic-perfectly plastic constitutive relation following the normality rule has been adopted, and interaction phenomena arising in the nonlinear range of behaviour are accounted for by means of an ellipse yield domain.

19.2 The Improved Non-linear Static Methods

19.2.1 The Extended N2 Method

According to the extended N2 method (Kreslin and Fajfar 2012) the inelastic seismic response of asymmetric structures can be conservatively predicted by adjusting the results of the original N2 method by means of correction factors

derived by a standard modal response spectrum analysis. The original N2 method is first applied to evaluate the displacement demand of the building. The pushover analyses can be performed on either two planar models (one for each direction of the seismic forces) or one 3-D model. The single pushover analysis is carried out until the displacement of the centre of mass of the roof reaches the displacement demanded by the assigned peak ground acceleration (target roof displacement).

Second, two modal response spectrum analyses of the 3-D model, one for each of the two horizontal directions of the seismic action, are performed. While the effects of the modes of vibration of the single modal response spectrum analysis are combined according to the CQC rule, those of the two modal response spectrum analyses are combined by the SRSS rule. The results of the modal response spectrum analysis are used to define two sets of correction factors to be applied to the results of the pushover analyses. One of the sets of correction factors refers to the heightwise distribution of the storey drifts and is not considered here because only single-storey systems are analysed. The second set of corrections factor refers to in-plan distribution of the displacements. Each correction factor is calculated as the ratio of the displacement at an arbitrary location to the displacement at the centre of mass C_M. In this chapter, the latter displacement is evaluated by the modal response spectrum analysis performed on two planar models (one for each direction of the seismic forces). The minimum value admitted for the correction factors is 1.0 because any favourable torsional effect arising from the elastic analysis is reduced in the inelastic range of behaviour.

19.2.2 The Corrective Eccentricity Method

The corrective eccentricity method predicts the displacement demand of asymmetric buildings through the envelope of the results of two nonlinear static analyses for each direction of the seismic action. The lateral forces are applied to two points of the deck that are generally different from the centre of mass C_M. The difference between the abscissa of the point where the force F is applied and the abscissa of C_M is named corrective eccentricity e_i. The corrective eccentricities are expressed as a function of the four parameters that mainly affect the torsional response of asymmetric structures (Goel and Chopra 1990; Hejal and Chopra 1987; Palermo et al. 2013). These parameters are the rigidity eccentricity e_r (distance between the centre of rigidity C_R and C_M), the ratio Ω_0 of the torsional to lateral frequencies of the corresponding torsionally balanced system (i.e. of the system obtained by shifting C_M into C_R), the strength eccentricity e_s (distance between the centre of strength C_S and C_M) and the ratio R_μ of the elastic strength demand to the actual strength of the *corresponding planar system*. This system is obtained by restraining the rotations of the deck.

The corrective eccentricities are calculated by means of analytical expressions (Bosco et al. 2012), which have been calibrated based on the results of a parametrical analysis. This analysis was performed on single-storey systems constituted by a rigid deck sustained by resisting elements, which provide lateral stiffness and strength along only one horizontal direction.

19.3 Analysed Systems

The analysed single-storey systems are mono-symmetric and are constituted by a rigid deck, which is rectangular in plan and is sustained by vertical resisting elements arranged along two orthogonal directions. The deck has dimensions, denoted as B and L in Fig. 19.1, equal to 12.5 m and 29.5 m, respectively. The systems are mass eccentric (MES). The mass m of the deck is equal to 1416 t and the mass radius of gyration r_m about C_M is equal to $0.312 L$. The systems are subdivided into three groups. The systems belonging to a single group have the same value of the uncoupled periods (i.e. the periods of the corresponding torsionally balanced system) along the x- and y-directions, as reported in Table 19.1.

Further, two models are adopted to represent the systems of each group. In the first model, which is suitable to simulate the behaviour of structures with braced frames or shear walls, the deck is supported by four resisting elements arranged along the x-axis of the assumed reference system (Fig. 19.1a) and by eight resisting elements arranged along the y-axis. All the resisting elements have lateral stiffness and strength in their plane only (*uni-axial resisting elements*). The force-displacement relationship of each vertical resisting element is bilinear with no strain hardening.

In the second model, which is suitable to simulate the behaviour of buildings with framed structure, the resisting elements are located at the points of the deck that are the intersection of the axes of the resisting elements adopted in the first model (Fig. 19.1b). Each resisting element provides lateral stiffness and strength in all the horizontal directions (*bi-axial resisting elements*). In particular, an elastic-perfectly plastic constitutive relation following the normality rule has been adopted, and interaction phenomena arising in the nonlinear range of behaviour are accounted for by means of an elliptical yield domain.
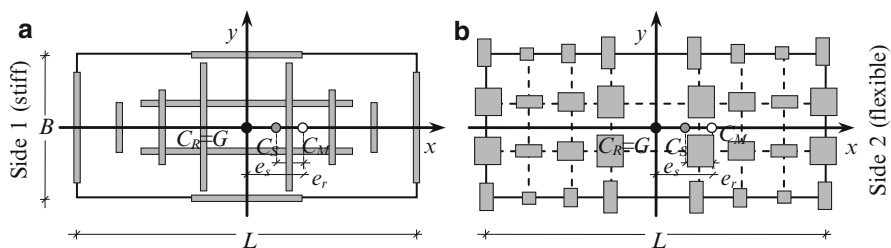
Fig. 19.1 Layout of systems with (**a**) uni-axial resisting elements; (**b**) bi-axial resisting elements

Table 19.1 Classification of the considered systems		Group		
	Resisting elements	01	02	03
	Uni-axial (U-)	$T = 0.6$ s	$T = 1.0$ s	$T = 1.4$ s
	Bi-axial (B-)	$T = 0.6$ s	$T = 1.0$ s	$T = 1.4$ s

For all the systems, the contribution γ_x of the resisting elements arranged along the x-axis to the total torsional stiffness about C_R is equal to 20 %. The systems belonging to each group are characterised by different values of the parameter e_r, e_s, Ω_θ and R_μ. Specifically, e_r is in the range from $-0.1\,L$ to 0 (step $0.025\,L$), e_s is in the range from $-0.1\,L$ to $0.10\,L$ (step $0.025\,L$), Ω_θ is in the range from 0.6 to 1.4 (step 0.05) and R_μ is in the range 1.0–6.0 (step 1.0). A further value $R_\mu = 0.5$ is considered to obtain also systems which exhibit an elastic behaviour.

19.4 Numerical Investigation

In this section, the effectiveness of the nonlinear static methods in estimating the maximum dynamic displacements of single-storey asymmetric systems is investigated. To this end, the single-storey systems described in the previous section are subjected to ten pairs of artificially generated ground motions and their seismic response is determined by nonlinear dynamic analysis. The Newmark method is used to evaluate the dynamic response of the analysed systems. The Rayleigh formulation is considered for damping. In particular, the viscous damping ratio is set equal to 5 % for the first and the third modes of vibration of the system. The average of the displacements along the y-direction obtained for the ten bi-directional ground motions is assumed as the benchmark for the nonlinear static methods. A computer program developed by the authors is used for the numerical analyses. This program can perform both the pushover and nonlinear dynamic analysis of 3D single-storey systems supported by uni- or bi-axial vertical resisting elements.

The errors committed by the nonlinear static methods (original N2 method, extended N2 method and corrective eccentricity method) in the estimate of the distribution of the maximum dynamic displacements are determined and analysed. As the object of this chapter is to test and compare the effectiveness of the analysed nonlinear static methods in predicting the in-plan distribution of the displacement demand, the errors in the estimate of the target displacement of the centre of mass (Bosco et al. 2009) are eliminated. To achieve this goal, the target displacement of the centre of mass of the asymmetric system is set equal to the average of the ten maximum (nonlinear) dynamic displacements of the corresponding planar system.

The effectiveness of the nonlinear static methods is quantified by means of the percentage difference between the displacement evaluated by the nonlinear static method and the corresponding value obtained by the dynamic analysis. Positive percentage differences indicate a conservative estimate provided by the nonlinear static method while negative values correspond to an unconservative estimate.

Three types of errors are calculated with regard to the whole system: (i) the maximum unconservative error (indicated as *max UCo error* in figures), (ii) the maximum conservative error (*max Co error* in figures), and (iii) the average absolute error, i.e. the average of the absolute values of the errors committed for all the resisting elements (*AAv error* in figures).

19.5   Discussion of the Results

To summarise the results obtained for the large number of structures analysed, each of the errors defined in the previous section is processed according to a procedure described in (Bosco et al. 2013) and reported in a compact form in Figs. 19.2 and 19.3. Grey, dark and white surfaces represent the errors committed by the original
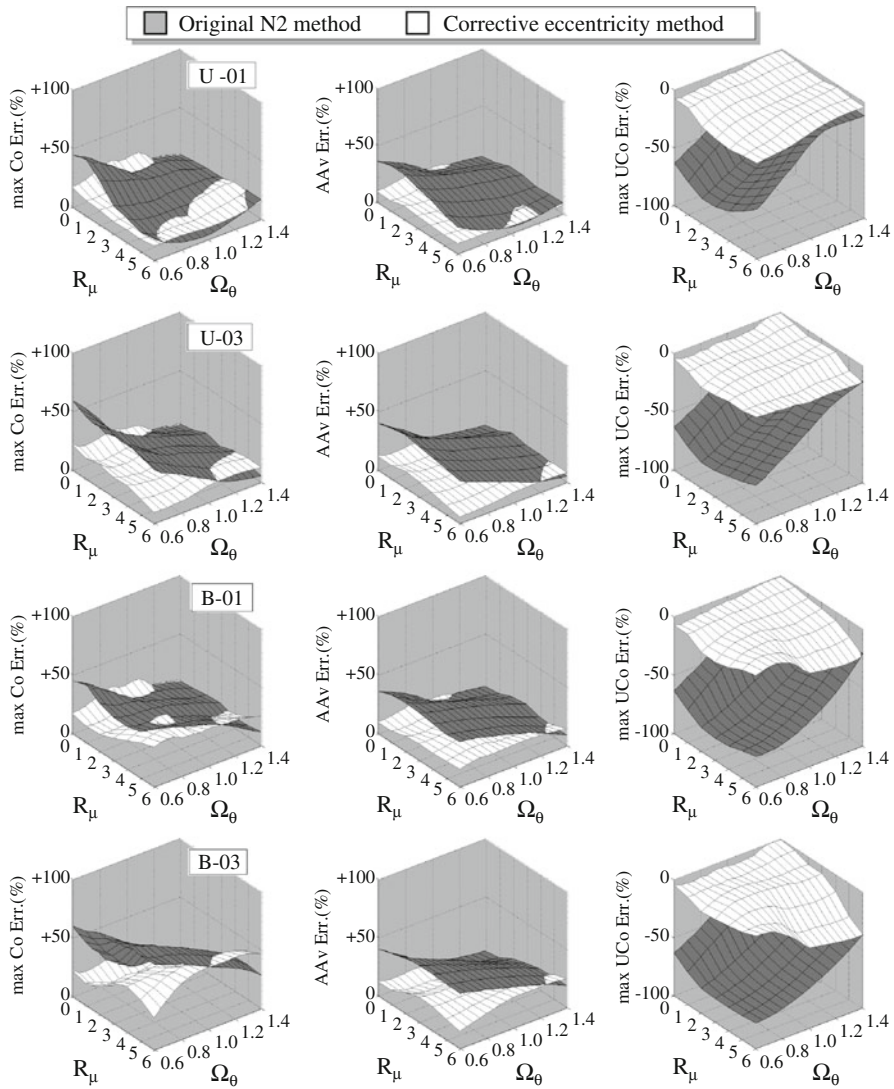
Fig. 19.2 Comparison between the errors committed by the original N2 method and the corrective eccentricity method (systems U-01, U-03, B-01, B-03)
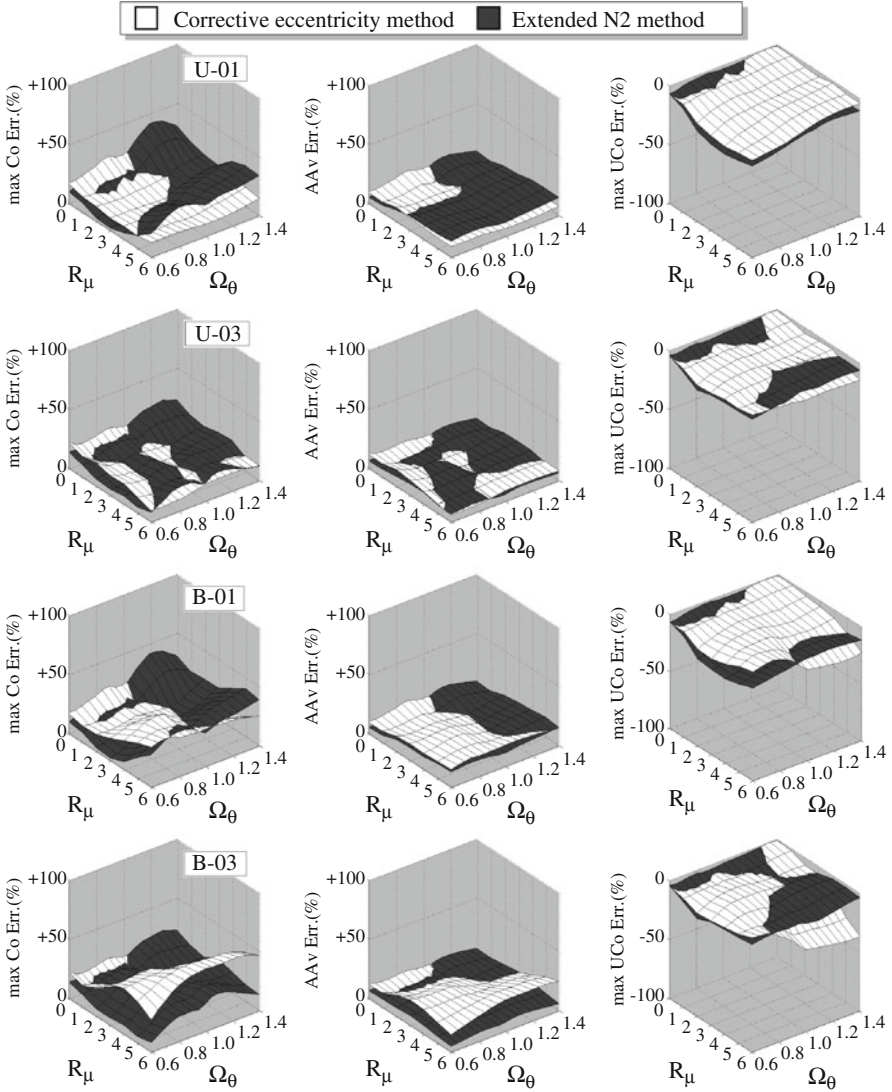
Fig. 19.3 Comparison between the errors committed by the improved nonlinear static methods (systems U-01, U-03, B-01, B-03)

N2 method, the extended N2 method and the corrective eccentricity method, respectively. Figure 19.2 shows that the standard N2 method is effective in the prediction of the seismic response of torsionally stiff structures (systems with Ω_θ larger than 1.2). In fact, for these systems all the considered errors are very low. Instead, the errors committed by this method of analysis (max Co, AAv and max UCo) are significant for all the other systems. For example, the maximum

unconservative errors committed for torsionally flexible systems are about 80 % ($\Omega_\theta = 0.6$, high value of the parameter R_μ). The use of the corrective eccentricity method enhances significantly the prediction of the displacement demand. In fact, this method leads to small unconservative and average errors for systems with uni-axial resisting elements. The errors are lower than those committed by the original N2 method but still significant for systems characterised by $\Omega_\theta > 1.0$, high value of the parameter R_μ and with bi-axial resisting elements. These errors are committed because the equations that provide the corrective eccentricities were calibrated neglecting the interactions phenomena that (1) modify significantly the prediction of the torsional response provided by nonlinear static analysis and that (2) modify only slightly the dynamic response (Bosco et al. 2015). Even if not shown in any figure, similar considerations apply to systems U-02 and B-02.

Figure 19.3 shows that the two improved nonlinear static methods are equally effective in the prediction of the seismic response of systems with uni-axial resisting elements even if the conservative errors provided by the extended N2 method are generally greater for torsionally stiff structures. The extended N2 method maintains its effectiveness for systems with bi-axial resisting elements. In fact, the prediction of the displacements provided by this method is equal for systems with uni- or bi-axial resisting elements.

19.6   Conclusions

The chapter investigates the effectiveness of two improved nonlinear static methods, namely the extended N2 method and the corrective eccentricity method, in predicting the seismic response of asymmetric single-storey systems. Their effectiveness is measured by the improvement that they can provide over the standard N2 method adopted in EC8. The investigation is conducted on a wide set of single-storey systems with uni- and bi-axial resisting elements, which are representative of buildings with braced frames (or shear walls) and framed structure, respectively.

The numerical investigation demonstrates that the standard N2 method is effective only in the prediction of the seismic response of very torsionally stiff structures (systems with Ω_θ larger than 1.2), but it leads to significant errors in the estimation of the displacement demand of the stiff side for other systems. For all the analysed systems, both the extended N2 method and the corrective eccentricity method provide an estimation of the displacement demand much closer to that determined by nonlinear dynamic analysis than that of the standard N2 method. When the two improved nonlinear static methods are compared each other, the extended N2 method, which is also easier to apply, generally appears more reliable than the corrective eccentricity method for systems with bi-axial resisting elements. Instead, the displacement demand predicted by the corrective eccentricity method is generally more accurate to that obtained by the extended N2 method for systems with uni-axial resisting elements.

References

Bento R, Bhatt C, Pinho R (2010) Verification of nonlinear static procedures for a 3D irregular SPEAR building. Earthq Struct 1(2):177–195

Bosco M, Ghersi A, Marino EM (2009) On the evaluation of seismic response of structures by nonlinear static methods. Earthq Eng Struct Dyn 38(13):1465–1482

Bosco M, Ghersi A, Marino EM (2012) Corrective eccentricities for assessment by the nonlinear static method of 3D structures subjected to bidirectional ground motions. Earthq Eng Struct Dyn 41(13):1751–1773

Bosco M, Ghersi A, Marino EM, Rossi PP (2013) Comparison of nonlinear static methods for the assessment of asymmetric buildings. Bull Earthq Eng 11(6):2287–2308

Bosco M, Ghersi A, Marino EM, Rossi PP (2015) Influence of the interaction yield domain on lateral-torsional coupling of asymmetric single-storey systems. In: Zbigniew Zembaty and Mario De Stefano (Eds) Seismic Behaviour and Design of Irregular and Complex Civil Structures II, vol 40, Chapter 18. Springer

Chopra AK, Goel RK (2004) A modal pushover analysis procedure to estimate seismic demands for unsymmetric-plan buildings. Earthq Eng Struct Dyn 33(8):903–927

Fajfar P (1999) Capacity spectrum method based on inelastic demand spectra. Earthq Eng Struct Dyn 28(9):979–993

Fajfar P, Gašperšič P (1996) The N2 method for the seismic damage analysis of rc buildings. Earthq Eng Struct Dyn 25(1):31–46

Fujii K (2014) Prediction of the largest peak nonlinear seismic response of asymmetric buildings under bi-directional excitation using pushover analyses. Bull Earthq Eng 12(2):909–938

Goel RK, Chopra AK (1990) Inelastic seismic response of one-story, asymmetric plan systems. Report No. UCB/EERC-90/14. University of California at Berkeley, Berkeley

Hejal R, Chopra AK (1987) Earthquake response of torsionally-coupled buildings. Earthquake Engineering Research Center, Report n° UCB/EERC-87/20. College of Engineering, University of California at Berkeley

Kreslin M, Fajfar P (2012) The extended N2 method considering higher mode effects in both plan and elevation. Bull Earthq Eng 10:695–715

Palermo M, Silvestri S, Gasparini G, Trombetti T (2013) Physically-based prediction of the maximum corner displacement magnification of one-storey eccentric systems. Bull Earthq Eng 11(5): 1467–1491

Peruš I, Fajfar P (2005) On the inelastic torsional response of single-storey structures under bi-axial excitation. Earthq Eng Struct Dyn 34(8):931–941

Chapter 20
Influence of the Rotational Mass Inertia on the Torsional Seismic Response

Dietlinde Köber and Dan Zamfirescu

Abstract Structures with uneven distributions of mass and stiffness (in the elastic range of behavior) and of mass and strength (in the inelastic range of behavior) are subjected to general torsion. These structures are called plan irregular ones. From a static elastic point of view general torsion may be described as a rotational movement around the center of stiffness, due to a given eccentricity (a distance between the center of stiffness, CR and the center of mass, CM). In order to describe more accurate the seismic behavior of plan irregular structures, at least a dynamic elastic point of view is needed. Under dynamic seismic input rotational mass inertia tries to overcome the rotation generated by the given eccentricity. Therefor a rotational inertial moment appears, as counterpart for the rotation around the CR. When moving to the nonlinear range of behavior, the rotational movement around CM takes place as counterpart of the rotational movement around the center of strength, CF. The authors aim to investigate how the rotational moment, due to mass inertia, changes for different structural layouts and seismic inputs. Because the rotational inertial moment is a measure for the elastic as well as for the inelastic structural behavior, it turns out to be a consistent way of describing the seismic response of plan irregular structures.

Keywords Rotational inertial moment • Plan irregularity • Inelastic behaviour • Torsional restrained structure • Dynamic nonlinear analysis

20.1 Introduction

Several past studies concerning plan irregular structures (Köber and Zamfirescu 2009, 2010; De La Llera and Chopra 1995; Garcia et al. 2004; Goel and Chopra 1990) showed a great sensitivity of their seismic response to the nature and intensity of the seismic input. According to former work in this field, the displacement demand turned out to be very different when changing the accelerogram applied

D. Köber (✉) • D. Zamfirescu
Reinforced Concrete Department, Technical University of Bucharest, B-dul Lacul Tei no. 122-124, 020396 Bucharest, Romania
e-mail: kober_dietlinde@yahoo.com; dzam@utcb.ro

Fig. 20.1 Definition of $M_{dynamic}$
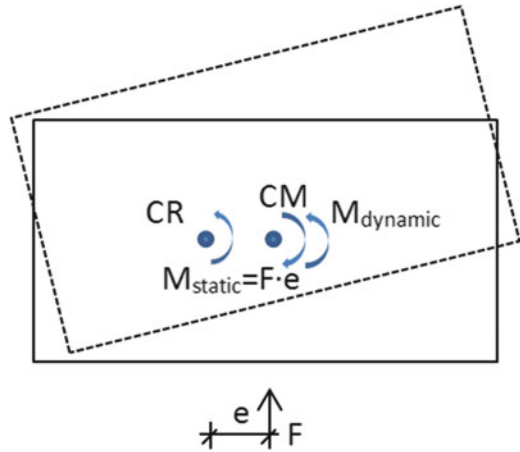
for dynamic calculation. Therefore consistent trends of behaviour for plan irregular structures are difficult to define in terms of structural displacement and rotation. A response measure having limited variation with respect to the seismic input and to the structural layout is needed. Former research in the field of plan irregular structures mentioned the rotary inertia of mass as an important parameter of the dynamic response (Paulay 2001). This study focuses on the effect of the inertial rotational moment, a measure suitable for the elastic range of behaviour as well as for the inelastic one, that may be described as follows (see Fig. 20.1):

$$M_{static} - M_{dynamic} = M_{total}$$

where:

$M_{static} = F{\cdot}e$ – static torsional moment equal to the seismic equivalent load (F) multiplied by the given eccentricity (e); gives a rotational movement around the centre of stiffness, CR;

$M_{total} = \Sigma(F_{yi}{\cdot}d_i + F_{yj}{\cdot}d_j)$ – torsional capacity defined as product of the yield forces of the structural elements and the distance between the structural elements and the centre of mass CM; "i" and "j" are the main directions of the layout;

$M_{dynamic}$ – counterpart of the static torsional moment, due to rotational mass inertia. A given eccentricity, e, produces the torsional moment M_{static}, which initiates a torsional movement around CM, $M_{dynamic}$. The two torsional components are withstand by the structural torsional capacity. $M_{dynamic}$ may be reflected only by dynamic calculation. In static calculation mass inertia is not mobilized.

The authors analyzed two different types of single-story plan irregular structures (twist restricted as well as twist unrestricted) subjected to a natural accelerogram and three spectrum compatible records, considering the design spectra of the Romanian Seismic Design Code and of the Eurocode 8. Several corner periods of the seismic input and structural eigen periods were considered. Dynamic nonlinear

calculation was applied for earthquake intensity values with a PGA of 0,2 g and of 0,4 g). The aim of the study is to investigate if the inertial torsional moment may be a predictable measure for the seismic response of plan irregular structures.

The study focuses especially on torsional restrained structures (having also structural elements perpendicular to the direction of the seismic input because they are practice suitable) and on structures with concentrated stiffness and strength (walls as lateral resisting elements).

Results from 720 cases (considering the variation of structural stiffness, corner period of the ground motion and seismic intensity level) were compared.

20.2 Analysed Structures

In this chapter two single story structures, having plan layouts of 11×44 m respective 22×22 m were investigated. Especially torsional stiff (twist restrained, TI) structures were analyzed due to the fact that most real structures have lateral load resisting elements on both main directions. For comparison also few torsional flexible structure (twist unrestrained, TL), were included in this study (see Fig. 20.2). Both structures in Fig. 20.2 are idealized structures with a rigid diaphragm floor and columns and walls as vertical structural elements. The vertical structural elements are disposed symmetric about the x and y axis. The structural mass is lumped at the center of mass (CM).

The structures of Fig. 20.2 are symmetric structures, being characterized through a coincidence between the center of stiffness (CR), the center of mass (CM) and the center of strength (CF). The corresponding eccentric systems are obtained by translating gradually CR and CF along the y axis, from its initial position up to ± 20 % of the plan dimension of the structure normal to the direction of the seismic input.
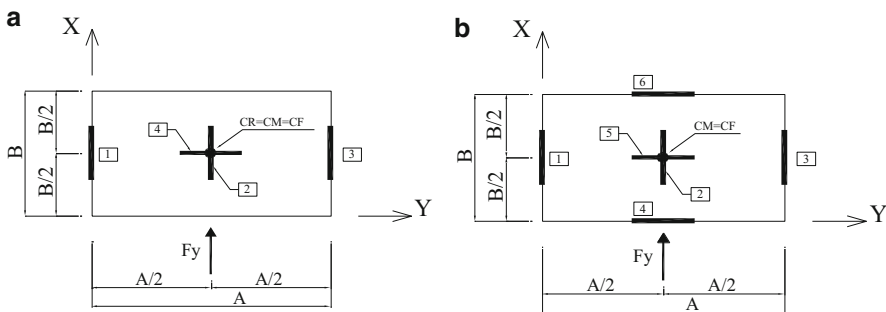
Fig. 20.2 Layout of symmetric structures: (**a**) torsional flexible (TL); (**b**) torsional stiff (TI)
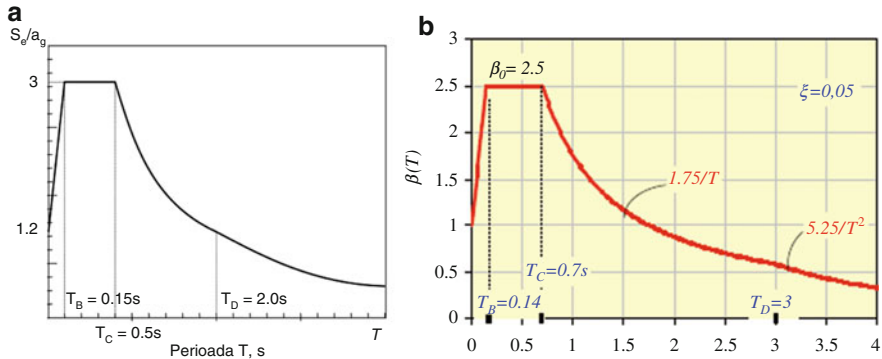
Fig. 20.3 Seismic design spectra: (**a**) EC8 – $T_c = 0.5$ s; (**b**) Romanian Seismic Design Code – $T_c = 0.7$ s

The total weight (G) of the floor is 4840 kN (considering a uniform load $p = 10$ kN/m^2). The structural walls were modeled as elastic-perfectly plastic springs acting on x and y direction (Zamfirescu 2000).

The stiffness of the structural elements was chosen for both main directions so that the initial translational period of the structure equals 0.7 s or 1.6 s. The stiffness and the strength of walls P2 and P4 (for TL) and of walls P2 and P5 (for TI) remain constant.

Structural static as well as dynamic rotations were computed.

20.3 Seismic Input

The seismic input for this study is unidirectional (along x direction) and is given by original records as well as by spectrum compatible accelerograms, acting along the x axis. Therefor design spectra from Eurocode 8 and the Romanian Seismic Design Code were used. Design spectra for corner periods equal to 0.5 s and 0.7 s were considered.

The results were obtained for two intensity levels of seismic input, scaling each accelerogram to a PGA of 0.2 g (Ultimate Limit State, SLU) and 0.4 g (Survivability Limit State, SVLS). For each seismic intensity level the authors considered an original record and three spectrum compatible accelerograms (see Fig. 20.3).

20.4 Case Study

The target of this case study was to identify a response measure suitable for plan irregular structures, that has a controlled variation with respect to the seismic input and to the structural layout. The authors interest focused on the torsional moment
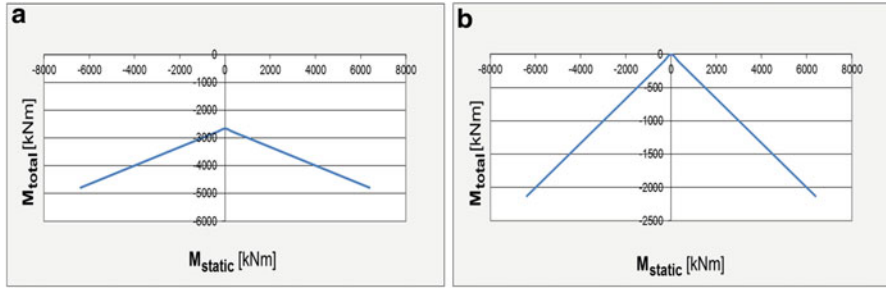
Fig. 20.4 Total torsional moment versus static torsional moment: (**a**) TI structure; (**b**) TL structure

around CM, $M_{dynamic}$ (due to rotational mass inertia), as counterpart of the static torsional moment, M_{static} (given by the static eccentricity). This choice may be explained by the fact that the torsional moment $M_{dynamic}$ is a structural response measure suitable for the elastic as well as for the inelastic range of behaviour and due to the fact that it may be calculated from static analysis.

Due to the fact that the torsional rotation around CM is reflected only by dynamic calculation the authors have chosen the name of $M_{dynamic}$.

Figure 20.4 shows the variation of M_{total} with respect to M_{static} for the 11×44 m structural layout and for the range of eccentricities considered (from -20 % up to 20 % of the plan dimension perpendicular to the direction of the seismic input in steps of 1 %). As expected, $M_{dynamic}$ is opposite to M_{static} (greater values for M_{static} than for M_{total}) and has greater values (twice in this case) for the TL structure compared to the TI structure.

In order to connect the computed $M_{dynamic}$ to the real behaviour of the analysed plan irregular structures, dynamic nonlinear calculation was applied and the variation of $M_{dynamic}$ with respect to the maximum rotation was investigated (see Fig. 20.5).

In Fig. 20.5 the variation of $M_{dynamic}$ with respect to the maximum rotation is shown for an original seismic input and three spectrum compatible accelerograms. The straight red line indicates the variation of $M_{dynamic}$ with the maximum rotation, having as slope the residual torsional stiffness (computed for the TI structure taking into account the lateral stiffness of the structural walls perpendicular to the direction of the seismic input). This estimation is sustained by the fact that the walls parallel to the direction of the seismic input yield because of translation and do not contribute to the structural torsional stiffness.

Graphics in Fig. 20.5 are representative for all analyzed cases and show the following main trends:

(a) $M_{dynamic}$ has a linear variation with respect to the maximum rotation;
(b) the residual torsional stiffness gives the slope of this variation (until yielding of all structural elements is achieved);
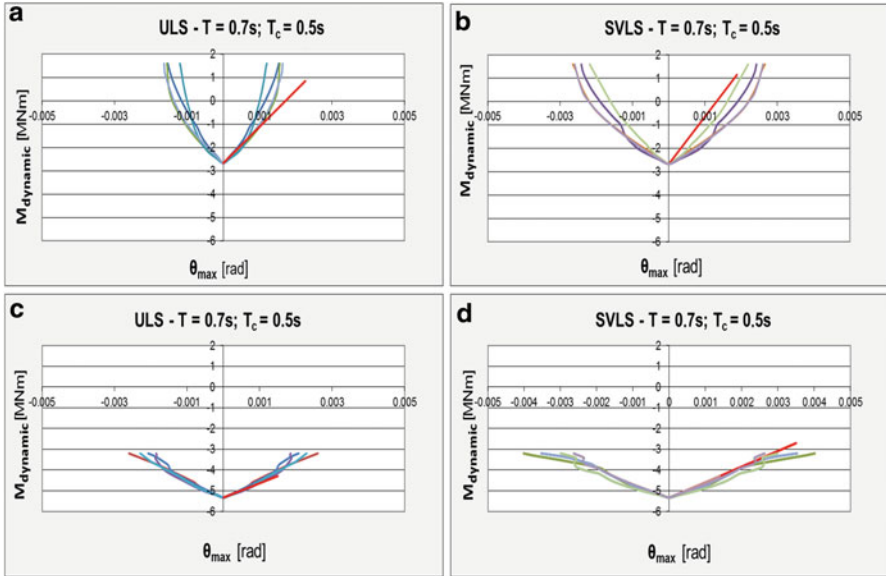
Fig. 20.5 Dynamic torsional moment versus maximum rotation; TI structure; T = 0.7 s; $T_c = 0.5$ s: (**a**) 11 × 44 ULS; (**b**) 11 × 44 SLSV; (**c**) 22 × 22 ULS; (**d**) 22 × 22 SLSV
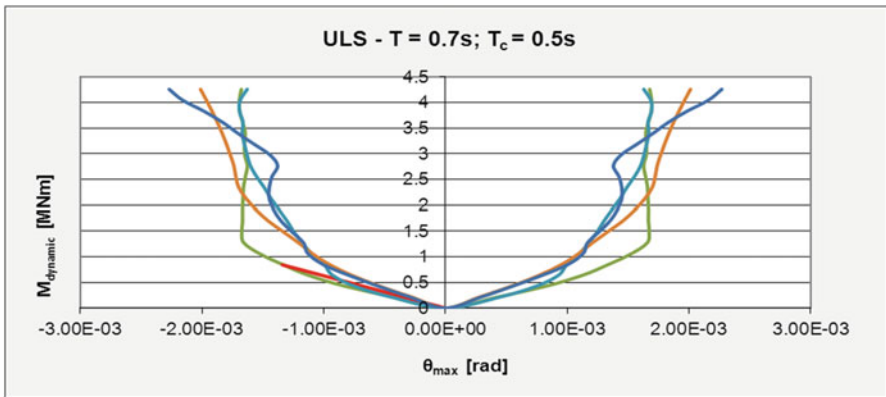
Fig. 20.6 Dynamic torsional moment versus maximum rotation for the 11 × 44 TL structure; T = 0.7 s; $T_c = 0.5$ s

(c) remarks (a) and (b) are valid for both analyzed structural layouts, both limit states and all seismic inputs considered.

Figure 20.6 shows an example of variation of $M_{dynamic}$ with the maximum rotation for a TL structure. Remarks made for the TI structures remain valid.

As expected, "yielding" of structural elements is reached earlier compared to the TI structure because walls parallel to the direction of the seismic input have to

Table 20.1 Eccentricity values for the 11 × 44 layout

			Eccentricity [%]	
	T [s]	T$_c$ [s]	ULS	SLSV
11 × 44 TI	0.7	0.5	8	8
		0.7	8	9
	1.6	0.5	15	9
		0.7	14	8
11 × 44 TL	0.7	0.5	5	–

Table 20.2 Eccentricity values for the 22 × 22 layout

			Eccentricity [%]	
	T [s]	T$_c$ [s]	ULS	SLSV
22 × 22 TI	0.7	0.5	11	8
		0.7	11	9
	1.6	0.5	17	12
		0.7	15	11

withstand translation and torsion. Once these walls yield, the structure has very low residual torsional stiffness (curves in Fig. 20.6 become asymptotic).

For the red line in Fig. 20.6 a residual stiffness of 5 % has been considered.

The linear variation of $M_{dynamic}$ with the maximum rotation is a first encourageable result of our study. Also the slope of this variation may be estimated by the residual torsional stiffness. Nevertheless, in order to use those results for current practice, the eccentricity range for which this estimation may be suitable should be determined. After "yielding" of walls in both main directions (for TI structures) this estimation is no more valid and explicit dynamic nonlinear analysis should be applied.

Tables 20.1 and 20.2 show eccentricity values up to which the residual torsional stiffness offers a good estimation of the variation of $M_{dynamic}$ with the maximum rotation. The eccentricity values are given as percentage from the plan dimension perpendicular to the direction of the seismic input.

Values in Tables 20.1 and 20.2 show that for T ≤ T$_c$ a suitable eccentricity value may be 10 % irrespective of the limit state, the seismic input or the structural layout. For T ≥ T$_c$ the eccentricity value may be 10 % for SVLS and may rise to 15 % for ULS.

This eccentricity limit may represent a suitable alternative to nowadays code provisions regarding the threshold between regular and irregular structures.

20.5   Concluding Remarks

This study showed that the inertial rotational moment may be a measure of plan irregularity suitable for practical design. It may be computed by static analysis and turned out to have a controlled variation with respect to the seismic input, the structural layout and the seismic intensity.

The residual torsional stiffness gives a good estimation of the variation of the inertial rotational moment with respect to the maximum structural rotation.

Further investigations need to be conducted considering also a bidirectional seismic input.

References

De La Llera JK, Chopra AK (1995) Understanding the inelastic seismic behavior of asymmetric plan – buildings. Earthq Eng Struct Dyn 24(4):549–572

EN 1998-1: 2004. Design of structures for earthquake resistance. General rules, seismic actions and rules for buildings, pp 45–69

Garcia O, Islas A, Ayala AG (2004) Effect of the in-plan distribution of strength on the non-linear seismic response of torsionally coupled buildings. In: Proceedings of the 13th WCEE, Lisbon, 24–28 September 2012, p 1891

Goel RK, Chopra AK (1990) Inelastic seismic response of one – story, asymmetric – plan systems. College of Engineering, University of California at Berkeley. UBC/EERC – 90/14

Köber D, Zamfirescu D (2009) Simplified methods used for evaluation of the displacement gain due to general torsion. Sci J Math Model Civ Eng 5(2):32–51

Köber D, Zamfirescu D (2010) Effects of general torsion on structural displacements. In: Proceedings 14 ECEE. Technical University Bucharest. ISBN 978-608-65185-1-6

Paulay T (2001) Some design principles relevant to torsional phenomena in ductile buildings. J Earthq Eng 5(3):273–308

P100 -1/ 2006. Cod de proiectare seismică. Prevederi de proiectare pentru clădiri, 32–61

Zamfirescu D (2000) *TORSDIN* – dynamic nonlinear analysis computer program. Reinforced Concrete Department. Technical University Bucharest

Chapter 21
Seismic Response Trends of SDOF Plan Irregular Structures. Simplified Approach

Dietlinde Köber and Dan Zamfirescu

Abstract Plan irregular structures experience a torsional seismic response even if the seismic input is unidirectional, due to an uneven distribution of mass and stiffness (in the elastic range of behavior) and of mass and strength (in the inelastic range of behavior). The seismic behavior of plan irregular structures is difficult to preview due to coupling between the translational and the rotational movement and to the change of the importance of stiffness and strength when moving from the elastic to the inelastic range of behavior. Past studies have also shown a high sensitivity of the seismic response of plan irregular structures to the characteristics of the ground motion. Therefor establishing trends of behavior for plan irregular structures is a goal very difficult to achieve but still it is a basic requirement for defining simplified approaches useful in current praxis. Dynamic nonlinear analysis and the simplified SESA method (Kober D, Zamfirescu D, Effects of general torsion on structural displacements. In: Proceedings 14 ECEE. ISBN 978-608-65185-1-6, 2010) were used for investigation. Structural displacements, rotations and rotational moments were checked and compared. The aim of the study is to establish behavior trends for plan irregular structures, looking especially at the variation of the rotation around CM, due to mass inertia.

Keywords General torsion • Inertial torsional moment • Response scattering dynamic nonlinear analysis • Statistic evaluation

21.1 Introduction

General torsion is a complex phenomenon that may be explained accurate by dynamic nonlinear analysis.

Because dynamic nonlinear analysis is too complicated for current practical design, research on general torsion focused during the last decades on defining simplified methods (as the N2 method or the MPA method) for computing the displacement amplification due to general torsion.

D. Köber (✉) • D. Zamfirescu
Reinforced Concrete Department, Technical University of Bucharest,
B-dul Lacul Tei no. 122-124, 020396 Bucharest, Romania
e-mail: kober_dietlinde@yahoo.com; dzam@utcb.ro

The authors proposed a simplified method for the estimation of the effects of general torsion on single story plan irregular structures under seismic action. The method (called SESA) is based on superposition of modal effects but it is extended to nonlinear behavior of the structure by using overdamped displacement response spectra. The method can be analytically applied for the estimation of the displacement amplification due to torsion (compared to translational only behavior) using the same steps of a regular spectral analysis.

Past studies (Köber and Zamfirescu 2009, 2010; De La Llera and Chopra 1995; Garcia et al. 2004) showed a high sensitivity of results from simplified design methods, with respect to the seismic intensity. Particularly, the observed variation of the accuracy of results from the SESA method compared to dynamic nonlinear analysis results is not monotone with the seismic intensity and differs for different structural assemblies. In order to apply SESA in practical design, the uncertainty of the accuracy of results should be investigated. Therefor the authors considered a study concerning the influence of the amount of nonlinearity on the response of plan irregular structures to be of interest.

Therefore the authors analyzed a large range of single-story plan irregular structures (twist restricted as well as twist unrestricted) subjected to a natural input and three spectrum compatible records, considering the design spectra of the Romanian Seismic Design Code and of the Eurocode 8 (P100 -1/2006; EN 1998-1, 2004). Three corner periods of the ground motion (0,5 s; 0,7 s; 1,6 s) were taken into account together with the variation of the structural stiffness (eigen periods of 0,3 s; 0,7 s; 1,6 s) and with the variation of the earthquake intensity (from elastic behavior until a PGA of 0,4 g). Eccentricity values (distances between the center of mass and the stiffness center, which coincides with the resistance center) of up to ± 20 % from the plan dimension perpendicular to the direction of the seismic input were considered.

Results from 324 cases (considering the variation of structural stiffness, corner period of the ground motion and seismic intensity level) were compared in order to answer the following questions:

1. How does the accuracy of results (from SESA compared to DNA) change with the seismic intensity, the structural type (TL or TI) and the corner period of the seismic input?
2. Is the accuracy of results equal for structural displacements, rotations and the inertial torsional moment?

21.2 Simplified Method for the Estimation of the Effects of General Torsion (SESA)

SESA is based on the estimation of the structural response under seismic action of an irregular single story system, by modal response spectrum analysis. In order to take into account the inelastic behavior, the capacity spectrum method is used, by equating the nonlinear system to an elastic one, equivalent in translation. The

resulting linear equivalent system is defined by the secant to maximum displacement stiffness, and the viscous damping properties are set through equivalence with the hysteretic damping properties of the initial system. The simplified method can be used to assess the displacement amplification due to general torsion maintaining the simplicity of the spectrum analysis (Goel and Chopra 1990).

The values of the equivalent damping ratio are set in order to obtain the same displacement of the equivalent linear system with the nonlinear displacement of the inelastic system.

It is important to mention that the simplified method is entirely consistent with the assumptions used for the capacity spectrum method. The substitution of the inelastic behavior by a translation equivalent elastic structure has shortcomings particularly for periods lower than the corner period of the ground motion (T_c). In order to minimize this influence the equivalent damping coefficient was determined by trial and error, iteratively, from the computed inelastic and elastic displacement spectra.

By applying the SESA method, results show a relatively good match to the structural response determined by dynamic nonlinear analysis and a better estimation of the structural response of irregular structures (influenced by general torsion) than the ones that can be obtained by using code provisions, for most of the cases (Köber and Zamfirescu 2009).

21.3 Analysed Structures

In this chapter two single story structures (layout 11×44 m), a twist unrestrained structure (TL) and a twist restrained structure (TI), were analysed (see Fig. 21.1). Both are idealized structures with a rigid diaphragm floor and columns and walls as vertical structural elements. The vertical structural elements are disposed symmetric about the x and y axis. The structural mass is lumped at the center of mass (CM).

The structures of Fig. 21.1 are symmetric structures, being characterized through a coincidence between the center of stiffness (CR), the center of mass (CM) and the
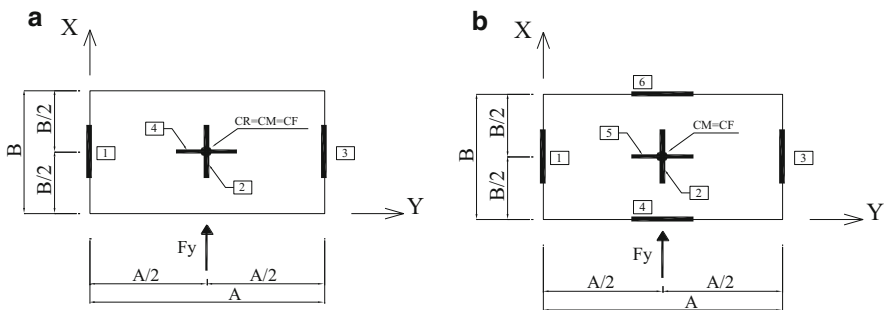
Fig. 21.1 Layout of symmetric structures: (**a**) twist unrestrained (TL); (**b**) twist restrained (TI)

center of resistance (CF). The corresponding eccentric systems are obtained by translating gradually CR and CF along the y axis, from its initial position up to ± 20 % of the plan dimension of the structure normal to the direction of the seismic input.

The total weight (G) of the floor is 4840 kN (considering a uniform load $p = 10$ kN/m^2). The structural walls were modeled as elastic-perfectly plastic springs acting on x and y direction.

The stiffness of the structural elements was chosen for both main directions so that the initial translational period of the structure equals 0.3 s, 0.7 s or 1.6 s. The stiffness and the strength of walls P2 and P4 (for TL) and of walls P2 and P5 (for TI) remain constant.

21.4   Seismic Input

The seismic input for this study is unidirectional (along x direction) and is given by original records as well as by spectrum compatible accelerograms, acting along the x axis. Therefor design spectra from Eurocode 8 and the Romanian Seismic Design Code were used. Design spectra for corner periods equal to 0.5 s, 0.7 s and 1.6 s were considered.

The results were obtained for elastic behavior (Serviceability Limit State, SLS) and four intensity levels of seismic input for the inelastic behavior. Therefor each accelerogram was scaled for four levels of strength: 0.1 g, 0.2 g (Ultimate Limit State, SLU), 0.3 g and 0.4 g (Survivability Limit State, SLSV). For each seismic intensity level the authors considered an original record and three spectrum compatible accelerograms.

21.5   Comparative Study

The target of this comparative study was to identify how well the SESA method based on modal analysis and overdamped response spectra can estimate the seismic response obtained by dynamic nonlinear calculation (using the Torsdin program), for different seismic intensity levels. The results of the SESA method were compared to the ones obtained by three-dimensional dynamic analysis (Zamfirescu 2000) in terms of displacement values at characteristic points of the structure (total displacement of the center of mass (u_x^{CM}), structural rotation (θ), displacements of walls P1 and P3 (u_{x1}, u_{x3})) and of inertial torsional moments (Fig. 21.2).

The inertial torsional moment was computed as difference between the static moment and the torsional capacity (torsional moment for yielding of structural elements).

Fig. 21.2 Definition of
$M_{dynamic}$
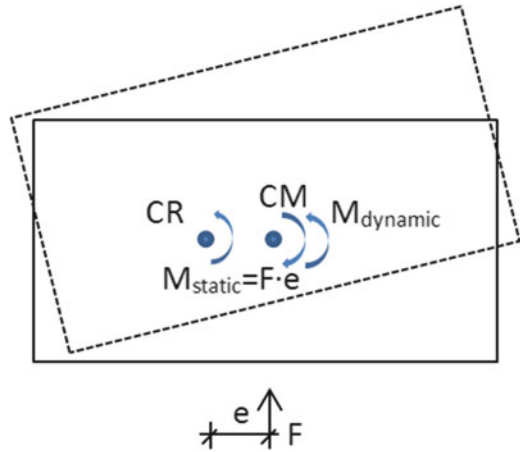
Results in terms of displacement values at characteristic points of the structure were gathered with respect to the seismic intensity level. Results in terms of inertial torsional moments were gathered with respect to the structural layout.

21.5.1   Structural Displacements and Rotations Gathered with Respect to the Intensity Level of the Seismic Input

For SLS, the SESA method mostly overestimates dynamic nonlinear analysis results. As expected, results are better for u_x^{CM} and θ as for u_{x1} and u_{x3}.

Figures 21.3 and 21.4 show results for the nonlinear range of behavior, separately for torsional unrestrained (TL) and for torsional restrained (TI) structures. The horizontal axes shows whether the SESA method overestimates (graphics right side, positive percentage) or underestimates (graphics left side, negative percentage) dynamic nonlinear analysis results. The vertical axes represents the percentage of results (from the total number of results) that fit into a range of accuracy.

For TL it was considered that the torsional stiffness of all walls is affected in the same way as their translational stiffness. For TI, the preliminary results showed that the walls situated perpendicular to the direction of seismic input yield also, and the consideration of their full lateral stiffness to the rotational stiffness of the structure leads to unconservative results. Consequently, for the comparative study the perpendicular walls participate with half of their lateral stiffness to the rotational stiffness of the structure to take into account the yielding effect.

For TL structures accuracy seems to drop with the rising of seismic intensity, although it is not a monotone variation. Structural displacements are estimated far better by the SESA method than structural rotations. Due to the fact that for
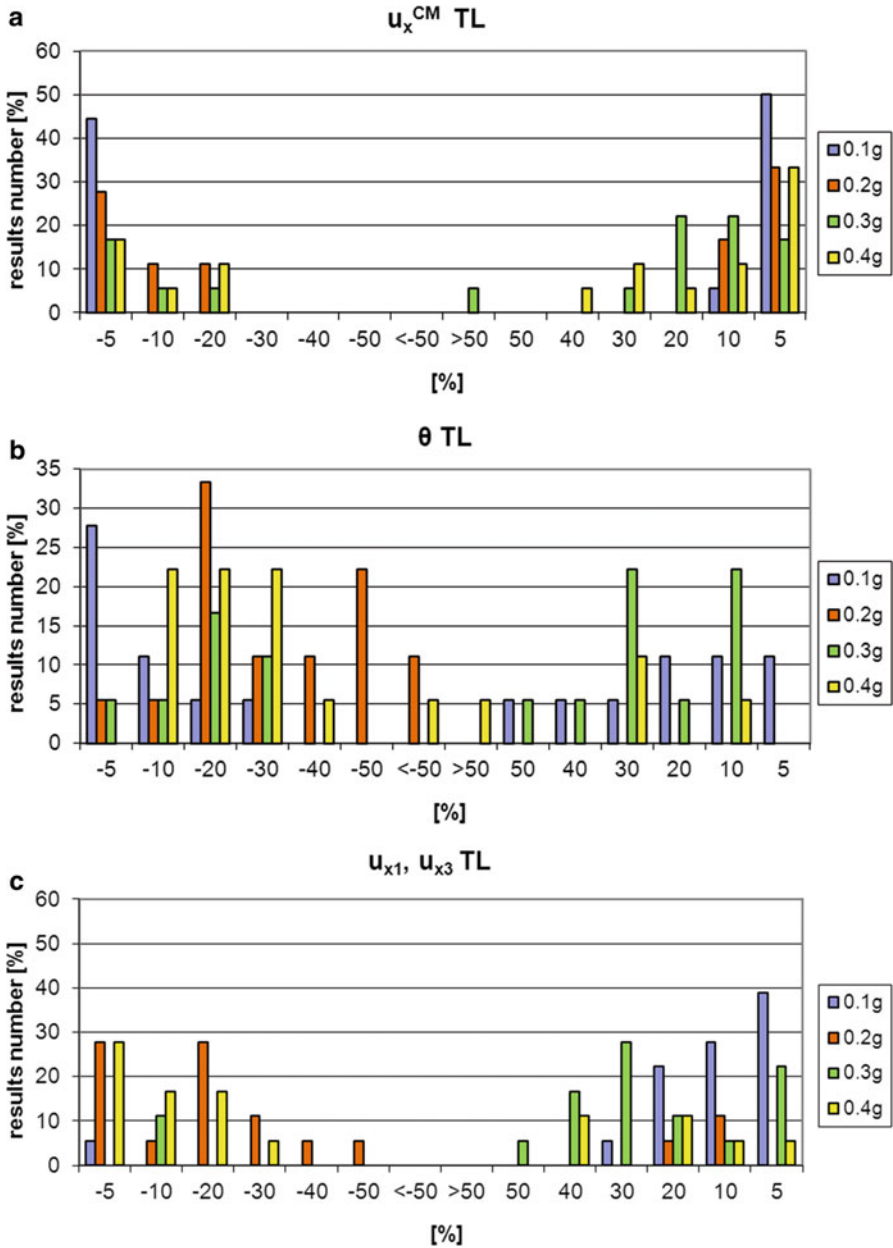
Fig. 21.3 Results for TL nonlinear behavior: (**a**) displacements of the mass center; (**b**) structural rotations; (**c**) displacements of walls P1 and P3
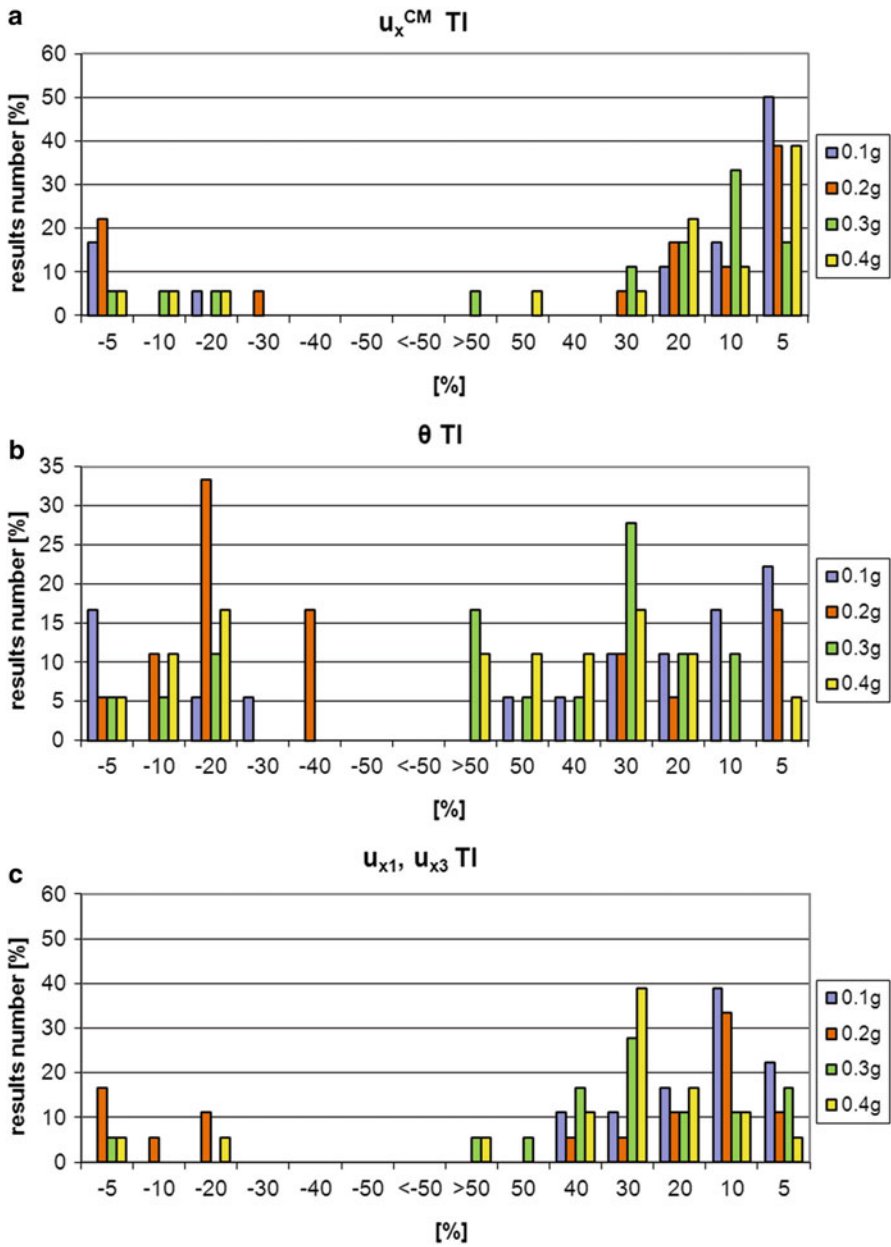
Fig. 21.4 Results for TI nonlinear behavior: (**a**) displacements of the mass center; (**b**) structural rotations; (**c**) displacements of walls P1 and P3

practical design usually displacements are needed, the rotations loss of accuracy is not inconvenient.

According to the Eurocode 8, the TL structures analyzed in this chapter experience torsional sensitivity for eccentricity values greater than ±12 % of the plan dimension perpendicular to the direction of seismic input. By restraining the statistic evaluation of results to eccentricities up to ±12 %, structural displacements are overestimated by less than 10 % by the SESA method in an amount of 85 % for 0.1 g seismic intensity and 65 % for 0.2 g, 0.3 g and 0.4 g seismic intensity.

Accuracy of results is better for TI structures due to the positive influence of the structural walls perpendicular to the direction of seismic input. The amount of overestimated results is greater than for TL structures. For 0.1 g seismic intensity and eccentricity values up to ±20 %, up to 70 % of the structural displacements are overestimated by less than 10 % by the SESA method. This percentage changes into 50 % for 0.2 g, 0.3 g and 0.4 g seismic intensity.

For this comparative study constant accuracy is obtained for seismic intensities greater than 0.1 g. This may be explained by the constancy of the structural response for the entire eccentricity range considered when getting more and more into the nonlinear range of behavior.

21.5.2   Inertial Torsional Moment for TL and TI

Following former research (Paulay 2001) the authors investigated the effect of the inertial rotational moment, a measure suitable for the elastic range of behaviour as well as for the inelastic one (Fig. 21.5).
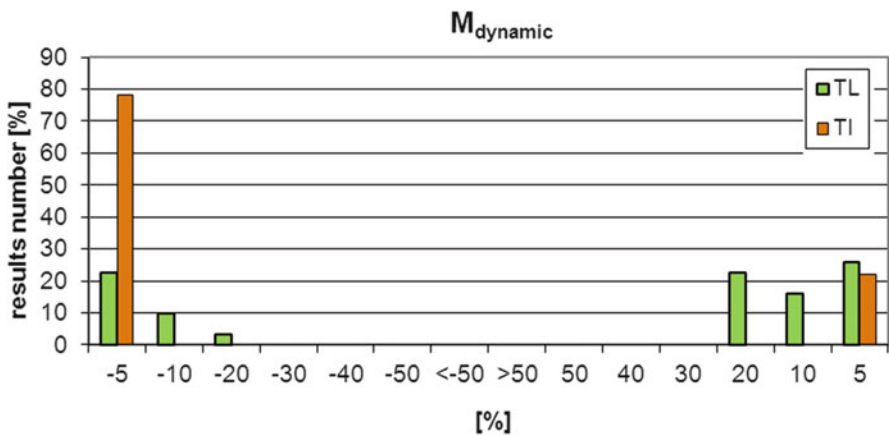
Fig. 21.5 Accuracy of $M_{dynamic}$

The relation between $M_{dynamic}$ and the maximum rotation showed complete yielding of all walls. For TL structures a residual stiffness of walls (after yielding) between 5 and 25 % turned out to be realistic.

By using $M_{dynamic}$ as behaviour measure, results show a much better accuracy than for displacements at different points of the structure. All results are estimated by less than $\pm 5\%$ for TI structures and 75 % of results are estimated by less than $\pm 10\%$ for the TL structure.

21.6   Concluding Remarks

The amount of nonlinearity (defined in this chapter as seismic intensity level) influences the accuracy of results from the SESA method for plan irregular structures, compared to dynamic nonlinear analysis results.

This study gives following answers to the questions in Chap. 1:

1. The accuracy of structural displacements and rotations (from SESA compared to DNA) doesn't have a monotonic variation with respect to the seismic intensity, is better for TI structures compared to TL structures and for $T > T_c$.

   For strong nonlinear behavior structural rotations remain nearly constant and the structural response tends to an upper limit.

   Structural displacements are estimated far better by the SESA method than structural rotations. For practical design usually displacements are needed, so the rotations loss of accuracy is not inconvenient.

2. The inertial torsional moment turned out to be the only behavior measure with controlled variability with respect to the seismic intensity, the structural layout or the corner period of the seismic input.

The results obtained in this and former studies make the authors confident in proposing the SESA method for practical design, as a simplified, analytical applicable design method for single story plan irregular structures.

References

De La Llera JK, Chopra AK (1995) Understanding the inelastic seismic behavior of asymmetric plan – buildings. Earthq Eng Struct Dyn 24(4):549–572

EN 1998-1 (2004) Design of structures for earthquake resistance. General rules, seismic actions and rules for buildings, 45–69

P100 -1/2006. Cod de proiectare seismică. Prevederi de proiectare pentru clădiri, 32–61

Garcia O, Islas A, Ayala AG (2004) Effect of the in-plan distribution of strength on the non-linear seismic response of torsionally coupled buildings. In: Proceedings of the 13th WCEE, Lisbon, 24–28 September 2012, p 1891

Goel RK, Chopra AK (1990) Inelastic seismic response of one – story, asymmetric – plan systems. College of Engineering, University of California at Berkeley. UBC/EERC – 90/14

Köber D, Zamfirescu D (2009) Simplified methods used for evaluation of the displacement gain due to general torsion. Sci J Math Model Civ Eng 5(2):32–51

Köber D, Zamfirescu D (2010) Effects of general torsion on structural displacements. In: Proceedings 14 ECEE. Technical University Bucharest. ISBN 978-608-65185-1-6

Paulay T (2001) Some design principles relevant to torsional phenomena in ductile buildings. J Earthq Eng 5(3):273–308

Zamfirescu D (2000) TORSDIN – dynamic nonlinear analysis computer program. Reinforced Concrete Department. Technical University Bucharest

Chapter 22
Maximum Corner Displacement Amplifications for Inelastic One-Storey In-Plan Asymmetric Systems Under Seismic Excitation

Michele Palermo, Stefano Silvestri, Giada Gasparini, and Tomaso Trombetti

Abstract The seismic behaviour of one-storey asymmetric structures has been extensively studied since 1970s by a number of research studies which identified the coupled nature of the translational-to-torsional response of this class of systems leading to severe displacement magnifications at the perimeter frames and to significant increase of local peak seismic demand to the structural elements. In previous research works, some of the authors introduced a simplified method, the so called "Alpha" method, for the estimation of the maximum torsional response of linear-elastic one-storey in-plan asymmetric systems. The present paper provides an extension of the "Alpha" method to inelastic systems. The main objective is to evaluate how the excursion of the structural elements in the inelastic range affects the seismic displacement demand. In detail, 3-D surfaces of corner displacement magnification factors for different force reduction factors are showed and comparisons with the results obtained from linear analysis are provided. The 3-D surfaces could be useful to assess the seismic displacement demand of asymmetric systems in a preliminary design phase.

Keywords One-storey asymmetric systems • Corner displacement amplifications • Elastic seismic response • Inelastic seismic response • Period shifting

M. Palermo (✉) • S. Silvestri • G. Gasparini • T. Trombetti
Department DICAM, University of Bologna, Viale Risorgimento 2, 40136 Bologna, Italy
e-mail: michele.palermo7@unibo.it; stefano.silvestri@unibo.it; giada.gasparini4@unibo.it; tomaso.trombetti@unibo.it

22.1 Introduction

Since the late 1970s it is well known that in-plan asymmetric systems, when subjected to dynamic excitation, develop a coupled lateral-torsional response that may considerably increase their local peak response, such as the corner displacements (Kan and Chopra 1987; Hejal and Chopra 1987; Rutenberg 1992).

In order to effectively apply the performance-based design approach to seismic design there is a growing need for code-oriented methodologies aimed at predicting deformation parameters. Thus, the estimation of the displacement demand at different locations, especially for eccentric structures, appears a fundamental issue. Furthermore, the ability to predict the torsional response of eccentric systems can be also useful to improve the capability of one of the most actually used seismic design approaches (i.e. push-over analysis, Perus and Fajfar (2005)).

Since the early 1990s, Nagarajaiah et al. (1993) observed that, for the specific class of torsionally-stiff asymmetric structures, the maximum center mass displacement can be well approximated by the maximum displacement of the equivalent not-eccentric system.

In previous research works, some of the authors identified a structural parameter, called "Alpha", related to the attitude of one-storey asymmetric linear systems to develop a rotational response in free vibration, and proposed a simplified procedure, called "Alpha" method, for the estimation of the maximum torsional response (Trombetti and Conte 2005; Trombetti et al. 2008). In its original formulation, based on the assumption of equal maximum center mass displacement response between the eccentric system and its not-eccentric counterpart, the "Alpha" method has been also used for the prediction of maximum corner side displacements. The assumption has been proven valid for torsionally-stiff systems only. More recently, the "Alpha" method has been extended to all classes of one-storey asymmetric systems, thus including both torsionally-stiff and torsionally-flexible systems, thanks to the introduction of some correction coefficients (Palermo et al. 2013). In detail, a coefficient accounting for the so-called "period shifting effect", leading to an increase in the center mass displacement between the eccentric system and its not-eccentric counterpart, has been introduced (Palermo et al. 2013).

In this paper a further generalization of the "Alpha" method is proposed by considering non-linear asymmetric systems. First, linear-elastic analyses are performed varying the damping ratio ξ from 0.02 to 0.30. Then, non-linear seismic analyses are performed by assuming an elastic-perfectly plastic response of the structural elements for various force reduction factors R. The main objective is to evaluate how the excursion of the structural elements in the inelastic field affects the displacement demand of one-storey in-plan asymmetric structures.

22.2 Problem Formulation and Summary of Previous Results

Let us consider the one-storey eccentric structure (i.e. a system characterized by non-coincident center of mass, CM, and center of stiffness, CK, leading to a one-way eccentricity $E_x = E$, $E_y = 0$) of Fig. 22.1 (the origin of the reference system is located at CM). It is assumed that the diaphragm is infinitely rigid in its own plane, and that the lateral-resisting elements are massless and axially inextensible. The self torsional stiffness (k_θ) of each lateral-resisting element is neglected. Under these assumptions, the system can be modelled as a 3-dof system: longitudinal center mass displacement, $u_{y,CM}$,; transversal center mass displacement, $u_{x,CM}$; center mass rotation, $u_{\theta,CM}$ (coincident with the floor rotation, u_θ). The case of one-way dynamic excitation (e.g. free vibrations or seismic input) along the longitudinal direction (namely, the y-direction) is treated in the next sections.

The longitudinal corner side displacements, i.e. the displacement of the so called stiff side $u_{y,s}$ (e.g. point B or B', the closer to CK) and of the flexible side $u_{y,f}$, (e.g. point A or A', the farther from CK), at any instant of time t, are given by:

$$u_{y,f}(t) = u_{y,CM}(t) - u_\theta(t) \cdot \frac{L}{2}$$
$$u_{y,s}(t) = u_{y,CM}(t) + u_\theta(t) \cdot \frac{L}{2}$$

(22.1)

Estimating corner displacements under seismic excitation according to Eq. 22.1 needs time-history analyses to be performed. Nonetheless, the practical engineer is
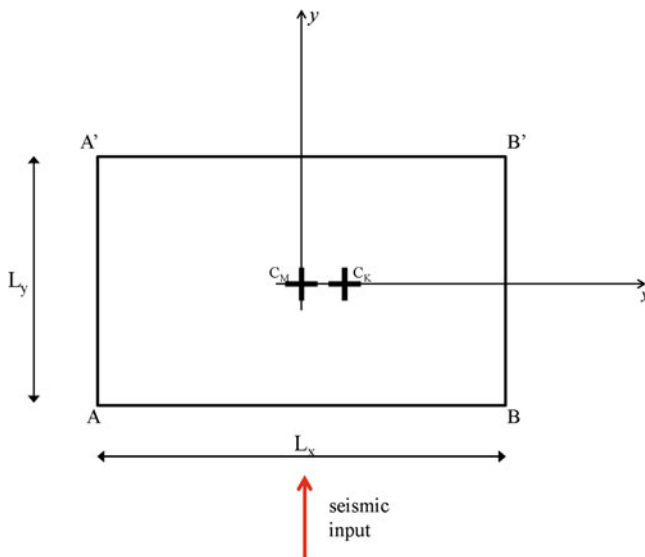
Fig. 22.1 Plan view of the studied system

mainly interested in the peak response, which, generally speaking, can be expressed as an appropriate combination of the longitudinal and rotational maximum responses. In a recent research work, the following expression for the estimation of the maximum corner side displacements, $u_{y,corner,max}$, has been introduced, leading to the so called "Alpha" method:

$$u_{y,corner,max} = \delta \cdot u_{y,CM,max,N-E} \cdot (1 + B \cdot A \cdot \alpha_u \cdot \phi) \tag{22.2}$$

The symbols have the following meaning:

- $\delta = \dfrac{u_{y,CM,max}}{u_{y,CM,max,N-E}}$ is the translational contribution providing the center mass displacement amplification with respect to that of the equivalent not-eccentric system (N-E), also referred to as "period-shifting effect".

- $A \cdot \alpha_u = \rho \dfrac{u_{\theta,max}}{u_{y,CM,max}}$ gives the rotational contribution (α_u is a parameter given in closed-form by Trombetti and Conte (2005) for the case of undamped free vibration response; ρ is the mass radius of gyration of the system, A is a parameter which accounts for the seismic nature of the input and has to be calibrated through numerical simulations).

- B is the correlation coefficient between the maximum displacement response and the maximum rotational response.

- $\phi = \sqrt{3(L_x/L_y)^2 / \left[1 + (L_x/L_y)^2\right]}$ is a geometric shape factor.

A closed-form estimation of δ has been provided by Palermo et al. (2013) by making use of the analytical expression of the natural periods and of a simplified response spectrum. It has been noted that torsionally-flexible systems are potentially prone to high center mass displacement amplifications which are caused by the shift of the fundamental period (the so-called "period shifting effect").

Since the late 1990s the ratio between the maximum rotational response and the maximum translational response in undamped free vibrations, the so-called "Alpha" parameter, has been derived in closed-form as a function of the normalized eccentricity ($e = E/D_e$, where D_e is the equivalent diagonal of the floor plan equal to $\sqrt{12}\,\rho$) and torsional-to-lateral frequency ratio Ω_θ (Goel and Chopra 1991) giving the name to the "Alpha" method (Trombetti and Conte 2005):

$$\alpha_u = \frac{\rho u_{\theta,max}}{u_{y,max}} = \frac{4e\sqrt{3}}{\sqrt{\left(\Omega_\theta^2 + 12e^2 - 1\right)^2 + 48e^2}} \tag{22.3}$$

The correlation coefficient B_u (subscript u standing for "undamped") is defined such as:

$$u_{y,flex} = u_{y,max} + B_u \cdot u_{\theta,max} \cdot \frac{L}{2} \tag{22.4}$$

leading to the following closed form expressions derived in the case of undamped free vibration:

$$
\begin{aligned}
B_u &= 1 - \frac{4A_3}{\alpha_u L_x} \rho_m \quad \text{for } A_1 \geq A_3 \\
B_u &= 1 - \frac{4A_1}{\alpha_u L_x} \rho_m \quad \text{for } A_1 < A_3
\end{aligned}
\tag{22.5}
$$

Note that $1 \geq B \geq 1 - \frac{2\rho}{\alpha_u L_x}$. A_1 and A_3 are coefficients depending on e and Ω_θ. See Trombetti and Conte (2005) for further details.

22.3   Linear Seismic Response

An ensemble of 50 ground motions selected from the PEER database has been used to perform the seismic analyses. The ground motions are selected with shear wave velocity $V_{s,30}$ in the range of 360–800 m/s (i.e. soil type B according to EC8 2002). The following response parameters are evaluated and analyzed (subscript eq stands for earthquake):

$$
\alpha_{d,eq} = \rho \frac{u_{\theta \max}}{u_{y,CM_{\max}}}
\tag{22.6}
$$

$$
B_{d,eq} = \frac{u_{y,\max} - u_{y,CM,\max}}{u_{\theta,\max} \cdot (L_x/2)}
\tag{22.7}
$$

$$
M_{CM,s} = \frac{u_{y,s,\max}}{u_{y,CM,\max}}
\tag{22.8}
$$

$$
M_{CM,f} = \frac{u_{y,f,\max}}{u_{y,CM,\max}}
\tag{22.9}
$$

$M_{CM,s}$ and $M_{CM,f}$ are the magnification factors (with respect to the center mass displacement) at the stiff side and flexible side, respectively. Figures 22.2 and 22.3 show 3-D surfaces of selected response quantities. The following observations arise:

- Peak values of $\alpha_{d,eq}$ are larger than 1.0 for small values of T_L and Ω_θ and for e around 0.2. The results indicate that the closed-form given in free vibration (α_u) is not always an upper bound. However, once the longitudinal period T_L increases, the peaks decrease and even vanish for T_L larger than 1.5 s.
- For fixed values of T_L, values of $\alpha_{d,eq}$ decrease as the damping ratio ξ increases.
- Torsionally-stiff systems are more sensitive to damping ratios than torsionally-flexible systems.
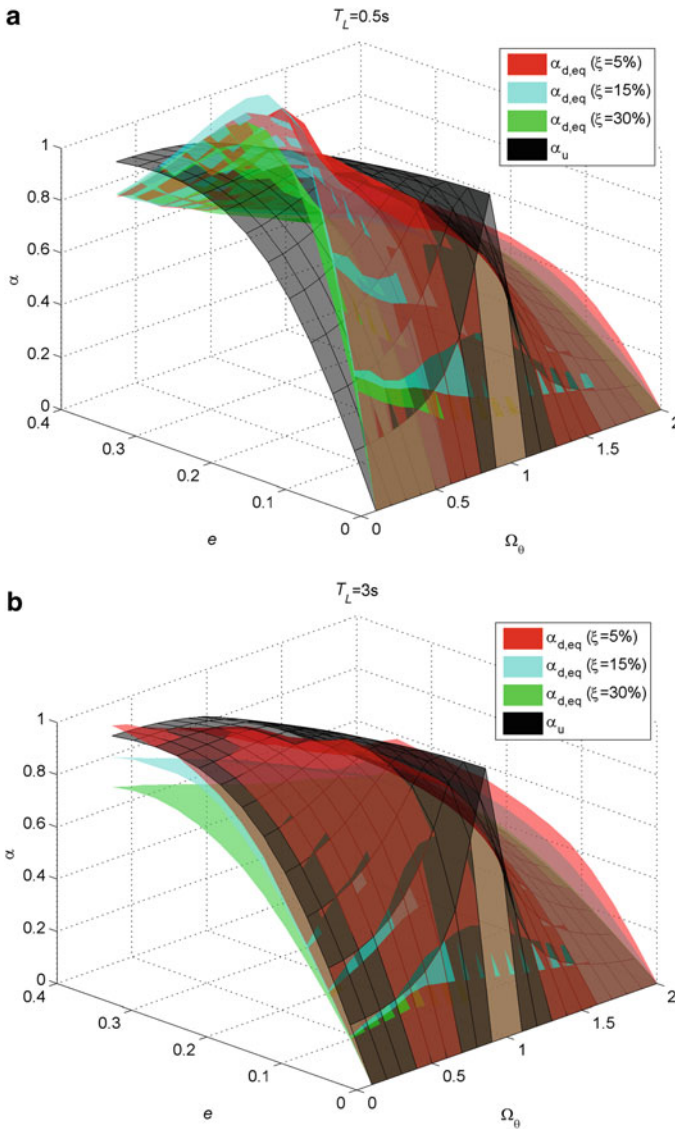
Fig. 22.2 "Alpha" rotational parameter as function of e and Ω_θ. (**a**) $T_L = 0.5$ s; (**b**) $T_L = 3.0$ s

- Values of $M_{CM,s}$ are between 0.4 and 1.8. The $M_{CM,s}$ surfaces are quite smooth for torsionally-stiff systems (values are less than 1.0), while they rapidly vary for torsionally-flexible systems (values are also larger than 1.0).
- For fixed values of T_L and ξ, the magnification factor at the stiff side $M_{CM,s}$ decreases once the eccentricity increases, except within an area characterized by small values of e and Ω_θ (high torsionally-flexible systems), where it exhibits peaks larger than 1.0 (maximum values are around 1.8). As the damping ratio increases, this area reduces.
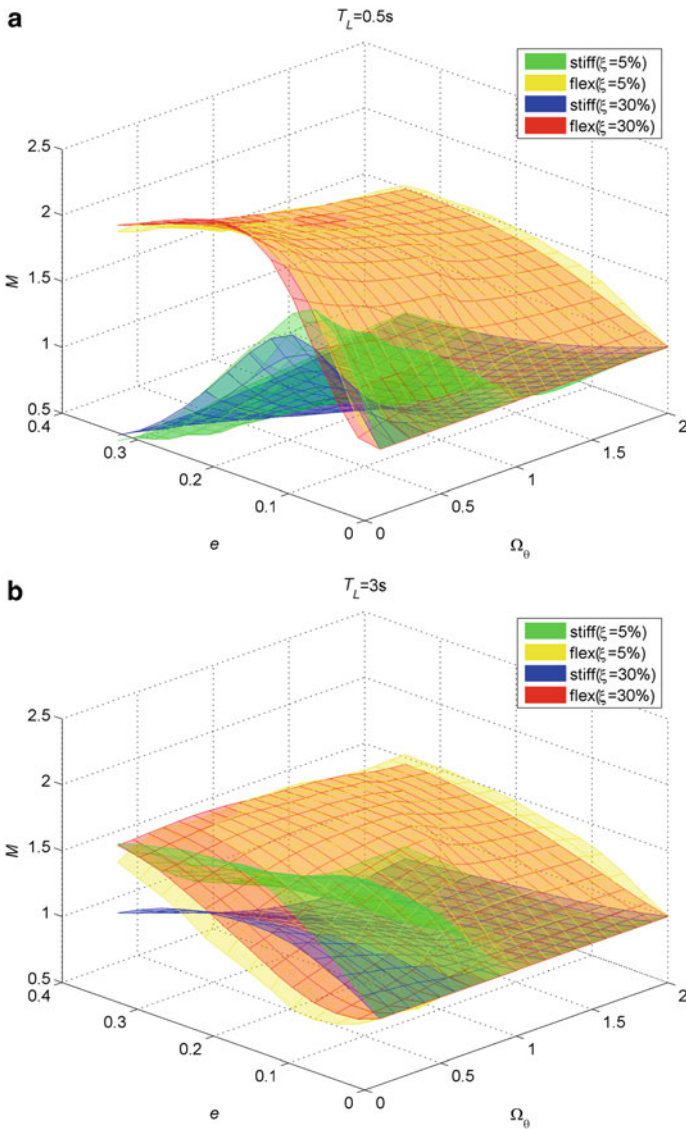
Fig. 22.3 Magnification factors of the stiff and flexible side as function of e and Ω_θ. (**a**) $T_L = 0.5$ s; (**b**) $T_L = 3.0$ s

- Values of $M_{CM,f}$ are between 0.9 and 2.2. $M_{CM,f}$ surfaces appear quite smooth within the entire domain.
- For fixed values of ξ and T_L, $M_{CM,f}$ increases with the eccentricity e, while the peak decreases as T_L increases.

For the sake of conciseness, the plots of the correlation coefficients $B_{d,eq}$ are not here displayed and discussed.
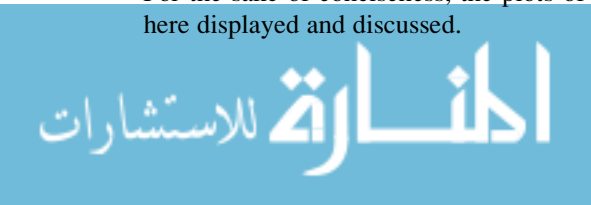
22.4   Nonlinear Seismic Response

The simple 3-dof system idealization adopted in the linear analyses cannot be used to study the non-linear response of planar asymmetric systems since, within the inelastic field, also the location of each resisting element and the number of resisting elements may affect the response. For this reason, the specific, but still simple, non-linear asymmetric model as proposed by Goel and Chopra (1991) is used to perform the non-linear analyses. It is clear that, in order to extend the results to realistic structures, a wide parametric analysis carried out on several idealised models is needed. The system consists of a roof diaphragm, assumed to be rigid in its own plane, supported by three frames, namely A, B and C (see Fig. 22.4).

Frame A is oriented along the y-direction, at a distance E from the center of mass (CM). Frames B and C are oriented along the x-direction, located at the same distance $D/2$ from the CM. Frames B and C are assumed to have the same lateral stiffness $(k/2)$ so that the system is not eccentric along the y-direction. Frame A is assumed to have a lateral stiffness equal to k. Along the x-direction the eccentricity is equal to E. The rigid motion of the roof can be described by the three degrees of freedom defined at the CM of the slab: displacements u_x (in the x-direction) and u_y (in the y-direction), and torsional rotation u_θ (about the vertical axis). The equations of motion of this specific system in the initial elastic range are given by:
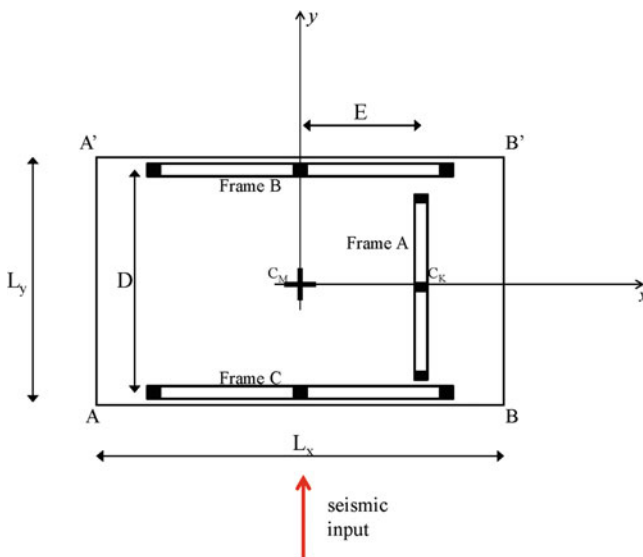
Fig. 22.4   Idealized non linear eccentric system used to perform non-linear analyses

$$
\begin{bmatrix} m & 0 & 0 \\ 0 & m & 0 \\ 0 & 0 & m \end{bmatrix} \begin{bmatrix} \ddot{u}_x(t) \\ \ddot{u}_y(t) \\ \rho\ddot{u}_\theta(t) \end{bmatrix} + [C] \begin{bmatrix} u_x(t) \\ u_y(t) \\ \rho u_\theta(t) \end{bmatrix}
$$

$$
+ \, m\omega_L^2 \begin{bmatrix} 1 & 0 & 0 \\ 0 & 1 & \sqrt{12}e \\ 0 & \sqrt{12}e & 12e^2 + d^2/4 \end{bmatrix} \begin{bmatrix} u_x(t) \\ u_y(t) \\ \rho u_\theta(t) \end{bmatrix} = \begin{bmatrix} p_x(t) \\ p_y(t) \\ \dfrac{p_\theta(t)}{\rho} \end{bmatrix}
\tag{22.10}
$$

where: m is the mass of the system; $[C]$ is the damping matrix (classical damping is assumed); $d = D/\rho$. Values of parameter Ω_θ distinguish in-plan asymmetric systems into: (i) torsionally-stiff systems: $\Omega_\theta \geq 1.0$; (ii) torsionally-flexible systems: $\Omega_\theta < 1.0$.

Each frame is characterized by an elastic-perfectly plastic response. The yield strength F_y is obtained by imposing a force reduction factor R between 2 and 5. Non-linear time-history analyses have been developed using the same ground motion ensemble used in the linear analyses. The response parameters computed from the non-linear analysis are indicated with subscript NL and represented in Figs. 22.5 and 22.6 through 3-D surfaces. The following observations arise:

- The $\alpha_{d,NL,eq}$ surfaces are qualitatively similar to those observed in the linear case. The largest values of $\alpha_{d,NL,eq}$ are observed for small values of T_L and Ω_θ and for e around 0.2. Again, peaks larger than 1.0 are observed (i.e. α_u is not always an upper bound estimation).
- As the longitudinal period T_L increases, the peaks decrease and they even vanish for $T_L = 1.5$ s.
- For a fixed longitudinal period T_L, the maximum rotational response tends to decrease as R increases. The dependence of $\alpha_{d,NL,eq}$ on R is larger for the class of torsionally-stiff structures.
- The surfaces of both $M_{CM,NL,s}$ and $M_{CM,NL,f}$ are qualitatively similar to those observed in the linear case. Peak values are slightly reduced.
- $M_{CM,NL,s}$ appears quite smooth for torsionally-stiff systems (values are less than 1.0), while it rapidly varies for torsionally-flexible systems (values are also larger than 1.0).
- For fixed values of T_L, the peaks of $M_{CM,NL,s}$ gradually decrease as R increases. On the contrary, for torsionally-stiff systems, $M_{CM,NL,s}$ tends to slightly increase (the surface becomes almost flat for $R = 5$ with values between 0.8 and 1.0).
- The magnification factor $M_{CM,NL,f}$ increases as the eccentricity increases. The peaks are observed for high torsionally-flexible systems and eccentricities e around 0.2.
- For fixed values of R, the peaks of $M_{CM,NL,f}$ decrease as T_L increases and the surface tends to flatten out.

For the sake of conciseness, the graphs of $B_{d,NL,eq}$ are not here displayed and discussed.
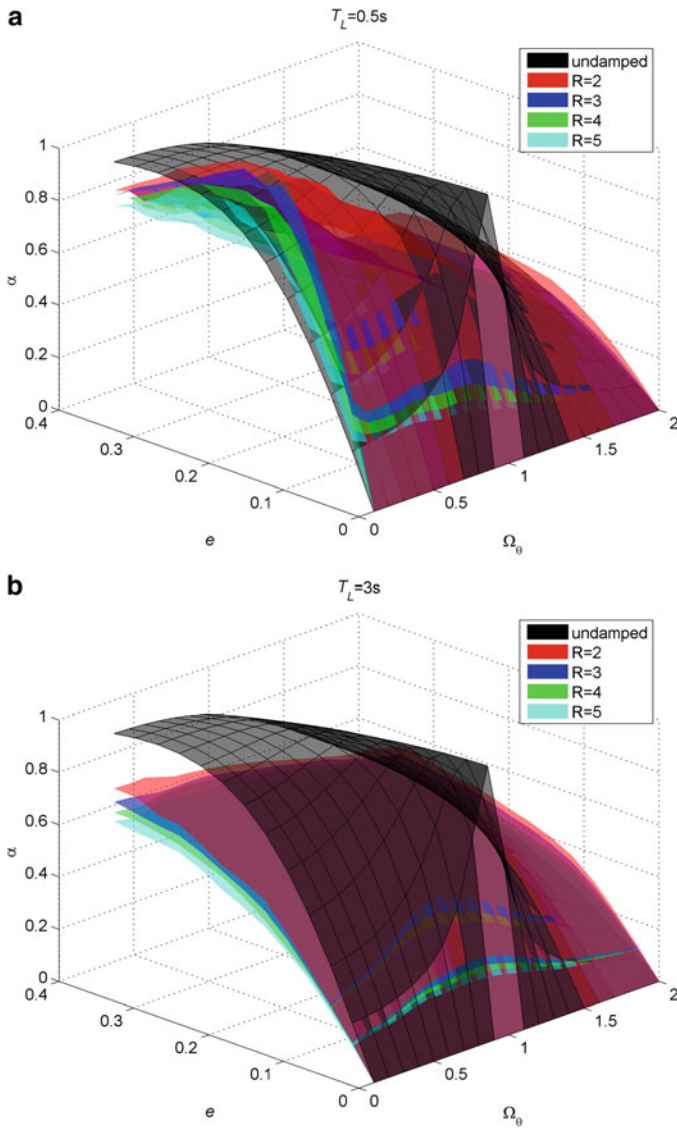
Fig. 22.5 "Alpha" rotational parameter as function of e and Ω_θ. (**a**) $T_L = 0.5$ s; (**b**) $T_L = 3.0$ s

22.5 Conclusions

This paper provides a further insight into the non-linear coupled lateral-torsional dynamic response of one-storey asymmetric systems through the development of a systematic parametric analysis aimed at exploiting the influence of the fundamental system parameters (e, Ω_θ, T_L, ξ, R) on the seismic displacement demand. In detail, 3-D surfaces of response parameters such as the normalized maximum rotational
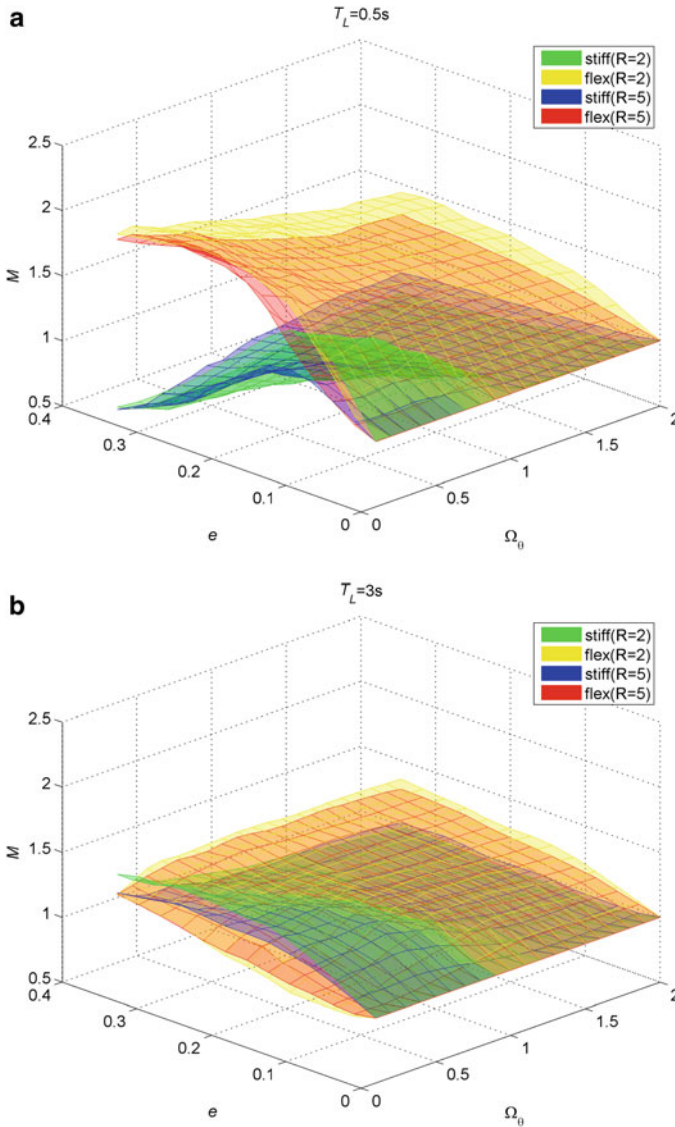
Fig. 22.6 Magnification factors of the stiff and flexible side as function of e and Ω_θ. (**a**) $T_L = 0.5$ s; (**b**) $T_L = 3.0$ s

response and the magnification factors of the maximum stiff and flexible side displacement have been obtained for both the linear and the non-linear case. These 3-D response surfaces could be used in the preliminary structural design phase in order to estimate the seismic displacement demand as a function of the normalized eccentricity and the torsional-to-lateral frequency ratio.

References

Eurocode 8 (2002) Design of structures for earthquake resistance. prEN 1998-1

Goel RK, Chopra AK (1991) Inelastic seismic response of one-storey, asymmetric-plan systems: effects of system parameters and yielding. Earthq Eng Struct Dyn 20(3):201–222

Hejal R, Chopra AK (1987) Earthquake response of torsionally coupled buildings. Report UCB/EERC 87/20, Earthquake Engineering Research Center, University of California, Berkeley, CA

Kan CL, Chopra AK (1987) Linear and non linear earthquake responses of simply torsionally coupled systems. Earthquake Engineering Research centre, University of California, Berkeley, CA

Nagarajaiah S, Reinhorn AM, Constantinou MC (1993) Torsion in base isolated structures with elastomeric isolation systems. J Struct Eng ASCE 119:2932–2951

Palermo M, Silvestri S, Gasparini G, Trombetti T (2013) Physically-based prediction of the maximum corner displacement magnification of one-storey eccentric systems. Bull Earthq Eng 11(5):1467–1491

Perus I, Fajfar P (2005) On the inelastic torsional response of single-storey structures under bi-axial excitation. Earthq Eng Struct Dyn 34:931–941

Rutenberg A (1992) Nonlinear response of asymmetric building structures and seismic codes: a state of the Art. Eur Earthq Eng VI(2):3–19

Trombetti T, Conte JP (2005) New insight into and simplified approach to seismic analysis of torsionally coupled one-storey, elastic systems. J Sound Vib 286:265–312

Trombetti T, Silvestri S, Gasparini G, Pintucchi B, De Stefano M (2008) Numerical verification of the effectiveness of the "Alpha" method for the estimation of the maximum rotational elastic response of eccentric systems. Eur Earthq Eng 12(2):249–280

Chapter 23
Earthquake-Induced Pounding Between Asymmetric Steel Buildings

Barbara Sołtysik and Robert Jankowski

Abstract Earthquake-induced pounding between buildings has been the subject of numerous numerical and experimental studies in the resent years. The phenomenon may cause severe damage to structural elements as well as may also lead to the total collapse of colliding structures. A major reason leading to pounding between adjacent, insufficiently separated buildings results from the differences in their dynamic properties. The aim of this paper is to show the results of the numerical analysis focuses on pounding between two L-shaped asymmetric steel buildings under earthquake excitation. In order to identify the dynamic characteristics of analyzed structures, the modal analysis has been first conducted. Then, the detailed dynamic analysis of interacting structures under earthquake excitation has been performed. The three components of the El Centro earthquake have been used in the study. The results of numerical analysis indicate that the earthquake-induced collisions between two asymmetric steel structures may substantially influence their behaviour leading to both increase and decrease in the response. The results also indicate that torsional vibrations (due to eccentric pounding) play an important role in the overall pounding-involved response of asymmetric steel buildings under earthquake excitations.

Keywords Structural pounding • Earthquakes • Steel buildings • Asymmetric structures • Numerical analysis

23.1 Introduction

Due to lack of space and high cost of land in the urban areas, buildings are often constructed with very small in-between separation gap. That situation may result in structural interactions during seismic excitations, known as the earthquake-induced structural pounding. Collisions between adjacent, insufficiently separated buildings have been repeatedly observed during moderate and strong ground motions (Kasai

---

B. Sołtysik (✉) • R. Jankowski
Faculty of Civil and Environmental Engineering, Gdańsk University of Technology, ul. Narutowicza 11/12, 80-233 Gdańsk, Poland
e-mail: barwiech@pg.gda.pl; jankowr@pg.gda.pl

and Maison 1997). For example, significant pounding damage on the parts of school buildings was observed after the Athens earthquake of September 7, 1999 (Vasiliadis and Elenas 2002). Also, the San Fernando earthquake in 1971 caused collisions between the main building of the Olive View Hospital and one of its independently standing stairway towers resulting in its permanent tilting (Bertero and Collins 1973). During the Kocaeli (Izmit) earthquake (17.08.1999), inadequate separation gap between buildings resulted in serious damage at the places of interactions.

The main reason of structural pounding between buildings is related to the difference in mass or stiffness of colliding structures (Anagnostopoulos 1988; Mahmoud et al. 2012; Mahmoud and Jankowski 2009). The difference in the natural vibration periods of neighbouring structures results in their out-of-phase vibrations. The phenomenon of earthquake-induced pounding between buildings has recently been intensively studied using various structural models and different models of collisions (see, for example, Anagnostopoulos and Karamaneas 2008; Anagnostopoulos and Spiliopoulos 1992; Jankowski 2005, 2007; Karayannis and Favvata 2005; Komodromos et al. 2007; Mahmoud et al. 2013; Mahmoud and Jankowski 2011; Maison and Kasai 1992). However, the analyses for asymmetric structures, which induce eccentric collisions, are very limited (see Leibovich et al. 1996). Also, the scientific interest was mainly focused on pounding-involved response of reinforced concrete buildings rather then on steel structures (Sołtysik and Jankowski 2013). Meanwhile, because of the lower stiffness and damping properties, steel structures usually experience vibrations with larger amplitudes which make then more vulnerable to structural pounding.

Therefore, the aim of this paper is to show the results of the numerical analysis dealing with structural pounding between two L-shaped asymmetric steel buildings under seismic excitation. In the first part of the work, the dynamic properties of both structures have been identified. Afterwards, the detailed dynamic analysis on earthquake-induced collisions between asymmetric steel structures has been conducted.

23.2 Numerical Model of Colliding Buildings

The research described in this paper has been focused on the pounding-involved response of two asymmetric steel buildings with different number of storeys. The 3-storey building (modelled by 10560 shell elements), as well as the 4-storey building (modelled by 14064 shell elements) with different dynamic properties have been considered in the analysis. The Finite Element (FE) model of both structures is presented in Fig. 23.1. All structural members have been modelled by four-node quadrilateral elements. Steel columns have been rigidly fixed to the ground and the soil-structure interaction has not been taken into account. Pounding between structures has been modelled using six three-dimensional gap-friction elements (two for each storey). These elements, placed between the corner nodes
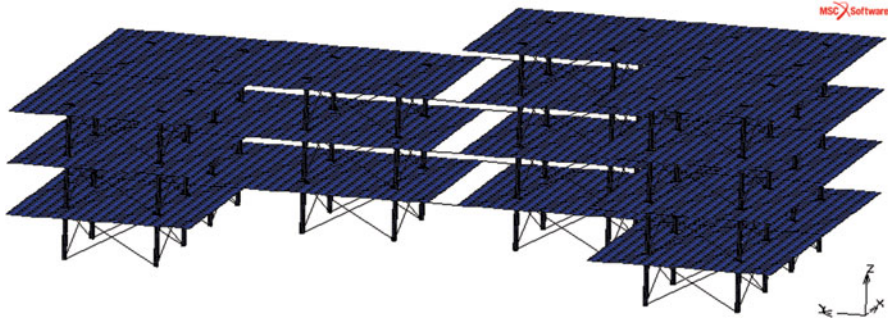
Fig. 23.1 FE model of two colliding asymmetric steel buildings

of the buildings at all storeys, assure frictional and gapping connection. When contact is detected, the nodes become fixed in the longitudinal direction and friction forces are imposed in the transverse and vertical directions. The initial separation gap between structures equal to 2 cm has been considered. The friction coefficient of 0.5 has been applied in the analysis. The numerical model has been implemented using the commercial software MSC Marc 2008.

23.3 Modal Analysis

The modal analysis has been first conducted in order to identify the dynamic properties of each asymmetric steel building. The results of the analysis showing the first three natural vibration modes of both structures are presented in Fig. 23.2. The corresponding natural frequencies for the modes of free vibrations are also summarized in Table 23.1.

23.4 Dynamic Analysis

The detailed dynamic analysis, focused on the response of interacting structures under seismic excitation, has been carried out in the second part of the study. The El Centro earthquake (18.05.1940) records have been used in the numerical analysis. The NS, EW and UD components of the ground motion have been applied in the longitudinal (Y), transverse (X) and vertical (Z) direction, respectively. The examples of the results of the analysis are shown in Figs. 23.3, 23.4, 23.5, and 23.6. In particular, Fig. 23.3 presents a comparison between the displacement time histories in the longitudinal direction for the 3-storey building (node no. 31650 at the corner of the third storey) with and without pounding (large separation gap); whereas Fig. 23.4 shows the corresponding results for the 4-storey building (node no. 27689 at the corner of the third storey). Furthermore, Figs. 23.5 and 23.6
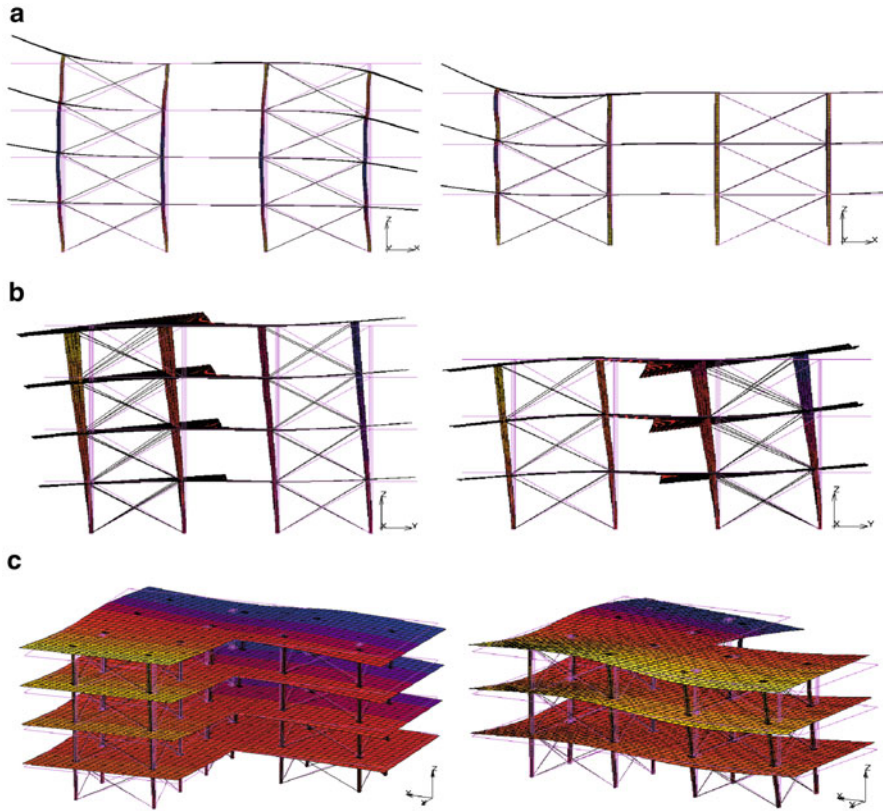
Fig. 23.2 Modes of free vibrations for 3-storey and 4-storey asymmetric steel buildings. (**a**) 1st modes of free vibrations (transverse direction). (**b**) 2nd modes of free vibrations (longitudinal direction). (**c**) 3rd modes of free vibrations (torsional vibrations)

Table 23.1 Natural frequencies for free vibration modes		Transverse	Longitudinal	Torsional
	3-storey building	5.526 Hz	3.002 Hz	3.309 Hz
	4-storey building	4.708 Hz	1.973 Hz	2.205 Hz

show the comparison between the pounding-involved and independent vibration time histories of the rotation angle at the top floor of the 3-storey and 4-storey building, respectively.

Figures 23.3 and 23.4 clearly show that structural pounding may substantially influence the response of two asymmetric steel buildings in the longitudinal direction under earthquake excitation. It can be seen from Fig. 23.3 that the peak response of the 3-storey structure increases due to collisions by 3.3 %. Also, Fig. 23.4 indicates that collisions between two asymmetric steel structures lead to the increase in the peak displacement of the 4-storey building, and this increase is as large as 14.8 %.
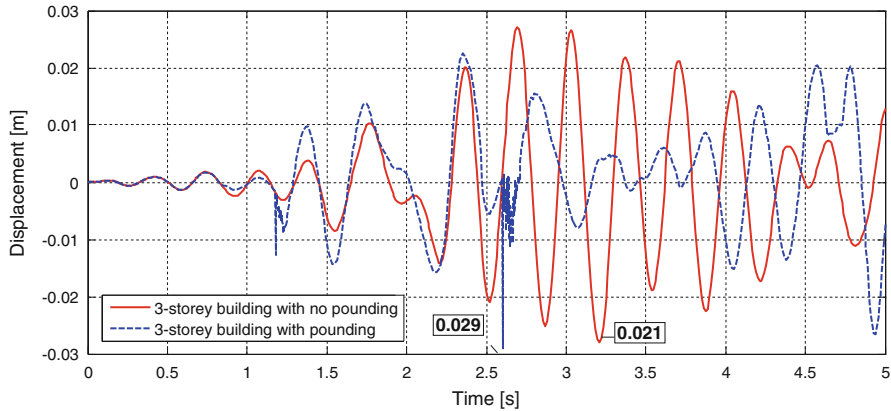
Fig. 23.3 Displacement time histories in the longitudinal direction for pounding-involved and independent vibration responses of 3-storey building
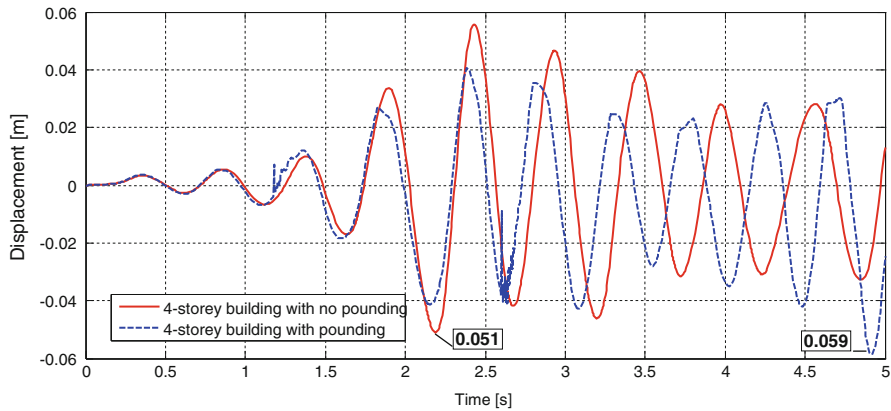
Fig. 23.4 Displacement time histories in the longitudinal direction for pounding-involved and independent vibration responses of 4-storey building

Figures 23.5 and 23.6 indicate that torsional vibrations of both buildings are important components of the overall structural responses, apart from the effect of pounding. They are induced during the earthquake as the result of structural eccentricity caused by asymmetric plan of the structures. The results indicate, however, that structural pounding may significantly influence the torsional behaviour of both structures and, what is more, it may play both positive and negative role. In the case of the 3-storey building, the increase in the peak value of the rotation angle at the top floor is equal to 13.9 % (see Fig. 23.5). On the other hand, Fig. 23.6 shows that the torsional response of the 4-storey building significantly decreases due to pounding. The change in the peak value of the rotation angle at the top floor of this structure during the earthquake is as large as 45.7 %.
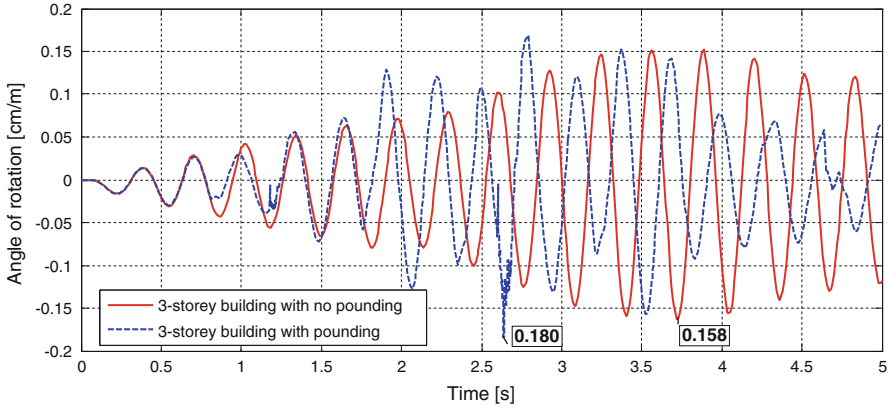
Fig. 23.5 Pounding-involved and independent vibration time histories of the rotation angle at the top floor of the 3-storey building
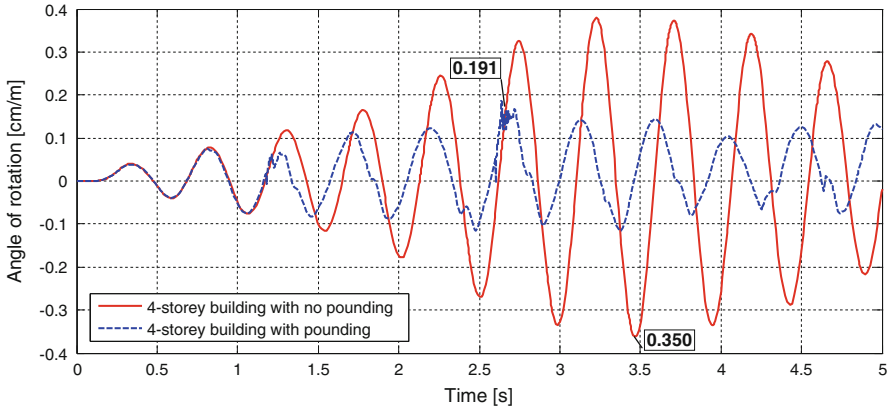
Fig. 23.6 Pounding-involved and independent vibration time histories of the rotation angle at the top floor of the 4-storey building

23.5   Concluding Remarks

The detailed numerical analysis, focused on pounding between two L-shaped asymmetric steel buildings under seismic excitations, has been considered in this paper.

The results of the study clearly indicate that earthquake-induced pounding may substantially influence the response of both asymmetric structures, especially in the longitudinal and torsional directions. In the case of the analysis conducted, it resulted in the considerable increase in the displacements of both structures. It also led to the increase in the torsional response of 3-storey building and significant decrease in the response 4-storey structure. The results of the study indicate that torsional vibrations (due to eccentric pounding) play an important role in the overall pounding-involved response of asymmetric steel buildings under earthquake excitations.

The results of the analysis focused on earthquake-induced pounding between the examples of two elastic steel buildings, for specified gap size, have been presented in this paper. Further studies are requires so as to extend our knowledge on the phenomenon. Such studies should consider the effects of different gap size values, inelastic responses as well as the influence of increasing the input excitation on the structural behaviour.

References

Anagnostopoulos SA (1988) Pounding of buildings in series during earthquakes. Earthq Eng Struct Dyn 16:443–456

Anagnostopoulos SA, Karamaneas CE (2008) Use of collision shear walls to minimize seismic separation and to protect adjacent buildings from collapse due to earthquake-induced pounding. Earthq Eng Struct Dyn 37:1371–1388

Anagnostopoulos SA, Spiliopoulos KV (1992) An investigation of earthquake induced pounding between adjacent buildings. Earthq Eng Struct Dyn 21:289–302

Bertero VV, Collins RG (1973) Investigation of the failures of the Olive View stairtowers during the San Fernando earthquake and their implications on seismic design. EERC Report No. 73-26, Earthquake Engineering Research Center, University of California, Berkeley

Jankowski R (2005) Impact force spectrum for damage assessment of earthquake-induced structural pounding. Key Eng Mater 293–294:711–718

Jankowski R (2007) Assessment of damage due to earthquake-induced pounding between the main building and the stairway tower. Key Eng Mater 347:339–344

Karayannis CG, Favvata MJ (2005) Earthquake-induced interaction between adjacent reinforced concrete structures with non-equal heights. Earthq Eng Struct Dyn 34:1–20

Kasai K, Maison B (1997) Building pounding damage during the 1989 Loma Prieta earthquake. Eng Struct 19:195–207

Komodromos P, Polycarpou PC, Papaloizou L, Phocas MC (2007) Response of seismically isolated buildings considering poundings. Earthq Eng Struct Dyn 36:1605–1622

Leibovich E, Rutenberg A, Yankelevsky DZ (1996) On eccentric seismic pounding of symmetric buildings. Earthq Eng Struct Dyn 25:219–233

Mahmoud S, Jankowski R (2009) Elastic and inelastic multi-storey buildings under earthquake excitation with the effect of pounding. J Appl Sci 9:3250–3262

Mahmoud S, Jankowski R (2011) Modified linear viscoelastic model of earthquake-induced structural pounding. Iran J Sci Technol 35 C1:51–62

Mahmoud S, Austrell PE, Jankowski R (2012) Simulation of the response of base-isolated buildings under earthquake excitations considering soil flexibility. Earthq Eng Vibration 11:359–374

Mahmoud S, Abd-Elhamed A, Jankowski R (2013) Earthquake-induced pounding between equal height multi-storey buildings considering soil-structure interaction. Bull Earthq Eng 11:1021–1048

Maison B, Kasai K (1992) Dynamics of pounding when two buildings collide. Earthq Eng Struct Dyn 21:771–786

Sołtysik B, Jankowski R (2013) Non-linear strain rate analysis of earthquake-induced pounding between steel buildings. Int J Earth Sci Eng 6:429–433

Vasiliadis L, Elenas A (2002) Performance of school buildings during the Athens earthquake of September 7 1999. In: 12th European conference on earthquake engineering, paper ref. 264, Elsevier Science Ltd.

Chapter 24
Dynamic Analysis of Irregular Multistorey Shear Wall Buildings Using Continuous-Discrete Approach

Jacek Wdowicki, Elżbieta Wdowicka, and Zdzisław Pawlak

Abstract The paper presents an analysis of coupled flexural-torsional vibrations of multi-storey shear wall buildings using continuous-discrete approach. A dynamic model with masses in the form of rigid floor slabs has been adopted. The mass matrix is generated exactly, according to real layout of walls, connecting beams and floor slabs. The flexibility matrix is generated on the basis of the solution of the governing differential equations for a three-dimensional continuous model. In order to verify the presented method, for the first example the free vibration analysis of non-planar, non-symmetrical coupled shear walls, previously analysed in the literature by SAP2000 program, has been chosen. In the second example, the possibility of seismic location of the multistorey building, designed originally in Poznań, stiffened by the asymmetrical system of coupled shear walls, was considered. The analysis, in which a continuous-discrete approach and the response spectrum technique were applied, was carried out by means of DAMB (Dynamic Analysis of Multistorey Buildings) program. The presented method is efficient and can be useful at the preliminary design stage when the solutions for a structure with many various geometrical and physical arrangements are required.

Keywords Tall buildings • Coupled shear walls • Continuous connection method • Flexural-torsional vibrations • Seismic analysis

J. Wdowicki (✉) • E. Wdowicka
Polytechnic Faculty, Higher Vocational State School (PWSZ) in Kalisz,
ul. Nowy Świat 4, 62-800 Kalisz, Poland
e-mail: jacek.wdowicki@put.poznan.pl; elzbieta.wdowicka@put.poznan.pl

Z. Pawlak
Institute of Structural Engineering, Poznań University of Technology,
ul. Piotrowo 5, 60-965 Poznań, Poland
e-mail: zdzislaw.pawlak@put.poznan.pl

24.1 Introduction

In multistorey buildings lateral loads that arise from effects of wind and earth-quakes are often carried by a system of shear walls acting as vertical cantilevers. Rutenberg (2013) reviews the literature on the seismic shear demand on reinforced cantilever walls. Such walls are usually perforated by vertical bands of openings, which are required for doors and windows, and they form a system of coupled shear walls. There are basically two approaches for analysis of coupled shear walls: discrete and continuous. In the continuous approach, which has been widely used for shear walls being uniform along the height, the discrete set of connecting beams is replaced by a continuous medium of equivalent properties.

The seismic design of multistorey buildings involves the dynamic analysis of structure. For the dynamic analysis it is convenient to use a hybrid approach, based on the analysis of an equivalent continuous medium and a discrete lumped mass system (Wdowicki and Wdowicka 1991; Li and Choo 1996). In this approach the continuous connection method is employed to find the structural flexibility matrix but the structure mass matrix is found with the lumped mass assumption.

When multistorey buildings with non-coincident centres of mass and stiffness are subjected to a ground motion due to earthquake they respond in coupled lateral and torsional vibrations. Torsional coupling may induce significant amplification of inertia force resulting from earthquakes and it is felt to be strongly influenced by building asymmetry (Glück et al. 1979; De Stefano and Pintucchi 2008; Yiu et al. 2014).

The paper presents an analysis of coupled flexural-torsional vibrations of multistorey shear wall buildings using continuous-discrete approach. The mass matrix including flexural and torsional inertia is generated. To find the flexibility matrix each lumped mass is loaded subsequently with a unit horizontal generalized force and the corresponding horizontal displacement vector for the whole structure is found by the continuous connection method. As a result of solving the eigenproblem, which corresponds to free vibrations of the system, the natural frequencies and mode shapes of vibration have been received.

To verify the presented method, the free vibration analysis of non-planar, non-symmetric coupled shear walls, previously analysed in the literature by the discrete method, has been presented. The results obtained by this method have been compared with those available in the literature.

The paper presents also the results of the seismic analysis based on discrete-continuous approach and the response spectrum technique. The subject of the analysis is the multistorey building, designed originally in Poznań, which is stiffened by the asymmetric system of coupled shear walls. The seismic analysis was carried out using DAMB program, as a part of an Integrated System (Wdowicki et al. 1995), using design spectrum for elastic analysis according to Eurocode 8 (EC8-1 2004).

24.2 Method of Analysis

The analysis is based on the following main assumptions:

1. The floor slabs are taken as diaphragms with infinite in-plane stiffness;
2. The out-of-plane stiffness of the floor slabs can be modelled by connecting beams of appropriate stiffness spanning between shear walls;
3. Vlasov's theory for thin walled beams of an open section is taken to be valid for the individual shear walls;
4. The walls and beams are assumed to be linearly elastic;
5. The geometric and mechanical properties of the structure are constant throughout the height of each segment (Wdowicki and Wdowicka 2012).

In our analysis the continuous connection method has been used in conjunction with Vlasov's theory of thin-walled beams. To simplify the analysis, the effect of St. Venant's torsion has been neglected. The dynamic model with masses in the form of rigid floor slabs has been adopted since over a half of the building total mass is usually concentrated on the floor levels. The coupled torsional-flexural vibrations have been taken into consideration. For shear wall multistorey structure it is more natural to determine the flexibility matrix $\mathbf{D}$ rather than the stiffness matrix $\mathbf{K}$ (Clough and Penzien 1993). To find the flexibility matrix $\mathbf{D}$ each lumped mass is loaded with a unit horizontal generalized force and the corresponding horizontal displacement vector is found using the continuous connection method.

The vibration of a structure is described by the following relation:

$$\mathbf{D}\,\mathbf{M}\,\ddot{\mathbf{x}} + \mathbf{D}\,\mathbf{C}\,\dot{\mathbf{x}} + \mathbf{x} = \mathbf{D}\,\mathbf{f} \tag{24.1}$$

where: $\mathbf{D}$ – flexibility matrix, $\mathbf{M}$ – mass matrix, $\mathbf{C}$ – damping matrix, $\mathbf{x}$ – d-element vector of generalised coordinates (d – number of dynamic degrees of freedom of the considered structure), f – d-element vector of generalised excitation forces, corresponding to the generalised coordinates.

The flexibility matrix $\mathbf{D}$ is generated on the basis of the exact solution of the governing differential equations for three-dimensional continuous model of the shear wall structure.

Also the mass matrix is generated exactly according to the real distribution of walls, connecting beams and floor slabs, including flexural and torsional inertia. Using mass properties of shear walls, connecting beam bands as well as floor slabs, a quasi-diagonal mass matrix of a whole structure is created:

$$\mathbf{M} = diag(\mathbf{M_k}), \quad (k = 1, \ldots, n_k) \tag{24.2}$$

where: n_k – number of storeys, $\mathbf{M_k}$ – the 3×3 symmetric matrix, which defines inertia properties of k-th storey.

The seismic response of the structure is estimated using the response spectrum technique (Chmielewski and Zembaty 1998). The involved stages of the analysis are as follows:

1. Determination of natural frequencies and corresponding mode shapes;
2. Evaluation of modal participation factors of modal loading of the structure using an appropriate design spectrum;
3. Estimation of response taking into account the contribution of all given modes for various parameters of interest, using three methods: SRSS – the square root of the sum of the squares, CQC – the complete quadratic combination or DSC – the double sum combination (Maison et al. 1983).

On the basis of the elaborated algorithm the software in Object Pascal of Delphi 5 environment has been implemented and included in the DAMB (Dynamic Analysis of Multistorey Buildings) program for the dynamic analysis of shear wall tall buildings.

24.3   Free Vibration Analysis of Non-planar Coupled Shear Walls

To verify the presented method, several examples have been solved. As the first example the non-planar, non-symmetric coupled shear wall system, presented by Aksogan et al. (2014), has been considered (Fig. 24.1). The total height of the shear wall is 48 m and the storey height is 3 m. The mass density and the elasticity and shear modules are as follows: $\rho = 2400$ kg/m^3, $E = 2.85$ GPa and $G = 1.056$ GPa. The height of the connecting beams is 0.4 m. The thickness of the connecting beams and walls is 0.4 m in the right part and 0.2 m in the left part of the structure. The mass of the typical storey, including a connecting beam, equals to 104.3×10^3 kg and the total mass of the building is 1669×10^3 kg. The mass of floor slabs has not been considered in this example for comparison purposes.

It may be noted that in the present analysis the shear deformation of the walls has been neglected due to the assumption in Vlasov's theory. The same assumption has been made in the analysis presented by Aksogan et al. (2014) and for comparison purposes the shear deformation was neglected in SAP2000 application as well.

In Table 24.1 the first ten natural frequencies corresponding to each mode found by the program DAMB are compared with the values given by Aksogan et al. (2014), obtained by SAP2000 structural analysis program, using MacLeod's frame method, for the case without a stiffening beam.

The torsional modes are omitted in the results given by Aksogan et al. (2014), but for the other frequencies a satisfactory match of results has been observed.

Figure 24.2 presents the first six mode shapes of the analysed non-planar shear wall structure found by the presented method, using DAMB program.
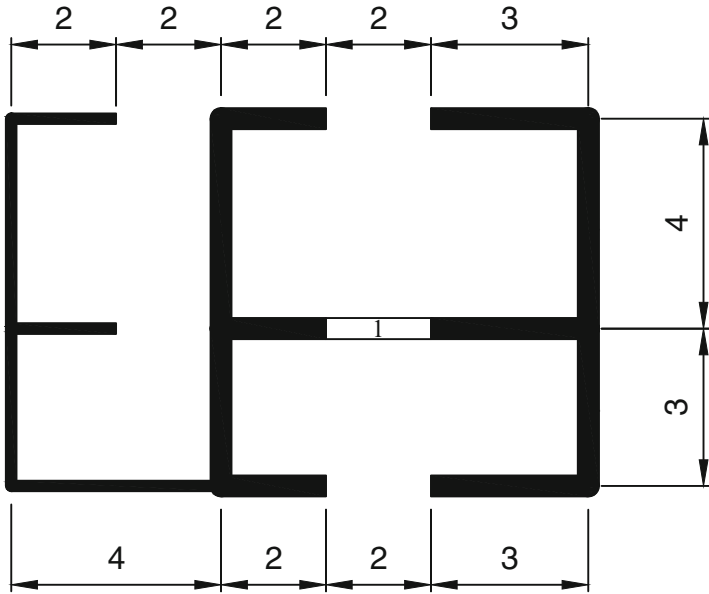
Fig. 24.1 Plan view of the non-planar shear wall structure [m]

Table 24.1 Comparison of the first ten natural frequencies found by the present method (program DAMB) and by SAP2000 program (Aksogan et al. 2014)

| Mode | Predominant mode | Natural frequencies [Hz] | | |
		Present method (program DAMB)	SAP2000	% difference
1	First mode X	0.4748	0.50047	−5.13
2	First mode Y	0.6656	0.66117	0.67
3	First torsional mode	1.0022	–	
4	Second mode X	2.4180	2.46396	−1.87
5	Second mode Y	4.1799	4.11839	1.49
6	Second torsional mode	6.2020	–	
7	Third mode X	6.4394	6.47507	−0.55
8	Third mode Y	11.729	11.45595	2.38
9	Fourth mode X	12.456	12.37532	0.65
10	Third torsional mode	17.265	–	

Functions: X, Y, F [f = 0.475 Hz T = 2.106 s]

max X = 1,000 z = 46,500

min F = -0,089 z = 46,500

Functions: X, Y, F [f = 0.666 Hz T = 1.502 s]

max Y = 1,000 z = 46,500

min X = -0,076 z = 46,500

Functions: X, Y, F [f = 1.022 Hz T = 0.978 s]

max X = 1,000 z = 46,500

min X = 0,000 z = 0,000

Functions: X, Y, F [f = 2.418 Hz T = 0.414 s]

max X = 1,000 z = 46,500

min X = -0,814 z = 22,500

Functions: X, Y, F [f = 4.180 Hz T = 0.239 s]

max Y = 1,000 z = 46,500

min Y = -0,840 z = 22,500

Functions: X, Y, F [f = 6.202 Hz T = 0.161 s]

max X = 1,000 z = 19,500

min Y = -0,867 z = 46,500

Fig. 24.2 The first six mode shapes of the non-planar shear wall structure, obtained by the DAMB program

24.4 Seismic Analysis of the Multi-storey Asymmetric Shear Wall Building

In the second example, the seismic analysis of the multistorey building, designed originally in Poznań, stiffened by the asymmetric system of coupled shear walls, has been presented. After the static analysis, the possibility of seismic location of the designed structure was considered. The investigated building is a multi-storey reinforced concrete structure. The elevation of the building and shear walls in the typical floor plan are shown in Figs. 24.3 and 24.4.

Fig. 24.3 The view of the analysed multistorey shear wall building

The building has 15 storeys above the ground level and 2 basement storeys. The total height of the building is 53.5 m. In the analysed building, lateral loads that arise as a result of winds and earthquakes are carried by the three-dimensional system of coupled shear walls. The dimensions of the central core are 3.15 m × 12 m. The thickness of walls equals to 0.3 m. The height of connecting beams is 0.7 m. The structural properties of shear walls and lintels are uniform along the building height. The slabs are 0.25 m thick.

A diaphragm action of all floor slabs is taken into consideration as the effect of the assumption of their in-plane infinite rigidity and negligible transverse one. The Young's modulus $E = 36$ GPa and the shear modulus $G = 15.4$ GPa are assumed for concrete. All the elements are assumed to be fully fixed in foundations. The static analysis was carried out on the basis of a variant of the continuous connection method (Wdowicki and Wdowicka 1993).
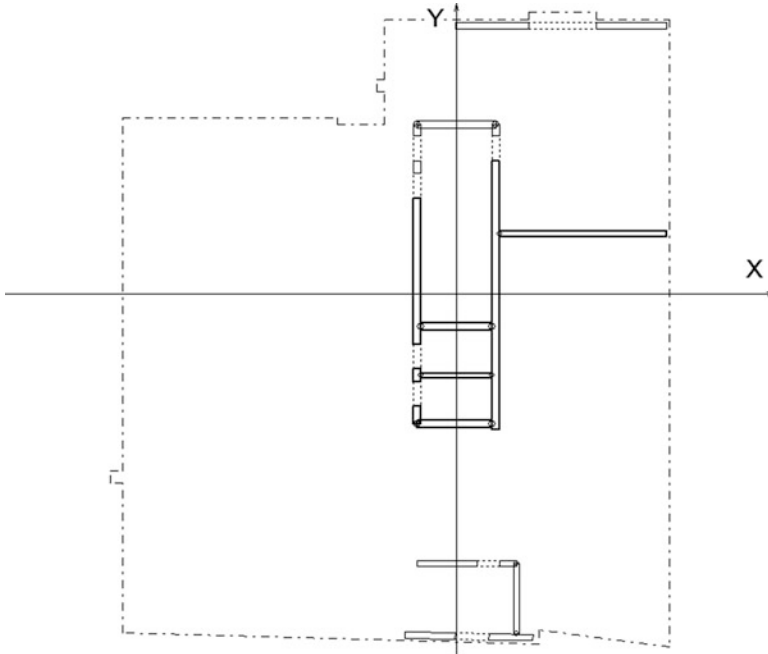
Fig. 24.4 The plan of the shear walls in typical floor (from the pre-processor of DAMB program)

Dynamic solutions have been obtained by treating the structure as a lumped parameter system with discrete masses in the form of rigid floor slabs, having flexural and torsional inertia. The floor masses are determined according to Eurocode 8. Complete masses resulting from the permanent load are considered, whereas the masses associated with the variable-live load are reduced using the factor $\Psi_{Ei} = \varphi \, \Psi_{2i}$. Factor Ψ_{2i} amounts to 0.3 in the case of an office building. Factor φ is equal to 1.0 for the roof slab and 0.5 for the other slabs. The total mass of the building is equal to $9\ 234 \times 10^3$ kg.

The analysis was made using DAMB program which gives a possibility to perform the dynamic analysis of three-dimensional shear wall structures. As a result of the first step the periods of vibration and the corresponding mode shapes have been received. The three fundamental periods of vibration of the building amount to 2.22 s, 1.60 s and 1.10 s. The first mode is predominantly torsional, the second mode is predominantly translational in the X direction and the third mode is predominantly translational in the Y direction. It may be noted that the analysed building can be classified as torsionally flexible (Fajfar et al. 2005).

The seismic action is represented by the Type 1 elastic response spectrum, recommended for high and moderate seismicity regions ($M_s > 5.5$), for subsoil class C (EC8-1 2004). The reference peak ground acceleration amounts to

$a_{gR} = 0.25$ g. The values of the periods (T_B, T_C, T_D) and the soil factor S, which describe the shape of the elastic response spectrum, amount to $T_B = 0.2$ s, $T_C = 0.6$ s, $T_D = 2.0$ s and $S = 1.15$. For the analysed building the importance category II, according to Eurocode 8, the corresponding importance factor $\gamma_I = 1.0$ and the reduction factor $v = 0.5$ were assumed. The value of viscous damping ratio $\xi = 5\%$ has been assumed in the analysis (Fajfar and Kreslin 2012).

Assuming that the specific provisions for all the structural elements are satisfied to provide the appropriate amount of ductility, the ductility class DCM (medium ductility) has been established. The value of behaviour factor $q = 2.0$ has been applied. In the analysis the design response spectrum according to Eurocode 8 has been applied (EC8-1 2004).

Modal response spectrum analysis was performed for the ground excitation in two horizontal directions, X (E-W) and Y (N-S), independently. The CQC rule for the combination of different modes was used.

The results of the analysis based on damage limitation state have been presented. It has been assumed that the analysed building has non-structural elements of brittle materials attached to the structure. The requirement of damage limitation is accomplished by Eurocode 8 when interstorey drifts d_r do not exceed the limited values, obtained using the following equation:

$$\frac{d_r}{h} \leq \frac{0.005}{v} = \frac{0.005}{0.5} = 0.01 \qquad (24.3)$$

where: d_r – difference between the lateral displacements occurring at the top and bottom of the storey, determined by the linear analysis based on the design response spectrum, h – the storey height.

The results of the displacement analysis, based on the response spectrum technique, for (E-W) seismic wave direction, are shown in Figs. 24.5 and 24.6.

The ratio of the actual top displacement and the total height of the building above the basement amounts to: $2.0 \times 0.123/53.5$ m $= 0.46\%$ and $2.0 \times 0.0844/53.5$ m $= 0.32\%$, for X and Y directions, respectively.

The obtained maximum value of interstorey drift d_r/h was equal to $2.0 \times 0.0176/3.45$ m $= 0.0102$.

The horizontal displacements of the shear wall structure due to the seismic wave parallel to X axis reveal the considerable influence of torsion. The torsional rigidity of the structure should be increased by the additional walls.

Using the software DAMB, it is easy to obtain the graphs of normal stresses for the entire cross-section of shear wall structure, for a selected three-dimensional shear wall as well as for a single wall (Fig. 24.7).

It seems advisable to consider the application of the presented method in the seismic analysis of the actual existing asymmetric, torsionally flexible shear wall buildings.
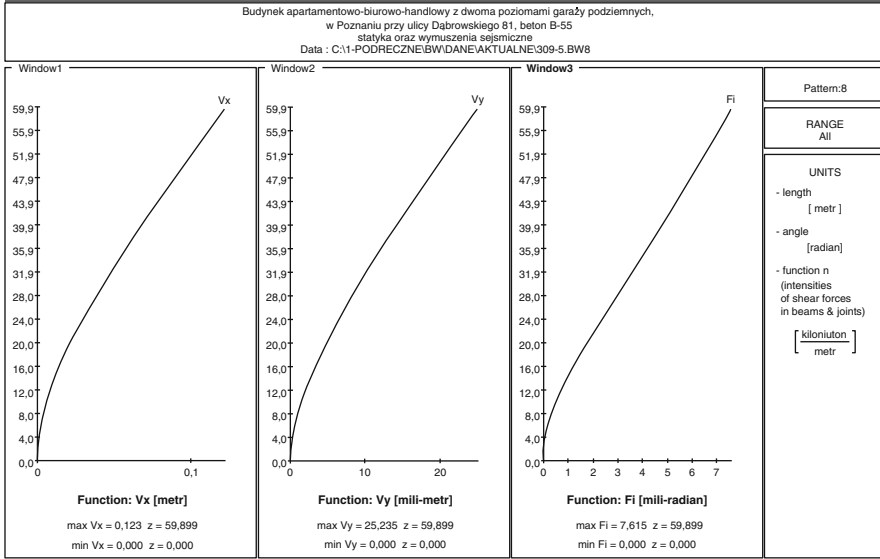
Fig. 24.5 Horizontal displacements of shear wall structure due to (E-W) seismic wave direction (parallel to X)
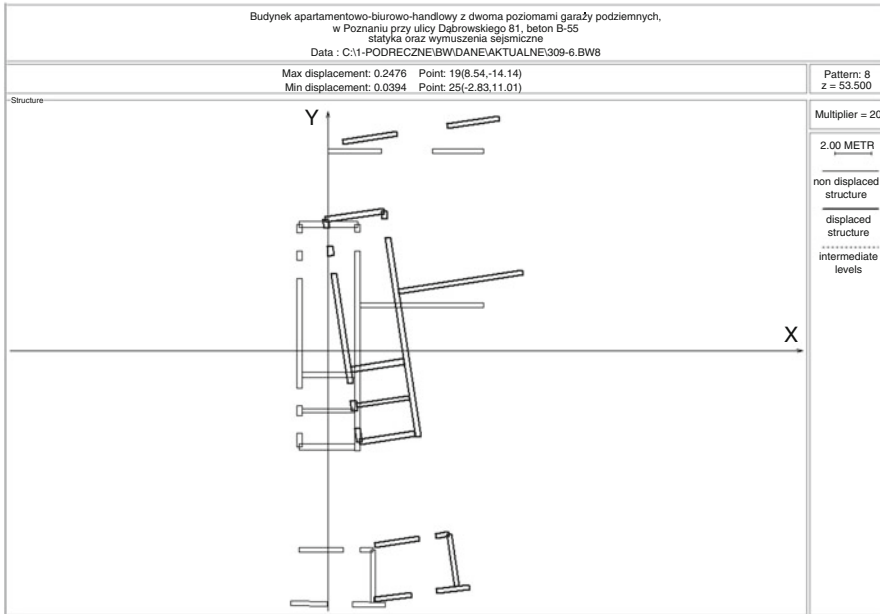
Fig. 24.6 View of the displacements of the shear wall structure due to (E-W) seismic wave direction; displacements are $20\times$ enlarged relative to the structure dimensions (from the post-processor of DAMB program)
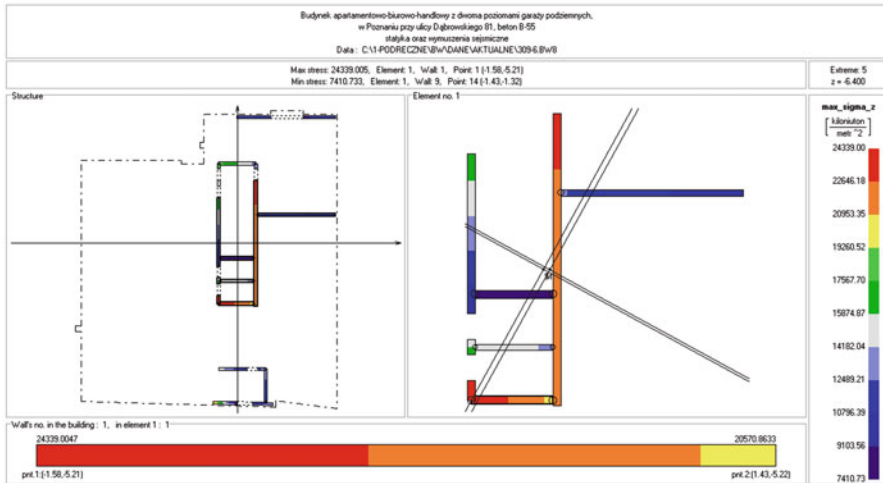
Fig. 24.7 Normal stresses at the base of the shear wall structure due to (N-S) seismic wave direction (from the post-processor of DAMB program)

24.5 Conclusions

In this study the seismic analysis of the shear wall tall building has been carried out using a continuous-discrete approach and the response spectrum technique. The coupled flexural-torsional vibrations have been taken into account. The results obtained by the abovementioned method have been compared with those obtained using the SAP2000 structural analysis program, given in the literature, and a satisfactory match has been observed. The proposed method is efficient and can be useful, particularly at the preliminary design stage when quick checks with different structural arrangements and dimensions are needed.

References

Aksogan O, Turkozer CD, Emsen R, Resatoglu R (2014) Dynamic analysis of non-planar coupled shear walls with stiffeners using a continuous connection method. Thin-Walled Struct 82:95–104

CEN. Eurocode 8 (EC8-1) Design of structures for earthquake resistance. Part 1: General rules, seismic actions and rules for buildings. EN 1998-1:2004, Comité Européen de Normalisation, Brussels, Belgium

Chmielewski T, Zembaty M (1998) Podstawy dynamiki budowli. Arkady, Warszawa

Clough RW, Penzien J (1993) Dynamics of structures. McGraw-Hill, New York

De Stefano M, Pintucchi B (2008) A review of research on seismic behaviour of irregular building structures since 2002. Bull Earthq Eng 6:285–308

Fajfar P, Kreslin M (2012) Introduction to the RC building example. Modeling and analysis of the design example. In: Eurocode 8: seismic design of buildings. Worked examples. JRC Scientific and Technical Reports, Eur 25204 EN- 2012, Chapter 2, pp 27–50, Ispra, Italy. Available from: http://eurocodes.jrc.ec.europa.eu/doc/WS_335/report/EC8_Seismic_Design_of_Buildings-Worked_examples.pdf

Fajfar P, Marusic D, Perus I (2005) Torsional effects in the pushover-based seismic analysis of buildings. J Earthquake Eng 9(6):831–838

Glück J, Reinhorn A, Rutenberg A (1979) Dynamic torsional coupling in tall building structures. Proc Inst Civ Eng Part 2 67:411–424

Li G-Q, Choo BS (1996) A continuous-discrete approach to the free vibration analysis of stiffened pierced walls on flexible foundations. Int J Solids Struct 33(2):249–263

Maison B, Neuss C, Kasai K (1983) The comparative performance of seismic response spectrum combination rules in building analysis. Earth Eng Struct Dyn 11(5):623–647

Rutenberg A (2013) Seismic shear forces on RC walls: review and bibliography. Bull Earthq Eng 11(5):1727–1751

Wdowicki J, Wdowicka E (1991) Integrated system for analysis of three-dimensional shear wall structures. Comput Methods Civ Eng 1(3–4):53–60

Wdowicki J, Wdowicka E (1993) System of programs for analysis of three-dimensional shear wall structures. Struct Des Tall Build 2(4):295–305

Wdowicki J, Wdowicka E (2012) Analysis of shear wall structures of variable cross section. Struct Design Tall Spec Build 21:1–15

Wdowicki J, Wdowicka E, Błaszczyński T (1995) Integrated system for analysis of shear wall tall buildings. In: Proceedings of the Fifth World Congress "Habitat and High- Rise: Tradition and Innovation", Council on Tall Buildings and Urban Habitat, Amsterdam, pp 1309–1324

Yiu C-F, Chan C-M, Huang M, Li G (2014) Evaluation of lateral-torsional coupling in earthquake response of asymmetric multistory buildings. Struct Design Tall Spec Build 23:1007–1026

Chapter 25
Analysis of the Dynamic Response of Masonry Buildings with Irregularities of Localization of Bearing Elements Due to Mining Shocks

Tadeusz Tatara and Filip Pachla

Abstract The study concerns the analysis of the impact of structural irregularities in the masonry buildings on their dynamic characteristics and dynamic response to kinematic loads. Several models of buildings deemed to be representative of this class of structures in the areas covered by the influence of mining tremors were analyzed. In areas Legnica-Głogów Copper District (LGCD) and the Upper Silesian Coal Basin (USCB) are the most numerous masonry buildings with a height of 1–5 storeys. The first part of the study refers to the adoption of 3-D dynamic models of buildings of different structural wall system. These were buildings with irregular, symmetrical and bisymmetrical system load-bearing walls. The second part concerns the dynamic characteristics of the building models and assessing the impact of irregularities in the load-bearing walls on the natural frequencies. Subsequently, using the response spectrum method and assuming different standard response spectra, dynamic responses of building models were determined. The level of dynamic principal and shear, depending on the adopted standard curve, describing the response spectrum and irregularities in the structural walls, were also evaluated. The results of numerical analyzes showed a significant influence of the structural irregularities on the natural frequencies of the analyzed models of buildings. It also showed the impact of the adopted standard response spectrum curve in the LGCD on the level of calculated stresses.

Keywords Mine tremors • Masonry buildings • Irregular structures • Response spectrum • Dynamic response • Eurocode 8

T. Tatara (✉) • F. Pachla
Institute of Structural Mechanics, Cracow University of Technology, ul. Warszawska 24, 31-155 Cracow, Poland
e-mail: ttatara@pk.edu.pl; fpachla@pk.edu.pl

25.1   Introduction

In Poland, Legnica-Głogów Copper District (LGCD) and the Upper Silesian Coal Basin (USCB) most intensive mining tremors are characterized by a power of up to 1E10 J and intensity of surface vibrations that reach even 0.3 g (g – acceleration due to gravity). Underground mining operations are conducted primarily in urban, heavily populated areas, so the influence of surface mining related vibrations on development and risk assessment is particularly important. Masonry buildings constitute the largest part of the residential development in the above areas. These are generally single-family or multi-family buildings (in lesser extent) which have from one to five floors. Repairs and reconstructions impose the necessity of structural changes in buildings. These changes often cause the appearance of symmetry or even bisymmetry of the load-bearing walls. However, the bearing wall systems of these buildings often represent abnormal structural systems as a result of extension works such as building external staircases. In this study the method of dynamic response spectrum Tatara (2012) was used. This method uses: (a) the adopted models of buildings treated as a representative for the considered class of objects, (b) standard response spectra characterizing the surface vibrations induced by mining tremors. These spectra were also compared with the standard response spectrum of EN 1998-1:2004 (2004).This comparison indicated the differences between the vibration-type surface mining and seismic (deriving from earthquakes) Tatara (2002, 2012). The numerical analysis includes simultaneous operations of two mutually perpendicular loads (parallel to the transverse and longitudinal axes of buildings' models) as described by standard response spectra. The vertical component has been omitted. Assessment of the impact of positioning the wall bearing elements in buildings on the responses was made by comparing the results of dynamic analysis of the models. The bases of this assessment were the additional maximum principal stress and maximum shear stress.

25.2   Analyzed Buildings and Their Structural Characteristics

All of the analyzed structures are masonry buildings of various height and design. Buildings can be considered as representative of this class of structures, residential single-family housing. It was built using the traditional method of unreinforced masonry. Floors and staircases and flights of stairs are made as a monolithic reinforced concrete. The first three are three-storey buildings; floor plans of their repetitive floors are shown in Fig. 25.1a–c.

Building from Fig. 25.1a is characterized by the symmetry of the load-bearing walls with respect to one axis, and the building from Fig. 25.2a is bisymmetrical.
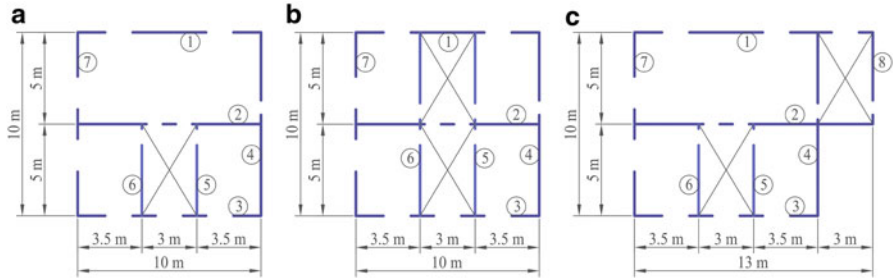
Fig. 25.1 Floor plans of three storey buildings: no. 1 (**a**), no. 2 (**b**), no. 3 (**c**)
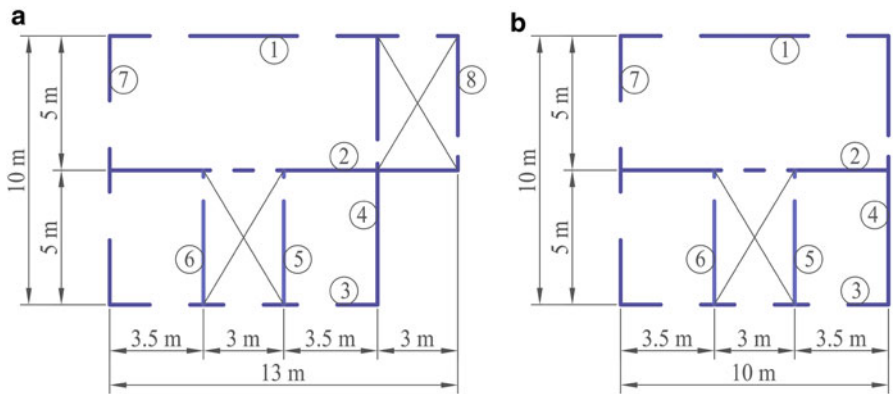
Fig. 25.2 Floor plans of five storey buildings: no. 4 (**a**), no. 5 (**b**)

There is no symmetry in building presented in Fig. 25.1c. Building from Fig. 25.1c differs in relation to the building in Fig. 25.1a due to addition of external staircase to one of the outer wall (gable wall). A characteristic feature is the lack of dilatation between the outer staircase and gable wall.

Buildings No. 4 and No. 5 – see Fig. 25.2 – have the same distribution of the bearing walls as buildings No. 3 and No. 1 respectively presented in Fig. 25.1a, c. Building No. 4 has two staircases, including one outside, not militated from the main part of the building – see Fig. 25.2a.

A five-storey building No. 6 has first three floors as building No. 4. The other two floors are of a different arrangement of bearing walls – see Fig. 25.3. Access to floors 1–3 is via an internal staircase – comp. Fig. 25.3a. Floors 4 and 5 can be accessed only using an external staircase located at the gable wall and not militated from the main part of the building – see Fig. 25.3b.
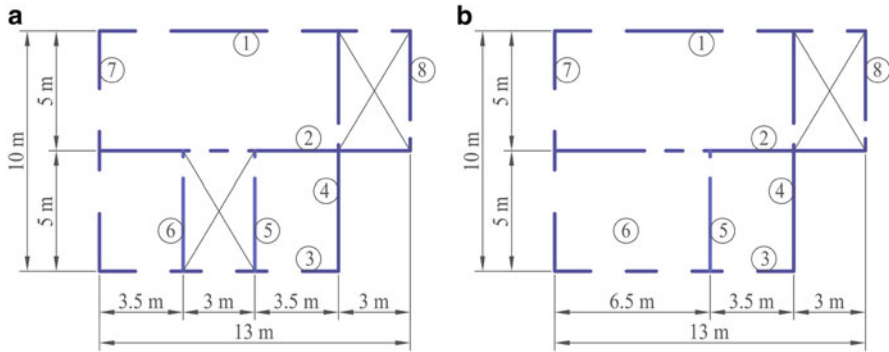
Fig. 25.3 Floor plans of five storey building no. 6

25.3 Assessment of Regularity of the Structural System of the Analyzed Buildings

Using the information provided e.g. in EN 1998-1:2004 (2004) buildings analyzed in the study can be characterized as structures in which:

- the ratio of height to width (length) is close to unity, which prevents the loss of stability of the structure and, consequently, its overturning,
- height of floors is the same, approximate carrying capacity due to the horizontal loads in two mutually perpendicular directions is similar,
- there is a uniform shape horizontally and vertically,
- there are stiffening rims and bearing walls on circuit of structure, which leads to a reduction in the effects of torsion,
- there is a lack of cantilever elements,
- there are no floors at different levels within the same storey,
- statically indeterminate structural system increases resistance and the possibility of transferring the loadings in case of damage to one or a group of bearing elements.

The presence of the factors listed above in the analyzed buildings provides that structures should be designed to carry additional dynamic loads caused by the mining related surface vibrations. The analyzed buildings shown in Figs. 25.1a–c and 25.2 are characterized by the regularity along the height. The center of gravity and the center of the shear remain in the vertical line. These buildings fulfill the conditions of regularity given in EN 1998-1:2004 (2004) – see Fig. 25.4.

a

$$\frac{L_1 - L_2}{L_1} \leq 0,20$$

b

$$\frac{L_3 + L_1}{L} \leq 0,20$$

(setback occurs above 0,15H)

c

$$\frac{L_3 + L_1}{L} \leq 0,50$$

(setback occurs below 0,15H)

d

$$\frac{L - L_2}{L} \leq 0,30$$

$$\frac{L_1 - L_2}{L_1} \leq 0,10$$
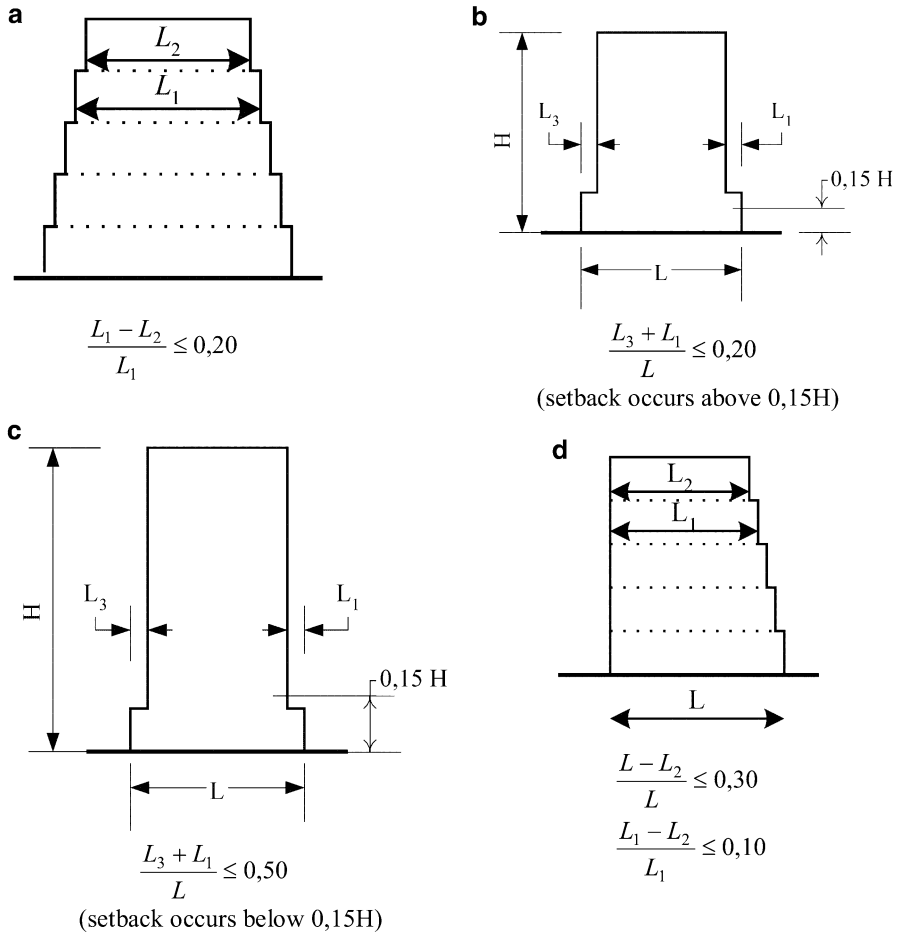
Fig. 25.4 Criteria for regularity of buildings EN 1998-1:2004 (2004)

25.4   Analyzed Models of Buildings and Their Dynamic Characteristics

The models take into account the different properties of building materials forming the bearing system, loads due to the weight of plasters and finishing elements, light warming of the roof and long-term part of the live load (40 %), according to polish standard PN-85/B-02170:1985 (1985). Assumption of only long-term part of the live load results from the fact that, during use of the building, occasionally this load reaches the maximum value, which in combination with the occurrence of mining shock is highly unlikely. In addition, the static load acting in accordance with the direction of gravitational acceleration plays reductive factor on the tensile stresses
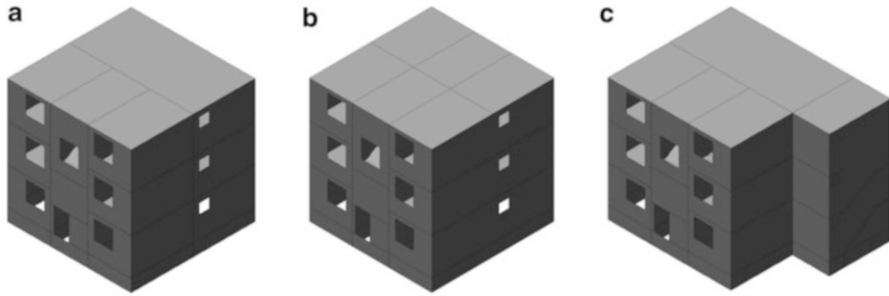
Fig. 25.5 Assumed geometric models of three storey buildings from Fig. 25.1a–c

caused by mining tremors, which leads to a safer estimate of the structure response to dynamic loads. When determining the value of the Young's modulus of the cement – limestone wall results of secant modulus of elasticity of the wall given in Kubica et al. (1999) and the standard PN-B-03002:1999 (1999) were used. The value of Poisson's ratio was adopted on the basis of the studies contained in Drobiec et al. (2000). Parameters for other materials were adopted on the basis of building standards PN-B-03002:1999 (1999), PN-B-03264:2002 (2002). In the analyzed models following values were used: reinforced concrete floors of the characteristics of materials – Young's modulus $E = 29$ GPa, Poisson's ratio $\nu = 0.2$, mass density $\rho_m = 2500$ kg/m^3, the walls of masonry cement mortar for masonry material characteristics – Young's modulus and $E = 2$GPa, Poisson's ratio $\nu = 0.25$, mass density $\rho_m = 1800$ kg/m^3.

The models of the analyzed buildings take into account all the elements relevant to the stiffness and mass of the buildings which include e.g. window and door openings, stairways, lintels. In the considered models masonry elements are viewed as homogeneous, treating such assumption as sufficiently accurate in terms of precise engineering calculations Tatara (2002). Finishing elements are not modeled using FEA for practical reasons. Models of elastic support building resulting from the foundation on the flexible ground were assumed. An influence of ground was taken into account by means of elastic mounting. Elastic support of the models was achieved by springs localized at the level of the bottom of the foundation. The stiffness of boundary elements was defined according to PN-80/B-03040:1980 (1980), as for substrate III category of medium stiffness, and the papers Sawinow (1964), Lipiński (1985). The dynamic coefficients of the substrate for the ground in a natural state of the residual amount up to 50 MPa/m. Adopted three storey building models from Fig. 25.1a–c are shown in Fig. 25.5a–c, and five storey building from Figs. 25.2 to 25.3 are presented in Fig. 25.6. These models will be the subject of further computational analyzes.

Table 25.1 summarizes, for example, the first three natural frequencies calculated for each of the analyzed masonry building models. Calculated mode shapes are complex. Therefore, determination of the sequence of natural frequency was guided by the dominant relative displacements in that direction.
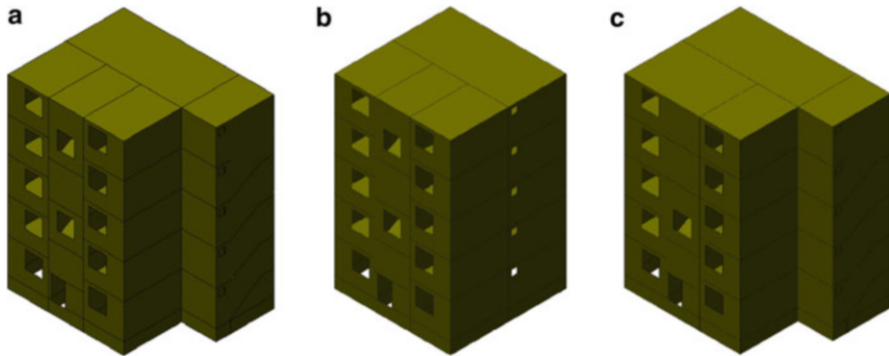
Fig. 25.6 Assumed geometric models of five storey buildings from Fig. 25.2 and 25.3

Table 25.1 First three calculated natural frequencies of analyzed models of masonry buildings

	f_1 [Hz]	f_2 [Hz]	f_3 [Hz]
Model no 1	7.08	7.57	11.22
Model no 2	7.34	7.73	10.92
Model no 3	6.93	8.04	10.51
Model no 4	3.70	4.42	6.14
Model no 5	3.81	4.07	6.54
Model no 6	3.73	4.46	6.18

In all models, first two calculated natural frequencies f_1 and f_2 correspond to the transverse vibration and the frequency f_3 to torsion vibration. In the case of building models with added staircase to the gable wall, regardless of their height, the value of the natural frequency f_2 is almost 20 % higher than the frequency f_1. This demonstrates the significant effect of irregularities in the position of the bearing walls on the stiffness of these buildings and consequently the value of the fundamental frequency of the vibrations in the transverse direction. In the case of other buildings impact of irregularities does not exceed 7 %.

25.5   The Dynamic Response of the Analyzed Models of Masonry Buildings

For further calculations, dynamic response spectrum method was used (RSA); described in detail in Tatara (2002). This method uses a structural model and corresponding computer software, which must implement the standard, relative acceleration response spectrum. The standard spectra contain information about the frequencies content of the recorded, mining related, surface vibrations. They may be used in the calculation of the design of dynamic structures exposed to kinematic load.
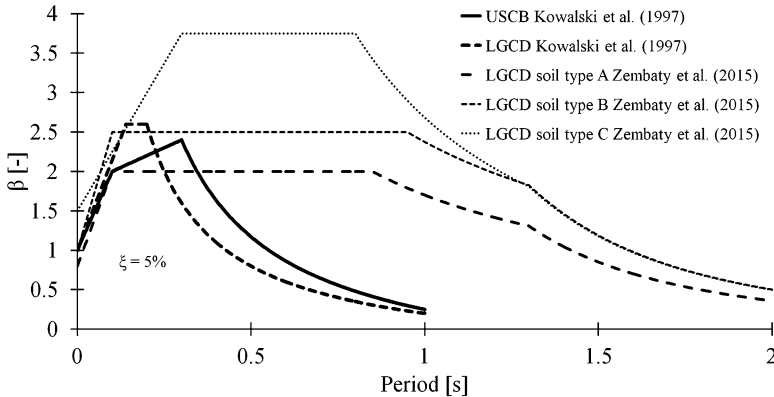
Fig. 25.7 Standard response spectra assumed as kinematic excitations

Figure 25.7 shows the standard spectra for the USCB and LGCD areas obtained by analysis of multiple horizontal components of the surface vibration accelerations. A comparison of the standard curves generated on the basis of investigation shows large variations. Application of dynamic curves proposed in Zembaty (2011, 2012), Zembaty et al. (2015), adapted from EN 1998-1:2004 (2004), to the analysis, can lead to erroneous solutions due to the very wide range of oscillation periods, where a constant maximum value of β is assumed. These curves are based on the EN 1998-1:2004 (2004), which refers only to the natural phenomena of earthquakes.

The studies carried out for many years at the Institute of Structural Mechanics in Cracow University of Technology related to construction of the standard response spectra for mining areas showed differences in the shape of the spectral curves corresponding to different regions of LGCD and USCB Ciesielski et al. (1996), Czerwionka and Tatara (2007), Kowalski et al. (1997), Kuźniar et al. (2010, 2006), Lipiński (1985), Tatara (2002, 2012). The results presented in these works indicated a significant effect of the ground properties on the shape of these curves. In Tatara (2002), there was a comparison made of standard curves for USCB and LGCD with the curve corresponding to response spectrum of the first type from EN 1998-1:2004 (2004). This comparison shows that in the case of a horizontal section of the curve from EN 1998-1:2004 (2004) is described by much wider range of periods, including much greater periods than in the case of mining tremors. Figure 25.8 shows the comparison of standard response spectra for USCB and LGCD area resulting from previous research and analysis Ciesielski et al. (1996), Kowalski et al. (1997), Tatara (2002) with type 2 spectral curves for different types of soil according to EN 1998-1:2004 (2004). The comparison indicates that standard curves correspond to different types of soil described in EN 1998-1:2004 (2004) are significantly different compared to the standard curves obtained for areas USCB and LGCD. It would be unreasonable to use these curves in the design of structures to dynamic loads of mining origin. It is difficult to assume that in the LGCD characteristics of the soil correspond to the rocky substrate (soil A) – for this type of substrate spectral curve of EN 1998-1:2004 (2004) is closest to the response
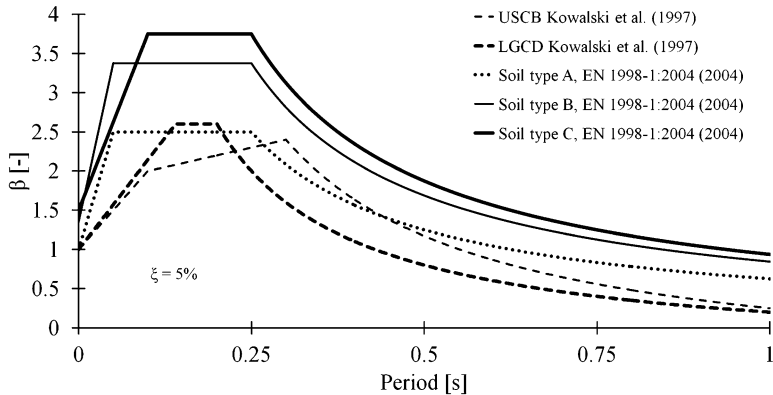
Fig. 25.8 Comparison of USCB and LGCD response spectra with response spectra of type 2 from EN 1998-1:2004 (2004) for different types of soils

curves from the LGCD and USCB – see Fig. 25.8. Similar comparative analysis of the standard curves obtained according to EN 1998-1:2004 (2004) with standard spectral curves from different mining areas of USCB (area KWK "Rydułtowy" and KWK "Anna") indicates a significant difference and demonstrates a significant effect of local soil conditions on the shape of the standard response spectra Tatara (2012).

These differences occur both for spectral curves drawn on the basis of horizontal and vertical components of the ground surface vibrations. These differences relate to the width of the horizontal portion of the spectrum ("plateau") and the value describing this part of curve. The horizontal part of the curve from EN 1998-1:2004 (2004) is described by much wider range of periods, including periods greater than these occurring in the case of mining tremors.

Dynamic calculations were performed assuming: (a) models of buildings shown in Chap. 4, (b) the ground acceleration $a_p = 1$ m/s^2, (c) the kinematic force in the form of a standard response spectrum applied in two mutually perpendicular horizontal directions. Calculations were done according to the procedure described in detail in Tatara (2012).

Tables 25.2 and 25.3 show for example calculated dynamic maximum principal stress in particular load-bearing walls in each of the analyzed models of buildings shown in Fig. 25.5b, c. Tables 25.4 and 25.5 present maximum dynamic shear stress. Calculated stresses showed in Tables 25.2, 25.3, 25.4, and 25.5 refer to cases without considering the impact of dead and live load.

From the analysis of exemplary calculations for LGCD area, listed in Tables 25.2 and 25.3, a significant influence of the type of the curve describing the standard response spectrum used for the dynamic calculations can be noted. Considering building in Fig. 25.1b (full symmetry), and taking into account the spectral curve given in Kowalski et al. (1997), Tatara (2002, 2012), an increase in the value of these stresses in the individual structural walls compared to the case of the use of the curves representing soil type A, B and C Zembaty (2011, 2012), Zembaty

Table 25.2 Maximum dynamic principal stress in bearing walls for model from Fig. 25.5b assuming $a_p = 1$ m/s^2

	Maximum dynamic principal stress in bearing walls [MPa]						
	1	2	3	4	5	6	7
GZW Kowalski et al. (1997)	0.26	0.42	0.57	0.37	0.33	0.42	0.14
LGCD Kowalski et al. (1997)	0.33	0.54	0.72	0.47	0.42	0.53	0.18
LGCD ground type A Zembaty et al. (2015)	0.21	0.34	0.46	0.30	0.27	0.34	0.11
LGCD ground type B Zembaty et al. (2015)	0.26	0.43	0.57	0.37	0.33	0.42	0.14
LGCD ground type C Zembaty et al. (2015)	0.26	0.43	0.58	0.38	0.34	0.42	0.14

Table 25.3 Maximum dynamic principal stress in bearing walls for model from Fig. 25.5c assuming $a_p = 1$ m/s^2

	Maximum dynamic principal stress in bearing walls [MPa]							
	1	2	3	4	5	6	7	8
GZW Kowalski et al. (1997)	0.37	0.40	0.37	0.35	0.28	0.34	0.17	0.44
LGCD Kowalski et al. (1997)	0.44	0.48	0.46	0.42	0.33	0.41	0.22	0.53
LGCD ground type A Zembaty et al. (2015)	0.30	0.32	0.30	0.29	0.22	0.27	0.14	0.36
LGCD ground type B Zembaty et al. (2015)	0.37	0.40	0.38	0.36	0.28	0.34	0.17	0.45
LGCD ground type C Zembaty et al. (2015)	0.36	0.39	0.37	0.35	0.27	0.33	0.18	0.44

Table 25.4 Maximum dynamic shear stress in bearing walls for model from Fig. 25.5b assuming that $a_p = 1$ m/s^2

	Maximum dynamic shear stress in bearing walls [MPa]						
	1	2	3	4	5	6	7
GZW Kowalski et al. (1997)	0.106	0.130	0.176	0.069	0.096	0.106	0.085
LGCD Kowalski et al. (1997)	0.135	0.165	0.135	0.088	0.121	0.134	0.107
LGCD ground type A Zembaty et al. (2015)	0.086	0.105	0.145	0.056	0.077	0.086	0.068
LGCD ground type B Zembaty et al. (2015)	0.108	0.131	0.178	0.070	0.097	0.107	0.086
LGCD ground type C Zembaty et al. (2015)	0.26	0.43	0.58	0.38	0.34	0.42	0.14

et al. (2015), reaches respectively, approximately 58, 27 and 22 %. In the case of the irregular arrangement of the building bearing walls – see Fig. 25.1c obtained results were larger of the average dynamic stress of about 50, 20 and 19 %. Practically in all bearing walls of considered models – comp. Fig. 25.1b, c, calculated maximum values of dynamic shear stress using spectral curves according to Kowalski

Table 25.5 Maximum dynamic shear stress in bearing walls for model from Fig. 25.5c assuming that $a_p = 1$ m/s^2

	Maximum dynamic shear stress in bearing walls [MPa]							
	1	2	3	4	5	6	7	8
GZW Kowalski et al. (1997)	0.115	0.118	0.132	0.086	0.107	0.077	0.081	0.083
LGCD Kowalski et al. (1997)	0.139	0.143	0.160	0.106	0.131	0.094	0.103	0.100
LGCD ground type A Zembaty et al. (2015)	0.094	0.096	0.108	0.070	0.087	0.063	0.066	0.067
LGCD ground type B Zembaty et al. (2015)	0.118	0.121	0.135	0.088	0.109	0.079	0.082	0.084
LGCD ground type C Zembaty et al. (2015)	0.115	0.117	0.132	0.086	0.107	0.077	0.084	0.082

et al. (1997), Tatara (2002, 2012) are larger than calculated from the curves of the studies Zembaty (2011, 2012), Zembaty et al. (2015) – see Tables 25.4 and 25.5.

In the area of LGCD and USCB in most of the structural walls in the bisymmetrical building higher calculated values of maximum principal stress than in a building with an irregular distribution of load-bearing walls were achieved. It is not possible to establish a clear trend indicating the impact of irregular bearing walls on the maximum value of shear stress – see Tables 25.4 and 25.5.

25.6 Conclusions

The study presents series of dynamic analysis of masonry buildings of a height of 3 and 5 floors. Buildings vary in terms of an angle of the load-bearing walls and show symmetry with respect to one or two axes. Models with an irregular localization of the building load-bearing walls are also analyzed. The results of numerical analysis show a significant effect of the irregular load-bearing walls on the rigidity of the system, hence on the value of the natural frequency. Buildings with irregularities, such as considered in the presented study, obtained up to 20 % higher natural frequency, compared to other models of buildings. The results of calculations show significant effect of the type of response spectrum curve taken into consideration on the calculated maximum values of dynamic stresses, regardless of the type of assumed bearing system of building. In both considered mining areas, there was no effect of irregular distribution of load-bearing walls on the calculated maximum dynamic values of principal and shear stresses.

References

Ciesielski R, Kowalski W, Maciąg E, Tatara T (1996) Response spectra of earthquakes, mining tremors, and their use (Spektra odpowiedzi od trzęsień ziemi i wstrząsów górniczych oraz ich zastosowanie). In: Proceedings of the 42nd conference of Committee of Civil Engineering of The Polish Academy of Sciences and the Science Committee of the Polish Association of Civil Engineers and Technicians, Kraków-Krynica, 17–22 September 1996

Czerwionka L, Tatara T (2007), Standard response spectra from chosen mining regions at Upper Silesian Coalfield (Wzorcowe spektra odpowiedzi z wybranych obszarów GZW). Czasopismo Techniczne z.6 seria Budownictwo z. 2-B:11–18

Drobiec Ł, Piekarczyk A, Kubica J (2000) Influence of the element shape and direction of the load on the value of the Poisson ratio of brick walls (Wpływ kształtu elementu badawczego oraz kierunku obciążenia na wartość współczynnika Poissona murów z cegły). In: Proceedings of the 46th conference of Committee of Civil Engineering of The Polish Academy of Sciences and the Science Committee of the Polish Association of Civil Engineers and Technicians, Wrocław – Krynica, 17–22 September 2000

Kowalski W, Maciąg E, Tatara T (1997) Influence of mining tremors on buildings and people staying in them (Wpływ wstrząsów górniczych na budynki i ludzi w nich przebywających). In: Kwiatek J (ed) Protection of buildings in mining areas (Ochrona obiektów budowlanych na terenach górniczych). GIG, Katowice, p 583

Kubica J, Drobiec Ł, Jasiński R (1999) Research of secant elasticity modulus of the brick walls (Badania siecznego modułu sprężystości murów z cegły). In: Proceedings of the 45th conference of Committee of Civil Engineering of The Polish Academy of Sciences and the Science Committee of the Polish Association of Civil Engineers and Technicians, Wrocław – Krynica, 13–18 September 1999

Kuźniar K, Maciąg E, Tatara T (2006) Acceleration response spectra from mining tremors, First European Conference on Earthquake Engineering and Seismology (a joint event of the 13th ECEE & 30th General Assembly of the ESC), Geneva, Switzerland, 3–8 September 2006, Paper Number: 665

Kuźniar K, Maciąg E, Tatara T (2010) Prediction of response spectra of foundation vibrations of buildings due to mining tremors using neural networks (Prognozowanie spektrów odpowiedzi drgań fundamentów budynków od wstrząsów górniczych z zastosowaniem sieci neuronowych), Prace Naukowe GIG, Górnictwo i Środowisko, Kwartalnik nr 4/4/2010, GIG, Katowice 2010:50–64

Lipiński J (1985) Foundations and supporting structures for the machines (Fundamenty i konstrukcje wsporcze pod maszyny). Arkady, Warszawa

Sawinow OA (1964) The modern design of foundations for machines and their calculations (Sowriemiennyje konstrukcii fundamientow pod maszyny i ich rascziot). Strojizdat, Moskwa

Tatara T (2002) An influence of surface mining-related vibration on low-rise buildings (Działanie drgań powierzchniowych wywołanych wstrząsami górniczymi na niską tradycyjną zabudowę mieszkalną), Zeszyty Naukowe Politechniki Krakowskiej, seria „Inżynieria Lądowa", nr 74, Kraków

Tatara T (2012) Dynamic resistance of buildings in mining tremors conditions (Odporność dynamiczna obiektów budowlanych w warunkach wstrząsów górniczych). Wydawnictwo Politechniki Krakowskiej, Kraków

Zembaty Z (2011) Adaptation of Eurocode 8 for the calculation of structures on influence of mining tremors (Adaptacja Eurokodu 8 do obliczeń budowli na wpływy wstrząsów górniczych), Inżynieria i Budownictwo Nr 3/2011:161–164

Zembaty Z (2012) The velocity conception of evaluation for mining tremors intensity to design of buildings exposed to mining tremors (Prędkościowa koncepcja oceny intensywności wstrząsów górniczych dla celów projektowania budowli narażonych na wstrząsy górnicze). In: Kabiesz J (ed) Risks and technologies (Zagrożenia i technologie). GIG, Katowice, p 405

Zembaty Z, Kokot S, Bozzoni F, Scandella L, Lai C, Kuś J, Bobra P (2015) A system to mitigate deep mine tremor effects in the design of civil infrastructure. Int J Rock Mech Min Sci, Elsevier, 74 (2015), 81–90

Standards and Other Materials

EN 1998-1:2004 Eurocode 8: Design of structures for earthquake resistant Part 1: Genaral rules, seismic actions and rules for buildings

PN-80/B-03040:1980 Foundations and supporting structures for the machines (Fundamenty i konstrukcje wsporcze pod maszyny)

PN-85/B-02170:1985 Evaluation of the harmfulness of building vibrations due to ground motion (Ocena szkodliwości drgań przekazywanych przez podłoże na budynki)

PN-B-03002:1999 Unreinforced masonry structures. Design and calculation (Konstrukcje murowe niezbrojone – projektowanie i obliczanie)

PN-B-03264:2002 Concrete, reinforced concrete and prestressed structures. Design and calculation (Konstrukcje betonowe, żelbetowe i sprężone. Obliczenia statyczne i projektowanie)

Chapter 26
Numerical and Experimental Prediction Methods for Assessment of Induced Vibrations in Irregular Buildings

Jan Benčat

Abstract The prediction models for the ground–borne vibrations and irregular buildings (IB) structure dynamic response due to traffic means have been introduced. For the free–field dynamic response at the distance (e.g. from railway track) and dynamic response of IB in the calculation procedures are described in this paper. The numerical model of the soils is modelled as a viscoelastic half-space. This model is used both for evaluation of the track–soil interaction forces as well as for prediction of the ground–borne vibrations. The numerical results in time domain are presented as the time histories damped amplitudes of the half-space vibration at the distance. In presented frequency domain free–field response is calculated via response spectra and frequency response function (FRF) of the viscoelastic soil medium. In the next step this functions are applied for building structure dynamic response calculation due to railway traffic (case study) via relevant computational building structure model.

Keywords Microtremor • Vibrations • Prediction • FEM • Experiments

26.1 Introduction

The growing traffic volume, the higher population density and the diminishing distance between the track and the structure can be considered to be responsible for increasing vibration nuisance due to railway traffic. Therefore, the development and validation of a numerical prediction model for traffic induced vibrations in buildings is treated in many works. Empirical models show a close relationship to a set of experimental data but the application of the model is limited to similar conditions. Also these models do not always provide insight in the influence of specific parameters. Numerical models allow the influence of various parameters to be

J. Benčat (✉)
University Research Centre, University of Žilina, Univerzitna 1,
SK 010 26 Žilina, Slovakia
e-mail: jan.bencat@gmail.com

investigated but a validation of the model with experimental data required to verify the underlying theoretical assumptions. Even though that validation is focuses on traffic induced vibrations, the numerical prediction model can be generally applicable to other types of vibration sources e.g. roadways Bencat J (1992, 2006), Bencat J et al (2009). The dynamic train–track interaction is a coupled problem, contrary to vehicle–road interaction problems, that requires the simultaneous solution of the equations of motion of the train and the track. The train–track interaction forces due to the track unevenness are computed using a flexibility formulation. A two–dimensional linear vehicle model with a limited number of DOF is coupled to a linear elastic longitudinal invariant track model, which allows a solution of the equations of motion in the frequency–wavenumber domain Bencat J (1992), The transfer functions Bendat J and Piersol A (1993) between the track and the soil and the computed interaction forces are used to compute the response at any arbitrary point in the free field. Finally, the building structure dynamic response at the distance calculation is performed using half – space output data (PSD, time history) as the input data into the IB structure foundations, see Bencat J et al. (2009), Fujikake T (1986), Ford R (1987), Grassie S and Cox S (1984), and Grundman H et al. (1999).

26.2   Track Model Description: Numerical Approach

A numerical prediction model for ground–borne vibrations due to railway traffic on ballasted track requires the modelling of several components, as indicated in Fig. 26.1. This paper presents a numerical prediction model which calculates the ground–borne vibration level due to railway traffic in two steps. The first step determines the dynamic track–soil interaction forces using a detailed train model and the dynamic behavior of the layered spring–damper system and the through–soil coupling of the sleepers are accounted for the soil model (Broeck and Roeck 1999; Grassie and Cox 1984; Grundman et al. 1999; Knothe and Wu 1998; Kotrasova 2009; Turek 1992).

The prediction of the ground–borne vibration level at the distance in the second step is based on the viscous–elastics soil model (Bencat 2006; Ford 1987).

The vehicle car–body, the bogie and the wheelset are modelled as rigid bodies connected by springs and dampers, Fig. 26.2e. The wheelset is connected to the rail with a linearized Hertzian spring. The rail is modelled as a hinged Rayleigh beam with rotational inertia. In the track model the rail is supported discretely by sleepers modelled as rigid bodies with spring–damper systems representing the rail pads. The sleeper is modelled as a short Rayleigh beam resting on flexural mass layer supported by discretely Pasternak spring–damper systems representing the elastic and attenuation characteristics of the railway ballast and substrate soils. As a result, the model evaluates the track–soil interaction forces in terms of the spectral density function which is often used as the statistical description of the rail roughness Turek J (1992).
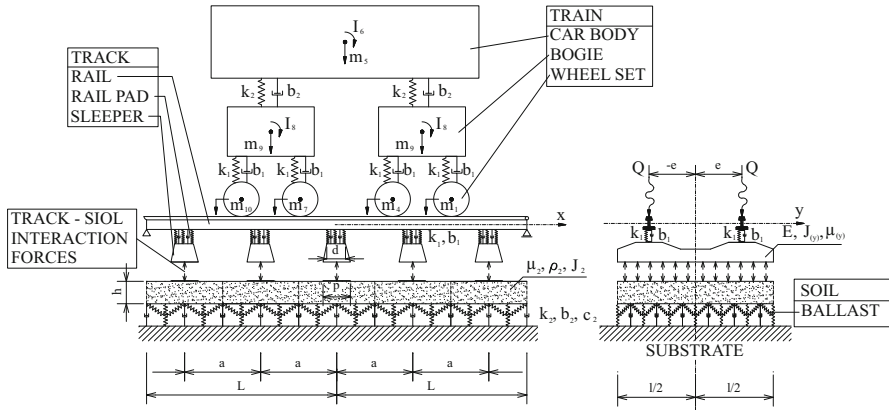
Fig. 26.1 Components of the train–track–soil system

This calculations followed by a second step in which the spectral density of the level of ground–borne vibrations is determined by FRF between track and unbounded soil. Proposed prediction theoretical model for vertical track vibration numerical program consists of three parts:

- model of vehicle
- model of train–track interaction
- model of track (sleepers/ballast and subsoil).

The frequency characteristics method (input–output) was used for calculation modelled feedback linear dynamic system train–track–soil system parameters, (program *Interaction*). Final products of the numerical calculations are: vehicle, rail, sleeper, railpads and ballast frequency response functions (also sleeper deflection and bending moment in time domain) using spectral density functions (SDF) of the rail roughness used by railway operators or experimentally measured in situ for case study.

An important example of non–linear behavior is the wheel–rail contact but also the rail pads and the suspension of the train can deflect in a non–linear manner. Nevertheless the results presented in this study are limited to linear analyses. Also in this model is accepted symmetrical dynamic response of the sleepers to longitudinal axis of the track (rail roughness coherence function for left and right rail is equals to ≈ 1).

26.2.1 Track Model

The track model commonly found in the literature represents the rail as infinite Timoshenko, Euler or Rayleigh beam, see also Grassie S and Cox S (1984) and Grundman H et al. (1999), on a continuous uniform support, Fig. 26.2a. The beam is
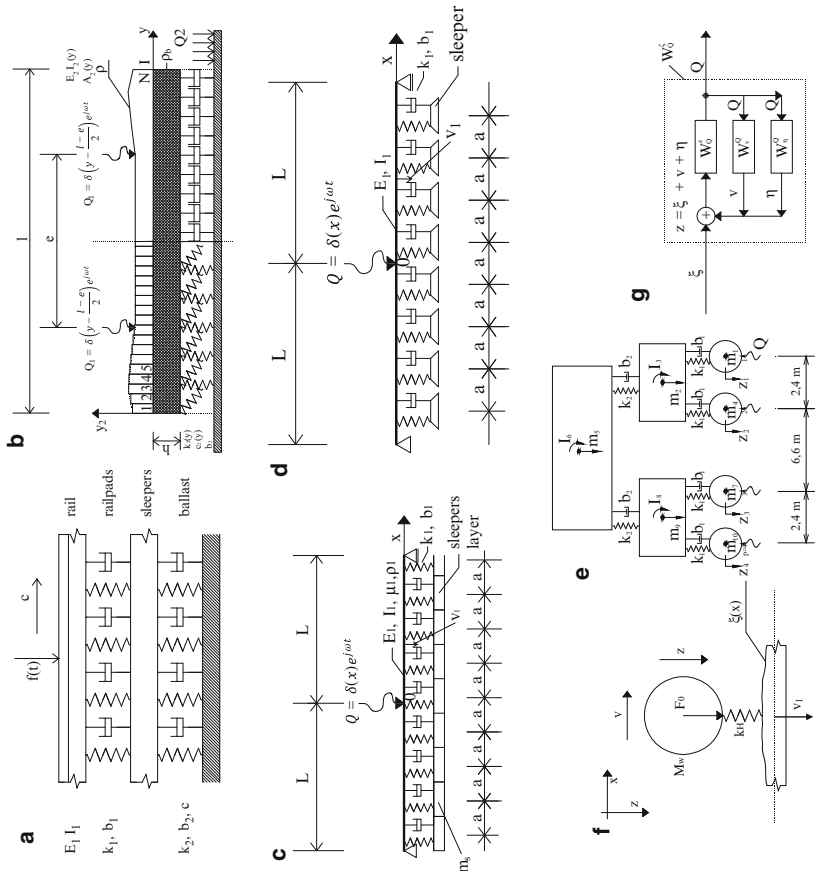
Fig. 26.2 The railway components model for numerical analysis

taken as uniform flexural rigidity EI, rail mass per unit m_r and distributed sleeper mass m_s. The railpad stiffness and viscous damping constant per unit length are taken to be k_1 and b_1 and the corresponding parameters for ballast are k_2 and b_2 respectively. An harmonic point force $p(t) = Pcos\omega t$ is assumed to run at constant velocity v along the rail. The FRF of the track excited to a harmonic force for proposed prediction model are discussed in this section. The track model consists of two parts: (i) model of sleeper with ballast and subballast, Fig. 26.2b and (ii) track model (rail supported discretely by sleepers modelled as rigid bodies with spring–damper systems representing the rail pads), Fig. 26.2c, d.

Finally, the solution for FRF of the linear dynamic system model e.g. in which on input are rail roughness ξ and on output are wheel forces Q enable calculations of the interaction matrix FRF according to scheme as shown Fig. 26.2g. The dynamic displacement of the wheel z is defined by $z = \xi + v + \eta$, where ξ represents rail roughness, v – rail vertical deflection and η – wheel and rail contact deformation in contact location.

The track irregularities are great source of the track and vehicles dynamic excitations. Such excitation arises from discrete irregularities such as wheel flats and rail joints as well as periodic irregularities such as corrugation of the railhead. It is assumed that excitation of the track arises from a wheel passing over a sinusoidal irregularity on the rail head (Fig. 26.2f). The stochastic theory analysis enables to define irregularities by PSD function by $S_\xi(\Omega) = A\Omega^{-a}$, where A, a are empirical (experimental) constants. The distance x is used as the independent variable to define $\xi(x)$.

26.2.2   Calculation of Track Component Arbitrary FRF

The frequency response function of arbitrary dynamic system part is calculated by rule of *FRF* summing as follows $W_Q^I = W_{Q1}^I . W_{Q2}^{Q1} . W_{Q3}^{Q2} \ldots \ldots . W_{Qi+1}^{Qi} \ldots . . W_Q^{Qn}$. The same way is used for summing of the arbitrary FRF matrix, e.g. consider a dynamic system with defined input rail roughness ξ producing output sleeper deflection v_2, than the FRF is given by equation

$$W_{v_2}^\xi = W_Q^\xi . W_{Q_1}^Q . W_{v_2}^{Q_1}.$$

26.2.3   The Response of Track Resting on a Continuous Rail Supports

An advantage of the continuous track model (Fig. 26.2c, d) is that enables for arbitrary track variables to calculate Turek J (1992): FRF, input spectra and standard deviations of the track dynamic response parameters – dynamic forces Q, Q_1, Q_2, dynamic deflections v_1, v_2, wheel center dynamic displacement z and

Fig. 26.3 The vertical
track receptance of v_1
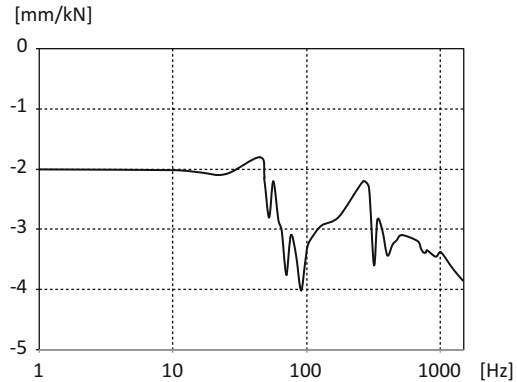
Fig. 26.4 The input PSD:
$G_{\ddot{v}_2\ddot{v}_2}(f)$
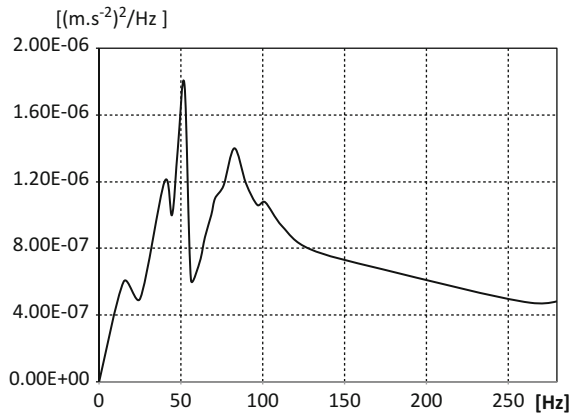
dynamic bending moment in rail and sleeper. As an example on Fig. 26.3 is plot of
numerical calculations results for vertical track receptance of rail deflection v_1 due
to wheel contact forces Q.

Parameters Used in Calculation:

Sleeper SB8: $k_2 = 49.40$ Mpa; $b_2 = 0.023$ Mpa.s; $c_2 = 0$; $h = 0.45$ m; $a = 0.55$;
$\rho_b = 0.0017$ kg.m^{-3}.

Rail R65: $L = 12.12$ m; $k_1 = 217{,}000$ Mpa; $b_1 = 0.037$ Mpa.s; $E = 210{,}000$ Mpa;
$I_1 = 3.6 \times 10^{-5}$ m^4; $m_r = 65$ kg.m^{-1}.

Vehicle: SKODA E 699; 10 degree of freedom; 4 axles; $k_H = 1.5 \times 10^9$ [N/m]; mass of
axle: 1,250 kg; mass of bogie: 4750 kg; mass of body casing: 23.500 kg; bogie inertia
moment: 5.5×10^3 kg m^2; bogie casing inertia moment: 5.10^5 kgm^2;
$k_1 = 7266.10^5$ Nm^{-1} spring stiffness: $k_2 = 9.5 \times 10^6$ Nm^{-1}; $k_1 = 7.266 \times 10^5$ Nm^{-1};
spring damping: $b_1 = 7.37 \times 10^4$ Nm^{-1}; $b_2 = 3.68 \times 10^4$ Nm^{-1}; axle base: 2.8 m;
boggie base: 10.3 m (Fig. 26.4). From the proposed model it is possible to calculate
also **sleepers** dynamic deflection, velocities and acceleration power spectral densi-
ties (PSD) as the input spectra or PSD into **the ballast and roadbed**, see Fig. 26.4.

26.3   Prediction Models for Ground Vibration from Railways

26.3.1   The Analytic–Experimental Approach

The analytic–experimental approach proposes the test and the theory data combination to calculate the prediction level of ground vibration (suitable in practical cases). In this process as an input signal can be used accelerations spectra (or spectral densities) derived from experimental data bank of authorized railway category with corresponding rail profile or accelerations spectrum $\overline{S}_{\ddot{w}\ddot{w}}(f)$ measured at nearest ground point to the track for individual case study. The frequency response function (or transfer function) of the ground can be derived via experimental *impulse seismic method* (ISM) Bencat J (1992, 2006) or *cross–hole test* data, *SASW* method, from which elastic and attenuation parameters of the ground can be obtained, too. The measuring output response acceleration spectrum (RAS) at the distance $S_{\ddot{w}\ddot{w}}(f)$ due to input accelerations spectrum $\overline{S}_{\ddot{w}\ddot{w}}(f)$ the FRF– $H(f)$ can be derived, see also Bencat J et al. (2009). In accordance with Bendat J and Piersol A (1993) then RAS is given by the formula: $S_{\ddot{w}\ddot{w}}(f) = H(f)S_{\ddot{w}\ddot{w}}(f)$.

26.3.2   In: Situ Soil Dynamic Parameter Tests Experimental Tests at Nearby Building IBM Region

To calculate prediction vibration level and dynamic response of the projected new building in the projected new railway line area it was needs to know the building site soils dynamic parameters, soil FRF and project building parameters. Therefore the in situ ISM tests in the IBM Data Centre building site were performed. The building site is situated in the same area in which the new Trans European Network (TEN–T) line is projected, too. After the both structures erection the distance between by them will be approximately 20 m. Hence the prediction of building vibration level and response spectra due to operating trains were required.

The building site is situated on level ground (sandy loam -3.5 m and gravel sand -12.0 m). This permits the ground to be modelled as a damped, viscoelastic half space. The viscoelastic model of soil simulation using the complex modulus conception $E^* = E(1 + \delta_E)$ and $G^* = G(1 + \delta_G)$ respectively, offers a very good approach to the actual soil behavior (E, G and $\delta_E \approx \delta_G$ are real and imaginary components of complex modulus). The *Raleigh's and shear waves propagation v_r and v_s* in half space in this form for the case study were analyzed in Bencat J (1992).

The experimental tests procedure for the purpose of the evaluation of elastic and attenuation soil parameters is described in Bencat J et al. (2009). The IBM building site layout, accelerometers and impact loading positions (I_i) during the experimental tests are shown in Fig. 26.5. *The ISM results are as follows*:

- $v_r = 145.10 \text{ ms}^{-1}$; $\delta_G = 0.117$; $E_0 = 109.20$ MPa; $G_0 = 41.10$ MPa,
- the ISM test No. 5 spectral analysis results example are plotted on Fig. 26.6.
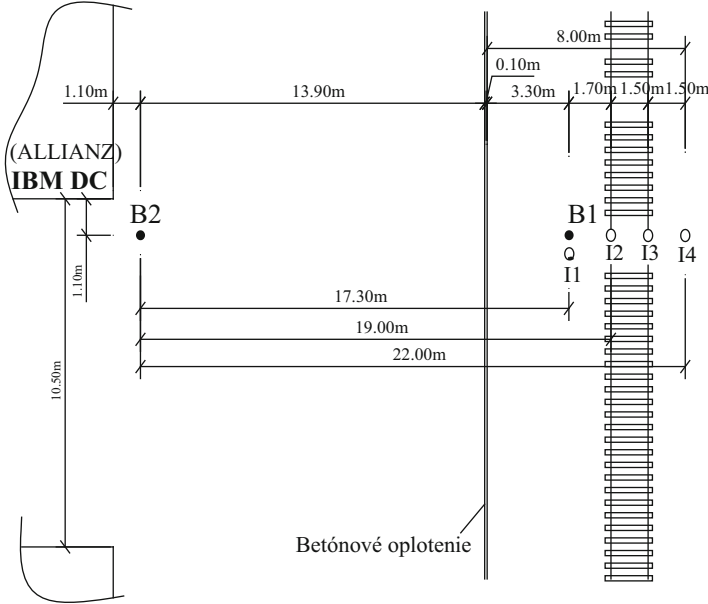
Fig. 26.5 Accelerometers and impacts (I1 – 4) position and projected building site layout
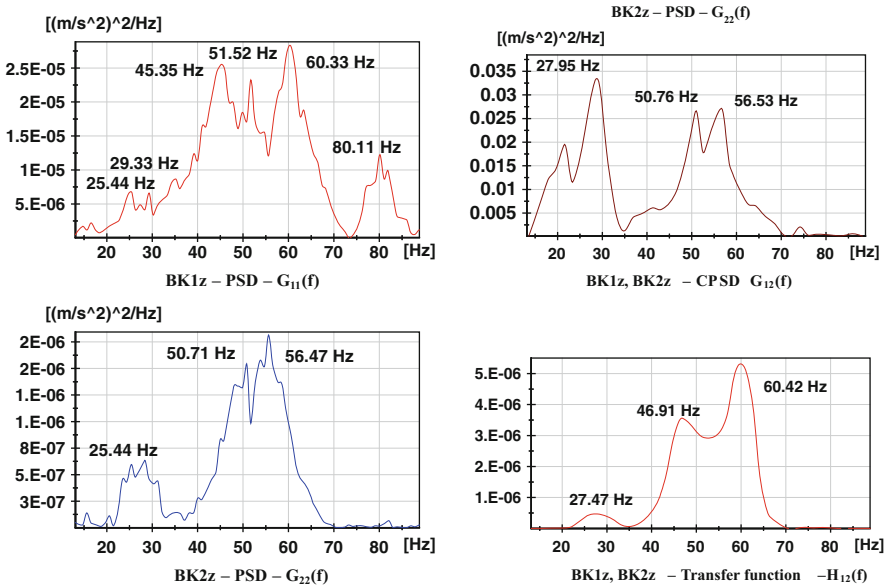
Fig. 26.6 The ISM5 test spectral analysis results at B1 and B2 points

The calculations includes data: $\lambda_R = 9.2$ m, (*Raleigh's wave length*); $\rho = 1950$ kgm^{-3}, (*soil mass density*); $\alpha = 0.0398$ m^{-1}, (*the attenuation coefficient obtained by standard deviations* σ_0, σ_y *of displacement amplitude vibration at the distance* l_0, l_y *from source of excitation using the displacement power spectral densities* $G_{ii}^{(0)}$ *and* $G_{kk}^{(y)}$).

26.3.3 Vibration Propagation Process Experimental Spectral Analysis

An experimental study of ground vibration transmission from a railway was carried out in the same region as the impact tests, adjacent to the ŽSR railway line *Bratislava – Vienna*, track No. 1 (No. 2) in the town district *Bratislava Trnávka*. The object of the experimental measurements was to find: *spectral characteristics* of the vibration components of the track near region soils by the acceleration power spectral densities $G_{ii}(f)$, $G_{kk}(f)$ and $G_{ik}(f)$. The pickups positions are shown in Fig. 26.7. The roadbed and ground accelerations of the vibrations were recorded using the portable computer with relevant software and hardware facilities. The test experimental procedure in details is described in Bencat J et al. (2009). As an example of the train induced vibrations accelerations spectral analysis results (PSD) in the ground at measured point BK1 are plotted on Fig. 26.8.
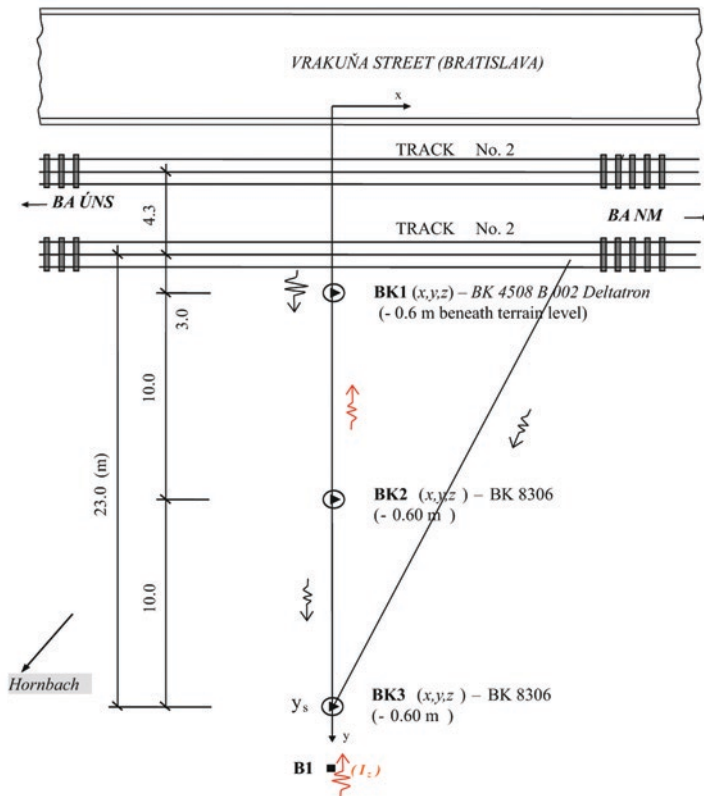
Fig. 26.7 The pickups and impacts positions in track region
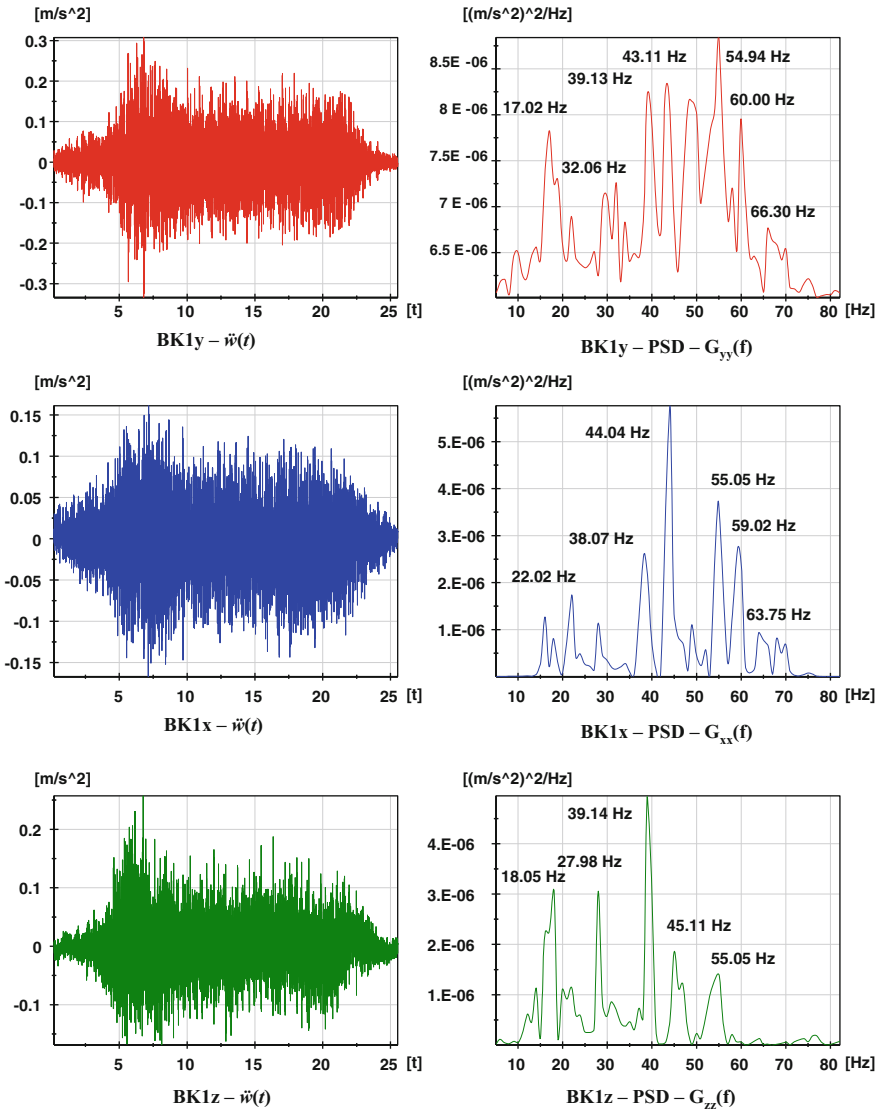
Fig. 26.8 The acceleration time histories and PSD at point BK1

26.4 Dynamic Response of the Building Structure Prediction

To calculate the prediction vibration level and the structure dynamic response of projected new IB structure situated at nearest area of the projected new railway line it was needs to know the building site soils dynamic parameters, site geological medium FRF and also the representative input accelerations spectra due to trains

Fig. 26.9 FEM model
render
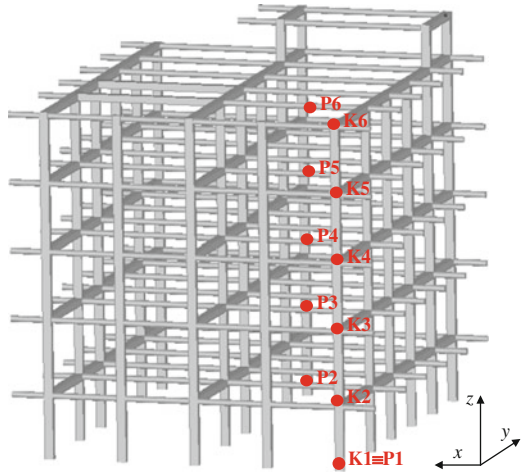
comparable to expected real train spectra due to trains in future traffic. For
calculation expected structure dynamic response it was used: (**i**) PSD – $G_{ii}(f)$ of
ground acceleration at the track nearest region (Fig. 26.7) with similar geological
medium data as the site geological medium input spectra (see Fig. 26.8), (**ii**) The
halfspace transfer function $H_{ik}(f)$ of the building site geological medium obtained
by ISM tests (see Fig. 26.6) and (**iii**) project of building structure.

The response PSD – $G_{kk}(f)$ of the halfspace point at the projected structure
foundations location was calculated and plotted on Fig. 26.11. In the next step these
spectra were used as the input spectra for expected building structure dynamic
response calculation due to train. The dynamic response of the building structure
numerical calculation was carried out by the *Visual Fea* program package. The
calculated values of natural frequencies and natural modes were used in the next
step of the IB structure dynamic response calculations. The structure FEM model
render and two natural modes examples are shown in Figs. 26.9 and 26.10.

In the next step the building structure dynamic response calculations were
performed in frequency domain. The spectral analysis was divided into two parts:
low frequency band (0–10 Hz) and *higher frequency band* (10–130 Hz). The low
frequency spectral analysis gives the basic building natural frequencies vibration
range which enables to predict possible resonance effects of structure vibration due
to traffic. Because of the vibration sensitive technologies installing in the IBM DC
building the power spectral densities are determined in the structure relevant points
(over columns and in the middle of beam spans) for the structure dynamic response
considering in the range of frequency band 10–130 Hz. The higher frequency
spectral analysis band is mainly required for vibration level assessment on moni-
tored frequency according to the IBM Corporate Standard C–S1–9711–002, 1990–
03 requirements. The accelerations PSD, displacements extreme and *rms* values
were numerically calculated at the selected render points (K1...K6, P1...P6) in the
three vibration directions *x*, *y*, *z*. The results of the IBM DC building structure
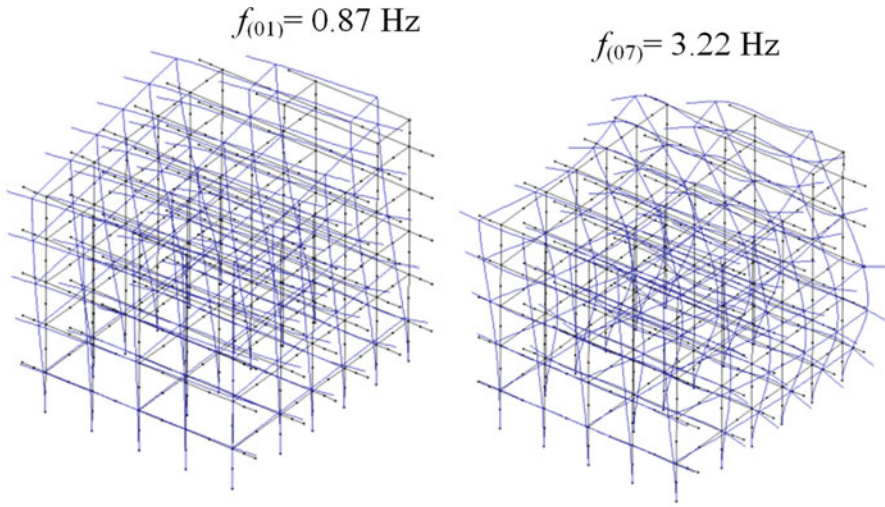
Fig. 26.10 Structure FEM natural modes examples
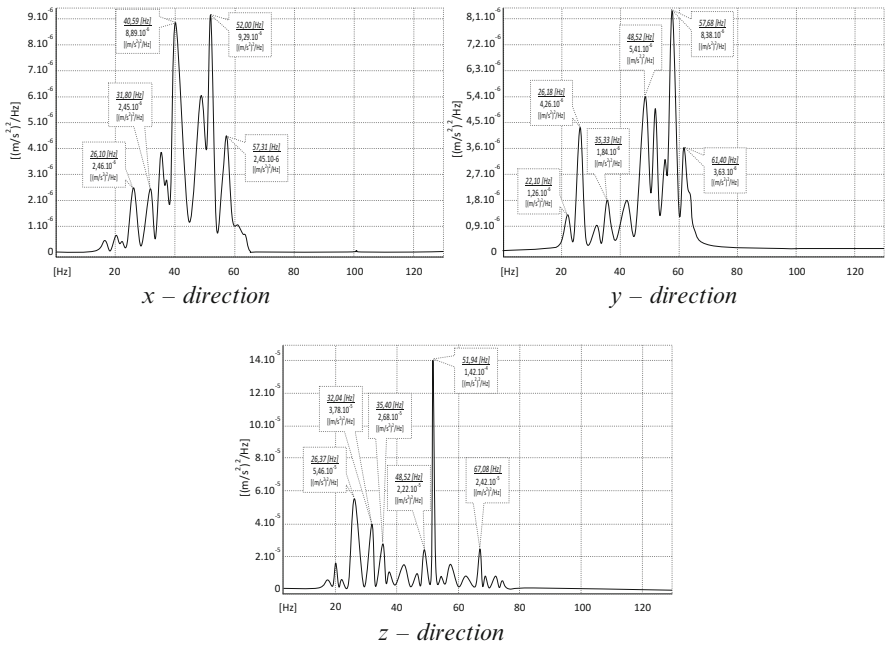
Fig. 26.11 The input acceleration PSD – $G_{11}(f)$ to foundation at point K1/10 – 130 Hz
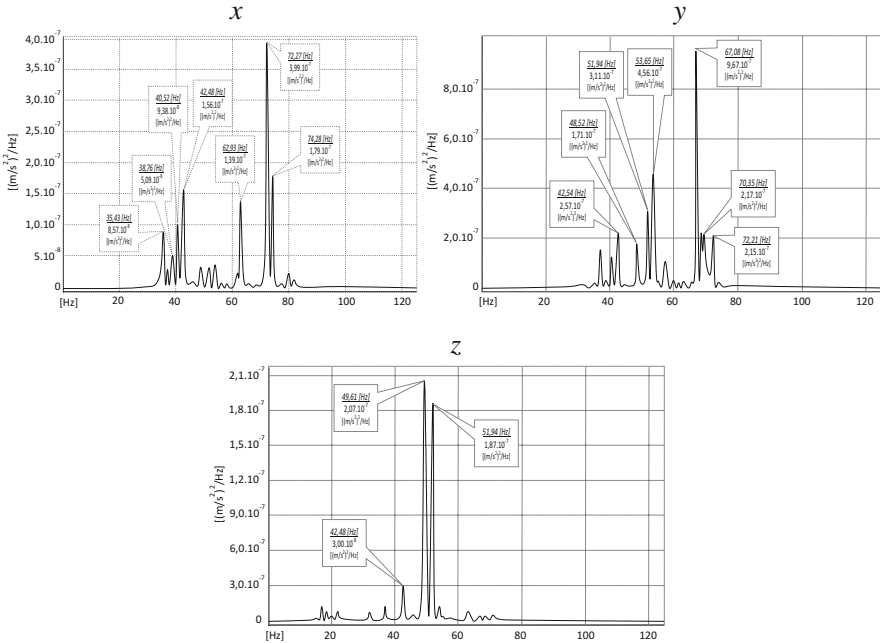
Fig. 26.12 The response acceleration PSD – $G_{66}(f)$ of roof at point K6/10 – 130 Hz

dynamic response calculations are presented in detail Bencat J et al. (2009). The adequate input load acceleration PSD – $G_{11}(f)$ into the foundation structure (render point K1) for x, y and z vibration directions are plotted in the Fig. 26.11 and the response acceleration PSD – $G_{66}(f)$ of the building roof structure (render point K6) is plotted in the Fig. 26.12.

26.5   Conclusions

Based on the results of this paper the following conclusions can be drawn:

(i) The numerical prediction model can account for many parameters of the train–track–soil interaction problem. Final products of the numerical calculations are vehicle, rail, sleeper, rail pads and ballast *frequency response functions* using spectral density functions of the rail roughness. To predict the level of ground vibration in the vicinity of railways it needs to calculate the response spectrum at distance point on the ground surface $S_{ww}(f)$ via the (FRF) – $H_{ik}(f)$ of the ground by a method involving integral transform.

(ii) The numeric–experimental approach process proposes the test and the theory data combination to calculate the prediction level of ground vibration. This approach is suitable for practical tasks and case studies (e.g. law studies, predictions).

(iii) The frequency response function $-H_{ik}(f)$ of the ground for the case study was derived via experimental impulse seismic method (ISM) test data, from which elastic and attenuation parameters of the ground were obtained, too.

(iv) The calculation results of the predicted *IBM Data Centre* building dynamic response using the relevant input experimental data are introduced, too. The relevant calculated data values following from spectral and amplitude analysis of the predicted IB dynamic response (spectral picks limit, vibration levels, etc.) were compared with relevant standards prescription values and criteria (IBM Corporate Standard C–S1, STN EN 1998 – 1/NA/Z1 (2010) Slovak Standard STN 73 0032 (2013), etc.). From this comparisons it follows that all relevant standards prescription values and criteria in future will be fulfilled.

References

Benčat J (1992) Microtremor due to traffic. In: Research report A – 4 – 92/b, UTC Žilina, 1992 (in Slovak)

Benčat J (2006) Microtremor from railway traffic. In: Proceedings of the 8th international conference on Computational Structures Technology, Gran Canaria

Benčat J et al (2009) Studies of the TEN–T railway traffic effects on IBM Data Centrum – ST Building in Bratislava. In: Report PC 16/SvF/2009, University of Žilina (in Slovak)

Bendat J, Piersol A (1993) Engineering applications of correlation and spectral analysis. Wiley, New York

Ford R (1987) The production of ground vibrations by railway trains. J Sound Vib 116(3):585–589

Fujikake T (1986) A prediction method for the propagation of ground vibration from railway trains. J Sound Vib 111(2):357–360

Grassie S, Cox S (1984) The dynamic response of railway track with flexible sleepers to high frequency vertical excitation. Proc Inst Mech Eng 198(2):117–124

Grundmann H et al (1999) The response of a layered half–space to traffic loads moving along its surface. Arch Appl Mech 69:55–67

Knothe K, Wu Y (1998) Receptance behaviour of railway track and subgrade. Arch Appl Mech 68:457–470

Kotrasová K (2009) Influence of category of sub-soil on liquid storage circular tanks during earthquake. In: Proceedings of 12th international scientific conference on structural mechanics. Brno University of Technology. In: Selected Scientific Papers, Journal of Civil Engineering, TU Košice (Slovakia), 3(1). ISSN 1336-9024.

Slovak Standard (2013) Calculation of building structures and foundations loaded by dynamic effect of machines (in Slovak). STN 73 0032. Slovak Institute of Standards, SUTN, Bratislava, 2010

Slovak National Annex to Eurocode 8 (2010) Design of structures for earthquake resistance. Part 1: General rules, seismic actions and rules for buildings (in Slovak). STN EN 1998 – 1/NA/Z1. Slovak Institute of Standards, SUTN, Bratislava

Turek J (1992) The interaction model of the vehicle–track system. In: Research report 245/92 VUŽ Prague

Van den Broeck, P, De Roeck G (1999) The vertical receptance of track including soil–structure interaction. In: Proceedings of the 4th European conference on structural dynamic: "Eurodyn 99", Prague, pp 849–853

Chapter 27
Stability Analysis of Żelazny Most Tailings Dam Loaded by Mining-Induced Earthquakes

Waldemar Świdziński, Aleksandra Korzec, and Kinga Woźniczko

Abstract The paper presents the stability analysis of Żelazny Most tailings dam subjected to mining-induced paraseismic events. The tailings dam as well as foundation have complex geotechnical structure. The foundation of the dam is built of series of tertiary and quaternary formations affected in the past by three glaciations whereas the complexity of tailings structure results from the method of its deposition within the pond. Simplified dynamic displacement analysis of the dam is performed based on Newmark's approach using GeoStudio2007 software. The paper highlights the necessity of proper domain and time discretization, especially in the case of complex geological structure. Dynamic response of the tailings dam was obtained for the equivalent linear one-phase soil model. Stability calculations were performed for Coulomb-Mohr model and Stress History And Normalized Soil Engineering Properties (SHANSEP). The applied input signals were selected by Arias intensity criterion from huge set of signals recorded on the ground surface caused by mining tremors. The peak ground acceleration value was scaled to the values predicted by hazard analysis. The results of the calculations carried out for three selected acceleration signals have revealed no permanent deformations.

Keywords Earth structure • Dynamic response • Dynamic properties • Stability analysis • Newmark's method

W. Świdziński • A. Korzec (✉)

Institute of Hydro-Engineering Polish Academy of Sciences, ul. Kościerska 7, 80-328 Gdańsk-Oliwa, Poland

e-mail: waldek@ibwpan.gda.pl; a.korzec@ibwpan.gda.pl

K. Woźniczko

DHV HYDROPROJEKT Sp. z o.o., ul. Dubois 7, 00-182 Warszawa, Poland

303

27.1 Introduction

Żelazny Most tailings dam is the only place to store huge amount of post-flotation mineral material coming from copper production in KGHM Polska Miedź S.A. Thus it is a key component of the production process. The depository is built by upstream method. The tailings-water mixture is discharged inside the depository surrounded by embankments. It needs to be continuously raised to accommodate subsequent batches of tailings. At present the maximum height of the depository is 66 m (East Dam). Other dams are lower due to natural morphology of the terrain on which they are founded. The development of the depository is based on observational method which needs well developed monitoring system to observe the response of the dams and foundation against increasing loadings. The monitoring system consist of thousands of various measuring points in which different measuring devices are installed (e.g.: benchmarks, vibrating-wire piezometers, deep inclinometers, seismic stations), Jamiolkowski et al. (2010). Due to extreme geotechnical complexity of both tailings and foundation, numerous laboratory and filed tests have been done.

The region of the Żelazny Most depository is characterized by very low natural seismicity Guterch (2009), however due to mining activity it is exposed to mining-induced tremors with close epicentral distances Lasocki (2011), Lasocki et al. (2012a) and Zembaty (2004), Fig. 27.1. Accelerometers that record three components of earthquake vibrations, are located in six cross-sections on the slope and at the toe of the dam, Fig. 27.1. Seismic hazard analysis has been carried out by
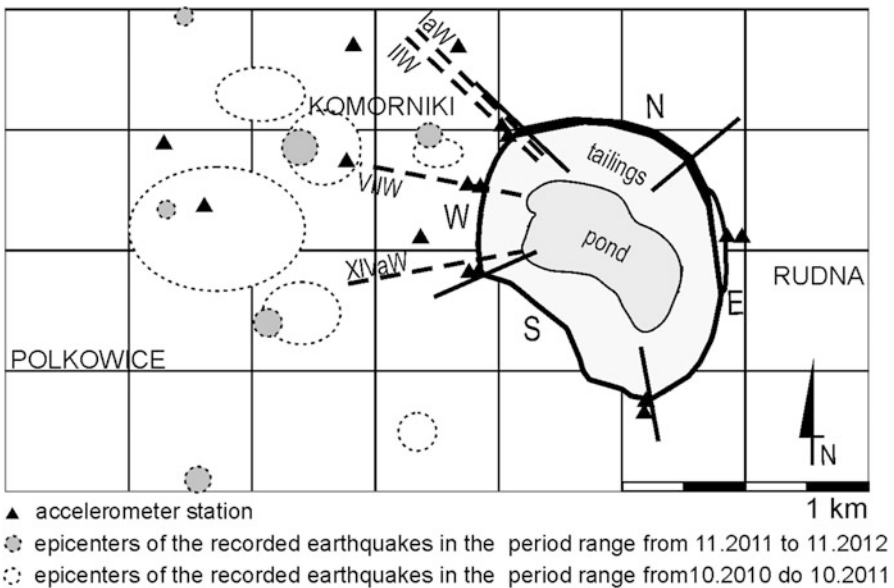
Fig. 27.1 Regions of epicentres near the Żelazny Most depository, based on Lasocki (2011) and Lasocki et al. (2012a)

Lasocki et al. based on collected records the seismic energy of which was greater than $1 \cdot 10^7$ J. For the mining activity plan in the period 2012–2042, the forecast of peak horizontal ground acceleration value (*PHA*) for one of the West Dam cross-sections was estimated to be 0.17 g, Lasocki et al. (2012b). This values with 5 % of exceedance over a period of 30 years has been assumed as *design acceleration*. High risk due to social, economic and environmental consequences of failure requires reliable dynamic stability analysis of the dams loaded by paraseismic events.

According to Eurocode 8 - EC8 (2003), pseudo-static stability analysis may be adopted for *PGA* lower than 0.08 g. Otherwise pseudo-dynamic or full dynamic analyses should be applied. One of the most popular pseudo-dynamic approaches is Newmark's concept which assess the dam stability in terms of permanent displacements produced during shaking, Newmark (1965). The original concept considers rigid mass sliding along surface when rigid perfectly plastic strength criterion is reached. The yield acceleration value that causes relative motion corresponds to factor of safety equal to one. The relative downward displacement occurs as long as relative velocity is non zero. Nowadays the modified Newmark's approach based on stress state derived from finite element method is being used.

In the paper the application of modified Newmark's approach to assess the stability of Żelazny Most tailings dam subjected to paraseismic loadings is presented. Simplified dynamic displacement analysis has been performed using GeoStudio2007 software reported in GEO-SLOPE (2010a, b). Dynamic response of the tailings dam is calculated based on the equivalent linear one-phase soil model. The attention was focused on the determination of differentiated material stiffness in order to reflect the soil structure complexity and also taking into account its stress and strain dependency. The paper highlights the necessity of proper domain and time discretization, as well as the numerical efficiency, which is not trivial issue in the case of complex geological structure.

27.2 Geotechnical Characterization of Żelazny Most Tailings Dam

One of typical cross-sections of the Żelazny Most depository dams is shown in Fig. 27.2. It consists of starter dam (2) and embankment (1), which create some kind of external shell for inside deposited tailings and they are made in the form of construction fill. Additionally, in order to improve the overall stability, in some parts of the depository the loading berms have been constructed (5). Hydraulically transported tailings are discharged from the top of the dam crest creating a beach that becomes the foundation for future embankments and deposited tailings. In the process of the gravitational flow the segregation of the tailings occurs, due to which the coarser materials (3) deposit close to embankment whereas the finer ones (4) flow towards the pond. Due to free water infiltration extensive mass of tailings if fully saturated, (saturated materials below the phreatic line have been marked as
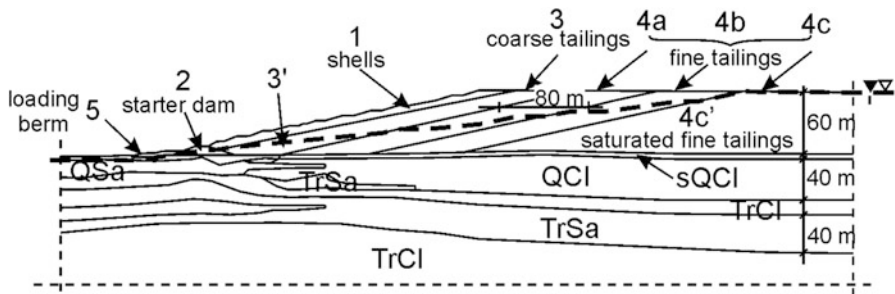
Fig. 27.2 Typical cross-section of ZM tailings depository

2′, 3′, 4′). The results of Cross-Hole tests have revealed large variability of tailings stiffness within the distance of 240 m from the embankment. Thus three additional zones (4a, 4b, 4c) have been distinguished for numerical simulations. The Żelazny Most tailings pond is founded on a very complex soil structure consisting of Tertiary (Tr) and Quaternary (Q) clays and sands affected by the three glaciations.

Dynamic calculations have been performed for equivalent linear model which takes into account hysteretic soil behaviour during cyclic loading and soil stiffness dependence on shear strain level. The hysteretic loop allows for the determination of a tangent shear modulus (equivalent modulus) and a damping ratio. The formula given by Ishibashi and Zhang (1993) was adopted in Quake/W to model normalized shear modulus degradation curves G/G_{max} depending on confining pressure (p') as well as plasticity index (*PI*) thus it is applicable for both cohesive and cohesionless soils. G/G_{max} curves were fitted based on experimental TX shearing test results for Tertiary clays and tailings, which is shown in Fig. 27.3a.

It is also well known that soil stiffness depends on stress state. Thus the maximum shear modulus G_{max} depending on vertical effective stress is considered by a modified version of the formula given by Seed and Idriss for non cohesive soils and a function proposed by Hardin for cohesive soils, Ishihara (2003). Respective curves for Tertiary clays and tailings (3, 4) were approximated based on numerous series of shear wave velocity measurements for undisturbed soils samples, made in TX with piezoelectric bender elements, at different level of confining stress, Fig. 27.3b.

Due to the lack of direct measurements of internal soil damping (according to the recommendation of EC8), constant damping ratio of 3 % has been assumed for foundation soils and 5 % for tailings. The Poisson ratio for dynamic calculations was defined as 0.495 for all soils under phreatic line which is the closest allowable approach to the constant volume condition in computational model.

Strength of the majority of soils in stability analysis has been modelled by Coulomb-Mohr yield condition, excluding fine tailings under phreatic line (4′) for which linear variation of strength with mean effective stress was assumed (SHANSEP model). Angle of internal friction of the dam's materials is equal to 34° and of foundation soils is varying from 17° to 34°.

a

G/G_{max} [−]

b

G_{max} [MPa]
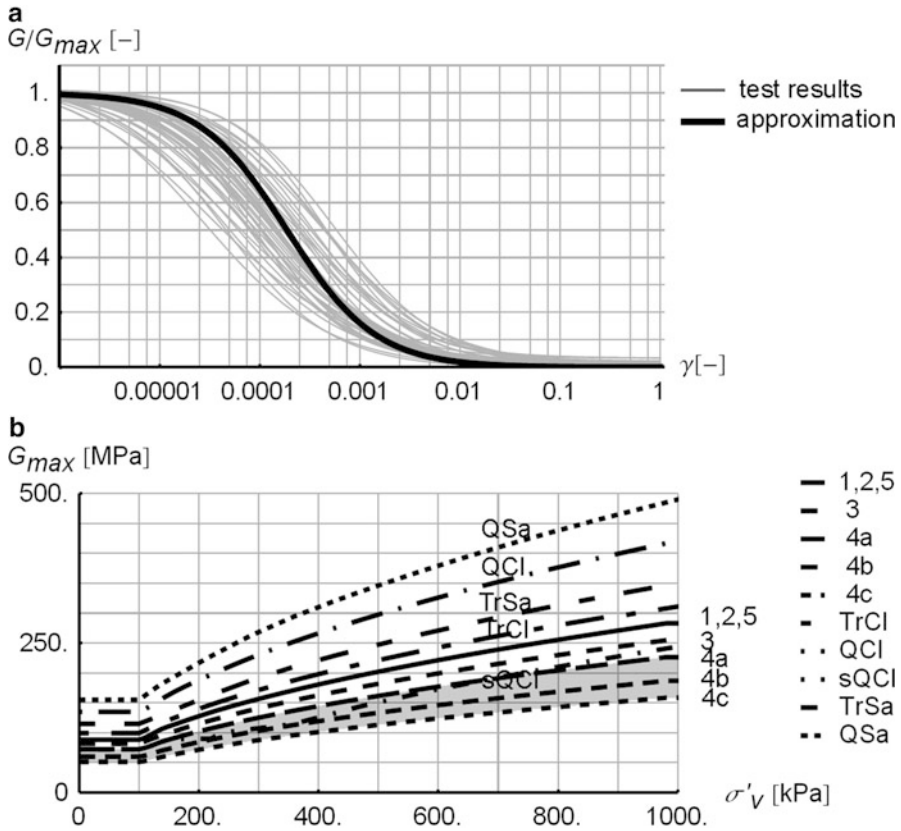
Fig. 27.3 (**a**) Normalized shear modulus against shear strain for tailings compared to laboratory tests. (**b**) Maximum shear modulus dependence on effective vertical stress

27.3 Dynamic Response of the ZM Dam

The 2D plane strain dynamic response of the dam was carried out based on finite element software Quake/W and Wilson-θ time integration method (GeoStudio2007 package). The size of the model was tested to minimize the boundary impact and wave reflections. Suggested geometry of the model dimensions is 5:1 (horizontal to vertical), Świdziński and Korzec (2013). The discrete model consist of 9571 triangular elements with 3 Gauss points. The mesh scheme is consistent with dynamic material properties and one period of shear wave described by at least five nodes. The conditions ensure that the distance between nodes is lower than the distance that the wave can travel in one single time step. Proposed approach gives almost constant value of Courant number in whole model. Due to memory and time restrictions only selected dynamic results are saved. Saving frequency must fulfil the Nyquist's criterion. After many tests the dynamic calculation times step was established as 0.013 s and saving time step as 0.052 s, Świdziński and Korzec (2013).
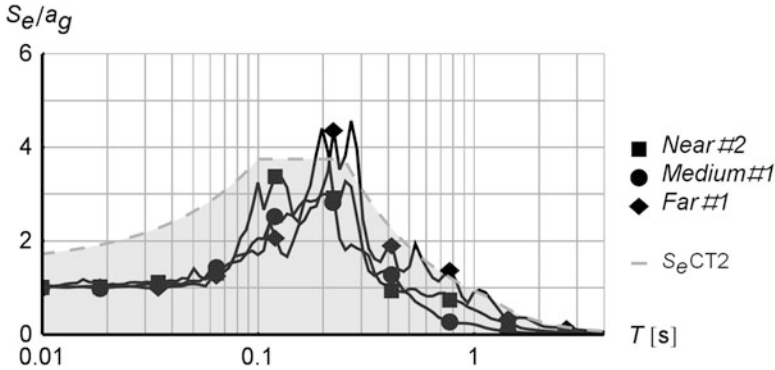
Fig. 27.4 Response spectra of selected signals compared to elastic spectrum proposed in EC8

The first stage in the stability analysis using FEM is to establish the initial static equilibrium stress state within the dam mass before earthquake. In this stage the initial shear modulus dependent on vertical effective stress is set for each element. For the sake of simplicity the stage construction and overconsolidation was neglected. Subsequently, the simplified one-phase dynamic calculations are done using equivalent linear procedure. Due to these assumptions, only elastic dynamic strains are expected and the pore pressure is not analysed. The model was loaded by three uniform horizontal acceleration time-histories that results from deconvolution procedure, Kramer (1996) and Dulińska (2012). Deconvolution allows to gain recorded free surface motions at the toe with designed *PHA*. The linear chirp signal which covers interested frequency range with the same amplitude was used to calculate the transmittance function. Accordance to EC8 recommendations, three accelerograms with waveforms representing *near*, *medium*, *far* field conditions have been applied. Peak acceleration ratio of these groups of signals has been assumed to be 1.0:0.5:0.3. An Arias intensity criterion has been used to select one signal from each group. Response spectra of selected accelerograms are quite compatible with type 2 of elastic response spectrum S_e given in EC8 for the ground type C, Fig. 27.4. To improve calculation efficiency, the important part of signal (denoted by t_a) was extracted using period criterion that covers an increase of Arias intensity from 1 to 95 %. Non-standard lower limit has been applied for the numerical stability purpose. The baseline correction and band-pass filtration were applied for the selected signals to ensure zero dynamic displacement at the end of vibration, reducing noise and high frequencies with very low amplitude, Boore and Bommer (2005).

There are two main steps of Newmark safety analyses using Slope/W. At first, an average acceleration history is determined based on shear forces mobilized along slip surface (from both static and dynamic FEM analysis), divided by the mass of sliding block. Next, the factor of safety is determined as the ratio of the available static resistance shear force to mobilized shear force along a slip surface. Knowing time-history of both the average acceleration and the factor of safety, yield acceleration a_y is determined. For the instability time periods (when the average

acceleration is greater than a_y) the positive relative average accelerations of the block arise. By double integration of the latter time-history, the relative velocity and then relative displacement time-history are determined. Around one hundred various slip surfaces were examined covering all admissible failure mechanisms; from shallow to deep surface, passing through the soft clays, and the boundary between saturated and unsaturated tailings.

27.4 Selected Calculation Results

Calculations of permanent displacements based on modified Newmark's approach have revealed that for predicted future mining induced seismic activity **no permanent displacements occur**. In order to verify and validate the model some additional calculations for scaled acceleration signals (design *PHA* multiplied by 3), applied to the base, have been carried out. Many various tests were performed and only selected results are presented. The main conclusions from validity tests and parametric study are as follows:

1. higher horizontal accelerations occur at the top part of the dam, however higher vertical accelerations are located in the middle part of the dam body;
2. higher initial shear modulus for the defined soils stronger response and higher wave reflection effect;
3. the permanent displacement for rigid base case should be calculated only for strong input signal duration;
4. the deconvolution procedure showed that due to horizontal loading applied to the base, vertical acceleration component appears which is mostly caused by differentiated elevation of model (the dam);
5. spatial variability of tailings should be considered, giving 30 % larger permanent deformation and different failure mechanism, Fig. 27.5.
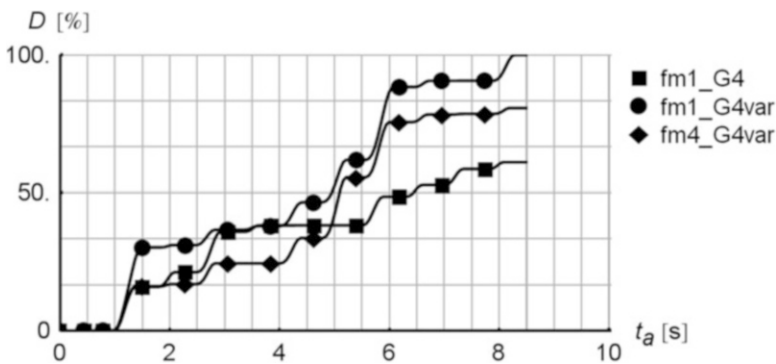
Fig. 27.5 The impact of tailings stiffness on the permanent displacements (G4 – constant stiffness of tailings; finl_G4var, fin4_G4var – various stiffness of tailings depending on its distance from the dam crest)

27.5 Conclusions

In the paper the assessment of the Żelazny Most tailings dam stability subjected to mining-induced paraseismic loading has been presented. Due to the fact that predicted peak ground accelerations for the mining plan up to 2042 are larger than given by EC8 allowable limit for application of pseudo-static approach, the assessment was carried out by simplified dynamic Newmark's analysis.

The Newmark approach coupled with FEM was chosen for stability analysis. The adopted methodology assumes one-phase equivalent linear shearing behaviour and it is correct for predicted *PHA* level and low cyclic mobility of saturated tailings. In the numerical analysis made by GeoStudio software the attention was focused on how to reflect the material complexity of dam and foundation. Such complexity required a determination of many material properties, which was based on the interpretation of large series of laboratory test results. The correctness and the efficiency of discrete model was proved by series of numerical tests. The proper simulation of the design motion was achieved by deconvolution procedure using linear chirp signal. The work should be continued to model compliant base case and check its influence to dynamic response.

For predicted design peak ground acceleration derived for the mining plan period from 2012 to 2042 no permanent displacements should occur.

References

Boore DM, Bommer JJ (2005) Processing of strong-motion accelerograms: needs, options and consequences. Soil Dyn Earthq Eng 25:93–115

Dulińska J (2012) Ziemne budowle hydrotechniczne na terenach sejsmicznych i parasejsmicznych w Polsce. Wybrane aspekty modelowania i obliczeń. Wydawnictwo PK, Kraków

Eurocode 8 (2003) Design of structures for earthquake resistance. Part 5: Foundations, retaining structures and geotechnical aspects. Final Draft. CEN

GEO-SLOPE International Ltd. (2010a) Dynamic modeling with QUAKE/W 2007. An Engineering Methodology

GEO-SLOPE International Ltd. (2010b) Stability modeling with SLOPE/W 2007 version. An Engineering Methodology

Guterch B (2009) Sejsmiczność Polski w świetle danych historycznych. Przegląd Geologiczny 57(6):513–520

Ishibashi I, Zhang X (1993) Unified dynamic shear moduli and damping ratios of sand and clay. Soils Found 33(1):182–191

Ishihara K (2003) Soil behaviour in earthquake geotechnics. Clarendon Press, Oxford

Jamiolkowski M, Carrier WD, Chandler RJ, Hoeh K, Swierczynski W, Wolski W (2010) The geotechnical problems of the second world largest copper tailings pond at Zelazny Most, Poland. Geotech Eng J SEAGS AGSSEA 41(1):1–15

Kramer SL (1996) Geotechnical earthquake engineering. Prentice-Hall, Upper Saddle River

Lasocki S (2011) Wybór rejestracji sejsmometrycznych zgodnie z zaleceniami Zespołu Ekspertów Międzynarodowych. IGF PAN, Warszawa

Lasocki S, Orlecka-Sikora B, Mirek J, Zarzycka E, Kozłowska M (2012a) Nadzór nad pomiarami oddziaływania sejsmicznego eksploatacji górniczej w zakresie sieci obserwacyjnej zapór OUOW „Żelazny Most" oraz stacji monitorujących zachodnie przedpole OUOW w 2012 roku. IGF PAN, Kraków

Lasocki S, Popiołek E, Zorychta A, Orlecka-Sikora B, Sopata P, Stoch T, Urban P (2012b) Szczegółowa prognoza oddziaływania wstrząsów indukowanych działalnością górniczą i deformacjami powierzchni terenu na OUOW „Żelazny Most" z uwzględnieniem jego rozbudowy oraz rozwoju wydobycia złoża rudy miedzi do roku 2042. IGF PAN, Warszawa

Newmark NM (1965) Effects of earthquakes on dams and embankments. Geotechnique 15(2):139–160

Świdziński W, Korzec A (2013) Opracowanie procedury projektowania zapór Obiektu Unieszko-dliwiania Odpadów Wydobywczych (OUOW) Żelazny Most do wyższych rzędnych metodą elementów skończonych oraz uproszczoną metodą Newmarka z uwzględnieniem obciążeń parasejsmicznych oraz zaleceń Eurokodu 8. IBW PAN, Gdańsk

Zembaty Z (2004) Rockburst induced ground motion – a comparative study. Soil Dyn Earthq Eng 24:11–23

Part III
Seismic Control and Monitoring of Irregular Structures

Chapter 28
Optimal Drift and Acceleration Control of 3D Irregular Buildings by Means of Multiple Tuned Mass Dampers

Yael Daniel and Oren Lavan

Abstract This chapter presents a formal optimization methodology for the seismic design of multiple tuned-mass-dampers (MTMDs) for the multi-modal control of 3D irregular buildings. The total weight of all TMDs is minimized while both inter-story drifts and total accelerations are constrained to allowable values so as to lead to a performance-based-design. The results reveal that, with the right design, MTMDs can mitigate both structural and nonstructural earthquake damage. Hence, they can potentially present a multi-hazard strategy to mitigate both winds and earthquakes.

Keywords Irregular structures • Multiple tuned mass dampers • Multi modal • Control • Seismic design of tall buildings • Acceleration control

28.1 Introduction

The main criterion in seismic design under strong ground motions (life safety) has long been limiting the amount of casualties following a severe earthquake. However, the financial consequences of recent ground motion (e.g. Northridge 1994; Kobe 1995; Christchurch 2011) led to the notion that financial criteria should also be considered. This understanding inspired the development of the performance-based design (PBD) philosophy, where limiting damage under less severe ground motions is also considered (see e.g. Fajfar and Krawinkler 1997, or Priestley 2000, for elaboration on the PBD concept). This also motivated retrofitting of existing structures to limit damage following ground motions of various levels.

Y. Daniel
AJS Consulting Engineers, Haifa, Israel
e-mail: yael.daniel@ajs-eng.co.il

O. Lavan (✉)
Faculty of Civil and Environmental Engineering, Technion – Israel Institute of Technology, Haifa, Israel
e-mail: lavan@tx.technion.ac.il

One of the advanced means for retrofitting such structures relies on tuned-mass dampers (TMD) (e.g. Den-Hartog 1940; Soong and Dargush 1997). Such devices can efficiently reduce the response of a linear system to a harmonic loading over a specific narrow band of frequencies. Therefore, the application to wind design is straight-forward (e.g. McNamara 1977; Luft 1979; Wiesner 1979). Under seismic events however, elastic behaviour is often experienced by tall buildings as well as buildings equipped with energy dissipation systems (Kasai et al. 2012). Here, limiting absolute acceleration, in addition to the traditional limitations on inter-story drifts, is of much importance (Kasai et al. 2012). As several modes often contribute to these responses, multiple TMDs (MTMDs), tuned to various frequencies have an advantage over a single TMD controlling only one mode of vibration (Clark 1988; Lavan and Daniel 2013; Daniel and Lavan 2014, 2015). This makes such devices attractive for multi-hazard mitigation of winds and earthquake hazards.

This chapter presents the main derivations and findings of Daniel and Lavan (2014). An optimization problem formulation suitable for the optimal design of such MTMDs in 3D irregular structures is first presented. The total mass of MTMDs is minimized, while local responses of interest of the peripheral frames are constrained to allowable values, each one individually. Hence, excessive local damage, which usually characterizes irregular structures, may be prevented, and elastic response could be ensured. Similarly, absolute accelerations at the perimeters of each floor are also constrained to allowable values, allowing the reduction of nonstructural damage levels. In turn, the derivation of a methodology that allows a formal optimal design for this PBD problem is presented. This methodology requires a relatively small computational effort, without predefining the amount of added devices, their locations, modes to be dampened, or sizes. An example of a design for retrofitting of an eight story asymmetric structure using the proposed methodology is presented, and its characteristics are thoroughly discussed.

28.2 Problem Formulation

28.2.1 Equations of Motion and Their Solution Using Lyapunov's Equation

The equations of motion of a general 3D linear asymmetric building were formulated and represented in state-space notation (see e.g. Soong 1990). Furthermore, a stochastic description of the ground motion hazard was adopted. This enabled a very efficient computation process by using Lyapunov's equation (see e.g. Kwakernaak and Sivan 1972), together with a more realistic representation of the ground motion input, by filtering a white noise input (Daniel and Lavan 2014).

28.2.2 Performance Measures

Inter-story drifts are well known to describe damage to structural elements, and therefore by limiting their value, the damage to these important elements can be effectively reduced (e.g. Williams and Sexsmith 1995; FEMA 356 2000; Charmpis et al. 2012). Inter-story drifts are a damage measure to some types of nonstructural components as well (e.g. partition walls). It is also important to note that by constraining the level of drifts, the structure can be brought to behave linearly, thus eliminating the problems associated with structural yielding and detuning of TMDs. When considering damage to other types of nonstructural elements (e.g. piping systems, air-conditioning systems, sensitive equipment), absolute accelerations are an important measure. Thus, these two parameters were chosen herein to describe the various aspects of seismic structural performance enhancement.

The measure of cost of TMDs is taken here as the amount of added mass. As more mass is added to the structure, the retrofit becomes more expensive and thus less cost-effective. Thus, this is taken as the objective function to be minimized.

28.2.3 Optimization Problem

In the problem to follow, TMDs are potentially allocated at each peripheral location (i.e. at the four edges) of each floor. At each location, multiple TMDs could be assigned, each tuned to a different frequency, aimed to control a different mode of the structure. The optimization problem is formulated so as to minimize the total amount of added mass in all TMDs while constraining root mean-square responses of the structure. These responses are measured at all peripheral locations of all floors, as they are the largest expected within story limits. These locations, that are also the potential locations for the TMDs, are shown in Fig. 28.1, for the story n, as: $(\mathbf{x}_{pyl})_n$, $(\mathbf{x}_{pyr})_n$, $(\mathbf{x}_{pxt})_n$ and $(\mathbf{x}_{pxb})_n$, and are the peripheral coordinates in the "y", "y", "x" and "x" directions, at the left, right, top and bottom edges of floor n,

Fig. 28.1 Definition of dynamic DOFs and peripheral coordinates of the nth floor (Daniel and Lavan 2014)
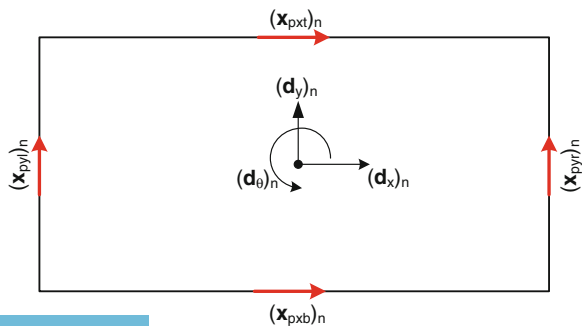
respectively. The responses at these locations can be found by using the transformation matrix, $\mathbf{T}$, from the DOFs of the original structure $((\mathbf{d}_x)_n, (\mathbf{d}_y)_n$ and $(\mathbf{d}_\theta)_n$ in Fig. 28.1) to peripheral coordinates.

The optimization problem is thus formulated as:

$$
\min_{\mathbf{m}_{TMD}} J = \sum_l^{\substack{\text{all} \\ \text{locations}}} \sum_f^{\substack{\text{all} \\ \text{frequencies}}} (\mathbf{m}_{TMD})_{l,f}
$$

$$
s.t.
$$

$$
\frac{RMS\left((\mathbf{r}_p)_l\right)}{\mathbf{r}_{all,l}^{RMS}} \leq 1.0 \quad \forall l = 1, 2, \ldots, N_{locations}
$$

(28.1)

where $(\mathbf{m}_{TMD})_{l,f}$ is the mass of the TMD located at peripheral location l tuned to frequency f, $RMS((\mathbf{r}_p)_l)$ is the root mean-square of the response of interest at each location, l, (the lth term of $RMS(\mathbf{r}_p)$ (such reference to a component of a vector or a matrix, $(\cdot)_l$, will be used throughout this chapter), $\mathbf{r}_{all,l}^{RMS}$ is the allowable root mean-square response at the location l, and $N_{locations}$ is the number of locations to be constrained ($=4N_{floors}$ where N_{floors} is the number of floors). Generally, the design variables in problems such as the one presented in Eq. (28.1) can be the masses of the TMDs, their stiffnesses and damping coefficients. Optimal frequencies (stiffnesses) and damping ratios (damping coefficients) for SDOF systems as a function of their mass were proposed by Den Hartog (1940). These could be applied to each mode separately as was proposed by Lavan and Daniel (2013). These are also adopted herein, thus, the masses of TMDs remain the only design variables.

28.3 Solution Scheme

A first order optimization method was adopted to solve to optimization problem. The required gradients were efficiently derived analytically. All constraints were first normalized by their allowable values and combined to a single constraint on their maximum value. The adjoint method was then utilized to efficiently derive its gradient. For further details of these derivations the reader is referred to Daniel and Lavan (2014).

28.4 Example

The following eight-story asymmetric setback reinforced concrete (RC) frame structure (Fig. 28.2) introduced by Tso and Yao (1994) is retrofitted using MTMDs. This structure was also adopted by Lavan and Daniel (2013) and
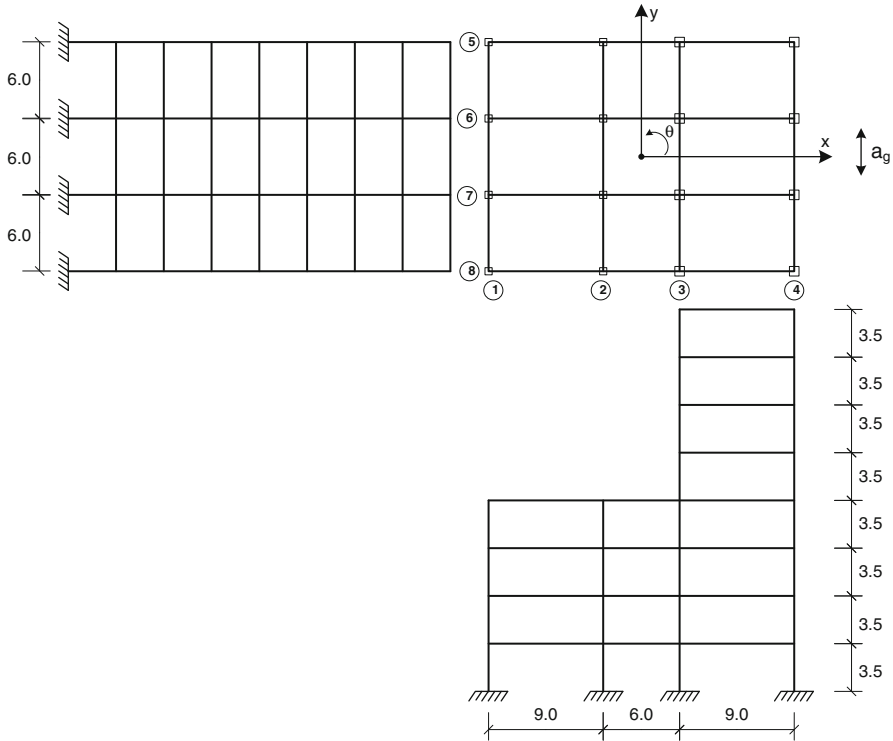
Fig. 28.2 Eight-story setback structure (Daniel and Lavan 2014)

retrofitted using MTMDs to limit total accelerations. Here, only the "y" direction component of the excitation is considered. A uniform distributed mass of 0.75 ton/m^2 was taken. The column dimensions are 0.5 m by 0.5 m for frames 1 and 2 and 0.7 m by 0.7 m for frames 3 and 4. The beams are 0.4 m wide and 0.6 m tall. Five percent Rayleigh damping for the first and second modes was used. The design variables are the locations and properties of the individual tuned mass dampers. The dampers are to potentially be located on the peripheral frames, where they are most effective, and as the excitation is in the "y" direction only, dampers will be assigned only to the peripheral frames 1 (lower 4 floors), 3 (upper 4 floors) and 4, to dampen frequencies of modes which involve "y" and "θ". The response is analysed under a Clough-Penzien filtered Kanai-Tajimi power-spectral density with parameters suited to match the SE 10/50 ground motion ensemble.

This example is solved for two constraints simultaneously: a constraint on RMS absolute accelerations and RMS inter-story drifts. Herein, it is desired to reduce the maximal responses by 45 % (i.e. the allowable RMS acceleration is 55 % of the max RMS acceleration of all locations at the bare structure's response, and the allowable RMS inter-story drift is 55 % of the max RMS inter-story drift of all locations at the bare structure's response).

Table 28.1 Natural frequencies of the structure in the coupled y,θ direction

Mode #	Angular frequency (rad/s)	Mode #	Angular frequency (rad/s)
2	7.36	9	43.48
3	10.37	11	57.41
5	17.88	12	67.27
6	22.61	13	71.95
8	35.96	15	94.66

Table 28.2 Final properties of added TMDs

Frame	Floor	Mode to dampen	Mass (ton)	Stiffness (kN/m)	Damping ratio
1	4	3	8.33	841.46	0.1041
3	8	2	122.44	4490.50	0.2120
3	8	3	15.05	1520.62	0.1041
3	8	5	3.68	1140.16	0.0759
4	8	2	18.99	696.47	0.2120

The first few natural frequencies and modes, associated with the "y" translation (and "θ" rotation) of the building, are shown in Table 28.1.

A 45 % reduction of both the absolute acceleration and the peripheral peak total inter-story drift in the bare structure is desired. 160 TMDs were added, as a first guess. These are comprised of 10 dampers each tuned to a different natural frequency (related to the "y" and "θ" modes) at each of the 16 peripheral locations of frames 1, upper 4 floors of frame 3, and frame 4. The initial frequencies and damping ratios were computed based on the initial masses of TMDs as per Den Hartog (1940). Using the Active Set algorithm for optimization, the mass converged to the final stiffness using 117 function/gradient evaluations. The final solution attained is given in Table 28.2.

Finally, an analysis of the retrofitted structure yields the peripheral RMS inter-story drifts and accelerations shown in Fig. 28.3. Also shown in Fig. 28.3 is the total amount of mass at each floor. As can be seen, in this case both constraints (i.e. accelerations and drifts) are active at the same time.

The convergence of the constraint as well as the performance index can be seen in Fig. 28.4.

28.5 Conclusions

This chapter presented a formal optimization methodology for the seismic retrofitting of 3D irregular structures. The proposed formulation minimizes the total mass of added MTMDs while constrains inter-story drifts and total accelerations to allowable values, thus limiting both structural and non-structural damage
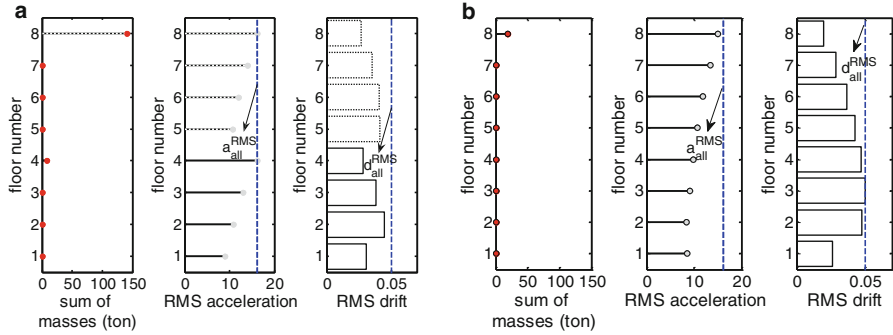
Fig. 28.3 Peripheral RMS accelerations and inter-story drifts of structure with final TMDs (*continuous* or *dashed*) and sum of added masses (*dots*) (**a**) frame 1 (floors 1–4) and 3 (floors 5–8) and (**b**) frame 4 (Daniel and Lavan 2014)
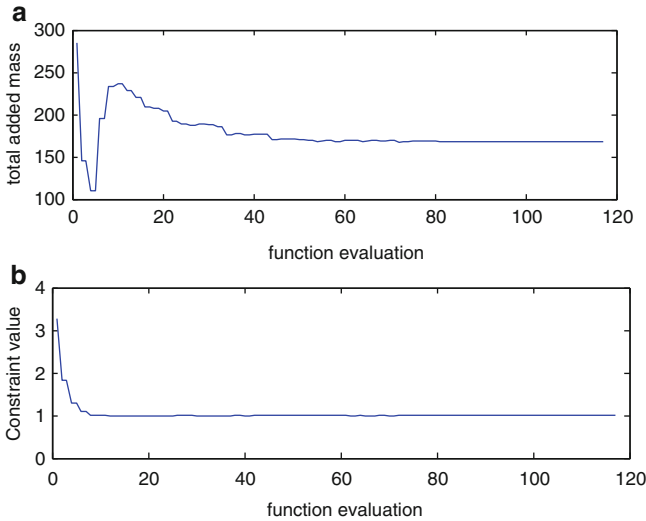
Fig. 28.4 Convergence of (**a**) performance index and (**b**) objective function, constraining absolute accelerations and inter-story drifts (Daniel and Lavan 2014)

levels. As responses of interest are constrained, the methodology could be used in the context of Performance-Based Design. It is believed by the authors that with the formulation of the optimization problem and the tools derived for its solution to assist in the design, a door is opened for a wider use of MTMDs for the seismic retrofitting of buildings.

References

Charmpis DC, Komodromos P, Phocas C (2012) Optimized earthquake response of multi-storey buildings with seismic isolation at various elevations. Earthq Eng Struct Dyn 41(15): 2289–2310

Clark AJ (1988) Multiple passive tuned mass dampers for reducing earthquake induced building motion. In: Proceedings of the 9th world conference on earthquake engineering, Tokyo-Kyoto, Japan, vol V, pp 779–784

Daniel Y, Lavan O (2014) Gradient based optimal seismic retrofitting of 3D irregular buildings using multiple tuned mass dampers. Comput Struct 139:84–97

Daniel Y, Lavan O (2015) Optimality criteria based seismic design of multiple tuned-mass-dampers for the control of 3D irregular buildings. Earthq Struct 8(1):77–100

Den-Hartog JP (1940) Mechanical vibrations, 2nd edn. McGraw-Hill Book Company, New York

Fajfar P, Krawinkler H (eds) (1997) Seismic design methodologies for the next generation of codes. Balkema, Rotterdam

FEMA 356 (2000) Pre-standard and commentary for the seismic rehabilitation buildings. Federal Emergency Management Agency, Washington, DC

Kasai K, Pu W, Wada A (2012) Response of passively-controlled tall buildings in Tokyo during 2011 Great East Japan Earthquake. In: Proceedings of the 15th world conference on earthquake engineering, Auckland, New Zealand, 2000

Kwakernaak H, Sivan R (1972) Linear optimal control systems. Wiley, New York

Lavan O, Daniel Y (2013) Full resources utilization seismic design of irregular structures using multiple tuned mass dampers. Struct Multidiscip Optim 43(3):517–532

Luft RW (1979) Optimum tuned mass dampers for buildings. ASCE J Struct Div 105:2766–2772

McNamara RJ (1977) Tuned mass dampers for buildings. ASCE J Struct Div 103:1785–1798

Priestley MJN (2000) Performance based seismic design. In: Proceedings of the 12th world conference on earthquake engineering, Lisbon, Portugal, 2012. Paper no. 2831

Soong TT (1990) Active structural control: theory and practice. Longman Scientific & Technical, Harlow

Soong TT, Dargush GF (1997) Passive energy dissipation systems in structural engineering. Wiley, Chichester

Tso WK, Yao S (1994) Seismic load distribution in buildings with eccentric setback. Can J Civ Eng 21:50–62

Wiesner KB (1979) Tuned mass dampers to reduce building wind motion. ASCE Convention and Exposition, Boston, pp 1–21

Williams MS, Sexsmith RG (1995) Seismic damage indices for concrete structures: a state-of-the-art review. Earthq Spectra 11(2):319–349

Chapter 29
Improved Seismic Performance of RCC Building Irregular in Plan with Water Tank as Passive TMD

Suraj N. Khante and Rutuja S. Meshram

Abstract The choices of building shapes and structural systems have significant effect on their seismic performance. Structures that have non-coincident centers of mass and stiffness are referred to as plan-irregular structures. Such structures could be highly vulnerable to earthquake damage due to torsional response. Regular buildings result in a fairly uniform distribution of seismic forces throughout its components, whereas irregular buildings result in highly indeterminate distribution of forces making the analysis prediction more complicated. This paper deals with analytical investigation of feasibility of implementing water tank as passive TMD on plan irregular building using SAP2000. The water tank was installed at the terrace level of L-shaped building. The response of building to earthquake data, namely, El-Centro 1940 and Bhuj 2001 were studied. The responses of the building with tank provided at three different locations of building were studied under five conditions, namely, tank empty, 0.25 h, 0.50 h, 0.75 h and full tank, where, h is the height of water level. It is concluded that water tank at top roof level in partially filled condition mitigate response of irregular buildings.

Keywords Plan irregularity • Water tank as Passive TMD • Nonlinear analysis • SAP2000

29.1 Introduction

To protect civil structures from significant damage, the response reduction during severe earthquakes has become an important topic in structural engineering. A building is said to be irregular when it lacks symmetry and discontinuity in geometry, mass or load resisting elements. There are two types of irregularities namely, Horizontal irregularities refers to asymmetrical plan shapes (L, T, U and F)

S.N. Khante (✉) • R.S. Meshram
Applied Mechanics Department, Government College of Engineering, Amravati, Maharashtra, India
e-mail: snkhante@yahoo.com; rutu.sm@gmail.com

or discontinuities in horizontal resisting elements and Vertical irregularities refer-
ring to sudden change of strength, stiffness, geometry and mass of a structure in
vertical direction.

An ideal multi-storey building designed to resist lateral loads due to earthquake
would consist of only symmetric distribution of mass and stiffness in plan at every
storey and a uniform distribution along height of the building. Such a building
would respond only laterally and is considered as torsionally balanced building. But
it is very difficult to achieve such a condition because of restrictions such as
architectural requirements and functional needs. The issue of mitigating the
response of such irregular structures due to seismic loads has drawn the interest
of many researchers in recent years.

Tuned mass dampers (TMD) have been widely used for the vibration control in
civil engineering structures. The concept of vibration control, using a mass damper,
dates back to the year 1909, when Frahm invented a vibration control device called
a dynamic vibration absorber. Through intensive research and development in
recent years, the TMD has been accepted as an effective vibration control device
for both new and existing structures. On similar lines TLD (Tuned Liquid Dampers)
have also proven themselves in the form of successful passive vibration mitigating
system. It is found to be a simple, effective, inexpensive and reliable means for
suppressing undesirable vibrations of structures caused by seismic excitations. It is
attached to a structure in order to reduce the dynamic response of the structure.

Since the water storage tanks are built-in component of buildings and mostly
these are constructed on the top roof level, hence they add dead load on the
structure. During earthquakes, this extra mass can be employed as damper to take
over the surplus energy transmitted to the structure.

Lin et al. (1994) studied vibration control effectiveness of passive tuned mass
dampers (PTMDs) for irregular buildings. The results verified that PTMDs are
capable of reducing building response effectively. Jaiswal (2004) employed Simple
Tuned Mass Damper to Control Seismic Response of Elevated Tanks. Mehboob
et al. (2013) carried out numerical investigation of water tank as TLD, installed at
the roof level of multi-storey building using ANSYS. Investigation was carried out
by locating water tank off the centre of mass of building and for different water
level conditions. Gulve and Murnal (2013) conducted study on implementation of
water tank as passive tuned mass damper. Three multi-storey regular structures,
three, seven and ten were taken for the study. Hemalatha and Jaya (2008) focused
on the feasibility of providing passive TMD on building when subjected to earth-
quake. The researchers had only varied water levels for analysis.

The studies available in literature mainly concentrate on regular buildings. More
so ever two mass model of water tank is missing in the structural modelling of water
tank. The present study bridges this gap. This study is an attempt to investigate
effect of different earthquake excitation on irregular building with varying height
on maximum displacement. Deliberately two earthquake spectra are employed for
excitation of building because of their typical characteristic signature. As the
purpose of study is to establish effectiveness of existing water tanks as TLD, the
parameters viz. frequency ratio, mass ratio which affect the performance of TLD
were not optimized. The water tanks were provided on bay of 3 m $\times$ 3 m.

29.2 Basic Principle

It was thought, modeling of water tank as two mass model will lead to more realistic dynamic response of the structure of which water tank is integral part. Two mass model for elevated tank was proposed by Housner (1963) which is more appropriate and is being commonly used in most of the international codes including IS 1893 (Part-II) (Liquid Retaining Tanks 2000). The pressure generated within the fluid due to the dynamic motion of the tank can be separated into impulsive and convective parts. For representing these two masses and in order to include the effect of their hydrodynamic pressure in analysis two-mass model is adopted for tanks. In spring mass model convective mass (m_c) is attached to the tank wall by the spring having stiffness (K_c), where as impulsive mass (m_i) is rigidly attached to tank wall. For elevated tanks two-mass model is considered, which consist of two degrees of freedom system. The two- mass model is shown in Fig. 29.1.

29.3 Building Description

The models of building considered for the analysis are G + 4 (M5), G + 7 (M8) and G + 12 (M13) storeys RCC structures. The buildings are irregular in plan as shown in Fig. 29.2. The building has bay width of 3 m in X and Y direction with 3 m storey height. Slab is modeled as rigid diaphragm. Tuned mass damper in the form of water tank is installed at three different locations at the top of the building.
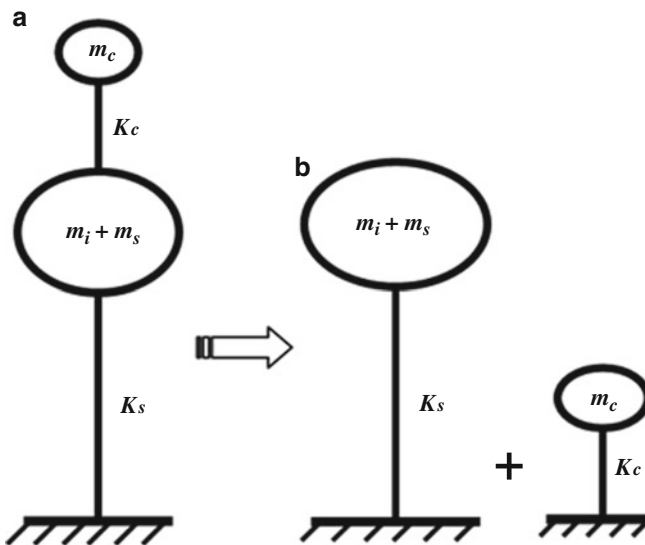
Fig. 29.1 Two mass model

a

b
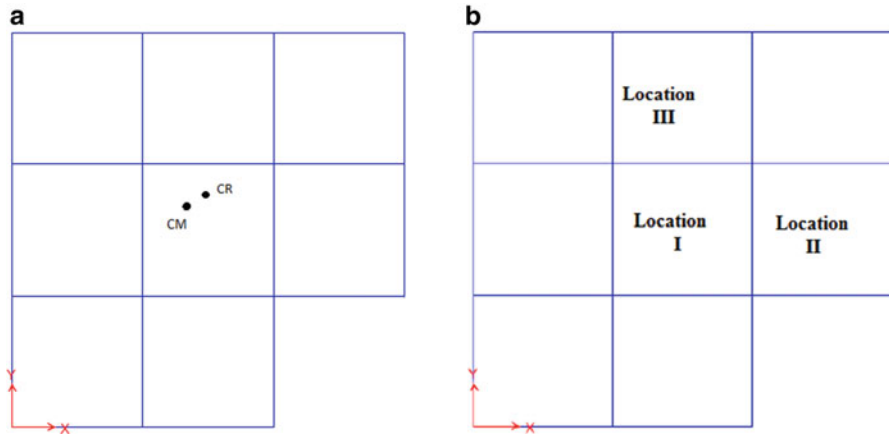
Fig. 29.2 Plan and location of water tank

Table 29.1 Details of the model

Model name	No. of floors	Dimension of column (m)	Dimension of beam (B x D) in m
M5	5	0.30×0.45	0.30×0.40
M8	8	0.40×0.40	0.30×0.40
M13	13	0.45×0.45	0.30×0.45

Non-linear time history analysis is carried out in SAP2000 software (Structural Analysis Program SAP 2000) using El Centro and Bhuj Earthquake records. CM (Centre of mass) is location where total mass of the system can be considered to be located. CR (Centre of rigidity) is the stiffness centroid within a floor diaphragm plan. When CM do not coincide with CR then eccentricity is created in structure i.e. distances between CM and CR. CM and CR are calculated by using ETABS software.

The scope of this study includes investigation of vibrational response of a 3D model of an irregular building provided with a water tank on the top roof level. Two random ground acceleration cases corresponding to past earthquake time-histories were applied to explore the dynamic response of buildings.

Plan irregular buildings i.e. L-shaped buildings were considered for the present study. Location of center of mass (CM) and center of rigidity (CR) along with different locations of water tank are shown in Fig. 29.2a, b. Table 29.1 shows their detail.

The material properties used for the analysis are Grade of concrete – M25, Poisson's ratio – 0.16 and Density of concrete – 2500 kg/m^3. The horizontal input ground motions, in the form of acceleration time-history are summarized in the Table 29.2.

Table 29.2 Time history record summary

Country/record	Station/year	Magnitude	PGA (g)
California/Imperial Valley	El-Centro (1940)	6.9	0.32
Bhuj	Ahmadabad (2001)	7.0	0.47
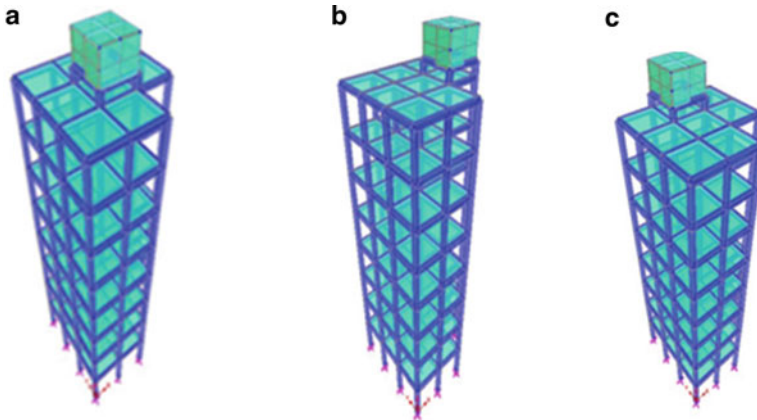
Fig. 29.3 Locations of water tank (**a**) Water Tank at Location I (**b**) Water Tank at Location II (**c**) Water Tank at Location III
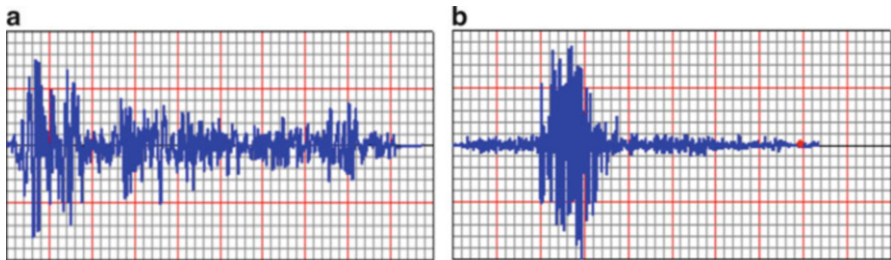
Fig. 29.4 Acceleration value for El-Centro earthquake and Bhuj earthquake. (**a**) El-Centro Earthquake (**b**) Bhuj Earthquake

In the present work the water tank was placed at three different locations. The tank had a plan dimension of 3×3 m and 2 m height for all the models and was placed over 1 m high columns. The beam-column supports for the tank were rectangular concrete sections and the walls and roof were modeled as concrete. Models of the tank with buildings are shown in Fig. 29.3.

Acceleration values for El-Centro and Bhuj earthquakes are shown in Fig. 29.4.

29.4 Results and Discussion

The location of water tank was changed and for each case of tank location, all three models were investigated for El-Centro and Bhuj earthquake data. The extreme recorded values of roof displacement are plotted and shown in Figs. 29.5, 29.6, and 29.7. From Fig. 29.5(a) (i) displacement of building M5 with empty tank at location I is lowest and displacement of building with 3/4th filled tank is adverse. The maximum displacement reduction of building with empty tank as compared to building without tank is 7.8 % for location II it is 9.4 % for El-Centro.

Generally it is observed that for buildings without water tank (Figs. 29.6(a)–(i), (a)-(ii), (b)-(i), (b)-(ii) and 29.7(a)-(i), (a)-(ii), (b)-(i), (b)-(ii)), with empty water tank (Figs. 29.6(a)-(iii) and 29.7(a)–(iii), (b)–(iii)) and with full water tank (Fig. 29.5(a)-(ii), (a)-(iii), (b)-(ii), (b)-(iii)) maximum displacement is more. On the contrary partially filled tank was found to be effective in mitigating response.

29.5 Conclusions

After the numerical investigation of water tank as TMD, for three different building models (difference in terms of height of building) irregular in plan, subjected to seismic excitation, following conclusions can be made:

- Water tank at top can be designed to serve as TMD provided the parameters i.e., plan location of water tank; water level and mass ratio are tuned properly.
- TMD (tank + water) located near the centre of mass and centre of rigidity of an irregular building shows maximum response reduction as compared to TMD (tank + water) located away from it. As the distance between water tank and centre of mass building increases the response of the building also increases.
- In higher building, maximum percentage reduction in response of plan irregular building is noted.
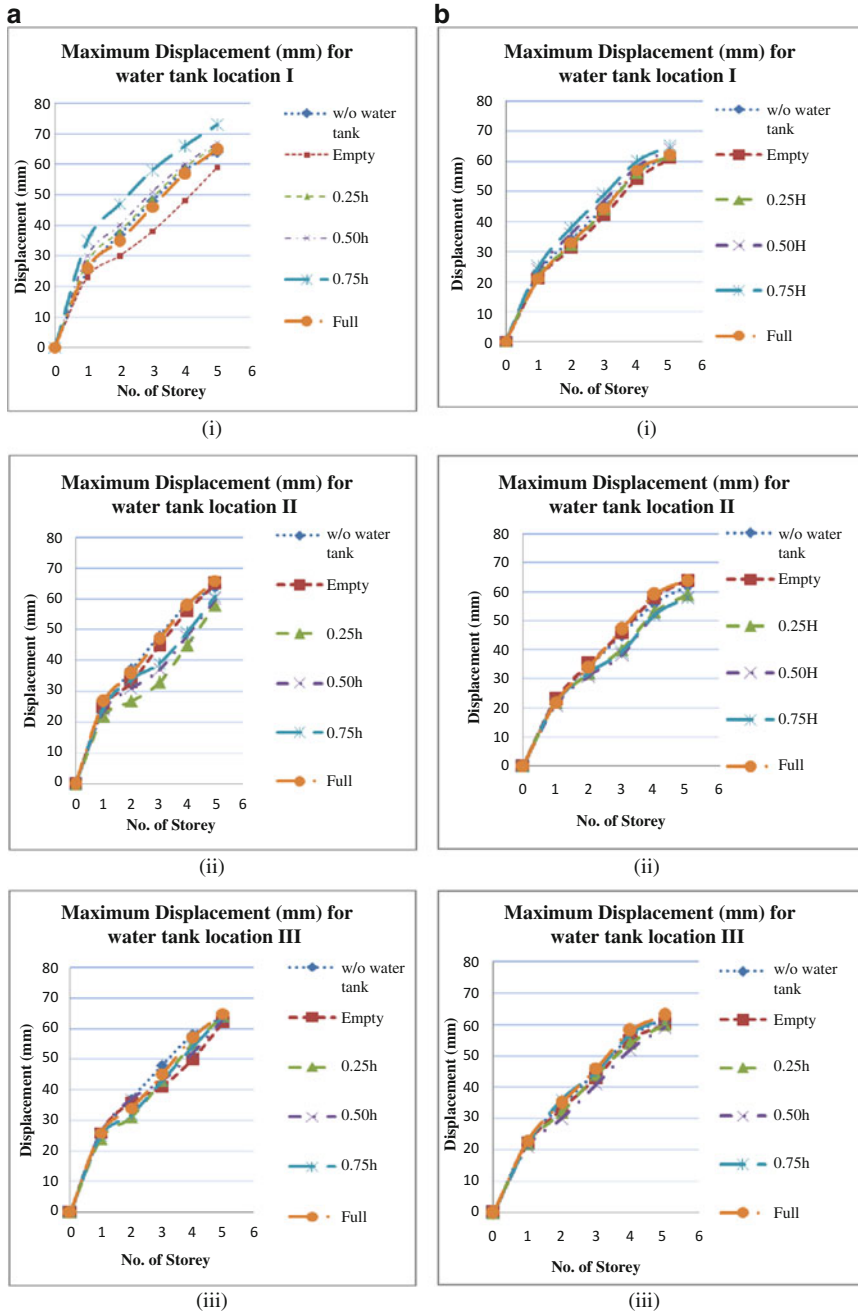
Fig. 29.5 Displacement of five storey building for El-Centro and Bhuj earthquake. (**a**) El-Centro Earthquake (**b**) Bhuj Earthquake
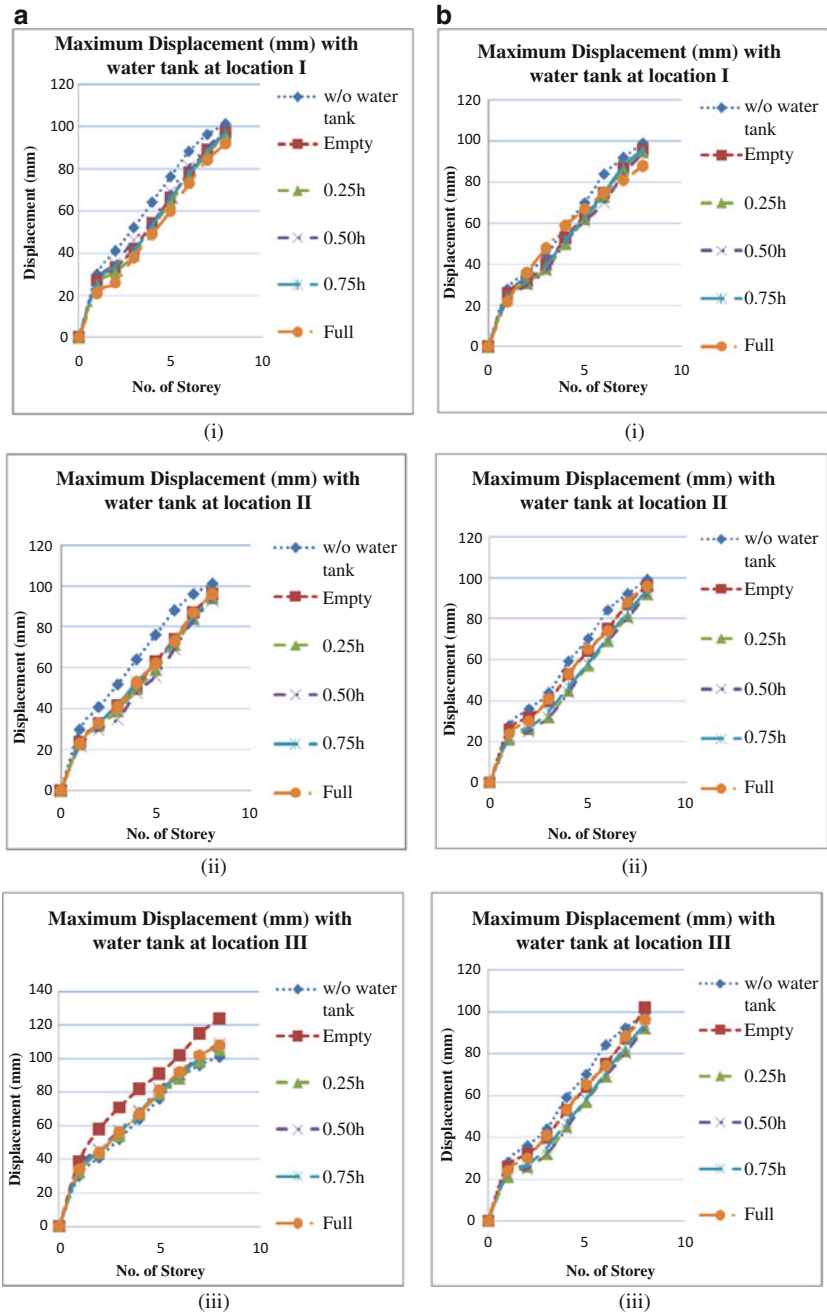
Fig. 29.6 Displacement of eight storey building for El-Centro and Bhuj earthquake. (**a**) El-Centro Earthquake (**b**) Bhuj Earthquake
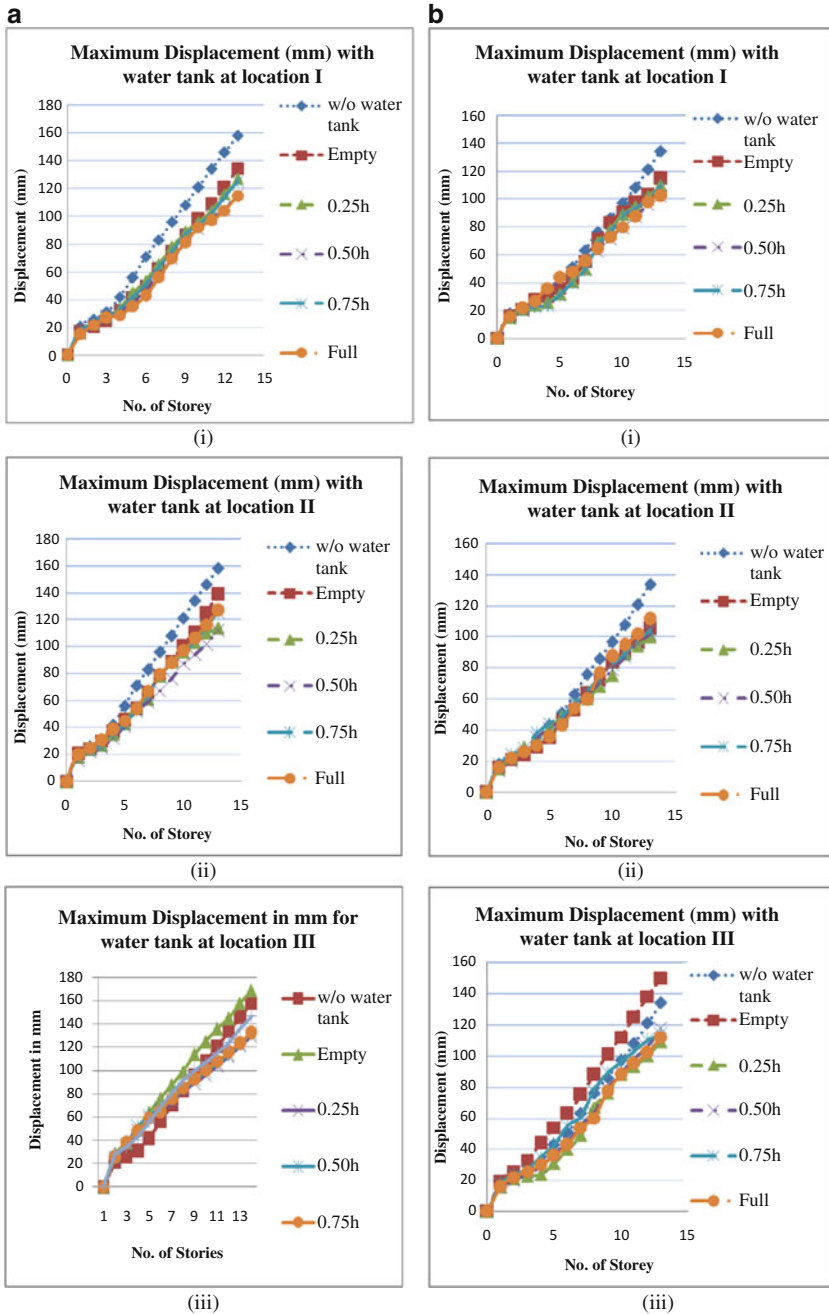
Fig. 29.7 Displacement of thirteen storey building for El-Centro and Bhuj earthquake. (**a**) El-Centro Earthquake (**b**) Bhuj Earthquake

References

Gulve TS, Murnal P (2013) Feasibility of implementing water tank as passive tuned mass damper. Int J Innov Technol Explor Eng (IJITEE) 3(3):12–19, ISSN: 2278-3075

Hemlatha G, Jaya KP (2008) Water tank as passive TMD for seismically excited structures. Asian J Civ Eng (Build Hous) 9(4):349–366

Housner GW (1963) The dynamic behavior of water tanks. Bull Seismol Soc Am 53(2):381–387

IS: 1893 (Part-II, Liquid Retaining Tanks) (2000) Criteria for earthquake resistant design of structures. Bureau of Indian Standards, New Delhi

Jaiswal OR (2004) Simple tuned mass damper to control seismic response of elevated tanks. In: Proceedings of the 13th world conference on earthquake engineering, Vancouver

Lin CC, Hu C-M, Wang JF, Hu R-Y (1994) Vibration control effectiveness of passive tuned mass damper. J Chin Inst Eng 17(3):367–376

Mehboob SS, Khan QZ, Tahir F, Ahmad MJ (2013) Investigation of water tank as TLD for vibration control of frame structures under seismic excitation. Life Sci J 10(7s):1182–1189, ISSN: 1097-8135

Chapter 30
Behaviour of Asymmetric Structure with Base Isolation Made of Polymeric Bearings

Tomasz Falborski and Robert Jankowski

Abstract Earthquake-induced ground motions are the most severe and unpredictable threats to the structures all around the world. Seismic excitations cause a lot of damage in a wide variety of ways, leaving thousands of casualties in their wake. Due to randomness of earthquake occurrence, lack of visible causes and their power of destructiveness, structural engineers need to develop new technical solutions and protection systems against earthquake forces and their devastating effects in order to minimize loss of life and property damage. Accordingly, designing seismic-resistant structures became an issue of great importance in many seismically active regions of the world. This concerns especially designing asymmetric structures, since their response under earthquake excitations is much more complex and often difficult to be predicted comparing with the symmetric ones. The present paper reports the results obtained from detailed finite-element analysis on a dynamic response of a base-isolated asymmetric multi-storey steel building under various seismic excitations. The numerical investigation aims to verify the effectiveness of Polymeric Bearings in suppressing vibrations of asymmetric structures under strong earthquakes.

Keywords Polymeric bearings • Seismic isolation • Asymmetric structures • Earthquakes • Numerical analysis

30.1 Base Isolation

Earthquakes produce large-magnitude forces of short duration that must be resisted by a structure without causing collapse and preferably without any significant damage to the structural members. It has been gradually being recognized that various methods of structural control are probably the most effective means of

T. Falborski (✉) • R. Jankowski
Faculty of Civil and Environmental Engineering, Gdańsk University of Technology, ul. Narutowicza 11/12, 80-233 Gdańsk, Poland
e-mail: tomfalbo@pg.gda.pl; jankowr@pg.gda.pl

protecting structures during seismic excitations (Buckle 2000). They are not only employed for mitigating earthquake forces, but are also equally useful in controlling undesirable structural vibrations produced due to wind loads and other minor dynamic excitations (Mayes and Naeim 2001).

Base isolation is considered to be one of the most popular passive structural control techniques of protecting structures against strong ground motions (Naeim and Kelly 1999). Base isolators, like Lead-Rubber Bearings (LRBs), High-Damping Rubber Bearings (HDRBs), and Friction Pendulum Systems (FPSs) are frequently used in practice in many earthquake-prone countries all around the world.

Base isolation systems work by decoupling the building from the horizontal components of the earthquake ground motion by interposing a layer with low horizontal stiffness between the structure and its foundation (Kelly 1993; Skinner 1993). The philosophy behind the concept of base isolation is to lengthen the period of vibration of the protected structure, so as to reduce the base shear induced by the earthquake, while providing additional damping to the system (Jankowski 2003; Mahmoud et al. 2012; Robinson 1982). This is why most seismic design codes suggest the use of base isolation systems that have the dual function of period elongation (period shift effect) and energy dissipation (increasing damping effect).

30.2 Numerical Model

Numerical simulation of the seismic behaviour of a multi-storey steel building, both fixed-base and base-isolated, under various seismic excitations has been performed using the Finite Element (FE) software MSC Marc® 2008. The FE model of the fixed-base asymmetric 4-storey steel structure building is composed of six steel rigid frames made of HEB 300 sections and 25 cm thick reinforced C25/30 concrete slabs (Fig. 30.1). In order to increase structural stiffness of the building, additional bracings in two sidewall vertical planes have been used. The spacing between the columns in the plane of steel frames is 6.0 m. The distance between the steel frames in longitudinal direction is 4.2 m. The height of each storey is 3.6 m. Accordingly, the analyzed structure is 12.6 m long, 12.0 m wide and its total height is 14.4 m. Steel frames as well as the reinforced concrete slabs have been modelled using 4-node shell elements (Zienkiewicz and Taylor 2002) available in MSC Marc® 2008. In order to generate bracings in vertical planes, 2-node truss elements have been employed. Both columns and girders are made of steel with the following elastic parameters: Young's modulus $E_s = 210$ GPa and Poisson's ratio $\nu_s = 0.3$. The material is isotropic and its mass density is $\rho_s = 7850$ kg/m^3, which corresponds to standard steel. Floor and roof slabs are made of concrete with the following elastic parameters: Young's modulus $E_c = 31$ GPa and Poisson's ratio $\nu_c = 0.2$, which is typical for C25/30 concrete. The material is also isotropic and its mass density is $\rho_c = 2400$ kg/m^3.

Fig. 30.1 FE model of a
fixed-base asymmetric
4-storey steel building
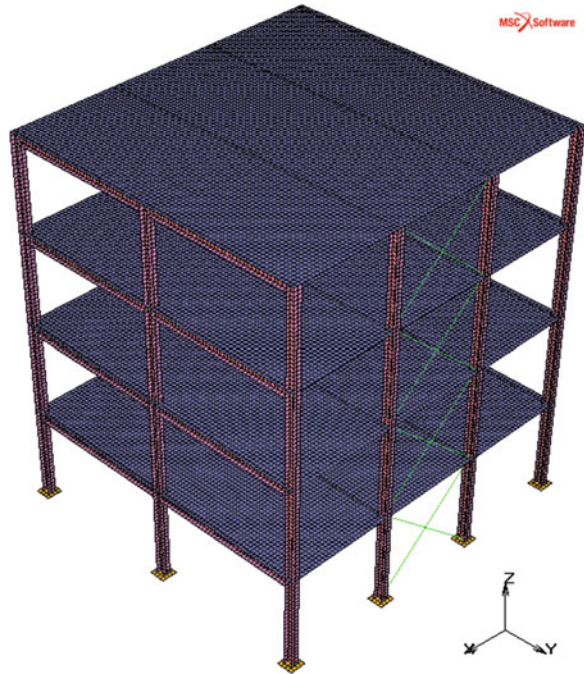
30.3 Polymeric Bearings

As indicated by Fig. 30.2, the analyzed 4-storey building has been decoupled from
the shaking ground with the Polymeric Bearings, which can be considered a
proposal of a new seismic isolation system. It consists of rectangular-shaped blocks
($600 \times 600 \times 400$ mm) made of a specially prepared flexible polymeric material
whose chemical composition includes certain additives so as to improve its
damping potential. The basic mechanical properties of this material have been
already determined in experimental studies and the results have been presented in
previous publications (Falborski 2012; Falborski et al. 2012a, b, c). Hysteresis
loops observed during the cycling testing have confirmed its relatively high
damping and energy-dissipation properties, which are extremely desirable for
materials used for seismic isolation devices. Moreover, shaking table experimental
study, using the prototype of the Polymeric Bearings supporting a 1.20 m high
single-storey and a 2.30 m high two-storey steel structure models, has also been
performed and the results have proven the effectiveness of this base isolation
system in suppressing structural vibrations during dynamic excitations (Falborski
and Jankowski 2012, 2013).

Rubber-like materials behave as hyperelastic, incompressible and, from a mac-
roscopic point of view, homogenous and isotropic solids. To analyze rubber
bearings, different analytical methods are available. In the present study, Polymeric
Bearings have been modelled using 8-node hexahedral solid elements available in

Fig. 30.2 FE model of a
base-isolated asymmetric
4-storey steel building
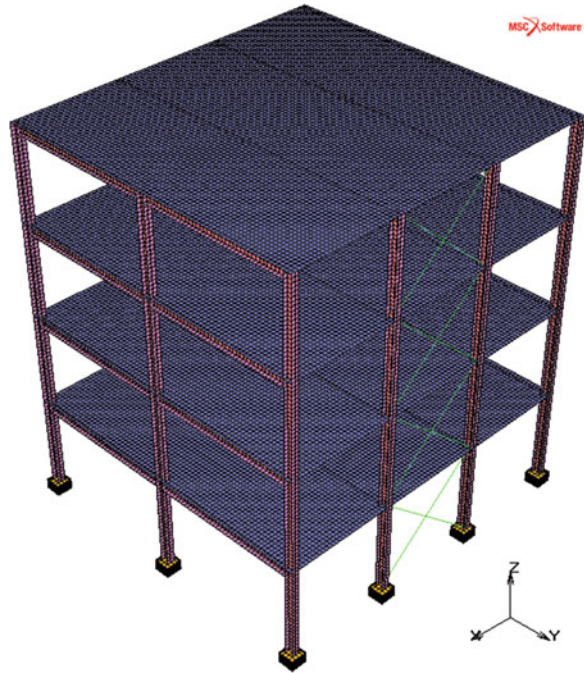
MSC Marc® 2008. The 5-parameter Mooney-Rivlin material has been adopted to
simulate the behaviour of seismic isolation bearings. This hyperelastic model pro-
vides the best fit with the previously obtained experimental results. Besides,
Mooney-Rivlin material model is counted among the most widely adopted consti-
tutive relationships in the stress analysis of polymers (Finney 2001). The following
material constants have been calculated based on the uniaxial tension and com-
pression test data: $C_{10} = 0.889$ MPa, $C_{01} = -0.246$ MPa, $C_{20} = -0.155$ MPa,
$C_{11} = 0.094$ MPa, $C_{30} = 0.011$ MPa and bulk modulus $G = 2.5$ GPa.

30.4   Modal Analysis

The first sequence in the numerical investigation has been focused on determination
of the dynamic properties of the 4-storey building, both fixed-base and base-
isolated. The results of the modal analysis are briefly summarized in Table 30.1.
The first dynamic mode of the base-isolated structure involves deformation only in
Polymeric Bearings, while the superstructure remains basically rigid, as indicated
by Fig. 30.3. The fundamental period corresponding to the first mode of the base-
isolated building has been shifted away and it has been calculated to be $T = 1.306$ s
($f = 0.766$ Hz).

Table 30.1 Results of the modal analysis

Vibration mode		Natural frequency (Hz)	Period of vibration (s)
Fixed-base structure	Transverse	1.594	0.627
	Longitudinal	2.132	0.469
	Torsional	2.736	0.365
Base-isolated structure	First mode	0.766	1.306

Fig. 30.3 Vibration mode of a base-isolated asymmetric 4-storey steel building
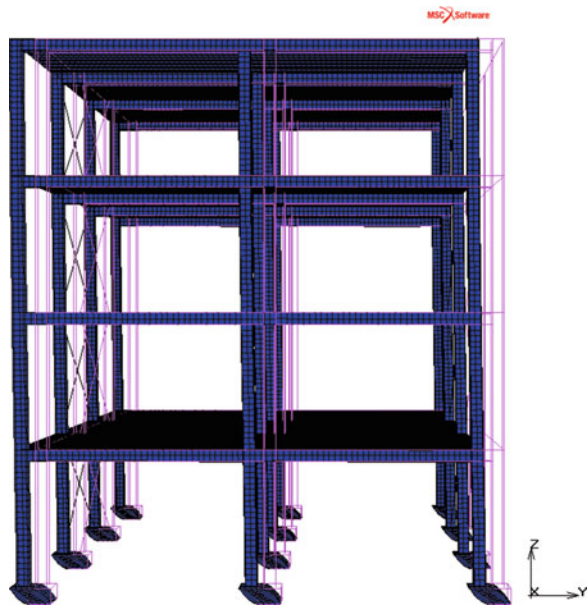
30.5 Dynamic Analysis

In the second stage of the numerical investigation, the dynamic transient analysis has been performed to investigate the response of the 4-storey building, both fixed-base and base-isolated, during a seismic excitation. Both structures, with and without base isolation system, have been subjected to the El Centro earthquake of 1940 (NS component, PGA = 3.070 m/s^2, EW component, PGA = 2.107 m/s^2) and the Northridge earthquake of 1994 (Santa Monica station, NS component, PGA = 3.628 m/s^2, EW component, PGA = 8.664 m/s^2). The NS and EW components of the ground motions have been applied along the Y and X direction, respectively. The first 20 s of the accelerograms, with a time step of 0.01 s, have been employed in this study.

The peak values of the seismic response of the analyzed building are briefly summarized in Table 30.2. Additionally, the time-acceleration histories recorded along the Y direction at the top of the structure, both fixed-base and base-isolated, are presented in Figs. 30.4, 30.5, 30.6, and 30.7.

Table 30.2 Results of the dynamic analysis

Dynamic excitation	Peak acceleration at the top (m/s^2)		Reduction (%)
	Base-isolated structure	Fixed-base structure	
El Centro earthquake of 1940	4.02	12.74	68.45
Northridge earthquake of 1994	6.50	11.38	42.88
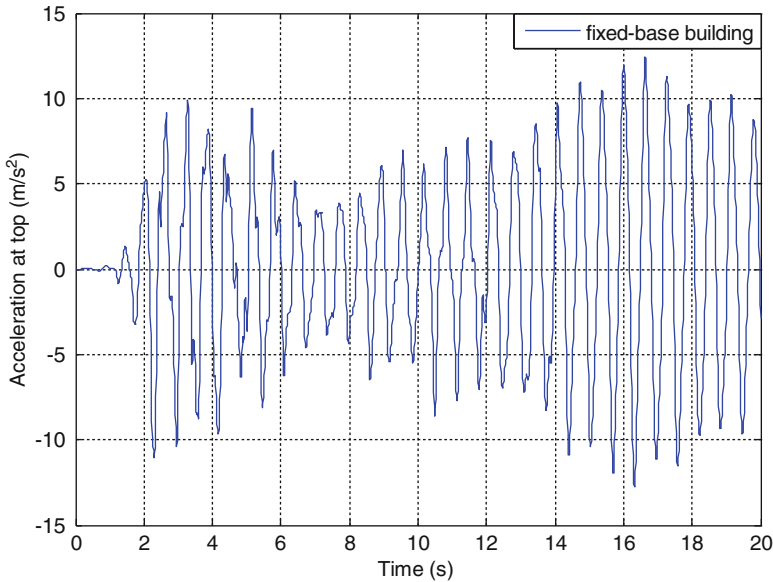
Fig. 30.4 Time-acceleration history plot for the fixed-base building during the 1940 El Centro earthquake (Y direction)

30.6 Results and Conclusions

The effectiveness of Polymeric Bearings in suppressing vibrations of asymmetric building under seismic excitations has been verified in this paper. The reduction in lateral response has been measured by comparing the peak accelerations of a 4-storey asymmetric steel building, both fixed-base and base-isolated. The peak lateral accelerations during the El Centro earthquake of 1940, and the Northridge earthquake of 1994 have been reduced by over 68 % and 42 %, respectively. The results obtained from the numerical analysis on seismic response of the analyzed multi-storey steel structure building indicate that Polymeric Bearings can be successfully used to reduce damage of structures during seismic excitations.

Nevertheless, further experimental studies and numerical analyses (including the nonlinear ones – see, for example, Mahmoud and Jankowski 2009; Jankowski
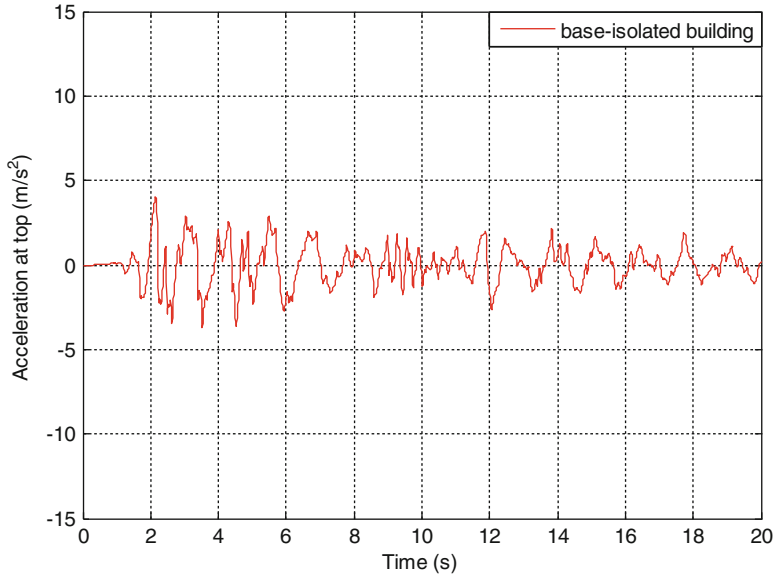
Fig. 30.5 Time-acceleration history plot for the base-isolated building during the 1940 El Centro earthquake (Y direction)
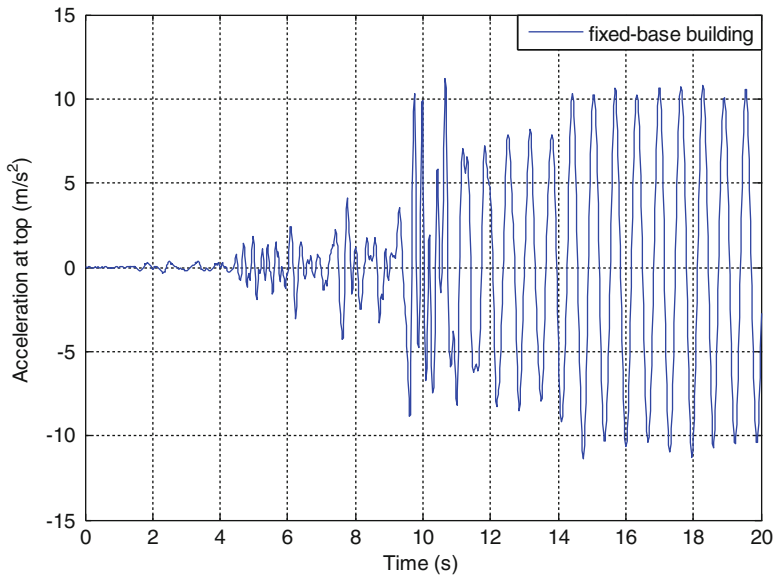
Fig. 30.6 Time-acceleration history plot for the fixed-base building during the 1994 Northridge earthquake (Y direction)
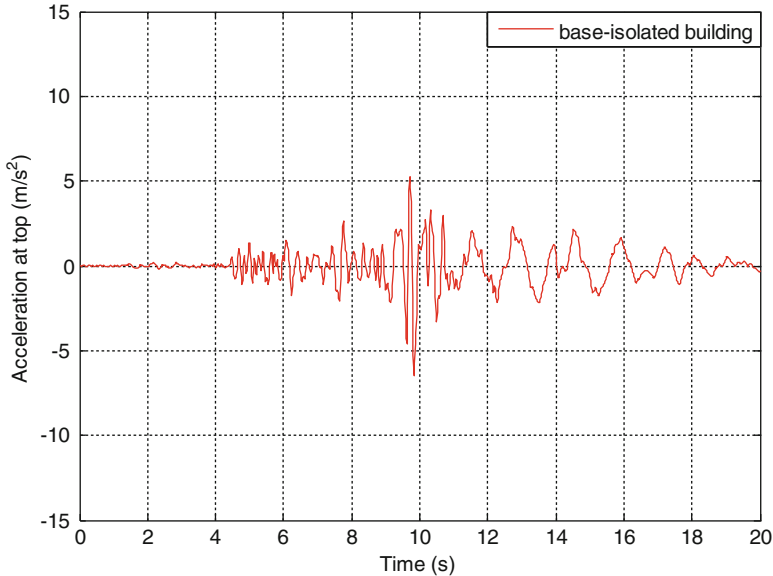
Fig. 30.7 Time-acceleration history plot for the base-isolated building during the 1994 Northridge earthquake (Y direction)

2007) are required to fully verify the efficiency of the Polymeric Bearings as a new base isolation system for asymmetric buildings.

References

Buckle IG (2000) Passive control of structures for seismic loads. In: Proceedings of the 12th world conference on earthquake engineering, Auckland, 30 January–4 February 2000

Falborski T (2012) Experimental determination of basic mechanical properties of elastomeric polymer. In: Fijało C, Fijało P (ed) Advances in chemical and mechanical engineering, Gdańsk University of Technology Publishers, Gdańsk, Poland, pp 147–150

Falborski T, Jankowski R (2012) Shaking table experimental study on the base isolation system made of polymer bearings, In: Proceedings of the 15th world conference on earthquake engineering, Lisbon, 24–28 September 2012

Falborski T, Jankowski R (2013) Polymeric Bearings – a new base isolation system to reduce structural damage during earthquakes. Key Eng Mater 569–570:143–150

Falborski T, Jankowski R, Kwiecień A (2012a) Experimental study on polymer mass used to repair damaged structures. Key Eng Mater 488–489:347–350

Falborski T, Kwiecień A, Strankowski M, Piszczyk Ł, Jankowski R (2012b) The influence of temperature on properties of the polymer flexible joint used for strengthening historical masonries. In: Jasieńko J (ed) Structural analysis of historical constructions. DWE, Switzerland, pp 816–822

Falborski T, Strankowski M, Piszczyk Ł, Jankowski R, Kwiecień A (2012c) Experimental examination of an elastomeric polymer. Technol Art 3:98–101

Finney RH (2001) The finite element method. In: Gent AN (ed) Engineering with rubber: how to design rubber components. Hanser, Berlin, pp 257–305

Jankowski R (2003) Nonlinear rate dependent model of high damping rubber bearing. Bull Earthq Eng 1:397–403

Jankowski R (2007) Assessment of damage due to earthquake-induced pounding between the main building and the stairway tower. Key Eng Mater 347:339–344

Kelly JM (1993) Earthquake-resistant design with rubber. Springer, New York

Mahmoud S, Jankowski R (2009) Elastic and inelastic multi-storey buildings under earthquake excitation with the effect of pounding. J Appl Sci 9:3250–3262

Mahmoud S, Austrell P-E, Jankowski R (2012) Simulation of the response of base-isolated buildings under earthquake excitations considering soil flexibility. Earthq Eng Eng Vib 11:59–374

Mayes RL, Naeim F (2001) Design of structures with seismic isolation. In: Naeim F (ed) The seismic design handbook, 2nd edn. Kluwer, Boston, pp 723–755

Naeim F, Kelly JM (1999) Design of seismic isolated structures: from theory to practice. Wiley, New York

Robinson WH (1982) Lead-rubber hysteretic bearings suitable for protecting structures during earthquakes. Earthq Eng Struct Dyn 10:593–604

Skinner RI (1993) An introduction to seismic isolation. Wiley, New York

Zienkiewicz OC, Taylor RL (2002) The finite element method. Butterworth-Heinemann, Oxford

Index